BIFURCATION ANALYSIS IN GEOMECHANICS

I. Vardoulakis and J. Sulem

BLACKIE ACADEMIC & PROFESSIONAL
An imprint of Chapman & Hall

Bifurcation Analysis in Geomechanics

Bifurcation Analysis in Geomechanics

I.VARDOULAKIS
Department of Engineering Science
National Technical University of Athens
Greece
and
J.SULEM
Centre d'Enseignement et de Recherche en Mécanique des Sols
Ecole Nationale des Ponts et Chaussées/LCPC
France

BLACKIE ACADEMIC & PROFESSIONAL
An Imprint of Chapman & Hall
London • Glasgow • Weinheim • New York • Tokyo • Melbourne • Madras

Published by
Blackie Academic & Professional, an imprint of Chapman & Hall,
Wester Cleddens Road, Bishopbriggs, Glasgow G64 2NZ

This edition published in the Taylor & Francis e-Library, 2005.

"To purchase your own copy of this or any of Taylor & Francis or Routledge's collection of thousands of eBooks please go to www.eBookstore.tandf.co.uk."

Chapman & Hall, 2–6 Boundary Row, London SEl 8HN, UK

Blackie Academic & Professional, Wester Cleddens Road, Bishopbriggs, Glasgow G64 2NZ, UK

Chapman & Hall GmbH, Pappelallee 3, 69469 Weinheim, Germany

Chapman & Hall USA, 115 Fifth Avenue, Fourth Floor, New York NY 10003, USA

Chapman & Hall Japan, ITP-Japan, Kyowa Building, 3F, 2–2–1 Hirakawacho, Chiyoda-ku, Tokyo 102, Japan

DA Book (Aust.) Pty Ltd, 648 Whitehorse Road, Mitcham 3132, Victoria, Australia

Chapman & Hall India, R.Seshadri, 32 Second Main Road, CIT East, Madras 600 035, India

First edition 1995

ISBN 0-203-69703-0 Master e-book ISBN

ISBN 0-203-69777-4 (Adobe eReader Format)
ISBN 0 7514 0214 1 (Print Edition)

A catalogue record for this book is available from the British Library

Library of Congress Catalog Card Number: 95–76795

Foreword

What is the use of bifurcation analysis in petroleum engineering rock mechanics?

This question no doubt will be asked by engineers working in this area with generally rather practical and application oriented portfolios.

> Is there any use at all, is it not just an academic subject, at best useful for well-controlled conditions such as those dealt with in structural engineering of surface facilities?
>
> Are subsurface rock conditions with inherent heterogeneity, anisotropy and layering not so uncertain that highly sophisticated numerical techniques with very precise determination of failure are out of balance?

Many sceptics, amongst whom I have found myself for some time, look upon bifurcation analysis in that way. Until recently there was definitely no strong business pull from petroleum engineering to develop bifurcation analysis in geomechanics because no operating company was really asking for improved production performance. Application of bifurcation analysis to petroleum engineering was clearly a technology push; a technique that was available and was (and is) waiting for people seeing opportunities to apply it.

Once these opportunities were found, this fine technology appears to be a lot more beneficial for our 'rough' business than initially anticipated. For instance, it allows us to solve the very important question of scale dependency of our rock mechanical tests, such as whether a hollow cylinder with a 8 mm hole can be representative for an 8½″ wellbore. Transition between different borehole failure and stabilisation mechanisms can now be understood, which significantly increases the scope for barefoot completions and exclusion or postponement of sand control.

Suddenly a technology that was initially regarded as rather academic contributes to millions of dollars savings.

This book gives an excellent overview and in-depth treatment of all aspects of bifurcation analysis in geomechanics. This is sophisticated and powerful technology, which can be exploited not only in petroleum engineering rock conditions but in many other geomechanical applications.

Cor Kenter

Preface

This book by Vardoulakis and Sulem is an outstanding contribution to the important field of geomechanics and will also be useful to the many branches of engineering and applied science, particularly those dealing with mechanical behavior.

Following a self-contained Introduction, chapter 2 introduces the basic concepts from continuum mechanics and thermodynamics before the incremental formulation of standard continuum mechanics, particularly useful for stability and bifurcation problems, is presented in chapter 3. This formalism is employed in chapter 4 to analyze in detail buckling and interface instabilities, including multilayered and cracked media which offer a natural stimulus for introducing the concept of Crosserat continuum.

Chapter 5 provides an updated contribution to the mechanics of water-saturated media. It takes Biot's original contribution to a new level of understanding, including important physical phenomena such as grain crushing and non-Darcean flow. It uses the essentials of mixture formalism but achieves a great economy of postulates and mathematical generalizations with no direct physical interpretation.

In the same spirit, chapters 6 to 8 provide self-contained reviews of the current plasticity theories and discuss in a systematic and thorough manner the problems of bifurcation and shear-band formation. The effects of non-coaxiality, confining pressure and grain characteristics are explained. The benchmark problems of the triaxial compression test, the biaxial compression test and the cavity inflation test are analyzed in detail as examples of loss of material stability and progressive failure.

The stage has now been set for the introduction of higher order continuum models to describe correctly bifurcation and periodic phenomena in granular materials. Standard theories of soil plasticity do not contain an internal length scale, and thus features such as thickness and spacing of shear bands, as well as the stress-strain response in the softening regime, cannot be addressed. As a result, finite element calculations do not converge and related boundary value problems are ill-posed. The authors were among the first to show that Cosserat and higher order gradient plasticity models can resolve these difficulties.

Self-contained accounts of Cosserat plasticity and second-grade plasticity are given in chapters 9 and 10, respectively. Bifurcation and shear-band analyses are performed and the necessity of higher order terms in removing ill-posedeness in the softening regime

with simultaneous determination of shear-band characteristics (not captured by standard continuum theory) is documented.

The book concludes with an account of stability of undrained deformations. This problem is complex and very little understood despite its practical importance. The authors demonstrate that fundamental work can intelligibly be applied to solve outstanding geomechanics problems with extended engineering implications. Careful laboratory tests are used to calibrate the theoretical models.

This well-organized volume is a substantial and valuable reference for civil engineers and geologists, as well as mechanical engineers and metal physicists. It should be of value to any junior or senior researcher with a keen interest in the stability of deformation.

Elias C.Aifantis
Center for Mechanics of Materials and Instabilities
Michigan Technological University
and Aristotle University of Thessaloniki

Contents

Acknowledgements

This book contains results from over two decades of research and teaching activity in the domain of geomechanics. The authors would like to use the opportunity to acknowledge here the major institutions who through their support have made this work possible:

1. ALERT Geomaterials
2. Commonwealth Scientific and Industrial Research Organization (CSIRO)
3. Commission des Communautés Européennes
4. Deutsche Forschungsgemeinschaft (DFG)
5. Ecole Nationale des Ponts et Chaussées
6. Elf Aquitaine (Production)
7. IKU Petroleum Research
8. Ministries of Foreign Affairs of Greece and France
9. National Science Foundation (NSF)
10. National Technical University of Athens
11. University of Minnesota

In addition we would like to acknowledge some of the individuals who over the years have helped us in this work, either through their collaboration in writing papers or through their valuable support, advice and constructive criticism.

Professor E.C.Aifantis, Dr J.Desrues, Professor A.Drescher, Dr M. Goldscheider, Professor G.Gudehus, Mr A.Guenot, Dr B.Graf, Professor A.Hettler, Professor B.Hobbs, Professor D.Kolymbas, Dr H.-B.Mühlhaus, Dr E.Papamichos, Dr P.Papanastasiou, Dr J.Tronvoll, Dr Ph.Unterreiner.

IV

JS

Commonly used symbols

Kinematics

Scalar	J	Jacobian of the deformation
	v^{p}	accumulated plastic volumetric strain
	g^{p}	accumulated plastic shearing strain intensity (3D model)
	γ^{e}, γ^{p}, γ	respectively, elastic, plastic and total shearing strain intensity for 2D model
Vector	(λ_i)	principal logarithmic strains
	(Δu_i)	infinitesimal displacement vector
	(k_α)	curvature in a 2D Cosserat continuum
Tensor	(F_{ij})	deformation gradient
	$(\Delta\varepsilon_{ij})$	infinitesimal strain tensor
	$(\Delta\omega_{ij})$	infinitesimal spin tensor
	$(\Delta\omega^{c}_{ij}$	infinitesimal Cosserat spin tensor
	(e_{ij})	deviatoric part of the strain tensor
	$I_{1\varepsilon-P}$	first invariant of plastic strain rate
	J_{2e-p}	second deviatoric invariant of plastic strain rate
	(γ_{ij})	relative deformation in a 2D Cosserat continuum
	$(\Delta\psi_{ij})$	microdeformation tensor
	$(\Delta\kappa_{ijk})$	microdeformation gradient

Statics

Scalar	P_w	pore-water pressure
	$I_{1\sigma}$	first invariant of stress tensor
	J_{2s}	second deviatoric invariant of stress tensor
	J_{3s}	third deviatoric invariant of stress tensor
	$p=I_{1\sigma}/3$	mean stress
	$T=\sqrt{J_{2s}}$	shearing stress intensity
	σ	mean stress for 2D model
	τ	shearing stress intensity for 2D model
	α_s	polar angle in deviatoric plane
	ϕ_σ	stress obliquity tan $\phi_\sigma = T/(q-p)$

Vector	(m_α)	couple stresses curvature in a 2D Cosserat continuum
Tensor	(σ_{ij})	Cauchy stress tensor
	(T_{ij})	Kirchhoff stress tensor
	(π_{ji})	first Piola-Kirchhoff stress tensor
	$(\mathbf{T}^{\mathrm{t}}_{ij})$	relative Kirchhoff stress tensor
	(S_{ij})	deviatoric part of the stress tensor
	(τ_{ij})	reduced stress tensor
	(α_{ij})	'back' stress tensor
	(m_{ijk})	double stress tensor

Constitutive functions

Scalar	F	plastic yield function
	Q	plastic potential function
	ψ	hardening parameter
	H	plastic modulus
	H_{t}	hardening modulus
	f	mobilized friction coefficient
	μ	mobilized friction function
	c	mobilized cohesion
	$q=cf$	tension cut-off
	ϕ_{m}	mobilized friction angle
	d	mobilized dilatancy coefficient
	β	mobilized dilatancy function
	ψ_{m}	mobilized dilatancy angle
	θ_{B}	shear-band orientation
Tensor	(Γ_{ji})	acoustic tensor
	$\mathbf{C}^{\mathrm{u}}_{ijkl}$	isotropic elastic stiffness tensor
	$\mathbf{C}^{\mathrm{e}}_{ijkl}$	plastic stiffness tensor
	$\mathbf{C}^{\mathrm{p}}_{ijkl}$	stiffness tensor of the lower-bound comparison solid
	$\mathbf{C}^{l}_{ijkl}$	stiffness tensor of the upper-bound comparison solid

Material parameters

Scalar	E	Young's modulus
	υ	Poisson's ratio
	G	elastic shear modulus
	K	elastic compression modulus

G'	elastic shear modulus for 2D model
K'	elastic compression modulus for 2D model
ρ	total density of saturated medium
ρ_{s}	density of the solid phase
ρ_{w}	density of the fluid phase

S	degree of water saturation
w	water content
n	porosity
e	voids ratio
c_s	particle compressibility
c	bulk compressibility
c_w	water compressibility
B	Skempton pore-water pressure
k_w	hydraulic conductivity
k	physical permeability
η_k	kinematic viscosity of water
η	dynamic viscosity of water
ℓ	characteristic material length

Miscellaneous

$\dot{\_}$	material time derivative
$\mathring{\_}$	Jaumann derivative
$[\_]$	jump of a quantity along a surface
(e_{ijk})	Levi-Civita permutation tensor

1
Introduction

1.1
A historical note

In the year 1900 Otto Mohr published his milestone paper with the title "Welche Umstände bedingen die Elastizitäsgrenze und den Bruch eines Materials?" ("Which conditions determine the elasticity limit and failure of a material?"). Mohr realized that his question cannot be answered without resorting to experiments performed carefully and systematically. However, he realized also that experiments do not give definite answers, since they are always subject to interpretation. In order to arrive at some conclusion one needs a solid theoretical framework within which the experiment is performed. Thus, Mohr developed his fundamental geometrical theory of stress analysis and allowed himself some answers to the original question he posed.

Figures 1.1.1 and 1.1.2 are taken from Mohr's (1900) paper. The former figure is very familiar to any geotechnical engineer and is usually referred to as the (graphical representation of the) 'Mohr-Coulomb' failure criterion, although in Mohr's original paper no explicit reference to Coulomb's (1773) work is made. Accordingly, Mohr's work contains the seeds of Prager's geometrical approach to plasticity theory (Drucker and Prager, 1952). The second figure from Mohr's paper was taken, as he acknowledges, from the *Handbuch der Materialkunde* of Martens. It shows nearly perfect patterns of slip lines (Fliessfiguren). Mohr is convinced that this regularity of the failure patterns, as it is characterized by almost constant relative inclination angles, can only be a result of material properties, which prior to 'failure' are the same everywhere in the tested material specimen. In more ductile metals, these 'yield lines' are more or less perpendicular to each other (upper plate), whereas for more brittle metals they form a rhombic pattern (lower plates). Similar regular rhombic patterns of 'shear bands' we encounter in clay specimens, as shown in Figure 11.4.2, in the last chapter of this book. In today's terminology Mohr's 'Fliessfiguren' would be called patterns of 'localized deformation'.

Mohr summarizes his observations by pointing to the following general property of 'localized' deformation:

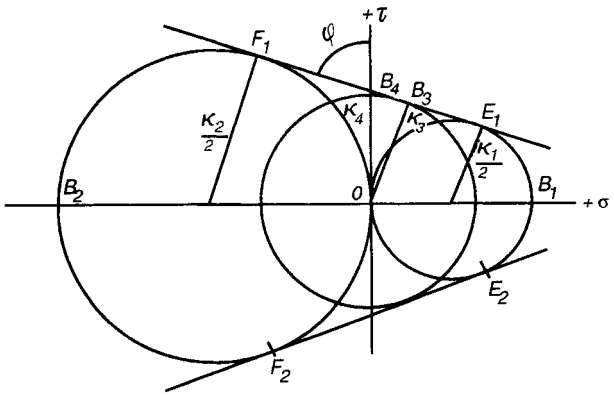

Figure 1.1.1 Mohr's original failure criterion for a frictional or Coulomb material (Mohr, 1900).

> …The deformations observed in a homogeneous body after the elasticity limit [is or less in the fact that parts of the body of finite dimensions, displace with respect reached] are not confined in the smallest domains of the body. They consist more to each other on two sets of slip bands…

Indeed, as we will see in the following sections one basic property of localization phenomena is some degree of discontinuity of the deformation.

There is no doubt that 100 years later, Mohr's original question is still challenging. More important, however, is Mohr's scientific method, which consists of the following steps: (a) Formulation of the mathematical framework; (b) formulation of the (mechanical) theory; (c) performance and interpretation of (critical) experiments according to the needs of the theory; (d) falsification or corroboration of the theory; and (e) possible return to steps (c), (b) or (a) for further iterations.

It is in this context that the title and structure of the book might find its justification. In trying to contribute towards some better description of the concept of 'failure' in solids, we use the term *equilibrium bifurcation analysis* as the name of the basic theoretical tool to be used in our analysis. *Geomechanics*, on the other hand, signifies the material of interest and our confinement to purely mechanical processes. Thus geomechanics is understood here as the mechanics of geomaterials, which in turn could be called 'Coulomb' materials, since these are materials with predominant internal friction in the sense of Mohr.

1.2 Observational background

Failure of many engineering structures is characterized by the formation and propagation of zones of localized shear deformation. In particular, failure and post-failure analyses are important in soil mechanics as well as in earthquake, mining and petroleum engineering design problems, where one is typically interested in ultimate and

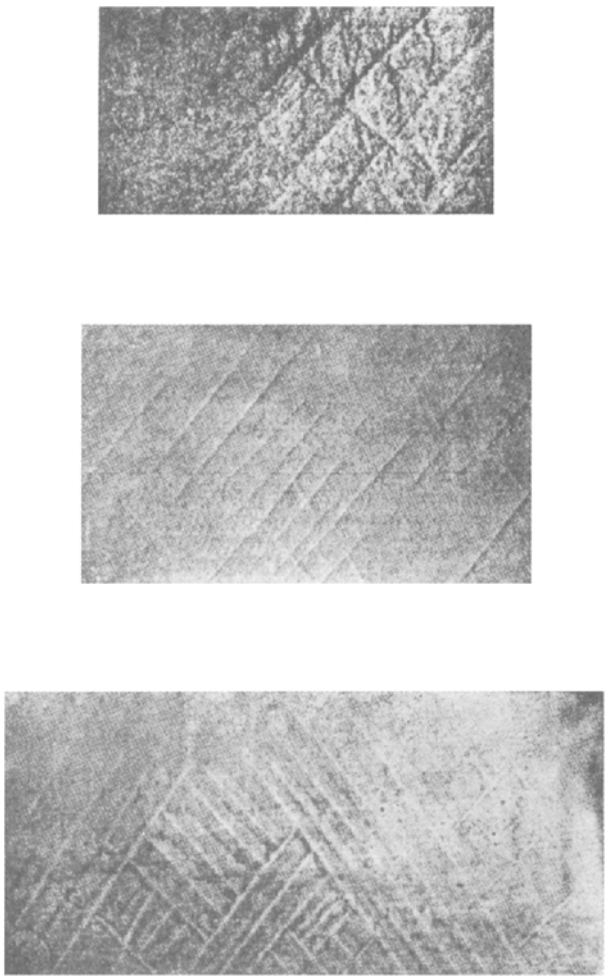

Figure 1.1.2 Marten's 'Fliessfiguren' for metals (Mohr, 1900).

residual bearing capacities of the various analyzed structures. There is also interest in structural geology, where shear bands appear as faults (Figure 1.2.1) which, among other things, give clues to the history, the magnitude and the orientation of tectonic stresses.

For most materials encountered in geomechanics, non-reversible deformation processes are involved in the course of loading history. Inelastic deformation in geomaterials is an inherently non-uniform process; i.e. whenever deformation occurs due to relative motions between grains or due to microcracking, there is a size scale below which the deformation is discontinuous. On size scales which encompass groups of grains or cracks, plastic deformation often appears uniform in specimens which are themselves subject to macroscopically uniform loading conditions. But even on this

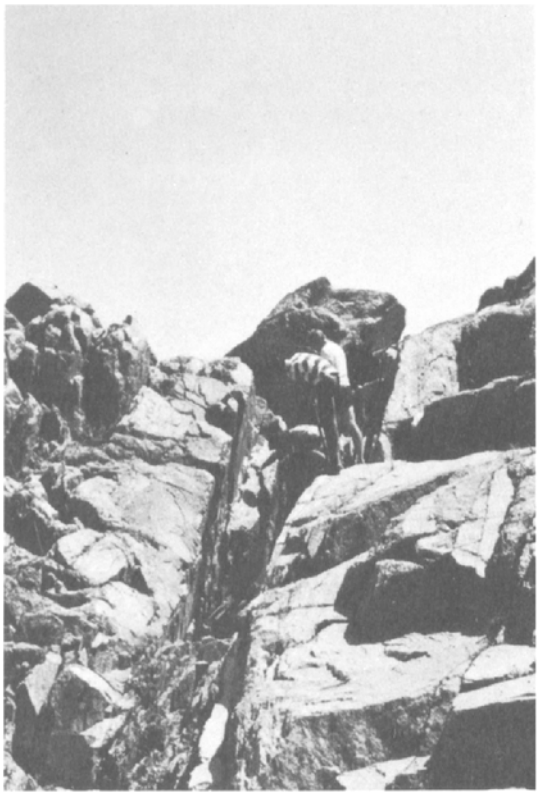

Figure 1.2.1 Shear zone in Wyangala gneiss, Australia (courtesy of Dr. Hobbs).

larger, macroscopic scale, a critical configuration of the deformed body may exist, where the homogeneous deformation breaks down into bands of localized shearing.

In granular, cohesionless solids, shear localization induces intense intergranular slip, which in turn leads to strong dilation of the material inside the localized zone. Figure 1.2.2(a) shows an X-ray radiography of a sand specimen prior to deviatoric loading, at a state of isotropic compression. In the middle of the specimen, a small lens of loose sand was placed to serve as a site of localized deformation. Figure 1.2.2(b) shows the same sand specimen at a later stage of deformation, at peak deviator, with a faint trace of localization of porosity crossing the soft-sand lens. With continued deformation, this localized zone is extending outwards to eventually reach the boundaries of the specimen; Figure 1.2.2(c). On the other hand, in coherent, brittle solids localization instabilities are the result of microcrack opening and slip, intergranular slip and rotation, and occasionally grain crashing (Figure 1.2.3 from Ord *et al.,* 1991), which all coalesce in the course of the post-critical deformation into macrofractures as shown in Figure 1.2.4.

Strong localized material dilatancy either due to grain rearrangement or due to microcracking leads to 'material softening' inside the localized zone, whereas outside

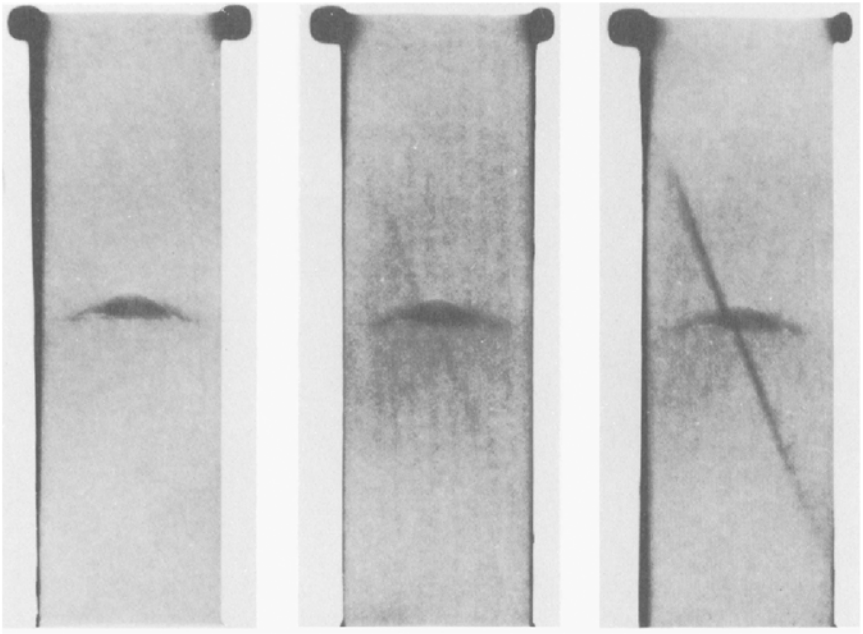

Figure 1.2.2 Evolution of a dilatancy localization in a sand specimen under biaxial compression. For explanation of parts (a) to (c) see text.

this zone elastic unloading is taking place. Thus, as a general observation, one may say that localization phenomena in geomaterials are characterized by material softening. On the other hand, in granular cohesionless solids, localization is mostly due to intense intergranular slip, which leads macroscopically to additional mismatch between internal friction and dilatancy of the granular medium (non-associativeness).

Shear-band formation is a typical example of a 'spontaneous' change of the deformation mode of a body whereas the boundary conditions of the considered structure are kept unchanged. Other examples may be observed at various scales and are usually related to buckling phenomena: buckling of pre-existing microcracks in a solid under uniaxial compression leading to axial splitting type of failure (Figure 1.2.5), barreling or necking of a specimen in a conventional axisymmetric compression or extension test (see Figure 7.1.3 in chapter 7), surface exfoliation and flaking at the wall of a borehole or a tunnel as observed in brittle rocks (Figure 1.2.6), folding or jointing with dominant wavelength spacing as observed in geological structures (Figure 1.2.7).

1.3
The frame of geomaterials constitutive modeling

Geomaterials usually exhibit predominant irreversible deformations and they are relatively rate insensitive. Thus geomaterials, in general, are good examples of 'plastic'

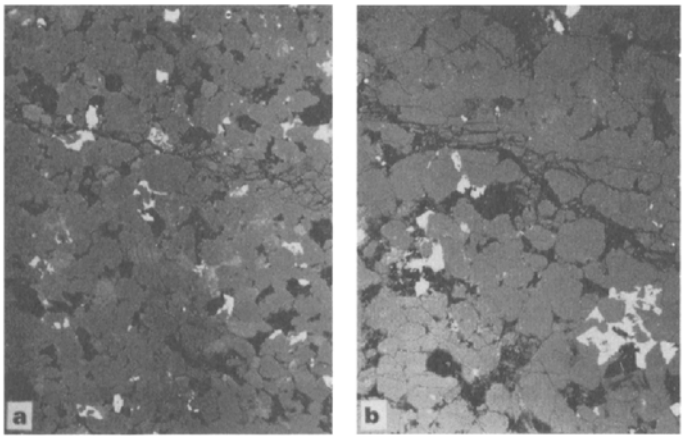

Figure 1.2.3 Micrographs of shear zone in Gosford sandstone under biaxial compression (from Ord *et al.,* 1991).

materials. However, the property which differentiates geomaterials from other 'plastic' solids like metals, is their pronounced *pressure sensitivity*: For pressure-sensitive materials under continued loading the stress deviator T is proportional to the mean normal stress *p,*

$$\mathrm{T} = f(-p) \qquad (p < 0) \tag{1.3.1}$$

where in turn the coefficient f is a function of internal friction, f_o, and cohesion c

$$f = f_0 + \frac{c}{|p|} + \dots \tag{1.3.2}$$

Thus under sufficiently high stresses, all geomaterials are behaving as purely frictional solids. Since sand is the ideal representative of purely frictional material, dry sand is usually selected as a model material to study the basic properties of geomaterials.

Geomaterials are also characterized by plastic or Reynolds' dilatancy, which is understood as a simple internal constraint between plastic volumetric strain increments $\mathrm{d}v^p$ and plastic shear increments $\mathrm{d}g^p$

$$\mathrm{d}v^p = d\,\mathrm{d}g^p \tag{1.3.3}$$

where d is the so-called dilatancy coefficient (Reynolds, 1885).

In frictional and dilatant material the (first-order) plastic work of the stressof the plastic strains is

$$\mathrm{d}w^p = (-p)(f - d)\,\mathrm{d}g^p \geqslant 0 \qquad (p < 0) \tag{1.3.4}$$

Thus from the point of view of energy dissipation, a frictional and dilatant material behaves like a purely frictional or Coulomb material with equivalent internal friction (Taylor, 1948)

$$\bar{f} = f - d \tag{1.3.5}$$

Figure 1.2.4 Macrofractures in a limestone under triaxial compression (courtesy of Dr. J.Labuz).

The above basic assumptions constitute the frame of constitutive modeling of geomaterials. The cohesive-frictional and dilatant character of geomaterials is quite satisfactorily modeled within the frame of elastoplasticity theory with strain hardening/ softening yield surface and non-associate flow rule as exposed, for example, in the comprehensive paper of Mróz (1963). Thus the particular problem of interest, that of localized deformation in geomaterials, must be treated within this theoretical framework.

The problem of modeling localized deformation in geomaterials is quite a challenging task, due to the difficulties which are encountered while dealing with softening materials and moving elastoplastic boundaries. It is, however, one of the most interesting bifurcation problems: Asking the question of possible spontaneous change of the deformation mode for a given loading history and subsequent evolution of this secondary deformation mode, one may search for the conditions of uniqueness and stability of the corresponding boundary value problem. Thus as first presented by

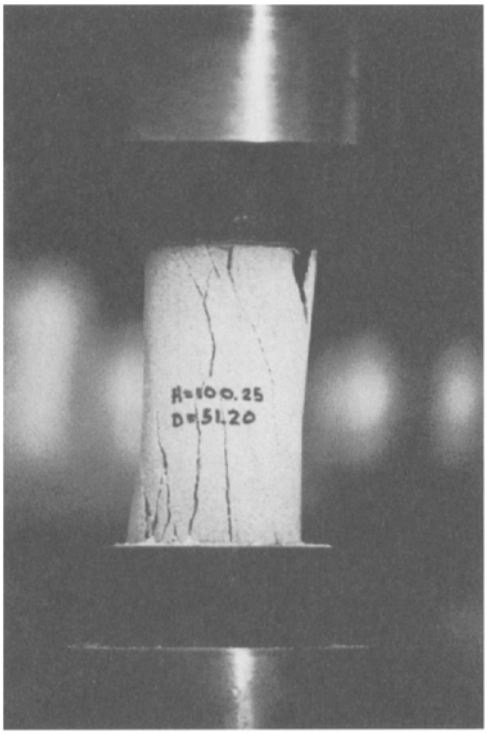

Figure 1.2.5 Failure by axial splitting of a Berea sandstone specimen loaded in uniaxial compression (courtesy of Dr. E.Papamichos).

Mandel (1964, 1966) questions of uniqueness and stability of solutions arise naturally within the context of shear-band analysis. It turns out that the result of such analyses dealing with geomaterials depends primarily on the assumed physical non-linearities which are inherent to the underlying constitutive description and is, in a lesser degree, influenced by geometrical non-linearities.

The various drawbacks and shortcomings of the classical continuum theory in connection with strain localization or, more generally, for the problem where a loss of ellipticity of the governing equations is taking place, have been discussed extensively in many recent papers; cf. Benallal *et al.* (1988, 1989). The origin of this undesirable situation can be traced back to the fact that conventional constitutive models do not contain material parameters with dimension of length, so that the shear-band thickness (i.e. the extent of the plastically softening region) is not determined. For example, for granular materials the observed shear-band thickness is of the order of 10 to 20 grain diameters (Roscoe, 1970). We can say that localization of deformation leads to a change in scale of the problem so that phenomena occurring at the scale of the grain cannot be ignored anymore in the modeling of the macroscopic behavior of the material. Then it appears necessary to resort to continuum models with microstructure to describe correctly localization phenomena. These generalized continua usually contain additional

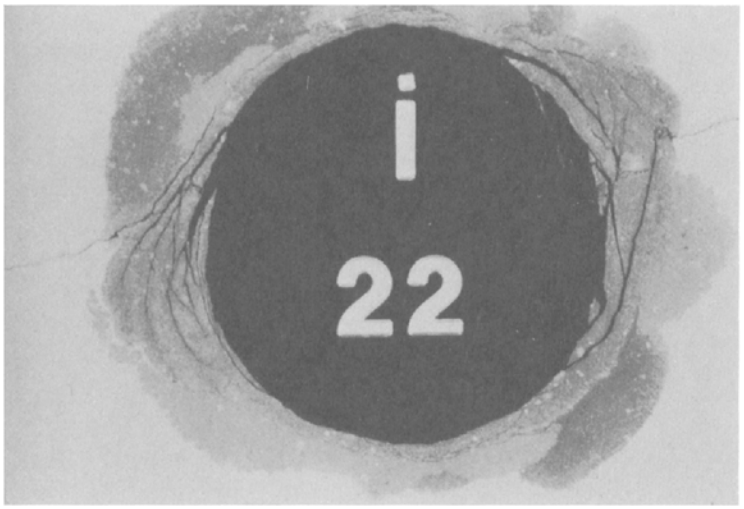

Figure 1.2.6 Failure of a hollow cylinder (courtesy of Dr. A.Guenot, Elf Aquitaine).

kinematical degrees of freedom (Cosserat continuum) and/or higher deformation gradients (higher-grade continuum). Cosserat continua and higher-grade continua belong to a general class of constitutive models which account for the materials *microstructure*.

Professor G.I.Barenblatt in the closing lecture of the 18th IUTAM Congress (Haifa, Israel, 1992) stated that: "Micromechanics is the branch of mechanics studying the phenomena for which the variations of microstructure are of governing influence for the macroscopic behavior of bodies". The description of statics and kinematics of continuous media with microstructure has been studied in a systematic way by Germain (1973a,b) through the application of the virtual work principle. In a classical description, a continuum is a continuous distribution of particles, each of them being represented geometrically by a point X and characterized kinematically by a velocity v. In a theory which takes into account the microstructure of the material, each particle is viewed as a continuum C(X) of small extent around the point X. Consequently, the deformation of the volume C(X) of the particle is called the *microdeformation*. For example, a Cosserat continuum is a 'micropolar' medium obtained by assuming that the particle C(X) moves as a rigid body, characterized by a velocity vector v and a particle rotation vector $\boldsymbol{\omega}^c$. The corresponding kinematical qualities, velocity and rotation gradient (curvature), $\nabla\mathbf{v}$ and $\nabla\boldsymbol{\omega}^c$,, are associated through the principle of virtual work with a non-symmetric stress tensor and couple stress tensor, respectively. Similarly, in a second gradient continuum trough, the principle of virtual work a symmetric second-order stress tensor and a third-order (double) stress tensor are defined which are dual in energy to $\nabla\mathbf{v}$ and $\nabla\nabla\mathbf{v}$ respectively.

Rotation gradients and higher velocity gradients introduce a material length scale into the problem, which as already mentioned is necessary for the correct modeling of

Figure 1.2.7 Folding and jointing.

localization phenomena. In this case, the underlying mathematical problem describing localization phenomena is 'regularized' and the governing equations remain elliptic. Moreover, this technique allows robust computations to follow the evolution of the considered system in the post-bifurcation regime and to extract additional information such as the shear-band thickness or to assess the effect of scale.

1.4
Considered topics

Although it is not possible to include in a single book a comprehensive analysis of bifurcation phenomena in geomechanics, it is our intention to present here the necessary theoretical tools and experimental facts which we believe are necessary for a rigorous and realistic description of 'failure' of soils and rocks.

Chapter 2 summarizes some of the basic concepts from classical continuum mechanics; this includes geometric non-linearity and large deformation analysis. This chapter, as all the others, is self-contained, and the reader can find at the end of each chapter references to additional literature. Chapter 3 deals with incremental continuum

mechanics in the frame of updated Lagrangian formulation. The emphasis lies here in the formulation of the linear bifurcation problem. Incremental continuum mechanics was first introduced in geomechanics by Biot (1965), in his pioneering work, which was mostly devoted to structural geology problems. As an application of the theoretical tools presented in chapter 3, we examine in chapter 4 buckling phenomena in elastic media as a typical bifurcation problem. The influence of microstructure of such media, like the existence of a periodic stratification or a double periodic crack array, on the buckling load and the dominant wavelength of the buckling mode is discussed as well.

Chapter 5 deals with the continuum mechanics of water-saturated granular materials where a mixture theory approach to modeling is followed. There one can find the derivation of pertinent balance laws, the discussion of Terzaghi's effective stress principle and its modifications as well as Darcy's law and its extension to the cases of turbulent and viscous dissipative flows.

Chapter 6 summarizes the basic concepts from plasticity theory as applied to granular soils and rocks. Starting from the basic concepts of classical flow theory of plasticity with a yield criterion and a plastic potential, we present, in a hierarchical manner, the possible extensions of isotropic hardening plasticity. We believe that an integral part of constitutive modeling is the calibration procedure. Since there is no unique strategy for calibration, examples given in chapter 6 should be understood as a suggestion which proved itself appropriate in number of applications.

Constitutive models are calibrated on 'element' tests performed in the laboratory by applying uniform loading to homogeneous specimens. However, experiments with 'perfect' boundary conditions and 'perfectly' homogeneous material do not generally secure homogeneous deformation. Spontaneous loss of homogeneity is possible and typically observed. This possibility is investigated in chapters 7 and 8 by asking for diffuse or localized modes under ideal boundary conditions. If solutions of the corresponding equilibrium bifurcation exist, it is reasonable to assume that imperfections only intensify this tendency. The reader will also find in chapter 8 additional information on the state of the art on shear banding in granular media with reference to open questions and its suggestions for possible modification of classical models.

Chapters 9 and 10 deal with higher order theories such as Cosserat continuum model and second-gradient model. The concepts discussed therein are applied to the problems of shear-band thickness and interface layers. The regularization of the original mathematically ill-posed boundary value problem with strain softening material is also demonstrated.

Finally, in the last chapter and as an application of the concepts presented in chapter 3 and 5–10, the coupled stability analysis of undrained deformations in water-saturated sand is discussed. The analysis uses an experimental database and seeks to shed some light in the phenomenon of soil 'liquefaction' and shear-banding under globally undrained conditions.

Literature

Textbooks and monographs

Biot, M.A. (1965). *Mechanics of Incremental Deformation.* John Wiley, New York.

Coulomb, Charles-Augustin. *'Essai sur une application des règles de Maximis et Minimis a quelques problèmes de statique, relatifs à I'architecture'* 1773. In: J.Heyman (1972), *Coulomb's Memoir on Statics,* Cambridge University Press, Cambridge.

Taylor, D.W. (1948). *Fundamentals of Soil Mechanics*. John Wiley, New York.

References

Barenblatt, G.I. (1992). Micromechanics of fracture. *Theoretical and Applied Mechanics*, Proc. 18th Int. Cong. Theor. Appl. Mech., Haifa, Israel (S.R.Bodner, J.Singer, A.Solan, eds), Elsevier, Amsterdam, 25–52.

Benallal, A., Billardon, R. and Geymonat, G. (1988). Some mathematical aspects of damage softening rate problem. In: *Cracking and Damage* (J.Mazars and Z.P.Bazant, eds), Elsevier, Amsterdam, 247–258.

Benallal, A., Billardon, R. and Geymonat, G. (1989). Conditions de bifurcation à l'intérieur et aux frontières pour une classe de matériaux non standards. *C.R. Acad. Sci., Paris,* **308,** série II, 893–898.

Drucker, D.C. and Prager, W. (1952). Soil mechanics and plastic analysis or limit design. *Quart. Appl. Math.,* **10,** 157–165.

Germain, P. (1973a). La méthode des puissances virtuelles en mécanique des milieux continus. Part 1. *J. de Méchanique,* **12,** 235–274.

Germain, P. (1973b). The method of virtual power in continuum mechanics. Part 2: Microstructure. *SIAM J. Appl. Math.*, **25,** 556–575.

Mandel, J. (1964). Propagation des surfaces de discontinuite dans un milieu élasto-plastique. In: *Stress Waves in Anelastic Solids,* Springer, Berlin, 331–341.

Mandel, J. (1966). Conditions de stabilité et postulat de Drucker. In: *Rheology and Soils Mechanics,* Springer, Berlin, 58–68.

Mohr, O. (1900). Welche Umstände bedingen die Elastizitäsgrenze und den Bruch eines Materials? *Zeitschr. Vereines deutsch. Ingenieure,* **44,** 1–12.

Mróz, Z. (1963). Non-associate flow laws in plasticity. *J. de Mécanique,* **2,** 21–42.

Ord, A., Vardoulakis, I. and Kajewski, R. (1991). Shear band formation in Gosford sandstone. *Int. J. Rock Mech. Min. Sci. Geomech. Abstr,* **28,** 5, 397–409.

Reynolds, O. (1885). On the dilatancy of media composed of rigid particles in contact. With experimental illustrations. *Phil. Mag.,* (2)**20,** 469–481. See also: Truesdell, C. and Noll, W. (1965). *The Non-Linear Field Theories of Mechanics, Handbuch der Physik, Vol. III/3,* section 119, Springer, Berlin.

Roscoe, K.H. (1970). The influence of strains in soil mechanics. *Géotechnique,* **16,** 129–170.

2
Basic concepts from continuum mechanics

2.1
Kinematic and static considerations

2.1.1
Lagrangian description of the deformation

Let a body B in an initial configuration $C^{(0)}$ be subjected to a given deformation which results in a configuration C, where the body B occupies the volume V and is surrounded by the boundary ∂V (Figure 2.1.1). Relative to a *fixed-in-space* Cartesian coordinate system a particle X has the coordinates ξ_i and x_i in $C^{(0)}$ and C, respectively. Let u_i denote the components of the displacement vector of the material point X with respect to its initial position in $C^{(0)}$

$$u_i = x_i - \xi_i \qquad (i = 1,2,3) \tag{2.1.1}$$

In the Lagrangian description of the deformation the coordinates x_i of point X in C are functions of the coordinates ξ_i of this point X in the reference configuration $C^{(0)}$ and of time t

$$x_i = x_i(\xi_k, t) \quad \text{with} \quad x_i(\xi_k, 0) \equiv \xi_i \tag{2.1.2}$$

The field $x_i(\xi_k, t)$ is called the deformation and its (material) spatial derivative is called the deformation gradient

$$F_{ij} = \frac{\partial}{\partial \xi_j} x_i(\xi_k, t) \tag{2.1.3}$$

which gives the change of the distance $d\xi_i$ between two neighboring material points $X(\xi_i)$ and $Y(\xi_i+d\xi_i)$

$$dx_i = F_{ij} d\xi_j \tag{2.1.4}$$

With equation 2.1.1, the deformation gradient can be expressed in terms of the displacement gradient

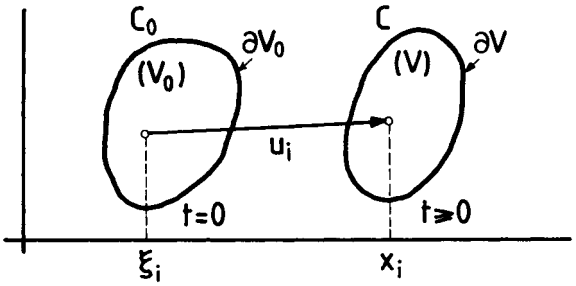

Figure 2.1.1 Initial and current configuration of a deforming solid.

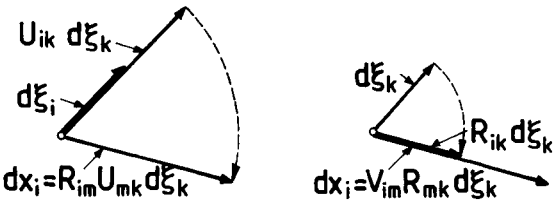

Figure 2.1.2 Schematic representation of the polar decompositions of F_{ij} (equations 2.1.6 and 2.1.25).

$$F_{ij} = \frac{\partial}{\partial \xi_j} u_i(\xi_k, t) + \delta_{ij} \tag{2.1.5}$$

where δ_{ij} is the Kronecker delta.

The right-polar decomposition of the deformation gradient F_{ij} results in an orthogonal part R_{ij} and into a symmetric part U_{ij}

$$F_{ij} = R_{ik} U_{kj} \tag{2.1.6}$$

with

$$R_{ik} R_{jk} = \delta_{ij};\ U_{ij} = U_{ji} \tag{2.1.7}$$

The orthogonal part of F_{ij} corresponds to a rigid-body rotation, i.e. $(R_{ij}) = +1$, whereas its symmetric part corresponds to pure stretching (Figure 2.1.2). Accordingly, R_{ij} is called the rotation tensor and U_{ij} the right-stretching tensor.

As already mentioned, the deformation gradient gives the change of the metric of the deformed body. Let $X(\xi_i)$ and $Y(\xi_i + d\xi_i)$ be two neighboring material points in $C^{(0)}$, which in C were to occupy the positions $X(x_i)$ and $Y(x_i + dx_i)$ respectively. The distance of these two points in $C^{(0)}$ is

$$dl^{(0)} = (d\xi_i\ d\xi_i)^{\frac{1}{2}} \tag{2.1.8}$$

which during the considered deformation $C^{(0)} \rightarrow C$ changes to

$$dl = (dx_i\ dx_i)^{\frac{1}{2}} \tag{2.1.9}$$

Since, according to equation 2.1.4, point differences transform like tensors we obtain

$$\begin{aligned} dl^2 &= F_{ij}d\xi_j F_{ik}d\xi_k \\ &= R_{il}U_{lj}R_{im}U_{mk}d\xi_j d\xi_k \\ &= U_{mj}U_{mk}d\xi_j d\xi_k \\ &= C_{ij}d\xi_j d\xi_k \end{aligned} \tag{2.1.10}$$

C_{ij} is called the right Cauchy-Green strain tensor

$$C_{ij} = F_{ki}F_{kj} = R_{km}U_{mi}R_{kn}U_{nj} = \delta_{mn}U_{mi}U_{nj} = U_{mi}U_{mj} \tag{2.1.11}$$

We notice that U_{ij} is not very convenient strain measure since its evaluation involves principal axes transformation of the tensor$C_{ij} = F_{ki}F_{kj}$. Furthermore, the eigenvalues of U_{ij} are the square roots of the eigenvalues of C_{ij}. Instead of C_{ij} the Green strain tensor Gij may be used

$$G_{ij} = (F_{ki}F_{kj} - \delta_{ij})/2 = (C_{ij} - \delta_{ij})/2 \tag{2.1.12}$$

If the deformation gradient tensor maps $C^{(0)}$ onto itself then the right Cauchy-Green tensor is the identity tensor and Green's tensor is zero; i.e. if

$$F_{ij} = F_{ji}^{-1} \rightarrow C_{ij} = \delta_{ij};\ G_{ij} = 0 \tag{2.1.13}$$

From equations 2.1.5 and 2.1.12 follows the well-known representation of Green's strain tensor in terms of the displacement gradient

$$G_{ij} = \frac{1}{2}\left[\frac{\partial u_i}{\partial \xi_j} + \frac{\partial u_j}{\partial \xi_i} + \frac{\partial u_k}{\partial \xi_i}\frac{\partial u_k}{\partial \xi_j}\right] \tag{2.1.14}$$

If the second-order terms in the right-hand side of equation 2.1.14 are negligible as compared to the first-order terms, then

$$G_{ij} = E_{ij} + 0(|\partial u_i/\partial \xi_j|^2) \tag{2.1.15}$$

where

$$E_{ij} = \frac{1}{2}\left[\frac{\partial u_i}{\partial \xi_j} + \frac{\partial u_j}{\partial \xi_i}\right] \tag{2.1.16}$$

is the infinitesimal Lagrangian strain tensor.

Another commonly used measure of finite strain is the logarithmic, right Hencky strain tensor, λ_{ij}^{r}. In order to evaluate the logarithmic strain one has first to find the principal axes of the right Cauchy-Green strain tensor and change coordinates into this system. Let

$$\bar{C}_{ij} = \delta_{ij}c_{(j)}$$

$$\bar{C}_{ij} = K_{ik}K_{jl}C_{kl}$$

with

be the right Cauchy-Green strain, transformed into principal axes. Then we define

$$(\ln C)_{ij} = K_{ki} K_{lj} (\ln \bar{C})_{kl}$$

$$(\ln \bar{C})_{ij} = \delta_{ij} \ln(c_{(j)})$$

and

$$\lambda^{r}_{ij} = \tfrac{1}{2}(\ln C)_{ij} \tag{2.1.17}$$

We must state here that the Lagrangian description of the deformation is mostly applied in the theory of finite elasticity. Here the Lagrangian formulation will not be exploited further since the emphasis lies on constitutive theories of the rate type among which the central place is occupied by the theory of plasticity as applied to geomaterials.

2.1.2
Eulerian description of the deformation

Here we will briefly review the Eulerian description of the deformation. Within this formulation, all fields are assumed to be functions of time and of the spatial coordinates x_i of a point X in C through the inverse mapping of equation 2.1.2

$$\xi_i = x_i^{-1}(x_k, t) \tag{2.1.18}$$

This results in the inverse deformation gradient

$$F_{ij}^{-1} = \frac{\partial}{\partial x_j} x_i^{-1}(x_k, t) \tag{2.1.19}$$

with

$$F_{ik} F_{kj}^{-1} = \delta_{ij};\ F_{ik}^{-1} F_{kj} = \delta_{ij} \tag{2.1.20}$$

With equations 2.1.1 and 2.1.18, the displacement vector can be expressed in terms of the Eulerian coordinates

$$u_i = u_i(\xi_k, t) = u_i(x_k^{-1}(x_l, t), t) = \hat{u}_i(x_l, t) \tag{2.1.21}$$

and the inverse deformation gradient becomes

$$F_{ij}^{-1} = \delta_{ij} - \partial_j u_i \tag{2.1.22}$$

where the notation $\partial_j \equiv \partial/\partial x_j$, for the differentiation with respect to the spatial coordinates x_i of X in C is used throughout and the superimposed (ˆ) is deleted. With

$$\mathrm{d}\xi_i = F_{ij}^{-1} \mathrm{d}x_j \tag{2.1.23}$$

the metric in C and $C^{(0)}$ is given by

$$\mathrm{d}\ell = (\mathrm{d}x_i\ \mathrm{d}x_i)^{\frac{1}{2}};\ \mathrm{d}\ell^{(0)} = (\mathrm{d}\xi_i\ \mathrm{d}\xi_i)^{\frac{1}{2}} = (F_{im}^{-1} F_{in}^{-1} \mathrm{d}x_m \mathrm{d}x_n)^{\frac{1}{2}} \tag{2.1.24}$$

On the other hand the left-polar decomposition of the deformation gradient F_{ij} results in Figure 2.1.2.

$$F_{ij} = V_{ik}R_{kj};\ R_{ik}R_{jk} = \delta_{ij};\ V_{ij} = V_{ji} \tag{2.1.25}$$

where R_{ij} is the same orthogonal tensor as in the right polar decomposition, equation 2.1.6. The symmetric tensor V_{ij} is called the left-stretching tensor which describes the relation between the metric in $C^{(0)}$ and the line elements in C

$$\begin{aligned} d\ell^{(0)} &= (R_{ki}V_{km}^{-1}dx_m R_{li}V_{ln}^{-1}dx_n)^{\frac{1}{2}} \\ &= (\delta_{kl}V_{km}^{-1}dx_m V_{ln}^{-1}dx_n)^{\frac{1}{2}} \\ &= (V_{km}^{-1}V_{kn}^{-1}dx_m dx_n)^{\frac{1}{2}} \\ &= (B_{mn}^{-1}dx_m dx_n)^{\frac{1}{2}} \end{aligned}$$

where B_{ij} is the left Cauchy-Green strain tensor

$$B_{ij} = F_{ik}F_{jk} = V_{im}R_{mk}V_{jn}R_{nk} = V_{im}V_{jm} \tag{2.1.26}$$

Alternatively, one may use the so-called Almansi strain tensor A_{ij}

$$A_{ij} = \tfrac{1}{2}(\delta_{ij} - F_{ki}^{-1}F_{kj}^{-1}) = \tfrac{1}{2}(\delta_{ij} - B_{ij}^{-1}) \tag{2.1.27}$$

If the deformation is a pure rigid-body rotation, then the Cauchy-Green strain tensor maps C onto itself and Almansi's strain tensor is null

$$F_{ij} = F_{ji}^{-1} \rightarrow B_{ij} = \delta_{ij} \quad \text{and} \quad A_{ij} = 0 \tag{2.1.28}$$

From equations 2.1.22 and 2.1.28 follows finally the well-known representation of Almansi's strain tensor in terms of the displacement gradient

$$A_{ij} = \tfrac{1}{2}(\partial_j u_i + \partial_i u_j - \partial_i u_k \partial_j u_k) \tag{2.1.29}$$

Again, if second-order terms are neglected, then A_{ij} coincides with the Eulerian infinitesimal strain

$$\varepsilon_{ij} = \tfrac{1}{2}(\partial_j u_i + \partial_i u_j) \tag{2.1.30}$$

in which case Lagrangian and Eulerian infinitesimal strains coincide, i.e.

$$\varepsilon_{ij} = \frac{1}{2}\left[\frac{\partial u_i}{\partial \xi_k}(\delta_{kj} - \partial_j u_k) + \frac{\partial u_j}{\partial \xi_k}(\delta_{ki} - \partial_i u_k)\right] \approx \frac{1}{2}\left[\frac{\partial u_i}{\partial \xi_j} + \frac{\partial u_j}{\partial \xi_i}\right] = E_{ij}$$

Similar to the definition 2.1.17, we may introduce the logarithmic left Hencky strain tensor,

$$\lambda_{ij}^{\ell} = \tfrac{1}{2}(\ln \mathbf{B})_{ij} \tag{2.1.31}$$

In the particular case of a rectilinear deformation, which is characterized by non-rotating principal strain directions, the left and right Hencky tensors coincide, $\lambda_{ij}^{\ell} = \lambda_{ij}^{r} = \lambda_{ij}$. As indicated in Figure 2.1.3 a cuboidal specimen undergoing a rectilinear deformation keeps its shape and only its sides are elongated or shortened. With initial and final dimensions of the specimen $\ell_i^{(0)}$ and $\ell_i = \ell_i^{(0)} + \Delta\ell_i\ (i = 1,2,3)$, in $C^{(0)}$ and C respectively, the principal logarithmic strains are

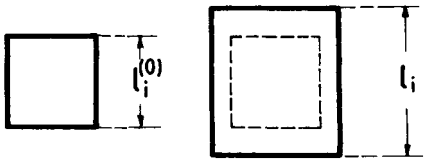

Figure 2.1.3 Rectilinear stretching of a cuboidal specimen.

$$\lambda_i = \ln(\ell_i^*) = \ln(1 + E_i);\ E_i = \varepsilon_i = \frac{\Delta \ell_i}{\ell_{(i)}^{(0)}} \tag{2.1.32}$$

and

$$\ell_i^* = \frac{\ell_i}{\ell_{(i)}^{(0)}} \qquad (i = 1, 2, 3) \tag{2.1.33}$$

are the principal stretches of the considered rectilinear deformation.

2.1.3
Deformation of surface and volume elements

Let $\mathrm{d}S_i^{(0)}$ be a surface element vector in $\mathrm{C}^{(0)}$ that is defined by the vector product of two line-element vectors $d_{\xi i}$, $d_{\psi i}$

$$\mathrm{d}S_i^{(0)} = e_{ijk}\,\mathrm{d}\xi_j\,\mathrm{d}\psi_k;\ \mathrm{d}S^{(0)} = (\mathrm{d}S_i^{(0)}\,\mathrm{d}S_i^{(0)})^{\frac{1}{2}} \tag{2.1.34}$$

where e_{ijk} is the Levi-Civita permutation tensor, i.e. the complete third-order antisymmetric tensor

$$\begin{aligned} &\text{if } (i, j, k) = \text{cyclic}(1, 2, 3) \text{ then } e_{ijk} = \ \ 1 \\ &\text{if } (i, j, k) = \text{cyclic}(2, 1, 3) \text{ then } e_{ijk} = -1 \\ &\qquad\qquad\qquad\qquad \text{else } e_{ijk} = \ \ 0 \end{aligned} \tag{2.1.35}$$

The line elements $\mathrm{d}\xi_i$ and $\mathrm{d}\psi_i$ are deformed to the line elements $\mathrm{d}x_i$ and $\mathrm{d}y_i$, respectively, and the surface element $\mathrm{d}S^{(0)}$ is deformed into the surface element $\mathrm{d}S$

$$\mathrm{d}S_i = e_{ijk}\,\mathrm{d}x_j\,\mathrm{d}y_k;\ \mathrm{d}S = (\mathrm{d}S_i\,\mathrm{d}S_i)^{\frac{1}{2}} \tag{2.1.36}$$

From

$$\mathrm{d}S_i^{(0)} = e_{ijk}F_{jm}^{-1}F_{kn}^{-1}\,\mathrm{d}x_m\,\mathrm{d}y_n$$

it follows that

$$\begin{aligned} F_{ip}^{-1}\,\mathrm{d}S_i^{(0)} &= e_{ijk}F_{ip}^{-1}F_{jm}^{-1}F_{kn}^{-1}\,\mathrm{d}x_m\,\mathrm{d}y_n \\ &= e_{ijk}F_{i1}^{-1}F_{j2}^{-1}F_{k3}^{-1}e_{pmn}\,\mathrm{d}x_m\,\mathrm{d}y_n \\ &= \det(F_{k1}^{-1})\,\mathrm{d}S_p \end{aligned}$$

and accordingly surface-element vectors are related to each other as

$$\mathrm{d}S_i = \mathrm{ad}(\mathbf{F})_{ki}\,\mathrm{d}S_k^{(0)} \tag{2.1.37}$$

where $\mathrm{ad}(\mathbf{F})_{ij}$ is the adjoint of F_{ij}

$$\mathrm{ad}(\mathbf{F})_{ij} = \det(F_{kl})F_{ij}^{-1}$$

Finally, let $\mathrm{d}V^{(0)}$ and $\mathrm{d}V$ be volume elements in $\mathrm{C}^{(0)}$ and C, respectively,

$$\mathrm{d}V^{(0)} = e_{ijk}\,\mathrm{d}\xi_i\,\mathrm{d}\psi_j\,\mathrm{d}\zeta_k;\ \mathrm{d}V = e_{ijk}\,\mathrm{d}x_i\,\mathrm{d}y_j\,\mathrm{d}w_k \tag{2.1.38}$$

The deformation rule for volume elements is then given by

$$\mathrm{d}V = J\,\mathrm{d}V^{(0)} \tag{2.1.39}$$

where the Jacobian of the deformation

$$J = \det(F_{ij}) = \mathrm{d}V/\mathrm{d}V^{(0)} > 0 \tag{2.1.40}$$

2.1.4
Static considerations

Let $\mathrm{d}t_i$ be the stress vector acting on a surface-element vector $\mathrm{d}S_i$ in C. The true or *Cauchy* stress tensor in C is defined through the mapping (Figure 2.1.4)

$$\mathrm{d}t_i = \sigma_{ki}\,\mathrm{d}S_k \tag{2.1.41}$$

In addition to the Cauchy stress tensor there are many other stress tensors which can be defined for describing the state of stress in the current configuration. The choice as to which one should be used mainly reflects convenience in the mathematical description of balance and/or constitutive equations. In addition to the Cauchy stress tensor we will discuss here another Eulerian stress tensor which is suitable for easy description of the behavior of materials undergoing large volumetric deformations. This stress tensor is called the *Kirchhoff* stress tensor and is related to the Cauchy stress σ_{ij} as follows

$$T_{ij} = J\sigma_{ij} \tag{2.1.42}$$

If the deformation is isochoric, then $\mathrm{d}V^{(0)} = \mathrm{d}V\ (J = 1)$, and the Kirchhoff and Cauchy stress tensors coincide.

In order to illustrate the usefulness of the Kirchhoff stress, we briefly comment here on the behavior of highly compressible geomaterials, like clays, and to the representation of corresponding experimental results. As it is common in the soil mechanics literature, the experimental data are plotted in terms of Cauchy stress and the infinitesimal strain resulting to non-linear stress-strain curves. Due to the highly non-linear character of the compression curves Terzaghi suggested representing the experimental results in a semi-logarithmic plot of engineering strain $|\varepsilon|$ versus the logarithm of the Cauchy stress $|\sigma|$. The engineering strain in uniaxial compression is defined as

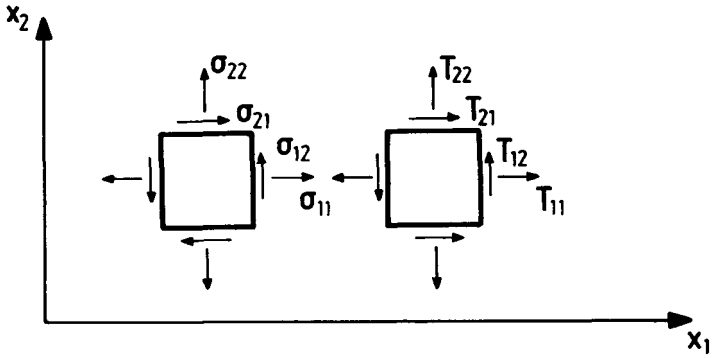

Figure 2.1.4 The components of the Cauchy and Kirchhoff stress tensors in two dimensions.

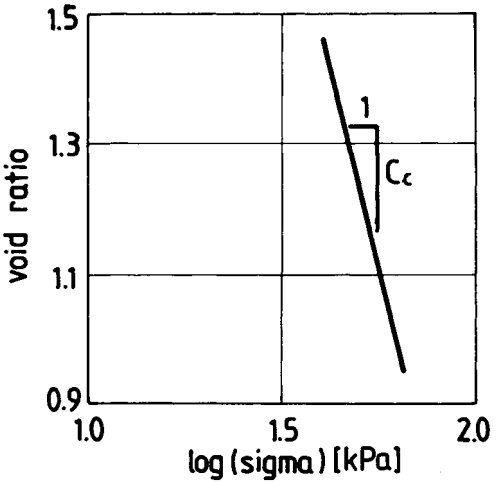

Figure 2.1.5 Conventional uniaxial compression curve of clay.

$$\varepsilon = -\Delta\ell/\ell^{(0)} \tag{2.1.43}$$

where $\ell^{(0)}$ and $\Delta\ell$ are the initial thickness of the specimen and its change, respectively. For a great variety of clays, the primary compression curve, the unloading (or swelling) curves and the recompression curves are then fairly approximated by straight lines. In a semi-logarithmic plot, these straight-line fits are characterized by their slopes, the so-called Terzaghi 'compression' and 'swelling' indices C_c and C_s, respectively. In most cases, straight-line fits are also generated if, instead of the ambiguous logarithmic stress and the inappropriate for large deformations engineering strain, one resorts to conjugate Eulerian measures like the Kirchhoff stress T_{ij} and the logarithmic strain λ. For example, a uniaxial or oedometric primary compression curve is shown for a typical clay in a conventional ($\log|\sigma|$, e) plot in Figure 2.1.5 (San Francisco Bay mud: initial voids ratio $e_0 = 1.46$, initial stress $|\sigma_0|$=40kPa, primary compression index $C_c = 1.063$; Holtz and Kovacs, 1981). If this result is transformed into the mechanically more meaningful

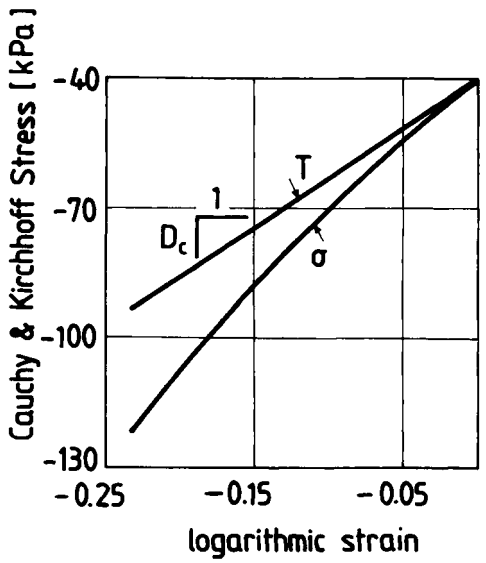

Figure 2.1.6 Uniaxial compression curve of clay in Eulerian description.

Eulerian stress and strain measures we obtain the graph shown in Figure 2.1.6. We see then that the primary compression data are best fit by a straight line in terms of the logarithmic strain and the Kirchhoff stress, i.e.

$$T = D_c \lambda \tag{2.1.44}$$

with $D_c = 230.3\,\mathrm{kPa}$, where

$$\lambda = \ln(1 + \varepsilon) \tag{2.1.45}$$

$$T = (1 + \lambda)\sigma \tag{2.1.46}$$

In the same figure, the non-linear (σ, λ) curve is also plotted for comparison.

2.2
Time derivatives and rates

2.2.1
Material time derivative and velocity

The velocity field gives the 'new' position $\bar{x}_i$ of a particle $X(\xi_k)$ at ime $\bar{t} = t + \Delta t$ relative to its 'old' position x_i at time t,

$$\Delta x_i = \bar{x}_i - x_i = x_i(\xi_k, t + \Delta t) - x_i(\xi_k, t) \approx v_i \Delta t \tag{2.2.1}$$

Accordingly, the following notations for the velocity are used

$$v_i = \lim_{\Delta t \to 0} \left\{ \frac{\Delta x_i}{\Delta t} \right\} = \frac{\partial x_i(\xi_k, t)}{\partial t} \tag{2.2.2}$$

Since the time differentiation is done in reference to a fixed material point X(ξ_k), it is commonly called the *material time derivative,* and the velocity becomes the material time derivative of the displacement

$$v_i = \frac{\partial}{\partial t} x_i(\xi_k, t) = \frac{\partial}{\partial t} \{ x_i(\xi_k, t) - x_i(\xi_k, 0) \} = \frac{\partial}{\partial t} u_i(\xi_k, t) \tag{2.2.3}$$

As already mentioned, with the inverse mapping (equation 2.1.18), we end up with the Eulerian description of the deformation. Accordingly, the velocity field v_i can be seen as a function of the current coordinates of X in C, i.e. $v_i = v_i(x_k, t)$. The material time derivative of an arbitrary field $\phi = \phi(x_k, t)$ in spatial coordinates is denoted as

$$\dot{\phi} = \frac{\mathrm{D}\phi}{\mathrm{D}t} = \lim_{\Delta t \to 0} \left\{ \frac{\Delta \phi}{\Delta t} \right\} \tag{2.2.4}$$

where

$$\Delta \phi = \phi(\bar{x}_k, \bar{t}) - \phi(x_k, t) \quad \text{for} \quad \Delta t \to 0 \tag{2.2.5}$$

With

$$\phi(\bar{x}_k, t + \Delta t) \approx \phi(\bar{x}_k, t) + \frac{\partial}{\partial t} \phi(\bar{x}_k, t) \Delta t \tag{2.2.6}$$

$$\phi(\bar{x}_k, t) \approx \phi(x_k, t) + \frac{\partial}{\partial x_l} \phi(x_k, t) \Delta x_l \tag{2.2.7}$$

and equation 2.2.2 we obtain the following expression for the Eulerian material time derivative of the considered field $\phi(x_k, t)$

$$\dot{\phi} = D_t \phi = \partial_t \phi + v_k \partial_k \phi \tag{2.2.8}$$

This means that the material time derivative in Eulerian description is a mixed differential operator $\dot{(\ )} \equiv D_t \equiv \partial_t + v_k \partial_k$ with $D_t \equiv \mathrm{D}/\mathrm{D}t$ and $\partial_t \equiv \partial/\partial t$. The first term of equation 2.2.8, called the 'local' variation, corresponds to the change of the field ϕ at a fixed-in-space position x_k. The second term, called the 'convective' term, is a correction, which accounts for the change of position of the considered material point in time. The convective term, being the inner product of the velocity and the spatial gradient of ϕ, is a 'non-linear' term and occasionally may be neglected. Indeed, if the velocity field and the gradient of ϕ are infinitesimal quantities, then the material time-derivative is approximated by the partial time derivative

$$\dot{\phi} = \partial_t \phi + 0(|v_k \partial_k \phi|) \tag{2.2.9}$$

As a first example let us consider the displacement field $u_i(x_k, t)$. In this case equation 2. 2.9 provides the following expression for the velocity

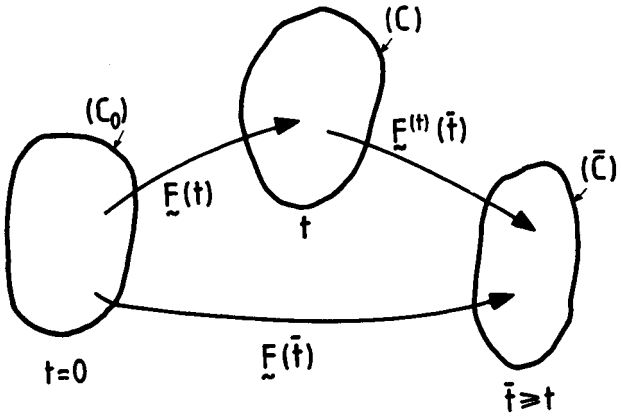

Figure 2.2.1 Relative deformation $\bar{t} \geqslant t$ with respect to current configuration C*(t)*.

$$v_i = \dot{u}_i = \partial_t u_i + v_k \partial_k u_i \tag{2.2.10}$$

or

$$v_i = (\delta_{ki} + \partial_i u_k)^{-1} \partial_t u_k \approx \partial_t u_i \tag{2.2.11}$$

Finally, the acceleration vector is computed as the material time derivative of the velocity

$$a_i = \dot{v}_i = \partial_t v_i + v_k \partial_k v_i \approx \partial_t v_i \approx \partial_{tt} u_i \tag{2.2.12}$$

2.2.2
Relative deformation gradient and its rate

The coordinates $\bar{x}_i$ of a point X in a configuration $\bar{C}$ at time $\bar{t} \geqslant t$ can be seen as functions of the coordinates x_i of X in C at time t

$$\bar{x}_i = \bar{x}_i(x_k, \bar{t}) \tag{2.2.13}$$

Accordingly, the deformation gradient, $\bar{F}_{ij} = F_{ij}(\xi_k, \bar{t})$, may be decomposed into the deformation gradient at time t, $F_{ij} = F_{ij}(\xi_k, t)$ and the relative deformation gradient $F^t_{ij} = F^t_{ij}(x_k, \bar{t})$, which describes the deformation $\mathbf{C} \rightarrow \bar{\mathbf{C}}$ with respect to the 'current' configuration C*(t)* (Figure 2.2.1)

$$\bar{F}_{ij} = \frac{\partial \bar{x}_i}{\partial \xi_j} = \frac{\partial \bar{x}_i}{\partial x_k} \frac{\partial x_k}{\partial \xi_j}$$

or

$$\bar{F}_{ij}(\xi_k, \bar{t}) = F^t_{ik}(x_m, \bar{t}) F_{kj}(\xi_m, t) \tag{2.2.14}$$

where

$$F^t_{ij} = \partial_j \bar{x}_i(x_k, \bar{t}) \quad \text{with} \quad F^t_{ij}(x_k, t) = \delta_{ij} \tag{2.2.15}$$

We observe that the velocity of the material point X, which at time t occupies the position x_k, is given by

$$v_i = \frac{\partial}{\partial \bar{t}}[\bar{x}_i(x_k, \bar{t})]_{x_k = \text{const}} = v_i(x_k, \bar{t}) \tag{2.2.16}$$

We consider now two neighboring points in C X(x_i) and Y(y_i), such that $y_i = x_i + \mathrm{d}x_i$. These points move instantaneously to new positions: and $\bar{y}_i = \bar{x}_i(x_k + \mathrm{d}x_k, \bar{t})$ such that $\mathrm{d}\bar{x}_i = \bar{y}_i - \bar{x}_i = F^t_{ij}\mathrm{d}x_j$The relative velocity of these points becomes

$$\frac{\partial}{\partial \bar{t}}[F^t_{ij}(x_k, \bar{t})\mathrm{d}x_j]_{\substack{x_k = \text{const} \\ \bar{t} = t}} = \dot{F}^t_{ij}(x_k, t)\mathrm{d}x_j$$

where

$$\dot{F}^t_{ij}(x_k, t) = \frac{\partial}{\partial \bar{t}}\frac{\partial \bar{x}_i}{\partial x_j}\bigg|_{\substack{x_k = \text{const} \\ \bar{t} = t}} = \frac{\partial}{\partial x_j}\frac{\partial \bar{x}_i}{\partial \bar{t}}\bigg|_{\substack{x_k = \text{const} \\ \bar{t} = t}} = \partial_j v_i(x_k, t) \tag{2.2.17}$$

The tensor

$$L_{ij} = \dot{F}^t_{ij}(x_k, t) = \partial_j v_i(x_k, t) \tag{2.2.18}$$

is called the spatial gradient of the velocity. From the right-polar decomposition of the relative deformation gradient

$$F^t_{ij}(\bar{t}) = R^t_{ik}(\bar{t})U^t_{kj}(\bar{t}) \tag{2.2.19}$$

we obtain that

$$\begin{aligned} L_{ij} &= \dot{R}^t_{ik}(\bar{t})|_{t=\bar{t}}U^t_{kj}(t) + R^t_{ik}(t)\dot{U}^t_{kj}(\bar{t})|_{t=\bar{t}} \\ &= \dot{R}^t_{ij}(t) + \dot{U}^t_{ij}(t) \end{aligned} \tag{2.2.20}$$

with

$$\dot{R}^t_{ij}(t) = -\dot{R}^t_{ji}(t);\ \dot{U}^t_{ij}(t) = \dot{U}^t_{ji}(t) \tag{2.2.21}$$

$\dot{R}^t_{ij}$ is an antisymmetric tensor and is called the spin or vorticity tensor; $\dot{U}^t_{ij}$ is symmetric and is called the rate of deformation tensor

$$W_{ij} = \dot{R}^t_{ij}(t) = \tfrac{1}{2}(L_{ij} - L_{ji}) = \tfrac{1}{2}(\partial_i v_j - \partial_j v_i) \tag{2.2.22}$$

$$D_{ij} = \dot{U}^t_{ij}(t) = \tfrac{1}{2}(L_{ij} + L_{ji}) = \tfrac{1}{2}(\partial_i v_j + \partial_j v_i) \tag{2.2.23}$$

Sometimes the rate of deformation tensor D_{ij} is confused with the material time derivative of the infinitesimal strain tensor. With

$$E_{ij} = \frac{1}{2}\left[\frac{\partial u_i}{\partial \xi_j} + \frac{\partial u_j}{\partial \xi_i}\right] \tag{2.2.24}$$

and

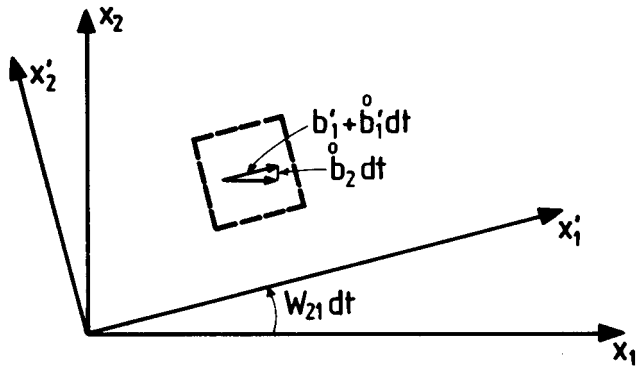

Figure 2.2.2 Corotating coordinate system *(Q_{ij}=−W_{ij})* and visualization of rigid body derivative of a vector field.

$$\frac{\partial v_i}{\partial \xi_j} = \frac{\partial}{\partial \xi_j}\frac{\partial x_i}{\partial t}\bigg|_{\xi_k = \text{const}} = \frac{\partial}{\partial t}\frac{\partial u_i}{\partial \xi_j}\bigg|_{\xi_k = \text{const}}$$

we obtain that

$$\dot{E}_{ij} = \frac{1}{2}\left[\frac{\partial v_i}{\partial \xi_j} + \frac{\partial v_j}{\partial \xi_i}\right] \tag{2.2.25}$$

The two tensors coincide of course when the displacements and the displacement gradients are infinitesimal. The rate of deformation tensor should be used whenever the displacements or their gradients are large.

2.2.3
Rigid-body or Jaumann derivative

Constitutive equations usually assume the form of evolution equations, i.e. equations for the rates of the various mechanical properties. In order to achieve objectivity in the material description one has to eliminate the rigid-body motion of the continuum from the material time derivative. For this purpose one introduces a 'corotating coordinate system' (x'_α), which is attached to the considered material point X and follows the rigid-body rotation of its neighborhood, described by the relative rotation tensor (Figure 2.2.2)

$$x'_\alpha = Q_{\alpha k}(\bar{t})x_k;\ Q_{ij} = R^t_{ji} \tag{2.2.26}$$

and accordingly a vector b_i will have the following components with respect to the corotating coordinate system

$$b'_\alpha = Q_{\alpha k} b_k \tag{2.2.27}$$

The material time derivative of this vector in the corotating system is

$$\dot{b}'_\alpha = \dot{Q}_{\alpha k} b_k + Q_{\alpha k}\dot{b}_k \tag{2.2.28}$$

If we transform this vector back to the 'fixed' coordinate system (x_i) we get

$$Q_{\alpha i}\dot{b}'_\alpha = Q_{\alpha i}\dot{Q}_{\alpha k}b_k + Q_{\alpha i}Q_{\alpha k}\dot{b}_k = -\dot{Q}_{\alpha i}Q_{\alpha k}b_k + \dot{b}_i \tag{2.2.29}$$

since

$$Q_{\alpha i}(\bar{t})Q_{\alpha k}(\bar{t}) = \delta_{ik} \rightarrow Q_{\alpha i}(\bar{t})\dot{Q}_{\alpha k}(\bar{t}) = -\dot{Q}_{\alpha i}(\bar{t})Q_{\alpha k}(\bar{t})$$

The *rigid-body* or *Jaumann* derivative of the vector b_i is now defined as the value of the above expression 2.2.29 evaluated at time t, i.e.

$$\mathring{b}_i = \lim_{\bar{t}\to t}\{Q_{\alpha i}\dot{b}'_\alpha\} = \dot{b}_i - \dot{Q}_{\alpha i}\delta_{\alpha k}b_k = \dot{b}_i - \dot{Q}_{ki}b_k \tag{2.2.30}$$

Finally, since

$$\dot{Q}_{ij}(t) = \dot{R}^t_{ji}(t) = W_{ji} = -W_{ij}$$

the rigid-body derivative of the vector field b_i is the objective derivative defined through the following expression,

$$\mathring{b}_i = \dot{b}_i - W_{ik}b_k \tag{2.2.31}$$

Similarly, the rigid-body or Jaumann derivative of a second-order tensor is defined through the material time derivative of this tensor with respect to the corotating coordinate system (x'_α) and its backwards transformation in the original 'fixed-in-space' coordinate system (x_i)

$$\mathring{S}_{ij} = \dot{S}_{ij} + S_{ik}W_{kj} - W_{ik}S_{kj} \tag{2.2.32}$$

2.2.4
Convective time derivative

We consider two Cartesian coordinate systems $x_i, i = 1,2,3$ and $(x'_\alpha, \alpha = 1,2,3)$. The x_i system is called 'fixed-in-space' and the x'_α system is called the 'moving' system. In particular we assume that the x'_α system is rotating with respect to the fixed one, e.g. with the third axis coinciding with the axis of relative rotation and for a coordinate system rotating with the angular velocity$\dot{\omega}$ we get the following coordinate transformation

$$\begin{aligned} x'_1 &= \cos(\dot{\omega}t)x_1 + \sin(\dot{\omega}t)x_2 = Q_{1i}(t)x_i \\ x'_2 &= -\sin(\dot{\omega}t)x_1 + \cos(\dot{\omega}t)x_2 = Q_{2i}(t)x_i \\ x'_3 &= x_3 = \delta_{3i}x_i = Q_{3i}(t)x_i \end{aligned} \tag{2.2.33}$$

In general, the coordinate transformation will be given by an orthogonal matrix corresponding to a rotation, i.e. by a proper orthogonal transformation

$$x'_\alpha = Q_{\alpha i}(t)x_i;\ \det(Q_{\alpha i}) = +1 \tag{2.2.34}$$

We observe that at any time

$$Q_{\alpha k}Q_{\beta k} = \delta_{\alpha\beta};\ Q_{\alpha i}Q_{\alpha j} = \delta_{ij} \tag{2.2.35}$$

During such a transformation the distance between two points does not change,

$$\begin{aligned} \Delta x_i &= x_i - y_i \rightarrow \Delta x'_\alpha = x'_\alpha - y'_\alpha = Q_{\alpha i}(x_i - y_i) = Q_{\alpha i}\Delta x_i \\ \Delta l'^2 &= \Delta x'_\alpha \Delta x'_\alpha = Q_{\alpha i}\Delta x_i Q_{\alpha j}\Delta x_j = \delta_{ij}\Delta x_i \Delta x_j = \Delta x_i \Delta x_i = \Delta l^2 \end{aligned} \tag{2.2.36}$$

A vector field b_i is called *objective or frame indifferent* if it does transform like a point difference

$$b'_\alpha = Q_{\alpha i} b_i \tag{2.2.37}$$

Similarly, a second-order tensor S_{ij} is called objective if its property to map an objective vector onto an objective vector remains valid also for the assumed coordinate transformation. In this case,

$$S'_{\alpha\beta} = Q_{\alpha i}Q_{\beta j}S_{ij} \tag{2.2.38}$$

With

$$v'_\alpha = \frac{\mathrm{D}}{\mathrm{D}t}(x'_\alpha) = \frac{\mathrm{D}}{\mathrm{D}t}(Q_{\alpha k}x_k) = \dot{Q}_{\alpha k}x_k + Q_{\alpha k}v_k \tag{2.2.39}$$

we observe that the velocity is not an objective vector field. Similarly, it can be shown that neither the acceleration a_t nor the velocity gradient L_{ij} are objective tensors. However, with

$$Q_{\alpha i} = \frac{\partial x_i}{\partial x'_\alpha} \quad \text{and} \quad L'_{\alpha\beta} = \dot{Q}_{\alpha k}Q_{\beta k} + Q_{\alpha i}Q_{\beta j}L_{ij} \tag{2.2.40}$$

we obtain that the rate of deformation tensor is objective,

$$D'_{\alpha\beta} = \tfrac{1}{2}(L'_{\alpha\beta} + L'_{\beta\alpha}) = \tfrac{1}{2}[\dot{(Q_{\alpha k}Q_{\beta k})} + Q_{\alpha i}Q_{\beta j}(L_{ij} + L_{ji})] = Q_{\alpha i}Q_{\beta j}D_{ij} \tag{2.2.41}$$

The physical meaning of this observation is appreciated by the fact that D_{ij} gives the change in the metric of the deformation

$$\frac{\mathrm{D}}{\mathrm{D}t}(\mathrm{d}l^2) = \frac{\mathrm{D}}{\mathrm{D}t}(\mathrm{d}x_i\,\mathrm{d}x_i) = L_{ik}\,\mathrm{d}x_k\,\mathrm{d}x_i + L_{jk}\,\mathrm{d}x_k\,\mathrm{d}x_j = 2D_{ij}\,\mathrm{d}x_i\,\mathrm{d}x_j \tag{2.2.42}$$

and accordingly

$$\frac{\mathrm{D}}{\mathrm{D}t}(\mathrm{d}l'^2) = 2D'_{\alpha\beta}\,\mathrm{d}x'_\alpha\,\mathrm{d}x'_\beta = 2Q_{\alpha i}Q_{\beta j}D_{ij}Q_{\alpha k}\,\mathrm{d}x_k\,Q_{\alpha l}\,\mathrm{d}x_l = \frac{\mathrm{D}}{\mathrm{D}t}(\mathrm{d}l^2) \tag{2.2.43}$$

From this property D_{ij} derives its characterization as the 'rate of the deformation'. Obviously the spin tensor W_{ij} is not objective. Finally, note that higher objective time derivatives of the stretching tensor can be derived through higher material time differentiation of the metric $\mathrm{d}l^2$, e.g. the second material time derivative of $\mathrm{d}l^2$ leads to the *convective time* derivative of the stretching tensor

$$\frac{\mathrm{D}^2}{\mathrm{D}t^2}(\mathrm{d}l^2) = D_{ij}^{(2)}\,\mathrm{d}x_i\,\mathrm{d}x_j \tag{2.2.44}$$

with

$$D_{ij}^{(2)} = \dot{D}_{ij} + D_{kj}L_{ki} + D_{ik}L_{kj} \tag{2.2.45}$$

We observe that $D_{ij}^{(2)}$ differs from the Jaumann derivative of the D_{ij} (cf. equation 2.2.32),

$$\mathring{D}_{ij} = \dot{D}_{ij} + D_{ik}W_{kj} - D_{ij}W_{kj} \tag{2.2.46}$$

only by an objective part,

$$D_{ij}^{(2)} - \mathring{D}_{ij} = D_{kj}D_{ik} + D_{ik}D_{kj} \tag{2.2.47}$$

This result is typical, meaning that there is no unique definition of an objective time derivative of a tensor S_{ij}. However all possible definitions differ from each other in terms of objective tensors, like the above indicated products $S_{kj}D_{ik}$ and $S_{ik}D_{kj}$. Of course, some authors prefer one definition over the other since some definitions of objective time derivatives have more meaning than others, i.e. they can be easily associated to a simple physical context. For example, the convective time derivative $D_{ij}^{(2)}$ describes the change in time of the metric, whereas $\mathring{D}_{ij}$ is less plausible. Moreover, further time differentiation of the metric $\mathrm{d}l^2$ leads easily to objective higher time derivatives of the rate of deformation.

2.2.5
Material derivative of volume integrals

Let us consider an arbitrary scalar field $\phi(x_i, t)$ defined over a volume V in the current configuration C and let $\psi(t)$ be its volume integral over V in C

$$\psi(t) = \int_V \phi(x_k, t)\,\mathrm{d}V \tag{2.2.48}$$

The material time derivative of ψ can be computed by changing the domain of integration from V in C to $V^{(0)}$ in $\mathrm{C}^{(0)}$ that is mapped onto V via the considered deformation. With equation 2.1.38 we obtain

$$\dot{\psi} = \int_{V^{(0)}} \frac{\mathrm{D}}{\mathrm{D}t}[\phi(x_i, t)J]\,\mathrm{d}V^{(0)} = \int_{V^{(0)}} \left[\frac{\mathrm{D}\phi}{\mathrm{D}t}J + \phi\frac{\mathrm{D}J}{\mathrm{D}t}\right]\mathrm{d}V^{(0)} \tag{2.2.49}$$

In order to evaluate this integral we consider first the material time derivative of the Jacobian of the deformation

$$\frac{\mathrm{D}J}{\mathrm{D}t} = \frac{\partial J}{\partial F_{ik}}\frac{\partial F_{ik}}{\partial t} = \frac{\partial J}{\partial F_{ik}}\frac{\partial}{\partial t}\left(\delta_{ik} + \frac{\partial u_i}{\partial \xi_k}\right) = \frac{\partial J}{\partial F_{ik}}\frac{\partial v_i}{\partial \xi_k} = \frac{\partial J}{\partial F_{ik}}F_{1k}\frac{\partial \hat{v}_i}{\partial x_1} \tag{2.2.50}$$

where

$$v_i = v_i(\xi_k, t) = v_i(\xi_k(x_l, t), t) = \hat{v}_i(x_l, t) \tag{2.2.51}$$

Making use of the identity

$$\mathrm{ad}(F)_{ik}F_{lk} = \delta_{il}J \tag{2.2.52}$$

and the fact that the adjoint of F_{ik} does not contain any of the F_{im}

$$\frac{\partial}{\partial F_{im}}(\mathrm{ad}(F)_{ik}F_{lk}) = \delta_{il}\frac{\partial J}{\partial F_{im}} \rightarrow \mathrm{ad}(F)_{lm} = \frac{\partial J}{\partial F_{lm}} \tag{2.2.53}$$

the above expression 2.2.49 for the $\dot{\psi}$ becomes

$$\dot{\psi} = \int_V (\dot{\phi} + \phi\,\partial_k v_k)\mathrm{d}V \tag{2.2.54}$$

This result is usually referred as *Reynolds' transport theorem*. Since the material time derivative of ϕ consists of both local and convective terms, equation 2.2.54 can be further transformed

$$\dot{\psi} = \int_V \{\partial_t\phi + \partial_k(\phi v_k)\}\mathrm{d}V \tag{2.2.55}$$

By using the divergence theorem equation 2.2.55 becomes

$$\dot{\psi} = \int_V \partial_t\phi\,\mathrm{d}V + \int_{\partial V} \phi v_k n_k\,\mathrm{d}S \tag{2.2.56}$$

where n_i is the outwards unit normal along the boundary ∂V. This means that the material time derivative of the integral quantity ψ consists also of local and convective terms, i.e. of a term that is due to changes of its density ϕ in V, and a term due to flux ϕv_i across the boundary ∂V of V.

Making use of the above general material time-differentiation formulae of volume integrals, the expression for conservation of mass, linear, and angular momenta, energy and entropy can be easily derived.

2.3
Balance equations

2.3.1
Mass balance

Let $\mathrm{d}m = \rho(x_k, t)\mathrm{d}V$ be the mass of material within the volume $\mathrm{d}V$ in C with ρ being the mass density. The total mass included in a finite volume V in C at time t is

$$m(t) = \int_V \mathrm{d}m = \int_V \rho(x_k, t)\mathrm{d}V \tag{2.3.1}$$

We observe that from equations 2.3.1 and 2.1.39 we obtain a useful expression or the Jacobian of the deformation in terms of the density in $C^{(0)}$ and C, respectively

$$J = \mathrm{d}V/\mathrm{d}V^{(0)} = (\mathrm{d}m/\mathrm{d}V^{(0)})/(\mathrm{d}m/\mathrm{d}V) = \rho^{(0)}/\rho \tag{2.3.2}$$

Mass balance in C is expressed by the condition

$$\dot{m} = 0 \tag{2.3.3}$$

On the other hand from equations 2.2.54 or 2.2.56 and 2.3.1 we obtain

$$\dot{m} = \int_V \partial_t \rho \, \mathrm{d}V + \int_{\partial V} \rho v_k n_k \, \mathrm{d}S = \int_V (\dot{\rho} + \rho \partial_k v_k) \, \mathrm{d}V \tag{2.3.4}$$

If this integral vanishes for arbitrary volume V and the integrand is continuous everywhere in V we obtain

$$\dot{\rho} + \rho \partial_k v_k = 0 \tag{2.3.5}$$

or

$$\partial_t \rho + \partial_k (\rho v_k) = 0 \tag{2.3.6}$$

which are the local forms of the mass balance law.

If the deformation is isochoric, then $\partial_k v_k = 0$,, and from the mass-balance equation 2.3. 5 follows that the density remains constant

$$\dot{\rho} = 0 \quad \text{or} \quad \partial_t \rho + v_k \partial_k \rho = 0 \tag{2.3.7}$$

As an application of the above mass balance law (equation 2.3.5) we consider a field ϕ which is originally defined per unit mass of the solid

$$\psi = \int_B \phi \, \mathrm{d}m = \int_V \rho \phi \, \mathrm{d}V \tag{2.3.8}$$

$\phi(x_k, t)$ is the specific value of the integral quantity ψ. By using Reynolds' transport theorem, equation 2.2.54, we obtain that

$$\dot{\psi} = \int_V \{(\rho \dot{\phi}) + \rho \phi \partial_k v_k\} \mathrm{d}V = \int_V \{\rho \dot{\phi} + \phi(\dot{\rho} + \rho \partial_k v_k)\} \mathrm{d}V \tag{2.3.9}$$

or due to the mass balance equation 2.3.5

$$\dot{\psi} = \int_B \rho \dot{\phi} \, \mathrm{d}V = \int_V \dot{\phi} \, \mathrm{d}m \tag{2.3.10}$$

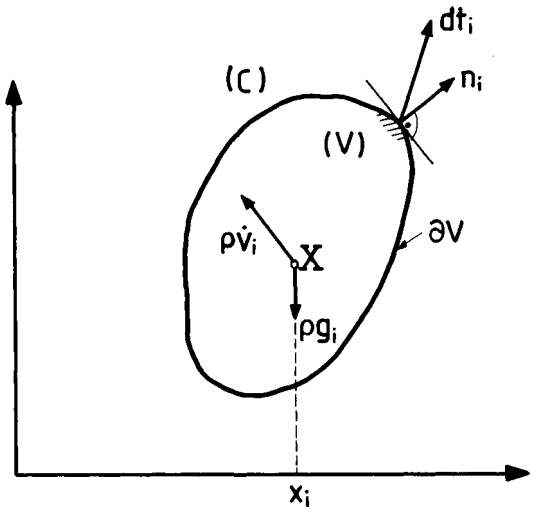

Figure 2.3.1 Mass forces, inertial forces and boundary tractions acting on the body B in C.

2.3.2
Balance of linear momentum

The total force F_i acting on a given body B is due to the contribution of all external forces, which are either volume forces, $\rho g_i dV$, like gravity forces and/or contact forces $\mathrm{d}t_i$ acting on the boundary ∂V of V (Figure 2.3.1)

$$F_i = \int_V \rho g_i \, \mathrm{d}V + \int_{\partial V} \mathrm{d}t_i \tag{2.3.11}$$

The stress vector $\mathrm{d}t_i$ acting in C on a surface element $\mathrm{d}S$ with unit outward normal n_i is related to the true or Cauchy stress tensor σ_{ij} as follows

$$\mathrm{d}t_i = \sigma_{ki} n_k \, \mathrm{d}S \tag{2.3.12}$$

From these equations and the divergence theorem one obtains

$$F_i = \int_V (\rho g_i + \partial_k \sigma_{ki}) \mathrm{d}V \tag{2.3.13}$$

On the other hand, the total momentum I_i of B in C is computed by summing up the momenta of all material points in V

$$I_i = \int_B v_i \, \mathrm{d}m = \int_V \rho v_i \, \mathrm{d}V \tag{2.3.14}$$

Balance of linear momentum is expressed by the following equation

$$F_i = \dot{I}_i \tag{2.3.15}$$

According to Reynolds' transport theorem the right-hand side of the above equation becomes

$$\dot{I}_i = \int_V \{\partial_t(\rho v_i) + \partial_k(\rho v_i v_k)\}\,\mathrm{d}V = \int_V \{(\partial_t \rho + \partial_k(\rho v_k))v_i + \rho \dot{v}_i\}\mathrm{d}V$$

Due to the mass balance equation 2.3.6 the first term of the integrand vanishes identically, and thus

$$\dot{I}_i = \int_V \rho \dot{v}_i\,\mathrm{d}V \tag{2.3.16}$$

By combining equations 2.3.15, 2.3.13 and 2.3.16 we finally obtain the local form of balance of linear momentum

$$\partial_k \sigma_{ki} + \rho g_i = \rho \dot{v}_i \tag{2.3.17}$$

2.3.3
Balance of angular momentum

In the absence of body couples and couple stresses, the total moment M_i acting on a given body B is the result of the contribution of the volume forces $\rho g_i \mathrm{d}V$ acting on V, and of the sum of all boundary tractions $\mathrm{d}t_i$ actingon ∂V

$$M_i = \int_V e_{ijk} x_j \rho g_k\,\mathrm{d}V + \int_{\partial V} e_{ijk} x_j\,\mathrm{d}t_k \tag{2.3.18}$$

On the other hand, the total angular momentum L_i of B in C is computed by summing up the angular momenta of all material points in V

$$L_i = \int_V e_{ijk} \rho v_k\,\mathrm{d}V \tag{2.3.19}$$

Balance of linear momentum is expressed by the following equation

$$M_i = \dot{L}_i \tag{2.3.20}$$

Considering that $e_{ijk}\dot{x}_j v_k = e_{ijk} v_j v_k = 0$ the right-hand side of equation 2.3.20 becomes

$$\dot{L}_i = \int_V \left[\frac{\mathrm{D}}{\mathrm{D}t}(e_{ijk} x_j \rho v_k) + e_{ijk} x_j \rho v_k \partial_l v_l \right] \mathrm{d}V$$

$$= \int_V \left[e_{ijk} x_j \frac{\mathrm{D}}{\mathrm{D}t}(\rho v_k) + e_{ijk} x_j \rho v_k \partial_l v_l \right] \mathrm{d}V$$

$$= \int_V e_{ijk} x_j \left\{ \{\partial_t \rho + \partial_l (\rho v_l)\} v_k + \rho \frac{\mathrm{D}v_k}{\mathrm{D}t} \right\} \mathrm{d}V$$

$$= \int_V e_{ijk} x_j \rho \frac{\mathrm{D}v_k}{\mathrm{D}t} \mathrm{d}V$$

On the other hand, the contribution of the boundary tractions yields

$$\int_{\partial V} e_{ijk} x_j \sigma_{lk} n_l \, \mathrm{d}S = \int_V \partial_l (e_{ijk} x_j \sigma_{lk}) \mathrm{d}V$$

$$= \int_V (e_{ijk} \delta_{jl} \sigma_{lk} + e_{ijk} x_j \partial_l \sigma_{lk}) \mathrm{d}V$$

$$= \int_V (e_{ijk} \sigma_{jk} + e_{ijk} x_j \partial_l \sigma_{lk}) \mathrm{d}V$$

and with this equation 2.3.20 becomes

$$\int_V e_{ijk} x_j \rho \dot{v}_k \, \mathrm{d}V = \int_V \{ e_{ijk} \sigma_{jk} + e_{ijk} x_j (\partial_l \sigma_{lk} + \rho g_k) \} \mathrm{d}V$$

which in connection with the balance of linear momentum, equation 2.3.17, finally results in the symmetry of the Cauchy stress tensor

$$\int_V e_{ijk} \sigma_{jk} \, \mathrm{d}V = 0 \rightarrow \sigma_{jk} = \sigma_{kj} \tag{2.3.21}$$

Due to the axiomatic nature of the symmetry of the Cauchy stress tensor, the continuum for which the symmetry condition 2.3.21 is holding is called a *Boltzmann* continuum. As opposed to a Boltzmann continuum, in a Cosserat continuum the Cauchy stress tensor is non-symmetric either due to the existence of couple boundary stresses and/or due to the existence of body couples, which in turn might be only due to inertia, stemming from the spinning of the unit cells (grains) of the material; cf. Schaeffer (1967).

2.3.4
Energy balance

The *first law of thermodynamics* requires that the change of the total energy E of a deforming solid body B with volume V and boundary ∂V in a configuration C consists of two contributions: (a) the power $\dot{W}$ of all external forces acting on B in C; and (b) of the energy $\dot{W}$ which is supplied at any time to B from the exterior domain, i.e.

$$\dot{E} = \dot{W} + \dot{Q} \tag{2.3.22}$$

The total energy of the body B in C consists in turn of two terms: (a) its kinetic energy K; and (b) its internal energy U, which does not depend on the relative motion of the observer with respect to the considered body, i.e.

$$\dot{E} = \dot{W} + \dot{Q} \tag{2.3.23}$$

where $e(x_k, t)$ is the specific internal energy of the body. Utilizing Reynolds' transport theorem, the time variation of the body's kinetic and internal energy become

$$E = K + U = \int_V \tfrac{1}{2}\rho v_k v_k \, \mathrm{d}V + \int_V \rho e \, \mathrm{d}V \tag{2.3.24}$$

cf. equations 2.3.8 to 2.3.10. On the other hand, the power of external forces acting in the volume V and on its boundary ∂V is

$$\dot{K} = \int_V \rho \dot{v}_k v_k \, \mathrm{d}V; \; \dot{U} = \int_V \rho \dot{e} \, \mathrm{d}V \tag{2.3.25}$$

where σ_{ij} is the Cauchy stress tensor in C and n_i is the unit outward normal vector on ∂V in C. Accordingly, the energy balance equation 2.3.22 becomes

$$\dot{W} = \int_{\partial V} v_k \, \mathrm{d}t_k + \int_V \rho g_k v_k \, \mathrm{d}V = \int_{\partial V} \sigma_{ik} n_i v_k \, \mathrm{d}S + \int_V \rho g_k v_k \, \mathrm{d}V \tag{2.3.26}$$

In order to evaluate the energy balance law (equation 2.3.26), we observe that the power of external and inertial forces is equal to the so-called stress power, i.e.

$$\dot{W} - \dot{K} = \int_{\partial V} n_k \sigma_{km} v_m \, \mathrm{d}S + \int_V (\rho g_k - \rho \dot{v}_k) v_k \, \mathrm{d}V = \int_V \sigma_{km} D_{km} \, \mathrm{d}V \tag{2.3.27}$$

This can be shown as follows: We consider the balance of linear momentum equation 2. 3.17, we contract it with v_i and integrate the resulting identity over the domain V

$$\int_V (\partial_k \sigma_{km} v_m + \rho g_k v_k \, \mathrm{d}V - \rho \dot{v}_k v_k) \, \mathrm{d}V = 0$$

and with

$$\int_V \partial_k \sigma_{km} v_m \, dV = \int_V \partial_k (\sigma_{km} v_m) \, dV - \int_V \sigma_{km} \partial_k v_m \, dV$$

$$= \int_V n_k \sigma_{km} v_m \, dS - \frac{1}{2} \int_V \sigma_{km} (\partial_k v_m + \partial_m v_k) \, dV$$

$$- \frac{1}{2} \int_V \sigma_{km} (\partial_k v_m - \partial_m v_k) \, dV$$

$$= \int_{\partial V} n_k \sigma_{km} v_m \, dS - \int_V \sigma_{km} D_{km} \, dV$$

we obtain equation 2.3.27. With the definition of the stress power

$$P = \sigma_{km} D_{km} \tag{2.3.28}$$

the equation of the power of internal and external forces including inertial forces (d'Alembert's principle) becomes

$$\dot{W} - \dot{K} = \int_V P \, dV = \int_B \rho^{-1} P \, dm \tag{2.3.27bis}$$

The quantity, $\rho^{-1}P$, is called the specific stress power (Elementarleistung). Accordingly, the Cauchy stress tensor σ_{ij} and the rate of deformation tensor D_{ij} are called dual in energy (Macvean, 1968). It should be noticed also that if in a continuum the stress power depends only on the rate of deformation tensor, then this continuum will be called a first-grade continuum. In chapter 10 a second-grade continuum will be discussed, where the stress power depends also on the gradient of the rate of deformation, $\partial_\kappa D_{ij}$ (Mindlin, 1964; Germain, 1973a,b).

Coming back to the energy balance equation 2.3.26, we observe that the total energy flux into V across ∂V can be expressed by the energy flux vector q_k, which is set positive whenever it is opposite to the unit outward normal vector n_k,

$$\dot{Q} = - \int_{\partial V} q_k n_k \, dS \tag{2.3.29}$$

For example, if non-mechanical energy transfer is only due to heat conduction, then q_k (x_1, t) becomes the heatfluxvector measured per unit surface dS in C.

Summarizing the above results we obtain the following global form

$$\int_V \rho \dot{e} \, dV = \int_V P \, dV - \int_{\partial V} q_k n_k \, dS = \int_V (P - \partial_k q_k) \, dV \tag{2.3.30}$$

and local form

$$\rho\dot{e} = P - \partial_k q_k \tag{2.3.31}$$

of the energy balance law.

If heat transfer is insignificant and all of the work done by the stresses is assumed to be converted into internal energy, then from equation 2.3.31 we obtain

$$\dot{e} = \rho^{-1}\sigma_{km}D_{km} \tag{2.3.32}$$

i.e. that the rate of specific internal energy is equal to the specific stress power.

2.3.5
Entropy inequalities and balance

Let Γ be the total entropy in a volume V in C

$$\Gamma = \int_V \rho s \, \mathrm{d}V \tag{2.3.33}$$

where s is the specific entropy. Let also q_k be the heat flux vector, and $\Theta>0$ be the absolute temperature. The total entropy flux across the boundary ∂V of the volume V in C due to conduction is

$$\int_{\partial V} \frac{q_k n_k}{\Theta} \mathrm{d}S$$

The *second law of thermodynamics* is the assertion that the rate of change of entropy cannot be less than the total entropy flux across ∂V due to conduction

$$\dot{\Gamma} \geqslant -\int_{\partial V} \frac{q_k n_k}{\Theta} \mathrm{d}S \tag{2.3.34}$$

Accordingly a local form of the second law of thermodynamics is proposed, the so-called *Gibbs-Clausius-Duhem Inequality* stating that the internal entropy production rate η per unit mass is non-decreasing, i.e.

$$\eta = \dot{s} + \frac{1}{\rho\Theta}\partial_k q_k - \frac{1}{\rho\Theta^2} q_k \partial_k \Theta_k \geqslant 0 \tag{2.3.35}$$

Due to the energy balance law (equation 2.3.31) the above entropy inequality is transformed to

$$-\rho(\dot{e} - \Theta\dot{s}) + P - (q_k/\Theta)\partial_k\Theta \geqslant 0 \tag{2.3.36}$$

Introducing the so-called Helmholtz free energy function f, i.e. the portion of the internal energy available for doing work at constant temperature

$$f = e - s\Theta \tag{2.3.37}$$

we obtain from equation 2.3.36 that

$$-\rho(\dot{f} + s\dot{\Theta}) + P - (q_k/\Theta)\partial_k\Theta \geqslant 0 \tag{2.3.38}$$

If one considers stationary (states $(\dot{\Theta} = 0)$ and rigid-body motions $(\dot{f} = 0, D_{ik} = 0)$ then from this inequality follows, in particular, that heat must flow opposite to the temperature gradient, i.e. that the entropy production by heat conduction is non-decreasing

$$\eta_{\text{con}} = -\frac{1}{\rho\Theta^2} q_k \partial_k \Theta \geqslant 0 \tag{2.3.39}$$

This result is reflected for example in Fourier's law of isotropic heat conduction

$$q_k = -K\partial_k\Theta \tag{2.3.40}$$

where K>0 is the thermal conductivity of an isotropic solid. In this case the entropy production by heat conduction is quadratic in the temperature gradient, and

$$\eta_{\text{con}} = (K/\rho\Theta^2)\partial_k\Theta\partial_k\Theta \geqslant 0 \tag{2.3.41}$$

If in turn we consider isothermal processes $(\partial_k\Theta = 0)$,, then inequality equation 2.3.38 yields that the local entropy production is also non-decreasing

$$\eta_{\text{loc}} = \frac{1}{\Theta}[\rho^{-1}P - (\dot{f} + s\dot{\Theta})] \geqslant 0 \tag{2.3.42}$$

It should be emphasized that the Gibbs-Clausius-Duhem inequality equation 2.3.35 for the internal entropy production as well as the inequalities and equations 2.3.39 and 2.3. 42 for the entropy production by heat conduction and the local entropy production have independent axiomatic character within continuum thermodynamics; cf. Truesdell and Noll (1965). In such a framework the local dissipation due to irreversibility of the deformation process becomes

$$D_{\text{loc}} = \rho(\Theta\eta_{\text{loc}}) = P - \rho(\dot{f} + s\dot{\Theta}) \geqslant 0 \tag{2.3.43}$$

The form of the restriction imposed by inequalities equation 2.3.42 or 2.3.43 depends mainly on the type of physical quantities which are assumed as thermodynamic state parameters. These usually are the stress, σ_{ij}, and the absolute temperature, Θ, but also a number of non-observables, the so-called hidden or internal parameters.

Finally from the energy balance equation 2.3.31 and the definitions of the free energy and local dissipation, equations 2.3.37 and 2.3.43 one obtains the following *balance law for local entropy production*

$$\Theta(\rho\dot{s}) = -\partial_k q_k + D_{\text{loc}} \tag{2.3.44}$$

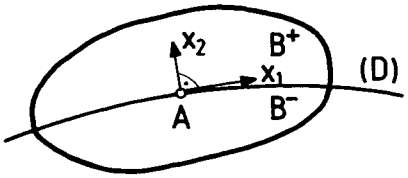

Figure 2.4.1 Compatibility of a field defined along D.

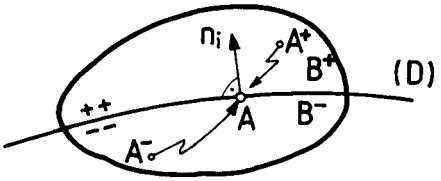

Figure 2.4.2 Domains of continuity.

2.4
Discontinuous fields and wave fronts

2.4.1
Geometric compatibility conditions

Let $z = z^-(x_1, x_2)$ be a function defined over a domain B^- in the (x_1, x_2) plane and let D be a smooth curve which subdivides B into B^+ and B^-, and over which the values of z are prescribed. The curve D is represented by the function $x_2 = f(x_1)$ and the function

$$z_D(x_1) = z^-(x_1, f(x_1)) \tag{2.4.1}$$

is assumed to be known. Such a restriction for the function z has some consequences on the possibility of restricting the function z in the neighborhood of D; namely, from equation 2.4.1 we have

$$\frac{dz_D}{dx_1} = \left.\frac{\partial z^-}{\partial x_1}\right|_D + \left.\frac{\partial z^-}{\partial x_2}\right|_D \frac{df}{dx_1} \tag{2.4.2}$$

It is always possible to choose the coordinate system in such a manner that the x_1-axis coincides with the tangent on a considered point A of D and the x_2-axis with the normal on D at point A of the considered curve. According to Figure 2.4.1 we then have

$$\left.\frac{df}{dx_1}\right|_A = 0 \tag{2.4.3}$$

and from equation 2.4.2 it follows that

$$\left.\frac{\partial z^-}{\partial x_1}\right|_A = \left.\frac{dz_D}{dx_1}\right|_A \tag{2.4.4}$$

Equation 2.4.4 is called *Hadamard's lemma* and means that prescribing the function z on D, by a condition like equation 2.4.1, restricts only the tangential derivative of z along D. Above results hold, of course, in three dimensions as well. Accordingly, we consider z as a function of x_i with i=1, 2, 3 and D as surface in three-dimensional space. By using the notation (Figure 2.4.2)

$$z^+ = \lim_{A^+ \to A} (z);\ z^- = \lim_{A^- \to A} (z) \tag{2.4.5}$$

we can define the *jump, [z]* of z along D as the difference of its one-side lines

$$[z] = z^+ - z^- \tag{2.4.6}$$

and applying equation 2.4.1 on both sides of D results in z being continuous along D

$$[z] = 0 \tag{2.4.7}$$

Equation 2.4.4, on the other hand, implies that only the normal derivative of z along D may be discontinuous, the latter being expressed by the conditions

$$[\partial_i z] = \zeta n_i \tag{2.4.8}$$

where n_i is the unit normal at a point A of D and ζ is the jump of the normal derivative of z with respect to D. With $x_n = n_i x_i$

$$\zeta = \left[\frac{\partial z}{\partial x_n}\right] \tag{2.4.9}$$

The above derivations can be summarized by the following,

Theorem of Maxwell: If a function z is continuous across a surface D, then only the normal derivative of z across D may be discontinuous, if

$$[z] = 0 \text{ then } [\partial_i z] = \zeta n_i \tag{2.4.10}$$

where the jump ζ of the normal derivative is unrestricted.

Equations 2.4.10 are called the *geometric compatibility conditions* for a weak discontinuity of the field $z(x_i)$. Theterm 'geometric' is used in order to express the fact that the corresponding compatibility conditions do not depend on the actual motion of the discontinuity surface. Conditions of the type of equation 2.4.10 hold for both stationary and moving discontinuity surfaces which are called also wave fronts.

Let D be for example a weak discontinuity surface of the displacement gradient field. Then according to Maxwell's theorem we have the following geometric compatibility conditions, if

$$[u_i] = 0 \quad \text{then} \quad [\partial_j u_i] = d_i n_j \tag{2.4.11}$$

For example, in plane strain all spatial derivatives of the displacement vector along a given direction, say the x_3-direction, vanish and thus if there is to be discontinuity of displacement gradient at all, then not all ζ_i can vanish, and the discontinuity surface of the displacement gradient is a cylindrical surface which is normal to the plane of deformation, i.e.

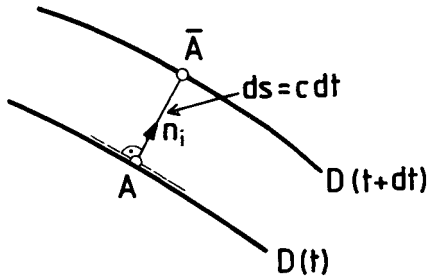

Figure 2.4.3 Propagating discontinuity surface.

$$[\partial_3 u_i] = d_i n_3 = 0 \quad \text{and} \quad |d_i| > 0 \rightarrow n_3 = 0 \tag{2.4.12}$$

2.4.2
Kinematic compatibility conditions

According to Figure 2.4.3 we consider a point A(x_i) on a wavefront D(t). At time $t + \Delta t$,, the wave surface is at position $\bar{\mathrm{D}} = \mathrm{D}(t + \Delta t)$. A point $\bar{\mathrm{A}}(x_i + \Delta x_i)$ on $\bar{\mathrm{D}}$ is considered with $\Delta x_i = \Delta s n_i$, where Δs is the normal distance of the surfaces D and $\bar{\mathrm{D}}$ at point A and n_i is the unit normal on D*(t)* at point A. The propagation velocity of the wavefront D is defined as

$$c = \lim_{\Delta t \to 0} \left\{ \frac{\Delta s}{\Delta t} \right\} \tag{2.4.13}$$

Notice that a discontinuity surface is called stationary if $c = 0$

Let $Z = [z]$ and $\bar{Z} = [\bar{z}]$ be the jumps of a function z across D and $\bar{\mathrm{D}}$ at times t and $\bar{t} = t + \Delta t$, and at the points A and $\bar{\mathrm{A}}$,, respectively. We define the δ time derivatives (Thomas, 1961)

$$\frac{\delta Z}{\delta t} = \lim_{\Delta t \to 0} \left\{ \frac{\Delta Z}{\Delta t} \right\}; \Delta Z = \bar{Z} - Z$$

$$\frac{\delta z^+}{\delta t} = \lim_{\Delta t \to 0} \left\{ \frac{\bar{z}^+ - z^+}{\Delta t} \right\}$$

$$\frac{\delta z^-}{\delta t} = \lim_{\Delta t \to 0} \left\{ \frac{\bar{z}^- - z^-}{\Delta t} \right\}$$

and

$$\frac{\Delta Z}{\Delta t} = \frac{Z - \bar{Z}}{\Delta t}$$

$$= \frac{(\bar{z}^+ - \bar{z}^-) - (z^+ - z^-)}{\Delta t}$$

$$= \frac{\bar{z}^+ - z^+}{\Delta t} - \frac{\bar{z} - z^-}{\Delta t}$$

From these definitions we obtain that

$$\frac{\delta[z]}{\delta t} = \left[\frac{\delta z}{\delta t}\right] \tag{2.4.14}$$

Moreover, from the above definitions we derive that

$$\frac{\delta x_i}{\delta t} = \lim_{\Delta t \to 0} \left\{\frac{\Delta x_i}{\Delta t}\right\} = \lim_{\Delta t \to 0} \left\{\frac{\Delta s}{\Delta t} n_i\right\} = c n_i \tag{2.4.15}$$

For the considered moving discontinuity surface the following first-order approximations hold

$$\frac{\bar{z}^+ - z^+}{\Delta t} = \partial_i z^+ \frac{\Delta x_i}{\Delta t} + \partial_t z^+$$

$$\frac{\bar{z}^- - z^-}{\Delta t} = \partial_i z^+ \frac{\Delta x_i}{\Delta t} + \partial_t z^-$$

and consequently

$$\frac{\delta z^+}{\delta t} = \partial_i z^+ c n_i + \partial_t z^+$$

$$\frac{\delta z^-}{\delta t} = \partial_i z^- c n_i + \partial_t z^-$$

From these equations, we finally derive an expression for the jump of the δ time derivative of a function z

$$\left[\frac{\delta z}{\delta t}\right] = [\partial_i z] c n_i + [\partial_t z] \tag{2.4.16}$$

or due to equation 2.4.14

$$[\partial_t z] = -[\partial_i z] c n_i + \frac{\delta[z]}{\delta t} \tag{2.4.17}$$

In the special case, when a function $z(x_i, t)$ is at all times continuous across a wavefront $D(t)$, we summarize the following compatibility conditions

$$[z] = 0;\ [\partial_i z] = \zeta n_i;\ [\partial_t z] = -\zeta c \tag{2.4.18}$$

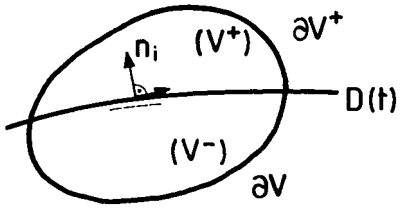

Figure 2.4.4 Domains of continuity.

As already mentioned, equation 2.2.11, if convective terms are neglected, the velocity is approximately equal to the time derivative of the displacement field, $v_i \approx \partial_t u_i(x_k, t)$. Forcontinuous displacementfield the above compatibility conditions yield

$$[v_i] = -\zeta_i c = -[\partial_k u_i] n_k c \tag{2.4.19}$$

From these conditions it follows that, if

$$c = 0 \rightarrow [v_i] = 0 \tag{2.4.20}$$

i.e. across a stationary discontinuity surface the velocity is continuous.

2.4.3
Dynamic compatibility conditions

Suppose that a volume V, whose motion is determined by the deformation of the material body B, is divided by a moving surface D(t) into two volumes, V^+ and V^-. Denote by ∂V^+ and ∂V^- the portions of the surface ∂V which form parts of the boundaries of V^+ and V^-, respectively; the remaining part of the boundary of V^+ and V^- will be furnished by the surface D(t) (Figure 2.4.4). The normal component of the velocity of V at points of its surface ∂V is $v_n = v_i n_i$, since the variation of the volume V is produced by the moving particles of the medium. Let D(t) be considered as part of the boundary of V^-. For an observer in V^+, D(t) is moving with the normal velocity $-c$. Accordingly equation 2.2.37 is modified by considering the flux of ϕ across D

$$\frac{\mathrm{D}}{\mathrm{D}t}\int_{V^+}\phi(x_i,t)\,\mathrm{d}V = \int_{V^+}\partial_t\phi\,\mathrm{d}V + \int_{\partial V^+}\phi v_n\,\mathrm{d}S - \int_{\mathrm{D}}\phi^+ c\,\mathrm{d}S$$

$$\frac{\mathrm{D}}{\mathrm{D}t}\int_{V^-}\phi(x_i,t)\,\mathrm{d}V = \int_{V^-}\partial_t\phi\,\mathrm{d}V + \int_{\partial V^-}\phi v_n\,\mathrm{d}S + \int_{\mathrm{D}}\phi^- c\,\mathrm{d}S$$

or

$$\frac{\mathrm{D}}{\mathrm{D}t}\int_{V}\phi(x_i,t)\,\mathrm{d}V = \int_{V}\partial_t\phi\,\mathrm{d}V + \int_{\partial V}\phi v_n\,\mathrm{d}S - \int_{D}[\phi]c\,\mathrm{d}S \tag{2.4.21}$$

The above generalization of Reynolds' transport theorem to discontinuous fields can be combined with the conservation laws of mechanics in order to derive useful compatibility conditions for the various fields. In particular, let ϕ be the density ρ of the solid, then from 2.4.21 and 2.3.4 we obtain

$$\dot{m} = \frac{\mathrm{D}}{\mathrm{D}t}\int_V \rho(x_i,t)\mathrm{d}V = \int_V \partial_t \rho \,\mathrm{d}V + \int_{\partial V^+} \rho v_n \,\mathrm{d}S + \int_{\partial V^-} \rho v_n \,\mathrm{d}S - \int_D [\rho] c \,\mathrm{d}S = 0$$

and consequently,

$$\int_V \partial_t \rho \,\mathrm{d}V + \int_{\partial V^+} \rho v_n \,\mathrm{d}S + \int_{\partial V^-} \rho v_n \,\mathrm{d}S - \int_D [\rho] c \,\mathrm{d}S = 0 \tag{2.4.22}$$

Now let V approach zero at a fixed time in such a way that it will pass, in the limit, into a part $\mathrm{D_o}$ of the surface D. The volume integral in the above equation will approach zero, and

$$\int_{\partial V^+} \rho v_n \,\mathrm{d}S \to -\int_{\mathrm{D_o}} \rho^+ v_n^+ \,\mathrm{d}S$$

$$\int_{\partial V^-} \rho v_n \,\mathrm{d}S \to \int_{\mathrm{D_o}} \rho^- v_n^- \,\mathrm{d}S$$

where v_n^+ and v_n^- denote the normal components of the particle velocities on the ($^+$) and ($^-$) sides of D along the normal direction from the ($^-$) to the ($^+$) side of it. Hence we obtain the *dynamic compatibility condition* for the density

$$-\int_{\mathrm{D_o}} \rho^+ \mathrm{v}_n^+ \,\mathrm{d}S + \int_{\mathrm{D_o}} \rho^- v_n^- \,\mathrm{d}S - \int_{\mathrm{D_o}} (\rho^+ - \rho^-) c \,\mathrm{d}S = 0$$

or

$$\rho^-(v_n^- - c) = \rho^+(v_n^+ - c) \tag{2.4.23}$$

By neglecting volume forces, balance of linear momentum is expressed by the conditions

$$\frac{\mathrm{D}}{\mathrm{D}t}\int_V \rho v_i \,\mathrm{d}V = \int_V \partial_k \sigma_{ki} n_j \,\mathrm{d}V = \int_{\partial V} \sigma_{ki} n_k \,\mathrm{d}S \tag{2.4.24}$$

Allowing again the volume V to approach zero, we obtain

$$\int_{\partial V} \sigma_{ij} n_j \,\mathrm{d}S \to \int_{\mathrm{D_o}} (\sigma_{ij}^+ - \sigma_{ij}^-) n_j \,\mathrm{d}S \tag{2.4.25}$$

If we put $\phi_i = \rho v_i$ in equation 2.4.21, we see that the left side of equation 2.4.24 becomes

$$\int_V \partial_t(\rho v_i)\,\mathrm{d}V + \int_{\partial V^+} \rho v_n v_i\,\mathrm{d}S + \int_{\partial V^-} \rho v_n v_i\,\mathrm{d}S - \int_D [\rho v_i] c\,\mathrm{d}S$$

and passing to the limit, the above sum of integrals reduces to

$$\int_{D_o} \rho^- v_i^- (c - v_n^-)\mathrm{d}S - \int_{D_o} \rho^+ v_i^+ (c - v_n^+)\mathrm{d}S \tag{2.4.26}$$

From equations 2.4.25 and 2.4.26, and the dynamic compatibility condition for the density, equation 2.4.23, we are led to the following dynamic compatibility conditions for the stress σ_{ij}:

$$[\sigma_{ij}]n_j = \rho^-(v_n^- - c)[v_i] \tag{2.4.27}$$

A *material discontinuity surface* is at all times moving as the underlying continuum, i.e. for a material discontinuity surface D*(t)* and for x_i on D, $v_n = c$.. For a material discontinuity surface compatibility, conditions 2.4.27 reduce to continuity of tractions across D

$$[\mathrm{d}t_i] = [\sigma_{ij}]n_j = 0 \tag{2.4.28}$$

which simply express the fact that across a material discontinuity surface the tractions must be in equilibrium.

2.4.4
Weak discontinuities

Let us consider a wavefront D*(t)* across which the velocity is continuous and consequently all first-order derivatives of the displacement must be also continuous. This means that across D*(t)* only second-order derivatives of the displacement vector may be discontinuous, and D*(t)* is called an acceleration wavefront

$$[\partial_j \partial_k u_i] = d_i n_j n_k;\ [\partial_t \partial_j u_i] = -d_i n_j c;\ [\partial_t \partial_t v_i] = d_i c^2 \tag{2.4.29}$$

With equations 2.2.10 and 2.2.12 the jump of the acceleration can be computed

$$[a_i] = d_i(c - v_n)^2 \tag{2.4.30}$$

Assuming that across D*(t)* density and stress are also continuous, the following geometrical and kinematical compatibility conditions hold

$$[\rho] = 0;\ [\partial_j \rho] = r n_j;\ [\partial_t \rho] = -rc \tag{2.4.31}$$

$$[\sigma_{ij}] = 0;\ [\partial_k \sigma_{ij}] = g_{ij} n_k;\ [\partial_t \sigma_{ij}] = -g_{ij} c \tag{2.4.32}$$

On both sides of the wave front D the balance equations of mass and linear momentum, equations 2.3.6 and 2.3.17 must hold

$$\partial_t \rho + v_k \partial_k \rho + \rho \partial_i v_i = 0 \tag{2.4.33}$$

$$\partial_k \sigma_{ki} + \rho g_i = \rho(\partial_t v_i + v_k \partial_k v_i) \tag{2.4.34}$$

and thus we can derive the following dynamical compatibility conditions

$$(c - v_n)(r + \rho d_k v_k) = 0 \tag{2.4.35}$$

$$g_{ij} n_j = \rho(c - v_n)^2 d_i \tag{2.4.36}$$

These conditions are restricting the jumps of the various fields across acceleration wavefronts.

Acceleration waves in isotropic linear elastic solids. For small strains, the constitutive equations for a linear, isotropic elastic solid are

$$\sigma_{ij} = 2G\{\varepsilon_{ij} + \nu/(1 - 2\nu)\varepsilon_{kk}\delta_{ij}\}$$

where G and ν are the elastic shear modulus and Poisson's ratio, and ε_{ij} the infinitesimal strain tensor. Utilizing the above compatibility conditions 2.4.35 and 2.4.36 one can determine the propagation velocity of acceleration waves in elastic solids. Thus the dynamic compatibility conditions 2.4.36 yield the following condition for the jump vector d_i

$$\{n_i n_k + G(\delta_{ik} + n_i n_k) - \rho(c - v_n)^2 \delta_{ik}\} d_k = 0 \qquad (i = 1, 2, 3)$$

Let us assume that the coordinate system is selected in such a way that the x_1-axis coincides with the normal on the propagating front at a considered point, pointing in the direction of its propagation, i.e. $n_i = \{1, 0, 0\}^T$. Furthermore, we assume that the propagation velocity of the wave is significantly larger than the normal velocity of the particles ($c \gg |v_n|$). Theabove equations provide, then, two types of acceleration waves: (a) waves which show a jump in longitudinal direction; $d_i = \{1, 0, 0\}^T$; and (b) waves which show a jump in the transverse direction; $d_i = \{0, 1, 0\}^T$ or $d_i = \{0, 0, 1\}^T$. Longitudinal waves propagate with velocity c_p and transversal waves with velocity c_s, given by

$$c_s = (G/\rho)^{\frac{1}{2}}; \; c_p = \{2(1 + \nu)/(1 - 2\nu)\}^{\frac{1}{2}} c_s$$

The dynamical compatibility condition 2.4.35, which was derived directly from mass balance, yields

$$r = -\rho d_i$$

This means that only across longitudinal wavefronts does the density gradient jump.

Literature

Textbooks and monographs

Holtz, R.D. and Kovacs, W.D. (1981). *An Introduction to Geotechnical Engineering.* Prentice-Hall Inc., Englewood Cliffs, New Jersey, 289–293.

Thomas, T.Y. (1961). *Plastic Flow and Fracture in Solids.* Academic Press, London.

Truesdell, C. and Noll, W. (1965). *Nonlinear Field Theories of Mechanics. Handbuch der Physik, Vol III/3,* sections 21–25 and 79. Springer, Berlin.

References

Germain, P. (1973a). La méthode des pulssances virtuelles en mécanique des milieux continus. Première partie: Théorie du second gradient. *J. de Mécanique,* **12**(2), 235–274.

Germain, P. (1973b). The method of virtual power in continuum mechanics. Part 2: Microstructure. *SIAM J. Appl Math.,* **25**(3), 556–575.

Macvean, D.B. (1968). Die Elementarleistung in einem Kontinuum und die Zuordnung von Spannungs- und Vezerrungstensoren. *ZAMP,* **19,** 157–184.

Mindlin, R.D. (1964). Micro-structure in linear elasticity. *Arch. Rat. Mech. Anal,* **10,** 51–77.

Schaeffer, H. (1967). Das Cosserat-Kontinuum. *ZAMM,* **47,** 485–498.

Further reading

Akivis, M.A. and Goldberg, V.V. (1977). *An Introduction to Linear Algebra and Tensors.* Dover Publications, New York.

Becker, E. and Bürger, W. (1975). *Kontinuumsmechanik.* Teubner, Stuttgart.

Bell, J.F. (1984). The experimental foundations of solid mechanics. In: *Mechanics of Solids,* Vol. I (C.Truesdell, ed.). Springer, Berlin.

Carslaw, H.S. and Jaeger, J.C. (1946). *Conduction of Heat in Solids.* Oxford Science Publishers, Oxford.

Malvern, L.E. (1969). *Introduction to the Mechanics of a Continuous Medium.* Prentice-Hall Inc., Englewood Cliffs, New Jersey.

Mróz, Z. (1966). On forms of constitutive laws for elastic-plastic solids. *Archiwum Mecaniki Stosowanej,* **1**(18), 3–35.

Prager, W. (1961). *Einführung in die Kontinuumsmechanik.* Birkhäuser.

Truesdell, C. and Toupin, R. (1960). *The Classical Field Theories of Mechanics. Handbuch der Physik, Vol III/1,* sections 173–194. Springer, Berlin.

3
Incremental continuum mechanics

3.1
Updated Lagrangian description

3.1.1
Kinematical considerations

Let a solid body B be at time t deformed to a given configuration C. In the so-called updated Lagrangian description of the motion, the current configuration (i.e. the configuration C at time t) of the considered solid body B with material points occupying positions with known spatial coordinates x_i is used as reference configuration. Let $\bar{\mathbf{C}}$ be the configuration of B at time $\bar{t} \geqslant t$ (Figure 3.1.1). The coordinates of a particle X in C and $\bar{\mathbf{C}}$, relative to a *fixed-in-space* Cartesian coordinate system are denoted by x_i and $\bar{x}_i$ in C and $\bar{\mathbf{C}}$, respectively. For small time increments, $\Delta t = \bar{t} - t$, the infinitesimal displacement vector of the material point X for the considered transition $\mathbf{C} \rightarrow \bar{\mathbf{C}}$ is

$$\Delta u_i = \bar{x}_i(x_k, \bar{t}) - \bar{x}_i(x_k, t) \approx v_i(x_k, t)\Delta t \tag{3.1.1}$$

Moreover, from equation 2.2.18 we obtain the following relationship between the relative deformation gradient and the infinitesimal displacement gradient

$$F^t_{ij}(x_k, \bar{t}) - F^t_{ij}(x_k, t) \approx \dot{F}^t_{ij}\Delta t = \partial_j(v_i \Delta t) \approx \partial_j \Delta u_i$$

or

$$\partial_j \Delta u_i \approx L_{ij}\Delta t \tag{3.1.2}$$

where $\partial_i = \partial/\partial x_i$, i.e. the gradient with respect to the coordinates in C*(t)*.

Within a *linearized continuum theory* we assume that the displacement gradient $\partial_j \Delta u_i$ is infinitesimal everywhere in C so that all terms of an order higher than one in $\partial_j \Delta u_i$ can be neglected in comparison to non-vanishing first order terms. Moreover, from equation 3.1.2 it follows that within a linearized theory, the relative deformation gradient can be additively decomposed into a part corresponding to rigid-body rotation and into a part corresponding to pure deformation

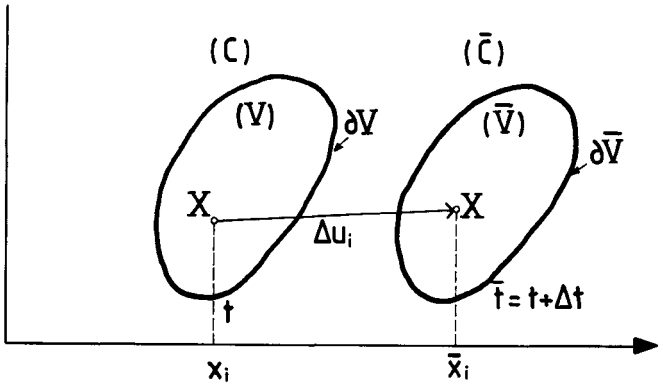

Figure 3.1.1 The updated Lagrangian description uses the current configuration as reference configuration.

$$\begin{aligned} F^t_{ij}(t+\Delta t) &\approx F^t_{ij}(t) + \partial_j \Delta u_i \\ &= \delta_{ij} + \tfrac{1}{2}(\partial_j \Delta u_i - \partial_i \Delta u_j) + \tfrac{1}{2}(\partial_j \Delta u_i + \partial_i \Delta u_j) \\ &= \delta_{ij} + \Delta\omega_{ij} + \Delta\varepsilon_{ij} \end{aligned} \tag{3.1.3}$$

where $\Delta\omega_{ij}$ and $\Delta\varepsilon_{ij}$ are the infinitesimal spin tensor and strain tensor, respectively

$$\Delta\omega_{ij} = \tfrac{1}{2}(\partial_j \Delta u_i - \partial_i \Delta u_j) \approx W_{ij}\Delta t \tag{3.1.4}$$

$$\Delta\varepsilon_{ij} = \tfrac{1}{2}(\partial_j \Delta u_i + \partial_i \Delta u_j) \approx D_{ij}\Delta t \tag{3.1.5}$$

3.1.2
Plane-strain deformations

In order to illustrate the decomposition 3.1.3 of the infintesimal relative deformation gradient, we consider the special case of *plane-strain* deformations. Plane strain is defined by the conditions that both the displacement vector and its derivatives in the x_3-direction vanish

$$\Delta u_3 = 0;\ \partial_3 \Delta u_i = 0 \quad (i = 1,2,3) \tag{3.1.6}$$

For a line element (AB) (Figure 3.1.2a), the displacement field at point B can be expressed in terms of the displacement at point A as follows

$$\Delta u_i(B) = \Delta u_i(A) + \partial_j \Delta u_i(A)\mathrm{d}x_j$$

where

$$\mathrm{d}x_i = m_i \mathrm{d}l;\ m_1 = \cos\alpha, m_2 = \sin\alpha \tag{3.1.7}$$

and $\mathrm{d}l$ is the length of the line element (AB). We introduce the displacement derivative vector

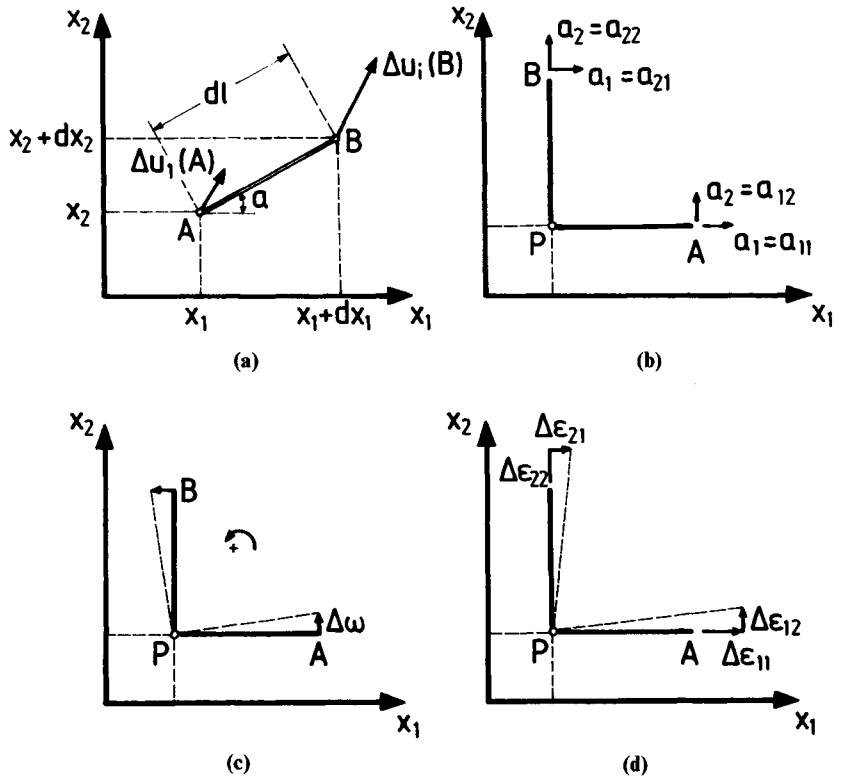

Figure 3.1.2 (a) Displacement of a line element; (b) the displacement derivative vectors; (c) incremental rigid-body rotation; (d) incremental strain.

$$a_i = \frac{\Delta u_i(B) - \Delta u_i(A)}{\mathrm{d}l} = \left.\frac{\mathrm{d}\Delta u_i}{\mathrm{d}l}\right|_m = \partial_j \Delta u_i(A) m_j \tag{3.1.8}$$

with

$$a_{ij} = \partial_i \Delta u_j \rightarrow a_i = a_{ki} m_k \tag{3.1.9}$$

In Figure 3.1.2(b) the geometrical meaning of the components of the displacement derivative vector is illustrated along line elements that are parallel to the coordinate axes.

Line element (PA): $m_1 = 1;\ m_2 = 0$

$$a_1 = a_{k1} m_k = a_{11} = \partial_1 \Delta u_1$$

$$a_2 = a_{k2} m_k = a_{12} = \partial_1 \Delta u_2$$

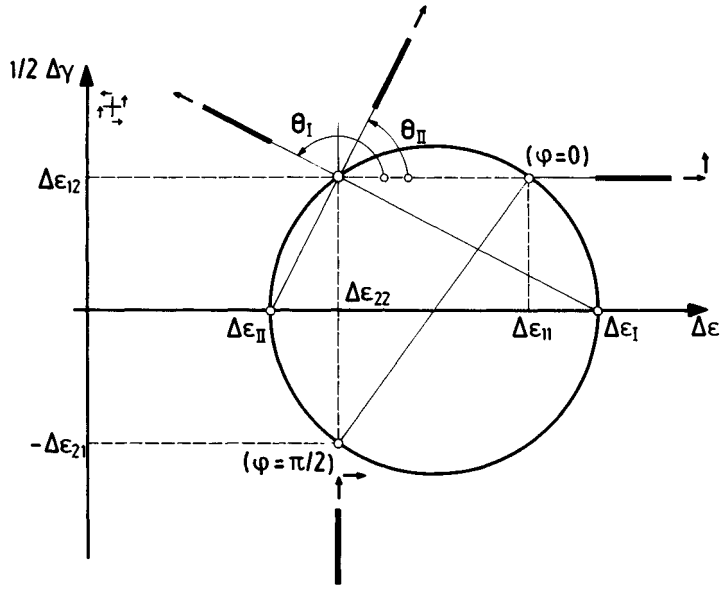

(e)

Figure 3.1.2 (e) Mohr's circle with pole of incremental strains.

$$\text{Line element (PB): } m_1 = 0;\ m_2 = 1$$

$$a_1 = a_{k1} m_k = a_{21} = \partial_2 \Delta u_1$$

$$a_2 = a_{k2} m_k = a_{22} = \partial_2 \Delta u_2$$

Within an infinitesimal theory, strain and spin are defined as follows

$$\Delta\varepsilon_{ij} = \tfrac{1}{2}(a_{ji} + a_{ij});\ \Delta\omega_{ij} = \tfrac{1}{2}(a_{ji} - a_{ij}) \tag{3.1.10}$$

or in matrix representation

$$\{\Delta\varepsilon_{ij}\} = \begin{bmatrix} \partial_1 \Delta u_1 & \tfrac{1}{2}(\partial_2 \Delta u_1 + \partial_1 \Delta u_2) \\ \tfrac{1}{2}(\partial_1 \Delta u_2 + \partial_2 \Delta u_1) & \partial_2 \Delta u_2 \end{bmatrix} \tag{3.1.10a}$$

$$\{\Delta\omega_{ij}\} = \begin{bmatrix} 0 & -\Delta\omega \\ \Delta\omega & 0 \end{bmatrix};\ \Delta\omega = \Delta\omega_{21} = \tfrac{1}{2}(\partial_1 \Delta u_2 - \partial_2 \Delta u_1) \tag{3.1.10b}$$

For the particular case where the deformation consists locally of a pure infinitesimal rigid-body rotation we have

$$a_{ij} = -a_{ji} \rightarrow \Delta\varepsilon_{ij} = 0;\ \Delta\omega_{ij} = -a_{ij}$$

This is illustrated in Figure 3.1.2(c).

$$\text{Line element (PA): } m_1 = 1;\ m_2 = 0$$

$$a_1 = a_{k1}m_k = a_{11} = 0$$

$$a_2 = a_{k2}m_k = a_{12} = -\Delta\omega_{12} = \Delta\omega$$

$$\text{Line element (PB): } m_1 = 0;\ m_2 = 1$$

$$a_1 = a_{k1}m_k = a_{21} = -\Delta\omega_{21} = -\Delta\omega$$

$$a_2 = a_{k2}m_k = a_{22} = 0$$

For the special case where the deformation is free of rigid-body rotations we have

$$a_{ij} = a_{ji} \rightarrow \Delta\varepsilon_{ij} = a_{ij};\ \Delta\omega_{ij} = 0$$

the deformation corresponds to pure stretching and distortion, Figure 3.1.2(d).

$$\text{Line element (PA): } m_1 = 1;\ m_2 = 0$$

$$a_1 = a_{k1}m_k = a_{11} = \Delta\varepsilon_{11}$$

$$a_2 = a_{k2}m_k = a_{12} = \Delta\varepsilon_{12}$$

$$\text{Line element (PB): } m_1 = 0;\ m_2 = 1$$

$$a_1 = a_{k1}m_k = a_{21} = \Delta\varepsilon_{21}$$

$$a_2 = a_{k2}m_k = a_{22} = \Delta\varepsilon_{22}$$

Remark on coordinate transformations. For reference purposes we summarize here in explicit form the simple transformation rules of a two-dimensional tensor like the above-discussed infinitesimal strain and spin tensors. Let us consider a coordinate transformation which corresponds to a counterclockwise rotation at an angle ϕ

$$x_1' = \cos\phi\, x_1 + \sin\phi\, x_2$$

$$x_2' = -\sin\phi\, x_1 + \cos\phi\, x_2$$

$$x_3' = x_3$$

The components of the infinitesimal strain tensor in the $x_{\bar{i}}'$-coordinate system become

$$\Delta\varepsilon_{1'1'} = \Delta\varepsilon_{11}\cos^2\phi + \Delta\varepsilon_{22}\sin^2\phi + 2\Delta\varepsilon_{12}\sin\phi\cos\phi$$

$$\Delta\varepsilon_{2'2'} = \Delta\varepsilon_{11}\sin^2\phi + \Delta\varepsilon_{22}\cos^2\phi - 2\Delta\varepsilon_{12}\sin\phi\cos\phi$$

$$\Delta\varepsilon_{1'2'} = \Delta\varepsilon_{2'1'} = -(\Delta\varepsilon_{11} - \Delta\varepsilon_{22})\sin\phi\cos\phi + \Delta\varepsilon_{12}(\cos^2\phi - \sin^2\phi)$$

or

$$\Delta\varepsilon_{1'1'} = \tfrac{1}{2}(\Delta\varepsilon_{11} + \Delta\varepsilon_{22}) + \tfrac{1}{2}(\Delta\varepsilon_{11} - \Delta\varepsilon_{22})\cos 2\phi + \Delta\varepsilon_{12}\sin 2\phi$$

$$\Delta\varepsilon_{2'2'} = \tfrac{1}{2}(\Delta\varepsilon_{11} + \Delta\varepsilon_{22}) - \tfrac{1}{2}(\Delta\varepsilon_{11} - \Delta\varepsilon_{22})\cos 2\phi + \Delta\varepsilon_{12}\sin 2\phi$$

$$\Delta\varepsilon_{1'2'} = \Delta\varepsilon_{2'1'} = -\tfrac{1}{2}(\Delta\varepsilon_{11} - \Delta\varepsilon_{22})\sin 2\phi + \Delta\varepsilon_{12}\cos 2\phi$$

Let Θ be the angle between the x_1-axis and the (I) principal direction of $\Delta\varepsilon_{ij}$. From the condition $\Delta\varepsilon_{1'2'}=0$ we obtain,

$$\tan 2\Theta = \frac{2\Delta\varepsilon_{12}}{\Delta\varepsilon_{11} - \Delta\varepsilon_{22}}$$

and the principal strains are computed from

$$\Delta\varepsilon_{\mathrm{I,II}} = \tfrac{1}{2}(\Delta\varepsilon_{11} + \Delta\varepsilon_{22}) \pm \tfrac{1}{2}\{(\Delta\varepsilon_{11} - \Delta\varepsilon_{22})^2 + 4\Delta\varepsilon_{12}^2\}^{\frac{1}{2}}$$

Figure 3.1.2(e) depicts the corresponding Mohr circle of infinitesimal strains, where we notice the sign convention.

Finally we remark that coordinate rotations do not affect the components of the spin tensor, i.e. the spin tensor is invariant towards coordinate rotations

$$\Delta\omega_{i'j'} = \Delta\omega_{ij}$$

3.1.3
Deformation of line, surface and volume elements

A line element in C and $\bar{\mathbf{C}}$ is described by the following line-element vectors (Figure 3.1.3a):

$$\begin{aligned} \mathrm{d}x_i &= m_i \mathrm{d}l;\ \mathrm{d}l = (\mathrm{d}x_i\,\mathrm{d}x_i)^{\frac{1}{2}} \\ \mathrm{d}\bar{x}_i &= \bar{m}_i \mathrm{d}\bar{l};\ \mathrm{d}\bar{l} = (\mathrm{d}\bar{x}_i\,\mathrm{d}\bar{x}_i)^{\frac{1}{2}} \end{aligned} \tag{3.1.11}$$

With

$$\mathrm{d}\bar{x}_i = F^t_{ij}(\bar{t})\mathrm{d}x_j$$

and

$$\mathrm{d}\bar{l} = \mathrm{d}l + \Delta\mathrm{d}l \tag{3.1.12}$$

the deformation rule for line elements can be derived

$$\begin{aligned} \mathrm{d}\bar{l} &= (F^t_{ij}\mathrm{d}x_j F^t_{ik}\mathrm{d}x_k)^{\frac{1}{2}} = (F^t_{ij}F^t_{ik}\mathrm{d}l^2 m_j m_k)^{\frac{1}{2}} \\ &= \mathrm{d}l\{(\delta_{ij} + \partial_j\Delta u_i)(\delta_{ik} + \partial_k\Delta u_i)m_j m_k\}^{\frac{1}{2}} \approx \mathrm{d}l(1 + 2\Delta\varepsilon_{jk}m_j m_k)^{\frac{1}{2}} \\ &\approx \mathrm{d}l(1 + \Delta\varepsilon_{jk}m_j m_k) \end{aligned}$$

i.e. within a linearized theory we obtain

$$\Delta\mathrm{d}l = \Delta\varepsilon_{ij}m_i m_j\,\mathrm{d}l = \partial_j\Delta u_i m_i m_j\,\mathrm{d}l \tag{3.1.13}$$

Similarly, the line-element unit vector deforms

$$\bar{m}_i = m_i + \Delta m_i \tag{3.1.14}$$

where

$$\Delta m_i = m_l(\delta_{ik} - m_i m_k)\partial_l\Delta u_k \tag{3.1.15}$$

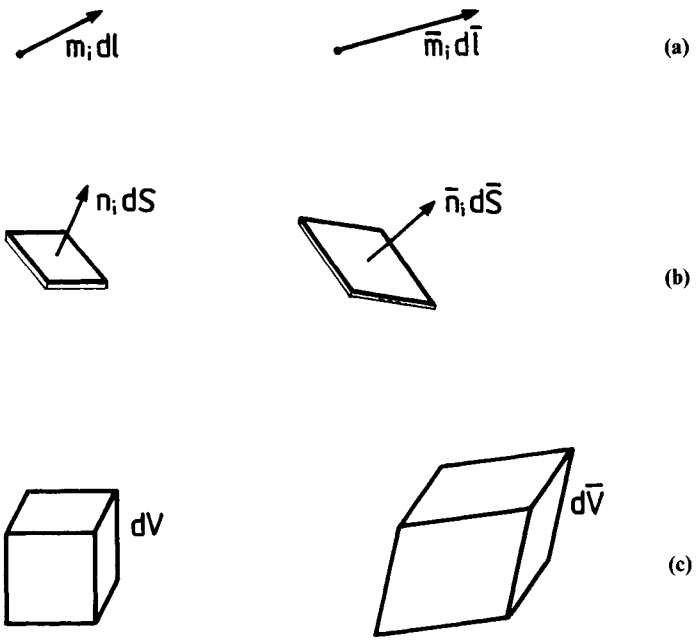

Figure 3.1.3 (a) Deformation of line element; (b) deformation of surface element; (c) deformation of volume element.

A surface-element vector in C and $\bar{\mathbf{C}}$ is given by the following expression (Figure 3.1.3b)

$$\begin{aligned} dS_i &= e_{ijk}\, dx_j\, dy_k = n_i\, dS;\ dS = (dS_i\, dS_i)^{\frac{1}{2}} \\ d\bar{S}_i &= e_{ijk}\, d\bar{x}_j\, d\bar{y}_k = \bar{n}_i\, d\bar{S};\ d\bar{S} = (d\bar{S}_i\, d\bar{S}_i)^{\frac{1}{2}} \end{aligned} \tag{3.1.16}$$

By replacing F_{ij} by F^t_{ij} in equation 2.1.36 we get

$$d\bar{S}_i = \mathrm{ad}(F^t)_{ki}\, dS_k \tag{3.1.17}$$

In order to linearize the above expression we consider the explicit form of $\mathrm{ad}(\mathrm{F}^t)_{ij}$:

$$\begin{aligned} \mathrm{ad}(\mathbf{F}^t)_{11} &= F^t_{22}F^t_{33} - F^t_{23}F^t_{32} = (1 + \partial_2\Delta u_2)(1 + \partial_3\Delta u_3) - \partial_3\Delta u_2\partial_2\Delta u_3 \\ &\approx 1 + \partial_2\Delta u_2 + \partial_3\Delta u_3 \\ \mathrm{ad}(\mathbf{F}^t)_{12} &= F^t_{32}F^t_{13} - F^t_{33}F^t_{12} \\ &= \partial_2\Delta u_3\partial_3\Delta u_1 - (1 + \partial_3\Delta u_3)\partial_2\Delta u_1 \\ &\approx -\partial_2\Delta u_1, \text{ etc.} \end{aligned}$$

or more generally

$$\mathrm{ad}(\mathbf{F}^t)_{ij} = (1 + \partial_k\Delta u_k)\delta_{ij} - \partial_j\Delta u_i \tag{3.1.18}$$

From equations 3.1.17 and 3.1.18 we obtain finally the deformation rule for surface elements

$$\mathrm{d}\bar{S} = \mathrm{d}S + \Delta\mathrm{d}S \tag{3.1.19}$$

where

$$\Delta\mathrm{d}S = (\Delta\varepsilon_{kk} - \Delta\varepsilon_{lm}n_l n_m)\mathrm{d}S \tag{3.1.20}$$

Similarly we obtain the transformation rule for the unit normal

$$\bar{n}_i = n_i + \Delta n_i \tag{3.1.21}$$

where

$$\Delta n_i = n_k(n_i n_l - \delta_{il})\partial_l \Delta u_k \tag{3.1.22}$$

Finally, let $\mathrm{d}V$ and $\mathrm{d}\bar{V}$ be volume elements in C and $\bar{\mathrm{C}}$ respectively (Figure 3.1.3c)

$$\mathrm{d}V = \mathrm{e}_{ijk}\,\mathrm{d}x_i\,\mathrm{d}y_j\,\mathrm{d}w_k;\ \mathrm{d}\bar{V} = e_{ijk}\,\mathrm{d}\bar{x}_i\,\mathrm{d}\bar{y}_j\,\mathrm{d}\bar{w}_k \tag{3.1.23}$$

The deformation rule for volume elements is then given by

$$\mathrm{d}\bar{V} = J^t\,\mathrm{d}V \tag{3.1.24}$$

where for a linear theory we find that the Jacobian of the deformation is

$$J^t = \det(F^t_{ij}) \approx 1 + \partial_k \Delta u_k = 1 + \Delta\varepsilon_{kk} \tag{3.1.25}$$

and consequently

$$\Delta\varepsilon_{kk} = \frac{\mathrm{d}\bar{V} - \mathrm{d}V}{\mathrm{d}V} = \frac{\Delta\mathrm{d}V}{\mathrm{d}V} \tag{3.1.26}$$

3.1.4
Stresses and stress increments

The state of stress in C and $\bar{\mathrm{C}}$ is primarily described by the true or Cauchy stress tensors σ_{ij} and $\bar{\sigma}_{ij}$, respectively. These stress tensors are defined as follows: Let $\mathrm{d}t_i$, $\mathrm{d}\bar{t}_i$ be the stress vectors acting on surface elements $\mathrm{d}S_k = n_k\,\mathrm{d}S$ and $\mathrm{d}\bar{S} = \bar{n}_k\,\mathrm{d}\bar{S}$ in C and $\bar{\mathrm{C}}$, respectively (Figure 3.1.4), then

$$\mathrm{d}t_i = \sigma_{ki}\,\mathrm{d}S_k;\ \mathrm{d}\bar{t}_i = \bar{\sigma}_{ki}\,\mathrm{d}\bar{S}_k \tag{3.1.27}$$

In finite strain analysis the nominal or *first Piola-Kirchhoff* (1. P.-K.) stress tensor T_{Rij} is defined by mapping the stress vector in the current configuration C onto the corresponding surface element in the initial configuration $\mathrm{C}^{(0)}$. In an updated Lagrangian analysis however the relative nominal or 1. P.-K. stress tensor in $\bar{\mathrm{C}}$ is introduced, denoted as $\pi_{ij} = T^t_{Rij}(\bar{t})$, by mapping the stress vector in $\bar{\mathrm{C}}$ onto the corresponding surface element in C

$$\mathrm{d}\bar{t}_i = \pi_{ij}\,\mathrm{d}S_j \tag{3.1.28}$$

where $\mathrm{d}S_i$ is related to $\mathrm{d}\bar{S}_i$ through the transformation 3.1.19 to 3.1.21. Accordingly we obtain the relation between the 1. P.-K. stress tensor and the corresponding Cauchy stress tensor

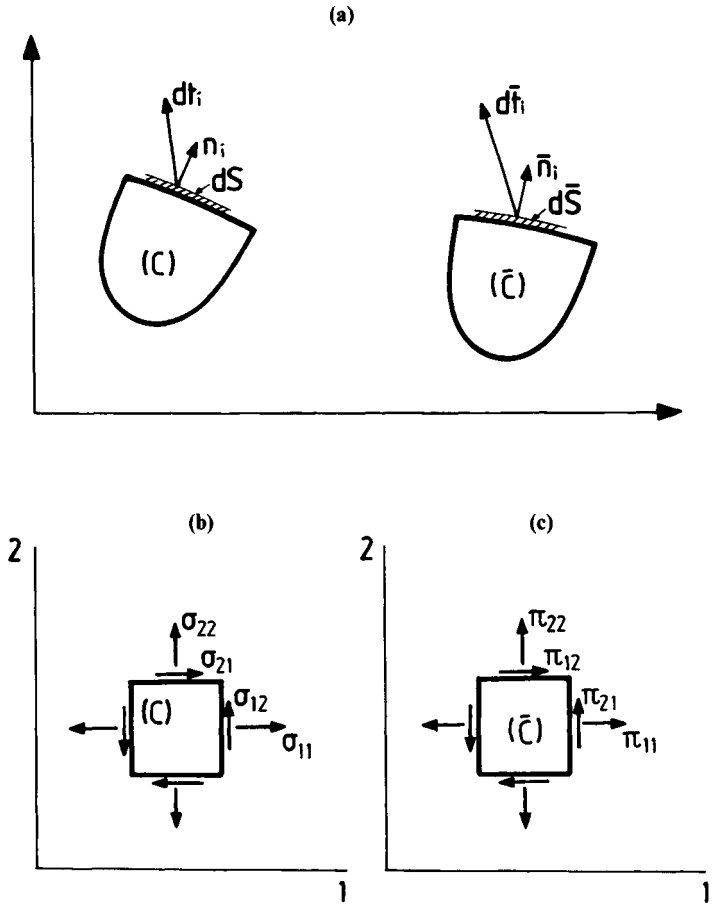

Figure 3.1.4 (a) Stress vectors in C and $\bar{C}$; (b) the components of the Cauchy stress tensor describing the state of stress in C; (c) the components of the 1. P.-K. stress tensor describing the state of stress in

$$\begin{aligned} \mathrm{d}\bar{f}_i &= \bar{\sigma}_{ki}\,\mathrm{d}\bar{S}_k = \bar{\sigma}_{ki}\,\mathrm{ad}(F^t)_{jk}\,\mathrm{d}S_j = J^t\bar{\sigma}_{ki}F^{t-1}_{jk}\,\mathrm{d}S_j \\ \pi_{ij} &= J^t\bar{\sigma}_{ki}F^{t-1}_{jk} \end{aligned} \tag{3.1.29}$$

By considering moment equilibrium of the tractions that act on the boundary of an arbitrary volume of material in C or $\bar{C}$ we find that the Cauchy stress tensor in a Boltzmann continuum is symmetric, cf. section 2.3.3,

$$\sigma_{ij} = \sigma_{ji} \quad \text{and} \quad \bar{\sigma}_{ij} = \bar{\sigma}_{ji} \tag{3.1.30}$$

However, according to equation 3.1.29, this is not true for the 1. P.-K. stress tensor, i.e. for $i \neq j$, $\pi_{ij} \neq \pi_{ji}$.

For infinitesimal transitions the Cauchy stress increment is given by

$$\bar{\sigma}_{ij} - \sigma_{ij} \approx \dot{\sigma}_{ij}(x_k, t)\Delta t = \Delta\sigma_{ij} \tag{3.1.31}$$

where $\dot{\sigma}_{ij}$ is the material time derivative of the Cauchy stress. The corresponding increment of the 1. P.-K. stress tensor is

$$\pi_{ij} - \sigma_{ij} \approx \dot{\pi}_{ij}(x_k, t) = \Delta\pi_{ij} \tag{3.1.32}$$

By using the definition 3.1.29 and the approximation for the adjoint of the deformation gradient, equations 3.1.18, the following expression is obtained

$$\Delta\pi_{ij} = \Delta\sigma_{ij} + \sigma_{ij}\partial_k\Delta u_k - \sigma_{ik}\partial_k\Delta u_j \tag{3.1.33}$$

The stress increment $\Delta\sigma_{ij}$ is directly related to the material time derivative of the Cauchy stress tensor, as indicated in equation 3.1.31, which according to equation 2.2.32 consists in turn of the rigid-body time derivative of the Cauchy stress and corrotational terms. Accordingly, the Jaumann stress increment of the Cauchy stress is introduced

$$\mathring{\Delta}\sigma_{ij} = \mathring{\sigma}_{ij}\Delta t \tag{3.1.34}$$

From the above definitions we find that

$$\Delta\sigma_{ij} = \mathring{\Delta}\sigma_{ij} + \Delta\omega_{ik}\sigma_{kj} - \sigma_{ik}\Delta\omega_{kj} \tag{3.1.35}$$

Substitution from equation 3.1.35 into equation 3.1.33 yields a decomposition of the increment $\Delta\pi_{ij}$ of the 1. P.-K. stress tensor in objective part and in a geometric correction term

$$\Delta\pi_{ij} = \mathring{\Delta}\sigma_{ij} + \Delta\omega_{ik}\sigma_{kj} - \sigma_{ik}\Delta\varepsilon_{kj} + \sigma_{ij}\Delta\varepsilon_{kk} \tag{3.1.36}$$

The Kirchhoff stress tensor T_{ij} in C and $\bar{\mathbf{C}}$ are defined as follows

$$T_{ij} = J\sigma_{ij};\ T_{ij} = \bar{J}\bar{\sigma}_{ij} \tag{3.1.37}$$

where J and $\bar{J}$ are the corresponding Jacobians of the deformation with respect to the initial configuration $C^{(0)}$,

$$\begin{aligned}\bar{J} &= \det(\bar{F}_{ij}) = \det(F^t_{ik}(\bar{t})F_{kj}(t)) = J^t J \\ &\approx J(1 + \Delta\varepsilon_{kk})\end{aligned} \tag{3.1.38}$$

and thus

$$\begin{aligned}T_{ij} &= JJ^t\bar{\sigma}_{ij} \approx J(1 + \Delta\varepsilon_{kk})(\sigma_{ij} + \Delta\sigma_{ij}) \\ &\approx T_{ij} + J\Delta\sigma_{ij} + T_{ij}\Delta\varepsilon_{kk}\end{aligned} \tag{3.1.39}$$

$$\Delta T_{ij} = \bar{T}_{ij} - T_{ij} \approx J\Delta\sigma_{ij} + T_{ij}\Delta\varepsilon_{kk} \tag{3.1.40}$$

In an updated Lagrangian analysis, however, the current configuration C is used as reference configuration. Accordingly, we define a relative Kirchhoff stress tensor, T^t_{ij}, such that

$$\begin{aligned} T_{ij}^t &= T_{ij}^t(t) = J^{-1} T_{ij} = \sigma_{ij} \\ \bar{T}_{ij}^t &= T_{ij}^t(\bar{t}) = J^{-1} \bar{T}_{ij} = J^t \bar{\sigma}_{ij} \end{aligned} \tag{3.3.41}$$

and

$$\begin{aligned} \Delta T_{ij}^t &= \bar{T}_{ij}^t - T_{ij}^t = J^{-1} \Delta T_{ij} \\ &\approx \Delta \sigma_{ij} + \sigma_{ij} \Delta \varepsilon_{kk} \end{aligned} \tag{3.1.42}$$

Accordingly, the Cauchy/Jaumann stress increment in equation 3.1.36 can be replaced by the relative Kirchhoff/Jaumann stress increment

$$\mathring{\Delta} \sigma_{ij} = \mathring{\Delta} T_{ij}^t - \sigma_{ij} \Delta \varepsilon_{kk} \tag{3.1.43}$$

Summarizing the above derivations we have

$$\Delta \sigma_{ij} = \mathring{\Delta} \sigma_{ij} + \Delta \omega_{ik} \sigma_{kj} - \sigma_{ik} \Delta \omega_{kj} \tag{3.1.35}$$

$$\Delta \pi_{ij} = \mathring{\Delta} \sigma_{ij} + \Delta \omega_{ik} \sigma_{kj} - \sigma_{ik} \Delta \varepsilon_{kj} + \sigma_{ij} \Delta \varepsilon_{kk} \tag{3.1.36}$$

$$\begin{aligned} \mathring{\Delta} \sigma_{ij} &= J^{-1} \mathring{\Delta} T_{ij} - \sigma_{ij} \Delta \varepsilon_{kk} \\ &= \mathring{\Delta} T_{ij}^t - \sigma_{ij} \Delta \varepsilon_{kk} \end{aligned} \tag{3.1.43}$$

$$\mathring{\Delta} T_{ij}^t = J^{-1} \mathring{\Delta} T_{ij} \tag{3.1.44}$$

$$\Delta T_{ij} = \mathring{\Delta} T_{ij} + \Delta \omega_{ik} T_{kj} - T_{ik} \Delta \omega_{kj} \tag{3.1.45}$$

$$\Delta T_{ij}^t = \mathring{\Delta} T_{ij}^t + \Delta \omega_{ik} \sigma_{kj} - \sigma_{ik} \Delta \omega_{kj} \tag{3.1.46}$$

$$\begin{aligned} \Delta \pi_{ij} &= \mathring{\Delta} T_{ij}^t + \Delta \omega_{ik} \sigma_{kj} - \sigma_{ik} \Delta \varepsilon_{kj} \\ &= J^{-1} \mathring{\Delta} T_{ij} + \Delta \omega_{ik} \sigma_{kj} - \sigma_{ik} \Delta \varepsilon_{kj} \end{aligned} \tag{3.1.47}$$

Thus we obtain a useful expression for the nominal stress increment in terms of the Kirchhoff stress and its Jaumann increment,

$$\Delta \pi_{ij} = J^{-1} (\mathring{\Delta} T_{ij} + \Delta \omega_{ik} T_{kj} - T_{ik} \Delta \varepsilon_{kj}) \tag{3.1.47bis}$$

We notice that for isochoric deformations ($J=J^t=1$) there is no difference between Cauchy and Kirchhoff stresses and their increments. For a comprehensive discussion of the various stress tensors and their increments which can be used in an updated Lagrangian analysis we refer to Bazant (1971).

Geometric correction terms for plane-strain deformations. First we recall that for isotropic material and plane-strain deformations the Cauchy shear stress on the x_3-plane is vanishing

$$\sigma_{13} = \sigma_{23} = 0$$

The principal stress, σ_{33}, is of course not necessarily zero.

With the current configuration being the reference configuration, and the notation

$$\Delta\sigma_{ij} = \mathring{\Delta}\sigma_{ij} + \bar{\Delta}\sigma_{ij};\ \bar{\Delta}\sigma_{ij} = \Delta\omega_{ik}\sigma_{kj} - \Delta\sigma_{ik}\Delta\omega_{kj}$$
$$\Delta T^t_{ij} = \mathring{\Delta}T^t_{ij} + \bar{\Delta}T^t_{ij};\ \bar{\Delta}T^t_{ij} = \Delta\omega_{ik}\sigma_{kj} - \Delta\sigma_{ik}\Delta\omega_{kj}$$
$$\Delta\pi_{ij} = \mathring{\Delta}\sigma_{ij} + \bar{\Delta}\pi_{ij};\ \bar{\Delta}\pi_{ij} = \Delta\omega_{ik}\sigma_{kj} - \sigma_{ik}\Delta\varepsilon_{kj} + \sigma_{ij}\Delta\varepsilon_{kk}$$

for plane-strain analysis we obtain the following expressions for the corotational terms $\bar{\Delta}\sigma_{ij} = \bar{\Delta}T^t_{ij}$ (cf. Vardoulakis, 1978)

$$\bar{\Delta}\sigma_{11} = -\bar{\Delta}\sigma_{22} = -2\sigma_{12}\Delta\omega$$
$$\bar{\Delta}\sigma_{12} = \bar{\Delta}\sigma_{21} = (\sigma_{11} - \sigma_{22})\Delta\omega$$
$$\bar{\Delta}\sigma_{3i} = 0 \quad (i = 1, 2, 3)$$

where

$$\Delta\omega = \tfrac{1}{2}(\partial_1\Delta u_2 - \partial_2\partial\Delta u_1)$$

is the only significant component of the incremental spin tensor. Similarly for the geometric correction terms of the nominal stress increment we obtain

$$\bar{\Delta}\pi_{11} = -\sigma_{12}\,\partial_1\Delta u_2 + \sigma_{11}\,\partial_2\Delta u_2$$
$$\bar{\Delta}\pi_{22} = -\sigma_{21}\,\partial_2\Delta u_1 + \sigma_{22}\,\partial_1\Delta u_1$$
$$\bar{\Delta}\pi_{33} = \sigma_{33}(\partial_1\Delta u_1 + \partial_2\Delta u_2)$$
$$\bar{\Delta}\pi_{12} = -\tfrac{1}{2}(\sigma_{11} - \sigma_{22})\partial_2\Delta u_1 - \tfrac{1}{2}(\sigma_{11} + \sigma_{22})\partial_1\Delta u_2 + \sigma_{12}\,\partial_1\Delta u_1$$
$$\bar{\Delta}\pi_{21} = -\tfrac{1}{2}(\sigma_{22} - \sigma_{11})\partial_1\Delta u_2 - \tfrac{1}{2}(\sigma_{22} + \sigma_{11})\partial_2\Delta u_1 + \sigma_{21}\,\partial_2\Delta u_2$$

The remaining components of $\bar{\Delta}\pi_{ij}$ and $\bar{\Delta}\sigma_{ij}$ are zero.

In the coordinate system of principal axes of the Cauchy stress, σ_{ij}, the above equations become

$$\bar{\Delta}\sigma_{11} = \bar{\Delta}\sigma_{22} = 0;\ \bar{\Delta}\sigma_{12} = \bar{\Delta}\sigma_{21} = (\sigma_1 - \sigma_2)\Delta\omega$$
$$\bar{\Delta}\pi_{11} = \sigma_1\Delta\varepsilon_{22};\ \bar{\Delta}\pi_{22} = \sigma_2\Delta\varepsilon_{11};\ \bar{\Delta}\pi_{33} = \sigma_3(\Delta\varepsilon_{11} + \Delta\varepsilon_{22})$$
$$\bar{\Delta}\pi_{12} = -\sigma_1\Delta\varepsilon_{12} + \sigma_2\Delta\omega;\ \bar{\Delta}\pi_{21} = -\sigma_2\Delta\varepsilon_{12} - \sigma_1\Delta\omega$$

We observe that for in-plane isotropic states the Cauchy corotational terms vanish.

Second-order continuum approximations. We consider the right-polar decomposition of the relative deformation gradient

$$F^t_{ij} = R^t_{ik}U^t_{kj}$$

where R^t_{ij} is the proper orthogonal rotation tensor and U^t_{ij} is the relative right-stretching tensor. Under plane-strain conditions we restrict the

demonstrations to the components in the plane of deformation

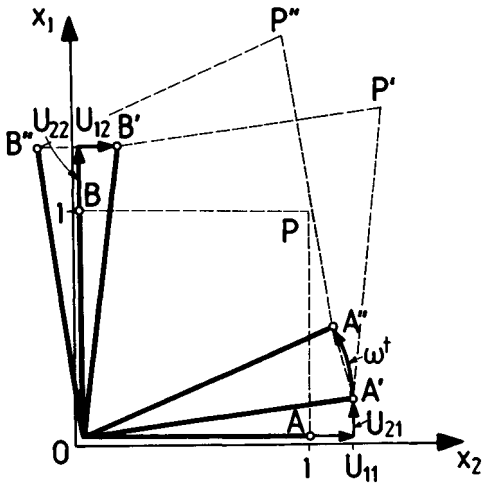

Figure 3.1.5 Polar decomposition of

$$\begin{bmatrix} F^t_{11} & F^t_{12} \\ F^t_{21} & F^t_{22} \end{bmatrix} = \begin{bmatrix} \cos\omega^t & -\sin\omega^t \\ \sin\omega^t & \cos\omega^t \end{bmatrix} \begin{bmatrix} U^t_{11} & U^t_{12} \\ U^t_{21} & U^t_{22} \end{bmatrix}$$

Let, again, $\Delta\varepsilon_{ij}$ be the symmetric part of the displacement gradient and $\Delta\omega$ the only non-zero component of its antisymmetric part, equations 3.1.10,

$$\Delta\varepsilon_{ij} = \tfrac{1}{2}(\partial_j \Delta u_i + \partial_i \Delta u_j);\ \Delta\omega = \tfrac{1}{2}(\partial_2 \Delta u_1 - \partial_1 \Delta u_2)$$

The rotation angle ω^t and the components of the right stretching tensor U^t_{ij} are given within a *second-order theory* by the following expressions (see Figure 3.1.5)

$$\omega^t \approx \Delta\omega - \tfrac{1}{2}\Delta\varepsilon_{kk}\Delta\omega$$

$$U^t_{11} \approx 1 + \Delta\varepsilon_{11} + \Delta\varepsilon_{12}\Delta\omega + \tfrac{1}{2}\Delta\omega^2$$

$$U^t_{12} \approx U^t_{21} = \Delta\varepsilon_{12} + \tfrac{1}{2}(\Delta\varepsilon_{22} - \Delta\varepsilon_{11})\Delta\omega$$

$$U^t_{22} \approx 1 + \Delta\varepsilon_{22} - \Delta\varepsilon_{21}\Delta\omega + \tfrac{1}{2}\Delta\omega^2$$

Similarly, expressions for the increment of the (relative) 1. P.-K. stress in $\bar{\mathbf{C}}$ can be derived. The increment, $\Delta\pi_{ij}$ of the 1. P.-K. stress can then be written as

$$\Delta\pi_{ij} \approx \mathring{\Delta}\sigma_{ij} + \Delta\pi^{(1)}_{ij} + \Delta\pi^{(2)}_{ij}$$

where $\Delta\pi^{(1)}_{ij} = \bar{\Delta}\pi_{ij}$ are linear correction terms, defined through equations 3.1.36, and

$$\Delta\pi_{11}^{(2)} = \mathring{\Delta}\sigma_{11}\,\partial_2\Delta u_2 - \mathring{\Delta}\sigma_{12}\,\partial_1\Delta u_2 + \{\sigma_{12}(\partial_1\Delta u_1 - \partial_2\Delta u_2) - \tfrac{1}{2}(\sigma_{11} - \sigma_{22})(\partial_2\Delta u_1 + \partial_1\Delta u_2)\}\Delta\omega$$

$$\Delta\pi_{12}^{(2)} = -\tfrac{1}{2}\mathring{\Delta}\sigma_{11}(\partial_2\Delta u_1 + \partial_1\Delta u_2) + \mathring{\Delta}\sigma_{12}\,\partial_1\Delta u_1 - \mathring{\Delta}\sigma_{22}\Delta\omega + \{\sigma_{12}(\partial_2\Delta u_1 + \partial_1\Delta u_2) + \tfrac{1}{2}(\sigma_{11} - \sigma_{22})(\partial_1\Delta u_1 - \partial_2\Delta u_2)\}\Delta\omega$$

are second-order geometric terms. Notice that the expressions for the remaining two components, $\Delta\pi_{21}^{(2)}$, $\Delta\pi_{22}^{(2)}$, can be obtained by interchanging above the indices 1 and 2. (For further reading see Novozhilov, 1961 and Biot, 1965.)

3.2
Infinitesimal strain superimposed upon finite strain

3.2.1
Plane rectilinear deformations

In this section we will outline the structure of constitutive equations of elastic materials which remain isotropic in finite strain (see Biot, 1965). We consider a rectangular block of elastic material in an undeformed configuration $C^{(0)}$ subjected to a rectilinear deformation $C^{(0)} \rightarrow C$

$$\begin{aligned} x_1 &= \ell_1^* \xi_1 \\ x_2 &= \ell_2^* \xi_2 \\ x_3 &= \ell_3^* \xi_3 \end{aligned} \tag{3.2.1}$$

where the principal stretches give the ratios of current to initial block dimensions (Figure 3.2.1)

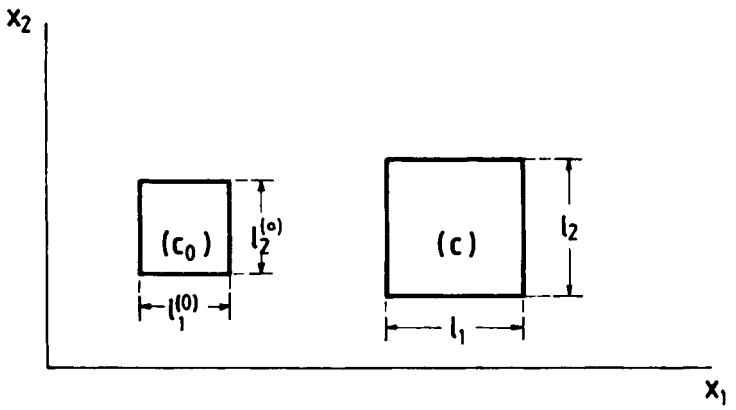

Figure 3.2.1 Rectilinear deformation $C^{(0)} \rightarrow C$.

$$\ell_i^* = \ell_i / \ell_{(i)}^{(0)} \qquad (i = 1,2,3) \tag{3.2.2}$$

A class of elastic materials is defined for which the specific strain (internal) energy is a function of the principal logarithmic strains

$$e = e(\lambda_1, \lambda_2, \lambda_3) \tag{3.2.3}$$

where

$$\lambda_i = \ln(\ell_i^*) \tag{3.2.4}$$

describe the finite strain of the considered rectilinear deformation $\mathbf{C}^{(0)} \rightarrow \mathbf{C}$. It should be remembered that for rectilinear deformations there is no distinction between left (Eulerian) and right (Lagrangian) logarithmic (Hencky) strain tensors.

3.2.2
Superposition of rectilinear deformations

We consider an infinitesimal continuation $\mathbf{C} \rightarrow \bar{\mathbf{C}}$ of the considered rectilinear deformation. During such a transition the principal axes of strain remain fixed, and the change of the logarithmic strain $\Delta\lambda_i = \bar{\lambda}_i - \lambda_i$ coincides with the infinitesimal strain,

$$\Delta\lambda_i = \frac{\Delta\ell_i}{\ell_{(i)}} = \Delta\varepsilon_i \tag{3.2.5}$$

cf. equation 3.1.13 and Figure 3.2.1. In elastic materials it is assumed that all the work done by the stresses is entirely stored in the form of recoverable internal energy. Then from local energy balance, equation 2.3.31, we obtain

$$\begin{aligned} \sigma_i \Delta\varepsilon_i &= \rho \Delta e \\ &= \rho \frac{\partial e}{\partial \lambda_i} \Delta\varepsilon_i \end{aligned} \tag{3.2.6}$$

where σ_i and $\Delta\varepsilon_i$ are the principal values of the Cauchy stress σ_{ij} and of the infinitesimal strain $\Delta\varepsilon_{ij} \approx D_{ij}\Delta t$. From this energy balance equation we obtain the expression of the principal Cauchy stresses in C in terms of the strain energy function

$$\sigma_i = \rho \frac{\partial e}{\partial \lambda_i} \tag{3.2.7}$$

Let $\mathrm{C}^{(0)}$ be the reference configuration of the considered finite deformation. This means that $\mathrm{C}^{(0)}$ is the unstrained configuration, characterized by $\lambda_i = \ln(1) = 0$. For an elastic material, which is defined by the strain energy function $e = e(\lambda_i)$, it is assumed that the unstrained configuration is also stress-free. Due to the definition 2.1.41 and equation 2. 3.2 for the Jacobian of the deformation, the above equation results in an expression for the Kirchhoff stresses

$$T_i = J\sigma_i = \frac{\rho^{(0)}}{\rho}\sigma_i = \rho^{(0)} \frac{\partial e}{\partial \lambda_i} \tag{3.2.8}$$

where $\rho^{(0)}$ is the density of the elastic material in the initial configuration $C^{(0)}$. Since $\rho^{(0)} = \text{const.}$, from the expression 3.2.8, the increments of the Kirchhoff stress can be computed through formal differentiation

$$\Delta T_{i(i)} = \frac{\partial T_i}{\partial \lambda_i}\Delta\varepsilon_{11} + \frac{\partial T_i}{\partial \lambda_2}\Delta\varepsilon_{22} + \frac{\partial T_i}{\partial \lambda_3}\Delta\varepsilon_{33} \tag{3.2.9}$$

The considered rectilinear continuations of the deformations are spinless and thus the increment of the Kirchhoff stress and its Jaumann increment coincide, and thus

$$\mathring{\Delta} T_{ij} = R_{ijkl}\Delta\varepsilon_{kl} \quad \text{for} \quad i = j,\ k = l \ \text{(no sum)} \tag{3.2.9bis}$$

where the components of the material stiffness tensor R_{ijkl} which relate the normal Kirchhoff/Jaumann stress increments to the normal components of the infinitesimal strain are given in terms of the strain energy function,

$$\begin{aligned} R_{1111} &= \frac{\partial T_1}{\partial \lambda_1} = \rho^{(0)}\frac{\partial^2 e}{\partial^2 \lambda_1} \\ R_{1122} &= \frac{\partial T_1}{\partial \lambda_2} = \rho^{(0)}\frac{\partial^2 e}{\partial \lambda_1 \partial \lambda_2} \ \text{etc.} \end{aligned} \tag{3.2.10}$$

3.2.3
Superposition of pure shear

In order to compute the shear stiffness, we consider a pure shear deformation, $\mathbf{C} \rightarrow \bar{\mathbf{C}}$ (Figure 3.2.2)

$$\begin{aligned} \bar{x}_1 &= \tfrac{1}{2}\Delta\gamma x_2 \\ \bar{x}_2 &= \tfrac{1}{2}\Delta\gamma x_1 \\ \bar{x}_3 &= x_3 \end{aligned} \tag{3.2.11}$$

superimposed upon the finite rectilinear stretching 3.2.1, resulting in

$$\begin{aligned} \bar{x}_1 &= \ell_1^* \xi_1 + \tfrac{1}{2}\Delta\gamma \ell_2^* \xi_2 \\ \bar{x}_2 &= \tfrac{1}{2}\Delta\gamma \ell_1^* \xi_1 + \ell_2^* \xi_2 \\ \bar{x}_3 &= \ell_3^* \xi_3 \end{aligned} \tag{3.2.12}$$

The corresponding deformation gradient $\bar{F}_{ij} = (\partial \bar{x}_i / \partial \xi_j)$ is decomposed according to 2.1.25 into left stretching tensor and spin tensor $\bar{F}_{ij} = V_{ik} R_{kj}$ (Figure 3.2.3)

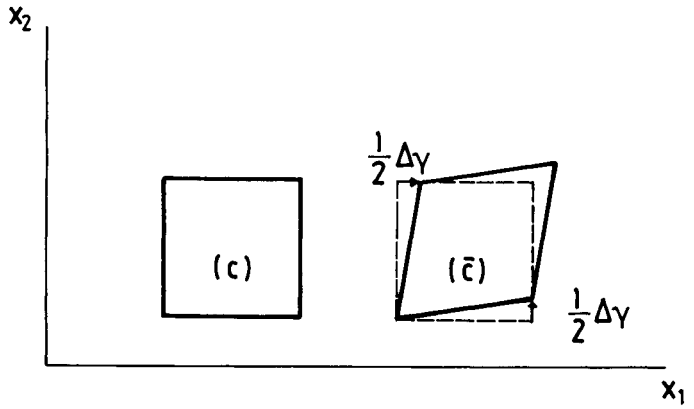

Figure 3.2.2 Pure shear $C \rightarrow \bar{C}$

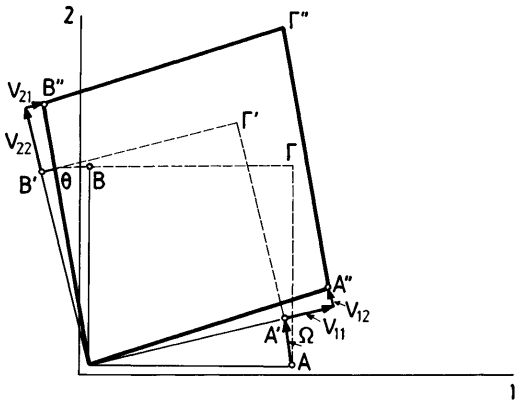

Figure 3.2.3 Polar decomposition of $\bar{F}_{ij}(C^{(0)} \rightarrow \bar{C})$

$$\{\bar{F}_{ij}\} = \begin{bmatrix} \ell_1^* & \frac{1}{2}\Delta\gamma\ell_2^* & 0 \\ \frac{1}{2}\Delta\gamma\ell_1^* & \ell_2^* & 0 \\ 0 & 0 & \ell_3^* \end{bmatrix} = \begin{bmatrix} V_{11} & V_{12} & 0 \\ V_{21} & V_{22} & 0 \\ 0 & 0 & V_{33} \end{bmatrix} \begin{bmatrix} \cos\Omega & -\sin\Omega & 0 \\ \sin\Omega & \cos\Omega & 0 \\ 0 & 0 & 1 \end{bmatrix} \tag{3.2.13}$$

resulting in

$$\begin{aligned} V_{11} &= \ell_1^* \cos\Omega - \tfrac{1}{2}\Delta\gamma \ell_2^* \sin\Omega \\ V_{22} &= \tfrac{1}{2}\Delta\gamma \ell_1^* \sin\Omega + \ell_2^* \cos\Omega \\ 2V_{12} &= \tfrac{1}{2}\Delta\gamma(\ell_1^* + \ell_2^*)\cos\Omega + (\ell_1^* - \ell_2^*)\sin\Omega \\ V_{33} &= \ell_3^* \end{aligned} \tag{3.2.14}$$

and

$$\tan\Omega = \frac{\ell_1^* - \ell_2^*}{\ell_1^* + \ell_2^*}(\tfrac{1}{2}\Delta\gamma) \tag{3.2.15}$$

Assuming that the superimposed shear strain is infinitesimal, $|\Delta\gamma| \ll 1$, then from equations 3.2.14 and 3.2.15 we obtain that

$$V_{11} \approx \ell_1^*;\ V_{22} \approx \ell_2^* \tag{3.2.16}$$

$$V_{12} \approx \frac{\ell_1^{*2} + \ell_2^{*2}}{\ell_1^* + \ell_2^*}(\tfrac{1}{2}\Delta\gamma) \tag{3.2.17}$$

$$\Omega \approx \frac{\ell_1^* - \ell_2^*}{\ell_1^* + \ell_2^*}(\tfrac{1}{2}\Delta\gamma) \tag{3.2.18}$$

Accordingly the principal strains are

$$V_{\mathrm{I,II}} = V_{11}\cos^2\Theta_v + V_{22}\sin^2\Theta_v + V_{12}\sin^2\Theta_v \tag{3.2.19}$$

where Θ_v is the orientation angle of the (I)-principal direction of the left stretching tensor V_{ij},

$$\tan^2\Theta_v = \frac{2V_{12}}{V_{11} - V_{22}} \tag{3.2.20}$$

resulting in

$$V_{\mathrm{I}} \approx V_{11} \approx \ell_1^*;\ V_{\mathrm{II}} \approx V_{22} \approx \ell_2^* \tag{3.2.21}$$

and

$$\Theta_v = \frac{\ell_1^{*2} + \ell_2^{*2}}{\ell_1^{*2} - \ell_2^{*2}}(\tfrac{1}{2}\Delta\gamma) \tag{3.2.22}$$

Assuming that the material is isotropic under finite strain, then the constitutive equations 3.2.9 hold for the principal directions, as indicated in Figure 3.2.4,

$$T_{\mathrm{I}} \approx T_{11};\ T_{\mathrm{II}} \approx T_{22} \tag{3.2.23}$$

We may resolve these principal stresses which are oriented along the principal directions (I) and (II) into x_1 and x_2 components. Since $T_{12} = 0$,

we find that

$$\Delta T_{12} = \frac{\ell_1^{*2} + \ell_2^{*2}}{\ell_1^{*2} - \ell_2^{*2}}(T_{11} - T_{22})(\tfrac{1}{2}\Delta\gamma) \tag{3.2.24}$$

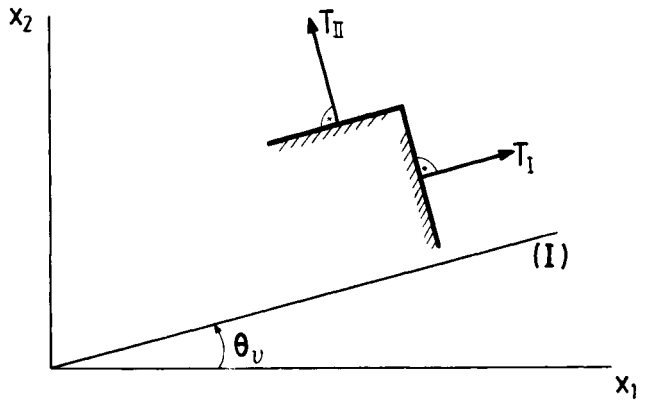

Figure 3.2.4 Principal stresses in

According to equation 3.1.45, the Jaumann increment of the Kirchhoff shear stress is

$$\mathring{\Delta}T_{12} = \Delta T_{12} - (T_{11} - T_{22})\Delta\omega \tag{3.2.25}$$

We observe from equation 3.2.11 that for the considered infinitesimal transition $\mathbf{C} \rightarrow \bar{\mathbf{C}}$, the infinitesimal rigid body rotation $\Delta\omega = 0$, and thus the Kirchhoff stress increment and its Jaumann increment coincide, and

$$\mathring{\Delta}T_{12} = R_{1212}\Delta\varepsilon_{12} + R_{1221}\Delta\varepsilon_{21} \tag{3.2.26}$$

where

$$R_{1212} = R_{1221} = \tfrac{1}{2}(T_{11} - T_{22})\frac{\ell_1^{*2} + \ell_2^{*2}}{\ell_1^{*2} - \ell_2^{*2}} \tag{3.2.27}$$

and the $T_{i(i)}$ are given by equations 3.2.8 (see also Hill, 1978). Equations 3.2.26 and 3.2.27 can be readily generalized by considering simple shears in the (x_1, x_3)-plane andthe (x_2, x_3)-plane as well.

3.2.4
Hypoelastic constitutive equations

According to the above derivations, the Jaumann increment of the Kirchhoff stress is found to depend linearly on the incremental strain

$$\mathring{\Delta}T_{ij} = R_{ijkl}\Delta\varepsilon_{kl} \tag{3.2.28}$$

where the components of the stiffness tensor are given according to equations 3.2.10 and 3.2.27 in terms of the strain energy function and the principal stretches, and obey the major symmetry conditions

$$R_{ijkl} = R_{klij} = R_{jikl} = R_{ijlk} \tag{3.2.29}$$

We remark that due to equation 3.1.43 the Cauchy/Jaumann stress increment is given by a constitutive equation of the form

$$\mathring{\Delta}\sigma_{ij} = C^e_{ijkl}\Delta\varepsilon_{kl} \tag{3.2.30}$$

where the stiifness tensor

$$C^e_{ijkl} = J^{-1}R_{ijkl} - \sigma_{ij}\delta_{kl} \tag{3.2.31}$$

does only obey minor symmetry conditions

$$C^e_{ijkl} = C^e_{jikl} = C^e_{ijlk} \tag{3.2.32}$$

This means that for large strain analysis, hypoelasticity laws should be expressed in terms of the Kirchhoff/Jaumann stress increment stress rather than in terms of the Cauchy/Jaumann one.

As an example, we refer here to a simple constitutive equation for compressible, isotropic elastic materials in finite deformations, which was discussed by Tvergaard *et al.* (1981) in connection with localization analyses. In this example, and for rectilinear deformations along the common principal directions of Kirchhoff stress and logarithmic strain, the following constitutive relations are established

$$T_i = 2G_s\left[\lambda_i + \frac{\nu_s}{1-2\nu_s}(\lambda_1 + \lambda_2 + \lambda_3)\right] \tag{3.2.33}$$

where ν_s and G_s are the 'effective' Poisson's ratio and shear modulus, respectively, which evolve during the deformation

$$\nu_s = \tfrac{1}{2} + (\nu - \tfrac{1}{2})E_s/E;\ G_s = E_s/(2(1+\nu_s)) \tag{3.2.34}$$

E is Young's modulus, ν is Poisson's ratio and E_s is the ratio of stress and strain for uniaxial Kirchhoff stress versus logarithmic strain curve. For large strains, the considered material becomes gradually less compressible$(\nu_s \to \frac{1}{2})$ since the secant Young's modulus diminishes $(E_s \to 0)$. For this model we obtain the following normal components of the stiffness tensor

$$R_{ijkl} = G_s\left[\delta_{ik}\delta_{jl} + \delta_{il}\delta_{jk} + \frac{2\nu_s}{1-2\nu_s}\delta_{ij}\delta_{kl} - \frac{E_s/E_t - 1}{E_s/E_t - (1-2\nu_s)/3}\frac{s^K_{ij}s^K_{kl}}{T^2_K}\right] \tag{3.2.35}$$

for $i = j$ and $k = l$ (no sum). In this expression

$$s^K_{ij} = T_{ij} - T_{kk}\delta_{ij}/3 \tag{3.2.36}$$

is the Kirchhoff stress deviator, E_t is the tangent Young's modulus, i.e. the slope of the uniaxial Kirchhoff stress/logarithmic strain curve, and

$$T_K = (s^K_{ij}s^K_{ij}/2)^{\frac{1}{2}} \tag{3.2.37}$$

is the effective Kirchhoff-Mises stress. We observe that the normalized deviators of the Kirchhoff and Cauchy stresses coincide,

$$m_{ij} = \frac{s^{K}_{ij}}{\sqrt{(2T_K)}} = \frac{s_{ij}}{\sqrt{(2T)}} \tag{3.2.38}$$

where s_{ij} and T are the corresponding Cauchy stress measures

$$s_{ij} = \sigma_{ij} - \sigma_{kk}\delta_{ij}/3 \tag{3.2.39}$$

$$T = (s_{ij}s_{ij}/2)^{\frac{1}{2}} \tag{3.2.40}$$

On the other hand, from equations 3.2.27 and 3.2.33 we obtain the following expressions for the shear moduli

$$R_{1212} = R_{2121} = R_{1221} = R_{2112} = G^* = G_s\frac{\lambda_1 - \lambda_2}{\tanh(\lambda_1 - \lambda_2)} \text{ etc.} \tag{3.2.41}$$

We observe that if the underlying uniaxial stress-strain curve is a straight line

$$E_s = E_t = E;\ v_s = v;\ G_s = G = E/(2(1 + v)) \tag{3.2.42}$$

then the normal stiffnesses

$$R_{ijkl} = G\left[\delta_{ik}\delta_{jl} + \delta_{il}\delta_{jk} + \frac{2v}{1 - 2v}\delta_{ij}\delta_{kl}\right] \quad \text{for} \quad i = j,\ k = l \text{ (no sum)} \tag{3.2.43}$$

An elastic material which is isotropic under finite strain develops a strain-induced anisotropy for shearing in axes parallel to the initial stretch (Biot, 1965). If in addition we assume that the normal stiifness of the Kirchhoff/Jaumann stress increments are constant, equations 3.2.42, then both the normal and shear stiffnesses for the relative Kirchhoff/Jaumann stress increment evolve as follows

$$\mathring{\Delta}T^t_{ij} = R^t_{ijkl}\Delta\varepsilon_{kl} \tag{3.2.44}$$

where

$$R^t_{ijkl} = G^t\left[\delta_{ik}\delta_{jl} + \delta_{il}\delta_{jk} + \frac{2v}{1 - 2v}\delta_{ij}\delta_{kl}\right] \quad \text{for} \quad i = j,\ k = l \text{ (no sum)} \tag{3.2.45}$$

$$R^t_{1212} = R^t_{2121} = R^t_{1221} = R^t_{2112} = G_* = G^t\frac{\lambda_1 - \lambda_2}{\tanh(\lambda_1 - \lambda_2)} \text{ etc.} \tag{3.2.46}$$

$$G^t = G/J;\ J = \exp(\lambda_1 + \lambda_2 + \lambda_3) \tag{3.2.47}$$

It should be mentioned that in several publications we find, instead of the above anisotropic hypoelastic constitutive equations 3.2.44 to 3.2.47, isotropic ones, which relate the relative Kirchhoff/Jaumann stress to the infinitesimal strain,

$$R^{t}_{ijkl} = G\left[\delta_{ik}\delta_{jl} + \delta_{il}\delta_{jk}\frac{2\nu}{1-2\nu}\delta_{ij}\delta_{kl}\right] \tag{3.2.48}$$

with G and ν constant.

The constitutive equation 3.2.44 for the Jaumann increment of the relative Kirchhoff stress with a stiffness tensor given by Hooke's law 3.2.48 is not truly elastic, i.e. hyperelastic; cf. the remark below, and the papers by Hutchinson (1973) and McMeeking and Rice (1975). This is generally not considered as a major deficiency of such a theory, and in large strain analyses equation 3.2.44 with equation 3.2.48 are used; cf. Dorris and Nemat-Nasser (1980). It should be noticed also that Christoffersen (1991) discussed a simple class of hyperelastic relations with isotropic rate forms. These rate equations do not involve the Jaumann derivative of the Kirchhoff stress but other suitably chosen objective stress rates.

Example: oedometric initial strain. Let us consider the example of oedometric compression

$$\lambda_2 = \lambda;\ \lambda_1 = \lambda_3 = 0 \tag{3.2.49}$$

We assume that the oedometric stress-strain curve is described by a power law for the Kirchhoff stress (cf. equation 2.1.44)

$$T_{\mathrm{K}} = \begin{cases} T_{\mathrm{K}0}(\Gamma/\Gamma_0) = G_0\Gamma & \text{for } \Gamma \leqslant \Gamma_0 \\ T_{\mathrm{K}0}(\Gamma/\Gamma_0)^N & \text{for } \Gamma \geqslant \Gamma_0 \end{cases} \tag{3.2.50}$$

where T_{K} is given by equation 3.2.37 and Γ is the corresponding measure for the shearing strain intensity, $\Gamma = \{2[(\lambda'_1)^2 + (\lambda'_2)^2 + (\lambda'_3)^2]\}^{\frac{1}{2}}$, where λ'_i are the principal deviatoric logarithmic strains. For oedometric compressions,

$$\Gamma = 2\lambda/\sqrt{3} \tag{3.2.51}$$

Moreover, we define the secant and tangent moduli by

$$G_{\mathrm{s}} = T_{\mathrm{K}}/\Gamma = G_0(\Gamma/\Gamma_0)^{N-1};\ G_{\mathrm{t}} = \mathrm{d}T_{\mathrm{K}}/\mathrm{d}\Gamma = NG_{\mathrm{s}} \tag{3.2.52}$$

For the considered initial state of strain we define plane-strain continuations in the (x_1, x_2)-plane. The incremental stress-strain relations for the *Kirchhoff stress* and for the constitutive law (3.2.33) of Tvergaard *et al.* (1981) are given by equation 3.2.28 with the following stiffness tensor

$$\begin{aligned} &\text{(i)} && R_{1111} = 3K_{\mathrm{s}} - 2\lambda_{\mathrm{s}} - G_{\mathrm{s}}(1-N)/3 \\ &\text{(ii)} && R_{2222} = 3K_{\mathrm{s}} - 2\lambda_{\mathrm{s}} - 4G_{\mathrm{s}}(1-N)/3 \\ &\text{(iii)} && R_{1122} = R_{2211} = \lambda_{\mathrm{s}} + 2G_{\mathrm{s}}(1-N)/3 \\ &\text{(iv)} && R_{1212} = R_{2121} = 2G_{\mathrm{s}}q;\ q = \lambda\coth(\lambda) \end{aligned} \tag{3.2.53}$$

In the above expressions K_{s} and λ_{s} are the secant compression modulus and Lamé moduli, respectively. Notice that the quantity q is a measure of strain-induced anisotropy. Its evolution with λ is depicted in Figure 3.2.5.

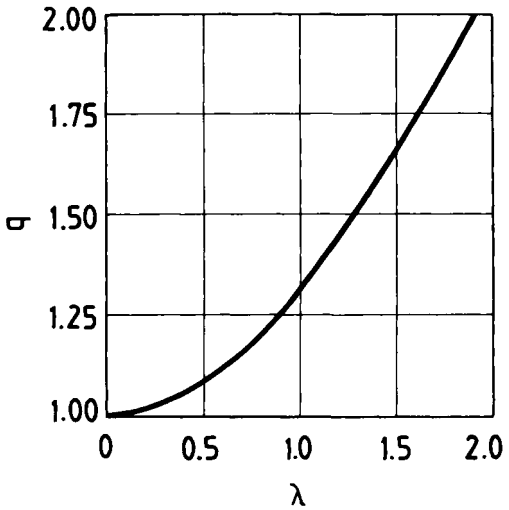

Figure 3.2.5 Large strain-induced anisotropy, equation 3.2.53.iv.

Remark on hyperelasticity, elasticity and hypoelasticity. We remark here on a few definitions and basic properties of elastic, hyper- and hypoelastic constitutive equations. A material is called elastic (a) if it possesses only one ground state $C^{(0)}$, i.e. a state that is undeformed and is also stress free, and (b) if the stress is a function of the deformation gradient. An elastic material is called isotropic if the stress is an isotropic tensor function of the deformation. This assumption results in a general constitutive equation of the form

$$T_{ij} = c_0\delta_{ij} + c_1 B_{ij} + c_2 B_{ik}B_{kj} \tag{El}$$

where the c_α $(\alpha = 0, 1, 2)$ are isotropic scalar functions of the invariants of B_{ij}, say the left Cauchy-Green tensor. B_{ij} in this equation can be replaced by any other convenient Eulerian deformation measure, for example the left Hencky (logarithmic) strain tensor.

More restrictive is the definition of the hyperelastic materials. In hyperelasticity, the Helmholtz free energy of the material is assumed to be a function of the corresponding measure of deformation, e.g.

$$\mathrm{f} = \mathrm{f}(B_{ij})$$

In hyperelastic materials the local entropy production at constant temperature is zero, and thus from equation 2.3.43 we obtain that the specific stress power is a Pfaffian form, since with $D_{ij} = \dot{B}_{ij}$ and $T_{ij} = J\sigma_{ij}$ from

$$(\rho^{(0)}/\rho)P = (\rho^{(0)}/\rho)\sigma_{ij}D_{ij} = T_{ij}\dot{B}_{ij} = \rho^{(0)}\dot{\mathrm{f}}$$

we obtain that

$$\rho^{-1}P = \dot{f} = \frac{\partial f}{\partial B_{ij}}\dot{B}_{ij}$$

Accordingly in hyperelasticity the Helmholtz free energy is the potential function of the Kirchhoff stress

$$T_{ij} = \rho^{(0)}\frac{\partial f}{\partial B_{ij}} \tag{Hpr}$$

(Hpr) is a slight generalization of equation 3.2.8. Using the representation theorem of isotropic tensor functions and the Cayley-Hamilton theorem, the form (El) for isotropic elastic materials follows from the form (Hpr), for hyperelastic materials. The converse is not generally true. If the material is hyperelastic, along a closed strain path, the total specific work done by the stresses is zero

$$\oint \rho^{-1}\sigma_{ij}\,dB_{ji} = \oint (\partial f/\partial B_{ij})dB_{ij} = 0$$

This is not generally true for elastic materials. However in closed stress paths in stress space both elastic materials and hyperelastic materials are characterized by zero residual strain.

We observe that both the constitutive equations of isotropic elastic materials (El) and for isotropic hyperelastic materials (Hpr) lead through formal rigid-body time differentiation to equations of the rate form

$$\mathring{T}_{ij} = R_{ijkl}D_{kl} \tag{HpoK}$$

or

$$\mathring{T}^{t}_{ij} = R^{t}_{ijkl}D_{kl} \tag{HpoKr}$$

$$\mathring{\sigma}_{ij} = L_{ijkl}D_{kl} \tag{Hpo}$$

Truesdell and Noll (1965) define a class of materials, which they call hypoelastic materials, and obey a rate constitutive equation like the ones above which are linear in D_{ij}, with the additional restriction that the corresponding fourth-order constitutive tensor is an isotropic tensor function of the Eulerian stress.

With equations 3.2.9 and 3.2.26 we have demonstrated a simple example, where hypoelasticity equations are derived from hyperelasticity. In general, however, hypoelastic constitutive equations are neither integrable to a finite form (El) nor connected to a free energy function through a constitutive equation of the form of (Hpr). Thus, hypoelastic equations will lead in general to residual strain, if integrated along closed stress paths and to violations of the second law of thermodynamics if integrated along closed strain paths (see Loret, 1985).

Finally, we want to refer to Kolymbas' (1978) generalizations of hypoelasticity equations in order to describe the behavior of granular materials. Kolymbas defines a class of

materials which he calls hypoplastic and which obey rate-type constitutive equations of the form

$$\mathring{\sigma}_{ij} = H_{ij}(\sigma_{kl}, D_{mn}) \tag{Hpl}$$

where the tensorial function H_{ij} is non-linear with respect to D_{ij}. If H_{ij} is linear in D_{ij}, then (Hpl) reduces to (Hpo). For example, starting from the representation theorem of isotropic tensor-valued functions of two symmetric tensorial arguments (Wang, 1970), Kolymbas' (1991) hypoplasticity of sand is a particular choice of (Hpl) which, in symbolic representation, reads as follows

$$\mathring{\boldsymbol{\sigma}} = c_1(\boldsymbol{\sigma}\mathbf{D} + \mathbf{D}\boldsymbol{\sigma}) + c_2\,\mathrm{tr}(\boldsymbol{\sigma}\mathbf{D})\mathbf{1} + \{c_3\boldsymbol{\sigma} + c_4\boldsymbol{\sigma}^2/(\mathrm{tr}\boldsymbol{\sigma})\}(\mathrm{tr}\mathbf{D}^2)^{\frac{1}{2}}$$

where $c_\alpha(\alpha=1,\ldots,4)$ are material constants, determined from the experiment.

3.3 Equilibrium bifurcation

3.3.1 The principle of virtual work

For any change of the volume forces and/or of the boundary conditions of a solid body B in its current configuration C body B deforms and assumes a new configuration $\bar{\mathbf{C}}$. Let $\delta\bar{u}_i$ be a virtual displacement of B in $\bar{\mathbf{C}}$ and let C* be the resulting virtual configuration (Figure 3.3.1). The virtual displacement field, $\delta\bar{u}_i$, must be piecewise differentiable and it must obey boundary constraints which will be specified below. The principle of virtual work in $\bar{\mathbf{C}}$ is expressed by an equation of the form

$$\delta\bar{W}^{(i)} = \delta\bar{W}^{(e)} \tag{3.3.1}$$

where $\delta\bar{W}^{(i)}$ and $\delta\bar{W}^{(e)}$ denote the virtual work done by the internal forces and external forces respectively. Let

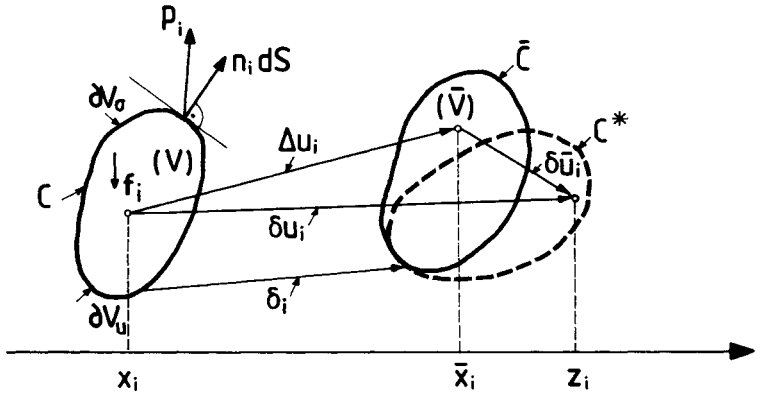

Figure 3.3.1 The definition of virtual configuration.

$$\delta \bar{W}^{(i)} = \int_{\bar{V}} \delta \bar{w}^{(i)} \, \mathrm{d}\bar{V} \tag{3.3.2}$$

where in a Boltzmann first-grade continuum the virtual work of the internal forces depends only on the Cauchy stress in $\bar{\mathbf{C}}$, and

$$\delta \bar{w}^{(i)} = \bar{\sigma}_{ij} \delta \bar{\varepsilon}_{ij} \tag{3.3.3}$$

with

$$2\delta \bar{\varepsilon}_{ij} = \frac{\partial \delta \bar{u}_i}{\partial \bar{x}_j} + \frac{\partial \delta \bar{u}_j}{\partial \bar{x}_i} \tag{3.3.4}$$

The virtual work of the external forces

$$\delta \bar{W}^{(e)} = \int_{\partial \bar{V}} \bar{p}_i \delta \bar{u}_i \, \mathrm{d}\bar{S} + \int_{\bar{V}} \bar{f}_i \delta \bar{u}_i \, \mathrm{d}\bar{V} \tag{3.3.5}$$

In these equations $\bar{p}_i$ are the boundary tractions acting on the boundary $\partial \bar{V}$ and $\bar{f}_i$ the body forces acting in $\bar{V}$. From the above virtual work equation 3.3.1 and Gauss' theorem, equilibrium conditions in $\bar{\mathbf{C}}$ can be derived, i.e. on $\partial \bar{V}$

$$\bar{n}_k \bar{\sigma}_{ki} = \bar{p}_i \tag{3.3.6}$$

and in $\bar{V}$

$$\frac{\partial \bar{\sigma}_{ki}}{\partial \bar{x}_k} + f_i = 0 \tag{3.3.7}$$

With the definition 3.1.29 of the relative 1. P.-K. stress tensor, π_{ij}, the expression for the virtual work of internal forces, equation 3.3.2, becomes

$$\delta \bar{W}^{(i)} = \int_{\bar{V}} \bar{\sigma}_{ij} \partial_k \delta \bar{u}_i F^{t\,-1}_{kj} J^t \, \mathrm{d}V = \int_V \pi_{ik} \partial_k \delta \bar{u}_i \, \mathrm{d}V \tag{3.3.8}$$

By defining nominal surface tractions and volume forces

$$\pi_i \, \mathrm{d}S = \bar{p}_i \, \mathrm{d}\bar{S}; \; b_i \, \mathrm{d}V = \bar{f}_i \, \mathrm{d}\bar{V} \tag{3.3.9}$$

from the virtual work equation 3.3.1 and Gauss' theorem we derive equilibrium equations in terms of the nominal stress tensor, i.e. on ∂V

$$n_k \pi_{ik} = \pi_i \tag{3.3.10}$$

and in V

$$\partial_k \pi_{ik} + b_i = 0 \tag{3.3.11}$$

The change of the tractions on ∂V and of the volume forces in V is defined by referring these changes to surface and volume elements in C

$$\pi_i \, \mathrm{d}S = (p_i + \Delta \pi_i) \mathrm{d}S; \; b_i \, \mathrm{d}V = (f_i + \Delta b_i) \mathrm{d}V \tag{3.3.12}$$

By using the above decompositions and equation 3.1.32, equations 3.3.8 and 3.3.5 become

$$\delta \bar{W}^{(i)} = \int_V (\sigma_{ij} + \Delta\pi_{ij}) \partial_j \delta \bar{u}_i \, \mathrm{d}V \tag{3.3.13}$$

$$\delta \bar{W}^{(e)} = \int_{\partial V} (p_i + \Delta\pi_i) \delta \bar{u}_i \, \mathrm{d}S + \int_V (f_i + \Delta b_i) \delta \bar{u}_i \, \mathrm{d}V \tag{3.3.14}$$

We assume that p_i and f_i are in equilibrium with the Cauchy stress σ_{ij} in C, i.e. on ∂V

$$n_k \sigma_{ki} = p_i \tag{3.3.15}$$

and in V

$$\partial_k \sigma_{ki} + f_i = 0 \tag{3.3.16}$$

Then from the virtual work equation 3.3.1 and the expressions 3.3.13 and 3.3.14 we obtain the following second-order virtual work equation,

$$\delta^2 W^{(i)} = \delta^2 W^{(e)} \tag{3.3.17}$$

where

$$\delta^2 W^{(i)} = \int_V \Delta\pi_{ij} \partial_j \delta \bar{u}_i \, \mathrm{d}V \tag{3.3.18}$$

$$\delta^2 W^{(e)} = \int_{\partial V} \Delta\pi_i \delta \bar{u}_i \, \mathrm{d}S + \int_V \Delta b_i \delta \bar{u}_i \, \mathrm{d}V \tag{3.3.19}$$

For deriving a useful form of the principle of virtual work for continued equilibrium, equation 3.3.17, we introduce the following notations: Let z_i be the coordinates of a material point X in the virtual configuration C*

$$z_i = \bar{x}_i + \delta \bar{u}_i \tag{3.3.20}$$

A virtual displacement field, δ_{ui}, is then introduced, which gives the virtual displacement of C* with reference to C

$$\delta u_i = z_i' - x_i = \delta \bar{u}_i + \Delta u_i \tag{3.3.21}$$

and within a linearized theory

$$\delta^2 W^{(i)} = \int_V \Delta\pi_{ij} (\partial_j \delta u_i - \partial_j \Delta u_i) \mathrm{d}V \approx \int_V \Delta\pi_{ij} \partial_j \delta u_i \, \mathrm{d}V \tag{3.3.22}$$

$$\begin{aligned}\delta^2 W^{(e)} &= \int_{\partial V} \Delta\pi_i(\delta u_i - \Delta u_i)\mathrm{d}S + \int_V \Delta b_i(\delta u_i - \Delta u_i)\mathrm{d}V \\ &\approx \int_{\partial V} \Delta\pi_i \delta u_i \,\mathrm{d}S + \int_V \Delta b_i \delta u_i \,\mathrm{d}V\end{aligned} \tag{3.3.23}$$

With these derivations, the principle of virtual work for continued equilibrium, equation 3.2.17, finally becomes (Vardoulakis, 1975)

$$\int_V \Delta\pi_{ij}\partial_j \delta u_i \,\mathrm{d}V = \int_V \Delta b_i \delta u_i \,\mathrm{d}V + \int_{\partial V} \Delta\pi_i \delta u_i \,\mathrm{d}S \tag{3.3.24}$$

For the evaluation of the above integrals, the virtual displacement field is imposed to the additional constraint that it obeys the kinematic constraints on that part ∂V_u of the boundary ∂V on which displacements are prescribed, i.e. on ∂V_u

$$\delta u_i = \Delta u_i \Big|_{x \in \partial V_u} = \delta_i \tag{3.3.25}$$

which *in* turn means that the original virtual displacement $\delta\bar{u}_i$ of $\bar{\mathbf{C}}$ must vanish on ∂V_u, sequations 3.3.21 and 3.3.25 we obtain

$$\delta\bar{u}_i = 0 \tag{3.3.26}$$

for x on ∂V_u.

From the complete variation of the virtual displacement field the local conditions for continued equilibrium can be derived, namely on ∂V_σ

$$n_k \Delta\pi_{ik} = \Delta\pi_i \tag{3.3.27}$$

and in V

$$\partial_k \Delta\pi_{ik} + \Delta b_i = 0 \tag{3.3.28}$$

Conditions for continued equilibrium in plane-strain deformations. As an example let us assume that $\partial_3 \equiv 0$, $\Delta b_i = 0$,, and that the initial stress σ_{ij} in C is constant. In the coordinate system of principal axes of initial stress σ_{ij} in the plane of the deformation, the conditions for continued equilibrium 3.3.28 can be written either in terms of the Cauchy/Jaumann stress increment

$$\begin{aligned}\partial_1 \mathring{\Delta}\sigma_{11} + \partial_2 \mathring{\Delta}\sigma_{12} + (\sigma_1 - \sigma_2)\partial_2 \Delta\omega = 0 \\ \partial_1 \mathring{\Delta}\sigma_{21} + \partial_2 \mathring{\Delta}\sigma_{22} + (\sigma_1 - \sigma_2)\partial_1 \Delta\omega = 0\end{aligned}$$

or of the relative Kirchhoff/Jaumann stress increment

$$\begin{aligned}\partial_1 \mathring{\Delta}T^t_{11} + \partial_2 \mathring{\Delta}T^t_{12} + (\sigma_1 - \sigma_2)\partial_2 \Delta\omega + \sigma_1 \partial_1 \Delta\varepsilon = 0 \\ \partial_1 \mathring{\Delta}T^t_{21} + \partial_2 \mathring{\Delta}T^t_{22} + (\sigma_1 - \sigma_2)\partial_1 \Delta\omega + \sigma_2 \partial_2 \Delta\varepsilon = 0\end{aligned}$$

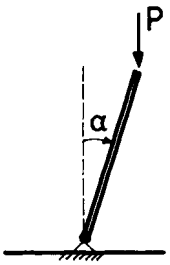

Figure 3.3.2 Trivial rotational instability of a rod in compression.

where $\Delta\omega$ and $\Delta\varepsilon$ are the only non-vanishing components of the infinitesimal rotation tensor and the infinitesimal volumetric strain, respectively

$$\Delta\omega = \tfrac{1}{2}(\partial_1 \Delta u_2 - \partial_2 \Delta u_1);\ \Delta\varepsilon = \partial_1 \Delta u_1 + \partial_2 \Delta u_2$$

We remark that: (a) For isochoric deformations $\Delta\varepsilon = 0$ e.g. for incompressible materials) the two formulations are identical; (b) for in-plane isotropic states of initial stress $\sigma_1 = \sigma_2$ the conditions for continued equilibrium in terms of the Cauchy/Jaumann stress increment do not introduce the effect of initial stress; in this case the second formulation in terms of the relative Kirchhoff/Jaumann stress increment is preferable.

3.3.2
The zero moment condition

In the virtual work equation 3.3.24, the virtual displacement field δu_i must be consistent with the displacement boundary conditions on ∂V_u, equation 3.3.25, but otherwise arbitrary. Beatty (1966), in his treatise on elastic stability, indicated that a general theory of uniqueness and stability can yield dubious results when the virtual displacements are considered entirely arbitrary. For example, a rod under constant compressive load is unstable for any load as soon as rigid body rotations of the rod in a plane containing its axis are allowed (Figure 3.3.2) (cf. Truesdell and Noll1965, Sect. 68 *bis*). In this section we briefly adapt into the present framework Beatty's main results, which in turn derive from global moment equilibrium.

In analogy to equations 3.3.13 and 3.3.14 we require that the resultant moment of all external forces acting on the considered body in the virtual configuration C* is zero

$$M_i = \int_{\partial V} e_{ijk} z_j \bar{p}_k \, \mathrm{d}\bar{S} + \int_V e_{ijk} z_j \bar{f}_k \, \mathrm{d}\bar{V} = 0 \tag{3.3.29}$$

or more explicitly

$$M_i = \int_{\partial V} e_{ijk}(x_j + \Delta u_j + \delta\bar{u}_j)(\sigma_{lk} + \Delta\pi_{lk})n_l \,\mathrm{d}S + \int_V e_{ijk}(x_j + \Delta u_j + \delta\bar{u}_j)(f_k + \Delta b_k)\,\mathrm{d}V = 0 \tag{3.3.30}$$

We observe that

$$\begin{aligned} I_2 &= \int_{\partial V} e_{ijk}\Delta u_j(\sigma_{kl} + \Delta\pi_{kl})n_l \,\mathrm{d}S + \int_V e_{ijk}\Delta u_j(f_k + \Delta b_k)\mathrm{d}V \\ &\approx \int_{\partial V} e_{ijk}\Delta u_j\sigma_{kl}n_l \,\mathrm{d}S + \int_V e_{ijk}\Delta u_j f_k \,\mathrm{d}V \\ &= \int_V e_{ijk}\partial_l\Delta u_j\sigma_{kl}\,\mathrm{d}V \end{aligned}$$

and that due to equation 3.1.33

$$I_1 + I_2 = \int e_{ijk}(\Delta\pi_{kj} + \partial_l\Delta u_j\sigma_{kl})\mathrm{d}V = \int e_{ijk}(\Delta\sigma_{kj} + \sigma_{kj}\partial_l\Delta u_l)\mathrm{d}V = 0$$

With these observations, the zero moment condition 3.3.30 becomes

$$\begin{aligned} M_i &= \int_{\partial V} e_{ijk}\delta\bar{u}_j(\sigma_{kl} + \Delta\pi_{kl})n_l \,\mathrm{d}S + \int_V e_{ijk}\delta\bar{u}_j(f_k + \Delta b_k)\mathrm{d}V \\ &= \int_V e_{ijk}\partial_l\delta\bar{u}_j(\sigma_{kl} + \Delta\pi_{kl})\mathrm{d}V = 0 \end{aligned} \tag{3.3.31}$$

Above zero moment condition for the virtual displacement field, $\delta\bar{u}_i$, can be written in the following alternative forms (Beatty, 1966):

$$M_i = \int_V e_{ijk}\partial_l\delta\bar{u}_j\pi_{kl}\,\mathrm{d}V = 0 \tag{3.3.31a}$$

or

$$M_i = \int_V e_{ijk}\frac{\partial\delta\bar{u}_j}{\partial\bar{x}_m}\bar{\sigma}_{im}\,\mathrm{d}\bar{V} = 0 \tag{3.3.31b}$$

The above conditions are not very useful for deriving restrictions for the virtual displacement field. Due to equation 3.3.21, however, we may only consider the leading term of condition 3.3.3 la

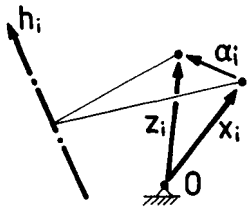

Figure 3.3.3 The definition of virtual rigid rotation.

$$M_i = \int e_{ijk}\partial_l \delta u_j \sigma_{kl}\,\mathrm{d}V + 0(|\Delta u_k|, |\Delta \pi_{k1}|) = 0 \tag{3.3.32}$$

We consider now a virtual displacement field

$$\delta u_i = \Omega_{ij} x_j \tag{3.3.33}$$

where Ω_{ij} is a uniform finite rigid rotation tensor, describing a rotation of an angle α ($0 \le \alpha \le \pi$) about a fixed-in-space axis whose unit vector is h_i (Figure 3.3.3), i.e.

$$\Omega_{ij} = e_{ijk} h_k \sin\alpha + (1 - \cos\alpha) h_{ij} \tag{3.3.34}$$

$$h_{ij} = h_i h_j - \delta_{ij} \tag{3.3.35}$$

With the notation

$$a_m = h_m \sin\alpha \tag{3.3.36}$$

$$S_{ij} = \int_V \sigma_{ij}\,\mathrm{d}V \tag{3.3.37}$$

the leading term of the zero moment condition becomes

$$\begin{aligned} M_i &= a_m e_{ijk} e_{imp} S_{jp} = a_m(\delta_{jm}\delta_{kp} - \delta_{km}\delta_{jp}) S_{jp} \\ &= a_j(S_{jk} - S_{pp}\delta_{jk}) = 0 \end{aligned} \tag{3.3.38}$$

For non-trivial solutions for a virtual rigid rotation, equation 3.3.33, a_i from equation 3. 3.38 must be non-zero, i.e. the volume average stress S_{ij} must satisfy the condition

$$\det(S_{ij} - S_{kk}\delta_{ij}) = 0 \tag{3.3.39}$$

In particular ai is an arbitrary vector if $S_{ij} = 0$. This is true for the stress-free state and for cases when the volume-average stress vanishes (for example, in any problem where body forces and surface tractions vanish). If on the other hand, the system of loads acting on the considered body in C does not exhibit an axis of equilibrium, then condition 3.3.39 does not hold, and $a_i = 0$ follows from equation 3.3.39. This means that in general the zero moment condition 3.3.32 will prohibit rigid-body rotations.

3.3.3
Configuration-dependent loading

Let us consider a body B in a given configuration C of it. By using the notation introduced above, we remark first that the body force increment Δb_i will consist of a Jaumann part and geometric correction terms

$$\Delta b_i = \mathring{\Delta} b_i + \bar{\Delta} b_i;\ \bar{\Delta} b_i = f_i \partial_k \Delta u_k + f_k \Delta \omega_{ik} \tag{3.3.40}$$

Conservative body forces like self-weight do not change, and

$$\Delta b_i = 0 \tag{3.3.41}$$

For $f_i = 0$ and by applying d'Alembert's principle, inertial body forces are given in terms of the acceleration and the density ρ of the solid in C

$$\Delta b_i = -\rho \partial_{tt} \Delta u_i \tag{3.3.42}$$

In order to properly define the linear bifurcation problem we must further clarify the type of contact forces which are acting on the boundary of the solid body B (Nemat-Nasser, 1972). Accordingly, a system of boundary tractions is called configuration-dependent if, for any point x_i on ∂V_σ, boundary tractions can be computed from assigned functions of the infinitesimal displacement and its gradient.

In the current configuration C, the surface element dS of the boundary ∂V_σ, with the exterior normal n_i is subjected to a surface load $\mathrm{d}t_i$

$$\mathrm{d}t_i = p_i \,\mathrm{d}S = p\alpha_i \,\mathrm{d}S \quad \text{with} \quad \alpha_i n_i > 0,\ \alpha_i \alpha_i = 1 \tag{3.3.43}$$

In this expression, α_i is the outwards pointing unit vector, in the direction of the applied boundary traction and p is the intensity of the boundary traction. According to the above definition p is positive as soon as the boundary traction is pointing outwards, i.e. $p>0$ if $p_i n_i>0$. Let m_i denote the unit vector tangent to the surface element dS and in the plane which contains n_i and α_i. According to the derivations of section 3.1 the vectors mi and n_i and the surface element transform according to the following rules:

$$\begin{aligned} \bar{m}_i &= m_i + \Delta m_i;\ \Delta m_i = m_l(\delta_{ik} - m_i m_k)\partial_l \Delta u_k \\ \bar{n}_i &= n_i + \Delta n_i;\ \Delta n_i = n_k(n_i n_l - \delta_{il})\partial_l \Delta u_k \\ \mathrm{d}\bar{S} &= \mathrm{d}S + \Delta \mathrm{d}S;\ \Delta \mathrm{d}S = (\Delta \varepsilon_{kk} - \Delta \varepsilon_{lm} n_l n_m)\mathrm{d}S \end{aligned} \tag{3.3.44}$$

Nominal surface transactions π_i in $\bar{\mathrm{C}}$ are defined through

$$\mathrm{d}\bar{t}_i = \bar{p}_i \,\mathrm{d}\bar{S} = \bar{p}\bar{\alpha}_i \,\mathrm{d}\bar{S} = \pi_i \,\mathrm{d}S \tag{3.3.45}$$

with

$$\pi_i = p_i + \Delta \pi_i \tag{3.3.46}$$

We remark that due to equation 3.3.27 $\Delta \pi_i$ is in equilibrium with the increment of the nominal $\Delta \pi_{ij}$.

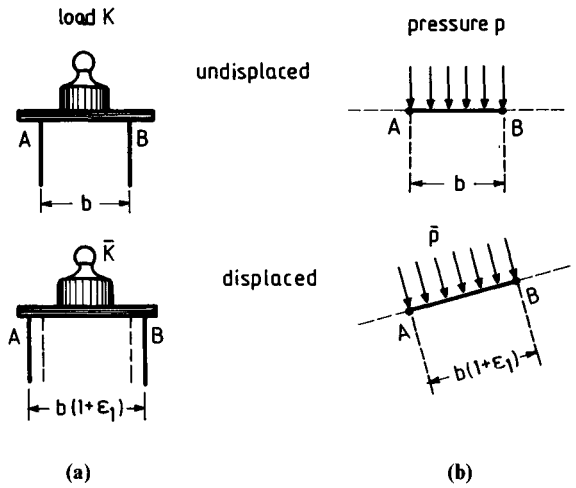

Figure 3.3.4 Examples of configuration-dependent loading: (a) dead loads; (b) hydrostatic pressure.

Dead loads. A system of boundary loads is called a system of dead loads if these loads keep their magnitude and orientation in space unchanged during the deformation, $\mathbf{C} \rightarrow \bar{\mathbf{C}}$ (Figure 3.3.4a):

$$\mathrm{d}t_i = \mathrm{d}\bar{t}_i \rightarrow p_i = \pi_i \rightarrow \Delta\pi_i = 0 \tag{3.3.47}$$

Follower loads. A system of boundary tractions is called a system of follower loads if these boundary loads follow the orientation of the surface upon which they are acting

$$m_i \alpha_i = \bar{m}_i \bar{\alpha}_i \tag{3.3.48}$$

If $\bar{p} = p$, then the system is said to constitute a system of follower tractions whereas if $\bar{p}\,\mathrm{d}\bar{S} = p\,\mathrm{d}S$ then a system of follower loads is considered. Of particular interest to applications are loads normal and tangential to the boundary. For normal loads α_i coincides with n_i whereas for tangential loads α_i is identical to m_i.

(i) Normal tractions of constant intensity $-p$. In this case, the boundary tractions act always perpendicular to the boundary of the solid and have a constant intensity $-p$ (Figure 3.3.4b). This case can be understood as the load produced on the boundary of a solid by hydrostatic fluid pressure:

$$\begin{aligned} \mathrm{d}t_i &= -pn_i\,\mathrm{d}S;\ \mathrm{d}\bar{t}_i = -p\bar{n}_i\,\mathrm{d}\bar{S} \\ \Delta\pi_i &= p(n_k\delta_{im} - n_i\delta_{km})\partial_m \Delta u_k \end{aligned} \tag{3.3.49}$$

(ii) Normal loads of constant magnitude: $p\,\mathrm{d}S = \bar{p}\,\mathrm{d}\bar{S}$

$$\begin{aligned} \mathrm{d}t_i &= -pn_i\,\mathrm{d}S;\ \mathrm{d}\bar{t}_i = -p\bar{n}_i\,\mathrm{d}S \\ \Delta\pi_i &= pn_k(n_i n_m - \delta_{im})\partial_m \Delta u_k \end{aligned} \tag{3.3.50}$$

(iii) Tangential tractions of constant intensity τ.

$$\begin{aligned} dt_i &= \tau m_i dS;\ d\bar{t}_i = \tau \bar{m}_i d\bar{S} \\ \Delta\pi_i &= \tau\{m_i(\delta_{kn} - m_k m_n - n_k n_i) + m_n \delta_{in}\}\partial_m \Delta u_k \end{aligned} \tag{3.3.51}$$

(iv) Tangential loads of constant magnitude: $\tau\, dS = \bar{\tau}\, dS$

$$\begin{aligned} dt_i &= \tau m_i dS;\ d\bar{t}_i = \tau \bar{m}_i dS \\ \Delta\pi_i &= \tau m_n(\delta_{ik} - m_i m_k)\partial_n \Delta u_k \end{aligned} \tag{3.3.52}$$

3.3.4
The linear bifurcation problem

Following the above considerations, we can formulate the general incremental boundary value problem and proceed to the formulation of the linear bifurcation problem: It is assumed that a solid body B has been already deformed to a given equilibrium configuration C. C is called the current configuration and is used as a reference configuration for subsequent continuations of the deformation of the body B. The boundary ∂V of B in C is divided into two complementary parts ∂V_σ and ∂V_u, suchthat on ∂V_σ tractions and on ∂V_u displacements are prescribed. In the volume V of B in C, volume forces are acting which could be understood as being for example gravitational or seepage forces. For any change of the boundary conditions and/or of the volume forces acting on B in C, there is a new configuration $\bar{\mathbf{C}}$ of it. Assuming that the kinematic constraints preclude any rigid-body motion of B, the incremental boundary value problem consists of determining the incremental displacement and stress fields which describe the transition $\mathbf{C} \rightarrow \bar{\mathbf{C}}$. Summarizing the theoretical results of the previous sections, we collect first the local equilibrium conditions which govern the considered incremental boundary value problem:

$$\partial_k \Delta\pi_{ik} + \Delta b_i = 0 \quad \text{in } V \tag{3.3.28}$$

with

$$n_k \Delta\pi_{ik} = \Delta\pi_i \quad \text{on } \partial V_\sigma \tag{3.3.27}$$

and

$$\Delta u_i = \delta_i \quad \text{on } \partial V_u \tag{3.3.25}$$

We may assume that boundary tractions and volume forces are either dead loads or configuration-dependent,

$$\Delta\pi_{ik} n_k = \pi_{ijk}\partial_k \Delta u_j;\ \Delta b_i = b_{ijk}\partial_j \Delta u_k \tag{3.3.53}$$

with known tensors π_{ijk} and b_{ijk} as demonstrated in the previous section. The 1. P.-K. stress increment is related to the infinitesimal displacement gradient

$$\Delta\pi_{ij} = C_{ijkl}\partial_l \Delta u_k \tag{3.3.54}$$

where according to equation 3.1.36 or 3.1.47 and for example equations 3.2.45 to 3.2.47, the stiffness tensor C_{ijkl} is expressed in terms of the initial stress and a constitutive tensor

$$C_{ijkl} = R^t_{ijkl} - \tfrac{1}{2}(\sigma_{ik}\delta_{jl} + \sigma_{kj}\delta_{il} + \sigma_{il}\delta_{jk} - \sigma_{jl}\delta_{ik}) \tag{3.3.55}$$

For investigating the uniqueness of solution for the considered incremental boundary-value problem, the displacement field is assumed to consist of two parts

$$\Delta u_i = \Delta \mathring{u}_i + \Delta \tilde{u}_i \tag{3.3.56}$$

such that the 'trivial' solution $\Delta \mathring{u}_i$, satisfies the kinematic constraints, i.e. on ∂V_u

$$\Delta \mathring{u}_i = \delta_i \tag{3.3.57}$$

and produces a stress field that satisfies equilibrium in V and on $\partial V\sigma$. Consequently, the 'non-trivial' solution, satisfies homogeneous boundary conditions on ∂V_u

$$\Delta \tilde{u}_i = 0 \tag{3.3.58}$$

Under these conditions the virtual work, equation 3.3.24, yields the weak formulation of the linear bifurcation problem

$$\int \{C_{ijkl}\partial_j \delta u_i \partial_l \Delta \tilde{u}_k + b_{ijk}\delta u_i \partial_j \Delta \tilde{u}_k\}\,\mathrm{d}V - \int \pi_{ikl}\delta u_i \partial_l \Delta \tilde{u}_k\,\mathrm{d}S = 0 \tag{3.3.59}$$

where δu_i is an admissible virtual displacement field. This means that δu_i is piecewise sufficiently differentiable, and satisfies (a) homogeneous displacement boundary condition on ∂V_u,

$$\delta u_i = 0 \tag{3.3.60}$$

(b) the zero-moment condition 3.3.32 in V. As already indicated in section 3.3.2, δu_i cannot be a rigid-body rotation.

A finite-element discretization of equations 3.3.59 with 3.3.58 would result in a homogeneous linear algebraic system of equations for the nodal displacements corresponding to the non-trivial field $\Delta \tilde{u}_i$, say of the form

$$[\mathbf{K}]\{\Delta \tilde{\mathbf{u}}\} = \{0\} \tag{3.3.61}$$

where **[K]** is the stiffness matrix and $\{\Delta\tilde{\mathbf{u}}\}$is the vector of nodal displacements corresponding to the non-trivial displacement field (Vardoulakis, 1975). In the case of a regular stiffness matrix

$$\det(\mathbf{K}) \neq 0 \rightarrow \{\Delta \tilde{\mathbf{u}}_i\} = \{0\} \tag{3.3.62}$$

and $\{\Delta\mathring{\mathbf{u}}\}$ is the unique solution of the problem. However, in the case of a singular system matrix

$$\det(\mathbf{K}) = 0 \tag{3.3.63}$$

at least a non-zero eigenvector field $\{\Delta\tilde{\mathbf{u}}\}$ exists. In this case, the displacement field corresponding to the infinitesimal transition $\mathbf{C} \rightarrow \bar{\mathbf{C}}$ is not uniquely determined and we

are dealing with an equilibrium bifurcation at state C, since more than one possible continuation of the considered deformation exist.

3.3.5
Uniqueness theorems under dead loading

Under dead loading the virtual work equation 3.3.24 becomes

$$\int_V \Delta\pi_{ij}\partial_j \delta u_i \, \mathrm{d}V = 0 \tag{3.3.64}$$

with $\delta u_i = \delta_i$ on ∂V_u. Let $\{\Delta\pi_{ij}, \Delta u_i\}^{(1)}$ and $\{\Delta\pi_{ij}, \Delta u_i\}^{(2)}$ be two solutions of the above incremental boundary value problem. Then their difference

$$\begin{aligned} \Delta\pi_{ij} &= \Delta\pi_{ij}^{(1)} - \Delta\pi_{ij}^{(2)} \\ \Delta u_i &= \Delta u_i^{(1)} - \Delta u_i^{(2)} \end{aligned} \tag{3.3.65}$$

satisfies equation 3.3.64 with the constraint 3.3.58, i.e.

$$\int_V \Delta\pi_{ij}\partial_j \Delta u_i \, \mathrm{d}V = 0 \tag{3.3.66}$$

$$\Delta u_i = 0 \quad \text{on} \quad \partial V_u \tag{3.3.67}$$

The integrand of the volume integral 3.3.66, is denoted here by the symbol

$$\Delta_2 w = \Delta\pi_{ij}\partial_j \Delta u_i \tag{3.3.68}$$

and it is called the *second-order work of stress*. Global uniqueness of the incremental boundary value problem is guaranteed if 3.3.66 and 3.3.67 hold only for the trivial solution $\Delta u_i = 0$ everywhere in V and on ∂V. In particular, a sufficient condition for global uniqueness is that for any admissible displacement field, the global second-order work of stresses is non-negative

$$\int_V \Delta_2 w \, \mathrm{d}V \geqslant 0 \tag{3.3.69}$$

with the equal sign holding only for the trivial solution $\Delta u_i = 0$. In the considered case, admissible is any field which satisfies the constraint 3.3.67 and which does not correspond to a rigid-body rotation. For hyperelastic materials, condition 3.3.69 is known as Hadamard's linearized, dead-load stability criterion (Beatty, 1966). Thus non-uniqueness implies (in the case of hyperelastic materials) instability in the sense of Hadamard. Of course, the converse does not hold, i.e. uniqueness does not imply Hadamard stability. A counterexample follows from the observation that

$$\int_V \Delta_2 w \, dV < 0 \tag{3.3.69bis}$$

implies uniqueness.

With

$$\Delta\pi_{ij} = C_{ijkl}\partial_l \Delta u_k \tag{3.3.70}$$

Hadamard (1903) has shown that for an equilibrium configuration C of a hyperelastic body under dead loads to satisfy the stability criterion 3.3.69, it is necessary that for all vectors g_i, n_i, thecondition

$$C_{ijkl} g_i g_k n_j n_l \geqslant 0 \tag{3.3.71}$$

hold at any point x_k of the considered body. For a rigorous proof of Hadamard's theorem see Truesdell and Noll (1965).

The above sufficient uniqueness condition (3.3.69) is satisfied if we impose the stronger condition, that the second-order work of stresses is positive everywhere in V for every non-zero displacement gradient field,

$$\Delta_2 w = C_{ijkl}\partial_i \Delta u_j \partial_l \Delta u_k > 0 \tag{3.3.72}$$

The positiveness of the second-order work of stresses is a stronger requirement than the so-called strong-ellipticity condition for the stiffness tensor

$$C_{ijkl} g_i g_k n_j n_l > 0 \tag{3.3.73}$$

which ensures that the differential equations governing the incremental boundary value problem are elliptic; cf. equations 3.3.28.

The increment $\Delta\pi_{ij}$ of the nominal stress is related to the Cauchy stress increment $\Delta\sigma_{ij}$ through equation 3.1.33. If the influence of initial stress is neglected, then $\Delta\pi_{ij} \approx \Delta\sigma_{ij}$, and the above sufficient local condition for uniqueness becomes

$$\Delta_2 w \approx \Delta\sigma_{ij}\Delta\varepsilon_{ij} > 0 \tag{3.3.74}$$

where the symmetry of the Cauchy stress was utilized. Accordingly, the inequality 3.3.74 means that positiveness of the second-order work of the Cauchy stresses implies uniqueness within a small strain theory. Obviously, from 3.3.72 similar restrictions for the Cauchy/Jaumann or relative Kirchhoff/Jaumann increments follow,

$$\Delta_2 w \approx \mathring{\Delta}\sigma_{ij}\Delta\varepsilon_{ij} > 0 \tag{3.3.75}$$

Inequality 3.3.75 is encountered in the literature as *'postulate for material stability'*, since it restricts the constitutive stress increment, so that within a small strain theory local uniqueness is guaranteed. However, it should be emphasized that positiveness of second-order work has no connection to the basic laws of continuum thermodynamics since, as already pointed out in section 2.3.5, the dissipation inequality is connecting the entropy production to the first-order work of the Cauchy stress, $\Delta w = \sigma_{ij}\Delta\varepsilon_{ij}$. Thus material stability does not follow from the Second Law of Thermodynamics and its

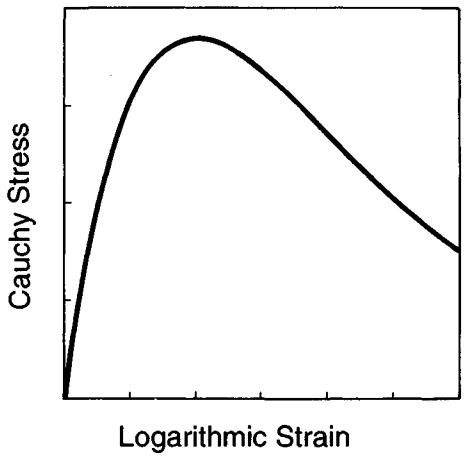

Figure 3.3.5 The stress-strain curve of a material violating the material stability postulate.

violation does not contradict this law. Materials which satisfy the postulate for material stability (3.3.75) are called stable materials. If, on the other hand, the second-order work of stresses is negative then the material is called unstable. Figure 3.3.5 shows the uniaxial stress-strain curve of a material, which shows a stable pre-peak branch ($\Delta\sigma\Delta\varepsilon>0$) and an unstable post-peak branch ($\Delta\sigma\Delta\varepsilon<0$). Within the terminology of plasticity theory, in the stable branch it is said that the material is hardening and in the unstable branch that it is softening.

According to equation 3.1.47 the second-order work of stress can be also expressed approximately in terms of the relative Kirchhoff/Jaumann stress increment,

$$\Delta_2 w \approx \mathring{\Delta} T^t_{ij} \Delta\varepsilon_{ij} \tag{3.3.76}$$

In isotropic elasticity, for example, the Kirchhoff/Jaumann stress increment is given through constitutive equations of the form 3.2.44 with a constitutive tensor which obeys major symmetry conditions. Thus, sufficient for small strain local uniqueness is that the requirement for positive definiteness of the constitutive tensor

$$R^t_{ijkl} g_{ij} g_{kl} > 0 \tag{3.3.77}$$

is holding for arbitrary, non-zero symmetric tensors g_{ij}. For elastic materials, inequality 3.3.77 implies in turn a convexity condition for the material strain energy function $e(\lambda_i)$,

$$\mathrm{d}^2 e = \frac{\partial^2 e}{\partial\lambda_i \partial\lambda_j} \mathrm{d}\lambda_i \, \mathrm{d}\lambda_j > 0 \tag{3.3.78}$$

Thus, stable hyperelastic materials are characterized by a convex strain energy function. A non-convex strain energy function resulting in an unstable stress-strain curve is shown in Figure 3.3.6.

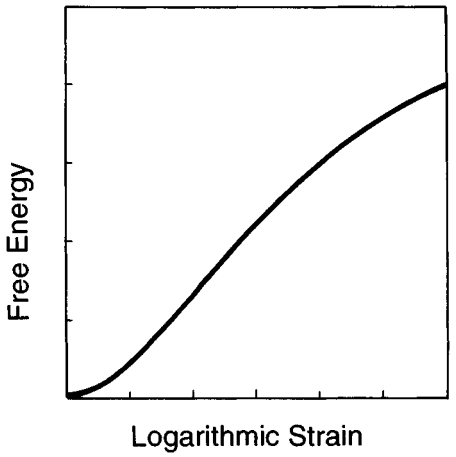

Figure 3.3.6 Non-convex strain energy function.

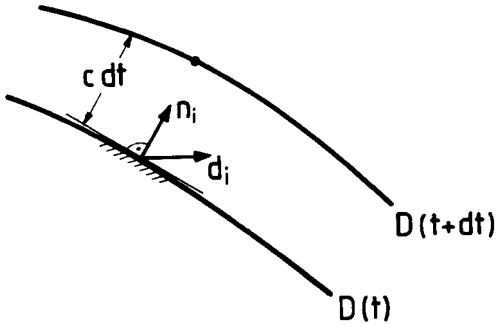

Figure 3.4.1 Acceleration wavefront.

3.4
Acceleration waves and stationary discontinuities

We consider here a solid body B at an equilibrium configuration C and study the propagation of acceleration waves, with C serving as reference configuration. Acceleration waves are weak discontinuities of the various mechanical fields across wavefronts D*(t)* which propagate with the speed c; cf. section 2.4.4. Across such wavefronts D*(t)* the following compatibility conditions hold for the displacement Δu_i, the density ρ and the nominal stress π_{ij}

$$[\partial_i \partial_k \Delta u_i] = d_i n_i n_k;\ [\partial_t \partial_i \Delta u_i] = -d_i n_i c;\ [\partial_t \partial_t \Delta u_i] = d_i c^2 \tag{3.4.1}$$

$$[\rho] = 0;\ [\partial_j \rho] = r n_j;\ [\partial_t \rho] = -rc \tag{3.4.2}$$

$$[\pi_{ij}] = 0;\ [\partial_k \pi_{ij}] = g_{ij} n_k;\ [\partial_t \pi_{ij}] = -g_{ij} c \tag{3.4.3}$$

where n_i is the unit normal on the wavefront, r, d_i and g_{ij} are the jumps of the density, velocity gradient and stress gradient respectively. Figure 3.4.1 illustrates the wave propagation and the velocity gradient discontinuity.

On both sides of the wavefront D*(t)* the balance equations of mass and linear momentum must hold

$$\dot{\rho} + \rho \partial_k v_k = 0 \tag{3.4.4}$$

$$\partial_k \pi_{ik} + b_i = \rho a_i \tag{3.4.5}$$

where

$$v_i = \Delta \dot{u}_i;\ a_i = \dot{v}_i \tag{3.4.6}$$

are the velocity and acceleration vectors, respectively.

For conservative body forces and due to the fact that C is an equilibrium configuration, the dynamic equations 3.4.5

$$\partial_k \Delta \pi_{ik} = \rho a_i \tag{3.4.7}$$

From the above balance equations we derive the following dynamic compatibility conditions

$$[\partial_t \rho] + v_k [\partial_k \rho] + \rho [\partial_k v_k] = 0 \tag{3.4.8}$$

$$[\rho_k \Delta \pi_{ik}] = \rho [a_i] \tag{3.4.9}$$

For moving wavefronts, from the above mass-balance relation 3.4.8 we derive the following compatibility condition, which is restricting the jump r of the density gradient such that across acceleration wavefronts

$$r = -\rho n_k d_k \tag{3.4.10}$$

On the other hand, in order to evaluate equation 3.4.9 we assume that the nominal stress increment is related to the incremental displacement gradient through a set of equations of the form

$$\Delta \pi_{ij} = C_{ijkl} \partial_l \Delta u_k \tag{3.4.11}$$

cf. equations 3.3.70. We assume in addition that the stiffness tensor C_{ijkl} is continuous across *D(t)*

$$[C_{ijkl}] = 0 \tag{3.4.12}$$

and notice that this assumption is true for elastic materials. From the above relations the following dynamical compatibility conditions are derived

$$\Gamma_{ik} d_k = \rho c_m^2 d_i \tag{3.4.13}$$

where

$$c_m = c - v_n \tag{3.4.14}$$

is the material wave propagation velocity, and $v_n = v_k n_k$ is the normal particle velocity, and

$$\Gamma_{ik} = C_{ijkl} n_j n_l \tag{3.4.15}$$

is the so-called *acoustic tensor*.

Equation 3.4.13 is the eigenvalue problem for the determination of the speed and jump properties (c_m, d_i) of acceleration waves which may propagate along the direction n_i. We notice that Hadamard's stability criterion (equation 3.3.71) guarantees that all material speeds c_m of acceleration waves are real. When all waves are able to propagate with real material speed, the material is stable in a dynamic sense. In the contrary, if one or more material wave speeds is not real, then the body is inherently unstable, i.e. unstable in the sense that a certain displacement may build up exponentially with time. This means that the eigenvalues of the acoustic tensor determine whether or not the considered body is locally dynamically stable or unstable.

If the material propagation velocity of the wavefront D*(t)* vanishes,

$$c_m = 0 \rightarrow c = v_n \tag{3.4.16}$$

then the wavefront is called *material* discontinuity surface. Existence of weak material discontinuities is guaranteed if

$$\det(\Gamma_{ik}) = 0 \tag{3.4.17}$$

According to equations 3.4.13 and 3.4.17, weak material discontinuity surfaces are characterized by the fact that the velocity gradient discontinuity vector d_i is the eigenvector of the acoustic tensor Γ_{ik}, which, for a given characteristic direction n_i that satisfies condition 3.4.17, corresponds to a zero eigenvalue of Γ_{ik}.

Hill (1962) in his famous paper on 'Acceleration waves in solids' suggested interpreting the condition for vanishing speed of acceleration waves along real characteristic directions n_i as the condition for shear-band formation. The discussion of Hill's proposition will be furthered in chapter 8 within the context of elastoplastic materials.

Literature

Textbooks and monographs

Biot, M.A. (1965). *Mechanics of Incremental Deformations.* Wiley, New York.

Hadamard, J. (1903). Leçons sur la propagation des ondes et les equations de l'hydrodynamique. Hermann, Paris. Reprinted by Chelsea Publishing Co., New York, 1949.

Hill, R. (1978). *Aspects of Invariance in Solid Mechanics.* In: *Advances in Applied Mechanics,* Vol. 18 (Chia-Shun Yih, ed.). Academic Press, New York, 1–75.

Kolymbas, D. (1978). Ein nichtlineares viskoplastisches Stoffgesetz für Böden. Dissertation Universität Karlsruhe, Veröffentlichungen IBF, Heft Nr. 77.

Novozhilov, V.V. (1961). *Theory of Elasticity.* Pergamon Press, Oxford.

Truesdell, C. and Noll, W. (1965). *Nonlinear Field Theories of Mechanics. Handbuch der Physik, Vol. III/3,* Sections 68, 68*bis,* 69, 99, 100. Springer, Berlin.

Vardoulakis, I. (1978). Equilibrium bifurcation of granular earth bodies. *Advances in Analysis of Geotechnical Instabilities,* University of Waterloo Press, SM Study No. 13, Paper 3, 65–120.

References

Bažant, Z.P. (1971). A correlation study of formulations of incremental deformation and stability of continuous bodies. *J. Appl. Mech.* (ASME), **38,** 919–928.

Beatty, M.F. (1966). Some static and dynamic implications of the general theory of elastic stability. *Arch. Rat. Mech. Anal,* **10,** 167–186.

Christoffersen, J. (1991). Hyperelastic relations with isotropic forms appropriate for elastoplasticity. *Eur. J. Mech. A/Solids,* **10,** 91–99.

Dorris, J.F. and Nemat-Nasser, S. (1980). Instability of a layer on a half space. *J. Appl Mech.,* **102,** 304–312.

Hill, R. (1962). Acceleration waves in solids. *J. Mech. Phys. Solids,* **10,** 1–16.

Hutchinson, J.W. (1973). Finite strain analysis of elastic-plastic solids and structures. In *Numerical Solution of Nonlinear Structural Problems* (R.F.Hartung, ed.). ASME, New York.

Kolymbas, D. (1991). An outline of plasticity. *Arch. Appl Mech.,* **61,** 143–151.

Loret, B. (1985). On the choice of elastic parameters for sand. *Int. J. Num. Anal Methods Geomech.,* **9,** 285–292.

McMeeking, R.M. and Rice, J.R. (1975). Finite-element formulations for problems of large elastic-plastic deformation. *Int. J. Solids Struct.,* **11,** 601–616.

Nemat-Nasser, S. (1972). On local stability of finitely deformed solid subjected to follower type loads. *Quart. Appl. Math.,* **26,** 119–129.

Tvergaard, V., Needleman, A. and Lo, K.K. (1981). Flow localization in the plane strain tensile test. *J. Mech. Phys. Solids,* **29,** 115–142.

Vardoulakis, I. (1975). Die lineare Naeherung des Prinzipes der virtuellen Verschiebungen. *Int. Conf. on Num. Meth. in Soil Rock Mech., Karlsruhe,* Universität Karlsruhe (G.Borm and H. Meissner, eds), 39–46.

Wang, C.C. (1970). On representation of isotropic functions. *Arch. Rat. Anal.,* **33,** 249–267.

4
Buckling of layered elastic media

4.1
Folding of elastic and viscoelastic media as a bifurcation problem

According to Hadamard (1903), a mathematical problem is called well-posed if it has (a) a solution, (b) not more than one solution and (c) a solution that changes only slightly with a slight change of data. These three conditions are known as conditions of existence, uniqueness and continuity (or stability). Within the theory of linear elliptic operators, Benallal *et al.* (1990) gave a precise mathematical definition for a well-posed mathematical problem. Such a definition does not only refer to the type of the governing differential equations but also makes use of boundary conditions and interfacial compatibility conditions. In this section we will simply address the problem of uniqueness of the incrementally linear boundary value problem which was treated in general terms in section 3.3.4. In particular, the constitutive equations of large strain elasticity theory will be utilized to study buckling of elastic layered media. These buckling modes can explain the occurrence of various periodic structures in geology such as folds and joints. Questions of uniqueness which relate to strain localization in the form of shear bands will be treated separately in chapter 8 within the context of elastoplasticity theory.

The analysis of the behavior of stratified elastic or viscoelastic media under compression is of great interest to the geologist. Biot has presented an analysis of folding of stratified sedimentary rock in a series of pioneering papers (1957, 1959a,b,c, 1961, 1965a, 1967) and in his reference book (1965b). The particular type of folding mechanism considered in Biot's theory is the spontaneous folding caused by instability under a compressive load acting in a direction parallel with the layers. The stability of an elastic layer embedded in an elastic medium has been studied by a number of authors in connection with the properties of sandwich panels (Gough *et al.,* 1940; Bijlaard, 1947). However, from the viewpoint of geology, a purely elastic theory is not sufficient to explain folding. Time-dependent phenomena such as viscous behavior must be taken into account. Biot (1957) developed a general theory of folding of a compressed viscoelastic layer embedded in an infinite medium of another viscoelastic material. He showed that, in general, there exists a lower and a higher critical load between which

folding occurs at a finite rate with a dominant wavelength. This is the wavelength whose amplitude increases at the fastest rate. The problem of interfacial adherence between the layer and the surrounding medium has been investigated in another paper (Biot, 1959b). It was shown that the influence of gravity in the case of a single layer is not significant and can be neglected. The influence of gravity on folding is important in certain situations with density contrasts and for a layer situated at the surface (Biot, 1959c). An experimental verification of Biot's theory of folding of stratified viscoelastic media in compression is presented in a paper by Biot *et al.* (1961).

Biot's theory of folding of layered media has provided the point of departure for many important studies on the modeling of rock folding (Ramberg, 1963, 1964; Ramberg and Stephansson, 1964; Ramsay, 1962, 1967; Chapple, 1968; Cobbold *et al.,* 1971; Dorris and Nemat-Nasser, 1980; Papamichos *et al.,* 1990; Martinod and Davy, 1992; Triantafyllidis and Lehner, 1993).

4.2
Surface and interfacial instabilities in elastic media

4.2.1
Buckling of a single layer under initial stress

4.2.1.1
Formulation of the eigenvalue problem.

The problem considered here is the non-homogeneous, plane-strain deformation of a layer of thickness $2h$, due to constant horizontal and vertical compressions σ_1 and σ_2, respectively, as shown in Figure 4.2.1. The theory used in this analysis is based on incremental plane-strain deformations superimposed on the large strain uniform compression. The problem is formulated in terms of the relative first Piola-Kirchhoff (1. P.-K.) stress π_{ij} with $\Delta\pi_{ij}$ being its increment referred to the deformed initially stressed state. In the case of constant body forces, the equations of equilibrium for the incremental problem take the form (see equations 3.3.27 and 3.3.28):

$$\partial_j \Delta\pi_{ij} = 0 \tag{4.2.1}$$

The incremental stress boundary conditions are

$$\Delta\pi_{ij} n_j = \Delta\pi_i \tag{4.2.2}$$

where $\Delta\pi_i$ are the components of prescribed traction increments referred to the initial stressed state and n_j are the components of the outward unit normal of the boundary.

Let $\Delta u_i(x, y)$ be the instantaneous incremental displacement components of typical material point in the current configuration. Then the incremental strain and spin are defined as

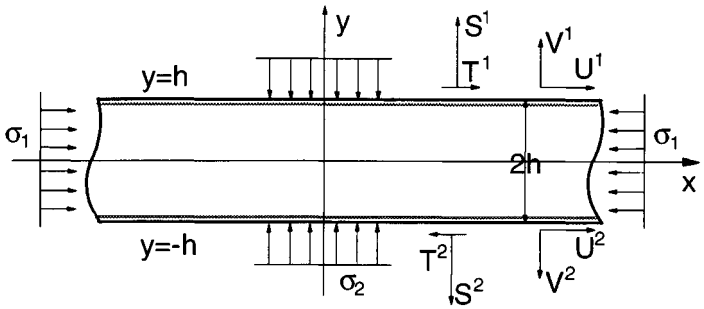

Figure 4.2.1 A single layer under initial stress σ_1 and σ_2.

$$\Delta\varepsilon_{ij} = (\partial_i \Delta u_j + \partial_j \Delta u_i)/2;\ \Delta\omega_{ij} = (\partial_i \Delta u_j - \partial_j \Delta u_i)/2 \tag{4.2.3}$$

The stress increment $\Delta\pi_{ij}$ is related to the Jaumann increments of the relative Kirchhoff stress, the initial stress field σ_{ij} and the incremental strain $\Delta\varepsilon_{ij}$ and spin $\Delta\omega_{ij}$ as follows (see equation 3.1.47):

$$\Delta\pi_{ij} = \mathring{\Delta} T^t_{ij} + \Delta\omega_{ik}\sigma_{kj} - \sigma_{ik}\Delta\varepsilon_{kj} \tag{4.2.4}$$

Using the equation 4.2.4, the equations of equilibrium (4.2.1) can be written as follows:

$$\partial_1 \mathring{\Delta} T^t_{11} + \partial_2 \mathring{\Delta} T^t_{12} + 2\tau\partial_2 \Delta\omega_{21} - (\sigma + \tau)\partial_1 \Delta\varepsilon_{kk} = 0$$
$$\partial_1 \mathring{\Delta} T^t_{21} + \partial_2 \mathring{\Delta} T^t_{22} + 2\tau\partial_1 \Delta\omega_{21} - (\sigma - \tau)\partial_2 \Delta\varepsilon_{kk} = 0$$

where

$$\tau = (\sigma_1 - \sigma_2)/2,\ \sigma = (\sigma_1 + \sigma_2)/2 \tag{4.2.6}$$

The Jaumann stress increments $\mathring{\Delta} T^t_{ij}$ of the relative Kirchhoff stress are related directly to the strain increments through constitutive relations for hyperelastic materials (see equations 3.2.44–3.2.47)

$$\begin{aligned} \mathring{\Delta} T^t_{11} &= C_{11}\Delta\varepsilon_{11} + C_{12}\Delta\varepsilon_{22} \\ \mathring{\Delta} T^t_{22} &= C_{21}\Delta\varepsilon_{11} + C_{22}\Delta\varepsilon_{22} \\ \mathring{\Delta} T^t_{12} &= 2G_*\Delta\varepsilon_{12} \end{aligned} \tag{4.2.7}$$

with

$$C_{11} = C_{22} = 2G^t(1 - \nu)/(1 - 2\nu),\ C_{12} = C_{21} = 2G^t\nu/(1 - 2\nu) \tag{4.2.8}$$

and the shear moduli G_* and G^t are expressed in terms of the logarithmic strains λ_1 and λ_2 by

$$G_* = G^t(\lambda_1 - \lambda_2)/\tanh(\lambda_1 - \lambda_2),\ G^t = G/J,\ J = \exp(\lambda_1 + \lambda_2) \tag{4.2.9}$$

By using the constitutive equations 4.2.7, the equilibrium equations 4.2.5 are written

$$\begin{aligned}(C_{11}-(\sigma+\tau))\partial_{11}^2\Delta u_1+(G_*-\tau)\partial_{22}^2\Delta u_1+(C_{12}+G_*-\sigma)\partial_{12}^2\Delta u_2=0\\(C_{21}+G_*-\sigma)\partial_{12}^2\Delta u_1+(G_*+\tau)\partial_{11}^2\Delta u_2+(C_{22}-(\sigma-\tau))\partial_{22}^2\Delta u_2=0\end{aligned}\tag{4.2.10}$$

For the considered non-homogeneous deformation mode, the displacement field is assumed to be given in terms of two unknown amplitude functions of the dimensionless coordinate *y*,

$$\begin{aligned}\Delta u_1&=\Delta U(y)\sin(\beta x);\ \Delta U(y)=A\exp(i\gamma y)\\\Delta u_2&=\Delta V(y)\cos(\beta x);\ \Delta V(y)=B\exp(i\gamma y)\end{aligned}\tag{4.2.11}$$

where $i=\sqrt{-1}$, $x=x_1/l$, $y=x_2/l$, l is a reference length and β is a dimensionless wave number. The wavelength W of the definition mode can then be written as $W=2\pi l/\beta$. By substituting the displacement field (4.2.11) in the differential equations 4.2.10, and letting $Z=\gamma/\beta$, we obtain a system of two linear homogeneous algebraic equations with respect to the integration constants *A* and *B*.

$$\begin{aligned}A[(C_{11}-(\sigma+\tau))+Z^2(G_*-\tau)]+B[(C_{12}+G_*-\sigma)iZ]=0\\A[(C_{21}+G_*-\sigma)iZ]-B[(C_{22}-(\sigma-\tau))Z^2+(G_*+\tau)]=0\end{aligned}\tag{4.2.12}$$

For non-trivial solution in terms of *A* and *B*, the determinant of the system of equations 4.2.12 must vanish. This leads to the following biquadratic equation for *Z*

$$aZ^4+bZ^2+c=0\tag{4.2.13}$$

where

$$\begin{aligned}a&=(C_{22}-(\sigma-\tau))(G_*-\tau)\\b&=(C_{11}-(\sigma+\tau))(C_{22}-(\sigma-\tau))+(G_*+\tau)(G_*-\tau)\\&\quad-(C_{12}+G_*-\sigma)(C_{21}+G_*-\sigma)\\c&=(C_{11}-(\sigma+\tau))(G_*+\tau)\end{aligned}\tag{4.2.14}$$

The four roots of equation 4.2.14 correspond to four solutions $\Delta u_k(y)$ and $\Delta v_k(y)$ $k=1,2,3,4$ for the displacement field amplitudes. The complete solution for *U(y)* and *V(y)* is then given as a linear combination of the functions base

$$\Delta U(y)=\sum_1^4 A_k\Delta U_k;\ \Delta V(y)=\sum_1^4 A_k\Delta V_k\tag{4.2.15}$$

where A_k are integration constants.

4.2.1.2
Classification of regimes and functions base.

Depending upon the values of the coefficients *a, b* and *c,* the biquadratic equation 4.2.13 has different types of solution in *Z* which correspond to different regimes of the system of differential equations 4.2.10:

1. *(EC) elliptic complex regime* when it has four complex roots, i.e. when

$$\delta = b^2 - 4ac < 0 \tag{4.2.16}$$

with $P = -b/2a$ and $Q = \sqrt{-\delta/2a}$ we define the following quantities

$$Z_1 = P + iQ;\ Z_2 = P - iQ;\ p = \mathrm{Re}(\sqrt{Z_1});\ q = \mathrm{Im}(\sqrt{Z_2}) \tag{4.2.17}$$

The functions base is

$$\begin{aligned} \Delta U_1 &= \cosh(\beta q y)\cos(\beta p y) \\ \Delta U_2 &= \sinh(\beta q y)\cos(\beta p y) \\ \Delta U_3 &= \sinh(\beta q y)\sin(\beta p y) \\ \Delta U_4 &= \cosh(\beta q y)\sin(\beta p y) \end{aligned} \tag{4.2.18}$$

and

$$\begin{aligned} \Delta V_1 &= r_1 \Delta U_2 - r_2 \Delta U_4 \\ \Delta V_2 &= r_1 \Delta U_1 - r_2 \Delta U_3 \\ \Delta V_3 &= r_2 \Delta U_2 + r_1 \Delta U_4 \\ \Delta V_4 &= r_2 \Delta U_1 + r_1 \Delta U_3 \end{aligned} \tag{4.2.19}$$

with

$$\begin{aligned} r_1 &= \frac{-(C_{11} - (\sigma + \tau) + (G_* - \tau)(p^2 + q^2)}{(C_{12} + G_* - \sigma)(p^2 + q^2)} q \\ r_2 &= \frac{(C_{11} - (\sigma + \tau)) + (G_* - \tau)(p^2 + q^2)}{(C_{12} + G_* - \sigma)(p^2 + q^2)} p \end{aligned} \tag{4.2.20}$$

2. *(EI) elliptic imaginary regime* when it has four imaginary roots, i.e. when

$$\delta = b^2 - 4ac \geqslant 0,\ b/a > 0 \quad \text{and} \quad c/a \geqslant 0 \tag{4.2.21}$$

with $P = b/2a$ and $Q = \sqrt{\delta/2a}$ we define the following quantities

$$Z_1 = P + Q;\ Z_2 = P - Q;\ p = \mathrm{Im}(\sqrt{-Z_1});\ q = \mathrm{Im}(\sqrt{-Z_2}) \tag{4.2.22}$$

The functions base is

$$\begin{aligned} \Delta U_1 &= \cosh(\beta p y) \\ \Delta U_2 &= \sinh(\beta p y) \\ \Delta U_3 &= \cosh(\beta q y) \\ \Delta U_4 &= \sinh(\beta q y) \end{aligned} \tag{4.2.23}$$

and

$$\begin{aligned}\Delta V_1 &= r_1 \Delta U_2 \\ \Delta V_2 &= r_1 \Delta U_1 \\ \Delta V_3 &= r_2 \Delta U_4 \\ \Delta V_4 &= r_2 \Delta U_3\end{aligned} \tag{4.2.24}$$

with

$$r_1 = \frac{-(C_{11} - (\sigma + \tau)) + (G_* - \tau)p^2}{(C_{12} + G_* - \sigma)p};\ r_2 = \frac{-(C_{11} - (\sigma + \tau)) + (G_* - \tau)q^2}{(C_{12} + G_* - \sigma)q} \tag{4.2.25}$$

3. *(P) parabolic regime* when it has two real and two purely imaginary roots, i.e. when

$$\delta = b^2 - 4ac > 0 \quad \text{and} \quad c/a < 0 \tag{4.2.26}$$

with $P = -b/2a$ and $Q = \sqrt{\delta/2a}$ we define the following quantities

$$Z_1 = \min(P - Q, P + Q);\ Z_2 = \max(P - Q, P + Q);\ p = \sqrt{-Z_1};\ q = \sqrt{Z_2} \tag{4.2.27}$$

The functions base is

$$\begin{aligned}\Delta U_1 &= \cosh(\beta p y) \\ \Delta U_2 &= \sinh(\beta p y) \\ \Delta U_3 &= \sin(\beta q y) \\ \Delta U_4 &= \cos(\beta q y)\end{aligned} \tag{4.2.28}$$

and

$$\begin{aligned}\Delta V_1 &= r_1 \Delta U_2 \\ \Delta V_2 &= r_1 \Delta U_1 \\ \Delta V_3 &= r_2 \Delta U_4 \\ \Delta V_4 &= -r_2 \Delta U_3\end{aligned} \tag{4.2.29}$$

with

$$r_1 = \frac{-(C_{11} - (\sigma + \tau)) + (G_* - \tau)p^2}{(C_{12} + G_* - \sigma)p};\ r_2 = \frac{(C_{11} - (\sigma + \tau)) + (G_* - \tau)q^2}{(C_{12} + G_* - \sigma)q} \tag{4.2.30}$$

4. *(H) hyperbolic* when it has four real roots, i.e. when

$$\delta = b^2 - 4ac \geqslant 0, \tag{4.2.31}$$

$$b/a \leqslant 0 \quad \text{and} \quad c/a \geqslant 0 \tag{4.2.32}$$

with $P = -b/2a$ and $Q = \sqrt{\delta/2a}$ we define the following quantities

$$Z_1 = P - Q;\ Z_2 = P + Q;\ p = \sqrt{-Z_1};\ q = \sqrt{Z_2} \tag{4.2.33}$$

The functions base is

$$\begin{aligned}\Delta U_1 &= \cos(\beta p y)\\ \Delta U_2 &= \sin(\beta p y)\\ \Delta U_3 &= \sin(\beta q y)\\ \Delta U_4 &= \cos(\beta q y)\end{aligned} \tag{4.2.34}$$

and

$$\begin{aligned}\Delta V_1 &= r_1 \Delta U_2\\ \Delta V_2 &= r_1 \Delta U_1\\ \Delta V_3 &= r_2 \Delta U_4\\ \Delta V_4 &= r_2 \Delta U_3\end{aligned} \tag{4.2.35}$$

with

$$r_1 = \frac{-(C_{11} - (\sigma + \tau)) - (G_* - \tau)p^2}{(C_{12} + G_* - \sigma)p};\ r_2 = \frac{-(C_{11} - (\sigma + \tau)) - (G_* - \tau)q^2}{(C_{12} + G_* - \sigma)q} \tag{4.2.36}$$

4.2.1.3
Eigendisplacements and tractions at layer boundaries.

The incremental displacement amplitudes at the upper and lower boundaries of the layer are obtained directly from equations 4.2.15:

$$\begin{aligned}\Delta U^1 &= \sum_1^4 A_k \Delta U_k(h/l);\ \Delta V^1 = \sum_1^4 A_k \Delta V_k(h/l)\\ \Delta U^2 &= \sum_1^4 A_k \Delta U_k(-h/l);\ \Delta V^2 = \sum_1^4 A_k \Delta V_k(-h/l)\end{aligned} \tag{4.2.37}$$

where the superscripts 1 and 2 denote the upper and lower faces of the layer, respectively. In this and following sections, *superscripts should not be confused with exponents*.

The boundary tractions $\Delta s = \Delta\pi_{22}$ and $\Delta t = \Delta\pi_{12}$ are written through expressions 4.2.2, 4.2.4, 4.2.7 and 4.2.11 as follows:

$$\Delta s = (\beta/l)\Delta S \cos(\beta x);\ \Delta t = (\beta/l)\Delta T \sin(\beta x) \tag{4.2.38}$$

with

$$\begin{aligned}\Delta S &= \sum_1^4 A_k \Delta S_k;\ \Delta S_k = C_{21}\Delta U_k + (C_{22} - (\sigma - \tau))\Delta V_k'/\beta\\ \Delta T &= \sum_1^4 A_k \Delta T_k;\ \Delta T_k = (G_* - \tau)\Delta U_k'/\beta - (G_* - \sigma)\Delta V_k\end{aligned} \tag{4.2.39}$$

The stress amplitudes ΔS and ΔT at the upper and lower faces of the layer are written, in accordance with expression 4.2.16, as

$$\Delta S^1 = \sum_1^4 A_k \Delta S_k(h/l);\ \Delta T^1 = \sum_1^4 A_k \Delta T_k(h/l)$$
$$\Delta T^2 = \sum_1^4 A_k \Delta T_k(-h/l);\ \Delta T^2 = \sum_1^4 A_k \Delta T_k(-h/l) \tag{4.2.40}$$

In matrix form the general solution for the upper (i=1) or lower (i=2) boundary displacement and traction amplitudes is written

$$\begin{bmatrix} \Delta U^i \\ \Delta V^i \\ \Delta S^i \\ \Delta T^i \end{bmatrix} = \begin{bmatrix} \Delta U_1^i & \Delta U_2^i & \Delta U_3^i & \Delta U_4^i \\ \Delta V_1^i & \Delta V_2^i & \Delta V_3^i & \Delta V_4^i \\ \Delta S_1^i & \Delta S_2^i & \Delta S_3^i & \Delta S_4^i \\ \Delta T_1^i & \Delta T_2^i & \Delta T_3^i & \Delta T_4^i \end{bmatrix} = \begin{bmatrix} A_1 \\ A_2 \\ A_3 \\ A_4 \end{bmatrix} \quad (i = 1, 2) \tag{4.2.41}$$

4.2.2
Buckling of a system of layers—the transfer matrix technique

In this section, we analyze the buckling of a system of layers and solve numerically the corresponding linear bifurcation problem by using the transfer matrix technique (Bufler, 1965). A system of n layers of different materials and different initial stresses on the layer axis, is considered. Such a medium is obtained by superposition of adhering layers, each of which can be viewed individually as a single layer. A global coordinate system is introduced, as shown in Figure 4.2.2. The layers are numbered from 1 to n starting at the top. By assuming perfect adherence at the interfaces, the incremental stresses and displacements have to be continuous all along the interfaces. Under these conditions, the equations for the buckling of the system of layers are derived immediately from the result obtained in section 4.2.1, provided that all local coordinates are expressed in the global coordinate system. In accordance with expression 4.2.20, the amplitude of the incremental stresses and displacements for the ith interface of the jth layer can be assembled in matrix form as follows:

$$\begin{bmatrix} \Delta U^{ij} \\ \Delta V^{ij} \\ \Delta S^{ij} \\ \Delta T^{ij} \end{bmatrix} = \begin{bmatrix} \Delta U_1^{ij} & \Delta U_2^{ij} & \Delta U_3^{ij} & \Delta U_4^{ij} \\ \Delta V_1^{ij} & \Delta V_2^{ij} & \Delta V_3^{ij} & \Delta V_4^{ij} \\ \Delta S_1^{ij} & \Delta S_2^{ij} & \Delta S_3^{ij} & \Delta S_4^{ij} \\ \Delta T_1^{ij} & \Delta T_2^{ij} & \Delta T_3^{ij} & \Delta T_4^{ij} \end{bmatrix} = \begin{bmatrix} A_1^j \\ A_2^j \\ A_3^j \\ A_4^j \end{bmatrix} \tag{4.2.42}$$

or

$$[X^{ij}] = [F^{ij}][A^j] \tag{4.2.43}$$

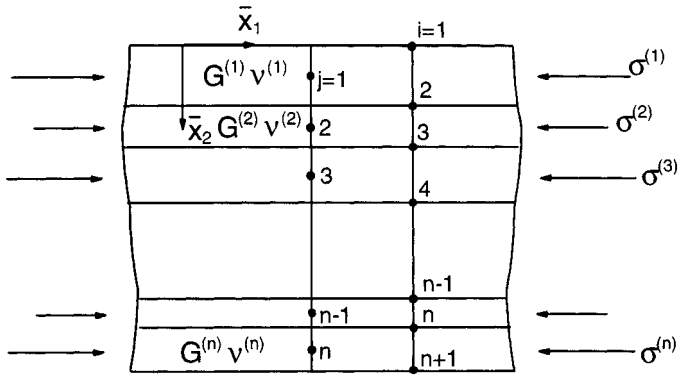

Figure 4.2.2 Arbitrary multilayered medium under compressive initial stress.

By requiring continuity of the incremental displacements and tractions at all interfaces, the integration constants of every layer are linked to the integration constants of the top layer as follows

$$[A^n] = [F][A^1],\ [F] = [F^n]\dots[F^1],\ [F^k] = [F^{k,k}]^{-1}[F^{k,k-1}] \tag{4.2.44}$$

In order to formulate the eigenvalue problem we have to consider boundary conditions only at the upper and lower boundary surfaces of the layered medium. As an example, the case of zero tractions at the upper boundary surface (i=1, j=1) and zero displacements at the lower boundary surface (i=n+1, j=n) is considered. These boundary conditions can be written in matrix form as

$$\begin{aligned}[Y^1][A^1] &= [0]\\ [Y^n][A^n] &= [0]\end{aligned} \tag{4.2.45}$$

where the $[Y^1]$ matrix contains the last two rows of the matrix $[F^{11}]$, and the matrix $[Y^n]$ the first two rows of the matrix $[F^{n+1,\,n}]$. By taking into account expression 4.2.44, the matrix equations 4.2.45 can be assembled in a homogeneous algebraic system of equations for the integration constants $[A^1]$,

$$\begin{bmatrix}[Y^n][F]\\ [Y^1]\end{bmatrix}[A^1] = [0],\quad \text{or}\quad [Y][A^1] = 0 \tag{4.2.46}$$

The resulting homogeneous system of equations has non-trivial solutions in terms of the integration constants involved only if the determinant of the system matrix is singular, i.e.

$$\det([Y]) = 0 \tag{4.2.47}$$

This provides an equation whose roots gives the corresponding eigenvalues. In this equation, we fix the wave number β and we consider it as an equation for the load. When monotonic loading is assumed, then the lowest loading level associated with the least eigenvalue provides the critical buckling load.

4.2.3
Surface instability of a homogeneous half-space

For the case of a homogeneous compressible half-space (Figure 4.2.3a), the analytical solution is easily calculated by requiring that the incremental displacement field decays with depth, vanishing at infinite distance from the free surface.

The eigenvalue problem is formulated in the same manner as in the case of the single layer discussed in section 4.2.1 and leads to the biquadratic equation 4.2.13. Let z_1 and z_2 correspond to the roots with positive imaginary part. The general solution for the incremental displacement field can be written as follows

$$\Delta U = A_1 \Delta U_1 + A_2 \Delta U_2;\ \Delta V = K_1 A_1 \Delta V_1 + K_2 A_2 \Delta V_2 \tag{4.2.48}$$

where (ΔU_i, ΔV_i, (i=1,2)) is the functions base

$$\begin{aligned} \Delta U_i &= \sin \beta x \exp(i\beta z_i y) \\ \Delta V_i &= K_i \cos \beta x \exp(i\beta z_i y) \qquad (i = 1,2) \end{aligned} \tag{4.2.49}$$

$$K_i = -((C_{11} - (\sigma + \tau)) + (G_* - \tau) z_i^2)/(C_{12} + G_* - \sigma) i z_i) \tag{4.2.50}$$

and A_i (i=1,2) are integration constants.

The boundary conditions at the surface require that

$$\Delta \pi_{22}(x,0) = 0 \quad \text{and} \quad \Delta \pi_{12}(x,0) = 0 \tag{4.2.51}$$

where

$$\begin{aligned} \Delta \pi_{22} &= C_{21} \partial_1 \Delta u_1 + (C_{22} - (\sigma - \tau)) \partial_2 \Delta u_2 \\ \Delta \pi_{12} &= (G_* - \tau) \partial_2 \Delta u_1 + (G_* - \sigma) \partial_1 \Delta u_2 \end{aligned} \tag{4 2 52}$$

Using the equation 4.2.42 for the incremental displacement field, the boundary conditions 4.2.52 lead to a homogeneous system of equations for the integration constants A_1 and A_2

$$\begin{aligned} [C_{21} + K_1 i z_1 (C_{22} - (\sigma - \tau))] A_1 + [C_{21} + K_2 i z_2 (C_{22} - (\sigma - \tau))] A_2 = 0 \\ [(G_* - \tau) i z_1 - (G_* - \sigma) K_1] A_1 + [(G_* - \tau) i z_2 - (G_* - \sigma) K_2] A_2 = 0 \end{aligned} \tag{4.2.53}$$

Asking for non-trivial solutions ($(A_1, A_2) \neq (0,0)$), we obtain the following buckling condition for the half-space

$$\begin{aligned} &[C_{21} + K_1 i z_1 (C_{22} - (\sigma - \tau))][(G_* - \tau) i z_2 - (G_* - \sigma) K_2] \\ &- [C_{21} + K_2 i z_2 (C_{22} - (\sigma - \tau))][(G_* - \tau) i z_1 - (G_* - \sigma) K_1] = 0 \end{aligned} \tag{4.2.54}$$

As shown on Figure 4.2.3(b) the critical buckling stress of an elastic half-space increases with the Poisson ratio of the medium.

Problem: Axisymmetric surface instabilities. Local instabilities are defined here as axisymmetric surface instabilities of a half-space subjected to a uniform radial initial stress, σ (Figure 4.2.4). Stresses and strains are measured with respect to a fixed-in-

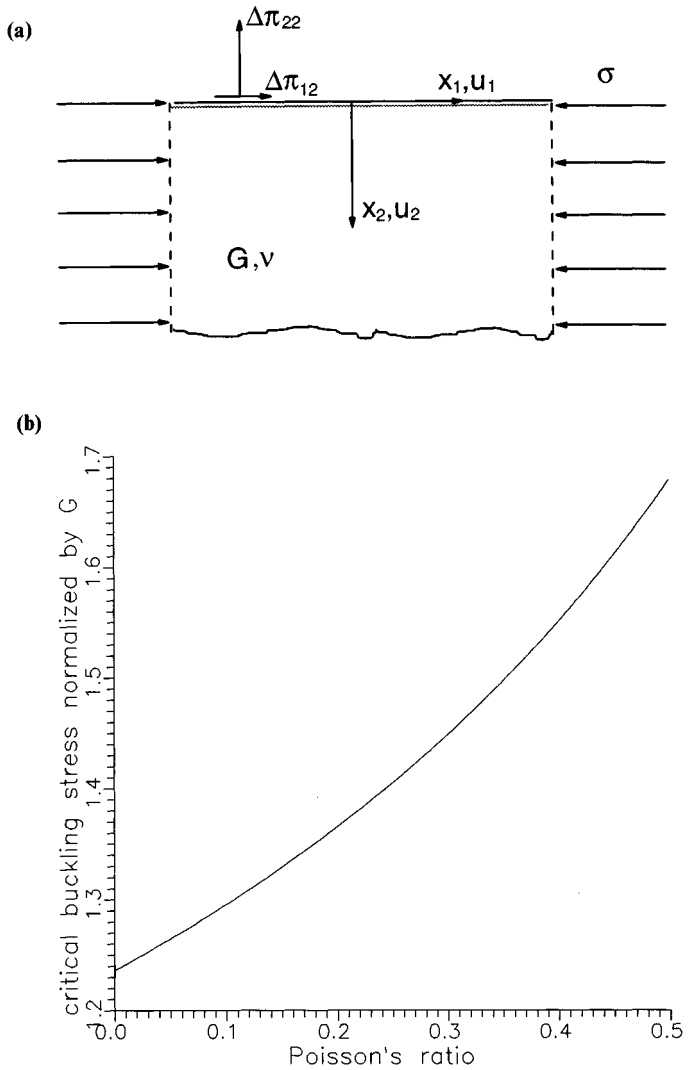

Figure 4.2.3 Surface instability of a homogeneous elastic half-space. (a) Geometric configuration; (b) normalized buckling load as a function of the Poisson ratio.

space polar coordinate system *(r, θ, z),* the *z*-axis being chosen normal to the free surface of the half-space and pointing to the exterior of it.

Let

$$\Delta u_r = \Delta u_r(r,z),\ \Delta u_\theta = 0,\ \Delta u_z = \Delta u_z(r,z) \tag{4.2.55}$$

be the physical components of the considered incremental displacement field. The corresponding physical non-zero components of the incremental strain and spin tensors in polar coordinates are:

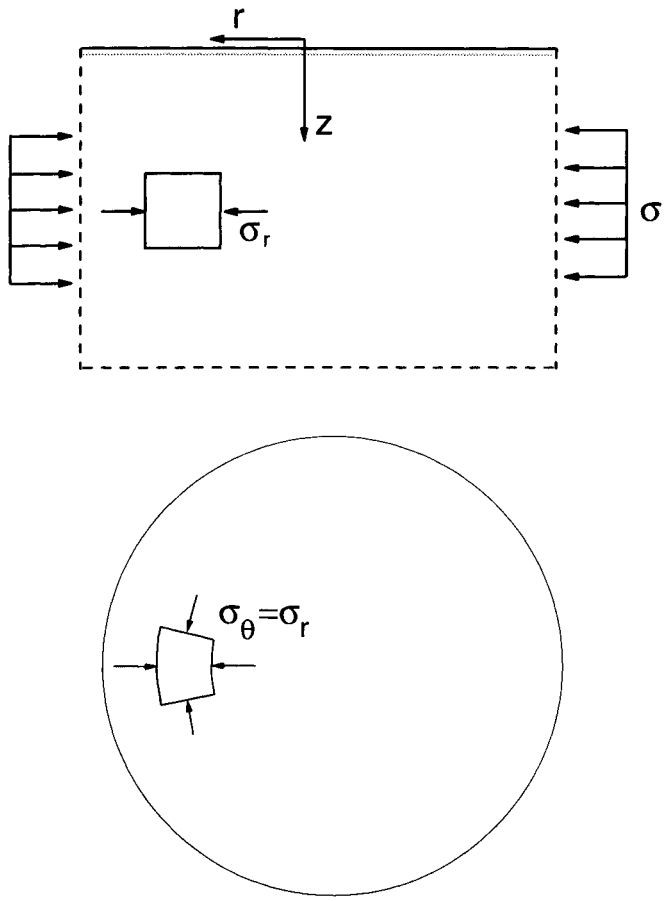

Figure 4.2.4 Half-space under constant radial stress.

$$\begin{aligned} \Delta\varepsilon_{rr} &= \partial_r \Delta u_r;\ \Delta\varepsilon_{zz} = \partial_z \Delta u_z;\ \Delta\varepsilon_{rz} = (\partial_r \Delta u_z + \partial_z \Delta u_r)/2 \\ \Delta\omega_{zr} &= -\Delta\omega_{rz} = \Delta\omega = (\partial_r \Delta u_z - \partial_z \Delta u_r)/2 \end{aligned} \tag{4.2.56}$$

Continued equilibrium is expressed in terms of the increment $\Delta\pi_i^k$ of the relative 1. P.-K. stress tensor

$$\Delta\pi_i^k|_k = 0 \tag{4.2.57}$$

where $(.)|_i$ denotes covariant differentiation.

For the considered state of prestress, the equations of equilibrium (equations 4.2.57) are given by

$$\begin{aligned} \partial_r \mathring{\Delta} T_{rr}^t + \partial_z \mathring{\Delta} T_{rz}^t + (\mathring{\Delta} T_{rr}^t - \mathring{\Delta} T_{\theta\theta}^t)/r + \sigma_r \partial_z \Delta\omega - \sigma_r \partial_r \Delta\varepsilon_{kk} = 0 \\ \partial_r \mathring{\Delta} T_{zr}^t + \partial_z \mathring{\Delta} T_{zz}^t + \mathring{\Delta} T_{zr}^t/r + \sigma_r(\partial_r \Delta\omega + \Delta\omega/r) = 0 \end{aligned} \tag{4.2.58}$$

where

$$\sigma_r = -\sigma, (\sigma > 0) \tag{4.2.59}$$

cf. Vardoulakis (1983).

The incremental constitutive equations for axisymmetric initial state of stress are

$$\begin{aligned} \mathring{\Delta} T^t_{rr} &= C_{11}\Delta\varepsilon_{rr} + C_{12}(\Delta\varepsilon_{\theta\theta} + \Delta\varepsilon_{zz}) \\ \mathring{\Delta} T^t_{zz} &= C_{21}(\Delta\varepsilon_{rr} + \Delta\varepsilon_{\theta\theta}) + C_{22}\Delta\varepsilon_{zz} \\ \mathring{\Delta} T^t_{rr} - \mathring{\Delta} T^t_{\theta\theta} &= 2G^t(\Delta\varepsilon_{rr} - \Delta\varepsilon_{\theta\theta}) \\ \mathring{\Delta} T^t_{12} &= 2G_*\Delta\varepsilon_{12} \end{aligned} \tag{4.2.60}$$

By using the constitutive equations 4.2.60, the equilibrium equations 4.2.57 are written

$$\begin{aligned} &(C_{11} - \sigma_r)L_r(\Delta u_r) + (G_* - \sigma_r)\partial^2_{zz}\Delta u_r + (C_{12} + G_* - \sigma_r)\partial^2_{rz}\Delta u_z = 0 \\ &(C_{21} + G_* - \sigma_r)(\partial^2_{rz}\Delta u_r + \partial_z\Delta u_r/r) \\ &\qquad + (G_* + \sigma_r)(\partial^2_{rr}\Delta u_z + \partial_z\Delta u_r/r) + C_{22}\partial^2_{zz}\Delta u_z = 0 \end{aligned} \tag{4.2.61}$$

where L_r is the Bessel function operator

$$L_r = \partial^2_{rr} + \partial_r/r - 1/r^2 \tag{4.2.62}$$

For axisymmetric surface instability we search for solution of the form

$$\Delta u_r(r,z) = AJ_1(\beta r)\exp(i\gamma z),\ \Delta u_z(r,z) = BJ_0(\beta r)\exp(i\gamma z) \tag{4.2.63}$$

where J_1 (respectively J_0) is the Bessel function of first kind and first order (respectively zero-th order) and A, B are integrations constants.

The eigenvalue problem is then reduced to the one studied in section 4.2.1 and leads to the biquadratic equation 4.2.13. Let z_1 and z_2 correspond to the roots with positive imaginary part. The general solution for the incremental displacement field can be written as follows

$$\Delta U = A_1\Delta U_1 + A_2\Delta U_2;\ \Delta V = K_1A_1\Delta V_1 + K_2A_2\Delta V_2 \tag{4.2.64}$$

where (ΔU_i, ΔV_i, $(i = 1,2)$)is the functions base

$$\begin{aligned} \Delta U_i &= J_1(\beta r)\exp(\beta z_i z) \\ \Delta V_i &= K_i J_0(\beta r)\exp(\beta z_i z) \quad (i = 1,2) \end{aligned} \tag{4.2.65}$$

and K_i are given by equation 4.2.50.

Using the boundary conditions (4.2.51) the same buckling condition (4.2.55) as for the half-space is obtained.

4.2.4
The problem of wavelength selection

We have seen in section 4.2.3 that the buckling condition for a homogeneous half-space is independent of the wavelength of the considered mode. This is due to the fact that no

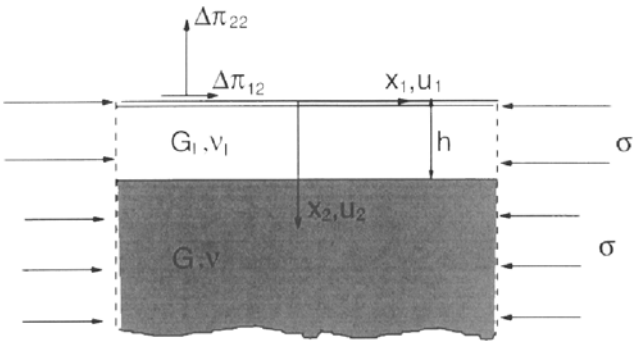

Figure 4.2.5 Layer lying on top of a half-space.

length appears in this problem and consequently the various modes corresponding to different wavelengths cannot be differentiated. We shall see in the next section various examples of problems with introduction of length that leads to the selection of a particular buckling mode.

4.2.4.1
Buckling of a layer on top of a half-space.

The problem considered is the buckling of a half-space covered by a layer due to a horizontal homogeneous strain field as shown in Figure 4.2.5. Both media are assumed isotropic and compressible with elastic parameters G, υ, and G_l, υ_l for the half-space and the layer respectively. Application of this problem corresponds to the folding of geological formation and crustal buckling under tectonic stresses.

Notice that a similar problem has been studied by Dorris and Nemat-Nasser (1980). However they consider in their paper a homogeneous stress field in the layer and the half-space. As pointed out by Dr. Bigoni, the problem solved by Dorris and Nemat-Nasser is kinematically ill-posed since homogeneous stress field implies discontinuous strain field at the boundary between the layer and the half-space. If we assume a continuous displacement field then according to the theorem of Maxwell (see section 2.4.1) ε_{11} must be continuous.

The results are presented in Figure 4.2.6. The wave number β is given by the expression $\beta = 2\pi h/W$, where h is the thickness of the layer and W the wavelength of the deformation field. For the two limiting cases of vanishingly short wavelength ($\beta \to \infty$) and infinitely large wavelength ($\beta \to 0$) the buckling stress corresponds to the one of a homogeneous half-space. In the first case for short wavelengths the layer behaves like a half-space whereas in the second case large wavelengths cannot 'see' the layer. If the layer is stiffer than the half-space then there is a dominant buckling mode, the wavelength of which depends upon the stiffness contrast G_l/G.

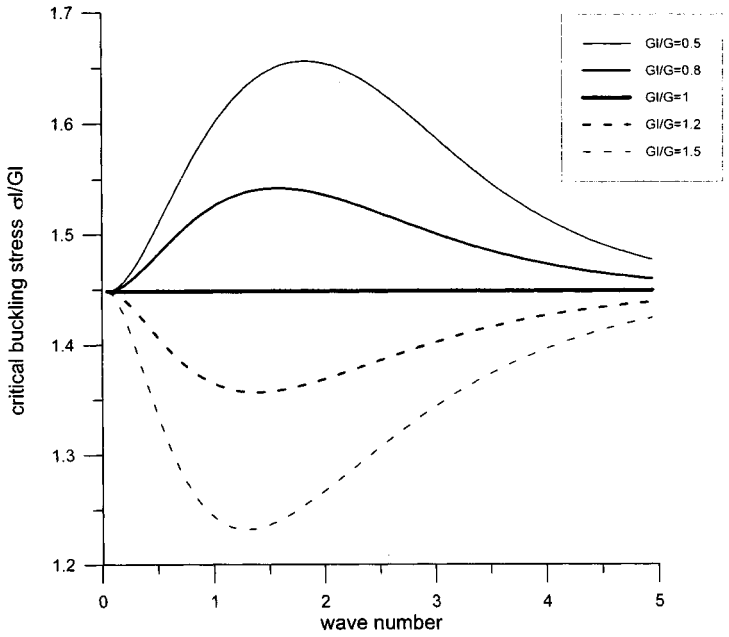

Figure 4.2.6 Buckling stress for the layer for indicated values of G_l/G.

4.2.4.2

Buckling of a homogeneous half-space under geostatic compression.

Surface instability in a homogeneous half-space under geostatic compression can be studied using the numerical method described in section 4.2.1.3. The results are shown on Figure 4.2.7 (curve B). The half-space buckles at the large wavelength limit. However, if we consider a single layer of finite thickness on a rigid base under constant horizontal stress, it buckles first at the short wavelength limit (curve A). Combination of these two competing factors is yielding to an intermediate critical wavelength (curve C). The selection of a dominant wavelength arises from the existence of two competing length scales.

4.2.4.3

Problem: Buckling of an incompressible Gibson half-space.

In a Gibson half-space the stiifness G of the medium increases linearly with depth according to the relation (Figure 4.2.8)

$$G = G_0(1 + x_2/\alpha) \tag{4.2.66}$$

The analytical solution for the buckling of an incompressible isotropic Gibson half-space under a horizontal compressive stress field $\sigma = -\sigma_{11}$ is presented here (Papamichos *et al.*, 1990). For an incompressible material, the Cauchy and the Kirchhoff stress tensors are identical. We use the incremental displacement field

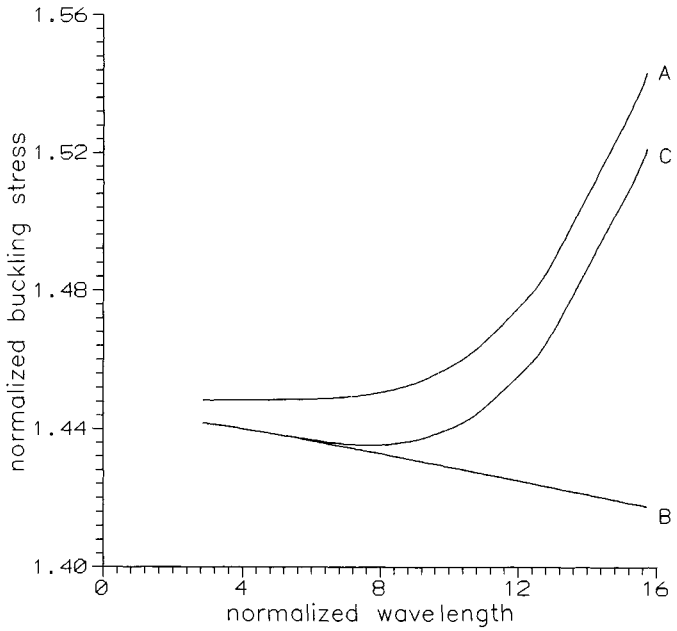

Figure 4.2.7 Buckling of a layer and a half-space under geostatic compression. (A) Buckling of a layer under constant horizontal load. (B) Buckling of a half-space under horizontal load increasing with depth. (C) Buckling of a layer under horizontal load increasing with depth.

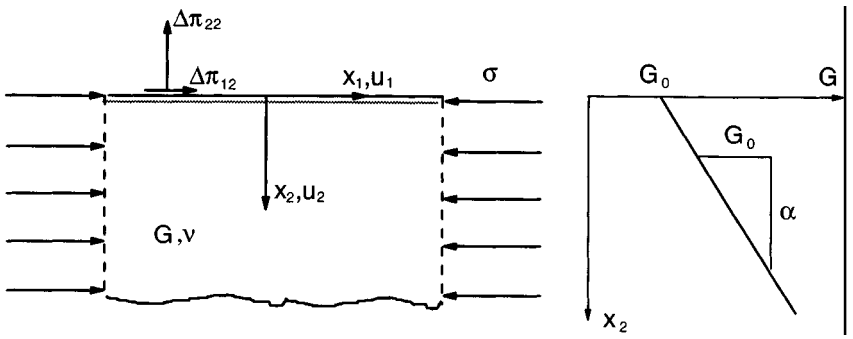

Figure 4.2.8 Gibson half-space under horizontal compression σ.

$$\Delta u_1 = \Delta U(y)\sin(x);\ \Delta u_2 = \Delta V(y)\cos(x) \tag{4.2.67}$$

where $x = \beta x_1/l, y = \beta(1 + x_2/l_G)/\lambda$ and $\lambda = l/l_G$. Then $G = G_0\lambda y/\beta$.. The stress-strain relations for elastic incompressible materials expressed in terms of the Jaumann stress $\mathring{\Delta}\sigma_{ij}$ are written

$$\mathring{\Delta}\sigma_{11} = 2G\Delta\varepsilon_{11} + \mathring{\Delta}p,\ \mathring{\Delta}\sigma_{12} = 2G\Delta\varepsilon_{12},\ \mathring{\Delta}\sigma_{22} = 2G\Delta\varepsilon_{22} + \mathring{\Delta}p \tag{4.2.68}$$

where

$$\mathring{\Delta}p = (\mathring{\Delta}\sigma_{11} + \mathring{\Delta}\sigma_{22})/2,\ \Delta\varepsilon_{11} + \Delta\varepsilon_{22} = 0 \tag{4.2.69}$$

For the displacement field (4.2.67), equations 4.2.68 yield

$$\begin{aligned} \mathring{\Delta}\sigma_{11} &= \lambda G_0(P - 2yV')\cos(x) \\ \mathring{\Delta}\sigma_{22} &= \lambda G_0(P + 2yV')\cos(x) \\ \mathring{\Delta}\sigma_{12} &= -\lambda y G_0(V'' + V)\sin(x) \end{aligned} \tag{4.2.70}$$

where $(.)' = \partial/\partial y$ and $\mathring{\Delta}p = \lambda G_0 P(y)\cos(x)$. Such a representation of $\mathring{\Delta}p$ is consistent with the displacement field (4.2.67) that was introduced above.

The equations for continued equilibrium of the incremental stresses are written

$$\begin{aligned} \mathring{\Delta}\sigma_{11,1} + \mathring{\Delta}\sigma_{21,2} - \sigma\Delta\omega_{,2} = 0 \\ \mathring{\Delta}\sigma_{12,1} + \mathring{\Delta}\sigma_{22,2} - \sigma\Delta\omega_{,1} = 0 \end{aligned} \tag{4.2.71}$$

By substituting equations 4.2.70 in the equations 4.2.71 and eliminating the term Δp, we end up with the following differential equation for the amplitude $\Delta V(y)$ of the vertical displacement:

$$(y + \xi)\Delta V'''' + 2\Delta V'' - 2y\Delta V'' - 2\Delta V' + (y - \xi) = 0 \tag{4.2.72}$$

where $\xi = \beta\sigma/2\lambda G_0$. The solution of this differential equation has to satisfy boundedness conditions, which require that the displacement field is vanishing at infinity. Taking this into account, the complete solution for ΔV reads (Vardoulakis, 1981)

$$\Delta V = [C_1 + C_2(y + \xi)U[(1 - \xi), 2, 2(y + \xi)]]e^{-y} \tag{4.2.73}$$

where $U\,[a, b, z]$ is a logarithmic confluent hypergeometric function (Abramowitz and Stegun, 1965) and C_1 and C_2 are integration constants.

The boundary conditions indicating that the half-space ($x_2 = 0$) is stress-free are as follows:

$$\Delta\pi_{12} = 0,\ \Delta\pi_{22} = 0 \tag{4.2.74}$$

By using equations 4.2.4 and 4.2.70 the above boundary conditions read

$$\begin{aligned} (y_0 + \xi)\Delta V'''' + \Delta V'' - (3y_0 + \xi)\Delta V' + \Delta V = 0 \\ \Delta V'' + \Delta V = 0 \end{aligned} \tag{4.2.75}$$

for $y = y_0$, where $y_0 = y(x_2 = 0) = \beta/\lambda$. The implementation of the solution 4.2.73 for V in equations 4.2.75 yields a linear, homogeneous system of equations in terms of the integration constants C_1 and C_2, which has a non-trivial solution if the determinant vanishes. This gives the following buckling condition:

$$P_1Q_2 - P_2Q_1 = 0 \tag{4.2.76}$$

where

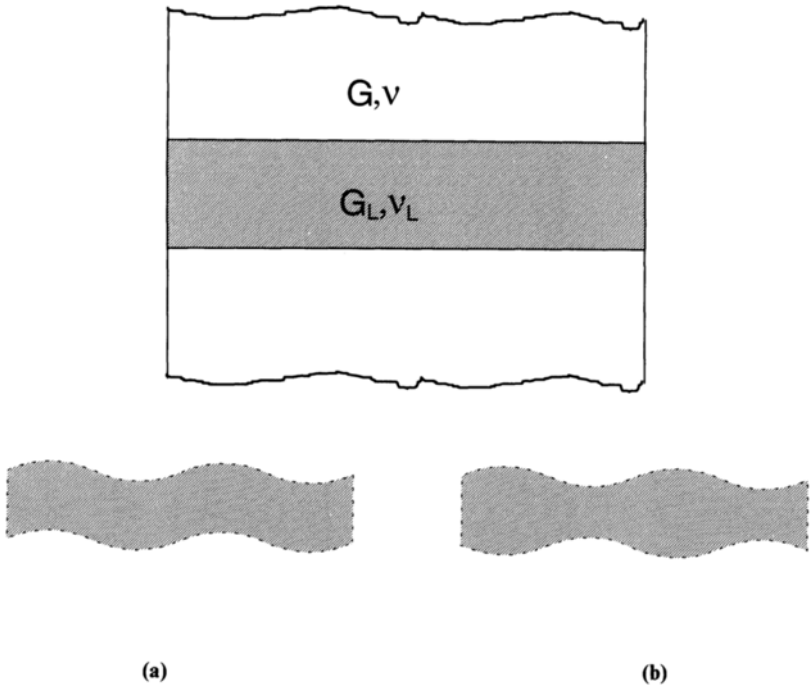

Figure 4.2.9 Interfacial instability. Geometric configuration. (a) Symmetric mode, (b) antisymmetric mode.

$$
\begin{aligned}
P_1 &= 2(1 + y_0) \\
Q_1 &= 2 \\
P_2 &= [(y_0 + \xi)W'''(y_0) + W''(y_0) - (3y_0 + \xi)W'(y_0) + W(y_0)]e^{y_0} \\
Q_2 &= [W''(y_0) + W(y_0)]e^{y_0}
\end{aligned}
\tag{4.2.77}
$$

and

$$
W(y) = e^{-y}(y + \xi)U[(1 - \xi, 2, 2(y + \xi)] \tag{4.2.78}
$$

4.2.5
Interfacial instability

In the previous sections we have emphasized the effect of the existence of a free surface. Here we consider the problem of a stiff layer embedded between two softer half-spaces emphasizing the effect of an interface and of the contrast of behavior between the layer and the surrounding medium (Figure 4.2.9). The considered system is submitted to a homogeneous horizontal strain field. The solution is based on the analysis of the buckling of single layer under initial stress as presented in section 4.2.1 and we

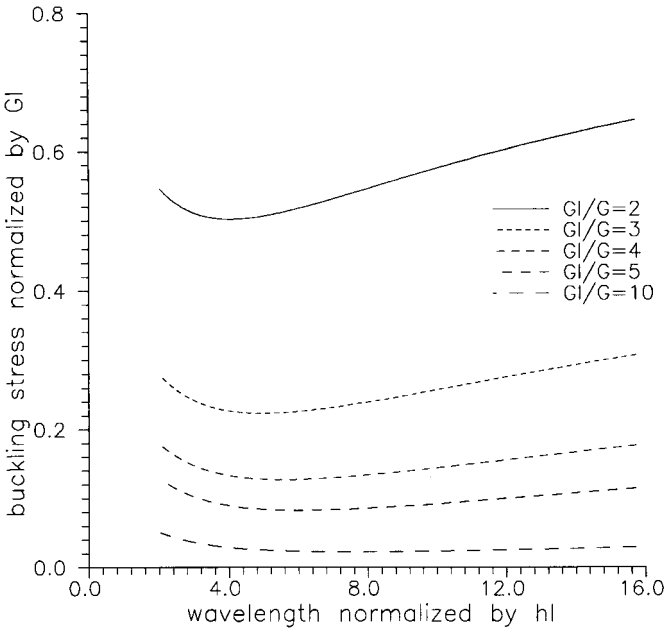

Figure 4.2.10 Buckling loads of a layer embedded between two half-spaces for indicated values of G_1/G.

discriminate in the eigendisplacements field between the symmetric mode corresponding to $\Delta V(-y) = \Delta V(y)$ (folding) and the antisymmetric mode corresponding to $\Delta V(-y) = -\Delta V(y)$ (boudinage). For the surrounding medium we impose in both cases continuity of eigenstresses and eigendisplacements at the layer boundaries and vanishing eigendisplacements at infinite distance from the interface. We have obtained that in compression $\sigma_1 < \sigma_2 < 0$ only the symmetric mode is possible (see also Martinod and Davy, 1992). As shown on Figure 4.2.10 there is a dominant buckling mode, the wavelength of which depends upon the stiffness contrast between the layer and the surrounding medium. We plot on Figure 4.2.11 the dominant wavelength W_d as a function of the ratio G_1/G. The computed results follow the well-known expression given by Biot:

$$W_d = 2\pi h_1 (G/6G_1)^{\frac{1}{3}} \tag{4.2.79}$$

4.3
Periodic elastic multilayered media

The mechanics of periodic media have been widely investigated because many engineering materials consist of alternating volumes of compounds with different

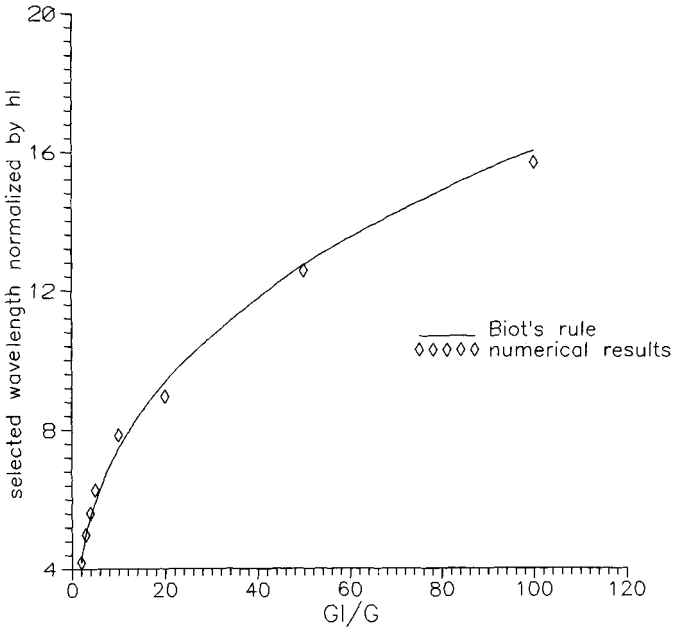

Figure 4.2.11 Selected wavelength as a function of the stiffness ratio.

properties (composite materials, layered rocks). Averaging processes have been developed in order to describe the mechanical behavior of such materials by an equivalent homogeneous medium with averaged (effective) characteristics (Bakhvalov and Panasenko, 1989). The question of calculation of effective characteristics of inhomogeneous media with periodic structures was already raised in the classical works of Poisson, Maxwell, Rayleigh, Voigt and Reuss. Voigt suggested calculation of effective characteristics by averaging the components of the stiffness tensor over the volume. Reuss on the other hand used averaging of the components of the reverse tensor (compliance). It is shown that Voigt's method gives the upper bound of effective parameters, whereas the method proposed by Reuss gives the lower bound. However the 'fork' between these approximations (Hill's fork) can be quite wide.

If the characteristic size of the recurrent cell of the periodic medium is small as compared to the size of the specimen or the characteristic size of the problem (e.g. the wavelength of the deformation field), a mathematically rigorous averaging method based on the asymptotic expansion of the solution can be developed.

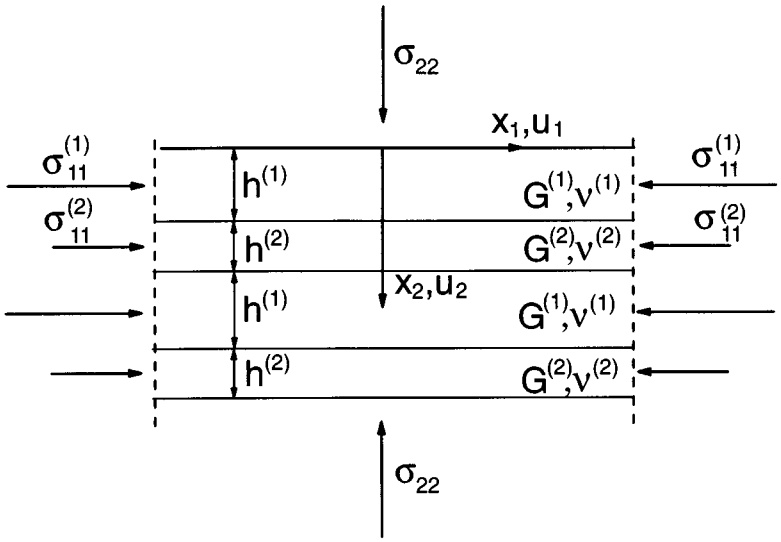

Figure 4.3.1 Periodic laminated half-space.

4.3.1
The asymptotic averaging method

Let us assume that for a laminated material, the constitutive coefficients C_{ij} and G_* in equation 4.2.7 are periodic functions of the spatial coordinate x_2 (Figure 4.3.1). The equilibrium equations (4.2.1)

$$\begin{aligned}
&\frac{\partial}{\partial x_1}\left((C_{11}-\sigma_1)\frac{\partial}{\partial x_1}\Delta u_1 + C_{12}\frac{\partial}{\partial x_2}\Delta u_2\right) \\
&\qquad + \frac{\partial}{\partial x_2}\left((G_*-\tau)\frac{\partial}{\partial x_2}\Delta u_1 + (G_*-\sigma)\frac{\partial}{\partial x_1}\Delta u_2\right) = 0 \\
&\frac{\partial}{\partial x_1}\left((G_*-\sigma)\frac{\partial}{\partial x_2}\Delta u_1 + (G_*+\tau)\frac{\partial}{\partial x_1}\Delta u_2\right) \\
&\qquad + \frac{\partial}{\partial x_2}\left(C_{21}\frac{\partial}{\partial x_1}\Delta u_1 + (C_{22}-\sigma_2)\frac{\partial}{\partial x_2}\Delta u_2\right) = 0
\end{aligned} \tag{4.3.1}$$

where σ_1 and σ_2 are the components of the initial stress tensor and σ and $\tau$are given by equation 4.2.6.

To investigate the solutions of equation 4.3.1, we use the method of many scales. Solution is sought in the form of series in power of a small parameter ε with coefficients depending both on the variables ($X = x_1$, $Y = x_2$), usually referred to as macroscopic variables, and $y = x_2/\varepsilon$ (microscopic variable). ε is, for example, the ratio between the thickness of the recurrent cell and the wavelength of the deformation field. The macroscopic variables *(X, Y)* correspond to the global structure of the fields and the microscopic variable y to their local structure.

$$\Delta u_1 = U_0(X, Y, y) + \varepsilon U_1(X, Y, y) + \varepsilon^2 U_2(X, Y, y) + \dots$$
$$\Delta u_2 = V_0(X, Y, y) + \varepsilon V_1(X, Y, y) + \varepsilon^2 V_2(X, Y, y) + \dots \tag{4.3.2}$$

The coefficients C_{ij}, G_* and the initial stresses σ_1 are periodic functions of the microscopic variable y. We do not restrict the problem by assuming that the period is 1 and $\varepsilon \ll 1$.

Spatial derivatives are calculated with the following rule

$$\frac{\partial}{\partial x_1} = \frac{\partial}{\partial X}; \frac{\partial}{\partial x_2} = \frac{\partial}{\partial Y} + \frac{1}{\varepsilon}\frac{\partial}{\partial y} \tag{4.3.3}$$

The asymptotic expansion of the incremental displacement fields (4.3.2) are substituted in the equations 4.3.1. By equating the terms of order ε^{-2}, ε^{-1}, ε^{-1}, ε^{0}, to zero we obtain the following differential system for the functions U_k and V_k(k=0,1,2)

$$\frac{\partial}{\partial y}\left((G_* - \tau)\frac{\partial U_0}{\partial y}\right) = 0 \tag{4.3.4.1}$$

$$\frac{\partial}{\partial y}\left((G_* - \tau)\frac{\partial U_1}{\partial y}\right) + \frac{\partial}{\partial y}\left((G_* - \tau)\frac{\partial U_0}{\partial Y}\right) + \frac{\partial}{\partial y}\left((G_* - \sigma)\frac{\partial V_0}{\partial X}\right) + \frac{\partial}{\partial Y}\left((G_* - \tau)\frac{\partial U_0}{\partial y}\right) + \frac{\partial}{\partial y}\left(C_{12}\frac{\partial V_0}{\partial y}\right) = 0 \tag{4.3.4.2}$$

$$\frac{\partial}{\partial y}\left((G_* - \tau)\frac{\partial U_2}{\partial y}\right) + \frac{\partial}{\partial y}\left((G_* - \tau)\frac{\partial U_2}{\partial Y}\right) + \frac{\partial}{\partial y}\left((G_* - \sigma)\frac{\partial V_1}{\partial X}\right) + \frac{\partial}{\partial Y}\left((G_* - \tau)\frac{\partial U_1}{\partial y}\right) + \frac{\partial}{\partial y}\left(C_{12}\frac{\partial V_1}{\partial y}\right) + \frac{\partial}{\partial X}\left((C_{11} - \tau)\frac{\partial U_0}{\partial X}\right) + \frac{\partial}{\partial X}\left(C_{12}\frac{\partial V_2}{\partial Y}\right) + \frac{\partial}{\partial Y}\left((G_* - \tau)\frac{\partial U_0}{\partial Y}\right) + \frac{\partial}{\partial Y}\left((G_* - \sigma)\frac{\partial V_0}{\partial X}\right) = 0 \tag{4.3.4.3}$$

$$\frac{\partial}{\partial y}\left((C_{22} - \sigma_2)\frac{\partial V_0}{\partial y}\right) = 0 \tag{4.3.4.4}$$

$$\frac{\partial}{\partial y}\left((C_{22} - \sigma_2)\frac{\partial V_1}{\partial y}\right) + \frac{\partial}{\partial y}\left(C_{21}\frac{\partial U_0}{\partial X} + (C_{22} - \sigma_2)\frac{\partial V_0}{\partial Y}\right) + \frac{\partial}{\partial Y}\left((C_{22} - \sigma_2)\frac{\partial V_0}{\partial y}\right) + \frac{\partial}{\partial X}\left((G_* - \sigma)\frac{\partial U_0}{\partial y}\right) = 0 \tag{4.3.4.5}$$

$$\begin{aligned}&\frac{\partial}{\partial y}\left((C_{22}-\sigma_2)\frac{\partial V_2}{\partial y}\right)+\frac{\partial}{\partial y}\left(C_{21}\frac{\partial U_1}{\partial X}+(C_{22}-\sigma_2)\frac{\partial V_1}{\partial Y}\right)\\&\quad+\frac{\partial}{\partial Y}\left((C_{22}-\sigma_2)\frac{\partial V_1}{\partial y}\right)+\frac{\partial}{\partial X}\left((G_*-\sigma)\frac{\partial U_1}{\partial y}\right)\\&\quad+\frac{\partial}{\partial X}\left((G_*-\tau)\frac{\partial V_0}{\partial X}\right)\\&\quad+\frac{\partial}{\partial Y}\left(C_{21}\frac{\partial U_0}{\partial X}+(C_{22}-\sigma_2)\frac{\partial V_0}{\partial Y}\right)=0\end{aligned}\tag{4.2.4.6}$$

By formally assuming X, Y and y to be independent variables, we consider the relations 4.3.4.i for i=1,6 as a recurrent chain of differential equations in y with unknown functions U_k and V_k(k=0,2) ar$(G_*-\tau)\frac{\partial U_0}{\partial y}$neters X and Y.

It follows from 4.3.4.1 that $(G_*-\tau)\frac{\partial U_0}{\partial y}$ is independent of y, i.e.

$$(G_*-\tau)\frac{\partial U_0}{\partial y}=F(X,Y)\quad\text{or}\quad\frac{\partial U_0}{\partial y}=F(X,Y)/(G_*-\tau)\tag{4.3.5}$$

We adopt the following notation for the average over period:

$$\langle F(X,Y,y)\rangle=\int_0^1 F(X,Y,y)\mathrm{d}y\tag{4.3.6}$$

Since U_0 is periodic function of y, then

$$\left\langle\frac{\partial U_0}{\partial y}\right\rangle=U_0(X,Y,y)\Big|_{y=0}^{y=1}=0\tag{4.3.7}$$

If we assume (G_*−τ)>0 which is natural for the applications, this implies $F(X,Y)=0$ and consequently U_0 is independent of y, i.e.

$$U_0=U_0(X,Y)\tag{4.3.8}$$

Similarly from equation 4.3.4.4 we obtain that V_0 is independent of y.

Considering 4.3.8 we write 4.3.4.2 as

$$\frac{\partial}{\partial y}\left((G_*-\tau)\left(\frac{\partial U_1}{\partial y}+\frac{\partial U_0}{\partial Y}\right)+(G_*-\sigma)\frac{\partial V_0}{\partial X}\right)=0\tag{4.3.9}$$

This implies that

$$\begin{aligned}&(G_*-\tau)\left(\frac{\partial U_1}{\partial y}+\frac{\partial U_0}{\partial Y}\right)+(G_*-\sigma)\frac{\partial V_0}{\partial X}=A(X,Y)\\&\frac{\partial U_1}{\partial y}+\frac{\partial U_0}{\partial Y}+\frac{G_*-\sigma}{G_*-\tau}\frac{\partial V_0}{\partial X}=\frac{A(X,Y)}{G_*-\tau}\end{aligned}\tag{4.3.10}$$

By applying the averaging operator <.> we get

$$\frac{\partial U_0}{\partial Y} + \tilde{G}\frac{\partial V_0}{\partial X} = \frac{A(X,Y)}{\hat{G}} \tag{4.3.11}$$

where

$$\tilde{G} = \int_0^1 \frac{G_* - \sigma}{G_* - \tau} \mathrm{d}y \tag{4.3.12}$$

and $\hat{G}$ is the harmonic mean of $G_* - \tau$

$$\hat{G} = \left\langle \frac{1}{G_* - \tau} \right\rangle^{-1} \tag{4.3.13}$$

Notice that for $\tau/G_* \to 0$, the Reuss model for the averaged shear modulus $\hat{G}$ is recovered.

Consequently

$$\frac{\partial U_1}{\partial y} = \left(\frac{\hat{G}}{G_* - \tau)} - 1 \right) \frac{\partial U_0}{\partial Y} + \frac{\tilde{G}\hat{G} - (G_* - \sigma)}{G_* - \tau} \frac{\partial V_0}{\partial X} \tag{4.3.14}$$

hence,

$$U_1 = N_1(y)\frac{\partial U_0}{\partial Y} + N_2(y)\frac{\partial V_0}{\partial X} \tag{4.3.15}$$

where

$$N_1(y) = \int_0^y \left(\frac{\hat{G}}{G_* - \tau} - 1 \right) \mathrm{d}u;\ N_2(y) = \int_0^y \frac{\tilde{G}\hat{G} - (G_* - \sigma)}{G_* - \tau} \mathrm{d}u \tag{4.3.16}$$

In the same manner we obtain from equation 4.3.4.5

$$V_1 = N_3(y)\frac{\partial U_0}{\partial Y} + N_4(y)\frac{\partial V_0}{\partial X} \tag{4.3.17}$$

where

$$N_3(y) = \int_0^y \frac{c_1 c_2 - C_{21}}{C_{22} - \sigma_2} \mathrm{d}u;\ N_4(y) = \int_0^y \left(\frac{c_2}{C_{22} - \sigma_2} - 1 \right) \mathrm{d}u \tag{4.3.18}$$

and

$$c_1 = \left\langle \frac{C_{12}}{C_{22} - \sigma_2} \right\rangle;\ c_2 = \left\langle \frac{1}{C_{22} - \sigma_2} \right\rangle \tag{4.1.19}$$

Integrating 4.3.4.3 and 4.3.4.6 with respect to y over [0,1] and considering the periodicity of U_1, V_1 and of the constitutive coefficients, we obtain

$$f_1\frac{\partial^2 U_0}{\partial X^2}+f_2\frac{\partial^2 U_0}{\partial Y^2}+f_3\frac{\partial^2 V_0}{\partial X\,\partial Y}=0$$
$$f_4\frac{\partial^2 U_0}{\partial X\,\partial Y}+f_5\frac{\partial^2 V_0}{\partial X^2}+f_6\frac{\partial^2 V_0}{\partial Y^2}=0 \tag{4.3.20}$$

with

$$f_1=\left\langle C_{11}-\sigma_1+\frac{C_{12}}{C_{22}-\sigma_2}(c_1c_2-C_{21})\right\rangle;\ f_2=\hat{G};$$
$$f_3=\left\langle\frac{c_2C_{22}}{C_{22}-\sigma_2}\right\rangle+\tilde{G}\hat{G} \tag{4.3.21}$$
$$f_4=c_1c_2+\tilde{G}\hat{G};\ f_5=\tilde{G}^2\hat{G}+\left\langle(G_*+\tau)-\frac{(G_*-\sigma)^2}{G_*-\tau}\right\rangle;\ f_6=c_2$$

Equations 4.3.20 are the system of averaged equations and $f_j(j=1,6)$ are the effective coefficients. These equations are called the solvability conditions as it is necessary for U_0 and V_0 to satisfy equations 4.3.20 in order that the problem 4.3.4.3 (respectively 4.3.4. 6) is solvable in U_2 (respectively V_2) in the class of periodic functions of y.

U_0 and V_0 which depend only on the macroscopic variables can be viewed as the average value of the displacement field. The solvability conditions (4.3.19) are the governing differential equations for this averaged displacement field and the coefficients f_i combine the effect of material properties and of initial stress. In general, this differential system cannot be derived from direct application of equilibrium equation on some equivalent stress-strain relationships.

As an example we consider here a layered medium with zero initial stress. We obtain as a result the following constitutive coefficients for the equivalent homogeneous continuum (Biot, 1965b):

$$C_{11}=a^{(1)}C_{11}^{(1)}+a^{(2)}C_{11}^{(2)}-\frac{a^{(1)}a^{(2)}(C_{12}^{(1)}-C_{12}^{(2)})(C_{21}^{(1)}-C_{21}^{(2)})}{a^{(2)}C_{22}^{(1)}+a^{(1)}C_{22}^{(2)}}$$
$$C_{12}=\frac{a^{(2)}C_{12}^{(2)}C_{22}^{(1)}+a^{(1)}C_{12}^{(1)}C_{22}^{(2)}}{a^{(2)}C_{22}^{(1)}+a^{(1)}C_{22}^{(2)}}$$
$$C_{21}=\frac{a^{(2)}C_{21}^{(2)}C_{22}^{(1)}+a^{(1)}C_{21}^{(1)}C_{22}^{(2)}}{a^{(2)}C_{22}^{(1)}+a^{(1)}C_{22}^{(2)}} \tag{4.3.22}$$
$$C_{22}=\frac{C_{22}^{(1)}C_{22}^{(2)}}{a^{(2)}C_{22}^{(1)}+a^{(1)}C_{22}^{(2)}}$$

where superscripts (1) and (2) relate to the two different layers. The thicknesses of the layers are denoted by $h^{(i)}$, (i=1,2) as shown in Figure 4.3.1. Each of the materials

occupies a fraction $a^{(i)} = h^{(i)}/(h^{(1)} + h^{(2)})$ of the total thickness. The value of G for the homogeneous medium is then given by

$$G = 1/(a^{(1)}/G_*^{(1)} + a^{(2)}/G_*^{(2)}) \tag{4.3.23}$$

4.3.2
Example: Surface instabilities in a multilayered periodic half-space

As an example we study here the problem of surface instabilities in a multilayered periodic half-space. Let us consider a half-space composed of two types of isotropic hyperelastic materials which alternate and are repeated periodically. In particular, we use the following values for the material parameters of the layers:

$$G^{(1)} = 2G^{(2)},\ \nu^{(1)} = \nu^{(2)} = 0.3 \tag{4.3.24}$$

In regard to fractions of the total thickness occupied by each layer, we assume that

$$a^{(1)} = a^{(2)} \tag{4.3.25}$$

Another parameter to also be considered is the influence of the upper layer. There are two possibilities:

(a) the hard layer is the upper layer of the half-space, or
(b) the soft layer is the upper layer of the half-space.

In the numerical solution we assume that the prescribed strain is homogeneous in the half-space, and consequently the corresponding initial stress $\sigma_{11}^{(i)}$ is different in each layer. An average initial stress is defined by $\sigma_{11} = a^{(1)}\sigma_{11}^{(1)} + a^{(2)}\sigma_{11}^{(2)}$. Notice that the case of prescribed homogeneous stress is kinematically ill-posed since continuity of strains is violated at layer boundaries.

For the multilayered half-space, the buckling load is computed using the transfer matrix technique as presented in section 4.2.2 for the two possibilities (a) and (b) of the upper layer. The numerical results are presented in Figure 4.3.2 where the buckling load is plotted versus the modal number of the considered mode. They show that the predicted buckling loads are lower when the stiff layer is on top. If the top layer of the half-space is a soft layer then it behaves as a confining medium for the stiff layer and therefore higher loads are required for the buckling of the half-space. In the other case, the stiff layer buckles without any restriction and therefore a lower buckling load is expected. In the large wavelength limit (small wave number) the deformation mode cannot 'see' the lamination and therefore the medium behaves as a homogeneous continuum without any differentiation between stiff or soft layer on top. In the short wavelength limit (large wave number) the buckling is restricted to a narrow zone close to the free surface. In that case, the top layer behaves as a half-space and therefore the same buckling loads are expected in cases (a) and (b).

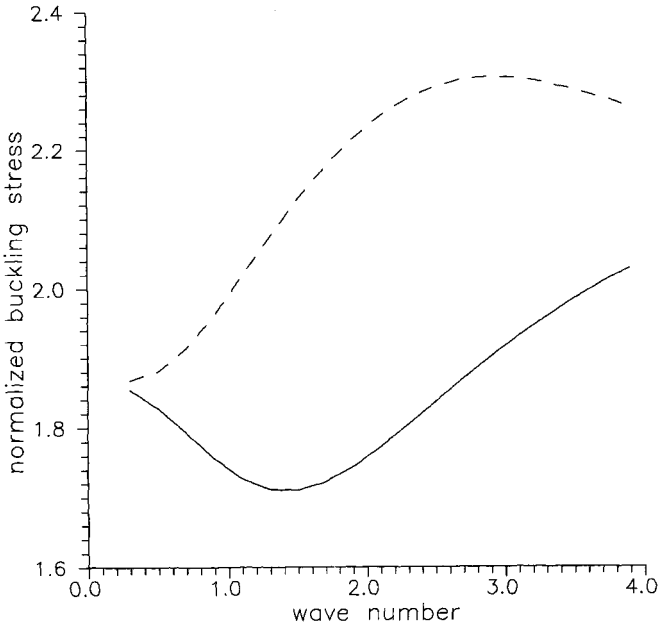

Figure 4.3.2 Buckling load of a layered half-space under homogeneous initial strain. (—) hard layer on top; (- -) soft layer on top.

The considered half-space can be represented by an equivalent homogeneous classical continuum as presented above. For the homogenized half-space the buckling condition is given by equation 4.2.6 which is already the same for all wavelengths. As we see in Figure 4.3.3 the representation of the laminated half-space is only valid for large wavelength deformation modes, i.e. when the layer thicknesses are sufficiently small with respect to the wavelength of the deformation mode. For small wavelength, the buckling load is underestimated. As we will see in the next section, the approximation can be refined by introducing higher order terms.

4.3.3
Limitations of the asymptotic averaging method

As noted above, the validity of the approximation of a laminated medium by a classical anisotropic continuum is restricted to cases where the rigidity contrasts between the layers are not too large and the layer thicknesses remain sufficiently small with respect to the wavelength dominating in the deformation field. In order to overcome these limitations, Biot (1967), Herrmann and Achenbach (1968), Mühlhaus (1985) and Mühlhaus and Vardoulakis (1986) proposed an alternative approach by representing a laminated half-space as a Cosserat medium.

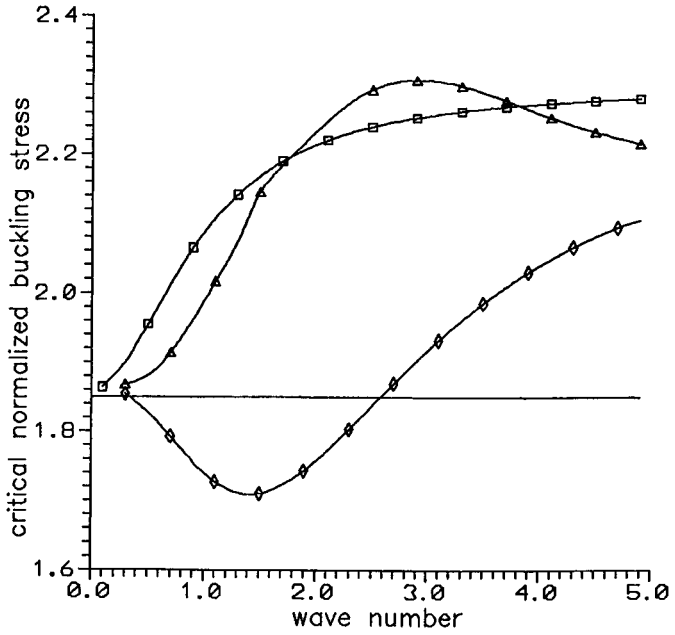

Figure 4.3.3 Buckling load of a layered half-space: layered solution and homogenization. $G^{(1)}/G^{(2)}=2$; $\upsilon^{(1)}/\upsilon^{(2)}=0.3$. (Δ) soft top layer; (◊) hard top layer; (□) Cosserat equivalent medium; (—) classical equivalent medium.

It is worth noting that by a mere mathematical averaging technique, no microstructural feature can be obtained unless it is already introduced at the microscopic level.

4.4
Elastic anisotropic Cosserat continuum

4.4.1
Basic concepts

Biot (1967) has extended his theory of folding of elastic or viscoelastic anisotropic solids under initial stress to the case of materials with bending stiffness. Bending stiffness gives rise to couple stresses, i.e. moment per unit area. As it is noted in Biot's paper, the use of couple stresses acting internally in an elastic continuum is found in implicit form in a paper by Cauchy as long ago as 1851. In that paper, the energy density is assumed to be a function of gradients of the displacements of any order. The idea of couple stress can also be traced to Voigt (1887, 1894). E. and F.Cosserat (1909) introduced explicitly the couple stresses in the analysis of a system with microelements undergoing rotations which may be different from the local rotation of the continuum.

In a Cosserat medium, each material point has three additional rotational degrees of freedom besides the three translational degrees of freedom which are considered in the classical continuum. In the present case, we will use the rotational degrees of freedom to describe the effect of bending of individual layers. Notice that the Cosserat rotations are treated here at the constitutive level as independent degrees of freedom, which are not directly related to the spin vector of the classical continuum. The structure of the resulting equations is quite similar to the equations of Reissner's theory of thick plates. Finally, it should be noted that the paper by Biot relates to a constraint Cosserat theory where the additional degree of rotation coincides with the macrorotation, that is, the antisymmetric part of the displacement gradient (Cosserat 'trièdre caché').

As mentioned in section 4.2.4, the critical buckling stress of a classical elastic half-space is independent of the wave number of the buckling mode. The Cosserat continuum theory has the advantage of allowing for an internal length to be considered in the constitutive relationships through the ratio of bending stiffness and elastic stiffness. As will be shown, incorporation of this internal length into the constitutive model results in a dependency of the critical buckling stress on the wave number.

In this section, an anisotropic elastic Cosserat continuum model for periodic layered media will be developed along the lines of a series of papers by Mühlhaus (1985, 1993) and Papamichos *et al.* (1990). In chapter 8, a Cosserat theory for elastoplastic materials will be discussed in relation to localized bifurcation in granular media.

4.4.2
The Cosserat model of a multilayered medium

In order to write constitutive relationships for a Cosserat material, we define the incremental (relative) strain tensor $\Delta\varepsilon_{ij}$. as

$$\Delta\varepsilon_{ij} = \Delta u_{i,j} - \Delta\omega^{c}_{ij} = \Delta\epsilon_{ij} + (\Delta\omega_{ij} - \Delta\omega^{c}_{ij}) \tag{4.4.1}$$

where $\Delta\varepsilon_{ij}$ and $\Delta\omega_{ij}$ are the classical infinitesimal strain and spin tensors given by equation 4.2.3. The tensor $\Delta\omega^{c}_{ij}$ is the infinitesimal Cosserat spin tensor whose components in 2D are calculated from the relation $\Delta\omega^{c}_{ij} = -e_{ij3}\Delta\omega^{c}$, where e_{ijk} is the permutation symbol. The difference $\Delta\omega_{ij} - \Delta\omega^{c}_{ij}$ can be interpreted as the infinitesimal relative rotation between an individual material point and its vicinity. Note that if this difference is zero then the incremental strain tensor $\Delta\varepsilon_{ij}$. coincides with the classical infinitesimal strain tensor $\Delta\varepsilon_{ij}$.

Generalizing the constitutive equations given by Schaefer (1962) (see also Mühlhaus, 1985; Mühlhaus and Vardoulakis, 1986; Mühlhaus and Triantafyllidis 1987; Papamichos *et al.,* 1990) we write

$$\mathring{\Delta}\sigma_{11} = C_{11}\Delta\varepsilon_{11} + C_{12}\Delta\varepsilon_{22};\ \mathring{\Delta}\sigma_{22} = C_{21}\Delta\varepsilon_{11} + C_{22}\Delta\varepsilon_{22} \tag{4.4.2}$$

$$\mathring{\Delta}\sigma_{12} = G(\Delta\varepsilon_{12} + \Delta\varepsilon_{21});\ \mathring{\Delta}\sigma_{21} = G(\Delta\varepsilon_{12} + \Delta\varepsilon_{21}) + G^c\Delta\varepsilon_{21}$$
$$\mathring{\Delta}m_1 = \tfrac{4}{12}T_1^c d_1^2 \Delta\omega_{,1}^c;\ \mathring{\Delta}m_2 = \tfrac{4}{12}T_2^c d_2^2 \Delta\omega_{,2}^c \tag{4.4.3}$$

where δm_i denotes the Jaumann increment of the moment stress vector. The moduli C_{ij} and G in equation 4.4.2 have the same significance as in a classical continuum. However, the present model also includes an additional shearing modulus G^c. The parameters d_1 and d_2 in equations 4.4.3 represent characteristic internal lengths of the layered material in the x_1 and x_2 directions, respectively, so that the moduli T_1^c and T_2^c have dimensions of stress. The internal length adds in the constitutive model information about the structure of the medium under consideration. Its order of magnitude has to be considered in every case of application with reference to an important length in the structure of the medium. In the material under consideration, δ_2 is of the order of magnitude of the layer thickness, whereas $d_1 \to 0$ since there is no 'structure' in the horizontal direction. In the following we replace $T_2^c d_2^2$ with $T^c d^c$. Then relations 4.4.3 read

$$\delta m_1 = \tfrac{4}{12}T^c d^2 \Delta\omega_{,1}^c;\ \delta m_2 = 0 \tag{4.4.4}$$

In the papers of Mühlhaus and co-authors (1985, 1986, 1987, 1990) the following relations have been derived between the moduli $G^{(1)}$ and $G^{(2)}$ of the individual layers and the Cosserat moduli G^c and T^c

$$G^c = T - G \tag{4.4.5}$$

$$T^c = \frac{Ta^{(1)}a^{(2)}}{a^{(2)}G^{(1)} + a^{(1)}G^{(2)}} \tag{4.4.6}$$

where G is given by equation 4.3.23 and

$$T = a^{(1)}G^{(1)} + a^{(2)}G^{(2)} \tag{4.4.7}$$

As we see G^c is simply the difference between the Reuss and Voigt moduli.

4.4.3
Example: Buckling of an homogeneous Cosserat half-space

The solution of this eigenvalue problem follows exactly the same methodology used in the solution for a classical material (section 4.2.2). However, since the Cosserat model includes couple stresses, we have to include the conditions for moment equilibrium:

$$\partial_1\mathring{\Delta}T_{11}^t + \partial_2\mathring{\Delta}T_{12}^t + 2\tau\partial_2\Delta\omega_{21} - (\sigma + \tau)\partial_1\Delta\varepsilon_{kk} = 0$$
$$\partial_1\mathring{\Delta}T_{21}^t + \partial_2\mathring{\Delta}T_{22}^t + 2\tau\partial_1\Delta\omega_{21} - (\sigma - \tau)\partial_2\Delta\varepsilon_{kk} = 0 \tag{4.4.8}$$
$$\partial_1\mathring{\Delta}m_1 + \partial_2\mathring{\Delta}m_2 + \mathring{\Delta}T_{21}^t - \mathring{\Delta}T_{12}^t = 0$$

Substituting the constitutive equations 4.4.3, 4.4.4 into the equilibrium equations 4.4.8, we obtain

$$
\begin{aligned}
&(C_{11} - (\sigma + \tau))\partial_{11}^2 u_1 + (G_* - \tau)\partial_{22}^2 u_1 + (C_{12} + G_* - \sigma)\partial_{12}^2 u_2 = 0 \\
&(C_{21} + G_* - \sigma)\partial_{12}^2 u_1 + (G_* + G^c + \tau)\partial_{11}^2 u_2 \\
&\qquad + (C_{22} - (\sigma - \tau))\partial_{22}^2 u_2 - G^c \partial_1 \Delta\omega^c = 0 \\
&\qquad \tfrac{1}{3} T^c d^2 \partial_{11}^2 \Delta\omega^c - G^c \Delta\omega^c + G^c \partial_1 u_2 = 0
\end{aligned}
\tag{4.4.9}
$$

Substituting the displacement field (4.2.11) in the third of equations 4.4.9 we obtain that

$$
\frac{T^c}{3G^c} d^2 \partial_{11}^2 \Delta\omega^c - \Delta\omega^c = \frac{\beta}{l} V(y)\sin(\beta x) \tag{4.4.10}
$$

From this equation $\Delta\omega^c$ can be expressed in terms of the function *V(y)*

$$
\Delta\omega^c = -\frac{\beta}{l} \frac{1}{1 + \dfrac{T^c}{3G^c}\left(\dfrac{\beta d}{l}\right)^2} V(y)\sin(\beta x) \tag{4.4.11}
$$

Considering the above expression of $\Delta\omega^c$ and substituting the displacement field (4.2.11) in the two first equations (4.4.8) we obtain the following linear homogeneous system of equations with respect to the integration constants *A* and *B*.

$$
\begin{aligned}
A[(C_{11} - (\sigma + \tau)) - Z^2(G_* - \tau)] + B[(C_{12} + G_* - \sigma)Z] = 0 \\
A[(C_{21} + G_* - \sigma)Z] + B[(C_{22} - (\sigma - \tau))Z^2 - (G_* + \tau + \xi_i)] = 0
\end{aligned}
\tag{4.4.12}
$$

where

$$
\xi_i = \frac{\dfrac{T^c}{3}\left(\dfrac{\beta d}{l}\right)^2}{1 + \dfrac{T^c}{3G^c}\left(\dfrac{\beta d}{l}\right)^2} \tag{4.4.13}
$$

For non-trivial solution in terms of *A* and *B*, the determinant of the system must vanish. This leads to the following biquadratic equation with respect to *Z*

$$
aZ^4 - b'Z^2 + c' = 0 \tag{4.4.14}
$$

where

$$
\begin{aligned}
a &= (C_{22} - (\sigma - \tau))(G_* - \tau) \\
b' &= (C_{11} - (\sigma + \tau))(C_{22} - (\sigma - \tau)) + (G_* + \tau + \xi_i)(G_* - \tau) \\
&\quad - (C_{12} + G_* - \sigma)(C_{21} + G_* - \sigma) \\
c' &= (C_{11} - (\sigma + \tau))(G_* + \tau + \xi_i)
\end{aligned}
\tag{4.4.15}
$$

Thus the equations derived from the classical continuum can be readily applied for the Cosserat continuum provided that the parameters *b* and *c* in equation 4.2.14 are replaced by *b′* and *c′* given by equations 4.4.15.

If we go back to the example of the buckling of a multilayered half-space as presented in section 4.3.2, we can compare the results obtained with the approximated Cosserat continuum to the ones obtained with the transfer matrix technique. In a Cosserat continuum, due to the existence of an internal length in the model, the buckling load depends upon the wave number of the considered mode (Figure 4.3.3). The approximated Cosserrat provides an exact solution in the large wavelength limit whereas in the short wavelength limit it provides an upper bound solution.

4.5 The effect of surface parallel Griffith cracks

In this section, a micromechanically motivated mechanism is presented, that views axial splitting and spalling in brittle materials like rock and concrete, as the result of a coupling effect between surface instabilities and surface parallel Griffith cracks. According to this mechanism, surface instabilities in a uniformly stressed half-space, produce secondary tensile stresses which, for material points close to the free surface, remain unbalanced in the direction normal to the surface. These tensile stresses cause latent, surface parallel cracks to open, and thus magnify the effect of diffuse bifurcation (see chapter 7). Tensile stress concentrations develop at the crack tips resulting in unstable crack growth and finally axial splitting and spalling of the material.

Unstable crack growth and axial splitting correspond to some critical crack surface density (distributed material damage) which manifests itself in the mean spacing of forming spalls. The fractured material becomes much weaker than the intact one due to the lower buckling stress of individual columns. Keeping this model in mind, we may consider that rock bursting, as well as borehole breakouts, are the result of buckling of flaked rock surfaces, the flaking itself being triggered by surface instabilities.

In order to investigate this mechanism, the buckling problem under plane-strain conditions due to a uniform compression of a semi-infinite medium containing surface parallel Griffith cracks is considered. Analytical solutions for these kind of problems have been presented by Keer *et al.* (1982), who solved the buckling problem in solids containing a periodic array of coplanar cracks and by Nazarenko, who considered the axisymmetric (1985) and plane-strain problem (1986). Vardoulakis and Papamichos (1991) have developed a numerical solution for solving the problems of an arbitrary number and/or geometry of surface parallel cracks in elastic, anisotropic media.

The analytical and numerical results summarized in this section are taken from Papamichos (1992). In particular, we present here an analytical solution for the single-crack problem. Furthermore, weakening of the medium due to the presence of additional periodic crack arrays is investigated and a Cosserat continuum representation of a semi-infinite medium containing periodic surface parallel crack arrays is presented. Finally, the influence of the initial stress field on crack propagation is discussed.

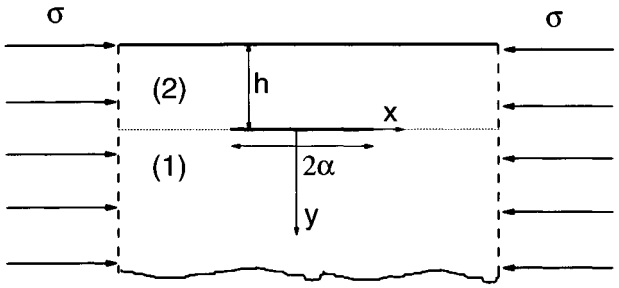

Figure 4.5.1 A half-space with a single surface parallel crack compressed by a uniform horizontal stress.

4.5.1
Analytical solution for a single crack

The problem specifically considered is shown in Figure 4.5.1, where a half-space containing a surface-parallel crack is compressed in the direction of the crack by a large uniform compression $\sigma = \sigma_{xx}$. For simplicity, the symmetric problem over the y-axis is considered and therefore only values $0 \leq x < \infty$ are taken. The boundary conditions of the problem have the form

$$\begin{aligned} &\Delta\pi_{yy} = 0,\ \Delta\pi_{xy} = 0,\ 0 \leqslant x < \alpha, \quad y = 0 \\ &\Delta\pi_{yy} = 0,\ \Delta\pi_{xy} = 0,\ 0 \leqslant x < \infty,\ y = -h \end{aligned} \tag{4.5.1}$$

The half-space is subdivided into two regions. The half-space ($y \geq 0$) is labeled (1) and the layer ($-h \leq y \leq 0$) is labeled (2). On the interface of the regions outside the crack, the following continuity conditions must be satisfied:

$$\Delta\pi_{yy}^{(1)} = \Delta\pi_{yy}^{(2)},\ \Delta\pi_{xy}^{(1)} = \Delta\pi_{xy}^{(2)},\ x > \alpha,\ y = 0 \tag{4.5.2}$$

$$u_y^{(1)} = u_y^{(2)},\ u_x^{(1)} = u_x^{(2)},\ x > \alpha,\ y = 0 \tag{4.5.3}$$

Continuity of the displacement u_x outside the crack requires that the derivative $u_{x,x}$ must also be continuous, that is

$$[u_{x,x}] = 0,\ x > \alpha,\ y = 0 \tag{4.5.4}$$

where [.] denotes the jump of the quantity across a discontinuity line. Equation 4.5.3 is valid through Maxwell's theorem which states that if a function is continuous across a geometrical discontinuity, then only the normal derivative of this function may be discontinuous across the discontinuity (see section 2.4).

Using the equilibrium equations 4.2.1, the constitutive equations 4.2.7 and the relations 4.2.4, the components of the incremental displacement vector Δu_x, $\Delta u_{y,}$ can be written in terms of two potential functions ϕ_1 and ϕ_2 as follows

$$\begin{aligned} \Delta u_x &= \phi_{1,x} + \phi_{2,x} \\ \Delta u_y &= q_1 \phi_{1,y} + q_2 \phi_{2,y} \end{aligned} \tag{4.5.5}$$

where

$$q_i = \frac{(c_{11} - 2\xi)\gamma_i - (1 + \xi)}{(c_{12} - 2\xi) + (1 - \xi)}, \quad (i = 1, 2) \tag{4.5.6}$$

and γ^2 are the two roots of the following characteristic quadratic equation in γ^2

$$\begin{aligned} (c_{11} + 2\xi)(1 - \xi)\gamma^4 + ((c_{12} + 2\xi)c_{21} + (c_{12} + 2\xi)(1 + \xi) + c_{21}(1 - \xi) \\ - (c_{11} + 2\xi)c_{22})\gamma^2 + c_{22}(1 + \xi) = 0 \end{aligned}$$

with

$$c_{ij} = C_{ij}/G_*, \; \xi = -\sigma_{xx}/2G_* \tag{4.5.8}$$

The potential functions $\phi_i(x,y)$, i=1,2, satisfy the relations

$$\phi_{i,xx} + \gamma_i^2 \phi_{i,yy} = 0 \tag{4.5.9}$$

By making the following substitution for the independent variable y

$$y_i = y/\gamma_i, \quad (i = 1, 2) \tag{4.5.10}$$

expression 4.5.9 is written

$$\phi_{i,xx} + \frac{\partial^2 \phi_i}{\partial y_i^2} = 0, \quad (i = 1, 2) \tag{4.5.11}$$

and the general solution for the displacement increments (4.5.5) becomes

$$\begin{aligned} \Delta u_x(x, y_i) &= (\phi_1 + \phi_2)_{,x} \\ \Delta u_y(x, y_i) &= \frac{q_1}{\gamma_1} \frac{\partial \phi_1}{\partial y_1} + \frac{q_2}{\gamma_2} \frac{\partial \phi_2}{\partial y_2} \end{aligned} \tag{4.5.12}$$

and for the first Piola-Kirchhoff stress increments $\Delta\pi_{ij}$

$$\Delta\pi^*_{xx}(x, y_i) = -(1+\xi)\left(\frac{1+q_1}{\gamma_1}\frac{\partial^2\phi_1}{\partial y_1^2} + \frac{1+q_2}{\gamma_2}\frac{\partial^2\phi_2}{\partial y_2^2}\right)$$

$$\Delta\pi^*_{yy}(x, y_i) = (1+q_1+(1-q_1)\xi)\frac{\partial^2\phi_1}{\partial y_1^2} + (1+q_2+(1-q_2)\xi)\frac{\partial^2\phi_2}{\partial y_2^2}$$

$$\Delta\pi^*_{xy}(x, y_i) = (1+\xi)\left(\frac{1+q_1}{\gamma_1}\frac{\partial^2\phi_1}{\partial x\,\partial y_1} + \frac{1+q_2}{\gamma_2}\frac{\partial^2\phi_2}{\partial x\,\partial y_2}\right) \tag{4.5.13}$$

$$\Delta\pi^*_{yx}(x, y_i) = (1+q_1+(1-q_1)\xi)\frac{1}{\gamma_1}\frac{\partial^2\phi_1}{\partial x\,\partial y_1} + (1+q_2+(1-q_2)\xi)\frac{1}{\gamma_2}\frac{\partial^2\phi_2}{\partial x\,\partial y_2}$$

where

$$\Delta\pi^*_{ij} = \Delta\pi_{ij}/G_* \tag{4.5.14}$$

By taking into account the boundary conditions (4.5.1) and expression 4.5.11, the continuity conditions 4.5.2 and 4.5.3 are written in terms of the potential functions ϕ_1, ϕ_2 as follows

$$(1+q_1+(1-q_1)\xi)\frac{\partial^2[\phi_1]}{\partial y_1^2} + (1+q_2+(1-q_2)\xi)\frac{\partial^2[\phi_2]}{\partial y_2^2} = 0, \quad 0 \leqslant x < \infty,\ y_i = 0 \tag{4.5.15}$$

$$\frac{1+q_1}{\gamma_1}\frac{\partial^2[\phi_1]}{\partial x\,\partial y_1} + \frac{1+q_2}{\gamma_2}\frac{\partial^2[\phi_2]}{\partial x\,\partial y_2} = 0, \quad 0 \leqslant x < \infty,\ y_i = 0$$

$$\frac{q_1}{\gamma_1}\frac{\partial[\phi_1]}{\partial y_1} + \frac{q_2}{\gamma_2}\frac{\partial[\phi_2]}{\partial y_2} = 0, \quad x > \alpha,\ y_i = 0 \tag{4.5.16}$$

$$[\phi_1]_{,x} + [\phi_2]_{,x} = 0, \quad x > \alpha,\ y_i = 0$$

Accordingly, condition 4.5.4 is written

$$-\frac{\partial^2[\phi_1]}{\partial y_1^2} - \frac{\partial^2[\phi_2]}{\partial y_2^2} = 0, \quad x > \alpha,\ y_i = 0 \tag{4.5.17}$$

This condition yields an additional requirement. By differentiating and integrating expression 4.5.12 with respect to x and using equation 4.5.11, the displacement increment $\Delta u_x^{(i)}$, $i = 1, 2$, at $y_i = 0$ can be written in the form

$$\Delta u_x^{(i)}(x, 0) = -\int_0^x \left\{\frac{\partial^2\phi_1^{(i)}}{\partial y_1^2} + \frac{\partial^2\phi_2^{(i)}}{\partial y_2^2}\right\} dx, \quad (i = 1, 2) \tag{4.5.18}$$

Then the jump $[\Delta u_x(x, 0)]$ can be written as

$$[\Delta u_x^{(i)}(x,0)] = -\int_0^{\alpha}\left\{\frac{\partial^2\phi_1^{(i)}}{\partial y_1^2}+\frac{\partial^2\phi_2^{(i)}}{\partial y_2^2}\right\}dx - \int_{\alpha}^{x}\left\{\frac{\partial^2\phi_1^{(i)}}{\partial y_1^2}+\frac{\partial^2\phi_2^{(i)}}{\partial y_2^2}\right\}dx \tag{4.5.19}$$

For $x>\alpha$ the second of conditions 4.5.3 requires that $\Delta u_x(x,0)=0$ while the second integral in equation 4.5.19 is equal to zero by virtue of condition 4.5.17. With this, equation 4.5.19 yields the following additional requirement for the functions $[\phi_1]$, $[\phi_2]$ at $y_i=0$

$$-\int_0^{\alpha}\left\{\frac{\partial^2\phi_1^{(i)}}{\partial y_1^2}+\frac{\partial^2\phi_2^{(i)}}{\partial y_2^2}\right\}dx = 0 \tag{4.5.20}$$

By representing the harmonic functions ϕ_1, ϕ_2 in the form of Fourier integral cosine expansions in the x-coordinate and changing to a dimensionless form, the system of equations 4.5.15, 4.5.16 and 4.5.20 is transformed to the following system of singular integral equations

$$\int_0^1 M_1(\eta,\tau)f(\tau)d\tau + \ln(1-\eta^2)\int_0^1 f(\tau)d\tau - \int_0^1 \ln|\eta^2-\tau^2|f(\tau)d\tau + \int_0^1 N_1(\eta,\tau)g(\tau)d\tau = 0$$

$$\int_0^1 M_2(\eta,\tau)f(\tau)d\tau + \int_0^1 N_2(\eta,\tau)g(\tau)d\tau - \int_0^1 \ln|\eta^2-\tau^2|g(\tau)d\tau - \text{const.} = 0$$

$$\int_0^1 g(\tau)d\tau = 0; \quad 0 \leqslant \eta < 1$$

where f (τ), g(τ) are unknown functions continuous along with their derivatives in the closed interval [0, 1]. The derivation of the above system of integral equations, together with expressions for kernels M_1, M_2 and N_1, N_2 are presented in the paper of Vardoulakis and Papamichos (1991).

Thus, the problem reduces to the investigation of eigenvalues of the system of equations 4.5.21 relative to the dimensionless initial stress parameter $\xi = -\sigma_{xx}/2G_*$. The parameter ξ appears implicitly in the kernels M_1, M_2, N_1, N_2. These equations contain expressions with the logarithmic singularity $\ln|\eta^2-\tau^2|$ in the domain of interest. This singularity is overcome by approximating the unknown functions f(τ), g(τ) by power series of the form

$$\begin{aligned} f(\tau) &= a_0 + a_1\tau + a_2\tau^2 + \ldots + a_N\tau^N \\ g(\tau) &= b_0 + b_1\tau + b_2\tau^2 + \ldots + b_N\tau^N \end{aligned} \tag{4.5.22}$$

By using these expressions, the singular integrals in 4.3.21 can be computed analytically.

Because of the complexity of the kernels M_1, M_2 and N_1, N_2 the integral equations are treated numerically by reducing them to a system of homogeneous algebraic equations

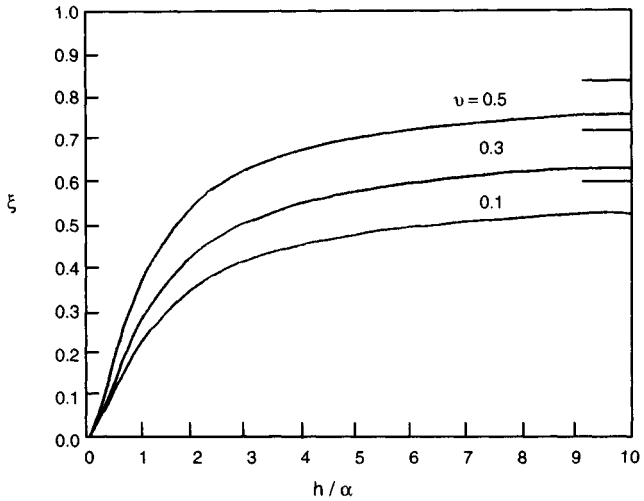

Figure 4.5.2 Critical buckling stress of the half-space with a single crack (analytical solution, υ=0.3).

in terms of the power series constants a_N, b_N and the integration constant appearing in the second of equation 4.5.21, using Gauss formulae of numerical integration. The collocation points used in computing the integral equations with respect to η are taken to be the same as the Gaussian points used in the integration scheme. In this system of equations, if the unknowns are to represent a non-trivial solution, then the matrix formed by the coefficients must have a vanishing determinant. This is achieved by fixing the material parameters and the geometry and varying the initial stress parameter ξ until the determinant becomes zero.

This analysis is used to calculate the critical buckling stress in an isotropic compressible material with shear modulus G and Poisson's ratio υ. The results are presented in Figure 4.5.2, where the dimensionless critical buckling stress ξ is plotted as a function of the geometric parameter $\beta = h/\alpha$, for three values of Poisson's ratio. For $\beta \rightarrow \infty$, the value of the buckling stress approaches asymptotically the buckling stress of the uncracked half-space (see section 4.2.3), which is also marked in the diagram. This diagram shows that the buckling stress is an increasing function of the parameter β and the Poisson's ratio υ.

4.5.2
Buckling of a half-space with a periodic array of coplanar cracks

We consider here the buckling problem of a half-space containing a periodic array of coplanar cracks and compare it with the analytical solution of Keer *et al.* (1982). A numerical solution for the eigendisplacements of the two crack faces and the free surface can be computed for the problem under consideration. The deformed shape of

the crack and the free surface for three values of the parameter β, is shown in Figure 4.5.3. At each point along the crack, the relative displacements between the two faces are the eigendisplacement discontinuities of the crack. It is shown that the two sides of the crack deform by different amounts and, as expected, the disturbed region of the free surface localizes with the crack approaching the free surface.

For the problem of the periodic crack array (Figure 4.5.4), the infinitely extended crack array is approximated here with ten 25-element cracks. Such an approximation is considered satisfactory since it was found that an increase in the number of cracks does not affect significantly the results. The results are presented in Figure 4.5.5, where the critical buckling stress parameter ξ is plotted as a function of the dimensionless depth with respect to the spacing between the cracks h/L, and the dimensionless crack length with respect to the spacing α/L. Poisson's ratio has the value of 0.3 in all calculations. This is the solution for the first bifurcation mode which is antisymmetric and corresponds to cracks tending to open and close alternately, as shown in Figure 4.5.5(a). The numerical results of the advanced solution for the symmetric mode of all open cracks are shown in Figure 4.5.5(b).

In order to investigate the differences between the first alternate mode and the advanced all open mode, the critical buckling stress parameter ξ is replotted in Figure 4.5.6 as a function of the dimensionless depth with respect to the spacing h/L, and the dimensionless depth with respect to the crack length h/α. Figure 4.5.6(a) shows that the critical stress is an increasing function of the spacing between the cracks and therefore, for the alternate mode, lower stress is required to buckle the medium when the spacing between the cracks diminishes. However, in Figure 4.5.6(b), an opposite behavior is predicted. The critical stress is a decreasing function of the spacing, meaning that higher stress is required to open all the cracks when the spacing diminishes.

Once the periodic crack array problem is solved, additional crack arrays are placed in the half-space, in the sense shown in Figure 4.5.7(a), in order to investigate the weakening of the medium due to the presence of the additional crack arrays. The crack arrays were approximated with ten 20-element cracks. In the results shown in Table 4.5.1, the ratio α/L is kept equal to 0.5, while the parameter β takes values from 0.5 to 5. They correspond to the lowest buckling mode. It is found that the second crack array reduces the critical buckling stress by approximately 6 per cent, while the third array reduces it by an additional 1.5 per cent. This means that the buckling load is mainly determined by the cracks closer to the free surface. Furthermore, the eigendisplacements at the critical state show that the buckling of the half-space affects primarily the crack array closer to the free surface, suggesting a progressive spalling behavior that starts close to the free surface and subsequently progresses deeper into the material. This spalling advancement was observed experimentally for example in Berea sandstone specimens tested in the surface instability detection apparatus, as discussed by Papamichos (1992).

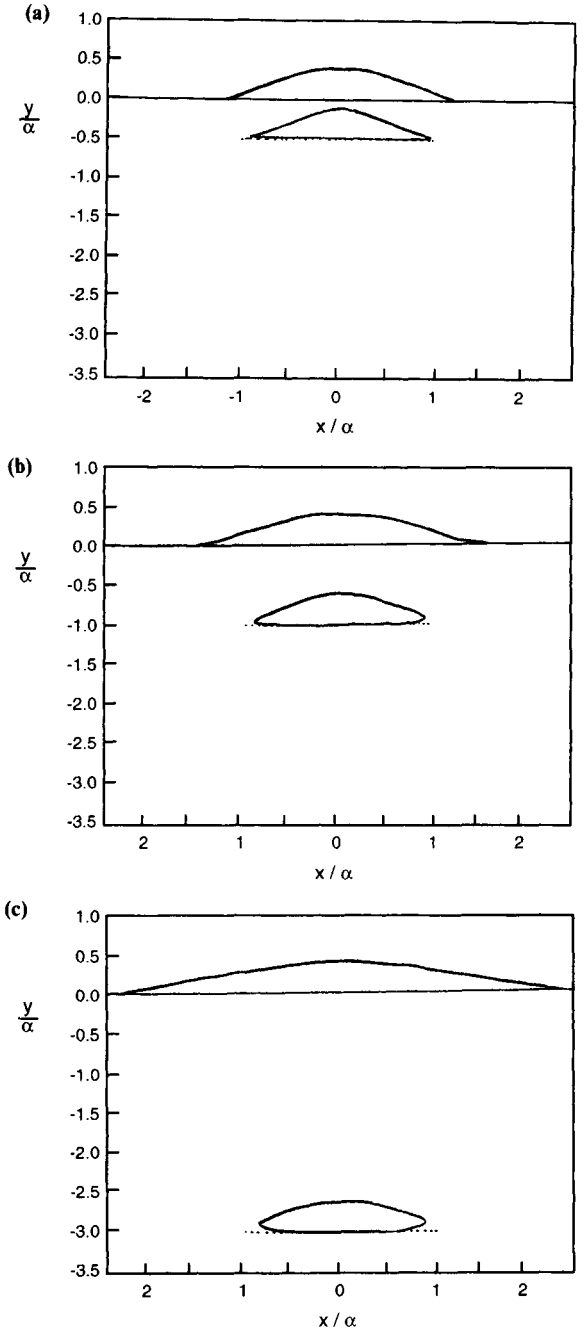

Figure 4.5.3 Deformed shape of the crack and the free surface due to buckling of the half-space, for (a) β=0.5, (b) β=1.0, and (c) β=3.0 (boundary element solution, υ=0.3).

4.5.3
A Cosserat continuum representation

In an attempt to combine micromechanical processes with continuum modeling, the

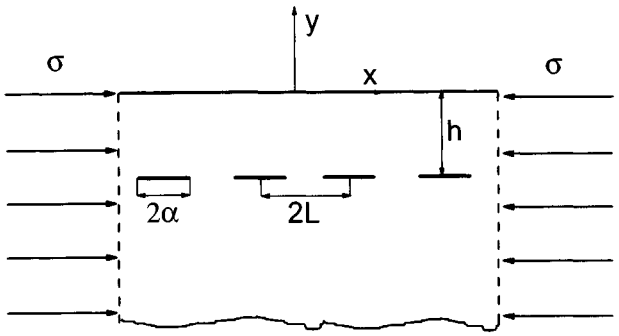

Figure 4.5.4 Half-space with periodic array of colinear cracks compressed by uniform horizontal stress.

effect of microcracks in the medium is viewed as a degradation of the elastic moduli. Based on this hypothesis, a Cosserat continuum model is constructed, using appropriate homogenization techniques (see section 4.4) and the critical buckling stress is compared with the numerical solution for a half-space containing periodic surface-parallel crack arrays.

The Cosserat continuum approach is based on the supposition that the generation of axial microcracks will markedly reduce the shear modulus of the rock, so that it behaves much as a multilayer of interbedded stiff and soft layers. Figure 4.5.7 depicts the original medium with the surface-parallel crack arrays and the corresponding periodic multilayered medium. Superscripts (1) and (2) denote quantities referred to the stiff and soft layer, respectively. The stiff layers are assumed to have the shear modulus of the intact material, $G^{(1)}=G$, while the soft layers have a reduced shear modulus $G^{(2)}=\lambda G$, depending on the extent of the damage, that is, the crack density in the medium. The crack density is expressed through the damage parameter λ, taken equal to $h/(h+2\alpha)$, with h being the distance between the crack arrays and 2α being the crack length. Furthermore, it is assumed that the stiff layer occupies a fraction $a^{(1)}=\lambda$ of the total thickness, while the soft layer occupies a fraction $a^{(2)}=1-\lambda$, such that $a^{(1)}+a^{(2)}=1$.

In the limiting case where the crack arrays approach the free surface ($h/\alpha\to 0$), the stiff layer vanishes ($a^{(1)}\to 0$), while the shear modulus of the soft layer reduces to zero ($G^{(2)}\to 0$). Such a medium has a zero buckling stress (Figure 4.5.5) satisfying the model's requirement at this limit. In the other limiting case where the crack arrays are far away from the surface ($h/\alpha\to\infty$), the soft layer vanishes ($a^{(2)}\to 0$), and the medium has the buckling stress of the half-space, satisfying the requirement at this limit as well.

The above-constructed multilayered medium is subsequently represented as a continuum with Cosserat structure. Using the Cosserat continuum, the critical buckling stress parameter $\xi=\sigma_{xx}/2G$ is calculated as a function of the distance h between the crack arrays, and the crack length α, where all of lengths are non-dimensionalized with the crack spacing L. The crack spacing in the Cosserat continuum is introduced by considering velocity fields with wavelength $2L$, such that the velocity fields have the

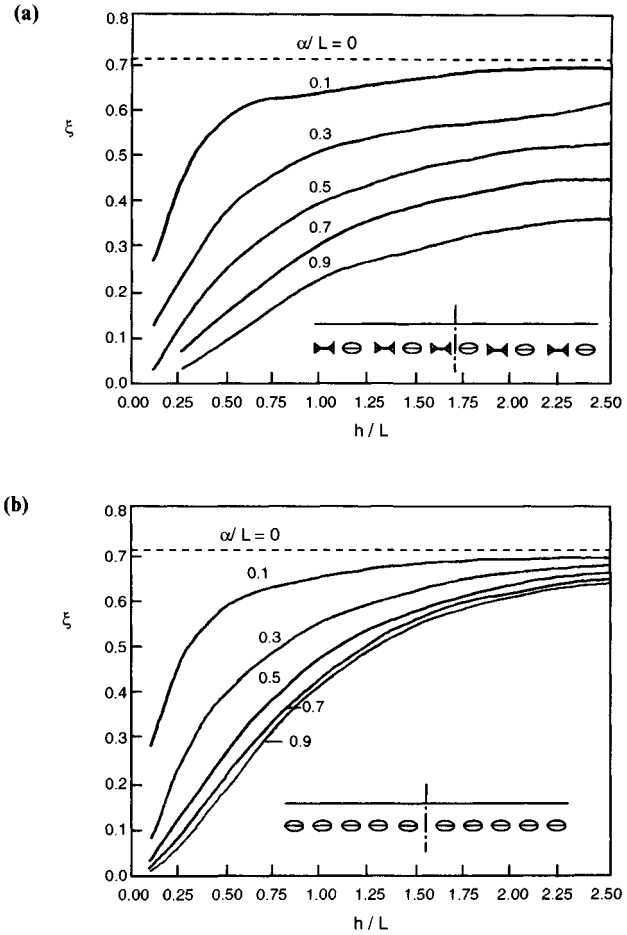

Figure 4.5.5 Critical buckling stress of a half-space with a periodic array of colinear cracks, for the (a) alternate open mode, (b) all open mode (boundary element solution, υ=0.3).

same wavelength in both media. Poisson's ratio has the value υ=0.3 in all calculations. The results from the numerical model and Cosserat continuum representation are presented in Figure 4.5.8. It is shown that the critical buckling stress decreases as the crack arrays approach the free surface ($h/L \rightarrow 0$) and as the crack spacing diminishes ($\alpha/L \rightarrow 1$). There is good agreement between the micromechanical and continuum results, especially when the crack length approaches the crack spacing ($\alpha/L \simeq 0.5$).

In conclusion, this analysis showed that continua with internal structure, such as the Cosserat continuum, in conjunction with appropriate homogenization techniques, are capable of capturing microstructural damage in the material.

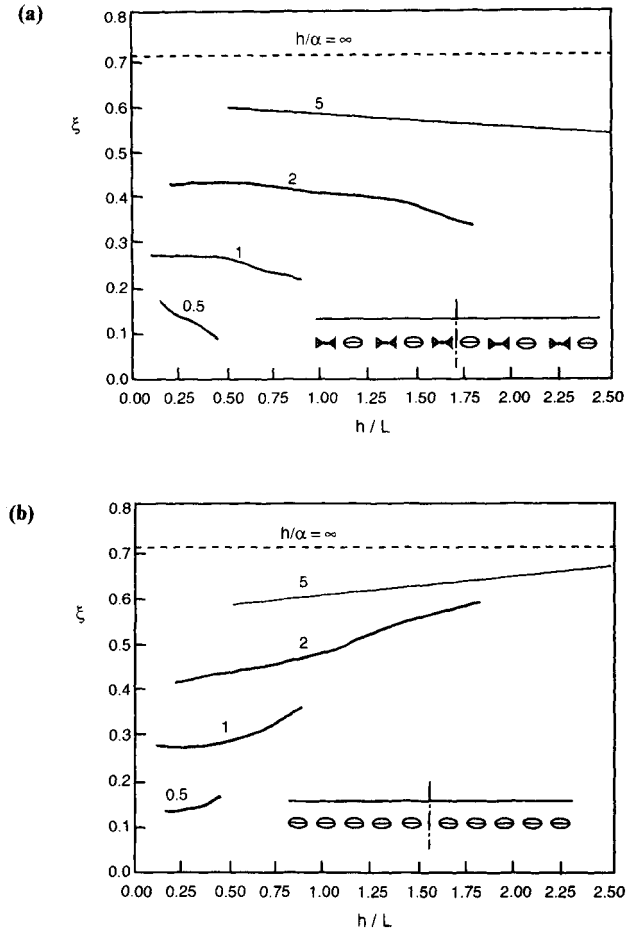

Figure 4.5.6 Critical buckling stress of a half-space with a periodic array of colinear cracks, for the (a) alternate open mode, (b) all open mode (boundary element solution, υ=0.3).

4.5.4
Influence of the initial stress field on crack propagation

An aspect of great significance in this micromechanical study is the investigation of crack propagation at the critical buckling state. In that respect, Biot (1972) indicated that in an infinite medium, the resistance to crack propagation is diminished when the condition corresponding to surface instability is approached. Papamichos and Vardoulakis (1989) have developed a numerical procedure that enables the analysis of crack propagation in anisotropic semi-infinite media by taking into account the non-linear influence of the initial stress field. In particular, effective stress intensity factors are calculated by applying a virtual internal pressure inside the cracks and calculating the energy release when a crack of length 2α is extended to a length $2(\alpha+\Delta\alpha)$.

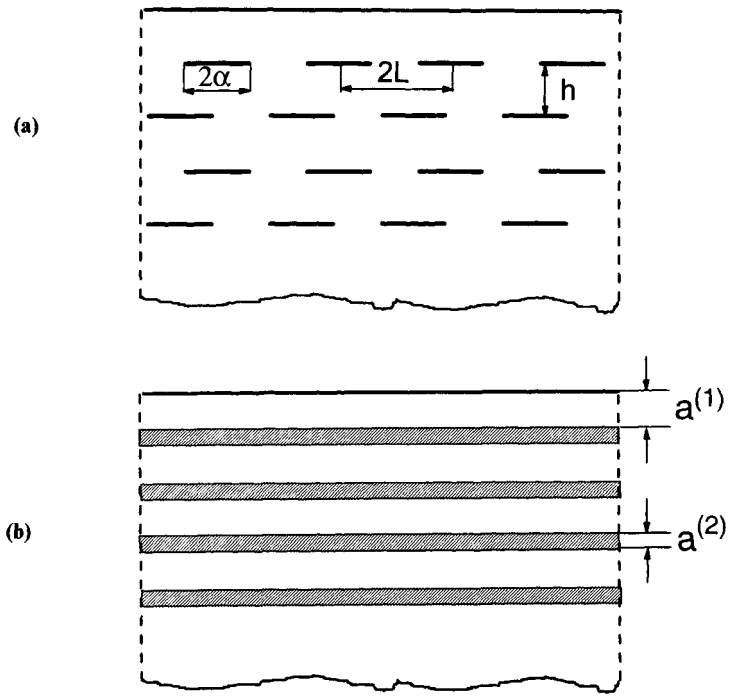

Figure 4.5.7 (a) Half-space with multiple periodic arrays of surface-parallel cracks; (b) corresponding periodic multilayered medium.

Table 4.5.1 Critical buckling stress of a half-space with multiple periodic arrays of colinear cracks (boundary element solution, $\alpha/L = 0.5$, $\nu = 0.3$)

h/α	$\xi = -\sigma_{xx}/2G$				
	1 array	2 arrays	3 arrays	4 arrays	5 arrays
0.5	0.133	0.125	0.123	0.121	0.119
1.0	0.267	0.246	0.242	0.240	0.239
2.0	0.399	0.375	0.367	0.365	0.363
5.0	0.529	0.506	0.498	0.495	0.493

The theory of linear elastic fracture mechanics is based, in part, upon the fact that the magnitude of stresses anywhere near the end of a Griffith crack are approximately proportional to the stress intensity factors (Kanninen and Popelar, 1985). The stress intensity factors are a function of the crack length and the distribution and magnitude of the boundary loads. The contention is that a fracture will propagate when the stress intensity equals a material property called the fracture toughness K_{IC}. The fracture toughness in general will be a function of the initial stress field. However, it is assumed that it remains always finite.

In order to investigate the influence of the initial stress field on crack propagation, a half-space containing a single coplanar crack of length 2α at depth $y = -h$ beneath the

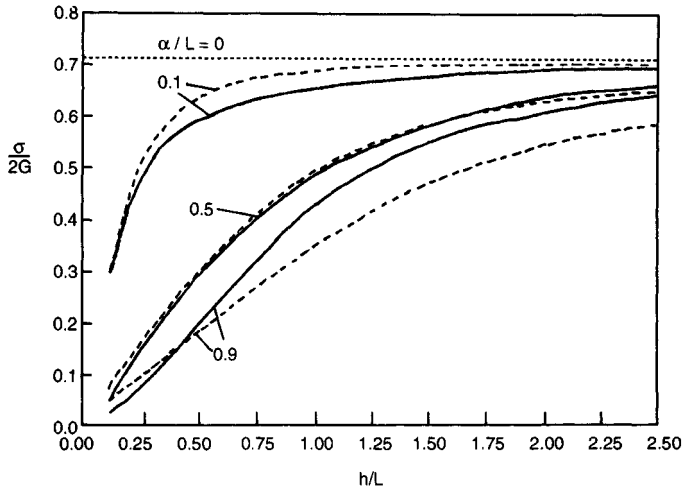

Figure 4.5.8 Critical buckling stress for a half-space with periodic arrays of colinear cracks. The solid line represents the numerical solution and the dashed line the Cosserat continuum solution.

surface, is considered. The half-space is compressed by an initial uniform horizontal stress $\sigma = -\sigma_{xx}$, and the crack is pressurized by a uniform internal pressure $-p(p>0)$.

A boundary element method for solution of crack problems in semi-infinite anisotropic media under initial horizontal stress is presented in the paper of Vardoulakis and Papamichos (1991). It is used to estimate the stress intensity factors at the crack tips. In this problem, the boundary conditions along the crack are written as

$$\Delta\pi_{xy} = 0,\ |x| < \alpha,\ y = -h$$

$$\Delta\pi_{yy} = -p,\ |x| < \alpha,\ y = -h$$

The numerical solution is represented as follows

$$\left.\begin{aligned} \Delta\pi^i_{xy} = 0 &= \sum_{j=1}^{N} A^{ij}_{xx} D^j_x + \sum_{j=1}^{N} A^{ij}_{xy} D^j_y \\ \Delta\pi^i_{yy} = -p &= \sum_{j=1}^{N} A^{ij}_{yx} D^j_x + \sum_{j=1}^{N} A^{ij}_{yy} D^j_y \end{aligned}\right\} i = 1 \text{ to } N \tag{4.5.24}$$

The above system of $2N$ simultaneous, linear equations is then solved for the unknown displacement discontinuities D^j_x and D^j_y.

A way of estimating stress intensity factors derives from the strain energy associated with the crack. For the pressurized crack problem, the strain energy for one-half crack is

$$W = -\tfrac{1}{2}p \int_0^{\alpha} \hat{u}_y(x)\mathrm{d}x = -\tfrac{1}{2}p \sum_{j=1}^{N} b^j D^j_y \tag{4.5.25}$$

where $\hat{u}_y$ is the relative normal displacement between the crack surfaces, and b^j is one-half the width of jth boundary segment.

Linear elastic fracture mechanics solutions which do not usually take into account the initial stress field give a standard relationship between the strain energy rate $\partial W/\partial\alpha$ and the stress intensity factor K. A derivation of this relationship is given, for example, by Kanninen and Popelar (1985). For the initially stressed media under consideration, the corresponding relationship can be derived by following the same procedure

$$\frac{\partial W}{\partial \alpha} = \frac{\pi(q_1 - q_2)/(\delta_1 - \delta_2)}{2G} K^2 \tag{4.5.26}$$

where q_i (i=1, 2) is given by equation 4.5.6 and

$$\delta_1 = \gamma_1(1 + q_1 + (1 - q_1)\xi)(1 + q_2),\ \delta_2 = \gamma_2(1 + q_2 + (1 - q_2)\xi)(1 + q_1) \tag{4.5.27}$$

For the case of an isotropic material and zero initial stress ($\xi = 0$), the term $(q_1-q_2)/(\delta_1 -\delta_2)$ in expression 4.5.26 reduces to $(1-\upsilon)$ (Rice, 1968; Kanninen and Popelar, 1985). By computing W for slightly different crack lengths, $\partial W/\partial\alpha$ can be estimated numerically as

$$\frac{\partial W}{\partial \alpha} = \frac{W(\alpha) - W(\alpha - \Delta\alpha)}{\Delta\alpha} \tag{4.5.28}$$

and equation 4.5.26 can be solved for the stress intensity factor K. The stress intensity factor K in expression 4.5.26 has to be interpreted as an effective stress intensity factor combining the magnitudes of both K_{I}, the mode I factor related to opening of the crack facets, and K_{II}, the mode II factor related to shear in the plane of the crack, $K^2 = K_{\mathrm{I}}^2 + K_{\mathrm{II}}^2$. In the results presented in the following, the factor K_∞ is used to normalize all stress intensity factors. K_∞ is the stress intensity factor corresponding to the case of pressurized crack in an infinite medium. In that case

$$K = K_\infty = K_{\mathrm{I}} = p\sqrt{\alpha},\ K_{\mathrm{II}} = 0 \tag{4.5.29}$$

Results obtained from this analysis are presented in Figure 4.5.9, where the normalized stress intensity factor K/K_∞ is plotted as a function of the initial stress parameter $\xi = -\sigma_{xx}/2G$, for three $h/\alpha = 1$. For $\xi = 0$, the analytical value of $K/K_\infty = 1.4968$ (Erdogan *et al.,* 1973) is marked in the diagram, together with the critical initial stress values for buckling of the half-space as predicted in section 4.2. The influence of the relative to the crack length depth, h/α, has been investigated by Pollard and Holzhausen (1979) for half-spaces without initial stress field ($\xi = 0$). Similar results are predicted for the initially stressed media.

Figure 4.5.9 shows that the resistance to crack propagation is diminished as the critical stress for surface instability is approached. The effective stress intensity factor increases rapidly near the surface instability condition. Furthermore, as has been shown by Pollard and Holzhausen, the effective factor K contains a non-zero mode II stress intensity factor K_{II}, which increases sharply as the crack approaches the free surface. This suggests that the propagation of a shallow crack will occur out of the original plane

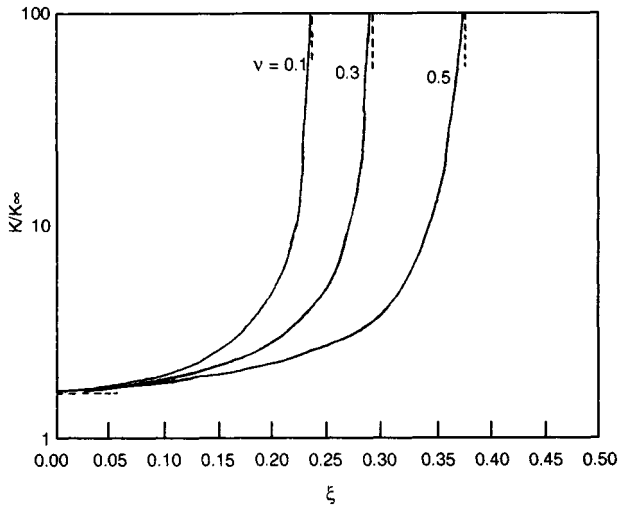

Figure 4.5.9 Stress intensity factor at the tips of a pressurized crack in a half-space under uniform horizontal compression.

of the crack and towards the free surface forming the echelon patterns observed by Ewy and Cook (1990a,b).

4.6
Concluding remarks and discussion

The present analysis shows that in elastic, semi-infinite media containing surface parallel Griffith cracks, the resistance to crack propagation is diminished as the critical stress for surface instability is approached. In particular, the effective stress intensity factor increases rapidly near the surface instability condition and therefore we may assume that any crack at this stress level will propagate. Furthermore, it is shown that the critical buckling stress of the media under consideration decreases rapidly with increases relative to the depth and length of the cracks. This suggests that in the case of a constant far-field stress (e.g. load control conditions in a laboratory setting), cracks close to the free surface will tend to become unstable once they begin to grow, leading to spalling of the surface. For a stable crack growth, a reduction in the value of the far-field stress will be necessary (e.g. displacement control conditions). Thus, a material with surface parallel cracks could be modeled as a softening material with respect to the crack length and spacing.

Literature

Textbooks and monographs

Abramowitz, M. and Stegun, I.A. (1965). *Handbook of Mathematical Functions.* Dover Publications, New York.

Bakhvalov, N. and Panasenko, G. (1989). *Homogenisation: Averaging Processes in Periodic Media.* Kluwer Academic Publishers, Dordrecht.

Biot, M.A. (1965b). *Mechanics of Incremental Deformations.* Wiley, New York.

Cosserat, E. and F. (1909). *Théorie des Corps Déformables,* A.Hermann et Fils, Paris.

Hadamard, J. (1903). *Leçons sur la propagation des ondes et les equations de l'hydrodynamique.* Hermann, Paris.

Kanninen, M.F. and Popelar, C.H. (1985). *Advanced Fracture Mechanics.* Oxford University Press, New York.

Papamichos, E. (1992). Surface Instability and Fracture: Theory and Experiment. PhD Thesis, University of Minnesota, 213 pp.

Ramsay, J.G. (1967). *Folding and Fracturing of Rocks.* McGraw-Hill, New York.

Truesdell, C. and Toupin, R.A. (1960). *Classical Field Theories of Mechanics. Handbook of Physics* III/1. Springer-Verlag, Berlin.

References

Benallal, A., Billardon, R. and Geymonat, G. (1990). Phénomènes de localisation a la frontière d'un solide. *C.R. Acad. Sci.,* Paris, **310,** série II, 670–684.

Bigoni, D. (1994). Private communication.

Bijlaard, P.P. (1947). On the elastic stability of thin plates supported by a continuous medium. *Koninkl Nederlandse Akad. Wetensch. Proc.,* **50**(1,2), 79–193.

Biot, M.A. (1957). Folding instability of a layered viscoelastic medium under compression. *Proc. Roy. Soc. London,* Ser. A., **242,** 444–454.

Biot, M.A. (1959a). Folding of a layered viscoelastic medium derived from an exact stability theory of a continuum under initial stress. *Appl. Math. Quart.,* **17**(2), 185–204.

Biot, M.A. (1959b). On the instability and folding deformation of a layered viscoelastic medium in compression. *J. Appl Mech.,* Ser. E, **26,** 393–400.

Biot, M.A. (1959c). The influence of gravity on the folding of a layered viscoelastic medium under compression. *J. Franklin Inst.,* **267**(3), 211–228.

Biot, M.A. (1965a). Theory of viscous buckling and gravity instability of multilayers with large deformations. *Bull. Geol. Soc. Am.,* **76,** 371–378.

Biot, M.A. (1967). Rheological stability with couple stresses and its application to geological folding. *Proc. Roy. Soc. London,* **A2298,** 402–423.

Biot, M.A. (1972). Non-linear effect of initial stress on crack propagation between similar and dissimilar orthotropic media. *Quart. Appl. Math.,* **30**(3) 379–406.

Biot, M.A., Odé, H. and Roever, W.L. (1961). Experimental verification of the theory of folding of stratified viscoelastic media. *Geol. Soc. Am. Bull.,* **72,** 1621–1632.

Bufler, H. (1965). Die Drucksstabilität rechteckiger Verbundplatten. *Ingenieur Archiv,* **34,** 109–128.

Chapple, W.M. (1968). A mathematical theory of finite amplitude folding. *Bull. Geol. Soc. Am.,* **79,** 47–68.

Cobbold, P.R., Cosgrove, J.W. and Summers, J.M. (1971). Development of internal structures in deformed anisotropic rocks. *Tectonophysics,* **11,** 329–375.

Dorris, J.F. and Nemat-Nasser, S. (1980). Instability of a layer on a half-space. *J. Appl Mech.,* 47, 304–312.

Erdogan, F., Gupta, G.D. and Cook, T.S. (1973). Numerical solutions of singular integral equations. In *Mechanics of Fracture 1, Methods of Analysis and Solutions of Crack Problems* (G.C.Sih, ed.), 368–425. Noordhoff International, Leyden.

Ewy, R.T. and Cook, N.G.W. (1990a). Deformation and fracture around cylindrical openings in rock. I. Observations and analysis of deformations. *Int. J. Rock Mech. Min. Sci. Geomech. Abstr.,* **27**(5), 387–407.

Ewy, R.T. and Cook, N.G.W. (1990b). Deformation and fracture around cylindrical openings in rock. II. Initiation, growth and interaction of fractures. *Int. J. Rock Mech. Min. Sci. Geomech. Abstr.,* **27**(5), 409–427.

Gough, G.S., Elam, C.F. and DeBruyne, N.A. (1940). The stabilization of a thin sheet by a continuous supporting medium. *J. Roy. Aero. Soc.,* **44,** 12–43.

Herrmann, G. and Achenbach, J.D. (1968). Applications of theories of generalized Cosserat continua to the dynamics of composite materials. *Proc. IUTAM Symp. Mechanics of Generalized Continua* (E.Kröner, ed.), 69–79. Springer-Verlag, Berlin.

Keer, L.M., Nemat-Nasser, S. and Oranratnachai, A. (1982). Surface instability and splitting in compressed brittle elastic solids containing crack arrays. *J. Appl. Mech.,* **49,** 761–767.

Martinod, J. and Davy, P. (1992). Periodic instabilities during compression or extension of the lithosphere. 1. Deformation modes from an analytical perturbation method. *J. Geophys. Res.,* **97,** 1999–2014.

Mühlhaus, H.B. (1985). Oberflächen-Instabilität bei geschichtetem Halbraum mit Biegesteifigkeit. *Ingenieur-Archiv,* **55,** 388–395.

Mühlhaus, H.B. (1990). Stress and couple stress in a layered half plane with surface loading. *Int. J. Num. Anal Geomech.,* **14,** 545–563.

Mühlhaus, H.B. (1993). Continuum models for layered and blocky rock. *Comprehensive Rock Eng.* (J.Hudson, ed.), **2,** 209–230.

Mühlhaus, H.B. and Vardoulakis, I. (1986). Axially-symmetric buckling of the surface of a laminated half-space with bending stiffness. *Mech. Materials,* **5,** 109–120.

Mühlhaus, H.B. and Triantafyllidis, N. (1987). Surface waves in a layered half-space with bending stiffness. *Dev. Geoth. End.* (A.S.Cakmak, ed.), **44,** 277–290. Elsevier and CMP, Amsterdam.

Nazarenko, V.M. (1985). Mutual effect of a circular surface crack and a free boundary in an axisymmetric problem of the fracture of an incompressible half-space in compression along the crack plane. *Soviet Appl. Mech.,* **21**(2), 133–138. The Faraday Press, New York.

Nazarenko, V.M. (1986). Theory of fracture of materials in compression along near surface cracks under plane-strain conditions. *Soviet Appl. Mech.,* **22**(12), 1192–1199. The Faraday Press, New York.

Papamichos, E. and Vardoulakis, I. (1989). The coupling effect of surface instabilities and surface parallel Griffith cracks in rocks. *Proc. Int. Symp. Rock Mech. Rock Physics at Great Depth, Pau, France* (V.Maury and D.Fourmaintraux, eds), Vol. 1, 481–487.

Papamichos, E., Vardoulakis, I. and Mühlhaus, H.B. (1990). Buckling of layered elastic media: A Cosserat continuum approach and its validation. *Int. J. Num. Anal. Mech. Geomech.,* **14,** 473–498.

Pollard, D.D. and Holzhausen, G. (1979). On the mechanical interaction between a fluid-filled fracture and the Earth's surface. *Tectonophysics,* **53,** 27–57.

Ramberg, H. (1963). Fluid dynamics of viscous buckling applicable to folding of layered rocks. *Bull Am. Assoc. Petrol Geologists,* **47,** 484–505.

Ramberg, H. (1964). Selective buckling of composite layers with contrasted rheological properties. A theory for simultaneous formation of several order of folds. *Tectonophysics,* **1,** 307–341.

Ramberg, H. and Stephansson, O. (1964). Compression of floating elastic and viscous plates affected by gravity, a basis for discussing crustal buckling. *Tectonophysics,* **1,** 101–120.

Ramsay, J.G. (1962). The geometry and mechanics of formation of 'similar' type folds. *J. Geol.,* **70,** 309–327.

Rice, J.R. (1968). Mathematical analysis in the mechanics of fracture. In: *Fracture and Advanced Treatise. II. Mathematical Fundamentals* (H.Liebowitz, ed.), 191–311. Academic Press, New York.

Schaefer, H. (1962). Versuch einer Elastizitätstheorie des zweidimensionalen ebenen Cosserat-Kontinuums. *Miszellaneen der Angewandten Mechanik, Festschrift Walter Tolmien,* 277–292. Academie Verlag, Berlin.

Triantafyllidis, N. and Lehner, F.K. (1993). Interfacial instability of density-stratified two-layer systems under initial stress. *J. Mech. Phys. Solids,* **41**(1), 117–142.

Vardoulakis, I. (1981). Surface waves in a half-space of submerged sand. *Earthquake Eng. Struct. Dyn.*, **9**, 329–342.

Vardoulakis, I. (1983). Rigid granular plasticity model and bifurcation in the triaxial test. *Acta Mechanica,* **49,** 57–73.

Vardoulakis, I. and Papamichos, E. (1991). Surface instabilities in elastic anisotropic media with surface parallel Griffith cracks. *Int. J. Rock Mech. Min. Sci. Geomech. Abstr.,* **28**(2/3), 163–173.

Voigt, W. (1887). Theorische Studien über die Elasticitätsverhaltnisse der Krystalle, *Abh. Ges. Wiss.* (Gottingen), **34.**

Voigt, W. (1894). Über Medien ohne innere Krafte und eine durch sie gelieferte mechanische Deutung der Maxwell-Hertzchen Gleichungen, *Gott. Abh.,* 72–79.

5
Mechanics of water-saturated granular materials

5.1
Definitions

A water-infiltrated granular material is considered as a mixture of a solid, an aqueous and a gaseous phase. The elementary volume dV of this material has a total mass dm and consists of the volume dV_s with mass dm_s of the solids of the volume dV_v of the voids. The void space is assumed to be partially occupied by water with mass dm_w and partially by air with mass dm_g ($dm_g/dm \ll 1$) (Figure 5.1.1)

$$dV = dV_s + dV_v;\ dm \approx dm_s + dm_w \tag{5.1.1}$$

The densities of the constituents are denoted by ρ_s and ρ_w

$$\rho_s = \frac{dm_s}{dV_s};\ \rho_w = \frac{dm_w}{dV_w} \tag{5.1.2}$$

and the relative density of the solids is called in soil mechanics the specific gravity denoted by,

$$G_s = \frac{\rho_s}{\rho_w} \tag{5.1.3}$$

For most soils the specific gravity G_s varies between 2.6 and 2.8.

The degree of water saturation of the voids is denoted by S, whereas the ratio of masses of the aqueous phase to the solid phase is called the water content and is denoted by w

$$S = \frac{dV_w}{dV_v};\ w = \frac{dm_w}{dm_s} \tag{5.1.4}$$

For a dry granular medium S=0, and for a fully saturated one S=1, in which case all the interconnected void space is occupied by water. The volume fraction of voids is usually expressed by the porosity n; however, in soil mechanics the void ratio e is also used

$$n = \frac{dV_v}{dV};\ e = \frac{dV_v}{dV_s} \tag{5.1.5}$$

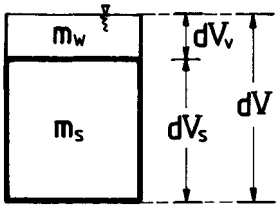

Figure 5.1.1 Phase diagram of a biphasic material.

In reservoir engineering, the symbol ϕ is used for the porosity; however, we will use this symbol for denoting the friction angle of a granular material, and thus we follow for the most part soil mechanics common notation. Porosity and void ratio are interrelated as follows

$$e = \frac{n}{1-n};\ n = \frac{e}{1+e} \tag{5.1.6}$$

Between the water content, the degree of saturation and the void ratio the following condition holds

$$w = \frac{eS}{G_s} \tag{5.1.7}$$

For a fully saturated medium, the total density and the relative densities

$$\rho = \frac{\mathrm{d}m}{\mathrm{d}V};\ \rho_1 = \frac{\mathrm{d}m_s}{\mathrm{d}V};\ \rho_2 = \frac{\mathrm{d}m_w}{\mathrm{d}V} \tag{5.1.8}$$

are related to the densities of the constituents according to the following expressions

$$\rho_1 = (1-n)\rho_s;\ \rho_2 = n\rho_w \tag{5.1.9}$$

$$\rho = \rho_1 + \rho_2 = (1-n)\rho_s + n\rho_w \tag{5.1.10}$$

The partial density for the solid phase is usually termed as the density of the dry soil ($\rho_1 = \rho_d$), whereas the total density of the 'mixture' is called the density of the saturated soil ($\rho = \rho_{sat}$).

Volume discharges $q_i^{(\alpha)}$ and velocities $v_i^{(\alpha)}$ are defined for each constituent, with the index $\alpha = 1$ indicating the solid and $\alpha = 2$ indicating the fluid (Figure 5.1.2)

$$q_i^{(\alpha)} = \frac{\mathrm{d}V_\alpha}{\mathrm{d}S_i\,\mathrm{d}t};\ v_i^{(\alpha)} = \frac{\mathrm{d}V_\alpha}{\mathrm{d}S_i^{(\alpha)}\,\mathrm{d}t} \tag{5.1.11}$$

$\mathrm{d}S_i$, $\mathrm{d}S_i^{(\alpha)}$ are the spatial and material surface element vectors, respectively, which are directed parallel to the x_i-Cartesian coordinate and $\mathrm{d}t$ is the time increment. Mass discharges $m_i^{(\alpha)}$ are defined as follows

$$m_i^{(1)} = \rho_s q_i^{(1)};\ m_i^{(2)} = \rho_w q_i^{(2)} \tag{5.1.12}$$

For a statistically isotropic porous medium, the ratio of void area to solid area is the same for all cross-sections. Hence the volume of the fluid in a thin slab of thickness $\mathrm{d}x$ is always a fraction n of the total volume. This means that the surface porosity equals

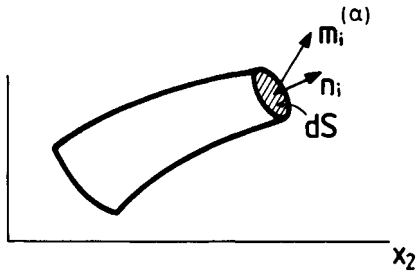

Figure 5.1.2 On the definition of the mass discharge vector.

the volume porosity. With this assumption, volume and mass discharges are easily expressed in terms of velocities

$$q_i^{(1)} = (1 - n)v_i^{(1)};\ q_i^{(2)} = nv_i^{(2)} \tag{5.1.13}$$

$$m_i^{(1)} = \rho_s q_i^{(1)} = \rho_s(1 - n)v_i^{(1)} = \rho_1 v_i^{(1)} \tag{5.1.14}$$

$$m_i^{(2)} = \rho_w q_i^{(2)} = \rho_w n v_i^{(2)} = \rho_2 v_i^{(2)} \tag{5.1.15}$$

In some continuum formulations of the fluid-infiltrated solid, the so-called barycentric velocity of the mixture, is used

$$v_i^{(m)} = (\rho_1/\rho)v_i^{(1)} + (\rho_2/\rho)v_i^{(2)} \tag{5.1.16}$$

and relative motions of the two constituents are measured with respect to it. Here we follow instead Gersevanov's proposition (Verruijt, 1969) according to which fluid flow is described by means of the relative specific discharge vector q_i, which reduces to the fluid discharge vector $q_i^{(2)}$ for a rigid solid skeleton

$$q_i = n(v_i^{(2)} - v_i^{(1)}) \tag{5.1.17}$$

Moreover, the velocity of the solid is denoted simply, as

$$v_i = v_i^{(1)} \tag{5.1.18}$$

so that the notation introduced in section 2.2.1 with respect to the relative deformation gradient, the spatial gradient of the velocity, the rate of deformation tensor and the spin tensor can be used invariantly for the solid phase.

With $u_i = u_i^{(1)}$ denoting the displacement of the solid, its velocity is computed from its material time derivative

$$v_i = \frac{D^{(1)}}{Dt} u_i \tag{5.1.19}$$

where, in general, $D^{(\alpha)}/Dt$ is the material time derivative with respect to the αth constituent

$$\frac{\mathrm{D}^{(\alpha)}}{\mathrm{D}t} = \partial_t + v_i^{(\alpha)}\partial_i \qquad (\alpha = 1,2) \tag{5.1.20}$$

We note that if the two species move in phase, then the two material time derivatives coincide, since

$$\frac{\mathrm{D}^{(2)}}{\mathrm{D}t} = \frac{\mathrm{D}^{(1)}}{\mathrm{D}t} + (v_k^{(2)} - v_k^{(1)})\partial_k \tag{5.1.21}$$

For the solid phase, where convection is inappreciable, one can neglect the convective term in the material time differentiation (i.e. $\mathrm{D}^{(1)}/\mathrm{D}t \approx \partial/\partial t$) and then

$$v_i \approx \partial_t u_i \tag{5.1.22}$$

5.2
Mass balance equations

Mass balance equations are derived for a fully fluid-saturated porous medium (S=1), since the mechanics of partially saturated porous media ($0 \leq S < 1$) are much more complex and somehow ambiguous (see Alonso *et al.,* 1989). Moreover, we assume here that in a given material body the masses of the two constituents (solid and fluid) are constant in time. This means that phenomena such as internal solids erosion (suffosion) or filtration of solids existing in suspension (colmatation or sluicing) are not considered here (cf. Sakthivadivel and Irmay, 1966; Vardoulakis *et al.,* 1995).

In the absence of mass generation terms, the mass of a given species (solid or fluid) contained in a volume V with boundary ∂V is

$$m^{(\alpha)}(t) = \int \rho_\alpha(x_i, t)\mathrm{d}V \tag{5.2.1}$$

Thus in the considered class of deformations, mass balance is expressed by the conditions

$$\frac{\mathrm{D}^{(\alpha)}}{\mathrm{D}t} m^{(\alpha)} = 0 \qquad (\alpha = 1,2) \tag{5.2.2}$$

which according to the derivations presented in chapter 2, section 2.3 result in

$$\int_V \left[\frac{\mathrm{D}^{(\alpha)}\rho_\alpha}{\mathrm{D}t} + \rho_\alpha \partial_k v_i^{(\alpha)}\right]\mathrm{d}V = 0 \tag{5.2.3}$$

or

$$\int_V (\partial_t \rho_\alpha + \partial_k(\rho_\alpha v_k^{(\alpha)}))\mathrm{d}V = 0 \tag{5.2.4}$$

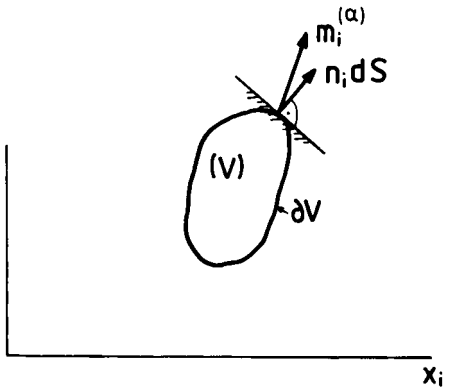

Figure 5.2.1 Mass balance in a finite volume.

Sometimes the following alternative form is used, that derives from equation 5.2.4 with 5.1.12

$$\int_V \partial_t \rho_\alpha \, dV + \int_{\partial V} m_k^{(\alpha)} n_k \, dS = 0 \tag{5.2.5}$$

where n_i is the unit outward normal to the boundary ∂V. This means that in absence of mass generation terms, changes in partial density within V are balanced by in- or outflux of mass across ∂V; see Figure 5.2.1.

By assuming that the balance equations 5.2.4 hold for arbitrary volumes V we derive their local form

$$\frac{D^{(\alpha)}\rho_\alpha}{Dt} + \rho_\alpha \partial_k v_k^{(\alpha)} = 0 \qquad (\alpha = 1,2) \tag{5.2.6}$$

or

$$\partial_t \rho_\alpha + \partial_k (\rho_\alpha v_k^{(\alpha)}) = 0 \qquad (\alpha = 1,2) \tag{5.2.6bis}$$

By adding these equations by parts we obtain that mass balance of the total mixture is expressed in terms of the barycentric velocity

$$\partial_t \rho + \partial_k (\rho v_k^{(m)}) = 0 \tag{5.2.7}$$

Considering the expressions of the partial densities, equations 5.1.9, and combining above balance equations 5.2.6 results in

$$-D_{kk} = \frac{1}{\rho_s} \frac{D^{(1)}\rho_s}{Dt} - \frac{1}{1-n} \frac{D^{(1)} n}{Dt} \tag{5.2.8}$$

$$-\partial_k q_k = \frac{1-n}{\rho_s} \frac{D^{(1)}\rho_s}{Dt} + \frac{n}{\rho_w} \frac{D^{(2)}\rho_w}{Dt} + D_{kk} \tag{5.2.9}$$

where

$$D_{ij} = \tfrac{1}{2}(\partial_i v_j + \partial_j v_i) \tag{5.2.10}$$

is the rate of deformation tensor of the solid.

The first simplification that can be introduced in the above mass balance equations 5. 2.8 and 5.2.9 results from neglecting convective terms in the material time derivations, i.e. by setting

$$\partial_t \approx \frac{\mathrm{D}^{(2)}}{\mathrm{D}t} \approx \frac{\mathrm{D}^{(1)}}{\mathrm{D}t} \tag{5.2.11}$$

we obtain the following mass balance equations

$$-D_{kk} = \partial_t\{\ln(\rho_s)\} - \frac{n}{1-n}\partial_t\{\ln(n)\} \tag{5.2.12}$$

$$-\partial_k q_k = (1-n)\partial_t\{\ln(\rho_s)\} + n\partial_t\{\ln(\rho_w)\} + D_{kk} \tag{5.2.13}$$

We note that in these equations D_{kk} is the rate of volumetric deformation of the solid phase. Equation 5.2.13 is usually called the *storage equation.*

The mass balance equations can be further simplified if the constituents of the solid phase (grains) are assumed to be incompressible, i.e. for ρ_s=const. these equations

$$D_{kk} = \frac{n}{1-n}\partial_t\{\ln(n)\} \tag{5.2.14}$$

$$-\partial_k q_k = n\partial_t\{\ln \rho_w\} + D_{kk} \tag{5.2.15}$$

Equation 5.2.14 is expressing the fact that for incompressible grains, volume changes in a porous granular medium are due only to changes in porosity. Using equation 5.1.6, the volume changes can be alternatively expressed in terms of the void ratio

$$D_{kk} = \frac{e}{1+e}\partial_t\{\ln(e)\} \tag{5.2.16}$$

In soil mechanics literature the use of the void ratio is preferred over the use of porosity, because due to the assumed incompressibility of the grains, changes in void ratio directly reflect changes in void space. Besides, the void ratio of a fully-saturated specimen can be easily determined experimentally by simply determining its water content; cf. equation 5.1.7.

On the other hand, the storage equation (5.2.15) is further simplified if the pore fluid is assumed to be incompressible (ρ_w=const.), which then reduces to the well-known *continuity equation,*

$$-\partial_k q_k = D_{kk} \tag{5.2.17}$$

5.3
Static considerations: partial and ‘effective’ stresses

Let $\mathrm{d}t_i$ be the total stress vector acting on a surface element $\mathrm{d}S_i$ in the current configuration of the porous, fluid-saturated medium. This medium is treated as a two-

phase mixture, which is equipped by a total (Cauchy) stress tensor σ_{ij} and by partial stress $\sigma_{ij}^{(\alpha)}$ assigned to the two phases. The total stress tensor is defined through the mapping

$$\mathrm{d}t_i = \sigma_{ki} n_k \,\mathrm{d}S \tag{5.3.1}$$

The traction $\mathrm{d}t_i$ is decomposed into two parts

$$\mathrm{d}t_i = \mathrm{d}t_i^{(1)} + \mathrm{d}t_i^{(2)} \tag{5.3.2}$$

with $\mathrm{d}t_i^{(\alpha)}$ being the part of the total traction which is acting on the αth phase ($\alpha = 1, 2$). Based on this decomposition, partial stresses $\sigma_{ij}^{(\alpha)}$ are defined such that

$$\mathrm{d}t_i^{(\alpha)} = \sigma_{ki}^{(\alpha)} n_k \,\mathrm{d}S \tag{5.3.3}$$

The total stress is then the sum of the partial stresses

$$\sigma_{ij} = \sigma_{ij}^{(1)} + \sigma_{ij}^{(2)} \tag{5.3.4}$$

The partial stress for the aqueous phase $\sigma_{ij}^{(2)}$ is directly related to the water pressure p_{w}. This can be shown by considering the definition of p_{w}

$$\mathrm{d}t_i^{(2)} = -p_{\mathrm{w}} \delta_{ki} n_k \,\mathrm{d}S_{\mathrm{v}} \qquad (p_{\mathrm{w}} > 0) \tag{5.3.5}$$

where $\mathrm{d}S_{\mathrm{v}}$ is the part of the surface element which corresponds to the voids. For statistically isotropic granular medium, the surface porosity is equal to the volume porosity, and consequently

$$\mathrm{d}t_i^{(2)} = -n p_{\mathrm{w}} \delta_{ki} n_k \,\mathrm{d}S \tag{5.3.6}$$

From equations 5.3.3 and 5.3.6 we obtain the relation between the partial fluid stress and the pore-water pressure

$$\sigma_{ij}^{(2)} = -n p_{\mathrm{w}} \delta_{ij} \tag{5.3.7}$$

Notice that Biot's (1941) poro-elasticity is based on the above definition of partial fluid stress.

A granular medium is considered that consists of loose particles in contact with each other at isolated contact points. In these points, contact forces can be transmitted from one particle to another. One of the basic principles of the mechanics of granular media is the notion that the deformations of the granular assembly are not so much determined by a summation of the deformation of the individual particles (i.e. by the elasticity of the grains), but rather by rearrangement of the particles, loss or gain of new grain contacts (dilatancy/contactancy) and due to sliding and rolling in the contact points (i.e. by the plasticity of the assembly). When the pores of the granular medium are filled with water of low compressibility, it is assumed that the particles are completely surrounded by water, so that an equal change of the total stress and of the pore-water pressure would entail an equal change of the stress in each particle, without any change of the forces transmitted in the isolated contact points. Along this line of

thought, Terzaghi (1936) proposed decomposing the total stress into an 'effective' stress, assigned to the soil skeleton, and into a pore-water pressure p_w

$$\sigma_{ij} = \sigma'_{ij} - p_w \delta_{ij} \tag{5.3.8}$$

Terzaghi's definition of effective stress, σ'_{ij}, is heuristic. Both the total stress σ_{ij} and the pore-water pressure p_w are measurable quantities, and thus equation 5.3.8 can be understood as an operational definition of effective stress. Terzaghi's effective stress principle was originally introduced for the description of limiting soil properties, such as classical Mohr-Coulomb type failure criteria for frictional materials. The usefulness of Terzaghi's effective-stress principle was demonstrated in numerous experimental investigations. Among those one could single out the most comprehensive study by Bishop and Skinner (1977) who performed drained tests with back pressure on a variety of water-saturated granular materials and for stress levels corresponding to the ones encountered in soil mechanics problems. The concept of Terzaghi's effective stress principle is generalized so as to describe the constitutive behavior of the soil skeleton as well. In other words, it is assumed that constitutive equations for the skeleton are expressed in terms of effective stresses. For example, for the description of soil consolidation phenomena, Verruijt (1969) related the effective stress to the strains of the skeleton via the equations of elasticity. In other applications, dealing with elastoplastic soils for example, rate-type equations for the skeleton are similarly described in terms of effective stresses.

Finally, from equations 5.3.4, 5.3.7 and 5.3.8 the relation between the partial stress for the solid $\sigma^{(1)}_{ij}$ and Terzaghi's effective stress can be derived

$$\sigma^{(1)}_{ij} = \sigma'_{ij} - (1 - n) p_w \delta_{ij} \tag{5.3.9}$$

From this equation the difference between Terzaghi's effective stress and the mixture's theory partial stress for the solid is obvious. As we will see in following sections, balance of momentum is primarily described in terms of partial stresses. With equations 5.3.7 and 5.3.9, however, partial stresses may be replaced by the pore-water pressure and Terzaghi's effective stress.

5.4
The influence of grain and fluid compressibility

Terzaghi's effective stress must be distinguished from Taylor's (1948) intergranular stress (Figure 5.4.1), where he states (p. 126):

> In concepts of stress…the surface that must be considered is one containing the points of grain-to-grain contact, in order to include the points of action of the forces which make up intergranular stress. Thus the unit area should be visualized as a wavy surface which is tangent to but does not cut through soil grains, and which at all points is as close as possible to a flat surface.

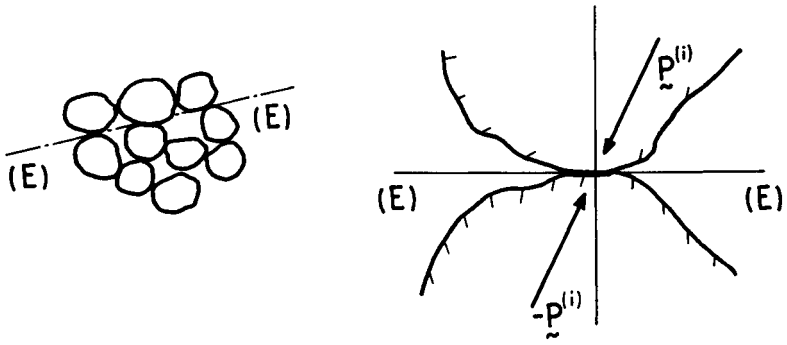

Figure 5.4.1 Taylor's definition of intergranular stress.

Based on this simple micromechanical argument Taylor is suggesting the definition of an intergranular stress

$$\sigma_{ij}^{(i)} = \sigma'_{ij} - n^* p_w \delta_{ij} \tag{5.4.1}$$

where n^* denotes the contact area of soil particles per unit area of the probing surface (and projected onto the surface). Taylor gives an estimate for $n^* \approx 0.03$. It is agreed that the correction term $n^* p_w$ is small in cohesionless soils and probably in clays, at the stress levels commonly encountered in soil engineering practice. However, in situations encountered in reservoir engineering, p_w may be very large as compared to the hydrostatic part of the effective stress, and Taylor's correction term may significant; cf. Garg and Nur (1973).

Bishop (1953, private comm.; see Bishop and Skenner, 1974) and later Verruijt (1982), modified Taylor's intergranular stress definition replacing n^* by the compressibility ratio

$$c^* = c_s/c \qquad (0 \leqslant c^* \ll 1) \tag{5.4.2}$$

where c_s is the particle compressibility and c the bulk compressibility, resulting in

$$\sigma_{ij}^{(i)} = \sigma'_{ij} - c^* p_w \delta_{ij} \tag{5.4.3}$$

For soils in the low effective stress range the bulk compressibility c is very large compared to the grain compressibility c_s. For the limiting case of incompressible grains $c_s = 0$, Bishop's intergranular stress and Terzaghi's effective stress coincide. Skempton (1960) has tabulated data (Table 5.4.1) showing that for soils ranging from normally consolidated clay to dense sand c^* lies in the range of 3.0×10^{-5} to 1.5×10^{-3} for an effective consolidation pressure of approximately l00 kPa. For clays and very high consolidation pressures of 20–60 MPa, Skempton (1960) and Bishop and Skinner (1977) suggested that c^* may rise to 0.4.

Verruijt (1982) proposed that for a fluid-saturated soil the density of solid constituent will be affected by both changes in the ambient pore-fluid pressure and the mean intergranular stress,

Table 5.4.1 Compressibilities of 100 kPa consolidation pressure (after Skempton, 1960)

Material	c (kPa^{-1})	c_s (kPa^{-1})	c^* (—)
Quartzitic sandstone	5.98×10^{-8}	2.75×10^{-8}	4.6×10^{-1}
Quincy granite	7.75×10^{-8}	1.93×10^{-8}	2.5×10^{-1}
Vermont marble	1.78×10^{-7}	1.43×10^{-8}	8.0×10^{-2}
Concrete*	2.12×10^{-7}	2.55×10^{-8}	1.2×10^{-1}
Dense sand	1.83×10^{-5}	2.75×10^{-8}	1.5×10^{-3}
Loose sand	9.17×10^{-5}	2.75×10^{-8}	3.0×10^{-4}
London clay (over-consolidated)	7.55×10^{-5}	2.04×10^{-8}	2.7×10^{-4}
Gosport clay (normally consolidated)	6.18×10^{-4}	2.04×10^{-8}	3.3×10^{-5}

* Approximate values.

$$\Delta\rho_s = \rho_s(c_s \Delta p_w - c_p p^{(i)}) \tag{5.4.4}$$

where according to equation 5.4.3 $p^{(i)}$ is the intergranular pressure,

$$p^{(i)} = p' - c^* p_w \tag{5.4.5}$$

and c_p is the compressibility of the solids due to concentrated forces

$$c_s/(1-n) \leqslant c_p \ll c \tag{5.4.6}$$

with $c_p/c = 0(c^*)$.

When, according to equation 5.2.11, convective terms are neglected one does not distinguish between material and time derivatives, and accordingly the notation $(\square)\equiv\partial t$ may be used unambiguously. In this case the mass balance equation 5.2.12 for the solid phase becomes (Vardoulakis and Beskos, 1986)

$$\frac{\dot{n}}{1-n} = \dot{\varepsilon}_{kk} - c_p \dot{p}' + (c_s + c^* c_p)\dot{p}_w \tag{5.4.7}$$

On the other hand, changes in water density are directly related to changes in pore-water pressure p_w

$$\Delta\rho_w = c_w \rho_w \Delta p_w \tag{5.4.8}$$

where c_w is the compressibility of water. At relatively low levels of pore-water pressure, soils are usually not perfectly saturated. Using mixtures theory, Verruijt (1982) demonstrated that a nearly saturated porous medium ($0<1-S\ll1$), can be replaced by a fully saturated one, whose fluid compressibility depends on the degree of saturation (see also Vardoulakis and Beskos, 1986), and accordingly

$$c_w = c_{wo} + (1-S)/p_w \tag{5.4.9}$$

where c_{wo} is the compressibility of de-aired water; $c_{wo} = 4.93 \times 10^{-7}\,kPa^{-1}$.

For compressible fluid and solid constituent, the storage equation 5.2.13 becomes

$$-\partial_k q_k = -c_1 \dot{p}' + c_2 \dot{p}_w + \dot{\varepsilon}_{kk} \tag{5.4.10}$$

where

$$c_1 = (1-n)c_p;\ c_2 = (1-n)(c_s + c^* c_p) + n c_w \tag{5.4.11}$$

For c*«1 and $c_p \approx c_s/(1-n)$, the storage equation 5.4.10 becomes

$$-\partial_k q_k = -c_s \dot{p}' + c_m \dot{p}_w + \dot{\varepsilon}_{kk} \tag{5.4.12}$$

where c_m is the compressibility of the mixture,

$$c_m = (1-n)c_s + n c_w \tag{5.4.13}$$

As an application of the above discussed concepts, we will discuss here the special case of *undrained deformation*: In undrained deformations, zero fluid flux across the specimen's boundaries is holding, which together with the assumption of homogeneity results in $q_i = 0$. Mass balance, as expressed in equations 5.4.12 and 5.4.7 for c^*«1, results in the prediction of small volumetric strains

$$\Delta\varepsilon = c_s \Delta p' - c_m \Delta p_w \tag{5.4.14}$$

$$\Delta n = (1-n)(\Delta\varepsilon - c_p \Delta p' + c_s \Delta p_w) \tag{5.4.15}$$

where $\Delta\varepsilon \approx D_{kk}\Delta t$, is the incremental volumetric strain.

Let

$$\Delta p' = \frac{1}{c}\Delta\varepsilon \tag{5.4.16}$$

be the constitutive relation which is describing the drained behavior of the soil material in isotropic compressions. From equation 5.4.14 we obtain an equation for the determination of the pore-water pressure increment

$$\Delta p_w = \frac{c^* - 1}{c_m}\Delta\varepsilon \approx -\frac{1}{c_m}\Delta\varepsilon \tag{5.4.17}$$

and thus the total pressure increment can be also computed

$$\Delta p = \Delta p' - \Delta p_w = \left(\frac{1}{c} + \frac{1}{c_m}\right)\Delta\varepsilon \tag{5.4.18}$$

We note that the degree of saturation S of a soil specimen is checked by means of the so-called B-test. After Skempton (1954) the ratio of excess pore-water pressure to the increment of isotropic total stress in undrained conditions is denoted by B. From the above expressions, Skempton's pore-pressure parameter B can be derived, resulting in the following expression

$$B = \frac{\Delta p_w}{|\Delta p|} = \frac{1}{1 + (c_m/c)} \tag{5.4.19}$$

Figure 5.4.2 demonstrates the well-known dependency of B on S for a medium dense sand ($c = 3.80 \times 10^{-5}\,\mathrm{kPa}^{-1}$), which in turn reflects the dependency of the water compressibility c_w on S; cf. equation 5.4.9.

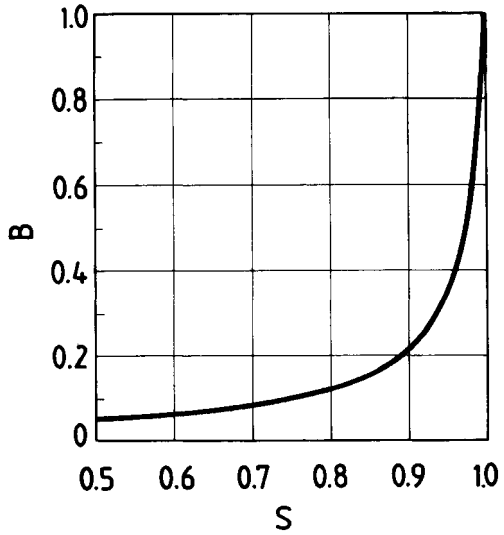

Figure 5.4.2 Skempton's pore-pressure parameter B for a medium dense sand; (n_0=0.4, c=3. 80×10^{-5}kPa^{-1}, p_{wo}=294.4 kPa).

A direct application of the above concepts can be found in the papers by Fragaszy and Voss (1984) and Vardoulakis (1987), who studied the phenomenon of *compression-induced liquefaction* of water-saturated, granular soils as a result of the different soil compressibility in (elastoplastic) loading and (elastic) unloading-reloading.

5.5
Balance of linear momentum

First we formulate the equations of balance of linear momentum in terms of partial stresses: the total force acting on the αth constituent is

$$F_i^{(\alpha)} = \int_V \rho_\alpha g_i \, dV + \int_V f_i^{(\alpha)} \, dV + \int_{\partial V} dt_i^{(\alpha)} \tag{5.5.1}$$

where $dt_i^{(\alpha)}$ is the partial surface traction vector, $p_\alpha g_i$ is the partial unit weight, g_i is the acceleration due to gravity in the ith direction, and

$$f_i^{(1)} = -f_i^{(2)} = f_i \tag{5.5.2}$$

is the interaction force exerted by the flowing fluid on the solid phase, whose nature depends on the fluid-flow characteristics and will be discussed in the following section. The partial momenta of the solid and aqueous phase can be written as follows

$$I_i^{(\alpha)} = \int_V \rho_\alpha v_i^{(\alpha)} \, \mathrm{d}V \tag{5.5.3}$$

where inertial mass coupling between the solid and fluid phase is disregarded; see below.

Balance of linear momentum for the αth constituent is expressed by the condition

$$F_i^{(\alpha)} = \frac{\mathrm{D}^{(\alpha)}}{\mathrm{D}t} I_i^{(\alpha)} \tag{5.5.4}$$

According to Reynold's transport theorem (2.2.56) and definition 5.1.20 the right-hand side of equation 5.5.4 becomes

$$\begin{aligned} \frac{\mathrm{D}^{(\alpha)}}{\mathrm{D}t} I_i^{(\alpha)} &= \int_V [\partial_t(\rho_\alpha v_i^{(\alpha)}) + \partial_k(\rho_\alpha v_i^{(\alpha)} v_k^{(\alpha)})] \, \mathrm{d}V \\ &= \int_V \left\{ [\partial_t \rho_\alpha + \partial_k(\rho_\alpha v_k^{(\alpha)})] v_i^{(\alpha)} + \rho_\alpha \frac{\mathrm{D}^{(\alpha)}}{\mathrm{D}t} v_i^{(\alpha)} \right\} \mathrm{d}V \end{aligned}$$

Due to the mass balance equation 5.2.6 the first term of the integrand vanishes identically, and thus

$$\frac{\mathrm{D}^{(\alpha)}}{\mathrm{D}t} I_i^{(\alpha)} = \int_V \rho_\alpha \frac{\mathrm{D}^{(\alpha)}}{\mathrm{D}t} v_i^{(\alpha)} \, \mathrm{d}V \tag{5.5.5}$$

According to equation 5.5.4, balance of linear momentum is thus expressed by

$$\int_{\partial V} \sigma_{ki}^{(\alpha)} n_k \, \mathrm{d}S + \int_V \rho_\alpha g_i \, \mathrm{d}V + \int_V f_i^{(\alpha)} \, \mathrm{d}V = \int_V \rho_\alpha \frac{\mathrm{D}^{(\alpha)}}{\mathrm{D}t} v_i^{(\alpha)} \, \mathrm{d}V$$

or in local form

$$\partial_k \sigma_{ki}^{(\alpha)} + \rho_\alpha g_i + f_i^{(\alpha)} = \rho_\alpha \frac{\mathrm{D}^{(\alpha)}}{\mathrm{D}t} v_i^{(\alpha)} \tag{5.5.6}$$

By adding the above equations for $\alpha = 1$ and $\alpha = 2$, and using the expressions of the total Cauchy stress tensor σ_{ij} and the total density ρ in terms of the corresponding partial quantities, equations 5.3.4 and 5.1.10, we derive the dynamic equation of the mixture

$$\partial_k \sigma_{ki} + \rho g_i = \rho_1 \frac{\mathrm{D}^{(1)}}{\mathrm{D}t} v_i^{(1)} + \rho_2 \frac{\mathrm{D}^{(2)}}{\mathrm{D}t} v_i^{(2)} \tag{5.5.7}$$

The right-hand side of equation 5.5.7 can be written also in terms of the barycentric velocity, defined through equation 5.1.16, resulting in the following form

$$\partial_k \sigma_{ki}^{*} + \rho g_i = \rho \frac{\mathrm{D}^{(\mathrm{m})}}{\mathrm{D}t} v_i^{(\mathrm{m})} \tag{5.5.8}$$

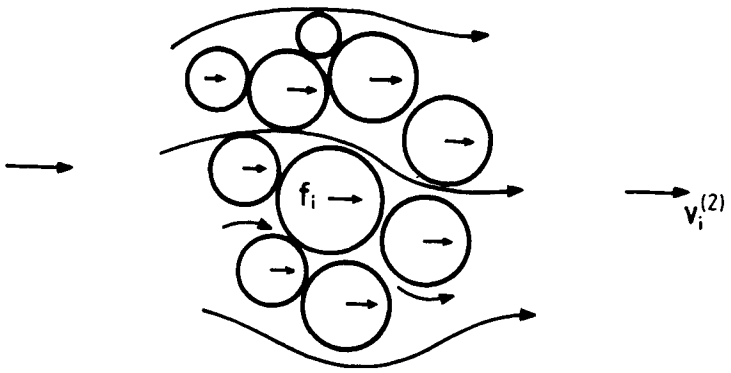

Figure 5.5.1 The seepage volume force.

where σ^*_{ki} is the so-called stress tensor of the mixture, which consists of an 'inner' part and a part due to diffusion,

$$\sigma^*_{ij} = \sigma_{ij} - R_{ij}$$

The inner part is identical with the total stress, defined through equation 5.3.4 and the diffusion term,

$$R_{ij} = \rho_1(v_i^{(m)} - v_i^{(1)})(v_j^{(m)} - v_j^{(1)}) + \rho_2(v_i^{(m)} - v_i^{(2)})(v_j^{(m)} - v_j^{(2)}) \tag{5.5.9}$$

is the so-called Reynold's stress.

For α=2, the dynamic equation 5.5.6 can be combined with equation 5.3.7 which defines the partial fluid stress in terms of the pore-water pressure. This results in a dynamic equation for the aqueous phase in terms of the pore-water pressure

$$-\partial_i p_w + \rho_w g_i - \{f_i/n + p_w \partial_i \ln(n)\} = \rho_w \frac{D^{(2)}}{Dt} v_i^{(2)} \tag{5.5.10}$$

The above momentum equations can be further simplified if one can neglect the convective terms in the material time derivatives. Moreover, for small spatial porosity changes the non-linear term $p_w \partial_i \ln(n)$ in equation 5.5.10can also be ignored. Accordingly, the dynamic equations are expressed in terms of the total stress, the effective stress and the pore-water pressure as follows

$$\partial_k \sigma_{ki} + \rho g_i = \rho_1 \partial_t v_i^{(1)} + \rho_2 \partial_t v_i^{(2)} \tag{5.5.11}$$

$$\partial_k \sigma'_{ki} + \rho_b g_i + \hat{f}_i = \rho_b \partial_t v_i^{(1)} - (1-n)\rho_w(\partial_t v_i^{(2)} - \partial_t v_i^{(1)}) \tag{5.5.12}$$

$$-\partial_i p_w + \rho_w g_i - \hat{f}_i = \rho_w \partial_t v_i^{(2)} \tag{5.5.13}$$

where ρ_b is the buoyant density of the soil skeleton

$$\rho_b = \rho - \rho_w = (1-n)\rho_s + n\rho_w - \rho_w = (1-n)(\rho_s - \rho_w) \tag{5.5.14}$$

and

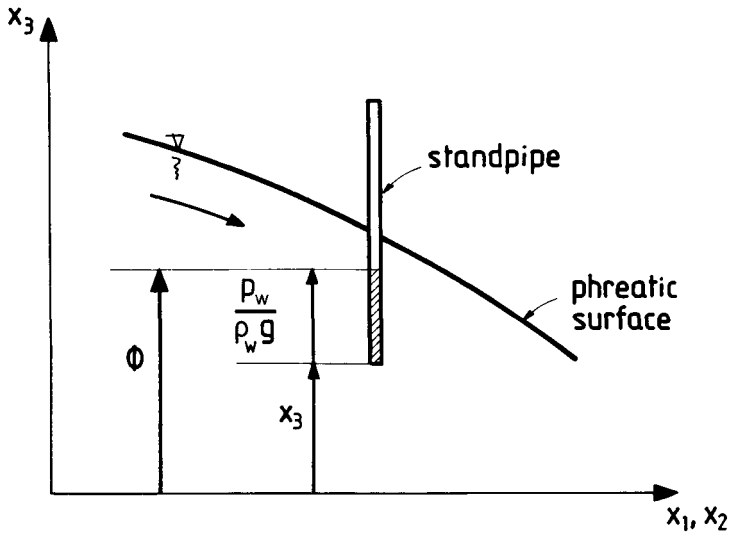

Figure 5.6.1 Definition of the hydraulic head Φ.

$$\hat{f}_i = f_i/n \tag{5.5.15}$$

is identified as the seepage volume force (Figure 5.5.1).

Finally, if inertial terms are also disregarded, we obtain the following well-known equilibrium equations

$$\partial_k \sigma_{ki} + \rho g_i = 0 \tag{5.5.16}$$

$$\partial_k \sigma'_{ki} + \rho_b g_i + \hat{f}_i = 0 \tag{5.5.17}$$

$$-\partial_i p_w + \rho_w g_i - \hat{f}_i = 0 \tag{5.5.18}$$

5.6
Laws governing fluid flow in porous media

5.6.1
Darcy's law

One-dimensional steady flow of a viscous, incompressible fluid through the interconnected pore space of a saturated homogeneous isotropic and rigid porous medium is described by Darcy's law which relates the specific discharge vector q_i to the gradient of the piezometric head Φ. Darcy's law can be used to identify the seepage force $\hat{f}_i$ which appears in the above equilibrium equations 5.5.17 and 5.5.18. With the x_3-axis vertical pointing upwards, gravity body forces are expressed as follows

$$g_i = -g\delta_{i3} \tag{5.6.1}$$

and accordingly the hydraulic head Φ is defined (Figure 5.6.1)

$$\Phi = \frac{p_w}{\rho_w g} + x_3 \tag{5.6.2}$$

Darcy's law becomes then

$$q_i = -k_w \partial_i \Phi \tag{5.6.3}$$

In this expression k_w is the hydraulic conductivity (dimensions LT^{-1}), which measures the permeability of the soil skeleton with respect to water. From equations 5.6.1 to 5.6.3 we derive the following form of Darcy's law

$$q_i = \frac{k_w}{\rho_w g}(-\partial_i p_w + \rho_w g_i) \tag{5.6.4}$$

Combining this equation with the equilibrium equation 5.5.18 for the aqueous phase we finally obtain the underlying constitutive law for the seepage force

$$\hat{f}_i = f q_i \tag{5.6.5}$$

where

$$f = \rho_w g / k_w \tag{5.6.6}$$

The constitutive equation 5.6.5 for the seepage force can be interpreted as follows: The drag exerted from the flowing fluid onto the skeleton grains is proportional to the relative motion of the fluid with respect to the grains and the proportionality coefficient f is inversely proportional to the permeability of the soil. Thus, from the continuum mechanics point of view it is preferable to introduce Darcy's law, equation 5.6.4 indirectly, by combining the equilibrium condition 5.5.18 for the aqueous phase and the constitutive law 5.6.5 for the drag force.

The permeability coefficient k_w in equation 5.6.6 is related to the Muskat or physical permeability k of the medium according to the following relation (Taylor, 1948)

$$k_w = \frac{g}{\eta_k} k \tag{5.6.7}$$

and thus

$$f = \rho_w \eta_k / k \tag{5.6.8}$$

In these expressions η_k the kinematic viscosity of water ($\eta_k = 1.0 \times 10^{-6}\,\mathrm{m^2\,sec^{-1}}$ at 20°C), and accordingly f is called the viscous drag coefficient.

The physical permeability k in equation 5.6.8 has the dimensions of surface, which means that k stands as a measure of the cross-sectional area of the microscopic channels in the interconnected void space. The physical permeability k is usually measured in millidarcy ($1\,\mathrm{md} = 0.987 \times 10^{-15}\,\mathrm{m^2}$). As far as the permeability coefficient kw is concerned, for sands Hazen's empirical rule is found to give a good estimate (Taylor, 1948)

$$k_w = 100 D_{10\%}^2 \tag{5.6.9}$$

where $D_{10\%}$ is the hydraulically (Hazen's) effective grain diameter in cm and k_w in cm/sec.

For example, for a fine sand $D_{10\%}$=0.0125 cm and k_w=156×10^4 cm/sec. From equations 5.6.7 and 5.6.8 we obtain then the following typical values: for the physical permeability $k = 15.9 \times 10^{-6}\,\mathrm{mm}^2 = 16.1\,\mathrm{d}$, and the viscous drag coefficient $f = 6.29 \times 10^4\,\mathrm{g\,cm^{-3}\,sec^{-1}}$.

If the gradient of elevation head s unimportant then Darcy's law, equation 5.6.4, becomes

$$q_i = -\frac{1}{f}\partial_i p_w \tag{5.6.10}$$

Finally, equation 5.6.10 can be combined with the storage equation 5.2.15 with 5.4.8, resulting for f=const., in

$$\nabla^2 p_w = f(nc_w \partial_t p_w + D_{kk}) \tag{5.6.11}$$

where $\nabla^2 = \partial_k^2$, is the Laplacian operator.

In soil mechanics one usually considers the incompressible pore-fluid limit, and equation 5.6.10 reduces to

$$\nabla^2 p_w = f D_{kk} \tag{5.6.11a}$$

on which the theory of soil consolidation is based. For example, with $\dot{p} = \dot{p}' - \dot{p}_w = 0$, and $D_{kk} = c\dot{p}'$, one obtains the consolidation equation

$$\partial_t p_w = c_v \nabla^2 p_w;\ c_v = 1/(fc) \tag{5.6.11b}$$

where c_v is the consolidation coefficient. In contrast, in reservoir engineering fluid compressibility dominates over skeleton compressibility, and equation 5.6.11 reduces into a pore-pressure diffusion equation

$$\partial_t p_w = c_f \nabla^2 p_w;\ c_f = 1/(fnc_w) \tag{5.6.11c}$$

For the above exemplary value of $f = 6.3 \times 10^4\,\mathrm{g\,cm^{-3}\,sec^{-1}}$, and for $c_w = 4.9 \times 10^{-7}\,\mathrm{kPa^{-1}}$, the pore-pressure diffusivity coefficient results in $c_f = (1/n) \times 3.2 \times 10^5\,\mathrm{cm^2\,sec^{-1}}$. Notice that the diffusivity coefficient for the pore pressure is inversely proportional to the fluid compressibility c_w, whereas the consolidation coefficient c_v is inversely proportional to the bulk (drained-skeleton) compressibility c.

Remarks on wave propagation. In soil mechanics one considers usually the limiting case of a water-saturated soil consisting of incompressible grains and fluid, obeying Terzaghi's effective stress principle and Darcy's law. The dynamic problem can then be formulated by using the corresponding balance and constitutive equations:

$$\partial_k q_k + \partial_k v_k^{(1)} = 0$$

$$\partial_k \sigma'_{ki} + \hat{f}_i = \rho_b \partial_t v_i^{(1)} - (1-n)\rho_w(\partial_t v_i^{(2)} - \partial_t v_i^{(1)})$$

where

$$\hat{f}_i = fq_i$$
$$q_i = n(v_i^{(2)} - v_i^{(1)})$$

This problem is complete, if, for example, one assumes for the effective stress the validity of the small strain equations of linear, isotropic elasticity

$$\sigma'_{ij} = \lambda\varepsilon_{kk}\delta_{ij} + 2\mu\varepsilon_{ij}$$

where $\mu = G$ and λ are the Lamé moduli.

In particular, waves for the dilatation, $\varepsilon = \partial_k u_k^{(1)}$, obey the *telegraphy equation*

$$\nabla^2\varepsilon = \frac{1}{c_p^2}\frac{\partial^2\varepsilon}{\partial t^2} + \frac{1}{c_f}\frac{\partial\varepsilon}{\partial t}$$

where

$$c_p = \{(\lambda + 2\mu)/\rho'\}^{\frac{1}{2}};\ \rho' = \rho_b + (1/n - 1)\rho_w$$

is a reference *p*-wave propagation velocity, and

$$c_v = (\lambda + 2\mu)/f$$

with c_v a consolidation coefficient.

It turns out that this theory produces only waves of the *second kind* in the terminology of Biot (1956a), i.e. slow, dispersive, attenuating *p*-waves:

$$\varepsilon = \exp(-\alpha z)\exp\{\text{is}\,(t - z/c)\}$$
$$c = c_p\{2/[(1 + (s_c/s)^2)^{\frac{1}{2}} + 1]\}^{\frac{1}{2}}: \text{ propagation velocity}$$
$$\alpha = sc_p\{2[(1 + (s_c/s)^2)^{\frac{1}{2}} - 1]\}^{\frac{1}{2}}: \text{ absorption}$$
$$s_c = c_p^2/c_v \qquad : \text{characteristic frequency}$$

5.6.2
Biot's modification of viscous and inertial drag

Biot (1956a,b) in a series of papers proposed a simple phenomenological theory of acoustic wave propagation in porous, fluid saturated media which can be easily embedded into the present framework, as a modification of the governing dynamic equations 5.5.11 and 5.5.12. First we consider here Biot's (1956a; cf. also Beskos, 1989 and Beskos *et al.,* 1989) modification of the viscous drag coefficient *f,* which in the present framework is given through equation 5.6.8. Poiseuille flow in the interconnected porosity network breaks down for frequencies higher than a cut-off frequency,

$$s_p = \frac{\pi\eta_k}{16R_H^2} \tag{5.6.12}$$

R_H is the hydraulic radius of the pores, which according to Taylor (1948) may be given in terms of the mean grain diameter $D_{50\%}$ and the void ratio by the Kozeny formula

$$R_H = eD_{50\%}/6 \tag{5.6.13}$$

Biot (1956b) also proved that, while for the low frequency range, i.e. for $s \leq s_p$, the dynamic viscosity $\eta = \rho_f \eta_k$ is constant, for the high-frequency range, $s > s_p$, η has to be replaced by a frequency-dependent viscosity $\eta F(\Theta)$, where

$$F(\Theta) = \frac{\Theta^2 T(\Theta)}{4\{\Theta + 2iT(\Theta)\}} \tag{5.6.14}$$

$$T(\Theta) = \frac{\mathrm{ber}'\Theta + i\,\mathrm{bei}'\Theta}{\mathrm{ber}\Theta + i\,\mathrm{bei}\Theta} \tag{5.6.15}$$

where $i = \sqrt{(-1)}$, berΘ and beiΘ denote Bessel-Kelvin functions of the first kind and order zero, a prime indicates differentiation with respect to the argument Θ, which in turn is related to the frequency through

$$\Theta = R_H(s/\eta_k)^{\frac{1}{2}} \tag{5.6.16}$$

$F(\Theta)$ allows for the fact that the effective damping changes when the viscous skin depth $\sqrt{(\eta_k/s)}$ becomes smaller than the pore size as the frequency s increases. It should be noted that there is also an upper bound for the frequency $s = s_c$ beyond which the continuum approach breaks down, since the wavelength becomes of the order of the pore size

$$s_c = \pi c/R_H \tag{5.6.17}$$

where c is the phase velocity of the wave.

The second significant modification of the governing dynamic equations introduced by Biot concerns the inertial drag, as follows

$$\begin{aligned} \partial_k \sigma_{ki}^{(1)} + \rho_1 g_i + f_i^{(1)} &= \rho_{11}\partial_t v_i^{(1)} + \rho_{12}\partial_t v_i^{(2)} \\ \partial_k \sigma_{ki}^{(2)} + \rho_2 g_i + f_i^{(2)} &= \rho_{21}\partial_t v_i^{(1)} + \rho_{22}\partial_t v_i^{(2)} \end{aligned} \tag{5.6.18}$$

where the coefficients $p_{\alpha\beta}$ are mass coefficients which take into account the fact that the relative fluid flow through the pores is not uniform, and describe the inertial drag that the fluid exerts on the solid as the latter is accelerated relative to the former and vice versa. The mass coupling coefficients are taken equal, $\rho_{12} = \rho_{21}$ and are assumed to represent the inertial coupling between fluid and solid even for a non-viscous pore fluid ($\eta F(\Theta) = 0$). By adding the dynamic equations we obtain the momentum equation in terms of the total stress

$$\partial_k \sigma_{ki} + \rho g_i = (\rho_{11} + \rho_{21})\partial_t v_i^{(1)} + (\rho_{12} + \rho_{22})\partial_t v_i^{(2)} \tag{5.6.19}$$

By comparing this expression with the dynamic equation 5.5.11 of the whole mixture we obtain the relations between the mass coefficients and the partial densities

$$\rho_1 = \rho_{11} + \rho_{21}$$
$$\rho_2 = \rho_{12} + \rho_{22} \tag{5.6.20}$$

In order to obtain some constitutive inequalities for the mass coefficients $\rho_{\alpha\beta}$ Biot is considering two special cases of motion of the mixture:

(a) If there is no relative motion between solid and fluid, i.e. if

$$v_i^{(1)} = v_i^{(2)} = v_i \tag{5.6.21}$$

then the total local kinetic energy of the mixture is:

$$k = \tfrac{1}{2}\rho v_i v_i = \tfrac{1}{2}(\rho_{11} + 2\rho_{21} + \rho_{22})v_i v_i$$

For the kinetic energy to be positive we require that

$$\rho_{11} + 2\rho_{21} + \rho_{22} > 0 \tag{5.6.22}$$

(b) If the fluid in some way is restrained so that

$$v_i^{(2)} = 0$$

then from the above dynamic equations we obtain the following expressions for the corresponding inertial forces

$$a_i^{(1)} = \rho_{11}\partial_t v_i^{(1)}$$
$$a_i^{(2)} = \rho_{21}\partial_t v_i^{(1)}$$

The second equation shows that when the solid is accelerated a force $a_i^{(2)}$ must be exerted on the fluid to prevent it from moving. This effect is measured by the coupling coefficient ρ_{21}. The force $a_i^{(2)}$ necessary to prevent the fluid motion is in a direction opposite to the acceleration of the solid; hence, we must always have

$$\rho_{21} < 0 \tag{5.6.23}$$

The same conclusion is reached by considering the first of the above equations, in which ρ_{11} represents the total effective mass of the solid moving in the fluid. This total mass must be equal to the mass proper of the solid ρ_1 plus an additional mass ρ_1 due to the fluid. Thus

$$\rho_{11} = \rho_1 + \rho_1;\ \rho_{21} = -\rho_1 \tag{5.6.24}$$

Similarly we obtain that,

$$\rho_{22} = \rho_2 + \rho_1';\ \rho_{12} = -\rho_1' \tag{5.6.25}$$

If moreover we choose, $\rho_i = \rho_i';$ i.e.

$$\rho_{21} = \rho_{12} = -\rho_1 < 0 \tag{5.6.26}$$

then the above restriction for the positiveness of the total, local kinetic energy of the synchronous moving phases is always satisfied as soon as also

$$\rho_{11} > 0;\ \rho_{22} > 0 \tag{5.6.27}$$

Plona and Johnson (1984) considered a simple model of porous medium to demonstrate the inertial mass coupling. In this model the pore space is a set of parallel cylindrical tubes. If the motion of the fluid is in a direction parallel to the tubes no coupling exists. If, however, the fluid is accelerated in a direction perpendicular to the tubes' axes, then there is an appreciable effect on the solid. Following this line of thought they finally derive an expression for the inertial mass coupling term,

$$\rho_{\mathrm{I}} = (\alpha - 1)n\rho_f \tag{5.6.28}$$

where α is a coefficient measuring the tortuosity of the pore-canal system. In the case of isolated spherical solid particles the tortuosity coefficient of the pore space a is given by the Berryman formula

$$\alpha = \frac{1}{2}\left(1 + \frac{1}{n}\right) \tag{5.6.29}$$

Johnson *et al.* (1987) have combined the two effects of inertial and viscous drag in the high frequency range and provided experimental backing of Biot's modification. It should be noted, however, that Biot's inertial drag correction is heuristic, since $\rho_{12} D_t^{(1)} v_{\mathrm{i}}^{(2)} \neq \rho_{21} D_t^{(2)} v_{\mathrm{i}}^{(1)}$, and a mixtures theory approach through the linear momentum conservation principle is not possible. In section 5.6.4 another approach for including an inertial drag on the basis of mixtures theory will be discussed.

5.6.3
Forchheimer's extension of Darcy's law

In pore-fluid flow, there is a slow transition from purely laminar flow to a mildly turbulent condition. A rough criterion of the limit of applicability of Darcy's law is expressed in terms of the Reynold's number of the flow referred to the mean grain diameter $D_{50\%}$ (Taylor, 1948)

$$\mathrm{Re} = \frac{qD_{50\%}}{\eta_k} \leqslant 1 \tag{5.6.30}$$

For higher Reynold's numbers the relation between head-loss and discharge velocity is non-linear. For one-dimensional flow with the discharge velocity q and hydraulic gradient $J = -\mathrm{d}\Phi/\mathrm{d}x$, Forchheimer suggested the following polynomial expression for the hydraulic gradient:

$$J = aq + bq^2 \tag{5.6.31}$$

where the first coefficient is identified with the hydraulic resistivity of the porous medium for laminar flow conditions

$$a = 1/k_{\mathrm{w}} \tag{5.6.32}$$

Considering the Navier-Stokes equations for the fluid and flow passing through a periodic array of spherical grains, Irmay (1958) justified a more general form of Forchheimer's law, which included inertial effects as well

$$J = aq + bq^2 + c\frac{\partial q}{\partial t} \tag{5.6.33}$$

where the various coefficients were given by the following expressions

$$a = c_1 \frac{(1-n)^2}{n^3} \frac{\eta_k}{gD_{50\%}^2} \tag{5.6.34}$$

$$b = c_2 \frac{1-n}{n^3} \frac{1}{gD_{50\%}} \tag{5.6.35}$$

$$c = \frac{1}{ng} \tag{5.6.36}$$

c_1 and c_2 are shape factors. As pointed out by Irmay (1958), the coefficient b depends on the porosity as $(1-n)/n^3$, and linearly on the inverse of the average grain diameter $D_{50\%}$. This means that the effect of the quadratic term in q in equation 5.6.33 will be more pronounced in the case of coarse-grained material, whereas for fine-grained material the linear term q should dominate. Irmay's law can be rewritten in terms of pore-water pressure gradient as follows

$$-\frac{\partial p_w}{\partial x} + \rho_w g = f_1 q + f_2 q^2 + \rho_w \frac{\partial v^{(2)}}{\partial t} \tag{5.6.37}$$

where

$$f_1 = c_1 \frac{(1-n)^2}{n^3} \frac{\eta_k \rho_w}{D_{50\%}^2} \tag{5.6.38}$$

$$f_2 = c_2 \frac{1-n}{n^3} \frac{\rho_w}{D_{50\%}} \tag{5.6.39}$$

By neglecting the quadratic term and comparing Irmay's law with the dynamic equation 5.5.13, we identify both dissipative and dynamic terms. Using equation 5.6.5 and $f_1 = f$, , the physical permeability of the soil is found to be proportional to the mean grain diameter

$$k = \frac{1}{c_1} \frac{n^3}{(1-n)^2} D_{50\%}^2 \tag{5.6.40}$$

cf. Hazen's rule (5.6.9). Equation 5.6.40 is known as the Karman-Kozeny equation (Dullien, 1979), with the constant c_1 given by

$$c_1 = c_o S_{vp} \tag{5.6.41}$$

Table 5.6.1 Typical values of a and b for uniform granular soils after Wittmann (1980)

$D_{50\%}$ (mm)	n (–)	k_w (m/s)	a (s/m)	b (s²/m²)	b/a (s/m)	f^* (s/m)
2–4	0.37	0.038	26.3	1445	55	31.7–63.5
4–6	0.38	0.123	8.1	806	100	64.5–96.8
6–8	0.36	0.200	5.0	630	126	93.7–125
5–10	0.38	0.243	4.1	575	140	80.6–161.3
9–16	0.40	0.807	1.2	318	265	150–266.6

where $S_{vp} = (2/R_H)$ is the specific surface of the pores, defined as the ratio between pore surface and pore volume; cf. equation 5.6.13. c_0 is the so-called Kozeny constant, which was assigned by Karman the value, $c_o = 5$. Bear (1972) indicates that Irmay adopted the values $c_1 = 180$ and $c_2 = 0.6$. Finally, we remark that Whitney and Evans (1989) give for f_2 empirical relationships distilled from a great number of tests on limestones and sandstones.

Irmay generalized Forchheimer's law in a similar fashion as the original Darcy law so as to describe two- or three-dimensional flow as well. In that sense equation 5.6.5 is extended to the non-linear flow regime as follows

$$\hat{f}_i = f\{1 + f^*(q_k q_k)^{\frac{1}{2}}\}q_i \tag{5.6.42}$$

where

$$f^* = \frac{c_2}{c_1}\frac{1}{1-n}\frac{D_{50\%}}{\eta_k} \tag{5.6.43}$$

Table 5.6.1 from Wittmann (1980) gives some typical results for the coefficients a and b for uniform sands. In this table the experimental value of b/a and its theoretical value f^*, predicted from Irmay's equation (5.6.43) are also listed.

5.6.4
Brinkman's and Aifantis modification of Darcy's law

On several occasions, the permeability of a granular medium is relatively high and grains are detached from the solid matrix and part of the pore fluid (fluidized bed). Also, fluid flow past permeable surfaces cannot be matched with Darcian flow within the porous medium. In these cases, the validity of Darcy's law is questionable and some modified form of it seems to be more appropriate. One possibility is to adopt Brinkman's (1947) generalization of Darcy's law, which allows for energy dissipation not only due to friction of fluid flowing around grains but also due to the viscous shearing stress which is acting within the fluid phase itself. This modification was done by adding to Darcy's law the corresponding viscous-stress term that is appearing in the Navier-Stokes equations. In our terminology, Brinkman's generalization of Darcy's law can be written in the following form

$$-\partial_i p_w = \rho_w \left[\frac{\eta_k}{k} q_i - \eta_k \nabla^2 q_i \right] = f(q_i - k\nabla^2 q_i) \tag{5.6.44}$$

For rigid solid $q_i = n v_i^{(2)}$, and equation 5.6.44 reduces to Navier-Stokes' equation as $k \to \infty$ and to Darcy's law if $kL^2 \ll 1$, where L denotes a spatial length scale.

On the other hand, for stability analyses of deformations in porous, fluid-saturated media, Aifantis (1984) proposed the following gradient modification of Darcy's law

$$-\partial_i (p_w - k_A \nabla^2 p_w) = f q_i \tag{5.6.45}$$

where the constant k_A has the dimension of length square. Using dimensional analysis argument similar to the one applied for deriving Brinkman's law (5.6.44), we observe that here the only significant material property is the physical permeability and due to lack of other information we set $k_A = c_A k$.

Brinkman's and Aifantis' modifications can be included in the mixtures theory formalism as follows (Vardoulakis and Aifantis, 1994): Starting from momentum balance for each phase separately, equation 5.5.1 is modified by considering volume as well as surface interaction terms

$$F_i^{(\alpha)} = \int_V \rho_\alpha g_i \, dV + \int_V f_i^{(\alpha)} \, dV + \int_{\partial V} dt_i^{(\alpha)} + \int_{\partial V} ds_i^{(\alpha)} \tag{5.6.46}$$

where

$$ds_i^{(1)} = -ds_i^{(2)} = ds_i \tag{5.6.47}$$

is the interaction traction exerted by the flowing fluid on the solid phase at the boundary ∂V of the considered volume V. These surface tractions can be related to a solid-fluid interaction stress tensor, as

$$ds_i^{(\alpha)} = s_{ki}^{(\alpha)} n_k \, dS \tag{5.6.48}$$

which then leads to the following modification of the corresponding dynamic equations

$$\partial_k (\sigma_{ki}^{(\alpha)} + s_{ki}^{(\alpha)}) + \rho_\alpha g_i + f_i^{(\alpha)} = \rho_\alpha \frac{D^{(\alpha)}}{Dt} v_i^{(\alpha)} \tag{5.6.49}$$

Under the same set of simplifying assumptions which have led to equation 5.5.13, equation 5.6.49 if applied for the fluid phase (α=2), leads to the following dynamic equation

$$-\partial_k (p_w \delta_{ki} - \hat{s}_{ki}) + \rho_w g_i - \hat{f}_i = \rho_w a_i^{(2)} \tag{5.6.50}$$

where

$$a_i^{(2)} = \frac{D^{(2)}}{Dt} (v_i^{(2)}) \tag{5.6.51}$$

is the fluid acceleration, and

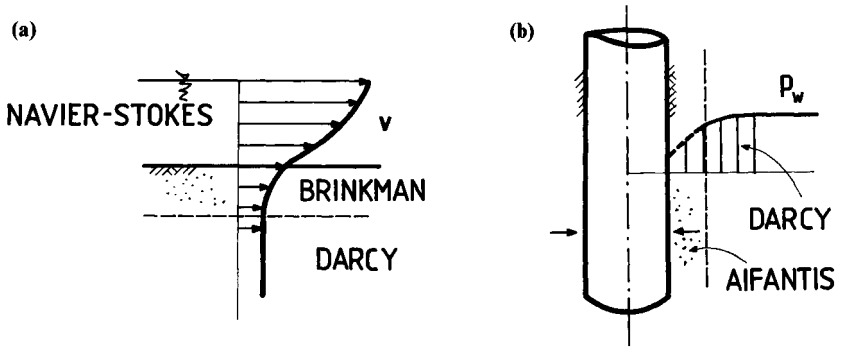

Figure 5.6.2 (a) Pore-fluid velocity variation for surface parallel flow; (b) pore-fluid pressure variation for surface normal flow.

$$\hat{s}_{ij} = s_{ij}/n \tag{5.6.52}$$

is Brinkman's viscous stress tensor.

We saw above, equation 5.6.5, that Darcy's law results in a constitutive equation for the seepage force, according to which the volume solid-fluid interaction force is proportional to the relative specific discharge

$$\hat{f}_i = fq_i \tag{5.6.53}$$

Brinkman's modification (5.6.44) suggests on the other hand that the solid-fluid interaction stress is proportional to the gradient of q_i

$$\hat{s}_{ki} = -\rho_w \eta_k \partial_k q_i \tag{5.6.54}$$

In this sense Brinkman's law is a gradient modification of Darcy's law, such that solid-fluid interaction at a small distance from the boundaries of a porous, water-saturated medium is considered in addition to their interaction in the interior domain. Brinkman's modification plays a role whenever one is interested in surface-parallel flows, where strong fluid velocity gradients are localized close to the boundary of the porous medium (Figure 5.6.2(a); Neale and Nader, 1974).

With the above constitutive assumptions 5.6.50 and 5.6.51 and within a linearized theory, the dynamic equation 5.6.49 becomes

$$-\partial_i p_w + \rho_w g_i - f(q_i - k\nabla^2 q_i) = \rho_w a_i^{(2)} \tag{5.6.55}$$

On the other hand, Aifantis' modification 5.6.45 suggests that the solid-fluid interaction stress is obeying a balance law of the form

$$\hat{s}_{ij} + \partial_k \hat{m}_{kij} = 0 \tag{5.6.56}$$

where $\hat{m}_{kij}$ are double stresses in the sense of Mindlin (1964). Thus, similar to Brinkman's law, Aifantis' modification is reinterpreted as applying only at small distances from the boundaries of a porous medium. Aifantis' rule (5.6.45) in particular

follows from the more general balance equation 5.6.56, if the double stresses are set proportional to the pressure gradient

$$\hat{m}_{kij} = k_{\mathrm{A}}(1/n)\partial_k(\sigma_{ij}^{(2)}) = -k_{\mathrm{A}}\partial_k p_{\mathrm{w}}\delta_{ij} \tag{5.6.57}$$

and thus

$$\hat{s}_{ij} = k_{\mathrm{A}}\nabla^2 p_{\mathrm{w}}\delta_{ij} \tag{5.6.58}$$

i.e. Aifantis' modification must play a role whenever one is interested in surface-normal flows where pore-pressure gradients are localized close to the boundary of the porous medium (Figure 5.6.2b). With these assumptions the dynamic equation 5.6.50 becomes

$$-\partial_i(p_{\mathrm{w}} - k_{\mathrm{A}}\nabla^2 p_{\mathrm{w}}) - fq_i = \rho_{\mathrm{w}} a_i^{(2)} \tag{5.6.59}$$

We observe that both Aifantis' and Brinkman's modifications fall within the context of balance equations for the intrinsic equilibrated body force $\hat{S}_{ij}$, like the one discussed by Cowin and Nunziato (1983) in their paper on linear elasticity of materials with voids, i.e.

$$\hat{s}_{ij} + \partial_k \hat{m}_{kij} + \hat{\Phi}_{ij} = \hat{I}_{ij} \tag{5.6.60}$$

accompanied by special constitutive assumptions for the double stresses

$$\hat{m}_{kij} = -k_{\mathrm{A}}\partial_k p_{\mathrm{w}}\delta_{ij};\ k_{\mathrm{A}} = c_{\mathrm{A}}k \tag{5.6.51\textit{bis}}$$

and the extrinsic equilibrated body force

$$\hat{\Phi}_{ij} = \rho_{\mathrm{w}}\eta_k\partial_k q_i \tag{5.6.54\textit{bis}}$$

For the equilibrated inertia one could try for example to include an effect similar to Biot's inertial drag in an objective manner

$$\hat{I}_{ij} = \rho_I k\hat{I}\delta_{ij} \tag{5.6.61}$$

As in the work of Cowin and Nunziato, the inertial drag $\hat{I}$ may be related to the second material time derivative of the porosity

$$\begin{aligned}\hat{I} &= \frac{\mathrm{D}^{(2)}}{\mathrm{D}t}\left[\frac{1}{n}\frac{\mathrm{D}^{(2)}}{\mathrm{D}t}(n)\right] = -\frac{\mathrm{D}^{(2)}}{\mathrm{D}t}\left[\partial_k v_k^{(2)} + \frac{1}{\rho_{\mathrm{w}}}\frac{\mathrm{D}^{(2)}}{\mathrm{D}t}(\rho_{\mathrm{w}})\right] \\ &= -\left[\partial_k a_k^{(2)} + c_{\mathrm{w}}\frac{\mathrm{D}^{(2)2}}{\mathrm{D}t^2}(p_{\mathrm{w}})\right]\end{aligned} \tag{5.6.62}$$

where the mass balance equation, equation 5.2.6 for $\alpha = 2$, and the constitutive law of equation 5.4.8 for the fluid phase were used. For incompressible fluid ($c_{\mathrm{w}} = 0$) the inertial drag is given only by the divergency of the fluid acceleration

$$\hat{I} = -\partial_k a_k^{(2)} \tag{5.6.63}$$

Accordingly, the complete extension of Darcy's law so as to include gradient effects follows

$$-\partial_i(p_w - k_A\nabla^2 p_w) - f(q_i - k_B\nabla^2 q_i) = \rho_w(a_i^{(2)} - k_I\partial_i\partial_k a_k^{(2)}) \tag{5.6.64}$$

where $k_A = c_A k$, $k_B = k$ and $k_I = (\rho_I/\rho_w)k$. It should be noted, however, that such gradient extensions of Darcy's law necessitate the study and formulation of extra boundary conditions which are in essence additional constitutive equations describing, for example, if a solid particle can move in or out of the solid matrix.

5.7
The incremental initial, boundary value problem

5.7.1
Governing equations

Let a fluid saturated soil body B at time t=0, be in a given configuration C. B is subjected to an infinitesimal deformation, and C is used as reference configuration. It is assumed that during this deformation process the various mechanical properties of the body change but little, e.g. the porosity changes from its value $n(x_k,0)$ in C to $\bar{n} = n + \Delta n(x_k, t)$ in $\bar{\mathbf{C}}$, with $\Delta n(x_k, 0) = 0$ and $|\Delta n|/n \ll 1$. The incremental displacement of the solid for the considered transition $\mathbf{C} \rightarrow \bar{\mathbf{C}}$ is Δu_i and the relative specific discharge vector of the fluid in $\bar{\mathbf{C}}$ is $\bar{q}_i = q_i + \Delta q_i$. Since convective terms will be neglected for both the fluid and the solid phase, material time derivatives coincide with partial time derivatives, and

$$v_i^{(1)} \approx \partial_t \Delta u_i \tag{5.7.1}$$

$$v_i^{(2)} = \partial_t \Delta u_i + \Delta q_i/n \tag{5.7.2}$$

For any time t>0 infinitesimal strain and spin of the solid are then given by

$$\Delta\varepsilon_{ij} = \tfrac{1}{2}(\partial_i \Delta u_j + \partial_j \Delta u_i);\ \Delta\omega_{ij} = \tfrac{1}{2}(\partial_i \Delta u_j - \partial_j \Delta u_i) \tag{5.7.3}$$

Mass balance is expressed here by equations 5.2.15 and 5.2.16, where one should bear in mind the underlying assumptions which have led to these forms

$$\Delta n = (1 - n)\Delta\varepsilon_{kk} \tag{5.7.4}$$

$$-\partial_k \Delta q_k = n c_w \partial_t \Delta p_w + \partial_t \Delta\varepsilon_{kk} \tag{5.7.5}$$

The partial stress of the fluid phase in C and $\bar{\mathbf{C}}$ is given through the following mappings which involve the pore-water pressure p_w and the porosity n,

$$\mathrm{d}t_i^{(2)} = \sigma_{it}^{(2)} n_k \,\mathrm{d}S = -n p_w \delta_{ik} n_k \,\mathrm{d}S \tag{5.7.6}$$

$$\begin{aligned} \mathrm{d}\bar{t}_i^{(2)} &= \bar{\sigma}_{ik}^{(2)} \bar{n}_k \,\mathrm{d}\bar{S} = -\bar{n}\bar{p}_w \delta_{ik} \bar{n}_k \,\mathrm{d}\bar{S} \\ &= \pi_{ik}^{(2)} n_k \,\mathrm{d}S \end{aligned} \tag{5.7.7}$$

The nominal fluid stress in $\bar{\mathbf{C}}$ is given as

$$\pi_{ik}^{(2)} = \sigma_{ik}^{(2)} + \Delta\pi_{ik}^{(2)} \tag{5.7.8}$$

and thus from equations 5.7.6 to 5.7.8 we obtain

$$\begin{aligned} -np_w\delta_{ik} + \Delta\pi_{ik}^{(2)} &= -(n+\Delta n)(p_w + \Delta p_w)\mathrm{ad}(F^t)_{ki} \\ &= -(n+\Delta n)(p_w + \Delta p_w)\{(1 + \partial_m \Delta u_m)\delta_{ki} - \partial_i \Delta u_k\} \end{aligned}$$

or with equation 5.7.4

$$\Delta\pi_{ij}^{(2)} = -n\Delta p_w \delta_{ij} + \bar{\Delta}\pi_{ij}^{(2)} \tag{5.7.9}$$

$$\bar{\Delta}\pi_{ij}^{(2)} = -p_w(\partial_m \Delta u_m \delta_{ij} - n\partial_i \Delta u_j) \tag{5.7.10}$$

Similarly the definition of the partial stress for the solid phase in C and $\bar{\mathbf{C}}$ involves the effective stress σ'_{ij} and the porosity n through the following mappings,

$$\mathrm{d}t_i^{(1)} = \sigma_{ik}^{(1)} n_k \,\mathrm{d}S = \sigma'_{ik} - (1-n)p_w \delta_{ik} n_k \,\mathrm{d}S \tag{5.7.11}$$

$$\begin{aligned} \mathrm{d}\bar{t}_i^{(1)} &= \bar{\sigma}_{ik}^{(1)} \bar{n}_k \,\mathrm{d}\bar{S} = \bar{\sigma}'_{ik} - \bar{n}\bar{p}_w \delta_{ik} \bar{n}_k \,\mathrm{d}\bar{S} \\ &= \pi_{ik}^{(1)} n_k \,\mathrm{d}S = (\sigma_{ik}^{(1)} + \Delta\pi_{ik}^{(1)}) n_k \,\mathrm{d}S \end{aligned} \tag{5.7.12}$$

where

$$\Delta\pi_{ij}^{(1)} = \Delta\sigma'_{ij} - (1-n)\Delta p_w \delta_{ij} + \bar{\Delta}\pi_{ij}^{(1)} \tag{5.7.13}$$

$$\bar{\Delta}\pi_{ij}^{(1)} = \sigma'_{ij}\partial_k \Delta u_k - \sigma_{ik}^{(1)} \partial_k \Delta u_j \tag{5.7.14}$$

The dynamic equations in $\bar{\mathbf{C}}$ are then expressed as follows

$$\partial_k \Delta\pi_{ik}^{(1)} + \Delta b_i^{(1)} = \rho_1 \partial_t v_i^{(1)} \tag{5.7.15}$$

$$\partial_k \Delta\pi_{ik}^{(2)} + \Delta b_i^{(2)} = \rho_2 \partial_t v_i^{(2)} \tag{5.7.16}$$

or

$$\partial_k(\Delta\sigma'_{ik} - \Delta p_w \delta_{ik}) + \partial_i(n\Delta p_w) + \partial_k \bar{\Delta}\pi_{ik}^{(1)} + \Delta b_i^{(1)} = \rho_1 \partial_{tt} \Delta u_i \tag{5.7.17}$$

$$-\partial_i(n\Delta p_w) + \partial_k \bar{\Delta}\pi_{ik}^{(2)} + \Delta b_i^{(2)} = \rho_2 \partial_t(\partial_t \Delta u_i + \Delta q_i/n) \tag{5.7.18}$$

where

$$\Delta b_i^{(1)} = -\Delta b_i^{(2)} = -\Delta b_i \tag{5.7.19}$$

is the nominal fluid-solid interaction force, which is computed as follows: The total fluid-solid interaction force in $\bar{\mathbf{C}}$ is

$$\bar{f}_i \,\mathrm{d}\bar{V} = b_i \,\mathrm{d}V = (f_i + \Delta b_i)\mathrm{d}V \tag{5.7.20}$$

cf. equation 3.3.12. With

$$f_i = n\hat{f}_i = nfq_i \tag{5.7.21}$$

$$\bar{f}_i = \bar{n}\bar{f}\bar{q}_i \approx f_i + f(n\Delta q_i + \Delta n q_i) \tag{5.7.22}$$

we obtain

$$\bar{f}_i \mathrm{d}\bar{V} = \{f_i + f(n\Delta q_i + \Delta n q_i)\}(1 + \Delta\varepsilon_{kk})\mathrm{d}V = (f_i + \Delta b_i)\mathrm{d}V$$

or

$$\Delta b_i = nf\Delta q_i + \hat{f}_i \Delta\varepsilon_{kk} \tag{5.7.23}$$

By adding the above partial dynamic equations by parts, we obtain the dynamic equation in terms of the total stress

$$\partial_k \Delta\pi_{ik} = \rho_1 \partial_t v_i^{(1)} + \rho_2 \partial_t v_i^{(2)} \tag{5.7.24}$$

where

$$\Delta\pi_{ij} = \Delta\sigma_{ij} + \sigma_{ij}\partial_k \Delta u_k - \sigma_{ik}\partial_k \Delta u_j \tag{5.7.25}$$

cf. equation 3.1.33.

If one neglects the influence of initial stress, the dynamic equations 5.7.24 in terms of the total stress increment

$$\partial_k \Delta\sigma_{ik} = \rho_1 \partial_t v_i^{(1)} + \rho_2 \partial_t v_i^{(2)} \tag{5.7.26}$$

whereas in terms of effective stress and pore-water pressure increment, equations 5.7. 17 and 5.7.18 yield,

$$\partial_k \Delta\sigma'_{ik} + \Delta\hat{b}_i = \rho_b \partial_t v_i^{(1)} - (1 - n)\rho_w(\partial_t v_i^{(1)} - \partial_t v_i^{(2)}) \tag{5.7.27}$$

$$-\partial_i \Delta p_w - \Delta\hat{b}_i = \rho_w \partial_t v_i^{(2)} \tag{5.7.28}$$

where according to equation 5.7.23 Darcy's law is recovered,

$$\Delta\hat{b}_i = f\Delta q_i \tag{5.7.29}$$

and the effective stress increment is given by a set constitutive equations for the 'drained' porous medium, of the form

$$\Delta\sigma'_{ij} = C_{ijkl}\Delta\varepsilon_{kl} \tag{5.7.30}$$

where C_{ijkl} is the appropriate stiffness tensor.

5.7.2
The incremental problem

The incremental initial, boundary value problem is governed by an appropriate set of balance and constitutive equations as outlined above. Time enters into the problem through the storage terms, equation 5.7.5, and the inertia terms in the dynamic equations. On some occasions one may emphasize the importance of one factor over the other. For demonstration purposes we will consider here the particular case which results from the following set of simplifying assumptions:

(1) The solid constituent is incompressible
(2) The fluid constituent is incompressible
(3) The effect of initial stress is negligible
(4) The effect of inertia is negligible
(5) Pore-fluid flow is governed by Darcy's law
(6) Deformation of the solid skeleton is governed by an incrementally linear constitutive equation for the effective Cauchy stress, as in equation 5.7.30 with constant stiffness tensor.

Accordingly, the set of governing equations becomes,

$$\Delta n = (1 - n)\partial_k \Delta u_k \tag{5.7.31}$$

$$-\partial_k \Delta q_k = \partial_t \partial_k \Delta u_k \tag{5.7.32}$$

$$C_{ijkl}\partial_j \partial_l \Delta u_k + f\Delta q_i = 0 \tag{5.7.33}$$

$$-\partial_i \Delta p_w - f\Delta q_i = 0 \tag{5.7.34}$$

The initial value problem is defined by specifying non-zero initial values

$$\Delta u_i(x_k, 0) = \Delta u_i^0(x_k);\ \Delta p_w(x_k, 0) = \Delta p_w^0(x_k) \tag{5.7.35}$$

Boundary conditions are usually expressed in terms of the total stress increment and the solid-phase displacement

$$n_k \Delta \sigma_{ki} = t_i \quad \text{on} \quad \partial V_\sigma;\ \Delta u_i = \delta_i \quad \text{on} \quad \partial V_u \tag{5.7.36}$$

and in terms either of the pore-pressure increment or the discharge vector for the fluid phase. For example, on a permeable boundary one may assume that the pore pressure is constant

$$\Delta p_w = 0 \quad \text{on} \quad \partial V_p \tag{5.7.37}$$

Across an impermeable boundary on the other hand no fluid flows,

$$\Delta q_i = 0 \quad \text{on} \quad \partial V_q \tag{5.7.38}$$

5.7.3
Linear stability analysis

In a fluid-saturated medium, local, short-term stability is studied with the so-called undrained deformation mode as the ground mode. Undrained deformations are characterized by remote boundary conditions which preclude in- or outflow of water. For incompressible fluid and solid such a type of boundary condition implies that under normal conditions the fluid flux vector is zero everywhere in the considered domain, i.e. the ground deformation mode is characterized by the condition,

$$\Delta \dot{q}_i = 0 \tag{5.7.39}$$

Thus from this condition and the continuity equation 5.7.32 it will follow that the ground deformation mode is volume preserving (isochoric)

$$\partial_k \Delta\dot{u}_k = 0 \tag{5.7.40}$$

The stability problem is now defined as follows: at any given state of an undrained deformation, small perturbations $\Delta\tilde{u}_i$, $\Delta\tilde{p}_w$ and $\Delta\tilde{q}_i$ of the displacements of the skeleton, the pore-water pressure and the relative specific discharge vector are considered and their evolution in time is studied; cf. Rice (1975) and Vardoulakis (1985, 1986). The total displacement, pore-water pressure and discharge are then the sum of the ground mode and the perturbation mode,

$$\Delta u_i = \Delta\dot{u}_i + \Delta\tilde{u}_i \quad \text{etc.} \tag{5.7.41}$$

We want to emphasize that the definition of stability discussed in this section refers to small perturbations around a ground state of undrained deformation. During such small perturbations, the 'drained' material behavior is assumed to be described by the constitutive tensor C_{ijkl} which in turn is assumed to be the same for all possible deformation continuations.

The considered stability problem is governed by the equilibrium equations 5.7.33 and 5.7.34 for both soil skeleton and fluid, the continuity equation 5.7.32 for the fluid flow, and the constitutive equations for the soil skeleton and the fluid flow. In particular, fluid flow in a porous medium is assumed here to be governed by Darcy's law. Finally the mass balance equation 5.7.31 permeability of the soil; cf. equation 5.6.40. Elimination of the relative specific discharge vector from the set of governing partial differential equations leads serves for the updating of the porosity, which in turn affects mostly the to the following governing equations for the perturbation mode

$$\partial_t \partial_k \Delta\tilde{u}_k = \frac{1}{f}\partial_m \partial_m \Delta\tilde{p}_w \tag{5.7.42}$$

$$C_{ijkl}\partial_j \partial_l \Delta\tilde{u}_k = \partial_i \Delta\tilde{p}_w \tag{5.7.43}$$

A simple class of perturbation modes corresponds to deformations which satisfy the zero drainage condition (5.7.39) and the incompressibility condition (5.7.40) in an average sense. Such modes correspond to spatially periodic patterns like the array of layers, the so-called roller bifurcation mode, which is shown in Figure 5.7.1. In this figure dark strips contract and expel water, whereas light strips dilate by an equal amount and suck water. The pore-water pressure in the contracting strips is increasing and the effective pressure is decreasing by an equal amount. The opposite is true for the dilating strips. The layer pattern is the simplest plane-strain perturbation of the isochoric motion and it is given by the following equations

$$\begin{aligned} \Delta\tilde{u}_i &= C_i \sin(Qn_k x_k)\exp(St) \qquad (i = 1, 2) \\ \Delta\tilde{p}_w &= C_3 \cos(Qn_k x_k)\exp(St) \end{aligned} \tag{5.7.44}$$

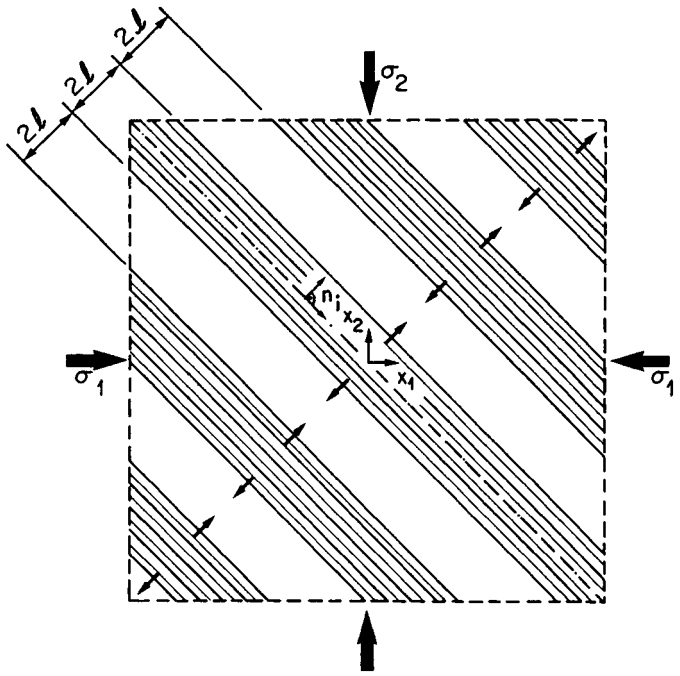

Figure 5.7.1 Layer pattern of dilating and contacting strips in water-saturated granular medium.

where $\{n_i\} = \{-\sin\Theta, \cos\Theta, 0\}^T$ is the normal to the direction of the layers, S is called the growth coefficient, Q the wavenumber of the instability and C_i are constants. Thus, according to equation 5.7.44 we are searching for spatially periodic solutions which are evolving exponentially in time.

It should be noted that besides the layer pattern other patterns are also possible; see Settinger (1979). The checkerboard pattern for example is defined as follows

$$\begin{aligned} \Delta\tilde{u}_1 &= C_1 \cos(Q_1 x_1)\sin(Q_2 x_2)\exp(St) \\ \Delta\tilde{u}_2 &= C_2 \sin(Q_1 x_1)\cos(Q_2 x_2)\exp(St) \\ \Delta\tilde{p}_w &= C_3 \cos(Q_1 x_1)\cos(Q_2 x_2)\exp(St) \end{aligned} \tag{5.7.45}$$

where the wavenumbers Q_i are related to wavelengths L_i of the instability,

$$Q_i = m_i \pi/(2L_i);\ m_i = 1, 3, \ldots \tag{5.7.46}$$

This mode is identical with Biot's (1965) internal buckling mode. The simplest case of square pattern corresponds to $Q_1 = Q_2 = Q$; see Figure 5.7.2. Another volume-preserving pattern is Benard's hexagonal pattern. It seems, however, that in most soil mechanics applications the strip pattern is the dominant one. In this case from equations 5.7.32 and 5.7.33 and the decomposition (5.7.41) we obtain the following homogeneous system for the determination of the constants C_i,

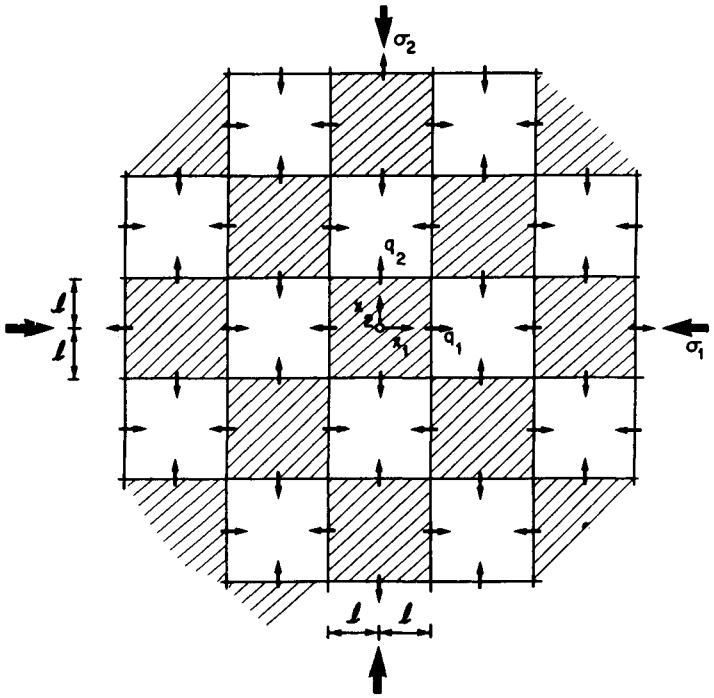

Figure 5.7.2 Checkerboard pattern of dilating and contacting cells in water-saturated granular medium.

$$\begin{bmatrix} Q\Gamma_{11} & Q\Gamma_{12} & -fn_1 \\ Q\Gamma_{21} & Q\Gamma_{22} & -fn_2 \\ Sn_1 & Sn_2 & Q \end{bmatrix} \begin{bmatrix} C_1 \\ C_2 \\ C_3 \end{bmatrix} = \{0\} \tag{5.7.47}$$

where

$$\Gamma_{ik} = C_{ijkl} n_j n_l \tag{5.7.48}$$

is identified with the 'acoustic' tensor, since it appears also in the acceleration waves propagation analysis.

The existence of non-trivial solutions of the homogeneous algebraic system of equations 5.7.47 requires the satisfaction of the following first-order 'dispersion' equation for the considered instability mode:

$$\Delta(n_1, n_2) Q(fS) + \Gamma(n_1, n_2) Q^3 = 0 \tag{5.7.49}$$

holding for $Q>0$. The coefficients Δ and Γ are biquadratic forms in the direction cosines n_i

$$\Delta = \Gamma_{11} n_2^2 - (\Gamma_{12} + \Gamma_{21}) n_1 n_2 + \Gamma_{22} n_1^2 \tag{5.7.50}$$

$$\Gamma = \det(\Gamma_{ik}) \tag{5.7.51}$$

The ground state (of undrained deformation) is called *stable* if for all directions and all wave numbers the considered perturbation of the isochoric motion decays exponentially with time, i.e. if $\forall n_i (fS)<0$. If $\Delta>0$ the sign of the growth coefficient is determined by the sign of Γ, the determinant of the acoustic tensor, i.e.

$$\{\forall n_i: \Delta > 0 \text{ and } \Gamma > 0\} \rightarrow -\infty < (fS) < 0 \tag{5.7.52}$$

As we will discuss in chapter 8, the condition

$$\Gamma = \det(\Gamma_{ik}) = 0 \tag{5.7.53}$$

is the classical shear-band bifurcation condition, i.e. a necessary condition for the existence of a particular type of non-uniqueness in the form of stationary discontinuities in the displacement gradients $\partial_j \Delta u_i$. If $\Delta>0$, the state (B) with $\Gamma = 0$ marks the first instability. Past this state the ground state becomes *unstable,* since exponential growth of an arbitrary small perturbation is predicted, i.e.

$$\{\forall n_i: \Delta > 0\} \quad \text{and} \quad \exists n_i / \Gamma < 0 \rightarrow 0 < (fS) < +\infty \tag{5.7.54}$$

In this case, the dispersion equation (5.7.49) predicts that instabilities with infinitesimal wavelength ($Q \rightarrow \infty$) grow with infinite pace. This shortcoming of classical continuum theory, which breaks down at the infinitesimal wavelength limit, can be remedied, for example, by resorting to Aifantis' (1984) gradient modification of Darcy's law.

The linear stability analysis becomes questionable, if for some directions n_i the coefficient Δ in equation 5.7.49 becomes zero. In this case, the algebraic dispersion equation 5.7.49 is meaningless, and the corresponding linear stability problem is called *mathematically ill-posed*.

5.8 Compaction instabilities

5.8.1 Grain crushing

Spacial instabilities under compression can only be explained by Biot's (1965) theory of internal buckling, if (a) significant deviators are applied, and (b) if the material possesses an adequate degree of anisotropy; cf. chapter 4. In particular, internal buckling theory cannot explain instabilities under isotropic compression. In other words, compaction instabilities are not explained by considering geometric non-linearities. They seem to be caused primarily by physical non-linearities, like material softening due to grain crushing or void collapse. (A typical value for grain crushing initiation in quartzitic sands is about 10 MPa; cf. Terzaghi and Peck, 1948.)

Compaction layering is observed in geomaterials at many scales, but it is more pronounced in porous geomaterials consisting of uniform particles and pores. It is

related mainly to sharp permeability variations in granular rock (sandstone; cf. Papamichos *et al.,* 1993) and to anomalous subsidence in porous rocks (chalks).

Garbrecht (1973) performed experiments with uniform glass beads and showed that under isotropic compression, non-uniform compaction can occur in association with sudden, spatially localized grain crushing. The externally applied pressure leads to interparticle stresses, which upon reaching a critical value, cause massive grain crushing. Spatially non-uniform grain crushing is accompanied by a catastrophic drop in bulk stiffness of the assembly, which after continued loading starts rising again only after substantial compaction has occurred. Figure 5.8.1 shows the experimental results of Garbrecht (1973). At the turning point of the stress-strain curve, considerable grain crushing was observed. This is shown in Figure 5.8.2 where the percentage F of broken glass spheres (original diameter 5 mm) is plotted as a function of the applied hydrostatic pressure. It is observed, however, that grain crushing reaches saturation, and stresses start to peak up again. This mechanism can be explained as follows: Initially a great population of intact grains exists, which is capable of load carrying, resulting in a net stress increase (strain hardening). In due course of loading grain crushing occurs, which results in further loading of the intact spheres, whereas broken spheres are in a more or less stress-free state. When the intergranular forces on the intact spheres reach a critical value, a catastrophic grain collapse occurs, which has as the result of annihilating (at least locally) the population of intact material. After that, broken material is reloaded, and thus an initial softening is followed by a restiffening. It should be noted that in the course of this process, irreversible compaction of the assembly takes place.

Following the above conceptual model, the simplest mechanism which can account for grain crushing is based on the assumption that the compaction curve of the material is S-shaped as shown in Figure 5.8.3. During the experiment the descending branch BC cannot be followed quasistatically, and thus there is a dynamic snap-through from A to D, resulting in the coexistence of broken and unbroken material and thus in compaction layering.

Figure 5.8.4 shows qualitatively the stiffness variation with volumetric strain. Accordingly, volumetric strain increments are related to the stress increments through a law similar to equation 5.4.10, where the stiffness $K_t = 1/c$ at the stage of grain-crushing drops significantly and it may also negative.

5.8.2
Stability of non-uniform compaction

As an application of the theory developed in section 5.7, we consider here the persistence of non-uniform compaction of a layer of collapsible, porous material which is saturated with fluid. The problem at hand is that of one-dimensional compaction and is formulated as follows: At any given state of stress σ_{xx}, a small increment of axial stress $\Delta\sigma_{xx}$ is added and consolidation of the layer is awaited. This type of loading may simulate a slow process of compaction due to sedimentation or a more rapid process of compaction

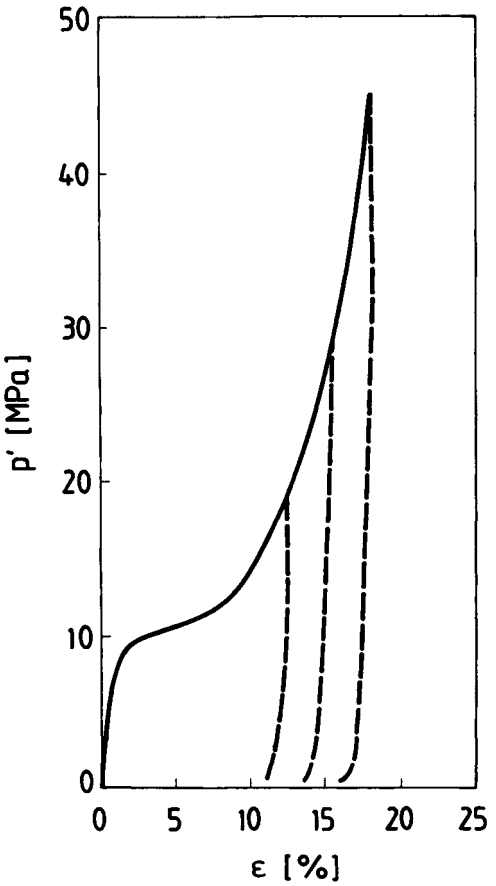

Figure 5.8.1 Isotropic compression of glass beads (Garbrecht, 1973).

due to pore-fluid pressure reduction in oil or earth-gas depletion processes. If the background behavior of the solid skeleton is strain hardening, then compaction is characterized by a slow consolidation process governed by the drainage conditions at remote boundaries. However, this is not the only possible mechanism, since, as shown in Figure 5.8.5, one may imagine, under continued loading conditions, the formation of a periodic pattern of layers of thickness d, which alternatively compact and expand by expelling or sucking pore fluid.

Starting from an equilibrium state (t=0) the linear stability problem is defined in terms of the increment of effective stress and excessive pore-fluid pressure for small initial values

$$\begin{aligned} \Delta\sigma'_{xx} &= \sigma'_{xx}(x,t) - \sigma'_{xx}(x,0) = \Delta\sigma'(x,t) \\ \Delta p_f &= p_f(x,t) - p_f(x,0) = \Delta p(x,t) \end{aligned} \tag{5.8.1}$$

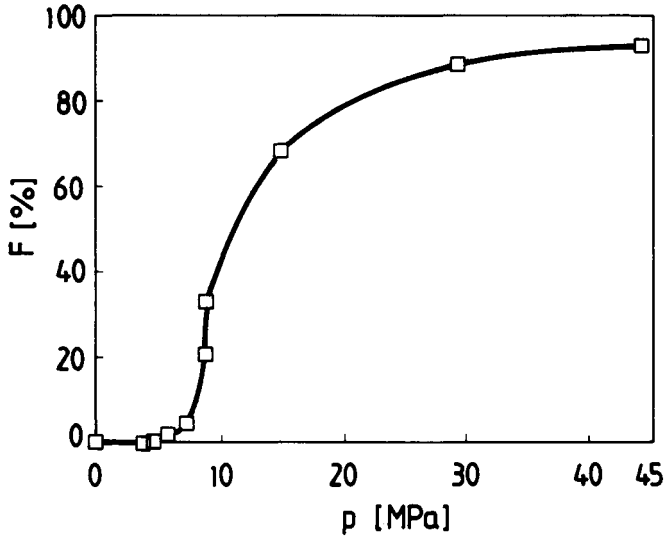

Figure 5.8.2 Grain breakage percentage as a function of applied pressure, during. hydrostatic compression of glass sphere assembly (Garbrecht, 1973).

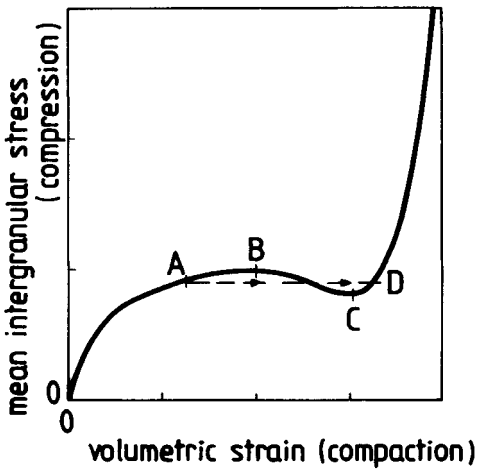

Figure 5.8.3 Stress variation of unstable material with volumetric strain.

The corresponding kinematic variables for the solid skeleton and the pore fluid are the incremental strain and the relative specific discharge of the fluid

$$\begin{aligned} \Delta\varepsilon_{xx} &= \varepsilon_{xx}(x,t) - \varepsilon_{xx}(x,0) = \Delta\varepsilon(x,t) \\ q_x &= q(x,t) \end{aligned} \tag{5.8.2}$$

The problem is governed by the equilibrium equations for both the solid skeleton and the fluid, and the continuity equation for fluid flow

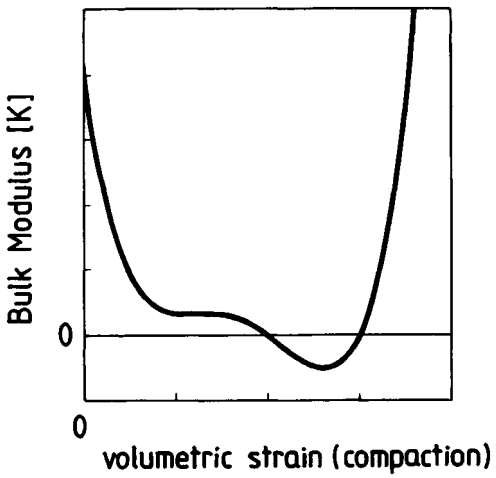

Figure 5.8.4 Stiffness variation of unstable material with volumetric strain.

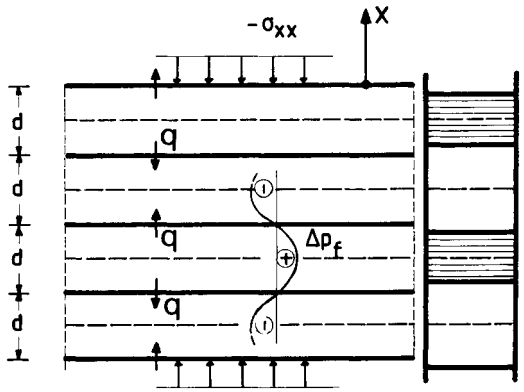

Figure 5.8.5 Periodic pattern of non-uniform compaction in fluid saturated porous medium.

$$\partial_x \Delta\sigma' = -fq;\ -\partial_x \Delta p = fq;\ -\partial_x q = \partial_t \Delta\varepsilon \tag{5.8.3}$$

The behavior of solid skeleton is described in terms of Terzaghi's effective stress increment through the constitutive equations of deformation theory of plasticity, equation 5.8.1

$$\Delta\sigma' = K_t \Delta\varepsilon \tag{5.8.4}$$

Within the frame of linear stability analysis, starting from a homogeneous state of deformation, the coefficient K_t is kept constant both in space and time. Combining the above governing equations yields the following governing differential equation for the excess pore-fluid pressure

$$\frac{\partial^2 \Delta p}{\partial x^2} = c_{vp} \frac{\partial \Delta p}{\partial t} \tag{5.8.5}$$

where c_{vp} is the coefficient of consolidation under continued plastic loading

$$c_{vp} = f/K_t \tag{5.8.6}$$

We observe that the standard continuum formulation of the considered linear stability leads to a consolidation (heat-conduction) equation for the excess pore-fluid pressure. In order to assess the stability of the incipient compaction process within such a layer of water-saturated material, we search for harmonic solutions in space which vary exponentially in time according to

$$\Delta p = \Delta p_o \cos(Qx)\exp(St) \tag{5.8.7}$$

$\Delta p_o>0$ is an arbitrary small initial value of the perturbation; Q is the wave number and S is the growth coefficient of the instability. From these equations we obtain the following dispersion law for the growth coefficient,

$$S = -(1/c_{vp})Q^2 \tag{5.8.8}$$

Within the range of validity of the linear stability analysis, the state of first instability is identical with the state of maximum intergranular stress (K_t=0). In the softening regime of the background drained behavior (K_t<0) the incipient non-uniform compaction of the material layer is highly unstable, since then S>0, and, consequently, any small perturbation of the pore-fluid pressure deviating from its initial uniform value will grow exponentially with time. Notice that for c_{vp}<0, equation 5.8.5 can be seen as an ordinary heat conduction equation (i.e. with positive diffusivity) but with time running backwards. The initial, boundary-value problem which is governed by the so-called backwards heat-conduction equation is mathematically ill-posed, because the growth coefficient S becomes infinite for infinite Q, meaning that the growth of infinitesimal instabilities is unbounded. As can be seen from equation 5.8.8, classical continuum theory cannot produce a statement about the extent of the individual strips. As explained in chapter 10, in the case of a non-classical continuum a material length ℓ is present in the constitutive description, and instead of the backwards heat-conduction equation 5.8.5, one obtains a higher-order diffusion equation which allows for wave-number selection, i.e. the determination of that particular 'wavelength' $1/Q$, which corresponds to the instability with maximum growth, $S(Q) = \max$.

Literature

Textbooks and monographs

Bear, J. (1972). *Dynamics of Fluids in Porous Media.* Dover, New York.
Biot, M.A. (1965). *Mechanics of Incremental Deformations.* John Wiley, New York.

Dullien, F.A.L. (1979). *Porous Media, Fluid Transport and Pore Structure.* Academic Press, New York.
Garbrecht, D. (1973). Kornbruch in irregulären Haufwerken aus elastischspröden Kugeln. Dissertation, Universität Karlsruhe. Veröffentlichungen IBF, Heft Nr. 56.
Sattinger, D.H. (1979). *Group Theory Methods in Bifurcation Theory.* Springer-Verlag, Berlin, Heidelberg, New York.
Taylor, D.W. (1948). *Fundamentals of Soil Mechanics.* John Wiley, New York.
Terzaghi, K. and Peck, R.B. (1948). *Soil Mechanics in Engineering Practice.* John Wiley, New York.
Verruijt, A. (1969). Elastic storage in aquifers. In: *Flow Through Porous Media* (R.J.M.De Wiest, ed.), 331–376. Academic Press, New York.
Wittmann, L. (1980). Filtrations- und Transportphänomene in porösen Medien. Dissertation, Universität Karlsruhe, Veröffentlichungen IBF, Heft Nr. 86.

References

Aifantis, E.C. (1984). Application of mixture theory to fluid saturated geologic media. In: *Compressibility Phenomena in Subsidence. Proc. of the Engineering Foundation Conference, New Hampshire, 1984* (S.K.Saxena, ed.), 65–78. New York Engineering Foundation, 1986.
Alonso, E.E., Gens, A. and Hight, D.W. (1989). *General Report: Groundwater Effects in Geotechnical Engineering. Proc. of the 9th Europ. Congr. on Soil Mechanics and Foundation Engineering,* 1087–1147. Balkema, Rotterdam.
Beskos, D.E. (1989). Dynamics of saturated rocks. 1. Equations of motion. *ASCE J. Eng. Mech.,* **115,** 982–995.
Beskos, D.E., Vgenopoulou, I. and Providakis, C. (1989). Dynamics of saturated rocks. II. Body Waves. *ASCE J. Eng. Mech.,* **115,** 996–1016.
Biot, M.A. (1941). General theory of three-dimensional consolidation. *J. Appl. Phys.,* **12**, 155–164.
Biot, M.A. (1956a). Theory of propagation of elastic waves in fluid-saturated porous solid. I. Low frequency range. *J. Acoust. Soc. Am.,* **28,** 168–178.
Biot, M.A. (1956b). Theory of propagation of elastic waves in fluid-saturated porous solid. II. Higher frequency range. *J. Acoust. Soc. Am.,* **28,** 179–191.
Bishop, A.W. and Skinner, A.E. (1977). The influence of high pore-pressure on the strength of cohesionless soils. *Phil. Trans. Roy. Soc. London,* **284,** 91–130. See also reference made to Bishop (1953) therein.
Brinkman, H.C. (1947). A calculation of the viscous force exerted by a flowing fluid on a dense swarm of particles. *Appl. Sci. Res., Al,* 27–34.
Cowin, S.C. and Nunziato, J.W. (1983). Linear elastic materials with voids. *J. Elast.,* **13**, 125–147.
Fragaszy, R.J. and Voss, M.E. (1984). Undrained Isotropic Compression Behavior of Eniwetok and Monterey Sands. AFWL-TR-83–126, Final Report.
Garg, S.K. and Nur, A. (1973). Effective stress laws for fluid-saturated porous rocks. *J. Geophys. Res.,* **78,** 5911–5921.
Irmay, S. (1958). On the theoretical derivation of Darcy and Forchheimer formulas. *Trans. Am. Geophysical Union*, **39,** 702–707.
Johnson, D.L., Plona, T.J. and Koijma, H. (1987). Probing porous media with 1st sound, 2nd sound, 4th sound, and 3rd sound. *AIP Conf. Proc. 154. Phys. and Chemistry of Porous Media. II* (R.Jayanth, J.Banavar and K.W.Winkler, eds), 243–277.
Mindlin, R.D. (1964). Micro-structure in linear elasticity. *Arch. Rat. Mech. Anal,* **10**, 51–77.

Neale, G. and Nader, W. (1974). Practical significance of Brinkman's extension of Darcy's law: Coupled parallel flows within a channel and a bounding porous medium. *Canad. J. Chem. Eng.,* **52,** 475–478.

Papamichos, E., Vardoulakis, I. and Quadfel, H. (1993). Permeability reduction due to grain crushing around a perforation. *Int. J. Rock Mech. Min. Sci. Geomech. Abstr.,* **30,** 1223–1229.

Plona, T.J. and Johnson, D.L. (1984). Acoustic properties of porous systems. I. Phenomenological description. *AIP Conf. Proc. 107. Phys. and Chemistry in Porous Media* (H.C.Wolfe, ed.), 89–104.

Rice, J.R. (1975). On the stability of dilatant hardening of saturated rock masses. *J. Geoph. Res.,* **80,** 1531–1536.

Sakthivadivel, R. and Irmay, S. (1966). A Review of Filtration Theories. University of California, Berkeley, Hydraulic Engineering Laboratory Rep., 15–4.

Skempton, A.W. (1954). Pore-pressure coefficients A and B. *Géotechnique,* **4**, 143–147.

Skempton, A.W. (1960). Effective stress in soils, concrete and rocks. *Conf. on Pore Pressure and Suction in Soils,* 4–16. Butterworths, London.

Schaeffer, D.G. (1990). Instability and ill-posedness in the deformation of granular materials. *Int. J. Num. Anal. Meth. Geomech.,* **14,** 253–278.

Terzaghi, K.V. (1936). The shearing resistance of saturated soils. *Proc. 1st ICSMFE, Cambridge,* Vol. 1, 54–56.

Vardoulakis, I. (1985). Stability and bifurcation of undrained, plane rectilinear deformations on water-saturated granular soils. *Int. J. Num. Anal. Meth. Geomech.,* **9**, 339–414.

Vardoulakis, I. (1986). Dynamic stability of undrained simple shear on water-saturated granular soils. *Int. J. Num. Anal. Meth. Geomech.,* **10,** 177–190.

Vardoulakis, I. (1987). Compression induced liquefaction of water-saturated granular media. *Constitutive Laws for Engineering Materials: Theory and Applications,* 647–656. Elsevier, Amsterdam.

Vardoulakis, I. and Aifantis, E. (1994). On the role of microstructure in the behavior of soils: Effects of higher order gradients and internal inertia. *Mech. Mater.,* **18,** 151–158.

Vardoulakis, I. and Beskos, D. (1986). Dynamic behavior of nearly saturated porous media. *Mech. Mater.,* **5,** 87–108.

Vardoulakis, I., Stauropoulou, M. and Papanostastou, P. (1995). Hydromechanical aspects of sand production problem. Submitted for publication.

Verruijt, A. (1982). Some remarks on the principle of effective stress. *IUTAM Conf. on Deformation and Failure of Granular Materials,* 167–172. Balkema, Delft.

Whitney, D.D. and Evans, R.D. (1989). The influence of temperature, effective stress and non-Darcy flow on the fracture flow capacity of propped fractures. *Rock at Great Depth* (V. Maury and D.Foumaintraux, eds), 947–954. Balkema, Rotterdam.

Appendix Characteristic soil properties

Symbols: M: mass
V: volume
W: weight

Subscripts: w: water
b: buoyant
d: dry
s: solid
sat: saturated
t: total
v: void

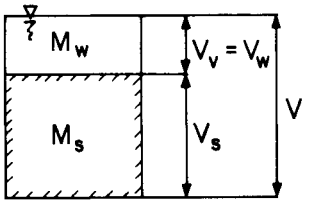

Porosity: $n = \dfrac{dV_v}{dV_t}$ $\quad n = \dfrac{e}{1+e};\ e = \dfrac{n}{1-n}$

Void ratio: $e = \dfrac{dV_v}{dV_s}$ $\quad e = \dfrac{\rho_s - \rho_d}{\rho_d}$

Degree of saturation: $S = \dfrac{dV_w}{dV_v}$ $\quad w = \dfrac{eS}{G_s}$

Water content: $w = \dfrac{dW_w}{dW_s}$

Specific gravity: $G_s = \dfrac{\rho_s}{\rho_w}$

Densities: $\rho_s = \dfrac{dM_s}{dV_s}$ $\quad (\rho_s = 2.6\text{–}2.7\,\text{g/cm}^3 \text{ for quartz})$

$$\rho_w = \frac{dM_w}{dV_w} \quad (\rho_w = 1.0\,\text{g/cm}^3)$$

$$\rho_t = \frac{dM_t}{dV_t};\ \rho_t = \frac{G_s + Se}{1+e}\rho_w = \frac{1+w}{1+e}\rho_s = (1+w)\rho_d = \rho_d + Sn\rho_w$$

$$\rho_d = \frac{dM_d}{dV_t};\ \rho_d = (1-n)\rho_s = \frac{G_s}{1+e}\rho_w = \frac{G_s}{1+wG_s/S}\rho_w$$

$$\rho_{sat} = \frac{dM_{sat}}{dV_t};\ \rho_{sat} = \frac{G_s + e}{1+e}\rho_w = \rho_d + n\rho_w$$

$$\rho_b = \frac{dM_b}{dV_t};\ \rho_b = \rho_{sat} - \rho_w = \frac{G_s - 1}{1+e}\rho_w = (1-n)(\rho_s - \rho_w)$$

6
Plasticity theory for granular materials

6.1
Micromechanical considerations

Granular media are among the best examples of 'plastic' materials, i.e. materials with vanishing elasticity and predominantly irreversible deformations. Thus, a discussion of the kinematics and statics of a simplified micromechanical model of granular media may facilitate the appreciation of mechanisms involved in plastic (irreversible) deformations of real frictional materials.

6.1.1
Kinematics

A two-dimensional random assembly of rods packed together as shown in Figure 6.1.1 is called Schneebelli material. The concepts developed for the Schneebelli material model can be readily generalized for three-dimensional assemblies. In general, the individual grains (rods) will slip and rotate with respect to each other and they will also deform and/or break. A macroscopic material element of the considered granular medium is assumed to be an assembly of a small number of grains (in two dimensions, we assume typically that a 'unit cell' of grains consists of 10×10 rods). These unit cells occupy a volume V^* with representative radius R^*. During a deformation process the motion of each individual rigid grain is given by the velocity $V_\alpha(\alpha=1,2)$ of its centroid and its spin w_3^c. The kinematic degrees of freedom of the individual grains are represented in the continuum description by their averages v_α and w_3^c, respectively, taken over the representative unit cell V^*

$$v_\alpha = \mathrm{avg}\{V^* | V_\alpha\};\ w_3^c = \mathrm{avg}\{V^* | W_3^c\} \tag{6.1.1}$$

In the following we will explore the properties of such a continuum by studying first various special cases of the general model. For example, in this chapter we will ignore the rotational degree of freedom of the grains and we will study a granular medium which is characterized only by particle displacement and particle deformation. In other words the granular medium is approximated here by a *Boltzmann* continuum. Moreover, we focus

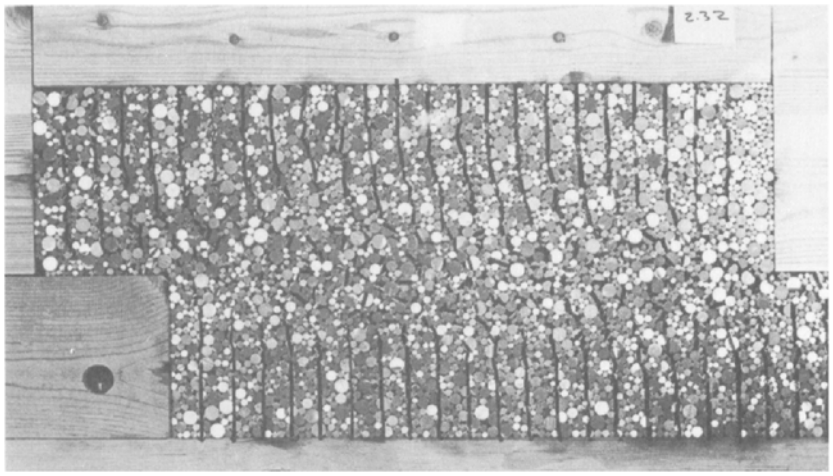

Figure 6.1.1 Shear band in direct shear of Schneebelli material. Test performed by Mr E. Dawson, University of Minnesota.

our attention on the particle displacement field and suppress particle deformation. This is the so-called 'rigid-granular' or 'psammic' limit which was proposed by Dietrich (1976) and Vardoulakis (1981a,b) in order to study problems with free boundaries where relatively low intergranular stresses develop and particle deformation is inappreciable. The study of the psammic limit is essential for establishing a micromechanically meaningful plasticity theory for granular media. Plastic deformation in granular media has its origin in two major microscopic mechanisms: (a) changes of the number of contacts per typical grain, i.e. changes of the coordination number k of the assembly of grains, and (b) interparticle slip which takes place at frictional particle contacts. The first mechanism is responsible for the phenomenon of irreversible volume change, which after Reynolds is called dilatancy, and the second mechanism is responsible for the frictional character of the strength of the granular assembly.

By assuming that the grains are embedded in a Boltzmann continuum let $v_\alpha(x_\beta, t)$ denote the velocity field at the center of a grain with global coordinates x_α ($\alpha,\beta=1,2$) and time t. We employ a local coordinate system (x'_α) which is rotating together with the neighborhood of the considered grain, i.e. the coordinate system rotates with the spin $w_3 = -e_{\alpha\beta 3}\omega_{\alpha\beta}$, where $\omega_{\alpha\beta} = \frac{1}{2}(\partial_\alpha v_\beta - \partial_\beta v_\alpha)$, and thus we may set

$$v'_\alpha = D'_{\alpha\beta} x'_\beta \tag{6.1.2}$$

where $D'_{\alpha\beta}$ is a symmetric tensor. In the following, for simplicity, we will refrain from repeating the ( )′, since all computations are meant to take place in the corotating coordinate system (x'_α). The relative velocity field which is characteristic for two grains at their periphery is given by

$$\Delta v_\alpha = 2R_g D_{\alpha\beta} n_\beta \tag{6.1.3}$$

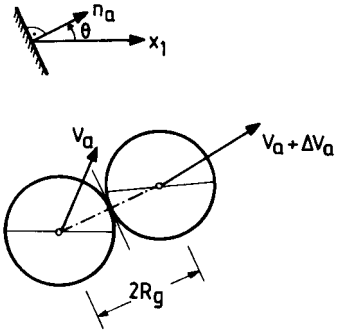

Figure 6.1.2 The kinematics of two non-rotating discs.

where R_g is the radius of the grain and $\{n_\alpha\} = \{\sin\Theta, -\cos\Theta\}^T$ is a unit vector originating at the center of the particle (Figure 6.1.2). The normal and tangential component of the relative velocity at the contact point are given by the following expressions

$$\begin{aligned} \Delta v^n_\alpha &= \Delta v^n n_\alpha;\ \Delta v^n = 2R_g D_{\alpha\beta} n_\alpha n_\beta \\ \Delta v^t_\alpha &= 2R_g (D_{\alpha\beta} - D_{\gamma\delta} n_\gamma n_\delta \delta_{\alpha\beta}) n_\beta \end{aligned} \tag{6.1.4}$$

In order to define average measures of the relative normal and tangential velocity at a contact between two grains the weighted average of the first and higher moments of the contact normal n_α must be computed, e.g.

$$\overline{n_\alpha n_\beta} = (1/2\pi) \int_0^{2\pi} f(\Theta) n_\alpha n_\beta \, d\Theta \tag{6.1.5}$$

For simplicity, the direction n_α of the contact normal is assumed to be completely random with a uniform probability distribution $f(\Theta) = \pi^2$ over the whole angle $0 \le \Theta \le 2\pi$. This may be a crude approximation of the real picture, since it is a well-established fact that the probability distribution of contact normals in a granular assembly under shear and normal stress is non-uniform (see for example Matsuoka, 1974; Kanatani, 1984; Mehrabadi *et al.,* 1982). By using definitions similar to equation 6.1.5, for the higher moments of the contact normal, the following identities are obtained

$$\begin{aligned} \overline{n_\alpha n_\beta} &= (\pi^2/2)\delta_{\alpha\beta} \\ \overline{n_\alpha n_\beta n_\gamma} &= 0 \\ \overline{n_\alpha n_\beta n_\gamma n_\delta} &= (\pi^2/8)(\delta_{\alpha\beta}\delta_{\gamma\delta} + \delta_{\alpha\gamma}\delta_{\beta\delta} + \delta_{\alpha\delta}\delta_{\beta\gamma}) = (\pi^2/8)\delta_{\alpha\beta\gamma\delta} \\ \overline{n_\alpha n_\beta n_\gamma n_\delta n_\varepsilon} &= 0, \text{ etc.} \end{aligned} \tag{6.1.6}$$

The continuum interpretation of the quantity Δv^n is the following: $\Delta v^n > 0$ means that a grain contact is lost and that the two considered grains are moving apart from each other. If, on the other hand, $\Delta v^n < 0$, then a new contact is generated and that the two grains are coming closer together (see Figure 6.1.3). The mean amplitude of the normal

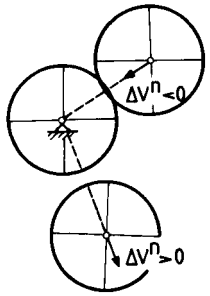

Figure 6.1.3 The gain or loss of contacts and its relation to dilatancy.

component of the relative velocity vector defines an average measure of the change of the distance of two grains in close proximity to each other, since

$$\frac{1}{\pi}\int_0^{2\pi}\frac{\Delta v^{\mathrm{n}}}{2R^{\mathrm{g}}}\,\mathrm{d}\Theta=\frac{1}{\pi}\int_0^{2\pi}D_{\alpha\beta}n_\alpha n_\beta\,\mathrm{d}\Theta=D_{\alpha\alpha} \tag{6.1.7}$$

The mean amplitude of the tangential component of the relative velocity vector defines an average measure of the relative slip of two grains in contact

$$\begin{aligned}\left[\frac{4}{\pi}\int_0^{2\pi}\frac{\Delta v_\alpha^{\mathrm{t}}}{2R^{\mathrm{g}}}\frac{\Delta v_\alpha^{t}}{2R^{\mathrm{g}}}\,\mathrm{d}\Theta\right]^{\frac{1}{2}}&=\left[\frac{4}{\pi}\int_0^{2\pi}(D_{\alpha\beta}D_{\alpha\gamma}n_\beta n_\gamma-D_{\alpha\beta}D_{\gamma\delta}n_\alpha n_\beta n_\gamma n_\delta)\mathrm{d}\Theta\right]^{\frac{1}{2}}\\&=[4\{D_{\alpha\beta}D_{\alpha\beta}-\tfrac{1}{4}(D_{\alpha\alpha}D_{\beta\beta}+D_{\alpha\beta}D_{\alpha\beta}+D_{\alpha\beta}D_{\beta\alpha})\}]^{\frac{1}{2}}\\&=[2D'_{\alpha\beta}D'_{\alpha\beta}]^{\frac{1}{2}}\end{aligned}$$

In equation 6.1.7 $D'_{\alpha\beta}$ denotes the 2D deviator of $D_{\alpha\beta}$

$$D_{\alpha\beta}=D'_{\alpha\beta}+D_{\gamma\gamma}\delta_{\alpha\beta}/2 \tag{6.1.9}$$

From 6.1.5 and 6.1.7 it follows that the first invariant of $D_{\alpha\beta}$

$$\dot{\varepsilon}=D_{\alpha\alpha} \tag{6.1.10}$$

is a measure for the change of contact points along the periphery of a grain and that its second deviatoric invariant

$$\dot{\gamma}=[2D'_{\alpha\beta}D'_{\alpha\beta}]^{\frac{1}{2}} \tag{6.1.11}$$

is measure of average slip along the periphery of a grain.

As already mentioned, the number of contacts per typical grain is the coordination number k of the assembly of grains. For example, assemblies of equal spheres show coordination numbers which vary between 6 and 12. In this context Rumpf (1958) found that k is inversely proportional to the porosity n of the assembly. As shown in section 5.2 changes in porosity are directly related to changes in volumetric strain. Thus for the rigid-particle limit, $\dot{\varepsilon}$ in equation 6.1.10 is a measure of irreversible (plastic) volume changes.

From equations 6.1.10 and 6.1.11, it follows that the most important microstructural changes in granular media are plastic dilatancy (or contractancy) and interparticle slip. A fundamental assumption is now introduced that sets the foundation for the microkinematics of granular media: In a deforming granular medium, plastic volume changes are predominantly linked to interparticle slip. In mathematical terms this assumption puts a constraint between $\dot{\varepsilon}$ and $\dot{\gamma}$

$$\dot{\varepsilon} = \beta\dot{\gamma} \tag{6.1.12}$$

This kinematic constraint is an essential part of the flow rule of a granular medium and is called the dilatancy constraint; the proportionality factor β in equation 6.1.12 is called the dilatancy coefficient of the granular material.

6.1.2 Statics

In order to define stresses in the granular assembly, the following procedure is envisioned: Let $\sum_{\alpha\beta}$ be the intergranular stress tensor defined over assemblies of grains that occupy domains with a radius $r<R^*$, where R^* represents the continuum particle. This stress tensor $\sum_{\alpha\beta}$ is defined via the intergranular forces $P_\alpha^{(\nu)}$ at αth contact between microelements with unit normal $n_\alpha^{(\nu)}$

$$\Sigma_{\alpha\beta} = \frac{1-n}{\pi R}\sum_{\nu=1}^{N} P_\alpha^{(\nu)} n_\beta^{(\nu)} \tag{6.1.13}$$

where N is the number of the contacts intersected by a closed surface that engulfs the considered microelement and n is the porosity of the medium. In general, this stress tensor will be varying over the range $2R_u$ of the considered macroelement. Accordingly, macroscopic stresses $\sigma_{\alpha\beta}$ can be defined that have the same effect as $\sum_{\alpha\beta}$ over the considered distance of the macroelement. Figure 6.1.4 shows an example of such a definition of the macroscopic stresses: The stress tensor $\sigma_{\alpha\beta}$ is the average of $\sum_{\alpha\beta}$ over the considered dimension $2R^*$, i.e.

$$\sigma_{11} = \int_{-R^*}^{R^*} \Sigma_{11}\, dx_2, \text{ etc.} \tag{6.1.14}$$

The continuum is now equipped with a stress tensor. Going back to the interaction among macroelements, intercellular contact tractions can be defined as follows:

$$t_\alpha = \sigma_{\alpha\beta} n_\alpha \tag{6.1.15}$$

With

$$t_\alpha^{n} = t^{n} n_\alpha;\; t^{n} = \sigma_{\alpha\beta} n_\alpha n_\beta;\; t_\alpha^{t} = (\delta_{\alpha\gamma} - n_\alpha n_\gamma)\sigma_{\gamma\beta} n_\beta \tag{6.1.16}$$

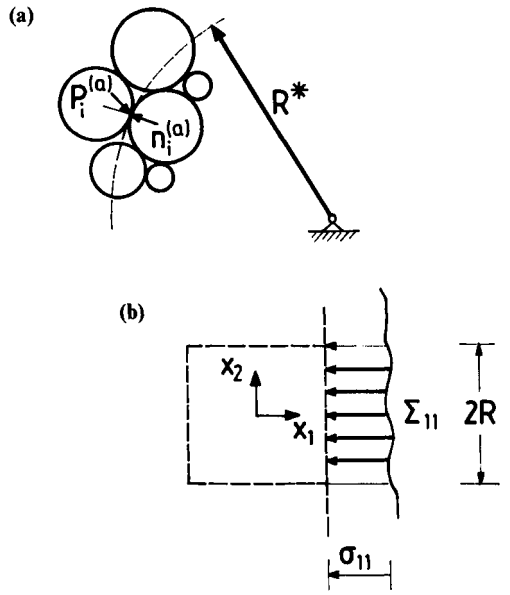

Figure 6.1.4 (a) The concept of intergranular force (b) First-order averaging procedure.

being the normal and tangential components of the intercellular tractions, invariant measures of average normal and shear contact tractions over the periphery of a macrocell result in the following definitions of mean normal and shear stress, respectively

$$\sigma = \frac{1}{\pi}\int_0^{2\pi} t^n \, d\Theta = \sigma_{\gamma\gamma}/2 \tag{6.1.17}$$

$$\tau = \frac{2}{\pi}\left[\int_0^{2\pi} t_\alpha^t t_\alpha^t \, d\Theta\right]^{\frac{1}{2}} = (\tfrac{1}{2} s_{\alpha\beta} s_{\beta\alpha})^{\frac{1}{2}} \tag{6.1.18}$$

where $s_{\alpha\beta}$ is the 2D-deviator of $\sigma_{\alpha\beta}$

$$\sigma_{\alpha\beta} = s_{\alpha\beta} + \sigma_{\gamma\gamma}\delta_{\alpha\beta}/2 \tag{6.1.19}$$

Accordingly, σ is interpreted as a measure for the intergranular normal forces and τ is understood as a measure for the intergranular shear forces (Gudehus, 1972). At isolated contact points of rigid grains, however, only normal and frictional tangential forces can develop. This leads to another fundamental assumption for the behavior of granular media: It is assumed that the shear stress intensity which is carried by the granular assembly cannot exceed a limiting value which is proportional to the normal stress intensity following a simple low of internal friction of the Coulomb type:

$$\tau \leqslant -\sigma\mu \quad \text{with} \quad \sigma < 0 \tag{6.1.20}$$

This inequality is called the yield condition of a granular medium and the coefficient μ>0 is the friction coefficient of the granular medium.

6.2
Flow theory of plasticity

6.2.1
The Mróz-Mandel non-associative elastoplasticity

In this section we discuss a simple elastoplastic constitutive model for cohesive-frictional, dilatant materials such as soils and rocks. This constitutive theory is known as the elastoplastic, isotropic-hardening, pressure-sensitive model with non-associate flow rule (Mróz, 1963, 1966). We notice that this model was discussed in the context of material stability and shear-band formation first by Mandel (1964).

According to the previous introductory remarks we focus our attention here on granular media. Thus σ_{ij} $(i,j=1,2,3)$ is used here invariably as an appropriate measure of intergranular stress. Moreover, granular media are porous and their void space may be filled by a fluid. For a fully saturated granular medium, in the presence of fluid pressure $p_f<0$ the intergranular stress is approximated by Terzaghi's effective stress, $\sigma'_{ij} = \sigma_{ij} - (-p_f)\delta_{ij}$, as discussed in section 5.3. Accordingly the behavior of the solid skeleton, usually termed 'drained behavior', is described here in terms of the effective Cauchy stress tensor σ'_{ij}. Since this section is devoted to the behavior of the solid skeleton only, stresses will be assumed to be always effective, and consequently the suffix $(\,)'$ will be avoided.

The stress tensor and its rate are decomposed into a deviatoric part and into a spherical part

$$\sigma_{ij} = s_{ij} + \sigma_{kk}\,\delta_{ij}/3 \tag{6.2.1}$$

$$\dot{\sigma}_{ij} = \dot{s}_{ij} + \dot{\sigma}_{kk}\,\delta_{ij}/3 \tag{6.2.2}$$

On the other hand, for an elastoplastic continuum, the strain-rate tensor is decomposed into an elastic and a plastic part

$$\dot{\varepsilon}_{ij} = \dot{\varepsilon}^{\mathrm{e}}_{ij} + \dot{\varepsilon}^{\mathrm{p}}_{ij} \tag{6.2.3}$$

which, in turn, are also split into spherical and deviatoric parts

$$\begin{aligned} \dot{\varepsilon}_{ij} &= \dot{e}_{ij} + \dot{\varepsilon}_{kk}\,\delta_{ij}/3 \\ \dot{\varepsilon}^{(\alpha)}_{ij} &= \dot{e}^{(\alpha)}_{ij} + \dot{\varepsilon}^{(\alpha)}_{kk}\,\delta_{ij}/3 \quad (\alpha = \mathrm{e},\mathrm{p}) \end{aligned} \tag{6.2.4}$$

For simplicity, it is assumed that the elastic strain rate is related to the stress rate through the equations of linear, isotropic elasticity

$$\dot{\sigma}_{ij} = C^{\mathrm{e}}_{ijkl}\,\dot{\varepsilon}^{\mathrm{e}}_{kl} \tag{6.2.5}$$

where C^{e}_{ijkl} is the isotropic elasticity tensor

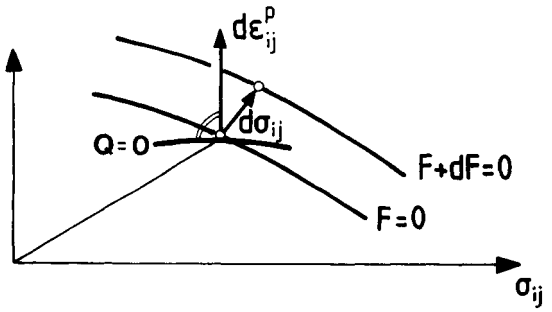

Figure 6.2.1 The concept of yield surface $F(\sigma_{ij}, \psi)=0$, and plastic potential surface $Q(\sigma_{ij}, \psi)=0$, in stress space.

$$C^{e}_{ijkl} = C\left(\delta_{ik}\delta_{jl} + \delta_{il}\delta_{jk} + \frac{2\nu}{1-2\nu}\delta_{ij}\delta_{kl}\right) \tag{6.2.6}$$

G and υ are the elastic shear modulus and the Poisson ratio, respectively. Alternatively, the elastic shear and compression moduli may be introduced, which relate the spherical and deviatoric parts of the corresponding tensors,

$$\begin{aligned} \dot{\sigma}_{kk} &= 3K\dot{\varepsilon}^{e}_{kk};\ \dot{s}_{ij} = 2G\dot{e}^{e}_{ij} \\ K/G &= (\tfrac{2}{3})(1+\nu)/(1-2\nu) \end{aligned} \tag{6.2.7}$$

Plastic strains are usually associated with a plastic potential function in stress space (Figure 6.2.1)

$$Q = Q(\sigma_{ij}, \psi) \tag{6.2.8}$$

which is assumed to be an isotropic function of the stress tensor. In the argument list of Q, ψ is a hardening parameter, i.e. a measure of plastic deformation. The flow rule of flow theory of plasticity becomes then

$$\dot{\varepsilon}^{p}_{ij} = \frac{\partial Q}{\partial \sigma_{ij}}\dot{\psi};\ \dot{\psi} \geqslant 0 \tag{6.2.9}$$

The above flow rule is called the co-axial flow rule, to denote that the principal axes of the plastic strain rate coincide with the principal axes of the stress. Notice also that the inequality 6.2.9 is essential for elastoplasticity, and defines the irreversible character of plastic deformations.

The material behavior is assumed to be 'local' and 'rate-independent'. The first assumption means that for a fixed-in-space material point (x_k), ψ is only a function of time. Rate independence, on the other hand, implies that the plastic hardening parameter ψ and the time t are simply two equivalent members of a class of parameters which may be used to identify the state of plastic deformation. Although real time flows continuously the intrinsic (endochronic) time of plasticity theory flows only whenever additional plastic deformation is taking place; Figure 6.2.2 shows that the variation of ψ

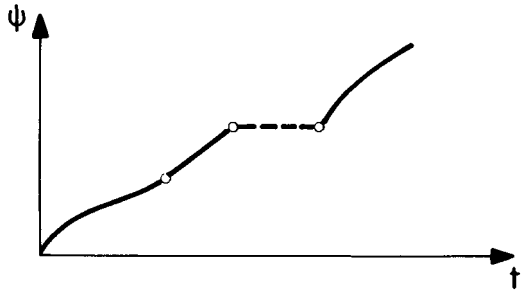

Figure 6.2.2 Endochronictime versus real time.

with real time may be discontinuous but never decreasing. Under these restrictions we identify ψ as a cumulative measure of plastic deformation,

$$\psi = \int_0^t \dot{\psi}\, \mathrm{d}t = \int_0^{\psi} \mathrm{d}\psi \tag{6.2.10}$$

Let

$$I_{1\varepsilon-p} = \dot{\varepsilon}^{\mathrm{p}}_{kk} \quad \text{respectively} \quad \dot{v}^{\mathrm{p}} = I_{1\varepsilon-p} \tag{6.2.11}$$

$$J_{2e-p} = \dot{e}^{\mathrm{p}}_{ij}\dot{e}^{\mathrm{p}}_{ji}/2 \quad \text{respectively} \quad \dot{g}^{\mathrm{p}} = 2\sqrt{(J_{2e-p})} = \sqrt{(2\dot{e}^{\mathrm{p}}_{ij}\dot{e}^{\mathrm{p}}_{ji})} > 0 \tag{6.2.12}$$

be the first invariant and the second deviatoric invariant of the plastic strain rate, respectively. According to the demonstrations in the previous section, $\dot{v}^{\mathrm{p}}$ and $\dot{g}^{\mathrm{p}}$ are interpreted as isotropic measures of irreversible dilatancy and of interparticle slip, respectively. According to the flow rule 6.2.9, they are directly related to $\dot{\psi}$,

$$\dot{v}^{\mathrm{p}} = Q_v\dot{\psi};\ Q_v = 3(\partial Q/\partial\sigma_{kk}) \tag{6.2.13}$$

$$\dot{g}^{\mathrm{p}} = Q_g\dot{\psi};\ Q_g = \left\{2\left[\frac{\partial Q}{\partial\sigma_{ij}} - \frac{\partial Q}{\partial\sigma_{kk}}\delta_{ij}\right]\left[\frac{\partial Q}{\partial\sigma_{ij}} - \frac{\partial Q}{\partial\sigma_{kk}}\delta_{ij}\right]\right\}^{\frac{1}{2}} \tag{6.2.14}$$

The state of plastic deformation can be measured either by ψ or its equivalent plastic-deformation measures

$$v^{\mathrm{p}} = \int_0^t \dot{v}^{\mathrm{p}}\, \mathrm{d}t = \int_0^{\psi} Q_v\, \mathrm{d}\psi \tag{6.2.15}$$

$$g^{\mathrm{p}} = \int_0^t \dot{g}^{\mathrm{p}}\, \mathrm{d}t = \int_0^{\psi} Q_g\, \mathrm{d}\psi \tag{6.2.16}$$

i.e. the accumulated plastic volumetric or shearing strain intensity, respectively. We note that the choice of the appropriate hardening parameter is a matter of judgement. For example, some combinations of isotropic stress and porosity of a granular medium lead to the so-called critical packing which deforms isochorically under continued shear, i.e. $\dot{v}^{\mathrm{p}} = 0$. In such a case vp is not a useful measure of plastic deformation. On the other

hand, under isotropic compressions $\dot{g}^p = 0$ and g^p as a hardening parameter is useless. Along these lines of thought sometimes we see that the arc length of the plastic strain path in strain space or the total plastic work is used as a measure for plastic deformation.

We notice that $\dot{\psi}$ in the flow rule 6.2.9 plays the role of the plastic multiplier of flow theory of plasticity, i.e. the flow rule 6.2.9 makes the plasticity problem 1D, since only the direction of the plastic strain rate and not its magnitude is determined. This indeterminacy is removed by resorting to the concept of yield surface in stress space,

$$F = F(\sigma_{ij}, \psi) = 0 \tag{6.2.17}$$

It is assumed that plastic strain rates are generated when (a) the state of stress lies on the yield surface and (b) if loading of that yield surface is taking place, i.e. if

$$F = 0; \dot{F} = 0 \quad \text{and} \quad \dot{\psi} > 0 \tag{6.2.18}$$

These restrictions must be consistent with the flow rule 6.2.9. This consistency requirement leads to the so-called Prager consistency condition of flow theory of plasticity

$$\dot{F} = \frac{\partial F}{\partial \sigma_{ij}} \dot{\sigma}_{ij} + \frac{\partial F}{\partial \psi} \dot{\psi} = 0 \tag{6.2.19}$$

Prager's consistency results in an algebraic equation for the plastic multiplier

$$\dot{\psi} = \langle 1 \rangle B_{kl} \dot{\varepsilon}_{kl} / H \tag{6.2.20}$$

where

$$B_{ij} = \frac{\partial F}{\partial \sigma_{kl}} C^e_{klij} \tag{6.2.21}$$

In equation 6.2.20 H is the plastic modulus

$$H = H_o + H_t > 0 \tag{6.2.22}$$

with

$$H_o = \frac{\partial F}{\partial \sigma_{kl}} C^e_{klmn} \frac{\partial Q}{\partial \sigma_{mn}} \tag{6.2.23}$$

$$H_t = -\frac{\partial F}{\partial \psi} \tag{6.2.24}$$

H_t is called the hardening (softening) modulus. In case of hardening $H_t>0$, while for $H_t<0$ softening is said to take place. In order to exclude locking behavior we assume that the plastic modulus H is strictly positive, i.e. in case of softening it is assumed that H_t never falls below its snap-back threshold value ($-H_o<H_t$; cf. Nguyen *et al.,* 1974).

In equation 6.2.20, the McAuley brackets, which, with $H>0$, are defined as follows

$$\langle 1 \rangle = \begin{cases} 1 \text{ if } F = 0 \text{ and } B_{kl}\dot{\varepsilon}_{kl} > 0 \\ 0 \text{ if } F < 0 \text{ or } F = 0 \text{ and } B_{kl}\dot{\varepsilon}_{kl} \leqslant 0 \end{cases} \tag{6.2.25}$$

Inserting the expression 6.2.20 into the flow rule 6.2.9, and utilizing the elasticity relationships 6.2.6 for the stress rate finally yields the well-known stress-strain relations of elastoplasticity (cf. Mróz, 1966)

$$\dot{\sigma}_{ij} = C^{ep}_{ijkl}\dot{\varepsilon}_{kl} \tag{6.2.26}$$

$$C^{ep}_{ijkl} = C^{e}_{ijkl} - C^{p}_{ijkl} \tag{6.2.27}$$

$$C^{p}_{ijkl} = \frac{\langle 1 \rangle}{H}(\partial Q/\partial\sigma_{mn})C^{e}_{mnij}(\partial F/\partial\sigma_{rs})C^{e}_{rskl} \tag{6.2.28}$$

Due to the McAuley brackets in the definition 6.2.28 of the plastic stiffness tensor, the elastoplastic stiffness tensor C^{ep}_{ijkl} is a quasilinear operator. Whenever the yield surface is used as a plastic potential surface ($Q \equiv F$), then the flow rule 6.2.9 is called an associate one. In this case the plastic strain rates are normal to the yield surface in stress space. The latter is also known as the normality condition of plasticity theory. From equation 6.2.28 we see directly that in case of associate plasticity the elastoplastic stiffness tensor is satisfying the major symmetry conditions,

$$(\partial F/\partial\sigma_{ij}) \equiv (\partial Q/\partial\sigma_{ij}) \rightarrow C^{ep}_{ijkl} = C^{ep}_{klij} \tag{6.2.29}$$

For granular media, non-associativity of the flow rule is usually restricted only for the volumetric component of the plastic strain rate. At the same time the deviatoric plastic strain rates are assumed to follow the normality rule. This property is called deviatoric normality (Gudehus, 1972; Lade and Duncan, 1973; Baker and Desai, 1982), and is expressed by the simple condition

$$(\partial F/\partial\sigma_{ij}) - (\partial Q/\partial\sigma_{ij}) = \lambda\,\delta_{ij} \tag{6.2.30}$$

where λ is a scalar. The ramifications of the non-linearity and non-symmetry of the elastoplastic stiffness tensor on equilibrium bifurcation will be addressed, in sections 6.4 and 6.5 below.

6.2.2
Stress-dependent elasticity

The elasticity of granular materials is found to be stress-dependent, and in the literature we encounter several proposals for modelling stress-dependent elastic behavior of geomaterials (cf. Loret, 1985; Lade and Nelson, 1987; Molenkamp, 1988). Accordingly, an elastic parameter, say the shear modulus G is assumed to depend, on both the mean stress p and the deviatoric stress T

$$G = G(p, T) \tag{6.2.31}$$

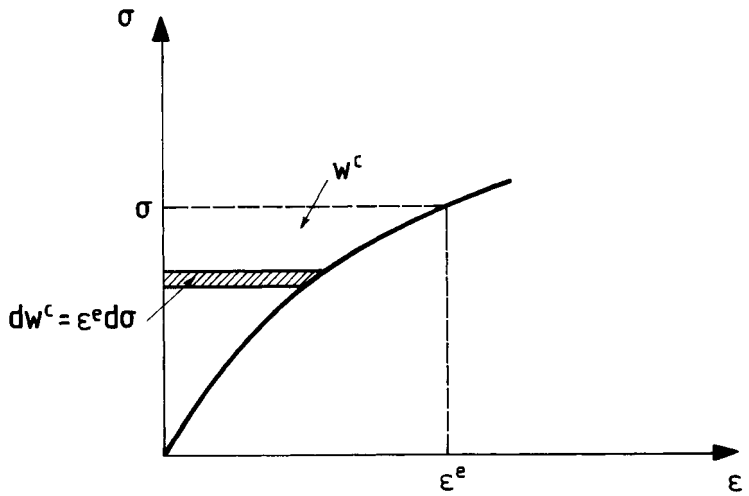

Figure 6.2.3 Definition of complementary energy density function w^c.

In rocks, for example, this type of stress dependence of the shear modulus can account for an initially convex upward stress-strain curve which is attributed to closing of cracks.

In order to account for stress dependence of elastic parameters, we assume that the underlying elasticity is a hyperelasticity, which is described by the corresponding complementary energy density function (Figure 6.2.3)

$$w^c(\sigma_{ij}) = \int_0^{\sigma_{ij}} \varepsilon^e_{ij}\, d\sigma_{ij} \tag{6.2.32}$$

Accordingly w^c is a stress potential function for the elastic strains

$$\varepsilon^e_{ij} = \frac{\partial w^c}{\partial \sigma_{ij}} \tag{6.2.33}$$

The existence of a complementary energy density function guarantees that in arbitrary, closed elastic stress cycles (i.e. stress cycles in the elastic domain) no energy is produced or dissipated.

For isotropic elasticity, the complementary energy density is a function of any three independent invariants of the stress tensor. Let

$$\begin{aligned} w^c &= w^c(I_{1\sigma}, J_{2s}, J_{3s}) \\ I_{1\sigma}/3 &= \sigma_{kk}/3;\ J_{2s} = s_{ij}s_{ji}/2;\ J_{3s} = s_{ij}s_{jk}s_{ki}/3 \end{aligned} \tag{6.2.34}$$

which together with equation 6.2.33 result according to the Cayley-Hamilton theorem in the general non-linear elasticity equation

$$\varepsilon^e_{ij} = a_1\delta_{ij} + a_2 s_{ij} + a_3 s_{ik}s_{kj} \tag{6.2.35}$$

where the coefficients a_i are functions of the stress invariants,

$$a_i = a_i(I_{1\sigma}, J_{2s}, J_{3s}) \tag{6.2.36}$$

Since the elastic strain is a unique function of stress, relationship 6.2.36 guarantees elastic strain reversibility.

Due to the lack of sufficient experimental data usually it is not possible to determine the influence of the third stress invariant, and thus the following identification is made

$$a_1 = \frac{I_{1\sigma}}{3K_s};\ a_2 = \frac{1}{2G_s};\ a_3 = 0 \tag{6.2.37}$$

where

$$K_s = K_s(I_{1\sigma}, J_{2s});\ G_s = G_s(I_{1\sigma}, J_{2s}) \tag{6.2.38}$$

are the (secant) elastic compression and shear modulus, respectively.

By decomposing the elastic strain in spherical and in deviatoric part the elasticity equation 6.2.35 with 6.2.37 yields

$$\varepsilon^e_{kk} = \frac{p}{K_s};\ e^e_{ij} = \frac{s_{ij}}{2G_s} \tag{6.2.39}$$

and with that

$$w^c = \int_0^p \frac{d(p^2)}{2K_s} + \int_0^T \frac{d(T^2)}{2G_s} \tag{6.2.40}$$

where $p = I_{1\sigma}/3$ and $T = \sqrt{J_{2s}}$.

Usually due to the scatter of the experimental data, one is forced to assume a constant Poisson's ratio, υ=const. (Lade and Nelson, 1987), and

$$K_s = \alpha G_s;\ \alpha = \frac{2(1+\nu)}{3(1-2\nu)} \tag{6.2.41}$$

In this case, equation 6.2.40 suggests defining the following stress measure which combines the effect of normal and shear stress and which may be called the 'elastic-equivalent' stress,

$$\sigma_e = [3(1-2\nu)p^2 + 2(1+\nu)T^2]^{\frac{1}{2}} \tag{6.2.42}$$

With

$$E_s = 2G_s(1+\nu) = 3K_s(1-2\nu) \tag{6.2.43}$$

where E_s is Young's secant modulus, we notice that for elastic-incompressible material, $K_s = \infty$, $\nu = \frac{1}{2}$, the elastic-equivalent stress is proportional to the shearing stress intensity, $\sigma_e = \sqrt{3}T$. If, on the other hand, the material is elastic shear rigid $G_s = \infty$, $\nu = -1$, then $\sigma_e = 3|p|$. In granular soils this is a common assumption, which is reflected in a pressure-dependent compression modulus (Terzaghi, 1925).

In general, from equations 6.2.40–6.2.42 we obtain

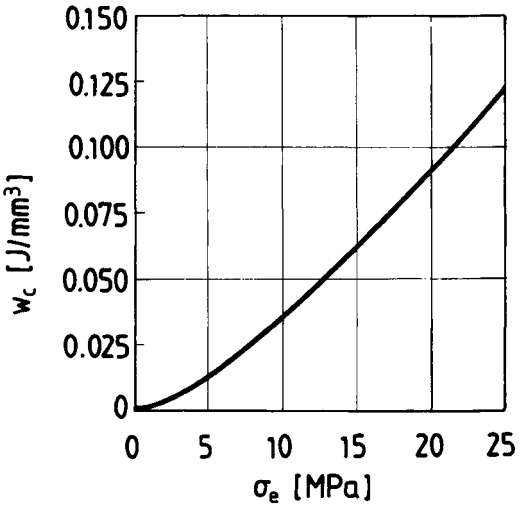

Figure 6.2.4 Complementary energy density for a sandstone as function of the elastic-equivalent stress σ_e.

$$w^c = \int_0^{\sigma_e} \frac{\sigma_e \, d\sigma_e}{E_s} \tag{6.2.44}$$

The simplest non-trivial model corresponds to the assumption that E_s is a linear function of σ_e

$$E_s = E_0 + E^* \sigma_e \tag{6.2.45}$$

With this representation for the secant shear modulus we obtain the following expression for the complementary energy density function

$$w^c = \frac{E_0}{E^{*2}} \{\overset{*}{\sigma}_e - \ln(1 + \overset{*}{\sigma}_e)\} \tag{6.2.46}$$

where $\overset{*}{\sigma}_e$ is a dimensionless equivalent stress

$$\overset{*}{\sigma}_e = E^*(\sigma_e / E_0) \tag{6.2.47}$$

For small stresses w^c is quadratic and for large stresses linear in σe (Figure 6.2.4)

$$\begin{aligned} w^c &\approx (E_0/E^{*2})(\overset{*}{\sigma}_e)^2 \quad \text{for} \quad \overset{*}{\sigma}_e \to 0 \\ w^c &\approx (E_0/E^{*2})(\overset{*}{\sigma}_e) \quad \text{for} \quad \overset{*}{\sigma}_e \to \infty \end{aligned} \tag{6.2.48}$$

With $(d^2 w^c / d\sigma_e^2) > 0$ at finite stress, w_c is a strictly convex function of σ_e and thus the underlying hyperelasticity is stable in the sense of Hadamard.

Starting from the finite elasticity equations 6.2.39, rate equations between the stress and elastic strain tensors can be derived by formal time differentiation

$$\dot{p} = K_s \dot{\varepsilon}^e_{kk} + p(\dot{K}_s/K_s) \tag{6.2.49}$$

$$\dot{s}_{ij} = 2G_s \dot{e}^e_{ij} + s_{ij}(\dot{G}_s/G_s) \tag{6.2.50}$$

With $3K_s = E_s/(1-2\nu)$, $2G_s = E_s/(1+\nu)$, and the stress dependence of E_s, and

$$\dot{G}_s = (\partial G_s/\partial p)\dot{p} + (\partial G_s/\partial T)\dot{T} \tag{6.2.51}$$

$$\dot{p} = \dot{\sigma}_{kk}/3;\ \dot{T} = (s_{lk}\dot{s}_{kl})/(2T) \tag{6.2.52}$$

the rate elasticity equations can be evaluated explicitly, resulting in the following equations

$$\dot{\sigma}_{ij} = C^e_{ijkl}\dot{\varepsilon}^e_{kl} \tag{6.2.53}$$

$$C^e_{ijk1} = G_s\left\{\delta_{ik}\delta_{jl} + \delta_{il}\delta_{jk} + \frac{2\nu}{1-2\nu}\delta_{ij}\delta_{kl} + 2(1+\nu)\frac{\xi}{1-\xi}\frac{\sigma_{ij}\sigma_{kl}}{\sigma_e^2}\right\} \tag{6.2.54}$$

with

$$\xi = \frac{\sigma_e}{G_s}\frac{dG_s}{d\sigma_e} \tag{6.2.55}$$

6.2.3 Finite strain formulations

In rigorous formulations, rate-constitutive equations are expressed in terms of an appropriate objective stress rate, say the Jaumann derivative of the Cauchy stress, $\mathring{\sigma}_{ij}$, and the rate of deformation tensor D_{ij}. However, in granular media, physical non-linearities dominate over geometric non-linearities. Elastic strains are very small whereas plastic strains may considerable. Thus within a small strain theory we do not distinguish between Jaumann and material time derivative of the Cauchy stress tensor and between the rate of deformation tensor and the rate of the infinitesimal Eulerian strain tensor,

$$\mathring{\sigma}_{ij} \approx \dot{\sigma}_{ij};\ D_{ij} \approx \dot{\varepsilon}_{ij} \tag{6.2.56}$$

On the other hand, within a finite strain theory this distinction must be made. Within this context D_{ij} is decomposed additively into an elastic and plastic part,

$$D_{ij} = D^e_{ij} + D^p_{ij} \tag{6.2.57}$$

In any case, the constitutive equations of elastoplasticity must be expressed in terms of an objective stress rate, and the selection of the appropriate stress rate is based on the argument that the underlying elasticity must be flawless. We note that in the case of isotropic elasticity in elastoplasticity, the underlying elasticity is a hypoelasticity, which in general does not derive from a hyperelasticity.

If one can justify that the overall elastic volumetric strains remain small then it is immaterial if one uses, say, the Jaumann derivative of the Kirchhoff stress or that of relative Kirchhoff stress. Moreover, for small elastic strains, one may assume that

$$\dot{T}^{t}_{ij} = R^{t}_{ijkl} D^{e}_{kl} \tag{6.2.58}$$

where according to equation 3.2.48 R^{t}_{ijkl} is the fourth-order isotropic elastic tensor

$$R^{t}_{ijkl} = G\left[\delta_{ik}\delta_{jl} + \delta_{il}\delta_{jk} + \frac{2}{1-2\nu}\delta_{ij}\delta_{kl}\right] \tag{6.2.59}$$

with constant G and ν.

Moreover, according to equation 3.1.43 the Jaumann derivatives of relative Kirchhoff and Cauchy stress differ only by the contribution of initial stress times the elastic volume deformation rate

$$\mathring{\sigma}_{ij} = \dot{T}^{t}_{ij} - \sigma_{ij} D^{e}_{kk} \tag{6.2.60}$$

Following the above remarks we consider here elastoplastic constitutive laws which are formulated on the basis of a Hooke-type hypoelasticity which relates the Jaumann derivative of the Cauchy stress to the rate of elastic deformation,

$$\mathring{\sigma}_{ij} = C^{e}_{ijkl} D^{e}_{kl} \tag{6.2.61}$$

where

$$C^{e}_{ijkl} = R^{t}_{ijkl} + 0(|\sigma_{ij}|/G) \tag{6.2.62}$$

The Jaumann derivative, $\mathring{\sigma}_{ij}$, differs from the material time derivative $\dot{\sigma}_{ij}$ by a corotational part which takes into account the initial stress (cf. sections 2.2.3 and 3.1.4),

$$\dot{\sigma}_{ij} = \mathring{\sigma}_{ij} + \overset{*}{\sigma}_{ij};\ \overset{*}{\sigma}_{ij} = W_{ik}\sigma_{kj} - \sigma_{ik}W_{kj} \tag{6.2.63}$$

We observe that the consideration of corotational terms, $\overset{*}{\sigma}_{ij}$, does not alter the essential structure of the constitutive equations of elastoplasticity. This can be shown as follows: The stress rate enters the constitutive description through the consistency condition 6.2.19, and in particular through the term

$$\frac{\partial F}{\partial \sigma_{ij}}\dot{\sigma}_{ij} = \frac{\partial F}{\partial \sigma_{ij}}(\mathring{\sigma}_{ij} + \overset{*}{\sigma}_{ij}) \tag{6.2.64}$$

Using the representation theorem of isotropic tensor functions and the Cayley-Hamilton theorem, it can be shown that any symmetric second-order tensor $F_{ij}(\sigma_{kl})$, which is an invariant of some other symmetric second-order tensor σ_{kl}, under a group of proper orthogonal transformations, is expressible in polynomial form, and accordingly

$$(\partial F/\partial \sigma_{ij}) = F_0\delta_{ij} + F_1\sigma_{ij} + F_2\sigma_{ik}\sigma_{kj} \tag{6.2.65}$$

where the coefficients F_i (i=0,1,2) are scalar invariants of the tensor σ_{ij}. Then it can be easily seen by inspection that,

$$\frac{\partial F}{\partial \sigma_{ij}} \overset{*}{\sigma}_{ij} = 0 \tag{6.2.66}$$

and thus

$$\frac{\partial F}{\partial \sigma_{ij}} \dot{\sigma}_{ij} = \frac{\partial F}{\partial \sigma_{ij}} \mathring{\sigma}_{ij} \tag{6.2.67}$$

Consequently consideration of initial stress leads to the following simple modification of the constitutive equations 6.2.26 of elastoplasticity

$$\mathring{\sigma}_{ij} = C^{ep}_{ijkl} D_{kl} \tag{6.2.68}$$

where the elastoplastic stiffness tensor is given by equations 6.2.27 and 6.2.28. Moreover the various definitions given through equations 6.2.20 and 6.2.25 hold by replacing if necessary $\dot{\varepsilon}_{kl}$ by D_{kl}.

It should be noted, finally, that if for some reason one chooses to formulate the elasticity law (6.2.58) in terms of an objective time derivative of stress, different from the rigid body derivative of an appropriate stress tensor, then, in general, through the consistency condition, additional terms will enter into the constitutive description.

6.2.4
The equation of thermoelastoplasticity

In the theory of rate-independent thermoelastoplastic materials it is assumed that the rate of deformation tensor is decomposed into a thermoelastic-elastic and a plastic part according to equation 6.2.57. If the underlying thermoelasticity is linear, then the local entropy production is linearly related to the rate of temperature change and to the thermoelastic strains (cf. Carlson, 1972)

$$\rho \dot{s} = \rho c \frac{\dot{\Theta}}{\Theta} - \frac{\Theta_0}{\Theta} M_{kl} D^e_{kl} \tag{6.2.69}$$

where c is the specific heat of the material and $\mathbf{M} = m\mathbf{1}$ is the (isotropic) stress-temperature tensor. Moreover, elastic deformations are linked to changes of the free energy through the Cauchy stress tensor

$$\rho(\dot{f} + s\dot{\Theta}) = \rho \dot{e} - \Theta(\rho \dot{s}) = \sigma_{ij} D^e_{ij} \tag{6.2.70}$$

For an isotropically hardening elastoplastic material, and according to section 2.3.5, equation 2.3.43, the local entropy inequality for stationary states yields a restriction for the local dissipation due to plastic deformation, which could be called plastic stress power,

$$\begin{aligned} P^p &= P - \rho(\dot{f} + s\dot{\Theta}) \\ &= \sigma_{ij} D_{ij} - \sigma_{ij} D^e_{ij} \\ &= \sigma_{ij} D^p_{ij} \geqslant 0 \end{aligned} \tag{6.2.71}$$

i.e. the whole plastic stress power is converted to heat. Within an incremental plasticity theory, the above dissipation inequality will reduce to a restriction for the so-called first-order plastic work

$$\Delta w^{p} = \sigma_{ij}\Delta\varepsilon_{ij}^{p} \geqslant 0 \tag{6.2.72}$$

In flow theory of plasticity, the rate of plastic deformation is given through the flow rule 6.2.9

$$D_{ij}^{p} = Q_{ij}\dot{\psi} \tag{6.2.73}$$

With $\dot{\psi} \geqslant 0$, from equation 6.2.71 we obtain the following constitutive inequality

$$Q_{ij}\sigma_{ij} \geqslant 0 \tag{6.2.74}$$

Finally from equation 6.2.69, the balance law for local entropy production, equation 2.3.44 and Fourier's law (equation 2.3.40) for heat conduction, we obtain the following heat conduction equation in thermoelastoplastic solids

$$\rho c\dot{\Theta} = K\nabla^{2}\Theta + \Theta_{0}M_{kl}D_{kl}^{e} + P^{p} \tag{6.2.75}$$

If, in particular, thermoelastic strains are disregarded, then the differential equation of heat conduction in a thermoplastic solid becomes

$$\rho c\dot{\Theta} = K\nabla^{2}\Theta + P^{p} \tag{6.2.76}$$

i.e. the plastic stress power is a source of heat supplied per unit time and per unit volume at any point of a deforming thermoplastic solid and can be independently determined experimentally. This is done on the basis of the theory of heat conduction for solids with internal heat sources (cf. Carslaw and Jaeger, 1946).

The classical experiments of Taylor and Farren (1925) (see for example Bell, 1973) on metals revealed that when the energy dissipated was calculated from the measured rise in temperature and was compared with the local dissipation due to deformation (obtained from the quasistatic stress versus strain curve) there is still an approximately 10% discrepancy which cannot be accounted for by the elastic strains, i.e. approximately 90% of the input energy appeared as measured thermal energy. This observation resulted in the so-called Taylor heat conduction equation of thermoplasticity where the source term was modified from P^{p} to $0.9P^{p}$.

6.2.5
Drucker's postulate

In section 3.3.4, we formulated the general equilibrium bifurcation problem emphasizing global and local sufficient conditions for uniqueness under dead loading conditions. The discussion was restricted to well-established theoretical results pertaining to the role of second-order work for hyperelastic materials. For elastoplastic solids, in the literature we encounter a constitutive inequality, which refers to the second-order stress power due

to plastic deformations, and is known as Drucker's stability postulate (Drucker, 1951, 1959)

$$ {}_2P^{\mathrm{p}} = \mathring{\sigma}_{ij} D^{\mathrm{p}}_{ij} \geqslant 0 \tag{6.2.77} $$

Since the elastic stiffness tensor is positive definite, the second-order elastic stress power is

$$ {}_2P^{\mathrm{e}} = \mathring{\sigma}_{ij} D^{\mathrm{e}}_{ij} = C^{\mathrm{e}}_{ijkl} D^{\mathrm{e}}_{ij} D^{\mathrm{e}}_{kl} \geqslant 0 \tag{6.2.78} $$

with the equal sign holding for $D^{\mathrm{e}}_{ij} = 0$. Thus Drucker's postulate (6.2.77) implies that the second-order stress power is non-negative, i.e.

$$ {}_2P^{\mathrm{p}} \geqslant 0 \rightarrow {}_2P = \mathring{\sigma}_{ij} D_{ij} \geqslant 0 \tag{6.2.79} $$

Of course, Drucker's postulate is not connected to the Second Law of Thermodynamics, which as we saw above, produces a statement for the positiveness of the first-order plastic work. Petryk (1991) examined the path dependence of second-order work in incrementally non-linear elastoplastic solids (in particular, yield vertex plasticity models). Based on the idea of thermodynamic potential and maximum dissipation principle, such an inequality may be derived and used to restrict the class of admissible incrementally non-linear models. Of course, both these thermodynamic postulates do not apply for frictional solids.

Within an incremental plasticity theory where the influence of initial stress is negligible, Drucker's postulate takes the following form

$$ \Delta_2 w^{\mathrm{p}} = \Delta\sigma_{ij} \Delta\varepsilon^{\mathrm{p}}_{ij} \geqslant 0 \rightarrow \Delta_2 w = \Delta\sigma_{ij} \Delta\varepsilon_{ij} \geqslant 0 \tag{6.2.80} $$

We saw in section 3.3.4, that this inequality is a local sufficient condition for uniqueness of the incremental boundary-value problem under dead loading. Thus Drucker's stability postulate is a sufficient local criterion for uniqueness under dead loading.

Finally, we observe that in case of strain hardening material obeying an associate flow rule, Drucker's postulate is satisfied, as indicated in Figure 6.2.5(a). However, Drucker's postulate is violated if material strain softening is taking place, since for continued plastic loading, the stress-rate vector is pointing into the interior domain of the yield surface (Figure 6.2.5b).

6.2.6
Uniqueness theorems for elastoplastic solids

Having in mind the formulation of the linear bifurcation problem discussed in section 3.3.4, and following the observations made in section 6.2.3, the constitutive equations of elastoplasticity may be expressed in terms of the Cauchy/Jaumann stress increment,

$$ \mathring{\Delta}\sigma_{ij} = C^{\mathrm{ep}}_{ijkl} \Delta\varepsilon_{kl} = (C^{\mathrm{e}}_{ijkl} - C^{\mathrm{p}}_{ijkl}) \Delta\varepsilon_{kl} \tag{6.2.81} $$

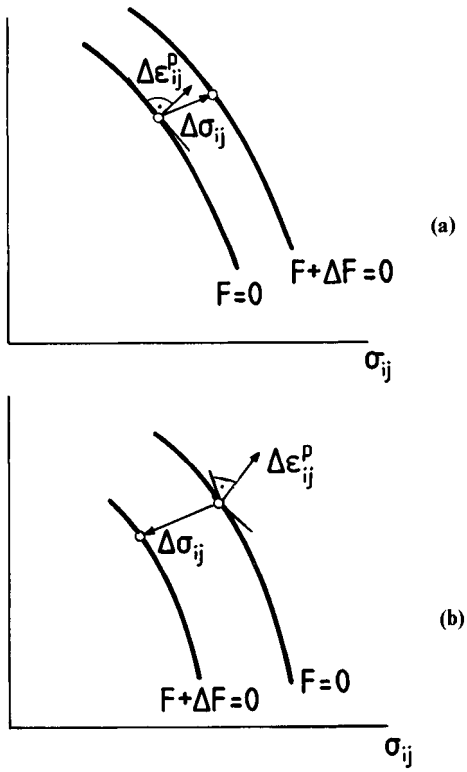

Figure 6.2.5 Drucker's postulate. (a) Hardening material obeying associative flow rule ($\Delta_2 w^p \geq 0$); (b) softening material ($\Delta_2 w^p \leq 0$).

where

$$C^p_{ijkl} = \frac{\langle 1 \rangle}{H} B^Q_{ij} B^F_{kl} \tag{6.2.82}$$

$$B^F_{ij} = F_{kl} C^e_{klij};\ F_{ij} = (\partial F / \partial \sigma_{ij}) \tag{6.2.83}$$

$$B^Q_{ij} = Q_{kl} C^e_{klij};\ Q_{ij} = (\partial Q / \partial \sigma_{ij}) \tag{6.2.84}$$

We recall at this point that the irreversibility of plastic deformation, originally expressed by the non-negativeness of the plastic multiplier ($\Delta\psi \geq 0$), is reflected in the above constitutive equations by the switch function which makes the elastoplastic operator quasilinear. On the other hand, due to the non-associativeness of the flow rule ($F_{ij} \neq Q_{ij}$), the stiffness tensor does not possess major symmetry, which makes the formulation of variational principles impossible even if a linearization of the problem is undertaken.

The 1. P.-K. stress increment is related to the Jaumann stress increment through equation 3.1.36, resulting in the following incremental stress-strain relationship

$$\Delta\pi_{ij} = C_{ijkl}\partial_l \Delta u_k \tag{6.2.85}$$

where

$$C_{ijkl} = C^{ep}_{ijkl} + A_{ijkl} \tag{6.2.86}$$

$$A_{ijkl} = \sigma_{ij}\delta_{kl} - \tfrac{1}{2}(\sigma_{ik}\delta_{jl} + \sigma_{kj}\delta_{il} + \sigma_{il}\delta_{jk} - \sigma_{lj}\delta_{ik}) \tag{6.2.87}$$

In section 3.3.5 we formulated a sufficient condition for global uniqueness for a solid body under dead loads

$$\int_V \Delta\pi_{ij}\partial_j \Delta u_i \, dV = \int_V C_{ijkl}\partial_j \Delta u_i \partial_l \Delta u_k \, dV \geqslant 0 \tag{6.2.88}$$

holding for any kinematically admissible virtual displacement field, with the equals sign holding only for the trivial solution $\Delta u_i = 0$. Although Hadamard's theorem, presented in section 3.3.5, does not apply directly to elastoplastic solids, Ryzhak (1987) has shown that necessary for condition 6.2.88 to hold is that for every non-zero g_i and n_i,

$$\begin{aligned}(C^{e}_{ijkl} + B^{Q}_{ij}B^{F}_{kl}/H + A_{ijkl})g_i n_j g_k n_l \geqslant 0 \\ (C^{e}_{ijkl} + A_{ijkl})g_i n_j g_k n_l \geqslant 0\end{aligned} \tag{6.2.89}$$

However Ryzhak's extension of Hadamard's theorem is not very practical.

In dealing with the linear bifurcation problem Raniecki and Bruhns (1981), generalized Hill's (1958) theory of uniqueness for elastoplastic solids obeying the normality flow rule so as to consider non-associative behavior as well. Within this theory, one can define a one-parameter family of linear *comparison* solids that has the following property: If uniqueness is certain for the comparison solid then bifurcation is precluded for the underlying elastic-plastic solid. The stiffness tensor for this linear comparison solid

$$C'_{ijkl} = C^{e}_{ijkl} - \frac{1}{4rH}(B^{Q}_{ij} + rB^{F}_{ij})(B^{Q}_{kl} + rB^{F}_{kl}) \tag{6.2.90}$$

is symmetric and it may be viewed as a one-parameter linearization of the underlying elastic-plastic stiffness tensor. The uniqueness criterion 6.2.88 in connection with the Raniecki solid (6.2.90) is shown to yield *lower bounds* to the magnitudes of primary bifurcation stresses. The parameter ($0 \leq r \leq 1$) is varied so as to optimize the estimate for the bifurcation stresses, resulting in the following optimal value

$$r^2 = \frac{Q_{ij}B^{Q}_{ij}}{F_{ij}B^{F}_{ij}} \tag{6.2.91}$$

In this context the following sufficient condition for uniqueness has been derived from Raniecki and Bruhns (1981)

$$\int_V (C'_{ijkl} + A_{ijkl})\partial_j \Delta u_i \partial_l \Delta u_k \, dV > 0 \tag{6.2.92}$$

for admissible non-zero displacement fields, satisfying homogeneous boundary constraints. Bigoni and Zaccaria (1992) observe that, based on Hadamard's theorem, a local necessary condition for condition 6.2.92 to hold is

$$(C'_{ijkl} + A_{ijkl})g_i n_j g_k n_l \geqslant 0 \tag{6.2.93}$$

It should be noticed that in the original Raniecki and Bruhns paper a sufficient uniqueness condition was derived for a general class of follower-type loading. Moreover, Hill's bifurcation criterion is deduced from the former one as a limiting case when normality holds.

The hypoelastic comparison solid that can be defined by a stiffness tensor always corresponding to loading has been proven to yield an *upper bound* to the true bifurcation stresses. Indeed, the first eigenstate of this solid may be identified with some bifurcation state of the underlying elastoplastic solid. This result is first utilized in Shanley's (1947) solution for plastic buckling of a column, who examined bifurcations which correspond to continued plastic loading through the column. In this case the comparison solid is defined by the following constitutive tensor

$$C^u_{ijkl} = C^e_{ijkl} - \frac{1}{H} B^Q_{ij} B^F_{kl} \tag{6.2.94}$$

If one assumes an associative flow rule, then the two linear comparison solids coincide (for r=1), and the bifurcation stress obtained from a linear bifurcation analysis coincides with the true bifurcation stress.

6.3
Simple constitutive models for frictional materials

6.3.1
Stress invariants

For the formulation of constitutive relations for frictional (Coulomb-type) materials use will be made of the following stress invariants (Figure 6.3.1):

(a) *The first stress invariant or the mean stress*

$$I_{1\sigma} = \sigma_{kk} \quad \text{respectively} \quad p = \sigma_{kk}/3 = (\sigma_1 + \sigma_2 + \sigma_3)/3 \tag{6.3.1}$$

where σ_i (i=1,2,3) are principal stresses. We remark that granular materials exist only in the compressive regime, p<0. More precisely, granular materials exist only for max $\{\sigma_{ij}\}$ <0.

It can be easily shown that p is the mean value of the normal stress over an elementary spherical surface

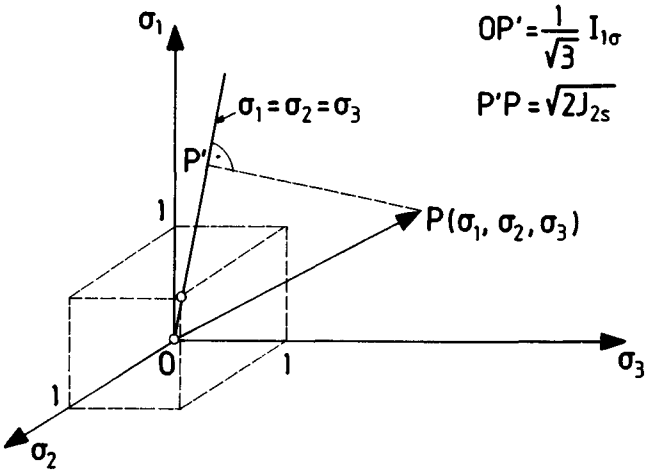

Figure 6.3.1 The Haigh-Westergaard principal stress space and the geometric meaning of the first- and second-stress invariants.

$$\langle t^{n} \rangle = \frac{1}{S} \int t^{n} \, dS = p \tag{6.3.2}$$

where

$$t^{n} = \sigma_{ik} n_i n_k \tag{6.3.3}$$

is the normal component of the stress vector acting on the surface element $n_i dS$ of the elementary sphere (cf. section 6.1.2). Note that in spherical coordinates (r, Θ, ϕ) the direction cosines of a normal to the sphere at an arbitrary point on its surface are given

$$n_1 = \sin\theta \sin\phi, \; n_2 = \sin\theta \cos\phi, \; n_3 = \cos\theta$$

and that

$$dS = r^2 \sin\theta \, d\theta \, d\phi; \; S = 4\pi r^2$$

(b) *The second deviatoric stress invariant or shearing stress intensity*

$$J_{2s} = s_{ij} s_{ji}/2 = (s_1^2 + s_2^2 + s_3^2)/2 \quad \text{respectively} \quad T = \sqrt{J_{2s}} \tag{6.3.4}$$

where s_i are principal deviatoric stresses. We observe that the mean tangential stress over $S \to 0$ an elementary spherical surface is directly proportional to T; i.e.

$$\langle t^{t} \rangle = \left[\frac{1}{S} \int t_i^{t} t_i^{t} \, dS \right]^{\frac{1}{2}} = \sqrt{\tfrac{2}{5}} T \tag{6.3.5}$$

where

$$t_i^{t} = (\delta_{ik} - n_i n_k) \sigma_{kl} n_l \tag{6.3.6}$$

is the tangential component of the stress vector acting on the surface element $n_i dS$ of the elementary sphere.

The above definitions of average normal and shear stress, equations 6.3.2 and 6.3.5, depend on the shape of the elementary volume as well as on the orientation of its bounding surface relative to the principal axes of stress. If we take for example an elementary volume in the form of a rectangular parallelepiped, the result of the integration in equation 6.3.5 will be different for different directions of the edges of this parallelepided. In particular, if its edges coincide with the principal directions of stress tensor then the computed value of $\langle t^t \rangle$ becomes zero.

In soil mechanics the stress ratio

$$\tan\phi_\sigma = -(T/p) \tag{6.3.7}$$

is used as a measure of average shear to normal stress over a spherical domain of integration; it is a measure of the so-called 'mobilized friction' at grain contacts. The minus sign in equation 6.3.7 is used in order to compute a positive stress obliquity ϕ_σ for $p<0$. Granular materials are the limiting case of cohesive-frictional materials with vanishing cohesion. However, cohesive forces among the grains may exist either due to slight cementation, capillary effects or, at the very low confining pressures, due to electrostatic intergranular attractions. In order to allow for cohesion, we have simply to replace in the above definition (equation 6.3.7) the intergranular pressure $(-p)$ by a quantity $(q-p)$, where q is related to the cohesion of the material, and thus

$$\tan\phi_\sigma = T/(q-p) \tag{6.3.7bis}$$

(c) *The third deviatoric stress invariant*

$$J_{3s} = s_{ik}s_{kj}s_{ji}/3 = (s_1^3 + s_2^3 + s_3^3)/3 \tag{6.3.8}$$

The principal deviatoric stresses are roots of the characteristic equation

$$s^3 - J_{2s}s - J_{3s} = 0 \tag{6.3.9}$$

The three (real) solutions of equation 6.3.9 are given by

$$\begin{aligned} s_1 &= (2T/\sqrt{3})\cos\alpha_s \\ s_2 &= -(2T/\sqrt{3})\cos\left(\frac{\pi}{3} - \alpha_s\right) \\ s_3 &= -(2T/\sqrt{3})\cos\left(\frac{\pi}{3} + \alpha_s\right) \end{aligned} \tag{6.3.10}$$

where α_s is the polar angle in the deviatoric plane, measured clockwise (Figure 6.3.2)

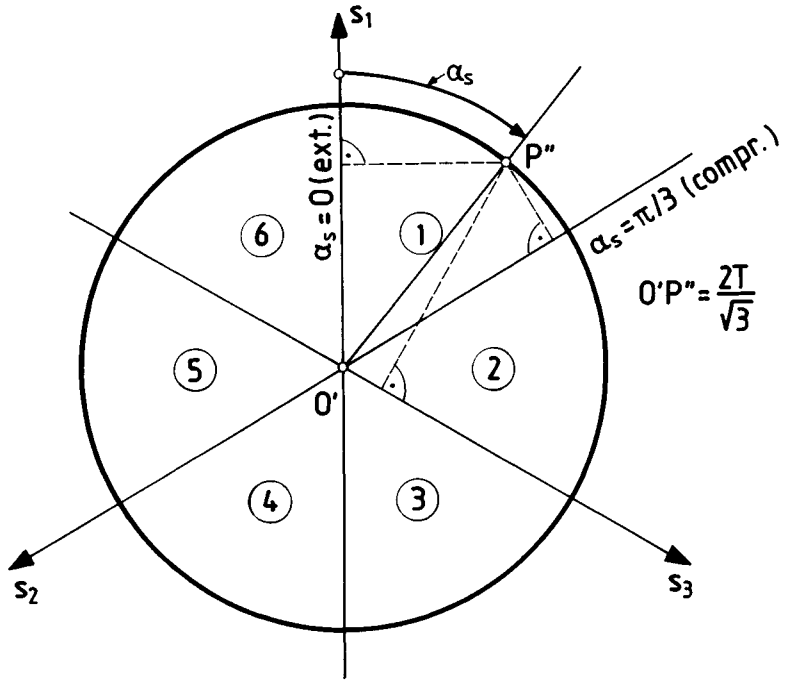

Figure 6.3.2 The definition of α_s in the principal deviatoric plane, and its relation to the principal deviatoric stresses.

$$
\begin{aligned}
&(1) && 0 \leqslant \alpha_s \leqslant \frac{\pi}{3}\ (s_2 \leqslant s_3 \leqslant s_1);\ \alpha_s = \alpha_{s0} \\
&(2) && \frac{\pi}{3} \leqslant \alpha_s \leqslant \frac{2\pi}{3}\ (s_2 \leqslant s_1 \leqslant s_3);\ \alpha_s = -\alpha_{s0} + \frac{2\pi}{3} \\
&(3) && \frac{2\pi}{3} \leqslant \alpha_s \leqslant \pi\ \ (s_1 \leqslant s_2 \leqslant s_3);\ \alpha_s = \alpha_{s0} + \frac{2\pi}{3} \\
&(4) && \pi \leqslant \alpha_s \leqslant \frac{4\pi}{3}\ (s_1 \leqslant s_3 \leqslant s_2);\ \alpha_s = -\alpha_{s0} + \frac{4\pi}{3} \\
&(5) && \frac{4\pi}{3} \leqslant \alpha_s \leqslant \frac{5\pi}{3}\ (s_3 \leqslant s_1 \leqslant s_2);\ \alpha_s = \alpha_{s0} + \frac{4\pi}{3} \\
&(6) && \frac{5\pi}{3} \leqslant \alpha_s \leqslant 2\pi\ (s_3 \leqslant s_2 \leqslant s_1);\ \alpha_s = -\alpha_{s0} + 2\pi
\end{aligned}
\tag{6.3.11}
$$

and α_{s0} is the stress invariant angle of similarity

$$\cos 3\alpha_{s0} = \frac{3\sqrt{3}}{2}\frac{J_{3s}}{(J_{2s})^{\frac{3}{2}}} \quad \text{with} \quad 0 \leqslant \alpha_{s0} \leqslant \frac{\pi}{3} \tag{6.3.12}$$

Notice that α_s is directly related to the Lode parameter L_σ,

$$L_\sigma = 2\frac{\sigma_3 - \sigma_2}{\sigma_1 - \sigma_3} - 1 = 2\frac{\sin\alpha_s}{\sin\left(\frac{\pi}{3} - \alpha_s\right)} - 1 \tag{6.3.13}$$

We observe also that according to equation 6.3.5, the angle α_s relates the maximum to the mean deviatoric stress; for example, for

$$T_{max} = |\sigma_1 - \sigma_2| \rightarrow \cos\left(\alpha - \frac{\pi}{6}\right) = T_{max}/(\sqrt{10\langle t^t\rangle})$$

In other words α_s is a measure of the deviation of the maximum from the mean shear stress (Novozhilov, 1961).

Stress invariants as statistical moments. According to Cauchy's fundamentaltheorem the traction vector at an elementary plane dS with unit normalvector n_i is a linear function of the vector n_i

$$dt_i = \sigma_{ki} n_k \, dS \quad \text{or} \quad t_i = \frac{dt_i}{dS} = \sigma_{ki} n_k$$

where σ_{ij} is the stress tensor. We assume that for a given microfabric of a granular material, the distribution of the tractions t_i is known for n_i taking all positions of the unit normal on a unit sphere.

In order to compute physically meaningful invariants of the stress tensor we consider the statistical properties of the traction vector t_i. For this reason we define the following:

scalar: $t^n = t_i n_i$

vector: $t_i^t = t_i - t^n n_i$

tensor: $t_{ij}^t = t_i^t t_j^t - (1/3) t_k^t t_k^t \delta_{ij}$

The problem then reduces in the computation of the following statistical moments:

(a) The mean value of the normal traction,

$$m_1 = \langle t^n \rangle$$

(b) The mean value of the intensity of the tangential traction,

$$m_2 = \langle t_i^t t_i^t \rangle$$

(c) The 'standard deviation' from this mean,

$$m_3 = \langle t_{ij}^t t_{jk}^t t_{ki}^t \rangle$$

In order to proceed with this computation we first note the following identities:

$$\langle n_i n_j \rangle = \int_0^{2\pi} \int_0^{\pi} n_i n_j \sin\theta \, d\theta \, d\phi = \frac{4\pi}{3} \delta_{ij}$$

$$\langle n_i n_j n_k n_l \rangle = \frac{4\pi}{3 \cdot 5} (\delta_{ij}\delta_{kl} + \delta_{ik}\delta_{jl} + \delta_{il}\delta_{jk}) = \frac{4\pi}{3 \cdot 5} \delta_{ijkl}$$

$$\langle n_i n_j n_k n_l n_m n_n \rangle = \frac{4\pi}{3 \cdot 5 \cdot 7} (\delta_{in}\delta_{jklm} + \delta_{jn}\delta_{klmi} + \delta_{kn}\delta_{lmij} + \delta_{ln}\delta_{mijk} + \delta_{mn}\delta_{ijkl})$$

$$= \frac{4\pi}{3 \cdot 5 \cdot 7} \delta_{ijklmn}$$

etc. All odd products are zero and contraction lowers the rank, since $n_i n_i = 1$. From the discussion in section 6.3.1 we already know that:

(a) The first invariant of the stress tensor σ_{ij} is proportional to the mean normal traction:

$$p = I_{1\sigma}/3 = \frac{1}{4\pi} m_1$$

(b) The second deviatoric invariant of σ_{ij} is proportional to the mean intensity of the tangential traction:

$$T = \sqrt{J_{2s}} = \left[\frac{5}{8\pi} m_2 \right]^{\frac{1}{2}}$$

(c) The interpretation of the third stress invariant is not straightforward. In order to arrive at such a statistical interpretation we define the dyad

$$M_{ij} = t_i^t t_j^t$$

Then with

$$M_{kk} = t_k^t t_k^t = m^2$$

we observe that

$$m_2 = \langle m^2 \rangle$$

and with that

$$m_3 = (M_{ij} - (\tfrac{1}{3})m^2 \delta_{ij})(M_{jk} - (\tfrac{1}{3})m^2 \delta_{jk})(M_{ki} - (\tfrac{1}{3})m^2 \delta_{ki})$$

Thus a 'standard deviation' σ can be introduced such that

$$\sigma^2 = \pm \{\langle m_3 \rangle\}^{\frac{1}{3}} > 0$$

From the considered averaging procedure over a unit sphere it turns out that this standard deviation from the mean tangential traction intensity is linked to all three stress tensor invariants, since:

$$\langle m_3 \rangle = \frac{2}{9}\frac{4\pi}{1\cdot 3\cdot 5\cdot 7\cdot 9\cdot 11\cdot 13}\{-3192 I_{1\sigma} I_{2\sigma} I_{3\sigma} + 2646 I_{2\sigma}^3 - 384 I_{2\sigma}^2 I_{1\sigma}^2 + 264 I_{3\sigma}^2 + 152 I_{3\sigma} I_{1\sigma}^3 + 9 I_{2\sigma} I_{1\sigma}^4 - I_{1\sigma}^6\}$$

where

$$I_{1\sigma} = \sigma_{kk}$$
$$I_{2\sigma} = \sigma_{ij}\sigma_{ji} = 2J_{2s} + (1/3)I_{1\sigma}^2;\ J_{2s} = (1/2)s_{ij}s_{ji}$$
$$I_{3\sigma} = \sigma_{ij}\sigma_{jk}\sigma_{ki} = 3J_{3s} + 2J_{2s}I_{1\sigma} + (\tfrac{1}{9})I_{1\sigma}^3;\ J_{3s} = (1/3)s_{ij}s_{jk}s_{ki}$$

Thus invariant σ^2, produces essentially a 'statistical' measure for the third invariant J_{3s}.

6.3.2
The Drucker-Prager and Mohr-Coulomb models

In the low-pressure regime friction and cohesion of a geomaterial may be assumed to be pressure insensitive. Moreover, under conditions of continuous plastic loading the so-called (secant) mobilized friction coefficient f, and mobilized cohesion c are evaluated directly from the stress ratio

$$f = \tan\phi_\sigma;\ c = qf \tag{6.3.14}$$

From these equations, we obtain the following expression for the yield surface in invariant stress space

$$F = T - f(q - p) = 0 \tag{6.3.15}$$

In general, both internal friction and cohesion coefficient are functions of the plastic hardening parameter, ψ. If f or c are monotonously increasing functions of the hardening parameter, then friction or cohesion *hardening* is said to be taking place, else *softening* is occurring.

For example, in sands, cohesion is vanishing, and isotropic friction hardening/softening is the rule (Figure 6.3.3a)

$$c = 0;\ f = f(n_o, g^p) \tag{6.3.16}$$

The variables n_o (porosity) and g^p (accumulated plastic shear strain) in the argument list of f indicate its dependency on the coordination number and on the average slip at grain boundaries, respectively.

Sandy rocks psammites = sandstones; ψάμμος = sand on the other hand are characterized by friction hardening and cohesion hardening/softening, which due to equation 6.3.15 is of the kinematic type (Figure 6.3.3b); for example

$$f = \begin{cases} f_o(g^p) & \text{for } 0 \leqslant g^p \leqslant g_p^p \\ f_p = \text{const} & \text{for } g_p^p \leqslant g^p \end{cases} \tag{6.3.17}$$

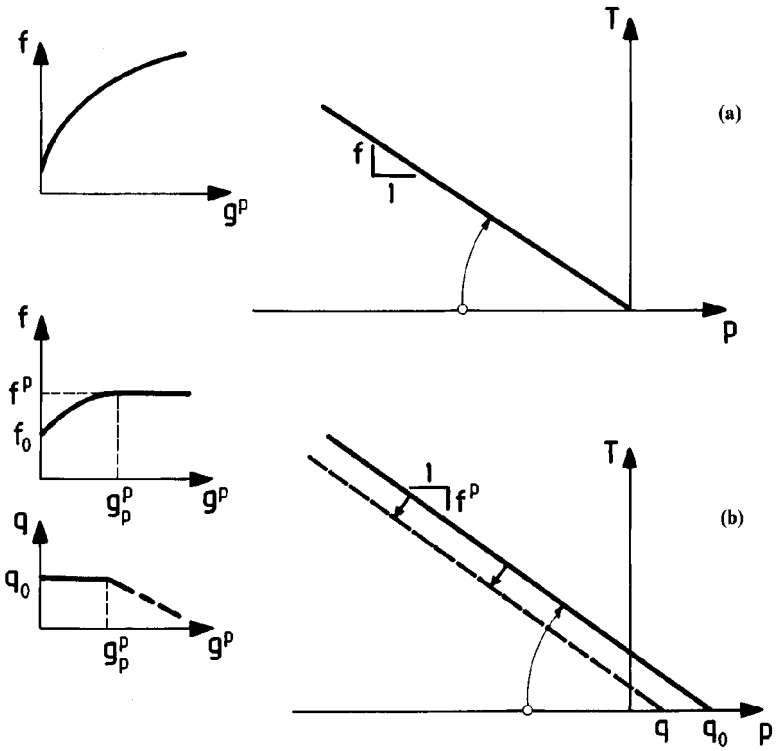

Figure 6.3.3 Coulomb models with linear material pressure sensitivity. (a) Isotropic or friction-hardening model for sand; (b) mixed isotropic/kinematic or friction hardening cohesion hardening/softening model for sandy rock.

$$q = q_o - \begin{cases} 0 & \text{for } 0 \leqslant g^p \leqslant g_p^p \\ r(g^p - g_p^p) & \text{for } g_p^p \leqslant g^p \ (r < 0, \text{linear softening}) \end{cases} \tag{6.3.18}$$

In this case g^p is identified as a measure for microslip, which is occurring at grain boundaries and microcracks.

In general the friction coefficient will depend also on the stress invariant angle of similarity α_{s0} (i.e. the third stress invariant)

$$f = f(\alpha_{s0}; g^p) \tag{6.3.19}$$

In particular, for a Drucker-Prager (D.-P.) model, no dependency of f on α_{s0} is assumed. This assumption results in conical surfaces in stress space with circular trace in the deviatoric plane (Figure 6.3.4). On the other hand for the Mohr-Coulomb (M.-C.) model, the dependence on α_{s0} is such that F=0 does not depend on the intermediate principal stress. This assumption together with the linear pressure dependence, results in surfaces in stress space which are hexagonal pyramids, whose trace in deviatoric plane

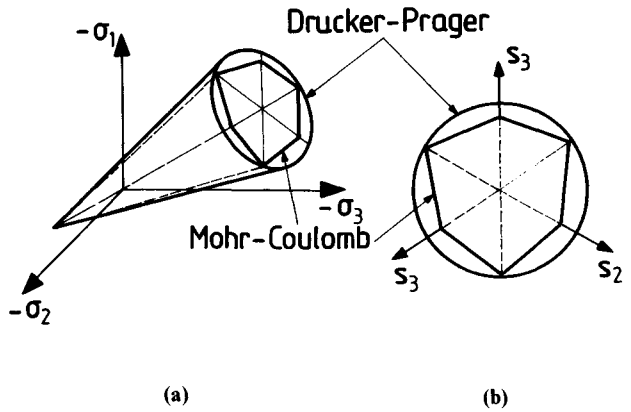

Figure 6.3.4 Drucker-Prager and Mohr-Coulomb models matched along the compression meridian in (a) principal stress space, and (b) in the deviatoric plane.

is a distorted hexagon. This means that for a M.-C. model f is given by the following expressions,

$$1/f = a(g^p)\cos\alpha_{s0} + b(g^p)\sin\alpha_{s0} \tag{6.3.20}$$

where, as will be shown below, a and b are interrelated functions of g^p.

In particular, the expressions for the yield and the plastic potential surface for the two above models are (see also Chen and Han, 1988):

(a) *Drucker-Prager yield surface:*

$$F = \sqrt{J_{2s}} - f(q - I_{1\sigma}/3) \tag{6.3.21}$$

In this case we have

$$\frac{\partial F}{\partial \sigma_{ij}} = \frac{1}{\sqrt{2}} m_{ij} + \frac{1}{3} f\delta_{ij};\ m_{ij} = \frac{s_{ij}}{\sqrt{(2J_{2s})}};\ m_{ij}m_{ij} = 1 \tag{6.3.22}$$

(b) Mohr-Coulomb yield surface:

$$F = \sqrt{J_{2s}}\left[\sin\left(\alpha_{s0} + \frac{\pi}{3}\right) + \cos\left(\alpha_{s0} + \frac{\pi}{3}\right)\sin\phi_m/\sqrt{3}\right] - (q - I_{1\sigma}/3)\sin\phi_m \tag{6.3.23}$$

where ϕ_m denotes the mobilized Mohr-Coulomb friction angle. In this case we have

$$\frac{\partial F}{\partial \sigma_{ij}} = B_0\delta_{ij} + B_1 s_{ij} + B_2 S_{ij};\ S_{ij} = s_{ik}s_{kj} - (2/3)J_{2s}\delta_{ij} \tag{6.3.24}$$

with

$$B_0 = \sin\phi_m/3 \tag{6.3.25a}$$

$$B_1 = \begin{cases} (3 + \sin\phi_m)/[4\sqrt{3}\sqrt{(J_{2s})}] & \text{for } \alpha_{s0} = 0 \\ \left[\sin\left(\alpha_{s0} + \frac{\pi}{3}\right)\Big/(2\sqrt{J_{2s}})\right]\left\{\left[1 + \cot\left(\alpha_{s0} + \frac{\pi}{3}\right)\cot 3\alpha_{s0}\right]\right. & \\ \qquad \left. + \sin\phi_m\left[\cot\left(\alpha_{s0} + \frac{\pi}{3}\right) - \cot 3\alpha_{s0}\right]\Big/\sqrt{3}\right\} & \text{for } 0 < \alpha_{s0} < \frac{\pi}{3} \\ (3 - \sin\phi_m)/[(4\sqrt{3}\sqrt{(J_{2s})}] & \text{for } \alpha_{s0} = \frac{\pi}{3} \end{cases} \tag{6.3.25b}$$

$$B_2 = \begin{cases} 0 & \text{for } \alpha_{s0} = 0 \\ \left[\sin\left(\alpha_{s0} + \frac{\pi}{3}\right)\sin\phi_m - \sqrt{3}\cos\left(\alpha_{s0} + \frac{\pi}{3}\right)\right]\Big/(2J_{2s}\sin 3\alpha_{s0}) & \text{for } 0 < \alpha_{s0} < \frac{\pi}{3} \\ 0 & \text{for } \alpha_{s0} = \frac{\pi}{3} \end{cases} \tag{6.3.25c}$$

(c) Drucker-Prager Potential Function:

$$Q = \sqrt{J_{2s}} + d(I_{1\sigma}/3) \tag{6.3.26}$$

where d is mobilized-dilatancy coefficient. In this case the plastic strain-rate gradient becomes

$$\frac{\partial Q}{\partial \sigma_{ij}} = \frac{m_{ij}}{\sqrt{2}} + \frac{1}{3}\mathrm{d}\delta_{ij}$$

whereas the conversion factors defined through equations 6.2.13 and 6.2.14 are

$$Q_v = d;\ Q_g = 1 \tag{6.3.28}$$

(d) Mohr-Coulomb Potential Function:

$$Q = \sqrt{J_{2s}}\left[\sin\left(\alpha_{s0} + \frac{\pi}{3}\right) + \cos\left(\alpha_{s0} + \frac{\pi}{3}\right)\sin\psi_m/\sqrt{3}\right] + (I_{1\sigma}/3)\sin\psi_m \tag{6.3.29}$$

where ψ_m denotes the mobilized Mohr dilatancy angle. The plastic strain-rate gradient is computed by expressions analogous to 6.3.24 to 6.3.25, where $\sin\phi_m$ is replaced by $\sin\psi_m$; for example,

$$\begin{aligned} \frac{\partial Q}{\partial \sigma_{ij}} &= Q_0\delta_{ij} + Q_1 s_{ij} + Q_2 S_{ij} \\ Q_0 &= \sin\psi_m/3;\ \text{etc.} \end{aligned} \tag{6.3.30}$$

Notice that between the dilatancy functions d and $\sin\psi_m$, the following relation holds

$$\begin{aligned} \sin\psi_m &= Q_g d \\ Q_g &= 2[Q_1^2 J_{2s} + 3Q_1 Q_2 J_{3s} + Q_2^2 J_{2s}^2/3]^{\frac{1}{2}} \approx 1 \end{aligned} \tag{6.3.31}$$

6.3.3
Data reduction and model calibration

Between the mobilized Mohr-Coulomb friction angle ϕ_m and the stress obliquity angle ϕ_σ defined above through equations 6.3.23 and 6.3.7, respectively, the following relationship holds

$$\sin\phi_m = \frac{\cos\left(\frac{\pi}{6} - \alpha_{s0}\right)\tan\phi_\sigma}{1 - \sin\left(\frac{\pi}{6} - \alpha_{s0}\right)\tan\phi_\sigma/\sqrt{3}} \tag{6.3.32}$$

In geomechanics the experimental data which are used to calibrate a constitutive model are obtained in most cases from triaxial compression tests. Sometimes data from triaxial extension tests are also included. We notice that according to Figure 6.3.2 and the formulae 6.3.11 these two tests correspond to the following configurations:

triaxial extensions	*triaxial compressions*
$\sigma_2 = \sigma_3 < \sigma_1 \leqslant 0\ (\alpha_s = 0)$	$\sigma_2 < \sigma_3 = \sigma_1 \leqslant 0\left(\alpha_s = \frac{\pi}{3}\right)$
$(*)\ \sigma_1 = \sigma_2 < \sigma_3 \leqslant 0\left(\alpha_s = \frac{2\pi}{3}\right)$	$\sigma_1 < \sigma_2 = \sigma_3 \leqslant 0\left(\alpha_s = \frac{3\pi}{3}\right)$
$\sigma_3 = \sigma_1 < \sigma_2 \leqslant 0\left(\alpha_s = \frac{4\pi}{3}\right)$	$(*)\ \sigma_3 < \sigma_1 = \sigma_2 \leqslant 0\left(\alpha_s = \frac{5\pi}{3}\right)$

(6.3.33)

With (*) we mark above the common notations in soil and rock mechanics. Accordingly, from equation 6.3.32 we obtain the following relations between the angular invariants ϕ_σ and ϕ_m

$$\sin\phi_m = \frac{3\tan\phi_\sigma}{2\sqrt{3} \pm \tan\phi_\sigma};\ \tan\phi_\sigma = \frac{(2\sqrt{3})\sin\phi_m}{3 \mp \sin\phi_m} \tag{6.3.34}$$

with the upper sign holding for triaxial compression and the lower sign for triaxial extension. As indicated in Figure 6.3.5, these expressions provide some restrictions for ϕ_σ and ϕ_m. If we assume the validity of D.-P. model, then tanϕσ assumes the same values in triaxial compression and triaxial extension. Then from equation 6.3.34 we obtain that for

$$\sin\phi_m < 1 \rightarrow f_{max} < \tan(41°) \approx 0.869 \tag{6.3.35}$$

i.e. a D.-P. model is applicable as soon as

$$\phi_{max,\,compr} < 37° \tag{6.3.36}$$

This is a considerable restriction as far as the applicability of the D.-P. model is concerned. For example, for medium-grained, uniform dense sands, the typical maximum (peak) value of the mobilized friction angle in triaxial compression is about 40°. Moreover, it is found that the mobilized friction angle shows a minor dependency on α_{s0}

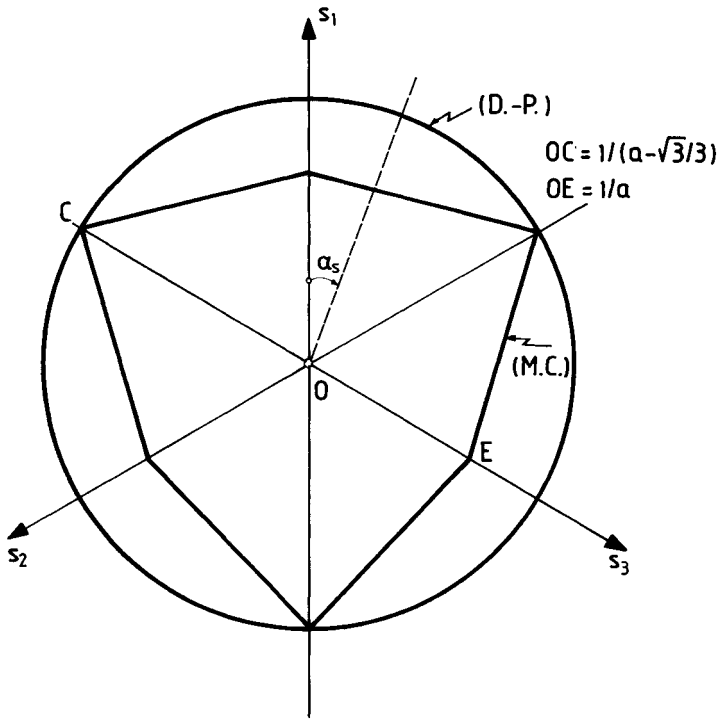

Figure 6.3.5 Traces of the D.-P. and M.-C. yield surfaces in the deviatoric plane for ϕ_m=30°.

and thus a M.-C. model is a good selection for a yield condition for granular materials (Goldscheider, 1976).

The M.-C. yield function 6.3.20 is defined through two material functions $a(n_o; g^p)$ and $b(n_o; g^p)$, which are interrelated as follows

$$a = \frac{3 + \sin\phi_m}{(2\sqrt{3})\sin\phi_m};\ b = \tfrac{1}{3}[(\sqrt{3})a - 2] \tag{6.3.37}$$

where the M.-C. friction coefficient

$$\sin\phi_m = \mu(n_o; g^p) \tag{6.3.38}$$

evaluated under full plastic loading conditions, is the assumed unique material function. Thus from equations 6.3.20, 6.3.37 and 6.3.38 we obtain,

$$f = \frac{2\sqrt{3}\mu}{(3 + \mu)\cos\alpha_{s0} + \sqrt{3}[(1 - \mu)\sin\alpha_{s0}]} \tag{6.3.39}$$

Example: Calibration of a M.-C. model for sand. A calibration procedure is sketched here using as example data from a triaxial compression test on dry sand. The material tested was a medium-grained, dense Karlsruhe sand of initial porosity $n_o = 0.350$. More information about the properties of this sand, tested under triaxial compression

conditions, can be found in the paper by Hettler and Vardoulakis (1984). In the experiment reported here the specimen was rather stout (initial height $H_o = 58.1\,\text{mm}$ and initial diameter $D_o = 69.4\,\text{mm}$), to suppress diffuse bifurcations, and precautions were taken so as to minimize end platen friction. Let $\sigma_r = \sigma_1 = \sigma_\theta = \sigma_2$ ($\lambda_r = \lambda_1 = \lambda_\theta = \lambda_2$ be the lateral and hoop Cauchy stresses (logarithmic strains) and $\sigma_z = \sigma_3$ ($\lambda_z = \lambda_3$) the axial stress (logarithmic strain) in the considered triaxial compression test. Under axisymmetric conditions the first and second stress and strain invariants

$$T = |\sigma_r - \sigma_z|/\sqrt{3};\ p = (2\sigma_r + \sigma_z)/3 \tag{6.3.40}$$

$$g = 2|\lambda_r - \lambda_z|/\sqrt{3};\ v = 2\lambda_r + \lambda_z \tag{6.3.41}$$

The corresponding experimental data are summarized in Table 6.3.1. The confining pressure during the first loading-unloading loop was $\sigma_c = 98.1\,\text{kPa}$, and was doubled for the subsequent reloading process. Figure 6.3.6 shows the variation of the shearing stress intensity T as a function of the shearing strain intensity g. Figure 6.3.7, on the other hand, shows the corresponding variation of the volumetric strain v with g.

From the unloading, reloading loops and the assumption of constant elastic moduli, it was estimated that the shear modulus and Poisson's ratio of the tested sand are: $G \approx 37.1$ MPa, $\nu \approx 0.1$.

For selecting a mobilized friction function, data points corresponding to loading have been used and the stress ratio

$$\tan\psi_\sigma = \frac{|\sigma_r - \sigma_z|/\sqrt{3}}{(2\sigma_r + \sigma_z)/3} \tag{6.3.42}$$

was plotted versus the cumulative plastic shear strain

$$g^p = \int \mathrm{d}g^p;\ \mathrm{d}g^p = 2|\mathrm{d}\varepsilon_r^p - \mathrm{d}\varepsilon_z^p|/\sqrt{3} \tag{6.3.43}$$

In the hardening regime, the test results were then fitted by a 'hyperbolic' law (Duncan and Chang, 1970)

$$\tan\psi_\sigma = f(g_p);\ f = g^p/(c_1 + c_2 g^p) \tag{6.3.44}$$

which provides continuous hardening and a maximum mobilized friction coefficient at infinite plastic strain $f_{\max} = 1/c_2$. A first estimate of the constants can be obtained by linear regression in a $(1/f,\ 1/g^p)$ diagram. A non-linear curve-fitting procedure has yielded: $c_1 = 3.007 \times 10^{-3}$; $c_2 = 9.667 \times 10^{-1}$. The corresponding $\tan\psi_\sigma = f(g_p)$ curve and data points are depicted in Figure 6.3.8(a).

According to the volumetric flow rule of flow theory of plasticity, equations 6.2.13 to 6.2.16, plastic volumetric strain increments

$$\mathrm{d}v^p = 2\mathrm{d}\varepsilon_r^p + \mathrm{d}\varepsilon_z^p \tag{6.3.45}$$

Table 6.3.1 Triaxial test data for Karlsruhe medium dense sand (initial porosity n_0=0.350) initial height H_o=58.1 mm; initial diameter D_o=69.4mm

no.	λ_z (—)	$\lambda_r = \lambda_\theta$ (—)	σ_z (kPa)	$\sigma_r = \sigma_\theta$ (kPa)
1	0.0	0.0	−0.9810E + 02	−0.9810E + 02
2	−0.2197E − 02	0.0000E + 00	−0.1745E + 03	−0.9810E + 02
4	−0.6467E − 02	0.4588E − 03	−0.2736E + 03	−0.9810E + 02
5	−0.1194E − 01	0.2292E − 02	−0.3527E + 03	−0.9810E + 02
6	−0.1633E − 01	0.4578E − 02	−0.3921E + 03	−0.9810E + 02
7	−0.2077E − 01	0.8226E − 02	−0.4218E + 03	−0.9810E + 02
8	−0.2586E − 01	0.1186E − 01	−0.4469E + 03	−0.9810E + 02
9	−0.3068E − 01	0.1548E − 01	−0.4663E + 03	−0.9810E + 02
10	−0.3548E − 01	0.1909E − 01	−0.4822E + 03	−0.9810E + 02
11	−0.4021E − 01	0.2313E − 01	−0.4945E + 03	−0.9810E + 02
12	−0.4536E − 01	0.2671E − 01	−0.5053E + 03	−0.9810E + 02
13	−0.5173E − 01	0.3162E − 01	−0.5172E + 03	−0.9810E + 02
14	−0.5963E − 01	0.3870E − 01	−0.5266E + 03	−0.9810E + 02
15	−0.6774E − 01	0.4443E − 01	−0.5328E + 03	−0.9810E + 02
16	−0.7215E − 01	0.4837E − 01	−0.5342E + 03	−0.9810E + 02
17	−0.7169E − 01	0.4881E − 01	−0.3531E + 03	−0.9810E + 02
18	−0.7073E − 01	0.4881E − 01	−0.2596E + 03	−0.9810E + 02
19	−0.6973E − 01	0.4881E − 01	−0.2041E + 03	−0.9810E + 02
20	−0.6849E − 01	0.4881E − 01	−0.1695E + 03	−0.9810E + 02
21	−0.6737E − 01	0.4881E − 01	−0.1481E + 03	−0.9810E + 02
22	−0.6661E − 01	0.4881E − 01	−0.1321E + 03	−0.9810E + 02
23	−0.6490E − 01	0.4881E − 01	−0.1217E + 03	−0.9810E + 02
24	−0.6379E − 01	0.4881E − 01	−0.2187E + 03	−0.1962E + 03
25	−0.6388E − 01	0.4881E − 01	−0.2431E + 03	−0.1962E + 03
26	−0.6439E − 01	0.4881E − 01	−0.2993E + 03	−0.1962E + 03
27	−0.6488E − 01	0.4881E − 01	−0.3543E + 03	−0.1962E + 03
28	−0.6539E − 01	0.4881E − 01	−0.4116E + 03	−0.1962E + 03
29	−0.6653E − 01	0.4881E − 01	−0.5284E + 03	−0.1962E + 03
30	−0.6786E − 01	0.4881E − 01	−0.6386E + 03	−0.1962E + 03
31	−0.6933E − 01	0.4881E − 01	−0.7282E + 03	−0.1962E + 03
32	−0.7086E − 01	0.4837E − 01	−0.8016E + 03	−0.1962E + 03
33	−0.7263E − 01	0.4837E − 01	−0.8608E + 03	−0.1962E + 03
34	−0.7710E − 01	0.4924E − 01	−0.9396E + 03	−0.1962E + 03
35	−0.8245E − 01	0.5230E − 01	−0.9786E + 03	−0.1962E + 03
36	−0.8793E − 01	0.5664E − 01	−0.9902E + 03	−0.1962E + 03
37	−0.9323E − 01	0.6054E − 01	−0.9950E + 03	−0.1962E + 03
38	−0.9349E − 01	0.6097E − 01	−0.9077E + 03	−0.1962E + 03
39	−0.9313E − 01	0.6097E − 01	−0.7815E + 03	−0.1962E + 03
40	−0.9265E − 01	0.6097E − 01	−0.6613E + 03	−0.1962E + 03
41	−0.9198E − 01	0.6140E − 01	−0.5390E + 03	−0.1962E + 03
42	−0.9135E − 01	0.6140E − 01	−0.4587E + 03	−0.1962E + 03
43	−0.9054E − 01	0.6183E − 01	−0.3909E + 03	−0.1962E + 03
44	−0.8906E − 01	0.6183E − 01	−0.3142E + 03	−0.1962E + 03

Note: E=exponential; E−01 =$\times 10^{-1}$ etc.

are directly related to the plastic shear strain increments through a dilatancy function

$$\mathrm{d}v^{\mathrm{p}} = \mathrm{d}(g^{\mathrm{p}})\mathrm{d}g^{\mathrm{p}} \tag{6.3.46}$$

For the selection of an appropriate dilatancy function $\mathrm{d}(g^{\mathrm{p}})$ we resort here to the realm of the so-called stress-dilatancy theories of soil mechanics (Taylor, 1948; Rowe, 1972),

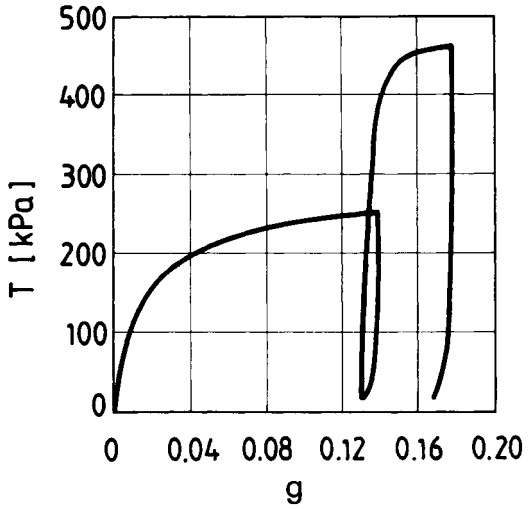

Figure 6.3.6 Triaxial compression of Karlsruhe sand (n_0=0.350). Deviatoric stress-strain curve. First loading at σ_c=100 kPa, second loading at σ_c=200 kPa.

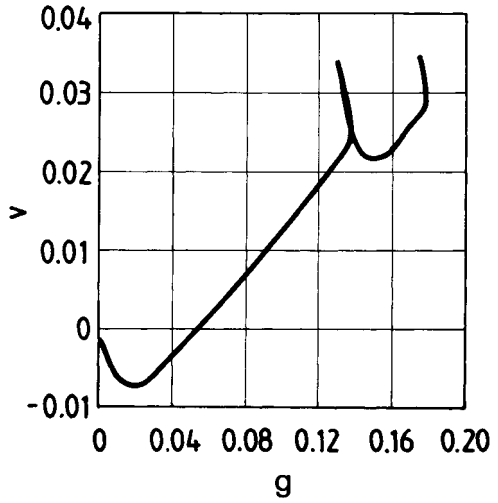

Figure 6.3.7 Triaxial compression of Karlsruhe sand (n_0=0.350). Volumetric stress-strain curve. First loading at σ_c=100 kPa, second loading at σ_c=200 kPa.

which can be reformulated in a more rational way as follows: For isotropically hardening, elasto-plastic materials the (first-order) plastic work of the stress on the plastic strains is dissipated into heat (see section 6.2.4). Accordingly, the Second Law of Thermodynamics requires that the first-order plastic work must be non-negative

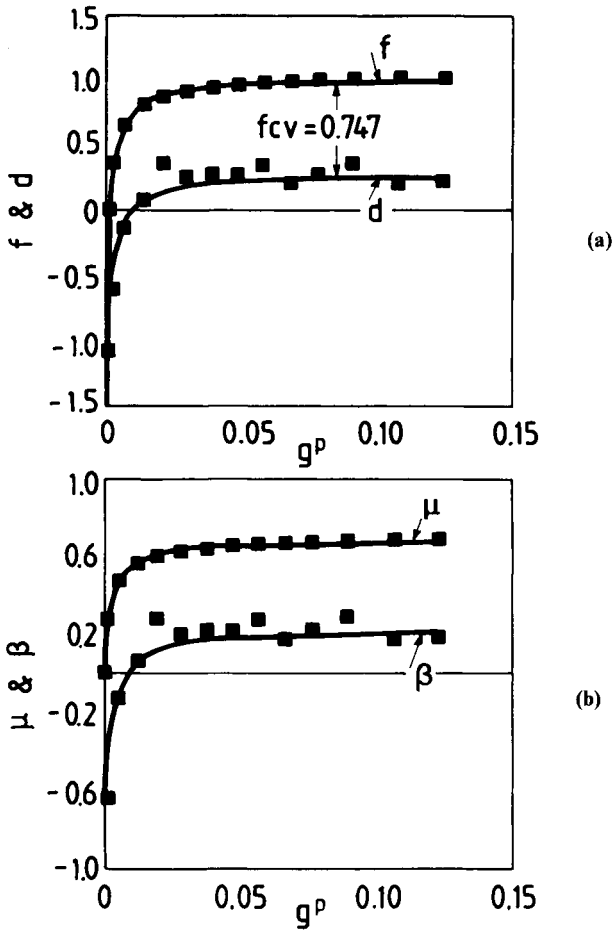

Figure 6.3.8 Mobilized friction and dilatancy coefficients: (a) f and d; (b) μ and β as functions of g^p.

$$\mathrm{d}w^p = \sigma_{ij}\,\mathrm{d}\varepsilon^p_{ij} = T\,\mathrm{d}g^p + p\,\mathrm{d}v^p \geqslant 0$$

$$\mathrm{d}w^p = (-p)(f-d)\mathrm{d}g^p \geqslant 0 \qquad (p<0) \tag{6.3.47}$$

Since during plastic loading $dg^p>0$ this results in a well-known constitutive inequality for the dilatancy coefficient

$$d \leqslant f \tag{6.3.48}$$

In Figure 6.3.9 the stress vector $\boldsymbol{\sigma} = \{p, T\}^T$ and the plastic strain increment vector $\mathrm{d}\boldsymbol{\varepsilon}^p = \{\mathrm{d}v^p, \mathrm{d}g^p\}^T$ are plotted for a typically dilatant soil. Inequality 6.3.48 determines the ultimate position of the plastic strain increment vector in stress space, which is that of

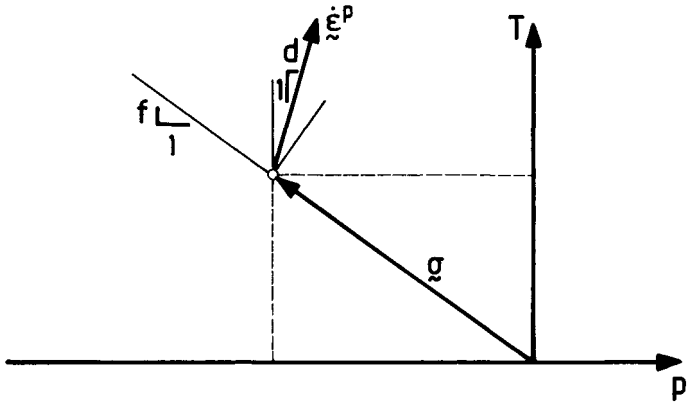

Figure 6.3.9 Geometric representation of a stress state at plastic yielding and of the corresponding plastic strain rate in invariant stress space for the visualization of the flow rule and of the first-order plastic work.

the *normal* $\boldsymbol{n}$ to the current yield surface. The so-called normality condition results here in the condition, $d=f$, i.e. requires the coincidence of the plastic potential function with the yield surface ($Q \equiv F$). (It is customary but rather misleading to call the corresponding behavior 'associative'.) We observe that for purely frictional materials the normality condition results in zero dissipation ($\mathrm{d}w^p/\mathrm{d}g^p = 0$). This is of course counter intuitive and has motivated the adoption of 'non-associative' plasticity models in soil mechanics.

In order to arrive at a simple mathematical description of the evolution of the mobilized dilatancy coefficient for the general non-associative case, $d<f$, we may generalize the above property of zero dissipation, holding for associative material behavior. We assume that from the point of view of energy dissipation a frictional and dilatant granular medium behaves like a purely frictional material with constant but reduced friction

$$\mathrm{d}w^p = \bar{T}\,\mathrm{d}g^p = -p\bar{f}\,\mathrm{d}g^p \tag{6.3.49}$$

where the corresponding 'effective' friction coefficient $\bar{f}$ assumed to be constant. This is known in the literature as Taylor's stress-ratio dilatancy theory (Taylor, 1948). From equations 6.3.47 to 6.3.49 then follows the simplest generalization of the normality condition of classical flow theory, which is included in it for the degenerate case of zero effective friction. It is customary, however, to call the corresponding flow-rule 'non-associated', although Taylor's rule provides a simple way to relate Q to F (the normals to the plastic potential and yield surface always produce the same angle, not necessarily zero).

For the evaluation of the effective friction coefficient we proceed with the observation that this constant can be identified with the stress ratio at which the soil behavior turns from contractant to dilatant. We may call this state also a state of isochoric plastic volumetric strain, and denote it by the abbreviation (cv)

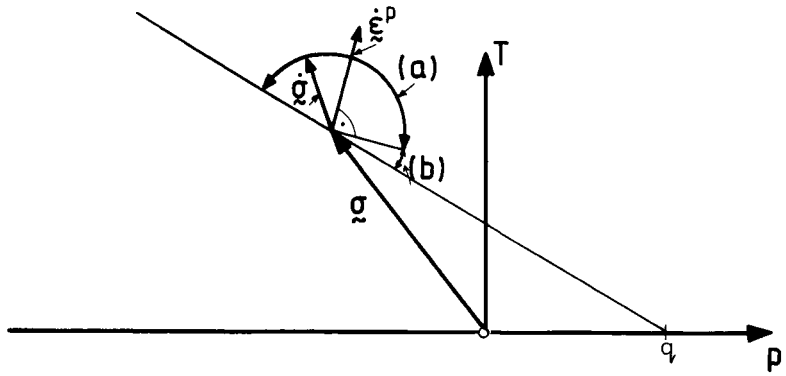

Figure 6.3.10 Stress probing in the various domains of positive or negative second-order plastic work for Coulomb material.

$$f = f_{cv};\ \mu_{cv} = \left.\frac{T}{p}\right|_{d=0} \tag{6.3.50}$$

Combining equations 6.3.47 to 6.3.50 we obtain the following simple 'stress-ratio dilatancy' formula

$$d = f - f_{cv} \tag{6.3.51}$$

In Figure 6.3.8 the data points d(g^p) are fitted by the corresponding shifted 'hyperbola', with $f_{cv} = 0.747$. We notice finally that the M.-C. yield condition and flow rule are making use of the mobilized friction and dilatancy angular functions

$$\sin\phi_m = \mu(g^p);\ \sin\psi_m = \beta(g^p) \tag{6.3.52}$$

respectively, which are related to the functions f and d as follows:

$$\mu = \frac{3f}{2\sqrt{3+f}};\ \beta = \frac{3d}{2\sqrt{3+d}} \tag{6.3.53}$$

In Figure 6.3.8(b) the measured and fitted M.-C. friction and dilatancy functions, μ and β, are plotted against the total plastic shear strain g^p. We notice that the maximum friction angle is $\phi_{max} = 43.6^\circ$, and that the mobilized friction angle at cv is $\phi_{cv} = 32.1^\circ$.

Remark on Drucker's postulate for geomaterials. We saw above that the thermodynamic requirement, that the local dissipation due to plastic deformation is strictly positive under fully loading conditions, restricts only the volumetric part of the flow rule, leading for frictional materials to a non-associative flow rule; cf. equation 6.3.48. Accordingly, within the framework of elastoplasticity theory, geomaterials are described by the constitutive equations for cohesive/frictional and dilatant media with *non-associated* flow rule. In this case, Drucker's postulate 6.2.54 is violated even in the *hardening* regime of the material behavior. As shown in Figure 6.3.10, for continued plastic loading the stress-rate vector is pointing into the exterior domain of the yield surface. Due to the

conical form of the yield surface there are then two distinct domains of material behavior: (a) a domain with $\Delta_2 w^p \geq 0$, and (b) a domain with $\Delta_2 w^p < 0$.

The existence of a set of stress probes with negative second-order plastic work in frictional materials was first pointed out by Mandel (1964) who clearly stated that Drucker's postulate is *not* a necessary condition for stability. We notice that Mandel's idea of stability is the one of linear, local stability analysis of the elastoplastic-dynamic initial value problem, i.e. it refers to the search for conditions for monotonic exponential growth of small perturbations out of a given equilibrium state. After the lecture of Jean Mandel (1964), Professor Drucker remarked however that "…the distinction between stability in the large and in the small is important. Professor Mandel's treatment of wave propagation and the friction example are based on stability in the small…".

6.3.4
Lade's yield surface model

Experiments show that the peak friction angle of a granular material in triaxial extension is typically a few degrees higher than that corresponding in triaxial compression (cf. Green, 1972). A simple one-parameter model of yield surface that accounts for such a behavior and does not deviate too much from the M.-C. model is a one-parameter model, originally proposed by Lade (1977). In case of cohesive-frictional material, Lade's model (L.) can be written as follows

$$F = I_{3\tau} - (1 - \eta(g^p))(I_{1\tau}/3)^3 \tag{6.3.54}$$

where $I_{1\tau}$ and $I_{3\tau}$ are the first and third invariant of a reduced stress tensor,

$$I_{1\tau} = \tau_{kk} \tag{6.3.55}$$

$$I_{3\tau} = \det(\tau_{ij}) \tag{6.3.56}$$

$$\tau_{ij} = \sigma_{ij} - q\delta_{ij} \tag{6.3.57}$$

In equation 6.3.57 q is the parameter related to the cohesion of the material; cf. equation *6.3.1bis* and Figure 6.3.3(b).

In terms of invariant angles, Lade's yield condition, $F = 0$, can be written as

$$-\eta \cot^3\phi_\sigma + \cot\phi_\sigma + \frac{2}{3\sqrt{3}}\cos 3\alpha_{s0} = 0 \tag{6.3.58}$$

which, for given $\eta = \eta(g^p)$, can be seen as an equation for determining ϕ_σ as a function of α_{s0}. Figure 6.3.11 depicts the typical trace of corresponding yield surface in the deviatoric plane. In particular for triaxial compression ($\alpha_{s0} = \pi/3$) and extension ($\alpha_{s0} = 0$) we have

$$\eta = \{\cot\phi_\sigma \mp 2/(3\sqrt{3})\}\cot^3\phi_\sigma \tag{6.3.59}$$

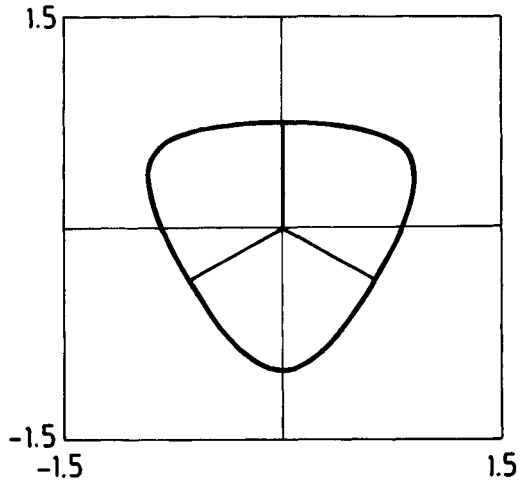

Figure 6.3.11 Deviatoric trace of the Lade (1977) yield surface.

We notice that implementation of a M.-C. yield surface may lead to numerical difficulties due to the existence of sharp corners. This is not the case with the L. model which, as can be seen from Figure 6.3.11, provides a smooth yield surface. Taking into account definition *6.3.1bis* for $\tan\phi_\sigma$, the gradient of the yield surface and the hardening modulus are computed as follows

$$\frac{\partial F}{\partial \sigma_{ij}} = \mathrm{ad}(\boldsymbol{\tau})_{ij} - (1-\eta)(I_{1\tau}/3)^2\,\delta_{ij} \tag{6.3.60}$$

$$H_t = -\frac{\partial F}{\partial g^{\mathrm{p}}} = \{\mathrm{ad}(\boldsymbol{\tau})_{ij} - 3(1-\eta)(I_{1\tau}/3)^2\}\frac{\mathrm{d}q}{\mathrm{d}g^{\mathrm{p}}} + (I_{1\tau}/3)^3\frac{\mathrm{d}\eta}{\mathrm{d}g^{\mathrm{p}}}$$

where $\mathrm{ad}(\tau)_{ij}$ is the adjoint of τ_{ij},

$$\mathrm{ad}(\boldsymbol{\tau})_{ij} = \begin{bmatrix} \tau_{22}\tau_{33} - \tau_{23}\tau_{32}, & \tau_{32}\tau_{13} - \tau_{33}\tau_{12}, & \tau_{12}\tau_{23} - \tau_{13}\tau_{22} \\ \tau_{23}\tau_{31} - \tau_{21}\tau_{33}, & \tau_{33}\tau_{11} - \tau_{31}\tau_{13}, & \tau_{13}\tau_{21} - \tau_{11}\tau_{23} \\ \tau_{21}\tau_{32} - \tau_{22}\tau_{31}, & \tau_{31}\tau_{12} - \tau_{32}\tau_{11}, & \tau_{11}\tau_{22} - \tau_{12}\tau_{21} \end{bmatrix} \tag{6.3.62}$$

6.4
Extensions of isotropic hardening plasticity

6.4.1
Non-potential flow rules

The flow rule of flow theory of plasticity, equation 6.2.9, is 'coaxial', i.e. the plastic strain rate tensor has the same principal axes as the Cauchy stress tensor. A co-axial flow rule

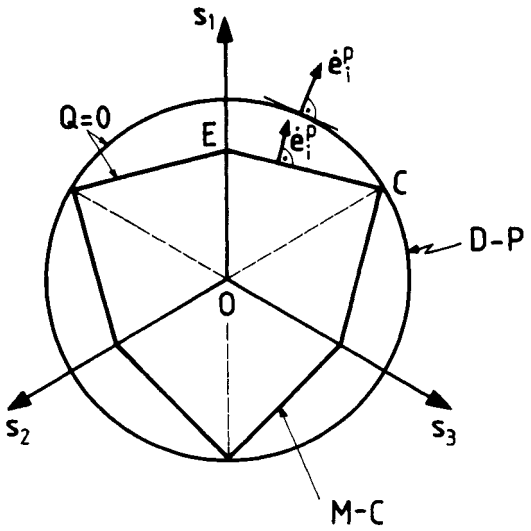

Figure 6.4.1 Geometric representation of the deviatoric flow rule.

may be represented graphically in the three-dimensional principal stress or any other stress-invariant space. For the models discussed above the flow rule derives from a potential function $Q(\sigma_{ij})$. For example, for a D.-P. model

$$\frac{\partial Q}{\partial \sigma_{ij}} = \frac{1}{3} d\delta_{ij} + \frac{1}{2\sqrt{J_{2s}}} s_{ij} \tag{6.4.1}$$

Accordingly, the flow rule is split into a volumetric and a deviatoric part. The volumetric part of the flow rule is represented in the *(p, T)* stress-invariant space, as already discussed in the previous section, cf. Figure 6.3.9. The qualitative difference between a D.-P., a M.-C. or a L. model is not seen in the *(T, p)* plane. For this we need to represent the flow rule in the principal-deviatoric plane, where the vector $(\dot{e}_1^p, \dot{e}_2^p, \dot{e}_3^p)^T$ is attached to the deviatoric trace of the corresponding plastic potential surface. As already mentioned, in the case of a D.-P. model this is a circle, whereas in the case of a M.-C. model it is a distorted hexagon (see Figure 6.4.1). In the latter case, of course, the potential function has corners and, accordingly, in the definition 6.2.9 of the flow rule, one must exclude these singular points, where separate values for the direction of the plastic strain rate must be prescribed; cf. equations 6.3.30. In order to avoid this peculiarity of the M.-C. model, several proposals exist like the above-discussed L. model, which interpolate between the circle and the hexagon (cf. Kim and Lade, 1988).

Historically, associative plasticity preceded non-asssociative plasticity, since for metals, the normality condition follows from pressure insensitivity and plastic strain-rate incompressibility. If one decides, however, to abandon

the concept of a flow rule associated to the yield surface F=0, through for example the simple normality condition, then one realizes that besides convenience, there is no

physical reason to assume that plastic strain rates are related to a potential function $Q(\sigma_{kl})$. Thus, one may generalize the flow rule 6.2.9, by assuming that the plastic strain rate is given by an isotropic tensor function of the stress tensor, which does not necessarily possess a potential function

$$\dot{\varepsilon}^{p}_{ij} = \dot{\psi}\, Q_{ij}(\sigma_{kl}) \tag{6.4.2}$$

Since Q_{ij} is an isotropic function of the stress tensor only, it follows that equation 6.4.2 is a co-axial flow rule as well. Dependence of the plastic strain rate on other tensors, like for example an objective stress rate may lead to non-linear or non-co-axial flow rules. Such non-potential flow rules will be discussed in chapter 8.

In order to discuss some interesting properties of the generalized linear and co-axial flow rule 6.4.2 we first observe that the invariant tensor-valued function Q_{ij} of the stress tensor σ_{k1} is expressible in polynomial form

$$\begin{aligned} Q_{ij} &= Q_0\delta_{ij} + Q_1\sigma_{ij} + Q_2\sigma_{ik}\sigma_{kj} \\ &= Q_0^{*}\delta_{ij} + Q_1 s_{ij} + Q_2 S_{ij} \end{aligned} \tag{6.4.3}$$

where

$$S_{ij} = s_{ik}s_{kj} - (\tfrac{2}{3})J_{2s}\delta_{ij} \tag{6.4.4}$$

and the coefficients Q_i $(i = 0, 1, 2)$ are scalar invariants of the tensor σ_{ij}. In view of representation 6.4.3, the simplest one-parameter realization of Q_{ij} is (cf. Vardoulakis, 1981a)

$$Q_{ij} = \frac{1}{3}d\delta_{ij} + \frac{1}{2\sqrt{(J_{2s})}}s_{ij} + \frac{1}{2\sqrt{(2J_{2s})}}CS_{ij} \tag{6.4.5.}$$

Notice that for $C = 0$, this flow rule coincides with the D.-P. rule. The deviatoric part of the flow rule 6.4.5 is rewritten as follows

$$\dot{e}^{p}_{ij} = \frac{\dot{\psi}}{2\sqrt{(J_{2s})}}Q'_{ij} \tag{6.4.6}$$

where

$$\begin{aligned} Q'_{ij} &= s_{ij} + R\{s_{ik}s_{kj} - (\tfrac{1}{3})s_{pq}s_{qp}\delta_{ij}\} \\ R &= C/(s_{pq}s_{qp})^{\frac{1}{2}} \end{aligned} \tag{6.4.7}$$

By using the notation

$$\begin{aligned} &\xi = s_{pq}s_{qp}; \quad \zeta = s_{pq}s_{qr}s_{rp} \\ &\overset{*}{\xi} = Q'_{pq}Q'_{qp}; \overset{*}{\zeta} = Q'_{pq}Q'_{qr}Q'_{rp} \end{aligned} \tag{6.4.8}$$

and the identities (cf. Thomas, 1961, p. 74)

$$\begin{aligned} \overset{*}{\xi} &= \xi + 2R\zeta + (R^2/6)\xi^2 \\ \overset{*}{\zeta} &= \zeta + (R\xi^2 + R^2\xi\zeta)/2 + R^3(\zeta^2 - \xi^3/12)/3 \end{aligned} \tag{6.4.9}$$

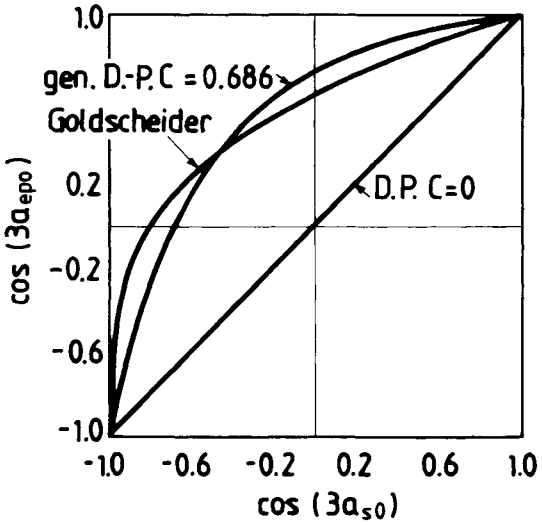

Figure 6.4.2 Relation between cos $3\alpha_{e\text{-}p0}$ and cos $3\alpha_{s0}$ for D.-P. flow rule (C=0) and generalized D.-P. flow rule C=0.686.

from the definitions

$$\cos 3\alpha_{s0} = \sqrt{6}\frac{\zeta}{\xi^{3/2}};\ \cos 3\alpha_{e-p0} = \sqrt{6}\frac{\overset{*}{\zeta}}{\overset{*}{\xi}^{\frac{3}{2}}} \tag{6.4.10}$$

we obtain the following relation between the two angles of similarity

$$\cos 3\alpha_{e-p0} = \frac{\cos 3\alpha_{s0} + C\sqrt{(\frac{3}{2})} + \cos 3\alpha_{s0} C^2/2 + (\cos^2 3\alpha_{s0} - \frac{1}{2})C^3/(3\sqrt{6})}{(1 + \cos 3\alpha_{s0} C\sqrt{(\frac{2}{3})} + C^2/6)^{\frac{3}{2}}} \tag{6.4.11}$$

The D.-P. model corresponds to $C = 0$ and it is represented by the condition

$$\cos 3\alpha_{e-p0} = \cos 3\alpha_s \tag{D.-P.}$$

which in the corresponding graph, Figure 6.4.2, is a straight line inclined at 45°, or a circle in the deviatoric plane, Figure 6.4.3. For increasing values of the parameter C, the corresponding integral curve in the deviatoric plane interpolates between the trace of a D.-P. and the M.-C. model or beyond towards a Rankine-type triangle with circular sides. For $C \geqslant \sqrt{6}$, cusps develop at $\alpha_s = (2k + 1)\pi/3$. Notice that for (cf. equation 6.2.14)

$$\dot{g}^p = Q_g \dot{\psi} > 0 \quad \text{for} \quad \dot{\psi} > 0 \tag{6.4.12}$$

$$Q_g = \{2[Q_{ij} - Q_{kk}\delta_{ij}][Q_{ij} - Q_{kk}\delta_{ij}]\}^{\frac{1}{2}} \tag{6.4.13}$$

For the generalized D.-P. flow rule

$$Q_g = \{1 + \sqrt{(\tfrac{2}{3})}C\cos(3\alpha_{s0}) + (\tfrac{1}{12})C^2\}^{\frac{1}{2}} \tag{6.4.14}$$

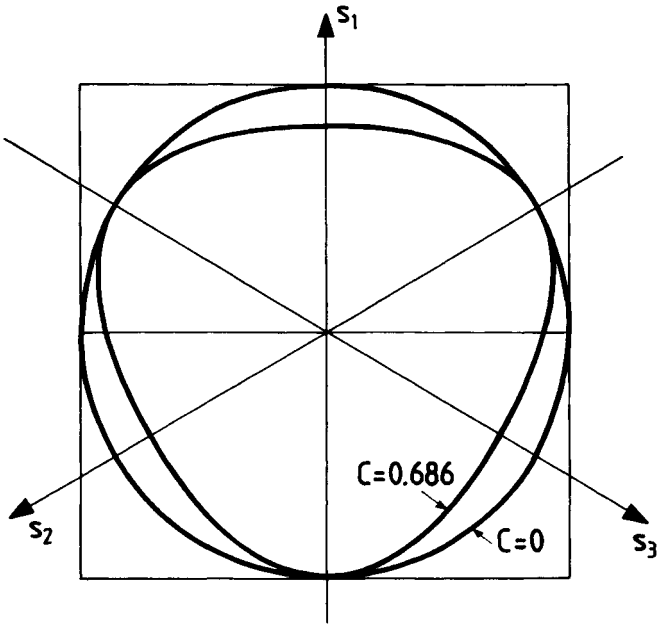

Figure 6.4.3 Integral curves for the non-potential flow rule (6.3.58) in deviatoric plane. (a) D.-P model, C=0; (b) best fit of Goldsheider's (1976) experimental results, C=0.686.

which restricts C further

$$0 \leqslant C \leqslant 2(\sqrt{6} - \sqrt{3}) \approx 1.43 \tag{6.4.15}$$

Within the frame of hardening plasticity theory, the parameter C is assumed to be a function of plastic state, i.e. $C = C(g^p)$. The experimental calibration of C necessitates the performance of experiments different than the triaxial compression or triaxial extension tests. For example one could perform *plane-strain* experiments with measurement of the (intermediate) principal stress, which is acting normal to the plane of deformation. Goldscheider (1976) studied experimentally the deviation from the D.-P. flow rule by using a true triaxial testing machine. Goldscheider's experiments can be seen as the soil mechanics counterpart of the classical Taylor and Quinney (1931) experiments on metals. Similar experimental results on sands are also reported by Kim and Lade (1988). Typically for sands, $C(0) = 0$, and C reaches a maximum value at peak strain. Figure 6.4.2 shows the above relationship 6.4.11 between $\cos 3\alpha_{s0}$ and $\cos 3\alpha_{e\text{-}p0}$ for $C = 0$ and $C = 0.686$ which corresponds to the best fit of Goldscheider's experimental data (Vardoulakis, 1981a). In Figure 6.4.3 the corresponding integral lines in deviatoric plane are plotted. The integration was carried for $0 \leq \alpha_{s0} \leq \pi/3$, and symmetry relations were used.

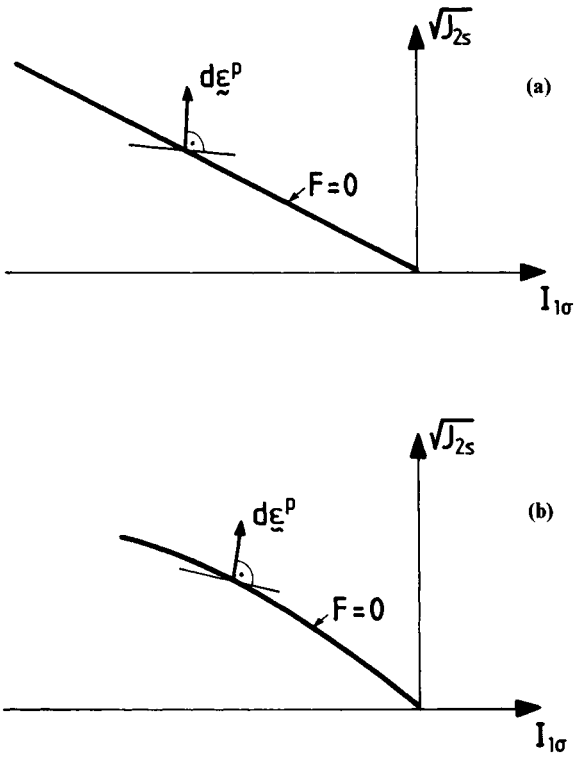

Figure 6.4.4 (a) Linear Mohr-Coulomb Model; (b) non-linear Mohr-Coulomb model.

6.4.2
Yield surface modifications

In the low stress limit, granular media are described by the so-called rigid-granular (psammic) material model, for which there is no material property with dimension of stress, and the behavior is given in terms of a set of non-dimensional properties, like the mobilized friction and dilatancy coefficients. In this limit the angles ϕ_m and ψ_m do not depend on the mean (intergranular) stress, and the corresponding yield and plastic potential surfaces are straight in a *(p, T)* stress space; Figure 6.4.4(a). However, there is experimental evidence suggesting that the friction and dilatancy characteristics of a soil are pressure sensitive, which in turn leads to modifications of the original linear Mohr-Coulomb model (Lade, 1977) (Figure 6.4.4(b)). It is important to note also, that within these non-linear Mohr-Coulomb models, even in the case of the non-associate flow rule, plastic volume changes are related to the yield surface indirectly through the common hardening parameter, namely a continuum isotropic measure of the average interparticle slip. Plastic volume changes in granular media are also caused by the increase of the mean intergranular stress due to compaction and grain crushing. This

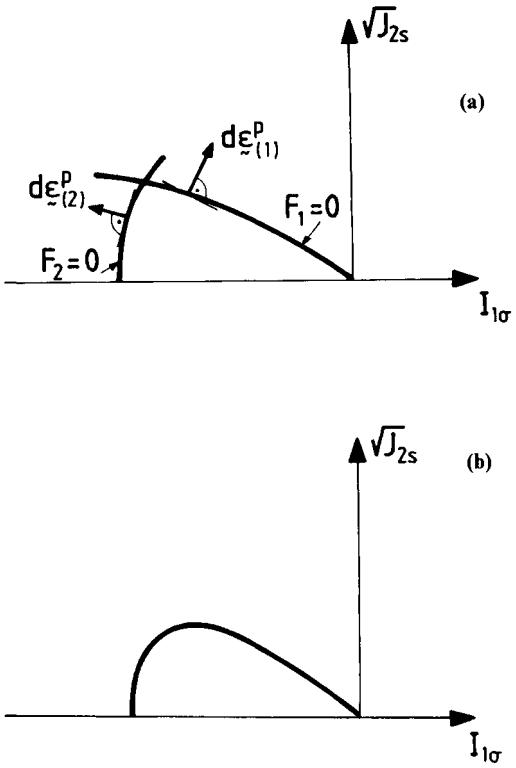

Figure 6.4.5 (a) The double hardening model with curved yield surfaces; (b) the work hardening model.

effect is usually accounted for in the so-called 'cap' models by the introduction of a second yield surface and a corresponding hardening parameter, which in turn is a measure of the compactive (inelastic) strain. If one wants to account for both dilation due to shear and compaction due to compression, one may resort to the so-called double-hardening elasto-plastic models (Koiter, 1953) with straight or curved yield surfaces (Vermeer, 1984); Figure 6.4.5(a). However, if plastic work is used as a hardening parameter one may simplify the model by choosing a single yield surface, which interpolates between the Mohr-Coulomb surface and the cap (Lade, 1988); Figure 6.4.5(b).

6.4.3
Modeling of strain softening

The model calibration discussed in section 6.3.3 is valid in the small strain regime which coincides with the strain hardening regime of the material behavior. As we will see in chapter 8, at some given state with small hardening rates, the deformation ceases to

be homogeneous turning 'spontaneously' into a localized one. In other words, prior to this equilibrium bifurcation the strains are moderate and the behavior is characterized in most cases by continuous strain hardening of a homogeneously deforming specimen (this is always true under plane-strain conditions). In the post-bifurcation regime the deformation localizes into one or more shear bands and usually leads to global softening. Accordingly, there is no direct way to measure the various material properties, like mobilized friction and dilatancy, in the softening regime. In order to overcome this difficulty, we discuss here a simple conceptual model of strain softening granular media that was motivated from the work of Frantziskonis and Desai (1987) and was discussed by Vardoulakis (1989), in relation to post-localization computations. It should be noted that a similar model was suggested later by Bardet (1992).

According to Dietrich (1976) we distinguish in a granular medium among two populations of grains: (i) the weak or frail fraction (f) with small coordination number, and (ii) the strong or competent fraction (c) with large coordination number. These two fractions can be easily identified in representations of granular assemblies with apparent intergranular forces; see for example Figure 6.4.6 from Cundall (1988). The granular medium is accordingly perceived as a mixture of these two fractions, such that during monotonous deformation processes of an 'overcritically' dense sand the average coordination number is decreasing which would mean here that competent granular fraction is irreversibly transformed into frail fraction.

As is usually the case in non-diffusing mixtures, the two fractions are assumed to share common strains but to have different stresses. In other words, we assign different partial stresses to the two phases, say σ^{c}_{ij} and σ^{f}_{ij}, whereas the partial strain rates are set equal, $\dot{\varepsilon}^{c}_{ij} = \dot{\varepsilon}^{f}_{ij} = \dot{\varepsilon}_{ij}$.

By introducing the volume fraction ratios

$$n^{f} = \frac{dV^{f}}{dV};\ n^{c} = \frac{dV^{c}}{dV} = 1 - n^{f} \tag{6.4.16}$$

and by assuming statistical isotropy, the total equilibrium stress becomes

$$\sigma_{ij} = (1 - n^{f})\sigma^{c}_{ij} + n^{f}\sigma^{f}_{ij} \tag{6.4.17}$$

Changes in n^{f} are assumed to be inversely proportional to changes in the average coordination number which in turn are related to changes of the porosity. In particular we assume here that the fraction ratio coincides with the relative porosity

$$n^{f} = \frac{n - n_{min}}{n_{max} - n_{min}} \qquad (0 \leqslant n^{f} \leqslant 1) \tag{6.4.18}$$

where n_{max} and n_{min} are the maximum and minimum porosity of the sand (here: n_{max}=0.45; n_{min}=0.35).

In granular media under shear elastic volumetric strains are small and thus changes of the porosity are mostly irreversible. From mass-balance considerations, equation 5.2.14, we then obtain that porosity changes are practically only due to plastic volume changes,

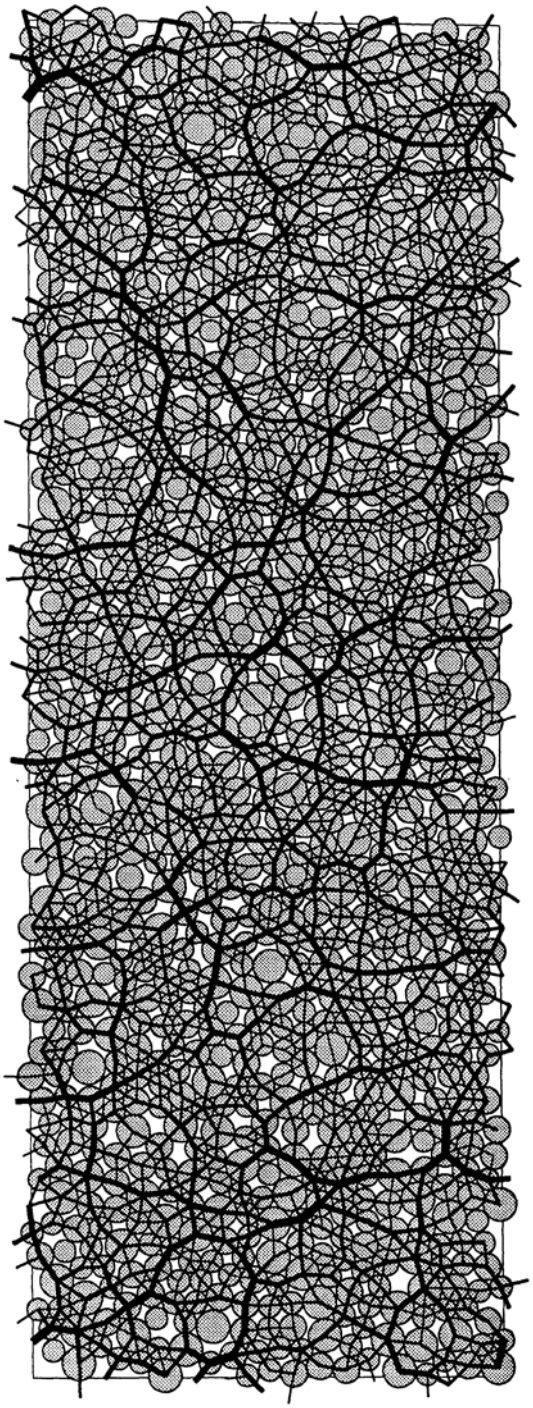

Figure 6.4.6 Distribution of contact forces in a 2D computer experiment by Cundall (1988).

$$\mathrm{d}n \approx (1-n)\mathrm{d}v^{\mathrm{p}} \tag{6.4.19}$$

with the initial value $n(v^{\mathrm{p}}=0)=n_o$ (here: $n_o=0.350$). In triaxial compression the plastic volumetric strains are linked to the plastic shear strains through the constraint 6.3.46 and Taylor's rule 6.3.51

$$\mathrm{d}v^{\mathrm{p}} = d\,\mathrm{d}g^{\mathrm{p}};\; d = f - f_{\mathrm{cv}} \tag{6.4.20}$$

The total equilibrium stress is decomposed into a deviatoric and into a spherical part. The behavior of the mixture is further specified by assuming that the mean pressure in both fractions is the same (Frantziskonis and Desai, 1987), resulting in

$$\sigma_{kk} = \sigma^{\mathrm{c}}_{kk} = \sigma^{\mathrm{f}}_{kk} = 3p;\; s_{ij} = (1-n^{\mathrm{f}})s^{\mathrm{c}}_{ij} + n^{\mathrm{f}}s^{\mathrm{f}}_{ij} \tag{6.4.21}$$

Furthermore we assume that the frail fraction is at 'critical state', which mathematically is described by the following conditions

$$s^{\mathrm{f}}_{ij} = \lambda\frac{s_{ij}}{\tau};\; \lambda\begin{cases} = |p|f^{\mathrm{f}} & \text{if} \quad \dot{g}^{\mathrm{p}} > 0 \\ \leqslant |p|f^{\mathrm{f}} & \text{if} \quad \dot{g}^{\mathrm{p}} = 0 \end{cases} \tag{6.4.22}$$

where the critical friction coefficient is identified with f_{cv} from Taylor's rule

$$f^{\mathrm{f}} = f_{\mathrm{cv}} \tag{6.4.23}$$

$f_{\mathrm{cv}} = 0.747$. From these assumptions we obtain the following expression for the mobilized friction coefficient

$$f = (1-n^{\mathrm{f}})f^{\mathrm{c}} + n^{\mathrm{f}}f^{\mathrm{f}} \tag{6.4.24}$$

With f^{c} and f_{cv} given, equations 6.4.19 and 6.4.20 can be integrated yielding the following expression for the porosity

$$\frac{1-n}{n_{\max}-n} = \frac{1-n_o}{n_{\max}-n_o}\exp\{E(g^{\mathrm{p}})\} \tag{6.4.25}$$

$$E = \frac{1-n_{\max}}{n_{\max}-n_{\min}}[(1/c_2 - f_{\mathrm{cv}})g^{\mathrm{p}} - (c_1/c_2^2)\ln\{1+(c_2/c_1)g^{\mathrm{p}}\}] \tag{6.4.26}$$

In the small strain regime we assume that the behavior is dominated by the response of the competent fraction, i.e. in a first approximation step, we may assume that $n \approx n_o n^{\mathrm{f}} \approx 0$ and $f \approx f^{\mathrm{c}}$. Within an iterative scheme it was found

$$f^{\mathrm{c}} = \frac{g^{\mathrm{p}}}{c_1 + c_2 g^{\mathrm{p}}} \tag{6.4.27}$$

with $c_1 = 3.5678E-3$; $c_2 = 9.1693E-1$. From this point of view, the competent fraction is always hardening with a maximum mobilized friction angle=45.9°. Figure 6.4.7 shows the evolution of f and f^{c} in the small strain regime.

As already mentioned, in the post-bifurcation regime the deformation localizes into a shear band, which leads to strain softening inside the band. Strain softening is modeled here according to the above two-fractions conceptual model. From equations 6.4.24 to 6.

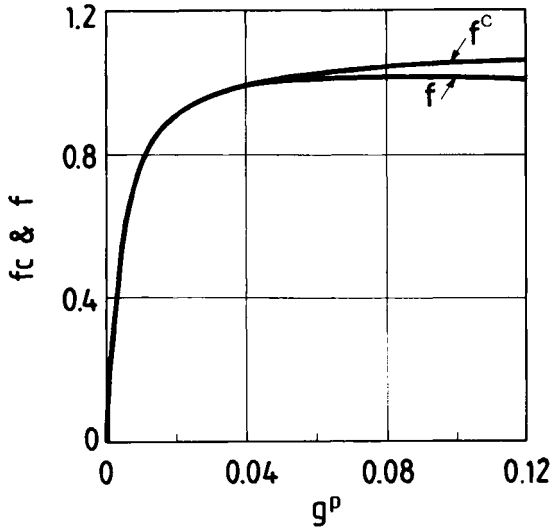

Figure 6.4.7 Small strain evolution of the friction functions f and f^c.

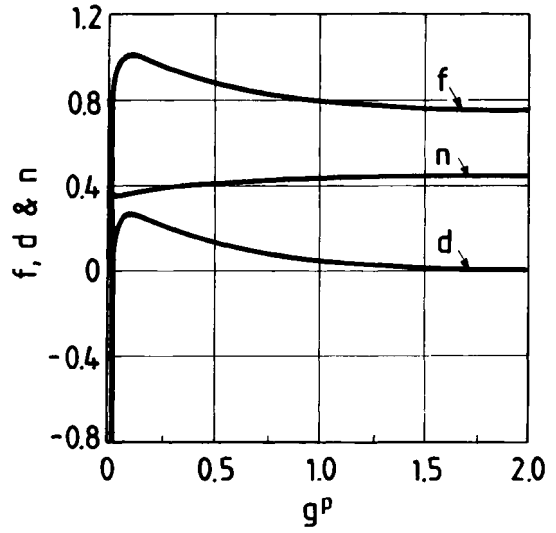

Figure 6.4.8 Large strain extrapolation of the experimental data for the mobilized friction and dilatancy coefficients in the softening regime.

4.27 we observe that for large values of n^f $(n^f \to 1)$ $f \to f^f$ and $d \to 0$. Figure 6.4.8 displays the large-strain evolution of the material functions f and d and n. Thus, the above presented material softening model contains implicitly the assumption that the critical state is reached asymptotically for strains of several hundred percent.

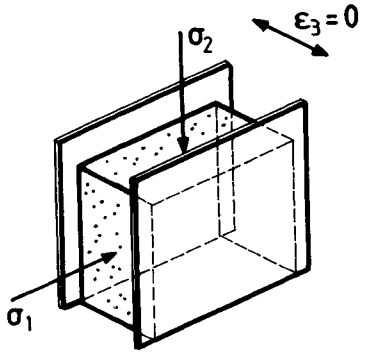

Figure 6.5.1 Rectangular specimen tested in plane-strain rectilinear compression.

6.5
2D-constitutive model for sand

6.5.1
Model justification

In many geo-engineering applications 'long' structures are studied (e.g. embankments, earth dams, tunnels, etc.) which suggests investigating the material behavior under plane-strain conditions. Accordingly, the behavior of the granular material in plane-strain deformations is of certain interest, and the following sections will focus on this subject. Ideally, for the analysis of plane-strain problems one should use data from plane-strain tests as well. However, such data are usually not readily available, and the behavior of the considered material under plane-strain conditions must be inferred theoretically from provided triaxial test data. In the previous sections we saw that we may have to select between competing models, e.g. the M.-C./D.-P. model (M.-C. yield surface and D.-P. plastic potential surface), and the M.-C./M.-C. model. The M.-C./M.-C. model is more attractive from the engineering application point of view, since in this case the concepts of friction and dilatancy are the same for all values of the intermediate principal stress and we do not have to distinguish, for example, between friction angle in compression, in extension and plane strain. In other words, within the M.-C./M.-C. model ϕ_m and ψ_m depend only on the initial porosity, and the accumulated plastic strain g^p, and not on the value of the intermediate principal stress σ_3.

Experimental results by Cornforth (1964) on sands tested under plane-strain conditions indicated that for the most part of the deformation the out-of-plane principal stress σ_3 is approximately in constant proportion to the sum of the other two

$$\sigma_3 \approx \text{const}\ (\sigma_1 + \sigma_2) \tag{6.5.1}$$

cf. Figure 6.5.1. This result is very useful in terms of defining a consistent and relatively simple way of describing plane-strain deformations: It suggests the application of a 2D-

flow theory of plasticity, whose material constants and functions are easily derived from or related to the ones of the corresponding 3D M.-C./M.-C. model. In order to demonstrate this assertion, let us consider plane-strain deformations, and let the x_α (α=1,2) be the Cartesian coordinates in the plane of deformation; then

$$\varepsilon_{33} = 0;\ \dot{\varepsilon}_{33} = 0 \tag{6.5.2}$$

if we assume the validity of a 3D elastoplastic M.-C./M.-C. constitutive model, then the plastic strain rates are given by the flow rule

$$\dot{\varepsilon}^{\mathrm{p}}_{ij} = \dot{\psi}\frac{\partial Q}{\partial \sigma_{ij}};\ \dot{\psi} \geqslant 0 \tag{M.-C.}$$

where the potential Q does not depend on the intermediate principal stress. If in addition we assume that the intermediate principal stress coincides with the stress normal to the plane of deformation, i.e. if

$$\sigma_3 = \sigma_{33} \quad \text{with} \quad \sigma_2 < \sigma_3 < \sigma_1 \tag{6.5.3}$$

then according to the M.-C. flow rule we obtain that

$$\dot{\varepsilon}^{\mathrm{p}}_{33} = 0 \tag{6.5.4}$$

Finally, this equation together with 6.5.2.2 results in

$$\dot{\varepsilon}^{\mathrm{e}}_{33} = 0 \tag{6.5.5}$$

From the elasticity equations

$$\dot{\varepsilon}^{\mathrm{e}}_{ij} = \frac{1}{2G}\left\{\dot{\sigma}_{ij} - \frac{\nu}{1-\nu}\dot{\sigma}_{kk}\delta_{ij}\right\} \tag{6.5.6}$$

and equation 6.5.5 we obtain

$$\dot{\sigma}_{33} = \nu(\dot{\sigma}_{11} + \dot{\sigma}_{22}) \tag{6.5.7}$$

Under these conditions, one may ignore the intermediate stress and study the behavior of the material within a 2D constitutive model. Such a model is also suitable for direct calibration on the basis of plane-strain (biaxial) test data, avoiding thus the complications and uncertainties concerning the influence of the third stress invariant.

Figures 6.5.2 to 6.5.4 show the computational results from plane-strain test simulations using the 3D constitutive laws discussed above in section 6.3 and for an assumed constant lateral stress $\sigma_c = 196.2\,\mathrm{kPa}$. From Figure 6.5.2 we discriminate the D.-P./D.-P. model which in most applications is yielding unacceptably high deviatoric stresses. As shown in Figures 6.5.3 and 6.5.4 for a M.-C.-type model condition (6.5.3) is met after some small initial strain (in our example for $|\varepsilon_2 - \varepsilon_1| > 1.25\%$). Finally we note that a M.-C.

model with a generalized D.-P. flow rule as discussed in section 6.4 provides smooth response.

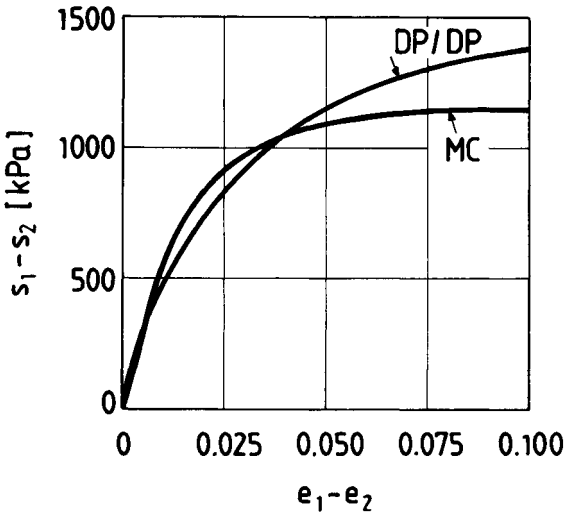

Figure 6.5.2 Computed stress-strain curve in the plane of deformation (σ_c=196.2 kPa): Models with a M.-C. yield condition collapse together whereas the model with a D.-P. yield condition shows higher strength.

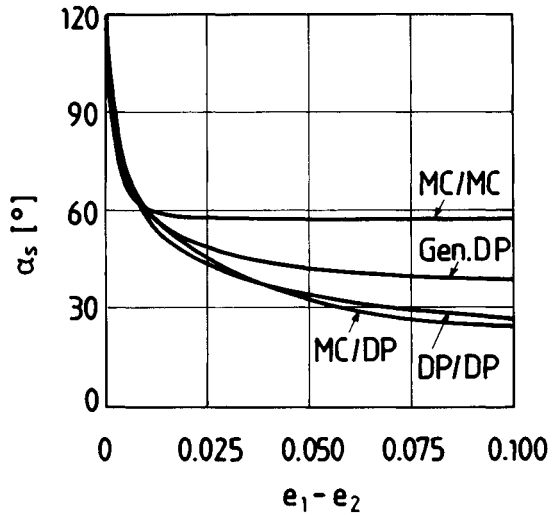

Figure 6.5.3 Evolution of the angle α_s for aM.-C./M.-C. and a M.-C./Gen.D.-P. (C=0.686) model.

6.5.2
Formulation

Considering only the components of the stress tensor $\sigma_{\alpha\beta}$ in the plane of deformation, we introduce a 2D stress tensor, whose components are again decomposed into spherical part and deviatoric part

$$\sigma_{\alpha\beta} = \sigma_{\gamma\gamma}\delta_{\alpha\beta}/2 + s_{\alpha\beta} \qquad (\alpha, \beta, \gamma = 1, 2) \tag{6.5.8}$$

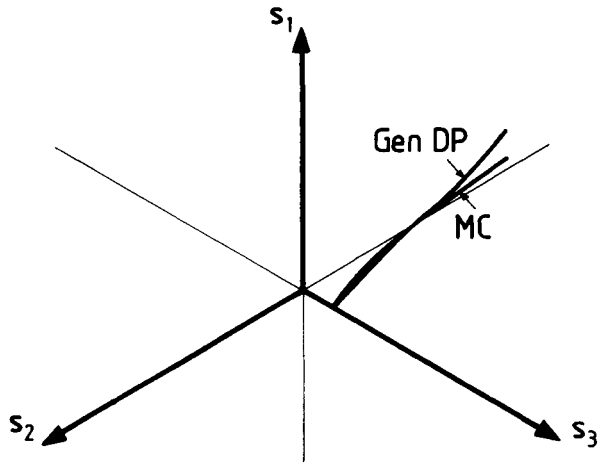

Figure 6.5.4 Stress paths in deviatoric plane for the M-C/M.-C. and the M.-C./Gen. D.-P. (C=0.686) model.

Furthermore, we introduce the so-called Roscoe stress measures, i.e. the mean stress σ and the shearing stress intensity τ in the plane of deformation are defined as follows

$$\sigma = \sigma_{\gamma\gamma}/2;\ \tau = \sqrt{(s_{\alpha\beta}s_{\alpha\beta}/2)} \tag{6.5.9}$$

Let also

$$\dot{\sigma}_{\alpha\beta} = \dot{s}_{\alpha\beta} + \dot{\sigma}\delta_{\alpha\beta};\ \dot{\sigma} = \dot{\sigma}_{\gamma\gamma}/2 \tag{6.5.10}$$

$$\dot{\varepsilon}_{\alpha\beta} = \dot{e}_{\alpha\beta} + \dot{\varepsilon}\delta_{\alpha\beta}/2;\ \dot{\varepsilon} = \dot{\varepsilon}_{\gamma\gamma} \tag{6.5.11}$$

be the corresponding 2D stress rate and 2D strain rate. The strain rate is decomposed again into an elastic and a plastic part, i.e.

$$\dot{\varepsilon}_{\alpha\beta} = \dot{\varepsilon}^{\mathrm{e}}_{\alpha\beta} + \dot{\varepsilon}^{\mathrm{p}}_{\alpha\beta} \tag{6.5.12}$$

which, in turn, are also split into spherical and deviatoric parts

$$\dot{\varepsilon}^{(\mathrm{k})}_{\alpha\beta} = \dot{e}^{(\mathrm{k})}_{\alpha\beta} + \dot{\varepsilon}^{(\mathrm{k})}\delta_{\alpha\beta}/2;\ \dot{\varepsilon}^{(\mathrm{k})} = \dot{\varepsilon}^{(\mathrm{k})}_{\gamma\gamma} \qquad (\mathrm{k} = \mathrm{e}, \mathrm{p}) \tag{6.5.13}$$

From 6.5.6 and 6.5.7, it follows that the 2D elastic shear and compression moduli are

$$G' \equiv G;\ K' = (3/2)K/(1+\nu) \tag{6.5.14}$$

and their ratio

$$k = K'/G' = 1/(1-2\nu) \tag{6.5.15}$$

Elastic strain rates are related to the stress rates through the equations of linear isotropic elasticity

$$\dot{e}^{\mathrm{e}}_{\alpha\beta} = \dot{s}_{\alpha\beta}/(2G);\ \dot{\varepsilon}^{\mathrm{e}} = \dot{\sigma}/K' \tag{6.5.16}$$

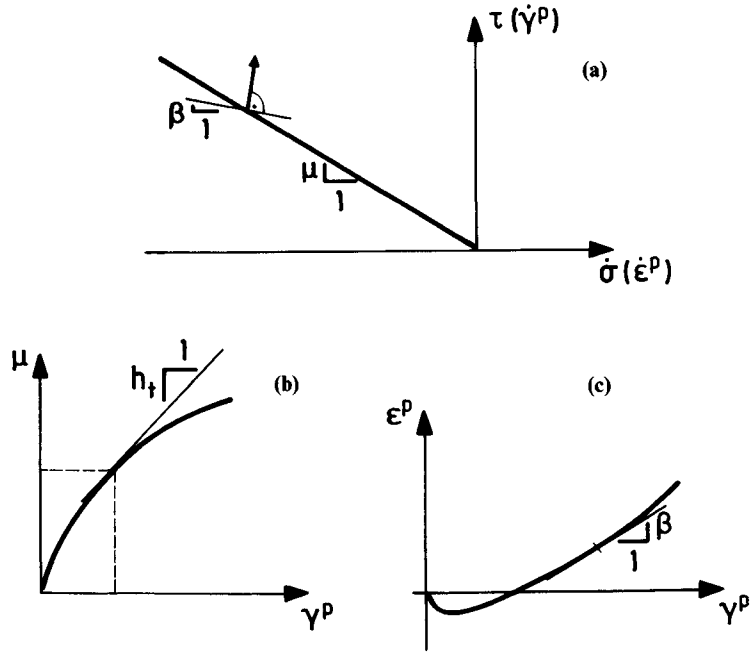

Figure 6.5.5 (a) Mohr-Coulomb yield surface and plastic strain-rate vector. (b) Mobilized friction function. (c) Mobilized dilatancy function.

The yield function and plastic strain rate potential functions are of the Coulomb type (Figure 6.5.5a),

$$F(\sigma_{\alpha\beta}, \psi) = \tau + \sigma\mu(\psi) \tag{6.5.17}$$

$$Q(\sigma_{\alpha\beta}, \psi) = \tau + \sigma\beta(\psi) \tag{6.5.18}$$

where $\mu(\psi)$ and $\beta(\psi)$ are the corresponding friction and dilatancy coefficients,which are both assumed to be functions of an appropriate hardeningparameter ψ. From these particular representations we derive the followingexpressions for the gradients of F and Q in stress space

$$f_{\alpha\beta} = \frac{\partial F}{\partial \sigma_{\alpha\beta}} = \frac{m_{\alpha\beta}}{\sqrt{2}} + \frac{1}{2}\mu\,\delta_{\alpha\beta};\; q_{\alpha\beta} = \frac{\partial Q}{\partial \sigma_{\alpha\beta}} = \frac{m_{\alpha\beta}}{\sqrt{2}} + \frac{1}{2}\beta\,\delta_{\alpha\beta} \tag{6.5.19}$$

where $m_{\alpha\beta}$ is the unit vector in deviatoric stress space co-axial to the stress

$$m_{\alpha\beta} = \frac{s_{\alpha\beta}}{\sqrt{2}\tau};\; m_{\alpha\beta} m_{\alpha\beta} = 1 \tag{6.5.20}$$

From the flow rule

$$\dot{\varepsilon}^{p}_{\alpha\beta} = \dot{\psi} q_{\alpha\beta} \tag{6.5.21}$$

and equation 6.5.19.2 it follows that in particular the deviatoric plastic strain rates are given by

$$\dot{e}^{p}_{\alpha\beta} = (m_{\alpha\beta}/\sqrt{2})\dot{\psi} \tag{6.5.22}$$

From equations 6.5.20 and 6.5.22, it follows that the plastic .hardening parameter is the second deviatoric invariant of the plastic strain rate

$$\dot{\gamma}^{p} = \sqrt{(2\dot{e}^{p}_{\alpha\beta}\dot{e}^{p}_{\alpha\beta})} = \dot{\psi} \tag{6.5.23}$$

and thus

$$\dot{e}^{p}_{\alpha\beta} = (m_{\alpha\beta}/\sqrt{2})\dot{\gamma}^{p};\ \varepsilon^{p} = \beta\dot{\gamma}^{p} \tag{6.5.24a}$$

or

$$\dot{\varepsilon}^{p}_{\alpha\beta} = (m_{\alpha\beta}/\sqrt{2} + \tfrac{1}{2}\beta\,\delta_{\alpha\beta})\dot{\gamma}^{p} \tag{6.5.24b}$$

It is worth noting that there is a formal difference between the 3D and 2D measures of plastic plane-strain hardening: If $i,j = 1,2,3$ and $\dot{e}^{p}_{\alpha\beta}$ $(\alpha,\beta = 1,2)$ are the corresponding principal plastic deviatoric strain rates, we have

$$\begin{aligned}\dot{g}^{p} &= \sqrt{\{2[(\dot{e}^{p}_{1})^2 + (\dot{e}^{p}_{2})^2 + (\dot{e}^{p}_{3})^2]\}} \\ &= (2/\sqrt{3})\sqrt{\{[(\dot{\varepsilon}^{p}_{1})^2 + (\dot{\varepsilon}^{p}_{2})^2 - \dot{\varepsilon}^{p}_{1}\dot{\varepsilon}^{p}_{2}]\}}\end{aligned} \tag{6.5.25a}$$

$$\dot{\gamma}^{p} = \sqrt{\{2[(\dot{e}^{p}_{1})^2 + (\dot{e}^{p}_{2})^2]\}} = |\dot{\varepsilon}^{p}_{1} - \dot{\varepsilon}^{p}_{2}| \tag{6.5.25b}$$

The friction and dilatancy coefficients are expressed in terms of the so-called mobilized angles of friction ϕ_{m} and dilatancy ψ_{m}. The term 'mobilized' is used to signify that ϕ_{m} and ψ_{m} are unique functions of the 2D measure for plastic shearing strain, $\gamma^{p} = \int \dot{\gamma}^{p}\,dt$ (Figure 6.5.5b,c)

$$\sin\phi_{m} = \mu(\gamma^{p});\ \sin\psi_{m} = \beta(\gamma^{p}) \tag{6.5.26}$$

From the consistency condition

$$F = 0 \quad \text{and} \quad \dot{F} = 0 \tag{6.5.27}$$

follows

$$\dot{\tau} + \mu\dot{\sigma} + \sigma h_{t}\dot{\gamma}^{p} = 0 \tag{6.5.21bis}$$

where h_{t} is the tangent modulus

$$h_{t} = \frac{d\mu}{d\gamma^{p}} \tag{6.5.28}$$

With

$$\begin{aligned}\dot{\tau} &= s_{\alpha\beta}\dot{s}_{\alpha\beta}/(2\tau)\\ &= 2G\dot{e}^{e}_{\alpha\beta}s_{\alpha\beta}/(2\tau)\\ &= Gs_{\alpha\beta}(\dot{e}_{\alpha\beta} - \dot{e}^{p}_{\alpha\beta})/\tau\\ &= G(s_{\alpha\beta}\dot{e}_{\alpha\beta}/\tau - \dot{\gamma}^{p})\end{aligned} \tag{6.5.29}$$

we obtain an expression for $\dot{\gamma}^{p}$ which is consistent with the flow rule 6.5.21, and the definition of the yield function 6.5.17

$$\dot{\gamma}^{p} = \frac{\langle 1\rangle}{H} b^{F}_{\alpha\beta}\dot{\varepsilon}_{\alpha\beta} \tag{6.5.30}$$

$b^{F}_{\alpha\beta}$ in equation 6.5.30 is derived from the gradient of the yield surface in stress space as follows

$$b^{F}_{\gamma\delta} = f_{\alpha\beta}L^{e}_{\alpha\beta\gamma\delta} = G(s_{\gamma\delta}/\tau + k\mu\delta_{\gamma\delta}) \tag{6.5.31}$$

where L^{e} is the 2D-elasticity tensor,

$$L^{e}_{\alpha\beta\gamma\delta} = G\{\delta_{\alpha\gamma}\delta_{\beta\delta} + \delta_{\alpha\delta}\delta_{\beta\gamma} + (k-1)\delta_{\alpha\beta}\delta_{\gamma\delta}\} \tag{6.5.32}$$

The plastic-, hardening- and snap-back moduli are expressed in terms of appropriate non-dimensional quantities

$$H = Gh^{*} = G(h + h_{o});\ h_{o} = 1 - h_{T} \tag{6.5.33}$$

$$h = \frac{|\sigma|}{G}h_{t};\ h_{T} = -k\mu\beta \tag{6.5.34}$$

where h_{T} is the value of the hardening modulus at maximum deviator in isochoric (constrained) motions. According to equation 6.5.34.1 h is a dimensionless hardening modulus. In the consistency condition 6.5.30, <·> are the McAuley brackets. Since G»|σ|, the hardening modulus $|h|$<<1. Moreover, for dilatant soils ψ_{m}>0 and thus h_{T}<0. From equation (6.5.23) it follows that indeed the plastic modulus H>0 and thus the switch function can be defined as follows

$$\langle 1\rangle = \begin{cases} = 1 & \text{if } F = 0 \text{ and } b^{F}_{\alpha\beta}\dot{\varepsilon}_{\alpha\beta} > 0\\ = 0 & \text{if } F < 0 \text{ or } \{F = 0 \text{ and } b^{F}_{\alpha\beta}\dot{\varepsilon}_{\alpha\beta} \leqslant 0\}\end{cases} \tag{6.5.35}$$

The plastic strain rates can be thus written in the following alternative form:

$$\dot{\varepsilon}^{p}_{\alpha\beta} = M^{p}_{\alpha\beta\gamma\delta}\dot{\sigma}_{\gamma\delta} \tag{6.5.36}$$

where the plastic compliances are given by the expression

$$M^{p}_{\alpha\beta\gamma\delta} = \frac{\langle 1\rangle}{Gh}q_{\alpha\beta}f_{\gamma\delta} \tag{6.5.37}$$

From the consistency condition 6.5.27bis and $\dot{\gamma}^{p} \geqslant 0$ we obtain the following alternative form for the plastic hardening parameter

$$\dot{\gamma}^{\mathrm{p}} = \frac{\langle 1 \rangle}{|\sigma| h_t}(\dot{\tau} + \mu \dot{\sigma}) \tag{6.5.38}$$

or, with equation 6.5.34.1 and the condition $F = 0$,

$$\dot{\gamma}^{\mathrm{p}} = \frac{\langle 1 \rangle}{Gh}\left[\frac{s_{\alpha\beta}}{2\tau}\dot{s}_{\alpha\beta} - \frac{\tau}{\sigma}\dot{\sigma}\right]$$

With this expression for $\dot{\gamma}^{\mathrm{p}}$ we obtain finally a simple generalization of the well-known Prandtl-Reuss equations in 2D:

$$2\dot{e}_{\alpha\beta} = \frac{\dot{s}_{\alpha\beta}}{G} + \frac{\langle 1 \rangle}{Gh}\frac{s_{\alpha\beta}}{\tau}\left[\frac{s_{\mu\tau}}{2\tau}\dot{s}_{\mu\tau} - \frac{\tau}{\sigma}\dot{\sigma}\right] \tag{6.5.40}$$

$$\dot{\varepsilon} = \frac{\dot{\sigma}}{K'} + \frac{\langle 1 \rangle}{Gh}\beta\left[\frac{s_{\mu\tau}}{2\tau}\dot{s}_{\mu\tau} - \frac{\tau}{\sigma}\dot{\sigma}\right]$$

In these expressions we recognize a 2D manifestation of the small strain version of the Rudnicki and Rice (1975) flow theory of plasticity for pressure sensitive and dilatant materials, which in their original paper was discussed in connection with localization of the deformation along a shear band.

Finally, by combining the expressions for the elastic and plastic part of the strain rate, equations 6.5.16 and 6.5.24 with 6.5.30, we obtain the following rate equations for the considered 2D flow theory of plasticity

$$\dot{\sigma}_{\alpha\beta} = L^{\mathrm{ep}}_{\alpha\beta\gamma\delta}\dot{\varepsilon}_{\gamma\delta} \tag{6.5.42}$$

where the elastoplastic stiffness tensor is given by

$$L^{\mathrm{ep}}_{\alpha\beta\gamma\delta} = L^{\mathrm{e}}_{\alpha\beta\gamma\delta} - L^{\mathrm{p}}_{\alpha\beta\gamma\delta} \tag{6.5.43}$$

$$L^{\mathrm{p}}_{\alpha\beta\gamma\delta} = \frac{\langle 1 \rangle}{H} b^{\mathrm{Q}}_{\alpha\beta} b^{\mathrm{F}}_{\gamma\delta} \tag{6.5.44}$$

The tensor $b^{\mathrm{Q}}_{\alpha\beta}$ is defined, in analogy to $b^{\mathrm{F}}_{\alpha\beta}$, equation 6.5.31, in terms of the mobilized dilatancy function

$$b^{\mathrm{Q}}_{\alpha\beta} = q_{\gamma\delta}L^{\mathrm{e}}_{\gamma\delta\alpha\beta} = G(s_{\alpha\beta}/\tau + k\beta\delta_{\alpha\beta}) \tag{6.5.45}$$

and is related to the normal in stress space on the plastic potential surface passing through the considered stress point. If we assume that the mobilized dilatancy angle coincides with the mobilized friction angle ($\psi_{\mathrm{m}} = \phi_{\mathrm{m}}$), then (i) $F \equiv Q$, the plastic strain rates are normal to the yield surface (normality condition), and the material obeys an associate flow rule, and (ii) since $b^{\mathrm{F}}_{\alpha\beta} \equiv b^{\mathrm{Q}}_{\alpha\beta}$ the elastoplastic stiffness tensor is symmetric. Otherwise the material obeys a non-associate flow rule and the stiffness tensor does not satisfy the major symmetry condition.

6.5.3
Example of model calibration

Let a homogeneous, cuboidal soil specimen in an undisturbed initial configuration C_o, be subjected to a monotonous, quasi-static homogeneous rectilinear deformation $C_o \rightarrow C$, Figure 6.5.6(a). Stress and strain at C are given by the Cauchy stress tensor $\sigma_{\alpha\beta}$ and the logarithmic strain $\lambda_{\alpha\beta}$, measured with respect to the isotropic configuration C_o. In the Cartesian coordinate system (x_1, x_2) ofthe fixed-in-space principal axes of these tensors the following representations hold:

$$\{\sigma_{\alpha\beta}\} = \begin{bmatrix} \sigma_1 & 0 \\ 0 & \sigma_2 \end{bmatrix} \qquad (\sigma_2 \leqslant \sigma_1 < 0) \tag{6.5.46}$$

$$\{\lambda_{\alpha\beta}\} = \begin{bmatrix} \lambda_1 & 0 \\ 0 & \lambda_2 \end{bmatrix} \qquad (\lambda_2 \leqslant \lambda_1) \tag{6.5.47}$$

where $\lambda_\alpha = \ln(\ell_\alpha/\ell_{\alpha 0})$ with $\ell_{\alpha 0}$ and ℓ_α (α=1,2) being the dimensions of the specimen in C_o and C, respectively. In the considered case, we obtain the following expressions for the mean stress, and the shearing stress intensity in the plane of deformation

$$\sigma = (\sigma_1 + \sigma_2)/2; \; \tau = |\sigma_1 - \sigma_2|/2 \tag{6.5.48}$$

Similarly, we define the total volumetric strain and shearing strain:

$$\varepsilon = \lambda_1 + \lambda_2; \; \gamma = |\lambda_1 - \lambda_2| \tag{6.5.49}$$

During loading and at a state C, the mobilized-friction coefficient becomes (Figure 6.5.6b):

$$\sin\phi_{\mathrm{m}} = \left|\frac{\sigma_1 - \sigma_2}{\sigma_1 + \sigma_2}\right| \tag{6.5.50}$$

where ϕ_{m} is called the mobilized Mohr-Coulomb friction angle.

For the considered rectilinear deformations,

$$\mathrm{d}\lambda_\alpha = \frac{\mathrm{d}\ell_\alpha}{\ell_\alpha} = \mathrm{d}\varepsilon_\alpha = \mathrm{d}\varepsilon_\alpha^{\mathrm{e}} + \mathrm{d}\varepsilon_\alpha^{\mathrm{p}} \tag{6.5.51}$$

and thus for the mobilized dilatancy angle ψ_{m} after Hansen and Lundgren (Figure 6.5.6c) we obtain the following expression

$$\sin\psi_{\mathrm{m}} = \frac{\mathrm{d}\varepsilon_1^{\mathrm{p}} + \mathrm{d}\varepsilon_2^{\mathrm{p}}}{\mathrm{d}\varepsilon_1^{\mathrm{p}} - \mathrm{d}\varepsilon_2^{\mathrm{p}}} \tag{6.5.52}$$

Example: In the following, the experimental results are presented from a biaxial test on a dry specimen of a fine-grained Dutch dune sand, the so-called Ostershelde sand (see Figure 6.5.7 and Table 6.5.1; Vardoulakis *et al.*, 1985; Vardoulakis, 1988). For the description of the biaxial experiment and its evaluation we refer to Vardoulakis and Goldscheider (1981) as well as to Drescher et al (1990). The initial porosity of the sand was $n_o = 0.383$ ($n_{\min} = 0.362$ and $n_{\max} = 0.482$ and $G_{\mathrm{s}} = 2.66$). During this test the confining

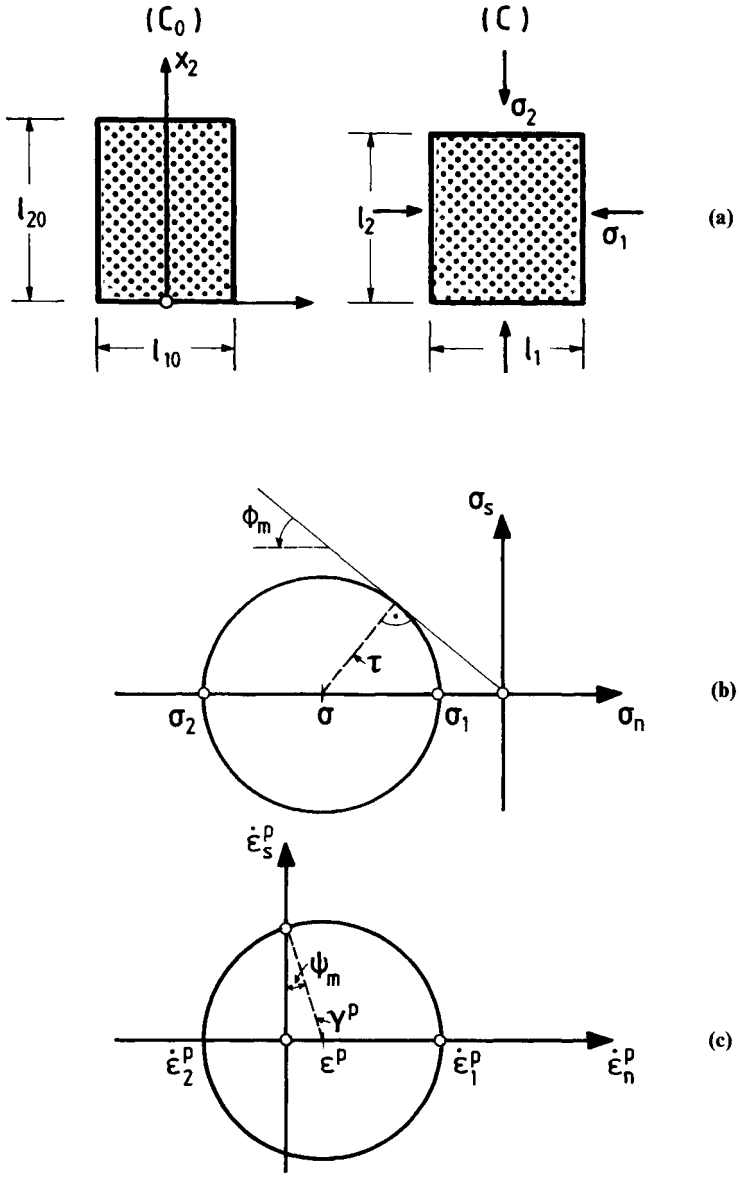

Figure 6.5.6 (a) Initial (C_o) and current *(C)* configuration of a rectangular specimen; Mohr circles (b) of stresses and (c) of plastic strain rates, with definition of mobilized friction angle ϕ_m and mobilized dilatancy angle ψ_m.

pressure was kept constant, $\sigma_c = 294.3\,\mathrm{kPa}$. In Figures 6.5.8(a,b) the measured mobilized friction coefficient $\sin\phi_m$ and volumetric strain ε for loading are plotted versus the shear strain γ and are approximated by the following functions

Table 6.5.1 Biaxial test data for Dutch dune sand dense sand (initial porosity n_o=0.383) initial height 1_{20}=40.93mm; initial width 1_{20}=41.03mm

no.	λ_1 (—)	λ_2 (—)	σ_1 (kPa)	σ_2 (kPa)
1	0.0000E + 00	0.0000E + 00	−0.2943E + 03	−0.2943E + 03
2	0.1849E − 05	−0.1882E − 03	−0.2943E + 03	−0.3101E + 03
3	0.7398E − 05	−0.4226E − 03	−0.2943E + 03	−0.3298E + 03
4	0.1595E − 04	−0.6440E − 03	−0.2943E + 03	−0.3482E + 03
5	0.3229E − 04	−0.9377E − 03	−0.2943E + 03	−0.3725E + 03
6	0.4856E − 04	−0.1161E − 02	−0.2943E + 03	−0.3909E + 03
7	0.1065E − 03	−0.1744E − 02	−0.2943E + 03	−0.4382E + 03
8	0.2278E − 03	−0.2572E − 02	−0.2943E + 03	−0.5039E + 03
9	0.3848E − 03	−0.3355E − 02	−0.2943E + 03	−0.5644E + 03
10	0.9177E − 03	−0.5202E − 02	−0.2943E + 03	−0.6997E + 03
11	0.1694E − 02	−0.7086E − 02	−0.2943E + 03	−0.8268E + 03
12	0.3102E − 02	−0.9618E − 02	−0.2943E + 03	−0.9799E + 03
13	0.4689E − 02	−0.1187E − 01	−0.2943E + 03	−0.1100E + 04
14	0.7028E − 02	−0.1462E − 01	−0.2943E + 03	−0.1226E + 04
15	0.1046E − 01	−0.1801E − 01	−0.2943E + 03	−0.1357E + 04
16	0.1390E − 01	−0.2095E − 01	−0.2943E + 03	−0.1450E + 04
17	0.1698E − 01	−0.2336E − 01	−0.2943E + 03	−0.1516E + 04
18	0.2021E − 01	−0.2572E − 01	−0.2943E + 03	−0.1572E + 04
19	0.2371E − 01	−0.2812E − 01	−0.2943E + 03	−0.1622E + 04
20	0.2726E − 01	−0.3043E − 01	−0.2943E + 03	−0.1664E + 04
21	0.3085E − 01	−0.3268E − 01	−0.2943E + 03	−0.1701E + 04
22	0.3402E − 01	−0.3459E − 01	−0.2943E + 03	−0.1729E + 04
23	0.3644E − 01	−0.3603E − 01	−0.2943E + 03	−0.1748E + 04

Note: E=exponential; *E*−01=×10^{-1} etc.

$$\sin\phi_m = \frac{\gamma}{d_1 + d_2\gamma} \tag{6.5.53}$$

with d_1=6.9980*E*−3, d_2=1.3083*E*0, and

$$\varepsilon = d_3\gamma + d_4 \ln(1 + d_5\gamma) \tag{6.5.54}$$

with d_3=4.5684−1, d_4=−1.6273*E*−2, d_5=8.9074*E*+1.

Data from first unloading-reloading loops were used to determine the elastic constants of the soil, resulting in a shear modulus, $G = 50.34\,\text{MPa}$ and a Poisson's ratio $\nu = 0.104$..

The mobilized friction and dilatancy functions,

$$\sin\phi_m = \mu(\gamma^p);\ \sin\psi_m = \beta(\gamma^p) \tag{6.5.55}$$

can be determined by using this database from loading and unloading stress paths. This procedure results in the following curve fits (Figure 6.5.9)

$$\mu = \frac{\gamma^p}{c_1 + c_2\gamma^p} \tag{6.5.56}$$

$$\beta = \mu - \mu_{cv} \tag{6.5.57}$$

with $c_1 = 1.7915E - 3$, $c_2 = 1.3930E + 0$ $(\phi_{max} = 45.9°)$, and $\mu_{cv} = 0.412(\phi_{cv} = 24.3°)$. We notice that the data support again Taylor's stress-dilatancyrule (cf. section 6.3.3).

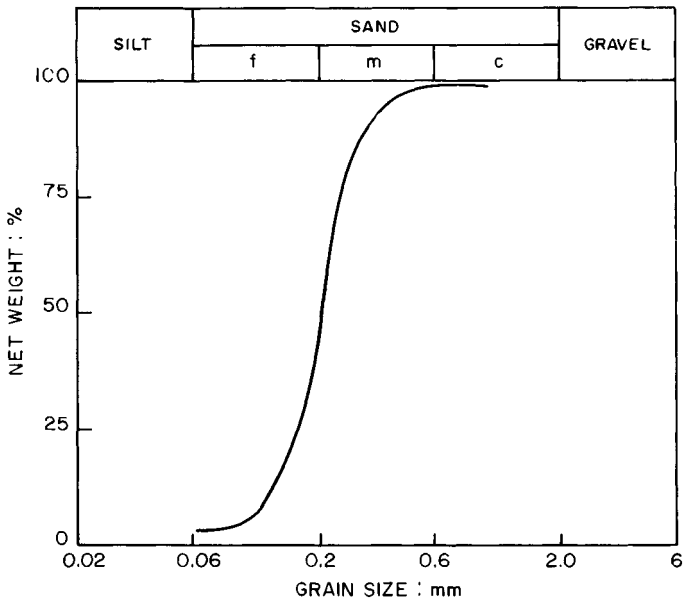

Figure 6.5.7 Grain size distribution curve of Dutch dune (Ostershelde) sand.

Literature

Textbooks and monographs

Bell, J.F. (1973). *Mechanics of Solids, Vol 1, The Experimental Foundations of Solids Mechanics.* Springer-Verlag, Berlin.

Carlslaw, H.S. and Jaeger, J.C. (1946). *Conduction of Heat in Solids.* Oxford Science Publications.

Chen, W.F. and Han, D.J. (1988). *Plasticity for Structural Engineers.* Springer-Verlag, Berlin.

Dietrich, Th. (1976). Der Psammische Stoff als mechanisches Modell des Sandes. Dissertation, Universität Karlsruhe.

Novozhilov, V.V. (1961). *Theory of Elasticity.* Pergamon, Oxford.

Taylor, D.W. (1948). *Fundamentals of Soil Mechanics.* John Wiley, New York, London.

Terzaghi, K.V. (1925). *Erdbaumechanik.* Franz Deuticke, Leipzig.

Thomas, T.Y. (1961). *Plastic Flow and Fracture in Solids.* Academic Press, New York.

References

Bardet, J.-P. (1992). Shear-band analyis in idealized granular material. *ASCE J. Eng. Mech.,* **118,** 397–415.

Baker, R. and Desai, C.S. (1982). Consequences of deviatoric normality in plasticity with isotropic strain hardening. *Int. J. Num. Anal. Meth. Geomech.,* **6,** 383–390.

Bigoni, D. and Zaccaria, D. (1992). Loss of strong-ellipticity in non-associative elastoplasticity. *J. Mech. Phys. Solids,* **40,** 1313–1331.

Cornforth, D.H. (1964). Some experiments on the influence of strain conditions on the strength of sand. *Géotechnique,* **14,** 143–167.

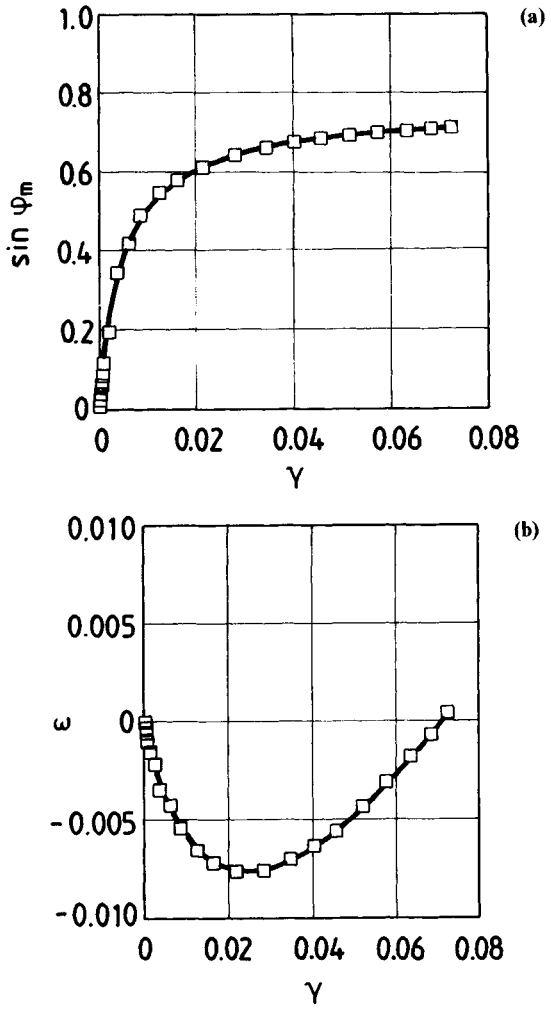

Figure 6.5.8 (a) Plane strain compression of sand: stress obliquity versus shear strain. (b) Plane strain compression of sand: volumetric strain versus shear strain.

Cundall, P. (1988). Numerical experiments on localization in frictional marterials. *Ingenieur Archiv.,* **59,** 148–159.

Drescher, A., Vardoulakis, I. and Han, C. (1990). A biaxial apparatus for testing soils. *Geotech. Test. J., GTJODJ,* **13**(3), 226–234.

Drucker, D.C. (1951). A more fundamental approach to stress-strain relations. *Proc. U.S. Nat. Congr. Appl. Mech., ASME,* 487–491.

Drucker, D.C. (1959). A definition of stable inelastic material. *J. Appl. Math.,* **26,** 101–106.

Duncan, J.M. and Chang, C.Y. (1970). Non-linear analysis of stress and strain in soils. *ASCE J. Geotech. Div.,* **96,** 1629–1653.

Frantziskonis, G. and Desai, C.S. (1987). Elastoplastic model with damage for strain softening geomaterials. *Acta Mechanica,* **68,** 151–170.

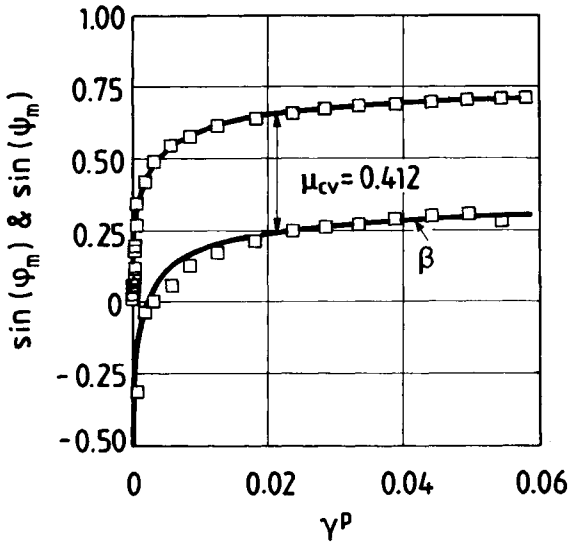

Figure 6.5.9 Mobilized friction and dilatancy functions for plane-strain tests utilizing Taylor's rule, equation 6.5.57.

Goldsheider, M. (1976). Grenzbedingung und Fliessregel von Sand. *Mech. Res. Comm.,* **3,** 463–468.

Green, G.E. (1972). Strength and deformation of sand in an independent stress control cell. *Proc. Roscoe Memorial Symposium* (R.H.G.Parry, ed.), G.T.Foulis & Co., Oxfordshire, pp. 285–323.

Gudehus, G. (1972). Elastic-plastic constitutive equations for dry sand. *Arch. Mech. Stosowanej,* **24,** 395–402.

Hettler, A. and Vardoulakis, I. (1984). Behavior of dry sand tested in a large triaxial apparatus. *Géotechnique,* **34,** 183–198.

Hill, R. (1958). A general theory of uniqueness and stability in elastic-plastic solids. *J. Mech. Phys. Solids,* **6,** 236–249.

Kanatani, K.I. (1984). Distribution of directional data and fabric tensors. *Int. J. Engng. Sci.,* **22,** 149–164.

Kim, M.K. and Lade, P. (1988). Single hardening constitutive model for frictional materials: I. Plastic potential function. *Comput. Geotech.,* **5,** 307–324.

Koiter, W.T. (1953). Stress-strain relations, uniqueness and variational theorems for elastic-plastic materials with singular yield surface. *Quart. Appl. Math.,* **11,** 350–354.

Lade, P.V. (1977). Elastoplastic stress-strain theory for cohesionless soil with curved yield surfaces. *Int. J. Solids Struct.,* **13**, 1019–1035.

Lade, P.V. (1988). Effects of voids and volume changes on the behavior of frictional materials. *Int. J. Num. Anal Meth. Geomech.,* **12,** 351–370.

Lade, P.V. and Duncan, J.M. (1973). Cubical triaxial tests on cohesionless soil. *J.Soil Mech. Found. Div., ASCE,* **99,** No. SM 10, 793–812.

Lade, P.V. and Nelson, B. (1987). Modelling the elastic behavior of granular materials. *Int. J. Num. Anal Meth. Geomech.,* **11,** 521–554.

Loret, B. (1985). On the choice of elastic parameters for sand. *Int. J. Num. Anal. Meth. Geomech.,* **9,** 285–287.

Mandel, J. (1964). Conditions de stabilité et postulat de Drucker. In: *Rheology and Soil Mechanics,* 58–68. Springer-Verlag, Berlin (1966).

Matsuoka, H. (1974). A microscopic study on shear mechanism of granular materials. *Soils and Foundations,* **14,** 29–43.

Mehrabadi, M.M., Nemat-Nasser, S. and Oda, M. (1982). On statistical description of stress and fabric in granular materials. *Int. J. Num. Anal. Meth. Geomech.,* **6,** 95–108.

Molenkamp, F. (1988). A simple model for osotropic non-linear elasticity of frictional materials. *Int. J. Num. Anal. Meth. Geomech.,* **12,** 467–476.

Mróz, Z. (1963). Non-associate flow laws in plasticity. *J. de Mécanique,* **2,** 21–42.

Mróz, Z. (1966). On forms of constitutive laws for elastic-plastic solids. *Arch. Mech. Stosowanej,* **18,** 3–35.

Nguyen, Q.S. and Bui, H.D. (1974). Sur les matériaux élastoplastiques a écrouissage positif ou négatif. *J. de Mécanique,* **3,** 322–432.

Petryk, H. (1991). On the second-order work in plasticity. *Arch. Mech.,* **43,** 377–397.

Raniecki, B. and Bruhns, O.T. (1981). Bounds to bifurcation stress in solids with non-associated plastic flow law at finite strain. *J. Mech. Phys. Solids,* **29,** 153–172.

Rowe, P.W. (1972). Theoretical meaning and observed values of deformation parameters for soil. *Proc. Roscoe Memorial Symposium, Cambridge University* (R.H.G.Parry, ed.), G.T.Foulis & Co., Oxfordshire, pp. 143–194.

Rudnicki, J.W. and Rice, J.R. (1975). Conditions for the localization of deformation in pressure-sensitive dilatant materials. *J. Mech. Phys. Solids,* **23,** 371–394.

Rumpf, H. (1958). Grundlagen und Methoden des Granulierens. *Chemie-Ingenieur-Technik*, Jg. **30,** 144–158.

Ryzhak, E.I. (1987). Necessity of Hadamard conditions for stability of elastic-plastic solids. *Izv. AN SSSR. Mekhanika Tverdogo Tela,* **22,** No. 4, 101–104.

Shanley, F.R. (1947). Inelastic column theory. *J. Aeronaut. Sci.,* **14,** 261–267.

Taylor, Sir G.I. and Farren, W.S. (1925). The heat developed during plastic extension of metals. *Proc. Roy. Soc. London,* Ser. A, **107,** 422–451.

Taylor, Sir G.I. and Quinney, H. (1931). The plastic distortion of metals. *Phil. Trans. Roy. Soc. London, Ser. A,* **230,** 323–362.

Vardoulakis, I. (1981a). Rigid granular constitutive model for sand and the influence of the deviatoric flow rule. *Mech. Res. Comm.,* **8,** 275–280.

Vardoulakis, I. (1981b). Bifurcation analysis of the plane rectilinear deformation on dry sand samples. *Int. J. Solids Struct.,* **17,** 1085–1101.

Vardoulakis, I. (1988). Theoretical and experimental bounds for shear-band bifurcation strain in biaxial tests on dry sand. *Res Mechanica,* **23,** 239–259.

Vardoulakis, I. (1989). Shear-banding and liquefaction in granular materials on the basis of a Cosserat continuum theory. *Ingenieur Archiv,* **59,** 106–113.

Vardoulakis, I. and Goldscheider, M. (1981). A biaxial apparatus for testing shear bands in soils. *10th ICSMFE, Stockholm,* **4/61,** 819–824. Balkema, Rotterdam.

Vardoulakis, I., Graf, B. and Hettler, A. (1985). Shear-band formation in a fine-grained sand. *5th Int. Conf. Num. Meth. Geomech.,* **1,** 517–521. Balkema, Rotterdam.

Vermeer, P. (1984). A five-constant model unifying well-established concepts. In: *Constitutive Relations for Soils* (G.Gudehus, F.Darve and I.Vardoulakis, eds), 175–197. Balkema, Rotterdam.

7
Bifurcation analysis of element tests

7.1
Observational background

Constitutive laws on soils and rocks are classically calibrated on element tests performed in the laboratory. Among them, the axisymmetric compression and extension tests and the plane-strain compression tests are the most commonly used. For example, Roscoe *et al.* (1963) have presented the results of so-called 'special' triaxial compression and extension tests, where very precise records of the failure patterns have been taken. These tests have shown that it is difficult to interpret the experimental data, due to appreciable bulging or necking of the samples. Kirkpatrick and Belshaw (1968) and Deman (1975) used an X-ray technique to investigate the strain field in cylindrical specimens on dry sand in triaxial compression with and without lubrication of the end platens. These experiments have shown that rough end platens support the development of rigid cones at the ends. Lubrication prevents formation of these cones (Figure 7.1.1 after Deman, 1975). The deformation is uniform for moderate strains, although bulging occurs at large strains. Bishop and Green (1965) studied the influence of the slenderness of the specimens and the end friction and arrived at similar conclusions. Non-uniform stress state in the specimen associated with non-uniform deformation causes geometric softening in addition to the material softening caused by the dilatancy of the material. Dresher and Vardoulakis (1982) have proposed an analysis of geometric softening in triaxial tests on a cohesionless material in order to evaluate the mobilized apparent friction angle. Their main conclusion is that non-lubricated end platens yield unsafe values of friction angle and give an erroneous indication of the extent of material softening.

As an improvement of the standard triaxial test, lubrication at the end platens has been used. The experimental evidence corroborated, however, the assertion that it is not possible to prevent inhomogeneous strain fields by refinements of the boundaries. Figure 7.1.2 from Hettler and Vardoulakis (1984) shows that diffuse bulging in triaxial compression tests on dry sand specimens. These tests were performed with lubricated, enlarged end platens and deformations were monitored optically with a theodolite. The initial dimensions of the specimens were $H_0 = 58.33\,\mathrm{mm}$ and $D_0 = 69.35\,\mathrm{mm}$ resulting in an

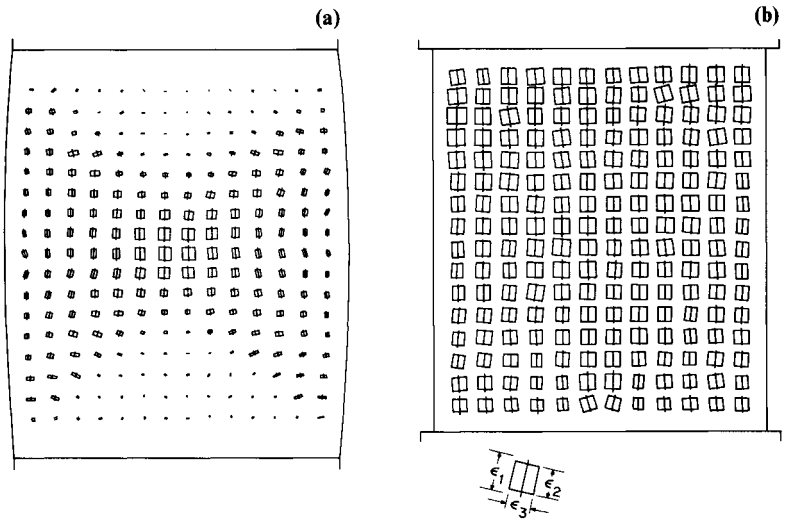

Figure 7.1.1 Internal deformation field for dense sand. (a) Non-lubricated end platens; (b) lubricated end platens (after Deman, 1975).

initial slenderness $H_0/D_0 = 0.8$ (notice that conventional triaxial testing for soils and rocks is done with $H_0/D_0 = 2$)). These figures show the results for a dense specimen ($n_0 = 0.362$) and a medium dense one ($n_0 = 0.411$). One observes that dense specimens are very sensitive and that from the constitutive point of view, volumetric strain measurements are difficult to interpret. Figure 7.1.3 shows pictures from an undeformed and a deformed specimen with clear indication of diffuse bulging and (post-peak) shear banding. These and other experiments on sand specimens with lubricated ends showed also a sensitivity of slender specimens towards diffuse bifurcations: the more slender a specimen is, the more it tends to bulge. For that purpose, Hettler and Vardoulakis (1984) performed a unique series of experiments with very large and stout specimens ($(H_0 = 280\,\text{mm}; D_0 = 780\,\text{mm},, H_0/D_0 = 0.4$) with lubricated ends, and proved that in this extreme setting diffuse bifurcations can be suppressed.

These results are forcing us to assume that spontaneous loss of homogeneity is possible. This possibility can be investigated by asking for bifurcation modes under ideal boundary conditions. If solutions of the corresponding equilibrium bifurcation problem exist, it is reasonable to assume that imperfections only intensify this tendency.

Theoretically bifurcation phenomena in axisymmetric conditions were first studied by Cheng *et al.* (1971) in an analysis of the tension and compression test of elastic-plastic cylinders. Hutchinson and Miles (1974) extended the analysis of necking bifurcation of an incompressible cylinder under uniaxial tension to include transverse anisotropy. Miles and Nuwayhid (1985) included compressibility. Axisymmetric bifurcations in frictional materials were studied in a series of paper by Vardoulakis (1979, 1981, 1983) and more recently by Chau and Rudnicki (1990). Chau (1992) extended the analysis to

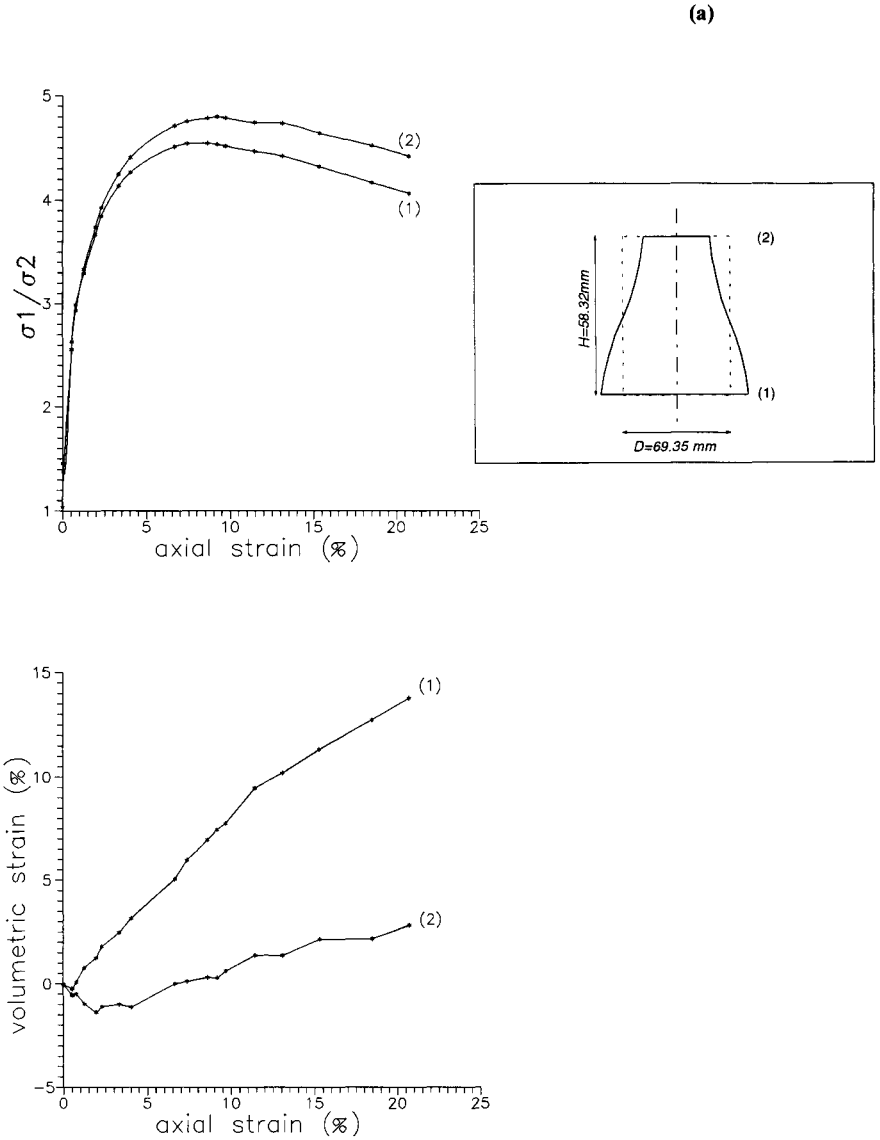

Figure 7.1.2 Optically recorded bulging in a specimen of (a) dense sand (n_0=0.362).

non-axisymmetric bifurcations of cylindrical specimens, whereas Sulem and Vardoulakis (1990) analyzed axisymmetric bifurcations in materials with microrotational degree of freedom (Cosserat continuum) (see chapter 9).

On the other hand, diffuse bifurcation modes of plane rectilinear deformations on dry samples have been discussed by Vardoulakis (1981). This bifurcation problem is the soil mechanics counterpart of the metal plasticity problems analyzed by Hill and Hutchinson (1975), Young (1976) and Needleman (1979). Complete analytical solutions for

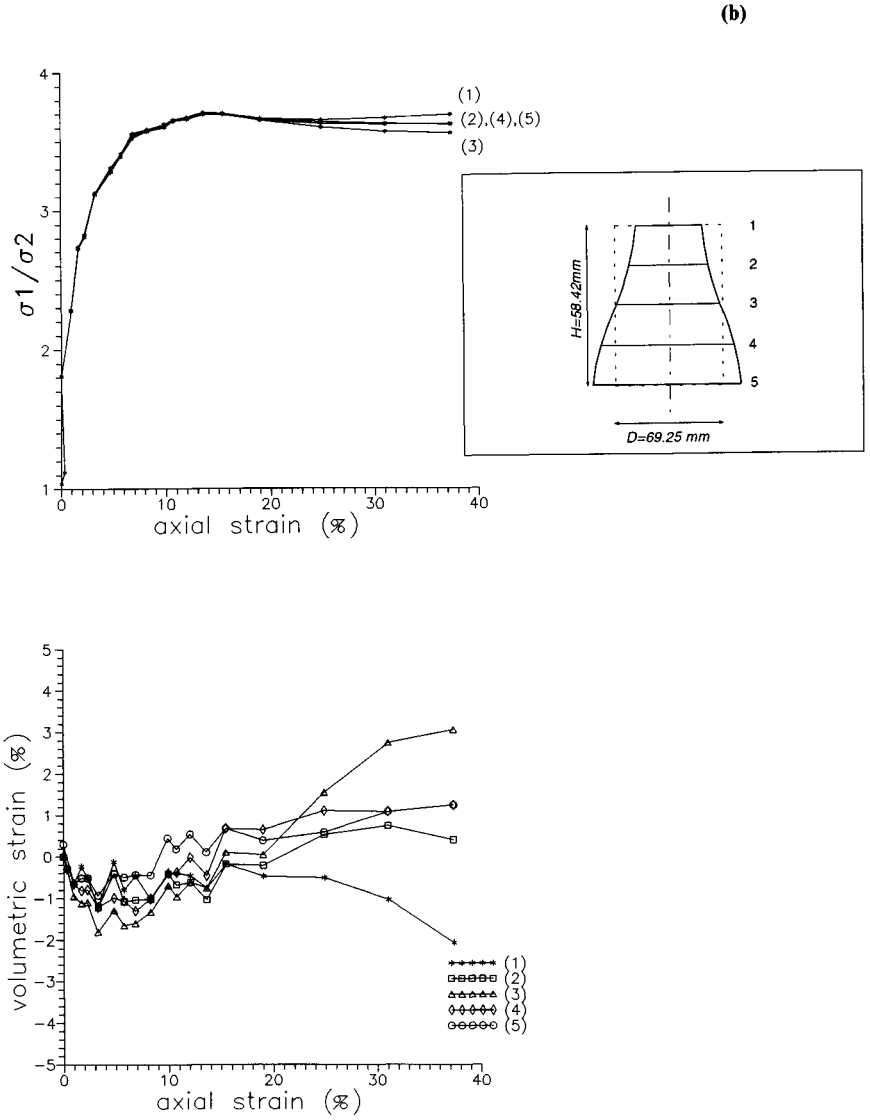

Figure 7.1.2 (continued) (b) Medium dense sand (n=0.411) (from Hettler and Vardoulakis, 1984).

compressible materials have been recently presented by Chau and Rudnicki (1990) and Bardet (1991).

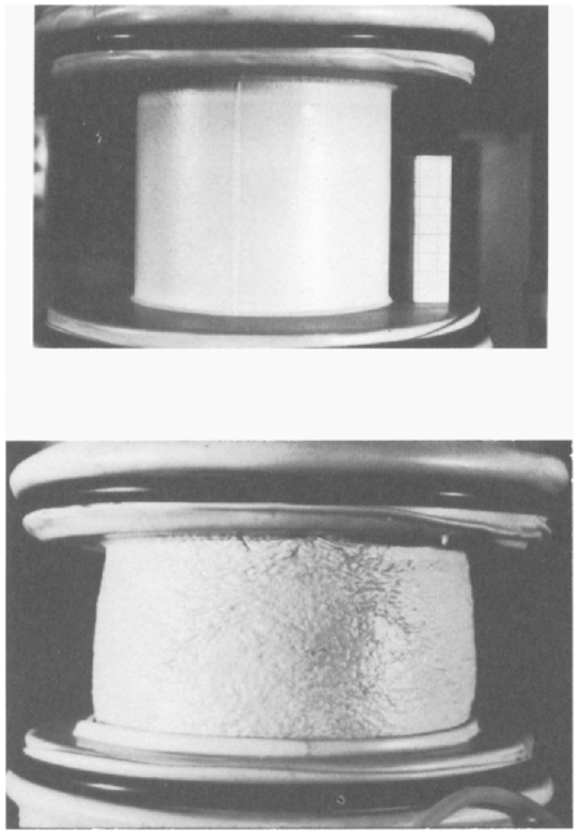

Figure 7.1.3 Initial and final shape of triaxial test sample with lubricated end surfaces (from Hettler and Vardoulakis, 1984).

7.2
Bifurcation analysis of the triaxial compression and extension tests

7.2.1
Problem statement

Let a homogeneous cylindrical rock specimen in an undistorted initial configuration C_o be subjected to a monotonic axisymmetric deformation $C_0 \rightarrow C$ (Figure 7.2.1). An equilibrium bifurcation mode is said to be taking place as soon as in addition to the fundamental homogeneous axisymmetric motion of compression or extension, another inhomogeneous perturbation solution exists that fulfils the same boundary conditions. The assumption is made here that the two end platens are perfectly lubricated so that the build up of frictional constraints is prevented. Stresses and strains at C are given by the Cauchy stress tensor σ_{ij} and the logarithmic strain λ_{ij}, measured with respect to the

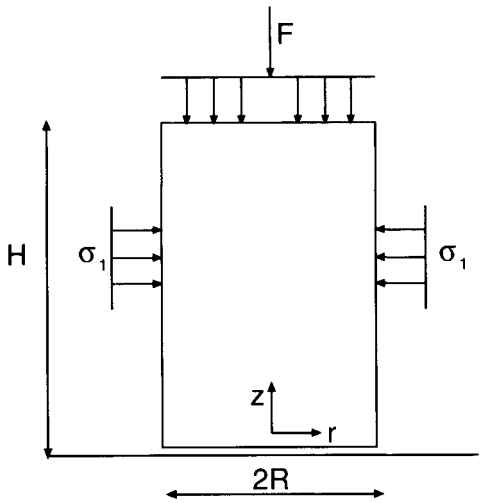

Figure 7.2.1 Geometry of a sample subjected axisymmetric triaxial compression.

isotropic configuration C_0. In a cylindrical coordinate system *(r, θ, z)* of the fixed-in-space principal axes of these tensors the following representations hold:

$$(\sigma_{ij}) = \begin{bmatrix} \sigma_1 & 0 & 0 \\ 0 & \sigma_1 & 0 \\ 0 & 0 & \sigma_3 \end{bmatrix} \quad \begin{matrix} (\sigma_3 \leqslant \sigma_1 \leqslant 0 \text{ in compression}) \\ (\sigma_1 \leqslant \sigma_3 \leqslant 0 \text{ in extension}) \end{matrix} \tag{7.2.1}$$

$$(\lambda_{ij}) = \begin{bmatrix} \lambda_1 & 0 & 0 \\ 0 & \lambda_1 & 0 \\ 0 & 0 & \lambda_3 \end{bmatrix} \tag{7.2.2}$$

where index 1 (index 3) is related to the radial (vertical) direction, $\lambda_1 = \ln(R/R_0)$ and $\lambda 3 = \ln(H/H_0)$, with R (R_0) and H (H_0) being the radius and the height of the sample in C (C_0). In the considered case we obtain the following expressions for the mean pressure and the shearing stress intensity:

$$p = (2\sigma_1 + \sigma_3)/2;\ T = \pm(\sigma_1 - \sigma_3)/\sqrt{3} \tag{7.2.3}$$

$$\tan\phi_\sigma = \frac{\pm(\sigma_1 - \sigma_3)/\sqrt{3}}{q + (2\sigma_1 + \sigma_3)/3} \tag{7.2.4}$$

In the above expression, the upper sign is holding for triaxial compression and the lower sign for triaxial extension.

7.2.2
A deformation theory of plasticity

Predictions of bifurcation phenomena depend strongly on the assumed constitutive model. As it is pointed out in several papers (Vardoulakis, 1983; Sulem and Vardoulakis, 1990), a classical flow theory of plasticity with a unique hardening modulus leads generally to unrealistic predictions for bifurcation phenomena in the axisymmetric compression test. Rudnicki and Rice (1975) have discussed a yield vertex plasticity model which leads to the introduction of a second hardening modulus in the incremental constitutive equations. We present in the following a similar constitutive model based on a small strain deformation theory of plasticity for elastoplastic, cohesive, frictional and dilatant materials (see also Vermeer and Schotman, 1986). The present theory could be viewed as a compromise between flow and damage (Krajcinovic, 1989) theories, that is, a flow theory of plasticity with elastic properties depending on plastic strain.

Deviatoric strain are related to deviatoric stresses through the following expression

$$e_{ij} = s_{ij}/(2G^*) \tag{7.2.5}$$

where

$$1/G^* = 1/G + 1/G_s \tag{7.2.6}$$

In this expression G is the elastic shear modulus, and G_s is another variable modulus which is defined as follows. As in chapter 6 for classical flow theory of plasticity, we introduce the concept of yield surface. For simplicity we adopt here a linear Drucker—Prager one:

$$F = T/(q - p) - f(g^p) = 0 \tag{7.2.7}$$

G_s is defined as a secant-type modulus, and its non-dimensional value $h_s = G_s/(q - p)$ is identified as the secant modulus to the assumed stress-ratio strain curve $f = f(g^p)$

$$G_s = (q - p)h_s;\ h_s = f/g^p \tag{7.2.8}$$

Similarly, an expression for the total volumetric strain is defined

$$v = p/K + D(g^p) \tag{7.2.9}$$

where K is the elastic compression modulus.

Rate constitutive equations can be derived through formal time differentiation of the above finite strain-stress relations 7.2.5 and 7.2.9. For the deviatoric strain rates we obtain

$$\dot{e}_{ij} = \frac{1}{2}\left(\frac{1}{G} + \frac{1}{G_s}\right)\dot{s}_{ij} + \frac{s_{ij}}{2T}\dot{g}^p - \frac{s_{ij}}{2G_s}\frac{\dot{T}}{T} \tag{7.2.10}$$

which, when contracted with s_{ij}, yields

$$\dot{T} = G(s_{ij}\dot{e}_{ij}/T - \dot{g}^p) \tag{7.2.11}$$

If we introduce this expression for $\dot{T}$ into the consistency condition.

$$\dot{T} + Kf\dot{v} - (Kfd + h_t(q - p))\dot{g}^p = 0;\ d = \mathrm{d}D/\mathrm{d}g^p;\ h_t = \mathrm{d}f/\mathrm{d}g^p \tag{7.2.12}$$

We end up with (see also equation 6.2.20)

$$\dot{g}^p = \frac{\langle 1 \rangle}{H} A^F_{ij}\dot{\varepsilon}_{ij} \tag{7.2.13}$$

where

$$A^F_{ij} = s_{ij}/T + \kappa f\delta_{ij};\ \kappa = K/G$$
$$\langle 1 \rangle = \begin{cases} 1 & \text{if } F = 0 \text{ and } A^F_{ij}\dot{\varepsilon}_{ij} > 0 \\ 0 & \text{if } F < 0 \text{ or } F = 0 \text{ and } A^F_{ij}\dot{\varepsilon}_{ij} \leqslant 0 \end{cases} \tag{7.2.14}$$

Similarly, through formal time differentiation of 7.2.9 we get

$$\dot{v} = \dot{p}/K + d\dot{g}^p \tag{7.2.15}$$

Inversion of equations 7.2.10 and 7.2.15 with 7.2.13 leads finally to the following form of the constitutive equations of a coupled flow-damage theory (or deformation theory) for an elastoplastic frictional and dilatant material:

$$\mathring{\sigma}_{ij} = L_{ijkl}\dot{\varepsilon}_{kl} = (L^e_{ijkl} - L^p_{ijkl})\dot{\varepsilon}_{kl} \tag{7.2.16}$$

where

$$L^e_{ijkl} = G\left\{\frac{1}{1 + 1/h_0}(\delta_{ik}\delta_{jl} + \delta_{il}\delta_{jk} - \delta_{ij}\delta_{kl}/3) + \frac{1}{(1 + h_0)}\frac{s_{ij}}{T}\frac{s_{kl}}{T} + \kappa\delta_{ij}\delta_{kl}\right\} \tag{7.2.17}$$

$$L^p_{ijkl} = G\frac{\langle 1 \rangle}{H} A^Q_{ij}A^F_{kl} \tag{7.2.18}$$

with

$$A^F_{ij} = s_{ij}/T + \kappa f\delta_{ij};\ A^Q_{ij} = s_{ij}/T + \kappa d\delta_{ij}$$
$$H = 1 + h - h_T > 0;\ h = (q - p)h_t/G;\ h_t = (\mathrm{d}f/\mathrm{d}g^p);\ h_T = -\kappa f d \tag{7.2.19}$$
$$h_0 = g^e/g^p = \{T/G\}/g^p = G_s/G$$

From these derivations it follows that a deformation theory of an elastoplastic material can be seen as a coupled elastoplastic flow theory. In such a theory the plastic stiffness tensor is the same with the one of classical flow theory (see equation 6.2.28 with 6.3.22 and 6.3.27), whereas the elastic stiffness tensor depends also on the total plastic shear strain. The elastoplastic coupling is introduced in 7.2.17 through the coefficient $1/h_0 = g^p/g^e$. For small plastic strains, i.e. in the close proximity of initial yielding $1/h_0 \simeq 0$, and the deformation theory coincides with the flow theory. For larger plastic strains, however, the elastoplastic coupling is significant and, as far as stability and uniqueness questions are concerned, it cannot be neglected.

For an initial state of axisymmetric, homogeneous deformation (triaxial test conditions), we can derive the corresponding incremental constitutive equations. Let (°) denote the

Jaumann time derivative and *(r, θ, z)* be the polar coordinates with the *z*-axis coinciding with the axis of symmetry, we obtain:

$$\begin{aligned} \mathring{\sigma}_{rr} &= L_{11}\dot{\varepsilon}_{rr} + L_{12}\dot{\varepsilon}_{\theta\theta} + L_{13}\dot{\varepsilon}_{zz} \\ \mathring{\sigma}_{zz} &= L_{31}\dot{\varepsilon}_{rr} + L_{32}\dot{\varepsilon}_{\theta\theta} + L_{33}\dot{\varepsilon}_{zz} \\ \mathring{\sigma}_{rr} - \mathring{\sigma}_{\theta\theta} &= 2Gh_1(\dot{\varepsilon}_{rr} - \dot{\varepsilon}_{\theta\theta}) \\ \mathring{\sigma}_{rz} &= 2Gh_1\dot{\varepsilon}_{rz} \end{aligned} \tag{7.2.20}$$

with:

$$\begin{aligned} L_{11} &= G[4h_1/3 + \kappa + h_2/3 - h_3((1/\sqrt{3} + \kappa d)(1/\sqrt{3} + \kappa f))] \\ L_{12} &= G[-2h_1/3 + \kappa + h_2/3 - h_3((1/\sqrt{3} + \kappa d)(1/\sqrt{3} + \kappa f))] \\ L_{13} &= G[-2h_1/3 + \kappa - 2h_2/3 - h_3((1/\sqrt{3} + \kappa d)(-2/\sqrt{3} + \kappa f))] \\ L_{31} &= G[-2h_1/3 + \kappa - 2h_2/3 - h_3((-2/\sqrt{3} + \kappa d)(1/\sqrt{3} + \kappa f))] \\ L_{32} &= L_{31} \\ L_{33} &= G[4h_1/3 + \kappa + 4h_2/3 - h_3((-2/\sqrt{3} + \kappa d)(-2/\sqrt{3} + \kappa f))] \end{aligned} \tag{7.2.21}$$

In the above equations h_1, h_2, h_3 are given by:

$$h_1 = \frac{h_0}{1 + h_0};\ h_2 = \frac{1}{1 + h_0};\ h_3 = \frac{1}{1 + h - h_T} \tag{7.2.22}$$

7.2.3 Governing equations

To study the possibility for existence of a non-homogeneous deformation mode under the boundary conditions presented above we consider the following fields

$$v_r = U(\rho)\cos\zeta;\ v_z = W(\rho)\sin\zeta \tag{7.2.23}$$

where ρ and ζ are dimensionless radial and axial coordinates:

$$\rho = r/R,\ \zeta = m\pi z/H\ (m = 1, 2\ldots) \tag{7.2.24}$$

R and H are the current radius and height of the cylindrical specimen, m is a modal number and K_m is a shape number:

$$K_m = m\pi R/\mathrm{H} \tag{7.2.25}$$

The equilibrium conditions, expressed in terms of the Jaumann derivatives of the Cauchy stresses read as follows (see section 3.1.4, equation 3.1.35):

$$\begin{aligned} \frac{\partial\mathring{\sigma}_{rr}}{\partial r} + \frac{\partial\mathring{\sigma}_{rz}}{\partial z} + \frac{1}{r}(\mathring{\sigma}_{rr} - \mathring{\sigma}_{\theta\theta}) + 2t\frac{\partial\dot{\omega}}{\partial z} &= 0 \\ \frac{\partial\mathring{\sigma}_{zr}}{\partial r} + \frac{\partial\mathring{\sigma}_{zz}}{\partial z} + \frac{1}{r}\mathring{\sigma}_{zr} + 2t\left(\frac{\partial\dot{\omega}}{\partial r} + \frac{\dot{\omega}}{r}\right) &= 0 \end{aligned} \tag{7.2.26}$$

where t is the stress difference

$$t = (\sigma_1 - \sigma_3)/2 \tag{7.2.27}$$

Using the constitutive equations 7.2.20 and considering equations 7.2.23 equilibrium equations 7.2.26 become:

$$\begin{gathered} a_1 L_\rho(U) - a_2 K_m^2 U + a_3 K_m W' = 0 \\ a_4 K_m \left(U' + \frac{U}{\rho} \right) - a_5 \left(W'' + \frac{W'}{\rho} \right) + a_6 K_m^2 W = 0 \end{gathered} \tag{7.2.28}$$

where L_ρ is the Bessel operator:

$$L_\rho(\cdot) = \frac{\partial^2}{\partial \rho^2} + \frac{1}{\rho} \frac{\partial}{\partial \rho} - \frac{1}{\rho^2} \tag{7.2.29}$$

and

$$\begin{gathered} a_1 = L_{11};\ a_2 = Gh_1 - t;\ a_3 = L_{13} + Gh_1 + t \\ a_4 = L_{31} + Gh_1 - t;\ a_5 = Gh_1 + t;\ a_6 = L_{33} \end{gathered} \tag{7.2.30}$$

The general form of the solution of the system of differential equation 7.2.28 is:

$$U = AJ_1(K_m \beta \rho);\ W = BJ_0(K_m \beta \rho) \tag{7.2.31}$$

where J_1 (respectively J_0) is the Bessel function of first kind and first order (respectively zeroth order), A and B are integration constants. From equations 7.2.28 and 7.2.31 we derive the following homogeneous system of equations.

$$\begin{pmatrix} a_1 \beta^2 + a_2 & a_3 \beta \\ a_4 \beta & a_5 \beta^2 + a_6 \end{pmatrix} \begin{pmatrix} A \\ B \end{pmatrix} = \begin{pmatrix} 0 \\ 0 \end{pmatrix} \tag{7.2.32}$$

The characteristic equation for β is derived from the requirement that non-trivial solutions for the integration constants A and B exist, resulting in:

$$a\beta^4 + b\beta^2 + c = 0 \tag{7.2.33}$$

with:

$$\begin{aligned} a &= a_1 a_5 \\ b &= a_1 a_6 + a_2 a_5 - a_3 a_4 \\ c &= a_2 a_6 \end{aligned} \tag{7.2.34}$$

Let Z_1, Z_2 be the roots of the characteristic equation 7.2.33; we distinguish among the following cases:

(I) *Elliptic complex regime (EC).* Equation 7.2.33 has two complex conjugate roots ($Z_1 = P + iQ$, $Z_2 = P - iQ$, $i = \sqrt{(-1)}$). Let

$$\beta_1 = p + iq;\ \beta_2 = p - iq \tag{7.2.35}$$

$$p = (((P^2 + Q^2)^{\frac{1}{2}} + P)/2)^{\frac{1}{2}};\ q = (((P^2 + Q^2)^{\frac{1}{2}} - P)/2)^{\frac{1}{2}} \tag{7.2.36}$$

The functions base is then:

$$U_1 = J_1(K_m\beta_1\rho);\ U_2 = J_1(K_m\beta_2\rho) \tag{7.2.37}$$

$$W_1 = w_1 J_0(K_m\beta_1\rho);\ W_2 = w_2 J_0(K_m\beta_2\rho) \tag{7.2.38}$$

and the proportionality factors $\omega_{1/2}$ are given by:

$$w_{1/2} = \frac{-1}{a_3\beta_{1/2}}(a_2 + a_1\beta_{1/2}^2) \tag{7.2.39}$$

(II) *Elliptic imaginary regime (EI).* Equation 7.2.33 has two real negative roots ($Z_i < 0,\ i = 1,2$). With:

$$\beta_i = \sqrt{|Z_i|} \tag{7.2.40}$$

the function base is:

$$U_i = I_1(K_m\beta_i\rho);\ W_i = w_i I_0(K_m\beta_i\rho) \qquad (i = 1,2) \tag{7.2.41}$$

where the coefficients ω_i are given by:

$$w_{1/2} = \frac{1}{a_3\beta_{1/2}}(a_2 - a_1\beta_{1/2}^2) \tag{7.2.42}$$

and

$$I_0(z) = J_0(iz);\ I_1(z) = -iJ_1(iz) \tag{7.2.43}$$

(III) *Hyperbolic regime (H).* Equation 7.2.33 has two real positive roots (Z_1>0, Z_2>0). With:

$$\beta_{\frac{1}{2}} = \sqrt{Z_{\frac{1}{2}}} \tag{7.2.44}$$

the functions base U_i W_i and the coefficients ω_i are given by equations 7.2.37, 7.2.38 and 7.2.39, respectively.

7.2.4
Bifurcation condition

In the considered case, the boundary conditions express the assumption that along the cylindrical surface of the specimen, a constant confining pressure σ_3 is acting. Mathematically, these conditions read

$$\sigma_3(n_k\delta_{il} - n_i\delta_{kl})v_{k|l} = 0 \tag{7.2.45}$$

where n_i is the unit outward normal on the cylindrical boundary of the specimen. In terms of amplitude functions *U, W* these conditions become:

$$\begin{aligned}\phi_1(U,W) &= \left\{L_{11}W' + L_{12}\frac{U}{\rho} + L_{13}K_mW\right\}\Big|_{\rho=1} = 0\\ \phi_2(U,W) &= \{-K_mU + W'\}|_{\rho=1} = 0\end{aligned} \tag{7.2.46}$$

The general solution for the diflferential system 7.2.28 has the following form:

$$U = \sum_{i=1}^{2} A_i W_i;\ W = \sum_{i=1}^{2} A_i W_i \tag{7.2.47}$$

The bifurcation condition is derived from the requirement of non-trivial solutions A_i, resulting in the following eigenvalue equation:

$$\det(\phi_{ij}) = 0 \tag{7.2.48}$$

where:

$$\phi_{ij} = \phi_i(U_j, W_j)|_{\rho=1} \tag{7.2.49}$$

7.2.5
Example of triaxial compression test on medium dense Karlsruhe sand

We refer here to experimental data of triaxial compression tests on medium dense Karlsruhe sand and to the calibration presented in section 6.3.3. Under axisymmetric loading conditions, diffuse bifurcation may be observed in the softening regime. We thus consider here the porosity softening theory discussed in section 6.4.3.

shear modulus:	$G = 37.1\ \mathrm{MPa}$
Poisson's ratio:	$\nu = 0.1$
mobilized friction of mixture:	$f = (1 - n^{\mathrm{f}})f^{\mathrm{c}} + n^{\mathrm{f}} f^{\mathrm{f}},\ f^{\mathrm{f}} = f_{\mathrm{cv}}$
mobilized friction of competent fraction:	$f = g^{\mathrm{p}}/(c_1 + c_2 g^{\mathrm{p}});\ c_1 = 3.5678 \times 10^{-3};\ c_2 = 9.1693 \times 10^{-1}$
mobilized dilatancy function:	$d = f - f_{\mathrm{cv}};\ f_{\mathrm{cv}} = 0.747$
relative porosity:	$n^{\mathrm{f}} = (n - n_{\min})/(n_{\max} - n_{\min})$
initial porosity:	$n_0 = 0.35$
maximum and minimum porosity:	$n_{\max} = 0.45;\ n_{\min} = 0.35$

On Figure 7.2.2 we plot the plastic shear strain at bifurcation corresponding to the mode m=1 versus the slenderness H/R of the sample for a confining pressure of 98.1 MPa. For slender specimens, diffuse bifurcation in the form of bulging is obtained for smaller accumulated plastic strains than for less slender ones which is in good accordance with the experimental observations. Bifurcation is obtained in the hardening regime close to the peak (see Figure 6.4.7), i.e. for small positive values of the hardening modulus. As shown in Figure 7.1.2, diffuse bulging was indeed observed at the peak of the stress—strain curve for medium dense Karlsruhe sand.

7.3
Bifurcation analysis of the biaxial test

Let a homogeneous, cuboidal sample in an undistorted initial configuration C_0 be subjected to a smooth, quasi-static, homogeneous rectilinear deformation (Figure 7.3.1).

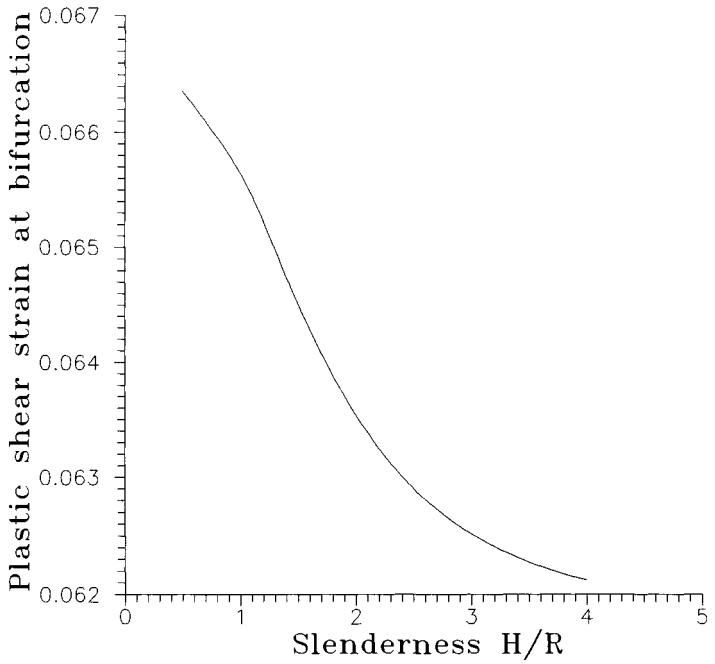

Figure 7.2.2 Effect of the slenderness of the sample on the computed plastic shear strain at bifurcation (m=1).

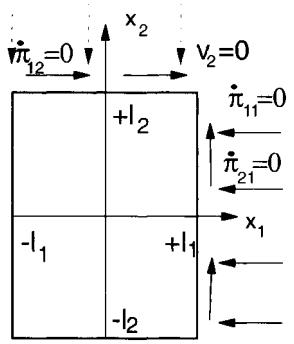

Figure 7 3.1 Geometry and boundary conditions of a sample subjected to plane strain compression.

We call the resultant configuration C. The boundaries of the sample in C are parallel to the principal axes of the Cauchy stress tensor σ_i in C. The boundary conditions are such that homogeneous deformation is possible. However, alternative solutions corresponding to non-uniform deformation are also possible and we investigate in this section the circumstances for which diffuse bifurcation modes such as bulging (symmetric bifurcation mode) or buckling (antisymmetric bifurcation) can appear (Figure 7.3.2).

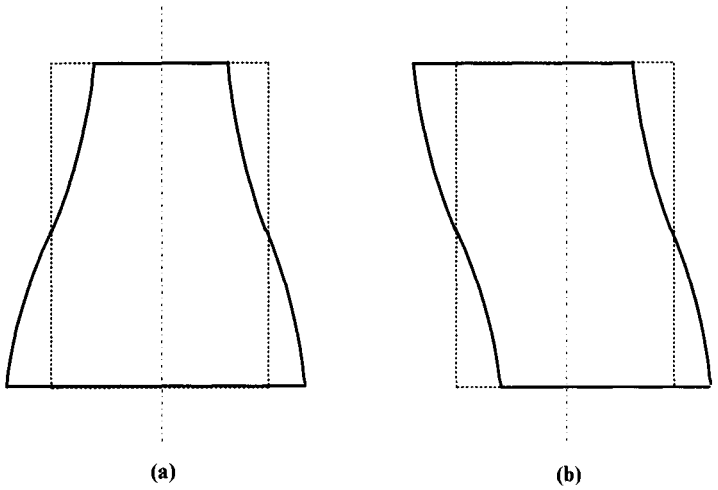

Figure 7.3.2 Biaxial test: (a) symmetric bifurcation mode (bulging); (b) antisymmetric bifurcation mode (buckling).

7.3.1
Formulation of the diffuse bifurcation problem

In the case of plane strain loading, the equilibrium conditions expressed in terms of the Jaumann derivatives of the Cauchy stresses read as follows:

$$\begin{aligned} \partial_1 \mathring{\sigma}_{11} + \partial_2 \mathring{\sigma}_{12} + 2t\,\partial_2 \dot{\omega}_{21} &= 0 \\ \partial_1 \mathring{\sigma}_{21} + \partial_2 \mathring{\sigma}_{22} + 2t\,\partial_1 \dot{\omega}_{21} &= 0 \end{aligned} \tag{7.3.1}$$

where t is the stress difference

$$t = (\sigma_1 - \sigma_2)/2 \tag{7.3.2}$$

The boundary conditions express that on the top and at the bottom edges ($x_2 = \pm l_2$), the velocity is prescribed in the x_2-direction without causing shear traction and that a constant stress σ_{11} is applied on the lateral surfaces ($x_1 = \pm l_1$) with l_α (α=1,2) being the dimensions of the specimen. Let $\dot{\pi}_{ij}$ be the rate of the first Piola-Kirchhoff stress tensor, the boundary conditions read:

$$\begin{aligned} &\text{for } x_2 = \pm l_2\text{: } v_2 = 0 \text{ and } \dot{\pi}_{12} = \mathring{\sigma}_{12} + \sigma_{22}\dot{\omega}_{12} - \sigma_{11}\dot{\varepsilon}_{12} = 0 \\ &\text{for } x_1 = \pm l_1\text{: } \dot{\pi}_{11} = \mathring{\sigma}_{11} + \sigma_{11}\dot{\varepsilon}_{22} = 0 \text{ and } \dot{\pi}_{21} = \mathring{\sigma}_{21} + \sigma_{11}\dot{\omega}_{21} - \sigma_{22}\dot{\varepsilon}_{21} = 0 \end{aligned} \tag{7.3.3}$$

We consider here a classical flow theory of plasticity as presented in section 6.5. The rate constitutive equations for the 'upper bound' linear comparison solid, corresponding to loading, are derived from equations 6.5.42 to 6.5.44. In the coordinate system of principal axes of initial stress we obtain

$$\begin{aligned}\mathring{\sigma}_{11} &= L^{u}_{1111}\dot{\varepsilon}_{11} + L^{u}_{1122}\dot{\varepsilon}_{22}\\ \mathring{\sigma}_{22} &= L^{u}_{2211}\dot{\varepsilon}_{11} + L^{u}_{2222}\dot{\varepsilon}_{22}\\ \mathring{\sigma}_{12} &= 2G\,\dot{\varepsilon}_{12}\end{aligned} \tag{7.3.4}$$

where for the considered 2D-continuum model

$$\begin{aligned}L^{u}_{1111} &= G\{k(1-\beta)(1-\mu) + (1+k)h\}/h^{*}\\ L^{u}_{1122} &= G\{k(1+\beta)(1-\mu) - (1-k)h\}/h^{*}\\ L^{u}_{2211} &= G\{k(1-\beta)(1+\mu) - (1-k)h\}/h^{*}\\ L^{u}_{2222} &= G\{k(1+\beta)(1+\mu) + (1+k)h\}/h^{*}\end{aligned} \tag{7.3.5}$$

The trivial solution of the above boundary value problem is a homogeneous stress and displacement field. In order to investigate the possibility of existence of a bifurcated velocity field corresponding to a non-homogeneous bifurcation mode we consider the following fields:

$$v_1 = U(x)\cos y;\; v_2 = V(x)\sin y \tag{7.3.6}$$

where x and y are dimensionless coordinates:

$$x = x_1/l_1,\; y = m\pi x_2/l_2 = \beta x_2 \qquad (m = 1,2\ldots);\; \beta = m\pi/l_2 \tag{7.3.7}$$

The perturbation fields 7.3.6 automatically fulfil the boundary conditions 7.3.3 for $x_2 = \pm l_2$.

Using the constitutive equations 7.3.5 and 7.3.6, the boundary value problem defined by equations 7.3.1, 7.3.3 and 7.3.4 becomes

$$\begin{aligned}a_1\,\partial^2_{11}v_1 + a_2\,\partial^2_{22}v_1 + a_3\,\partial^2_{12}v_2 &= 0\\ a_4\,\partial^2_{12}v_1 + a_5\,\partial^2_{11}v_2 + a_6\,\partial^2_{22}v_2 &= 0\end{aligned} \tag{7.3.8}$$

with boundary conditions:

$$\begin{aligned}\text{for } x = \pm 1\text{:}\; a_1\,\partial_1 v_1 + a_7\,\partial_2 v_2 &= 0\\ a_8\,\partial_2 v_1 + a_5\,\partial_1 v_2 &= 0\end{aligned} \tag{7.3.9}$$

In the above equations the coefficients a_i (i=1,8) are given by

$$\begin{aligned}&a_1 = L^{u}_{1111};\; a_2 = G - t;\; a_3 = L^{u}_{1122} + G + t\\ &a_4 = L^{u}_{2211} + G - t;\; a_5 = G + t;\; a_6 = L^{u}_{2222}\\ &a_7 = L^{u}_{1122} + p + t;\; a_8 = G - p\end{aligned} \tag{7.3.10}$$

The general solution of the differential system 7.3.8 is

$$U(x) = A\exp(i\gamma x);\; V(x) = B\exp(i\gamma x) \tag{7.3.11}$$

where A and B are integration constants. From equations 7.3.8 and 7.3.11 we derive the following homogeneous system of equations.

$$\begin{pmatrix} a_1Z^2 + a_2 & a_3(-iZ) \\ a_4(iZ) & a_5Z^2 + a_6 \end{pmatrix} \begin{pmatrix} A \\ B \end{pmatrix} = \begin{pmatrix} 0 \\ 0 \end{pmatrix} \tag{7.3.12}$$

where

$$Z = \gamma/\beta l_1 \tag{7.3.13}$$

The characteristic equation for Z is derived from the requirement that non-trivial solutions for the integration constants A and B exist, resulting to:

$$aZ^4 + bZ^2 + c = 0 \tag{7.3.14}$$

with:

$$\begin{aligned} a &= a_1a_5 \\ b &= a_1a_6 + a_2a_5 - a_3a_4 \\ c &= a_2a_6 \end{aligned} \tag{7.3.15}$$

7.3.2
Classification of regimes and bifurcation condition

As we have seen in section 7.2.3 in the bifurcation analysis of the triaxial test, depending on the values of *a, b,* and *c,* equation 7.3.14 has four different types of solution in *Z*:

EI elliptic imaginary when it has four imaginary roots,
EC elliptic complex when it has four complex roots,
P parabolic when it has two real and two purely imaginary roots,
H hyperbolic when it has four real roots.

In the following we shall distinguish between symmetric and antisymmetric solutions in x_1 and give the bifurcation condition for the various regimes of the solutions.

Elliptic imaginary regime (EI). This is the case when

$$\Delta = b^2 - 4ac \geqslant 0,\ b/a > 0 \text{ and } c/a \geqslant 0 \tag{7.3.16}$$

The general form of the symmetric bifurcation velocity field is:

$$\begin{aligned} v_1 &= [A_1 \sinh(\beta Z_1 x_1) + A_2 \sinh(\beta Z_2 x_1)]\cos(\beta x_2) \\ v_2 &= [B_1 \cosh(\beta Z_1 x_1) + B_2 \cosh(\beta Z_2 x_1)]\sin(\beta x_2) \end{aligned} \tag{7.3.17}$$

with

$$B_\alpha = r_\alpha A_\alpha;\ r_\alpha = (a_2 - a_1Z_\alpha^2)/(a_3Z_\alpha) \qquad \alpha = 1, 2 \tag{7.3.18}$$

From the boundary conditions 7.3.9 we deduce the following bifurcation condition for symmetric velocity in the EI regime:

$$(a_1Z_1 + a_7r_1)(a_5r_2Z_2 - a_8)\tanh(\beta Z_2 l_1) - (a_1Z_2 + a_7r_2)(a_5r_1Z_1 - a_8)\tanh(\beta Z_1 l_1) = 0 \tag{7.3.19}$$

The general form of the antisymmetric bifurcation velocity field is:

$$\begin{aligned} v_1 &= [A_1\cosh(\beta Z_1 x_1) + A_2\cosh(\beta Z_2 x_1)]\cos(\beta x_2) \\ v_2 &= [B_1\sinh(\beta Z_1 x_1) + B_2\sinh(\beta Z_2 x_1)]\sin(\beta x_2) \end{aligned} \tag{7. 3.20}$$

with

$$B_\alpha = r_\alpha A_\alpha;\ r_\alpha = (a_2 - a_1 Z_\alpha^2)/(a_3 Z_\alpha) \qquad \alpha = 1,2 \tag{7.3.21}$$

The same analysis as for the symmetric modes leads to the following bifurcation condition for antisymmetric velocity in the EI regime:

$$(a_1Z_1 + a_7r_1)(a_5r_2Z_2 - a_8)\operatorname{cotanh}(\beta Z_2 l_1) - (a_1Z_2 + a_7r_2)(a_5r_1Z_1 - a_8)\operatorname{cotanh}(\beta Z_1 l_1) = 0 \tag{7.3.22}$$

Remark: For the short wave length limit ($\beta \to \infty$) we obtain the following bifurcation condition:

$$(a_1Z_1 + a_7r_1)(a_5r_2Z_2 - a_8) - (a_1Z_2 + a_7r_2)(a_5r_1Z_1 - a_8) = 0 \tag{7.3.23}$$

Elliptic complex regime (EC) This case emerges when

$$\Delta < 0 \tag{7.3.24}$$

The characteristic equation 7.3.14has two complex conjugate roots $Z_1=P+iQ$, $Z_2=P-iQ$. Let

$$\begin{aligned} \chi &= \mathrm{Re}(\sqrt{Z_1}) = [((P^2 + Q^2)^{\frac{1}{2}} + P)/2]^{\frac{1}{2}} \\ \zeta &= \mathrm{Im}(\sqrt{Z_1}) = [((P^2 + Q^2)^{\frac{1}{2}} - P)/2]^{\frac{1}{2}} \end{aligned} \tag{7.3.25}$$

The functions base of the solutions is then

$$\begin{aligned} U_1 &= \cosh(\beta\zeta x_1)\cos(\beta\chi x_1) & V_1 &= r_1U_2 - r_2U_4 \\ U_2 &= \sinh(\beta\zeta x_1)\cos(\beta\chi x_1) & V_2 &= r_1U_1 - r_2U_3 \\ U_3 &= \sinh(\beta\zeta x_1)\sin(\beta\chi x_1) & V_3 &= r_2U_2 + r_1U_4 \\ U_4 &= \cosh(\beta\zeta x_1)\sin(\beta\chi x_1) & V_4 &= r_2U_1 + r_1U_3 \end{aligned} \tag{7.3.26}$$

with

$$\begin{aligned} r_1 &= [-a_1(\chi^2 + \zeta^2) + a_2]\zeta/[a_3(\chi^2 + \zeta^2)] \\ r_2 &= -[a_1(\chi^2 + \zeta^2) + a_2]\chi/[a_3(\chi^2 + \zeta^2)] \end{aligned} \tag{7.3.27}$$

The general form of the symmetric bifurcation velocity field is:

$$\begin{aligned} v_1 &= (A_1U_2 + A_2U_4)\cos(\beta x_2) \\ v_2 &= (A_1V_2 + A_2V_4)\sin(\beta x_2) \end{aligned} \tag{7.3.28}$$

From the boundary conditions 7.3.9 we deduce the following bifurcation condition for symmetric velocity in the EC regime:

$$(f_1 f_4 - f_2 f_3)\sinh(2\beta\zeta l_1) + (f_1 f_3 + f_2 f_4)\sin(2\beta\chi l_1) = 0 \tag{7.3.29}$$

with

$$\begin{aligned} f_1 &= a_1\zeta + a_7 r_1 \\ f_2 &= a_1\chi + a_7 r_2 \\ f_3 &= -a_8 + a_5(r_1\zeta - r_2\chi) \\ f_4 &= a_5(r_1\chi + r_2\zeta) \end{aligned} \tag{7.3.30}$$

The general form of the antisymmetric bifurcation velocity field is:

$$\begin{aligned} v_1 &= (A_1 U_1 + A_2 U_3)\cos(\beta x_2) \\ v_2 &= (A_1 V_1 + A_2 V_3)\sin(\beta x_2) \end{aligned} \tag{7.3.31}$$

From the boundary conditions 7.3.9 we deduce the following bifurcation condition for antisymmetric velocity in the EC regime:

$$(f_1 f_4 - f_2 f_3)\sinh(2\beta\zeta l_1) - (f_1 f_3 + f_2 f_4)\sin(2\beta\chi l_1) = 0 \tag{7.3.32}$$

Parabolic regime (P): This case emerges when

$$\Delta > 0 \quad \text{and} \quad c/a < 0 \tag{7.3.33}$$

Let

$$Z_1 = [(b - \sqrt{\Delta})/(2a)]^{\frac{1}{2}};\ Z_2 = [-(b - \sqrt{\Delta})/(2a)]^{\frac{1}{2}} \tag{7.3.34}$$

The functions base of the solutions is then

$$\begin{aligned} U_1 &= \cosh(\beta Z_1 x_1) & V_1 &= r_1 U_2 \\ U_2 &= \sinh(\beta Z_1 x_1) & V_2 &= r_1 U_1 \\ U_3 &= \cos(\beta Z_2 x_1) & V_3 &= r_2 U_4 \\ U_4 &= \sin(\beta Z_2 x_1) & V_4 &= -r_2 U_3 \end{aligned} \tag{7.3.35}$$

with

$$\begin{aligned} r_1 &= [-a_1 Z_1^2 + a_2]/a_3 Z_1 \\ r_2 &= [-a_1 Z_2^2 + a_2]/a_3 Z_2 \end{aligned} \tag{7.3.36}$$

The general form of the symmetric bifurcation velocity field is:

$$\begin{aligned} v_1 &= (A_1 U_2 + A_2 U_4)\cos(\beta x_2) \\ v_2 &= (A_1 V_2 + A_2 V_4)\sin(\beta x_2) \end{aligned} \tag{7.3.37}$$

From the boundary conditions 7.3.9 we deduce the following bifurcation condition for symmetric velocity in the P regime:

$$(a_1Z_1 + a_7r_1)(a_5r_2Z_2 - a_8)\tan(\beta Z_2 l_1) - (a_1Z_2 - a_7r_2)(a_5r_1Z_1 - a_8)\tanh(\beta Z_1 l_1) \tag{7.3.38}$$

The general form of the antisymmetric bifurcation velocity field is:

$$v_1 = (A_1U_1 + A_2U_3)\cos(\beta x_2)$$
$$v_2 = (A_1V_1 + A_2V_3)\sin(\beta x_2) \tag{7.3.39}$$

From the boundary conditions 7.3.9 we deduce the following bifurcation condition for antisymmetric velocity in the P regime:

$$(a_1Z_1 + a_7r_1)(-a_5r_2Z_2 - a_8)\tanh(\beta Z_1 l_1) + (a_1Z_2 + a_7r_2)(a_5r_1Z_1 - a_8)\tan(\beta Z_2 l_1) \tag{7.3.40}$$

Hyperbolic regime (H). This is the case when

$$\Delta \geqslant 0,\ b/a \leqslant 0 \text{ and } c/a \geqslant 0 \tag{7.3.41}$$

Let

$$Z_1 = \sqrt{(-b - \sqrt{\Delta})/2a};\ Z_2 = \sqrt{(-b + \sqrt{\Delta})/2a} \tag{7.3.42}$$

The general form of the symmetric bifurcation velocity field is:

$$v_1 = [A_1\sin(\beta Z_1 x_1) + A_2\sin(\beta Z_2 x_1)]\cos(\beta x_2)$$
$$v_2 = [B_1\cos(\beta Z_1 x_1) + B_2\cos(\beta Z_2 x_1)]\sin(\beta x_2) \tag{7.3.43}$$

with

$$B_\alpha = r_\alpha A_\alpha;\ r_\alpha = -(a_2 + a_1Z_\alpha^2)/(a_3Z_\alpha) \qquad \alpha = 1,2 \tag{7.3.44}$$

From the boundary conditions 7.3.9 we deduce the following bifurcation condition for symmetric velocity in the H regime:

$$(a_1Z_1 + a_7r_1)(a_5r_2Z_2 + a_8)\tan(\beta Z_2 l_1) - (a_1Z_2 + a_7r_2)(a_5r_1Z_1 + a_8)\tan(\beta Z_1 l_1) = 0 \tag{7.3.45}$$

The general form of the antisymmetric bifurcation velocity field is:

$$v_1 = [A_1\cos(\beta Z_1 x_1) + A_2\cos(\beta Z_2 x_1)]\cos(\beta x_2)$$
$$v_2 = [B_1\sin(\beta Z_1 x_1) + B_2\sin(\beta Z_2 x_1)]\sin(\beta x_2) \tag{7.3.46}$$

with

$$B_\alpha = r_\alpha A_\alpha;\ r_\alpha = (a_2 + a_1Z_\alpha^2)/(a_3Z_\alpha) \qquad \alpha = 1,2 \tag{7.3.47}$$

The same analysis as for the symmetric modes leads to the following bifurcation condition for antisymmetric velocity in the H regime:

$$(a_1 Z_1 - a_7 r_1)(-a_5 r_2 Z_2 + a_8)\text{cotan}(\beta Z_2 l_1) - (a_1 Z_2 - a_7 r_2)(-a_5 r_1 Z_1 + a_8)\text{cotan}(\beta Z_1 l_1) = 0 \tag{7.3.48}$$

7.3.3
Example: Biaxial compression test on a Dutch sand

For numerical examples we refer here to experimental data of biaxial test on a Dutch sand as described in section 6.5. The constitutive equations of 2D flow theory of plasticity were calibrated on the basis of pre-failure data from the considered biaxial tests. The corresponding material constants and functions are summarized below (see section 6.5.3):

shear modulus:	$G = 50.34\,\text{MPa}$
Poisson's ratio:	$\nu = 0.1$
mobilized friction function:	$\mu = \gamma^p/(c_1 + c_2\gamma^p)$; $c_1 = 1.7915 \times 10^{-3}$; $c_2 = 1.3930$
mobilized dilatancy function:	$\beta = \mu - \mu_{cv}$; $\mu_{cv} = 0.412$

For this example, the parabolic regime is never met. The boundary between the elliptic complex regime and the hyperbolic regime is shown on Figure 7.3.3 as a function of the confining pressure. This boundary corresponds to shear band formation as we shall see in chapter 8. This figure shows that the critical plastic shear strain corresponding to shear banding increases with confining pressure which corroborates experimental observation (see Figure 8.3.3). For a given value of the confining pressure ($\sigma_{11} = -294.3\,\text{kPa}$), the critical plastic shear strain for the occurrence of symmetric and antisymmetric modes with $m = 1$ is shown on Figure 7.3.4 as a function of the slenderness l_2/l_1. This function has a quasi-periodic shape related to the periodic form of the bifurcation condition in the hyperbolic regime (equations 7.3.45 and 7.3.48). The diffuse bifurcation modes occur always in the hyperbolic regime except for large values of the slenderness where antisymmetric mode is possible. Consequently shear band formation which occurs at the transition between the elliptic complex and the hyperbolic regime (see chapter 8) precedes diffuse bifurcation. We can thus conclude like Vardoulakis (1981) and Bardet (1991) that the sand specimens may deform under plane strain rectilinear deformation without occurrence of diffuse bifurcation.

References

Bardet, J.P. (1991). Analytical solutions for the plane-strain bifurcation of compressible solids. *J. Appl Mech.*, **58,** 651–657.

Bishop, A.W. and Green, G.E. (1965). The influence of end restraint on the compression strength of a cohesionless soil. *Géotechnique,* **15**(3), 243–266.

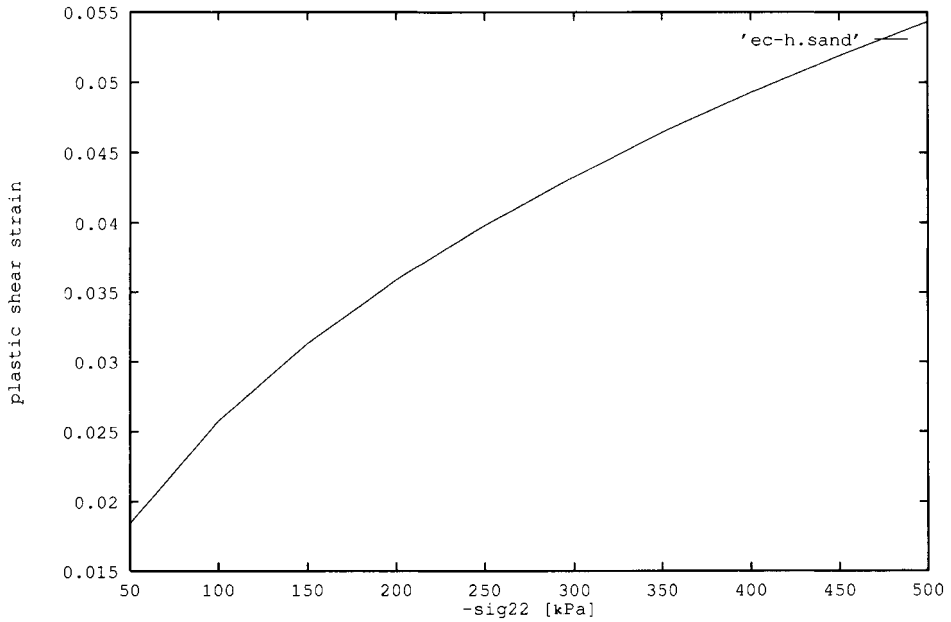

Figure 7.3.3 Elliptic complex/hyperbolic boundary as a function of the confining pressure.

Chau, K.T. (1992). Non-normality and bifurcation in a compressible pressure sensitive circular cylinder under axisymmetric tension and compression. *Int. J. Solids Structures,* **7,** 801–824.

Chau, K.T. and Rudnicki, J.W. (1990). Bifurcation of compressible pressure sensitive materials in plane strain tension and compression. *J. Mech. Phys. Solids,* **38**(6), 875–898.

Cheng, S.Y., Ariaratnam, S.T. and Dubey, R.N. (1971). Axisymmetric bifurcation in an elastic-plastic cylinder under axial load and lateral hydrostatic pressure. *Quart. Appl Math.,* **29,** 41–51.

Deman, F. (1975). Achsensymmetrische Spannungs- und Verformunggsfelder in trockenem Sand. *Veröffentlichungen des Instituts für Bodenmechanik und Felsmechanik der Universität Karlsruhe,* Heft 62.

Drescher, A. and Vardoulakis, I. (1982). Geometric softening in triaxial tests on granular material. *Géotechnique,* **32**(4), 291–303.

Hettler, A. and Vardoulakis, I. (1984). Behaviour of dry sand tested in a large triaxial apparatus. *Géotechnique,* **34**(2), 183–198.

Hill, R. and Hutchinson, J.W. (1975). Bifurcation phenomena in the plane tension test. *J. Mech. Phys. Solids,* **23,** 239–264.

Hutchinson, J.W. and Miles, J.P. (1974). Bifurcation analysis of the onset of necking in an elastic-plastic cylinder under uniaxial tension. *J. Mech. Phys. Solids,* **22,** 61–71.

Kirkpatrick, W.M. and Belshaw, D.J. (1968). On the interpretation of the triaxial test. *Géotechnique,* **18,** 336–350.

Krajcinovic, D. (1989). Damage mechanics. *Mech. Mater.,* **8,** 117–197.

Miles, J.P. and Nuwayhid, U.A. (1985). Bifurcation in compressible elastic-plastic cylinder under uniaxial tension. *Appl Sci. Res.,* **42,** 33–54.

Needleman, A. (1979). Non-normality and bifurcation in the plane strain tension and compression. *J. Mech. Phys. Solids,* **27,** 231–254.

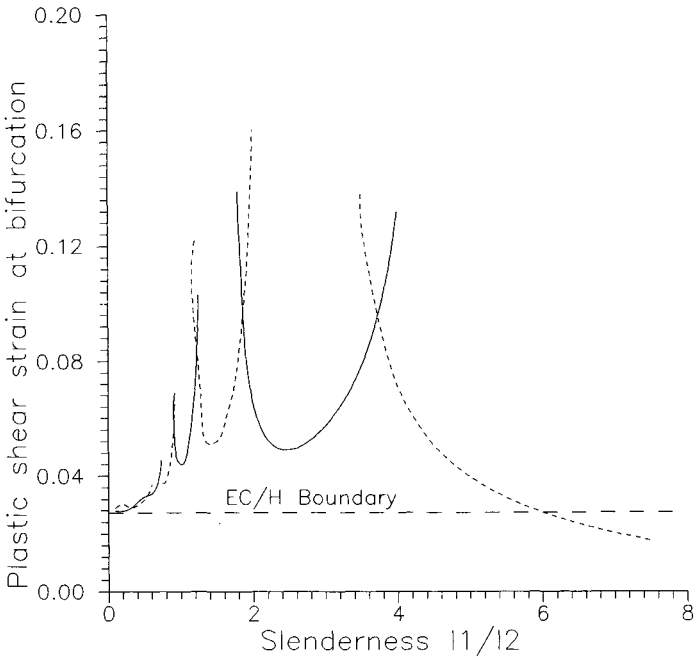

Figure 7.3.4 Effect of the slenderness of the sample on the computed plastic shear strain at bifurcation for symmetric and antisymmetric modes (m=1).——, Symmetric mode; ------, antisymmetric mode.

Roscoe, K.H., Schofield, A.N. and Thurairajah, A. (1963). An evaluation of test data for selecting a yield criterion for soils. *Laboratory Shear Testing of Solids, ASTM Special Publications,* **361,** 111–128.

Rudnicki, J.W. and Rice, J.R. (1975). Conditions for the localization of deformation in pressure-sensitive dilatant materials. *J. Mech. Phys. Solids,* **23,** 371–394.

Sulem, J. and Vardoulakis, I. (1990). Analysis of the triaxial test on rocks specimens. A theoretical model for shape and size effect. *Acta Mechanica,* **83,** 195–212.

Vardoulakis, I. (1979). Bifurcation analysis of the triaxial test on sand samples. *Acta Mechanica,* **32,** 35–54.

Vardoulakis, I. (1981). Bifurcation analysis of the plane rectilinear deformation on dry sand samples. *Int. J. Solids Structures,* **17**(11), 1085–1101.

Vardoulakis, I. (1983). Rigid granular plasticity model and bifurcation in the triaxial test. *Acta Mechanica,* **49,** 57–79.

Vermeer, P.A. and Schotman, G.J. (1986). An extension of the deformation theory of plasticity. In: *Proc. 2nd Int. Symp. Numer. Models Geomech.,* pp. 33–41. Balkema, Rotterdam.

Young, N.J.B. (1976). Bifurcation phenomena in the plane compression test. *J. Mech. Phys. Solids,* **24,** 77–91.

8
Shear-band bifurcation in granular media

8.1
Equilibrium bifurcation and stability

8.1.1
The Thomas-Hill-Mandel shear-band model

Localization of deformation into shear bands is one of the most interesting bifurcation problems in solid mechanics. In this section the so-called Thomas-Hill-Mandel shear-band model is presented, based on the assumption that shear banding may be described as an equilibrium bifurcation from a homogeneous deformation. According to Rice (1976), this approach investigates whether the constitutive description of homogeneous deformation can admit a solution which is compatible with boundary conditions for further homogeneous deformation, but which corresponds to non-uniform deformation in a plane shear-band (see also Vardoulakis, 1976). In other words, we examine the existence of discontinuous deformation modes as possible continuations of homogeneous deformations and we examine their relation to particular constitutive assumptions within the frame of elastoplasticity.

According to the definition proposed by Hill (1962), a shear band is viewed as a thin layer that is bounded by two parallel material discontinuity surfaces of the incremental displacement gradient (Figure 8.1.1). These material discontinuity surfaces $D^{(1)}$ and $D^{(2)}$ are called shear-band boundaries and their distance, $2d_B$, is the thickness of the shear band. Within the frame of constitutive theories without material length, the shear-band thickness d_B is indetermined. The solutions obtained from such constitutive theories are assumed to correspond to the limit $d_B \to 0$ of a corresponding higher grade extension of the underlying classical constitutive theory, which is equipped with a material length scale. Such continuum theories are discussed in chapters 9 and 10.

The incremental displacement field outside the band, $\Delta\mathring{u}_i$, and that inside the shear band, $\Delta\tilde{u}_i$, differ drastically, since inside the band a rapid change is assumed to take place. Accordingly, in the vicinity of the shear band the exterior displacement field is varying slowly, and thus, as the shear-band thickness tends to zero, $\Delta\tilde{u}_i$ is only a

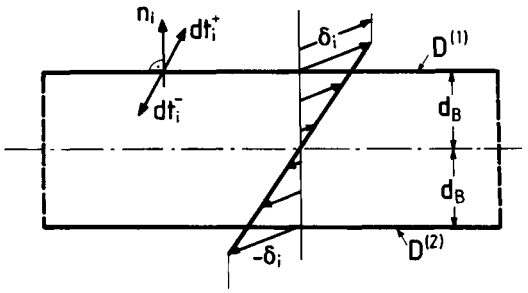

Figure 8.1.1 Linear approximation of the shear-band kinematic field $\Delta\tilde{u}_i$

function of distance across the band. The displacement field in the domain of interest is thus seen as a superposition of the two fields,

$$\Delta u_i = \Delta\mathring{u}_i + \Delta\tilde{u}_i \tag{8.1.1}$$

Let $\pm\delta_i$ be the incremental displacements at the shear-band boundaries (Figure 8.1.1). With $\delta_2 \neq 0$, we do not imply separation but dilatancy of the material inside the band. Under these conditions, the inhomogeneous displacement gradient field $\Delta\tilde{u}_i$ is given by the following expressions

$$\Delta\tilde{u}_i = \begin{cases} -\delta_i & \text{for } d_B \leqslant n_k x_k \\ -\dfrac{1}{d_B}\delta_i n_k x_k & \text{for } -d_B \leqslant n_k x_k \leqslant d_B \\ \delta_i & \text{for } n_k x_k \leqslant -d_B \end{cases} \tag{8.1.2}$$

where n_i is the unit vector normal to the shear-band axis. With

$$[\partial_j \Delta\mathring{u}_i] = 0;\ [\partial_j \Delta u_i] = [\partial_j \Delta\tilde{u}_i] \tag{8.1.3}$$

across the shear-band boundaries the displacement field is continuous and only the displacement gradient jumps. Accordingly, on $D^{(v)}$ (v=1,2) the following kinematic compatibility conditions hold (cf. section 2.4)

$$[\Delta u_i] = 0 \quad \text{and} \quad [\partial_j \Delta u_i] = \zeta_i^{(v)} n_j \tag{8.1.4}$$

Finally from equations 8.1.2 and 8.1.4 follows that

$$\zeta_i^{(1)} = -\zeta_i^{(2)} = -\delta_i / d_B \tag{8.1.5}$$

For a material discontinuity surface D the tractions across it must be in equilibrium. By assuming equilibrium across a material discontinuity surface in the reference configuration C, and by requiring equilibrium in the adjacent configuration $\bar{C}$, we have (Figure 8.1.1)

$$d\bar{t}_i^+ = d\bar{t}_i^- \tag{8.1.6}$$

or by using the definition 3.1.28 of the 1. P.-K. stress tensor

$$\mathrm{d}\bar{t}_i^+ = \pi_{ik}^+ n_k \,\mathrm{d}S;\ \mathrm{d}\bar{t}_i^- = \pi_{ik}^- n_k \,\mathrm{d}S \tag{8.1.7}$$

we have

$$[\mathrm{d}t_i] = [\pi_{ik}]n_k = 0 \tag{8.1.8}$$

By assuming that the initial stress, σ_{ij}, is continuous across D in C,

$$[\sigma_{ij}] = 0 \tag{8.1.9}$$

from the above equations derive the following static compatibility conditions for the increment of the 1. P.-K. stress tensor,

$$[\Delta\pi_{ik}]n_k = 0 \tag{8.1.10}$$

The increment of the 1. P.-K. stress tensor can be expressed, for example, in terms of the increment of the Jaumann stress increment of the Cauchy stress tensor $\mathring{\Delta}\sigma_{ij}$, cf. equation 3.1.36. It is assumed now that the constitutive behavior is expressed by the constitutive equations 6.2.59 of elastoplastic materials with smooth yield and plastic potential surfaces and in terms of the Jaumann increment of the Cauchy stress tensor, and thus

$$\begin{aligned} \Delta\pi_{ij}^+ &= C_{ijkl}^+ \partial_k \Delta u_l \\ \Delta\pi_{ij}^- &= C_{ijkl}^- \partial_k \Delta u_l \end{aligned} \tag{8.1.11}$$

where

$$C_{ijkl}^{\pm} = C_{ijkl}^{\pm \mathrm{ep}} + A_{ijkl} \tag{8.1.12}$$

and A_{ijkl} is given by equation 6.2.61.

We observe that there are two possibilities, namely that the constitutive behavior across the shear band boundaries is either continuous or discontinuous. Concerning continuous bifurcations a lower bound is obtained by identifying the stiffness tensor C_{ijkl}^{ℓ} of the 'lower bound' linear comparison solid of Raniecki, given here by equation 6.2.90, cf. Vardoulakis (1988). Concerning discontinuous bifurcations one has to examine the possibility that elastic unloading occurs outside the shear band while continued elastic-plastic loading occurs within the band. If the elastoplastic constitutive law admits a single smooth yield surface and plastic potential, Rice and Rudnicki (1980) have shown that continuous bifurcation analyses on the basis of the 'upper bound' linear comparison solid, described by the stiffness tensor C_{ijkl}^{u} equation 6.2.94, provide the lower limit to the range of deformations for which discontinuous bifurcations can occur. Accordingly, we restrict ourselves here to the first possibility of continuous constitutive behavior

$$[C_{ijkl}] = 0 \tag{8.1.13}$$

with

$$C_{ijkl} = C_{ijkl}^{\mathrm{u}} + A_{ijkl} \tag{8.1.14}$$

From the above *assumption* that the stiffness tensor C_{ijkl} is continuous across $D^{(v)}$, the static compatibility conditions 8.1.10

$$C_{ijkl}[\partial_l \Delta u_k] n_j = 0 \tag{8.1.15}$$

By combining the above compatibility conditions with geometric compatibility conditions for the incremental displacement gradient, equations 8.1.4, we finally obtain

$$\Gamma_{ik} \zeta_k^{(\alpha)} = 0 \tag{8.1.16}$$

where Γ_{ik} is the acoustic tensor

$$\Gamma_{ik} = C_{ijkl} n_j n_l \tag{8.1.17}$$

In accordance with the general result obtained in section 3.4 concerning acceleration waves, from the static compatibility conditions 8.1.16 it follows that weak stationary discontinuities for the incremental displacement exist only if the acoustic tensor is singular

$$\det(\Gamma_{ij}) = 0 \tag{8.1.18}$$

Equation 8.1.18 is the characteristic equation in terms of the direction cosines n_i of a statically, kinematically and materially admissible discontinuity surface. If the characteristic equation provides real solutions for the direction cosines n_i, discontinuity surfaces for the incremental displacement gradient exist and may also develop in due course of the deformation. In the contrary the condition

$$\det(\Gamma_{ij}) > 0 \tag{8.1.19}$$

is sufficient for the exclusion of discontinuous solutions for the incremental displacement field (Hill, 1962).

For elastoplastic solids, the threshold to the bifurcation stress which satisfies the characteristic equation 8.1.18 is usually expressed in terms of hardening modulus H_t; cf. section 6.2.1. Because H_t is a decreasing function of the cumulative plastic strain, as indicated in Figure 8.1.2, we seek the orientation (given by the direction cosines n_i of the discontinuity surface $D^{(v)}$) for which the value of H_t is maximum (Rudnicki and Rice, 1975). For example, if geometric terms A_{ijkl} are neglected, and if linear isotropic elasticity, characterized by a shear modulus G and Poisson's ratio υ, is assumed, then the critical hardening modulus for shear-band bifurcation is computed as the solution of the following constrained maximization problem (Rice, 1976)

$$H_t^{cr}/(2G) = \max\{L(n_i)\};\ n_i n_i = 1 \tag{8.1.20}$$

$$L(n_i) = 2F_{ik}Q_{il}n_k n_l - F_{ij}Q_{kl}n_i n_j n_k n_l - F_{ij}Q_{ij} - \frac{\upsilon}{1-\upsilon}(F_{ij}n_i n_j - F_{kk})(Q_{kl}n_k n_l - Q_{mm}) \tag{8.1.21}$$

where

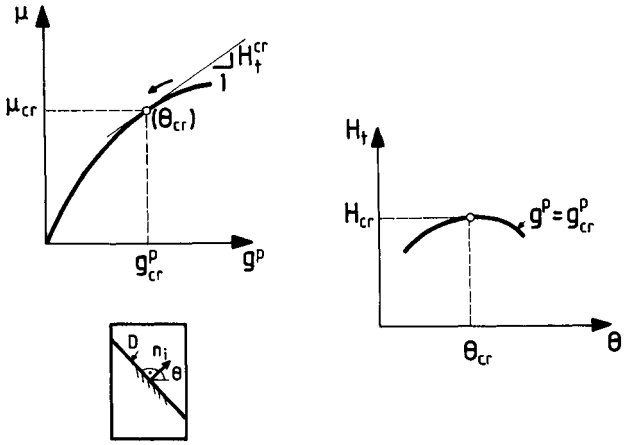

Figure 8.1.2 The constrained maximization problem for the determination of the critical hardening rate H_t (Rudnicki and Rice, 1975).

$$F_{ij} = (\partial F/\partial \sigma_{ij});\ Q_{ij} = (\partial Q/\partial \sigma_{ij}) \tag{8.1.22}$$

Computational results for the critical hardening modulus and the corresponding critical orientation angles of shear bands for various constitutive models for non-associative, frictional elastoplastic materials are given by Molenkamp (1985). Ortiz *et al.* (1987) provided numerical procedures for evaluating the above constrained maximization problem, whereas analytic solutions of it are given by Bardet (1990) and Bigoni and Hueckel (1990,1991).

Remark on rigid-plastic laws. Rigid plastic models for granular materials have been studied extensively in connection with shear band formation and equilibrium bifurcation by Vardoulakis (1980, 1981, 1983). In these models the constitutive equation which relates the (plastic) volume change to the (plastic) shear strain increment is postulated as an internal constraint, which is called the dilatancy constraint

$$d\varepsilon - \beta(\gamma)d\gamma = 0$$

The dilatancy constraint is in general a non-linear differential form. Vardoulakis (1981) has demonstrated, however, that the non-linear dilatancy constraint can be linearized for deformations which deviate only slightly from a straight ahead continuation of a previous loading history. These linearized forms of the dilatancy constraint belong to the class of internal constraints which are Pfaffian forms of the strain increment

$$P_{ij}(\varepsilon_{kl})d\varepsilon_{ij} = 0$$

For example, with $P_{ij} \equiv \delta_{ij}$, one recovers the well-known incompressibility constraint

$$d\varepsilon_{kk} = 0$$

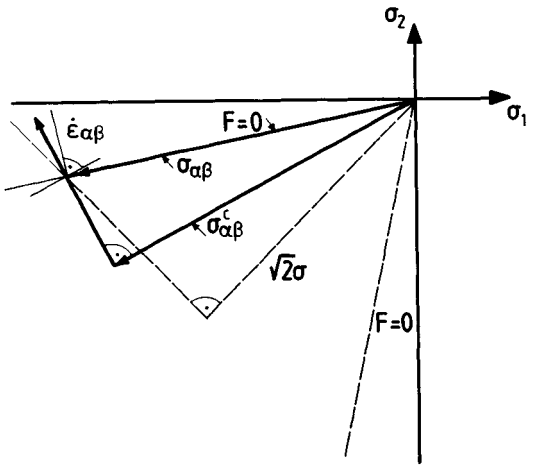

Figure 8.1.3 Use of mean stress as the indeterminate quantity.

In case of incompressibility, it is also well known that the spherical stress $(1/3)\sigma_{kk}\delta_{ij}$ is indeterminate. In general, from the principle of determinism for simple materials subject to internal constraint, it follows that the stress σ_{ij} at any time is determined by the deformation history only within a stress $\overset{c}{\sigma}_{ij}$ that does not work in any motion satisfying the constraints; cf. Truesdell and Noll (1965, section 30). In case of a linear differential constraint form, this is expressed by an equation of the form

$$\overset{c}{\sigma}_{ij} = \lambda P_{ij}$$

where λ is an indeterminate scalar; see also Kanatani (1982).

In the special case of 'psammic' material behavior, absence of an elastic domain, a linear Mohr-Coulomb yield surface, and the dilatancy constraint restrict only the direction of the stress vector in stress space. In other words, in this limit one cannot distinguish between two stress states which only differ by a scalar multiplier. Thus for a convenient formulation of rate-constitutive equations the mean stress $p = \sigma_{kk}/3$ can be used instead of the constraining (workless) stress $\overset{c}{\sigma}_{ij}$ as the indeterminate quantity. This is illustrated in Figure 8.1.3 in invariant stress space for the case of rigid-plastic frictional/dilatant granular material.

In the aforementioned publications of Vardoulakis, it was demonstrated that shear banding in the rigid-plastic model occurs earlier than in the corresponding elastoplastic model corroborating the stabilizing effect that has on the constitutive description the existence of an elastic domain.

Following a remark by Professor Lippmann, Rice and Rudnicki (1980) examined also the rigid-plastic limit of the elastoplastic shear-band analysis. If normality is not satisfied, localization in the rigid-plastic limit appears to be possible at values of the hardening modulus which are not admitted by the direct rigid-plastic analysis. Rice and

Rudnicki demonstrated, however, that modes which appear to be possible in the rigid-plastic limit of the elastoplastic model involve rigid components and are in fact inadmissible. Thus a rigid-plastic model for frictional materials is not a good approximation of the corresponding elastoplastic model with high values for the elasticity constants.

8.1.2
Mandel's dynamic stability analysis

Linear dynamic stability analysis for elastoplastic solids obeying non-associative flow rule was discussed first by Mandel (1964). Within the present framework, Mandel's stability analysis reads as follows: Starting from a state C of a solid body, an infinitesimal transition $\mathbf{C} \rightarrow \bar{\mathbf{C}}$ is considered which is described by the displacement field $\Delta u_i(x_k, t)$. This displacement field is assumed to be a linear combination of a 'trivial' mode, $\Delta \mathring{u}_i(x_k)$, and of another, yet to be determined, 'non-trivial' mode, $\Delta \tilde{u}_i(x_k, t)$,

$$\Delta u_i = \Delta \mathring{u}_i + \Delta \tilde{u}_i \tag{8.1.23}$$

It is assumed that the trivial mode produces an incremental stress field which causes loading everywhere in the considered body. On the other hand, the amplitude of the non-trivial mode is assumed to be small as compared to that of the trivial mode. This assumption permits the use of the same constitutive description for both modes and is met in order to overcome the difficulties arising from the non-linearity of an elastoplastic constitutive model. This construction is analogous to Shanley's (1947) solution for elastoplastic buckling of a rod, and corresponds here to the use of the constitutive equations 6.2.94 of the 'upper-bound' linear comparison solid.

Since the trivial mode satisfies equilibrium, the dynamic linear stability problem is formulated in terms of the non-trivial mode

$$C^{\mathrm{u}}_{ijkl}\partial_j\partial_l\Delta\tilde{u}_k = \rho\partial_{tt}\Delta\tilde{u}_i \tag{8.1.24}$$

A simple class of perturbation modes corresponds to the so-called roller bifurcation mode of a periodic pattern of layers under shear (cf. section 5.7.3)

$$\Delta\tilde{u}_i = C_i \sin(Qn_k x_k)\exp(St) \tag{8.1.25}$$

where n_i is the normal to the direction of the layers, S is the growth coefficient, Q the wavenumber of the instability and C_i are constants. Thus, according to 8.1.25 we are searching for spatially periodic solutions which are evolving exponentially in time. By inserting 8.1.25 into 8.1.24 we obtain

$$\{Q^2\Gamma_{ik} - (-\rho S^2)\delta_{ik}\}C_i = 0 \tag{8.1.26}$$

First we notice the affinity between the dynamic stability problem and of the problem of acceleration wave propagation. By comparing equation 8.1.26 and 3.4.13, we obtain

$$S^2 = -c_{\mathrm{m}}^2 Q^2 \tag{8.1.27}$$

where c_m is the material wave propagation velocity. From equation 8.1.27 we observe that if acceleration waves propagate with real speed (c_m>0), then the underlying continuum is locally, dynamically stable. In general, however, the acoustic tensor Γ_{ik} will be non-symmetric and real eigenvalues will not be guaranteed. This is because, even in the case when the geometric terms A_{ijkl} are neglected, due to non-associativity, the stiffness tensor C^{u}_{ijkl} wiSll not possess major symmetry property. Thus, in general, the eigenvalue ($-\rho S^2$) from 8.1.26 may turn out complex (Rice, 1976). In any case, the sign of the real part of the growth coefficient, S, will determine whether or not the considered equilibrium state C is inherently stable or not. That is if Re(S)≤0 then C will be stable, whereas if Re(S)>0, C will be unstable. Since in the latter case $(S)\rightarrow\infty$ for $Q\rightarrow\infty$, Schaeffer (1990) has called the underlying perturbation problem mathematically ill-posed.

Complex growth coefficient with positive real part, corresponds to a 'flatter-type' instability. Loret *et al.* (1990) have shown, however, that for a great class of materials, obeying deviatoric normality (cf. equation 6.2.30), flatter instability is excluded. Consequently Mandel's stability analysis for non-associative elastoplastic solids obeying deviatoric normality provides a neccessary condition for stability. This is the requirement that all eigenvalues of every acoustic tensor are real and positive. In this context, shear-band (continuous) bifurcation, characterized by the nullity of the determinant of the acoustic tensor, equation 8.1.18, marks the end of the stable regime. Past the shear-band bifurcation point, equilibrium of the ground state is unstable.

It is worth noticing that the theory of acceleration waves in elastoplastic solids was first developed in the two milestone papers by Hill (1962) and Mandel (1962). The first reference of Mandel's (1964) stability analysis in relation to soil mechanics applications is due to Professor Serrano (1972) in a panel discussion of the 5th European Conference on Soil Mechanics and Foundation Engineering in Madrid, Spain. The research in the mathematical foundations of bifurcation analysis in elastoplastic materials is ongoing. For a detailed discussion of localization, uniqueness and stability in associative and non-associative plasticity, the reader is referred to the research papers by Bigoni and Hueckel (1991) and Bigoni and Zaccaria (1992a,b).

8.2
Shear-band formation in element tests

8.2.1
Shear-band analysis in plane strain rectilinear deformations

As an application we restrict our demonstrations here to the 2D-constitutive model for sands discussed in section 6.5. Assuming that the initial stress $\sigma_{\alpha\beta}$ is continuous in C, in the coordinate system of principal axes of initial stress, the statical compatibility conditions are given here in terms of the Cauchy/Jaumann stress increment and the jump of incremental spin

$$
\begin{aligned}
[\mathring{\Delta}\sigma_{11}]n_1 + ([\mathring{\Delta}\sigma_{12}] + (\sigma_1 - \sigma_2)[\Delta\omega])n_2 = 0 \\
([\mathring{\Delta}\sigma_{21}] - (\sigma_2 - \sigma_1)[\Delta\omega])n_1 + [\mathring{\Delta}\sigma_{22}]n_2 = 0
\end{aligned}
\tag{8.2.1}
$$

where $\Delta\omega = (\partial_1 \Delta u_2 - \partial_2 \Delta u_1)/2$ is theonly significant component of the incremental spin tensor.

The incremental constitutive equations for the 'upper-bound' linear comparison solid, corresponding to loading, are derived frorn equations 6.5.42. In the coordinate system of principal axes of initial stress we obtain

$$
\begin{aligned}
\mathring{\Delta}\sigma_{11} &= L^{u}_{1111}\Delta\varepsilon_{11} + L^{u}_{1122}\Delta\varepsilon_{22} \\
\mathring{\Delta}\sigma_{22} &= L^{u}_{2211}\Delta\varepsilon_{11} + L^{u}_{2222}\Delta\varepsilon_{22} \\
\mathring{\Delta}\sigma_{12} &= 2G\Delta\varepsilon_{12}
\end{aligned}
\tag{8.2.2}
$$

where for the considered 2D-continuum model

$$
\begin{aligned}
L^{u}_{1111} &= G\{k(1-\beta)(1-\mu) + (1+k)h\}/h^* \\
L^{u}_{1122} &= G\{k(1+\beta)(1-\mu) - (1-k)h\}/h^* \\
L^{u}_{2211} &= G\{k(1-\beta)(1+\mu) - (1-k)h\}/h^* \\
L^{u}_{2222} &= G\{k(1+\beta)(1+\mu) + (1+k)h\}/h^*
\end{aligned}
\tag{8.2.3}
$$

By using these constitutive equations, the compatibility conditions 8.2.1 together with conditions 8.1.4

$$
\begin{bmatrix}
L^{u}_{1111}n_1^2 + G(1-\xi)n_2^2 & (L^{u}_{1122} + G(1+\xi))n_1n_2 \\
(L^{u}_{2211} + G(1-\xi))n_1n_2 & L^{u}_{2222}n_2^2 + G(1+\xi)n_1^2
\end{bmatrix}
\begin{bmatrix}
\zeta_1^{(v)} \\ \zeta_2^{(v)}
\end{bmatrix} = \{0\}
\tag{8.2.4}
$$

The influence of initial stress is given by the normalized stress difference

$$
\xi = (\sigma_1 - \sigma_2)/(2G)
\tag{8.2.5}
$$

which in most cases turns out to be negligible ($|\xi| \ll 1$).

For non-trivial solutions for the jumps of the incremental displacement gradient, from equation 8.2.4 we obtain the following characteristic equation for the shear-band inclination angle θ

$$
a\tan^4\theta + b\tan^2\theta + c = 0
\tag{8.2.6}
$$

where θ is measured with respect to the minor principal stress direction (Figure 8.1.2)

$$
\tan\theta = -(n_1/n_2)
\tag{8.2.7}
$$

and

$$
\begin{aligned}
a &= G(1+\xi)L^{u}_{1111} \\
b &= L^{u}_{1111}L^{u}_{2222} - L^{u}_{1122}L^{u}_{2211} - G(1+\xi)L^{u}_{2211} - G(1-\xi)L^{u}_{1122} \\
c &= G(1-\xi)L^{u}_{2222}
\end{aligned}
\tag{8.2.8}
$$

The condition for shear-band bifurcation is derived from the requirement that the above characteristic equation 8.2.6 has real solutions. This condition is firstly met at a state C_B (B for bifurcation) for which

$$b/a < 0 \quad \text{and} \quad D = b^2 - 4ac = 0 \tag{8.2.9}$$

For any state beyond C_B, there are four solutions for the shear-band orientation. According to the experimental evidence, however, the observed shear bands usually belong to a single family of symmetric solutions. This observation justifies the selection of 8.2.9 as the shear-band bifurcation condition. At C_B only two symmetric shear-band directions exist, given by

$$\theta_{1,2} = \theta_{3,4} = \pm\theta_B;\ \theta_B = \arctan(c^{\frac{1}{2}}) \qquad (b < 0) \tag{8.2.10}$$

For the considered linear comparison solid, equation 8.2.2 can be solved in terms of the critical hardening rate h_B at the bifurcation point, resulting in (Mandel, 1964):

$$h = h_B;\ h_B = \frac{(\mu_B - \beta_B)^2}{8(1-\nu)} \tag{8.2.11}$$

Similarly, from equation (8.2.10) we obtain

$$\theta_B = \arctan\left[\frac{(1+\mu_B)(1+\beta_B) + (1+1/k)h_B}{(1-\mu_B)(1-\beta_B) + (1+1/k)h_B}\right]^{\frac{1}{2}} \tag{8.2.12}$$

As already pointed out in chapter 6, in granular materials $\mu > \beta$ (cf. equation 6.5.57), which suggests that shear banding in plane-strain deformations always takes place in the hardening regime ($h_B > 0$). As first observed by Vardoulakis (1980), the dimensionless hardening modulus at bifurcation is a relatively small number ($h_B \ll 1$). This observation, considerably simplifies equation 8.2.12 for the shear-band orientation resulting in

$$\theta_B \approx \arctan\left[\frac{1+\sin\bar{\phi}}{1-\sin\bar{\phi}}\right]^{\frac{1}{2}} \tag{8.2.13}$$

where

$$\sin\bar{\phi} = \frac{\sin[(\phi_B + \psi_B)/2]}{\cos[(\phi_B - \psi_B)/2]} \tag{8.2.14}$$

Usually, $(\phi_B - \psi_B) < 30°$, and the denominator in equation 8.2.14 can be approximately equalized to unity: $\cos\{(\phi_B - \psi_B)/2\} \geq \cos(15°) = 0.96$. This second approximation step yields a simple formula for the shear-band orientation

$$\theta_B \approx \theta_V;\ \theta_V = 45° + (\phi_B + \psi_B)/4 \tag{8.2.15}$$

that was first proposed by Arthur *et al.* (1977) on the basis of experimental observations and was subsequently proven theoretically and supported experimentally by Vardoulakis (1980).

Let C_C (C for Coulomb) be the state of maximum stress obliquity. In this state the mobilized friction is maximum ($h = h_C = 0$). The experimental observation suggests that also the dilatancy angle is maximum at C_C. Let

$$\phi_C = \max\{\phi_m(\gamma^p)\};\ \psi_C = \max\{\psi_m(\gamma^p)\} \tag{8.2.16}$$

It can be easily shown that at C_C, two symmetric solutions for the shear-band orientations exist, namely (Vardoulakis, 1978):

$$\theta_{1,2} = \pm\theta_C;\ \theta_C = 45^\circ + \phi_C/2 \tag{8.2.17}$$

$$\theta_{3,4} = \pm\theta_R;\ \theta_R = 45^\circ + \psi_C/2 \tag{8.2.18}$$

The first solution is the classical Coulomb solution whereas the second one is called the Roscoe solution. In case of associative plasticity, according to equation 8.2.11 C_B coincides with C_C, i.e. if $\mu = \beta$ then

$$h_B = h_C = 0 \quad \text{and} \quad \theta_B = \theta_C = \theta_R = \theta_V \tag{8.2.19}$$

This means that for associated flow rule, Coulomb's failure criterion is derived from a bifurcation analysis. Coulomb's criterion states that shear banding occurs at the state of maximum stress obliquity and that the orientation of the shear bands coincides with the planes across which the ratio of shear to normal stress is maximum.

The bifurcation analysis presented above applies to a full-space domain under uniform state of stress, like the one shown in Figure 8.2.1(a). In the case, however, of a half-space domain under uniform stress, a shear band will intersect in general the free boundary, as shown in Figure 8.2.1(b). As pointed out by Benallal *et al.* (1990), the effect of pressure-like boundary conditions at the free boundary can be accounted for in the analysis by requiring that the same tractions exist at both sides of the shear-band boundaries. This gives the additional condition

$$[\Delta\pi_{ik}]m_k = \Delta\pi_i \tag{8.2.20}$$

where m_i is the exterior unit normal vector on the half-space boundary, and $\Delta\pi_i$ is defined according to a follower-load type law, equations 3.3.49 or 3.3.50. If one neglects the influence of initial stress, then instead of condition 8.2.20 one has

$$[\Delta\sigma_{ik}]m_k = 0 \tag{8.2.20\textit{bis}}$$

With $\mathring{\Delta}\sigma_{ij}$, the considered problem results in the following condition

$$\begin{bmatrix} Gn_1 & Gn_2 \\ L^u_{1122}n_1 & L^u_{1111}n_2 \end{bmatrix} \begin{bmatrix} \zeta_1^{(v)} \\ \zeta_2^{(v)} \end{bmatrix} = \{0\} \tag{8.2.21}$$

For non-trivial solutions for the jumps $\zeta_\alpha^{(v)}$, the determinant of the algebraic system 8.2.21 must vanish, resulting in the characteristic equation

$$\tan^2\theta_B = \frac{(1+\mu_B)(1+\beta_B) + (1+1/k)h_B}{(1+\mu_B)(1-\beta_B) - (1+1/k)h_B} \tag{8.2.22}$$

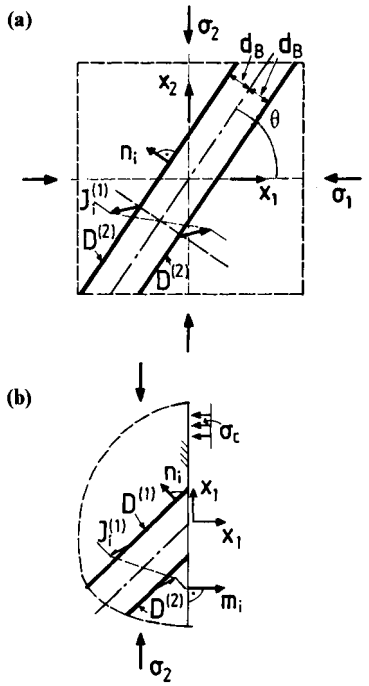

Figure 8.2.1 Shear banding in domains under uniform state of stress. (a) Full-space solution; (b) half-space solution.

which for small values of the hardening modulus yields the Roscoe solution,

$$\theta_B \approx \pm\theta_R;\ \theta_R = 45° + \psi_C/2 \tag{8.2.23}$$

Remark on non-associate perfect-plastic laws. Starting with Hill (1950), non-associated flow rules in frictional materials have been widely discussed in the context of rigid, perfectly-plastic, or elastic, perfectly-plastic material behavior (cf. Shield, 1953). The idea was to approximate true material behavior with the relatively simple constitutive law of perfect plasticity. All these models lead to two sets of distinct characteristics, the so-called statical and kinematical characteristics; cf. equations 8.2.17 and 8.2.18. Accordingly, the domains of solution for stresses and velocities do not coincide. The existence of two sets of characteristics triggered extensive experimental investigations aiming at determination as whether or not the zero-extension lines in soils coincide with the static characteristics of the perfectly plastic solid; cf. Bransby and Milligan (1975).

A simple shear-band analysis for a hardening material obeying a non-associate flow rule, proves that shear banding in plane strain occurs at positive hardening rates. Perfect plasticity presumes, however, that plastic deformation and formation of slip lines occurs at zero hardening rate. Thus, the perfectly plastic non-associate model cannot be a good approximation of the hardening non-associate plastic model. This point has been

overlooked in the literature, where perfect plasticity was adopted regardless of the flow rule. Apparently, the adoption of perfect plasticity for soils has been borrowed from metal plasticity, where the associative flow rule satisfactorily describes plastic deformation; it results directly from incompressibility, pressure insensitivity and coaxiallity. In all other materials, perfect plasticity is justified only if the flow rule is associative.

8.2.2
Analysis of a biaxial compression test on sand

Figure 8.2.2 shows the 'raw' experimental data from a biaxial compression test, on fine Dutch dune sand (cf. section 6.5.3), namely the variation of the axial force P and of the lateral displacement, $u_1 = u_{1L} + u_{1R}$, with the axial displacement u_2. The initial dimensions of the tubular shaped specimen were: l_{10}=41.03mm, l_{20}=140.93mm, l_{30}=79.10mm. The specimen was loaded in plane strain under constant confining pressure, $\sigma_c = 294.3\,\mathrm{kPa}$. The force-displacement curve consists of one major loading path with two unloading loops. Before first loading and after each unloading, X-ray radiographs were taken in order to investigate the homogeneity of the specimen. The specimen contained a small density imperfection of loose sand; (Figure 8.2.3a). At the state of maximum axial load, a shear band was seen to emerge from the density disturbance (Figure 8.2.3b). The evaluation of a series of X-ray plates from experiments with the same sand (Vardoulakis and Graf, 1985; Vardoulakis *et al.,* 1985) prompted the suggestion that homogeneous deformations are disrupted at a shearing strain intensity which is bounded as follows,

$$\gamma_E^{(l)} \leqslant \gamma \leqslant \gamma_E^{(u)} \tag{8.2.24}$$

The lower bound of the bifurcation strain, ($\gamma_E^{(l)} \approx 0.06$) corresponded to that value of the overall shear strain for which a first indication for shear-band formation could be seen in the X-ray plate. Eventually the growing density in homogeneity reached the specimen faces, leading to separation by a fully formed shear band. The upper bound for the overall strain that corresponded to separation was estimated as, $\gamma_E^{(u)} \approx 0.10$.

We remark that X-ray detection of shear banding is an observation of porosity localization. As explained in section 6.4.3, strong porosity changes must be accompanied with local strain softening, i.e. with states of stress which lie past the bifurcation limit of continuous bifurcations, which for plane strain and according to equation 8.2.11 is in the hardening regime. This means that shear-band *formation* is a post-bifurcation phenomenon within the frame of a classical non-associative plasticity theory and that the theoretical shear-band bifurcation strain must be always less than any estimate that stems from direct porosity localization observations.

In section 6.5.3, the constitutive equations of 2D flow theory of plasticity were calibrated on the basis of pre-failure data from the considered here biaxial tests. The corresponding material constants and functions are summarized below:

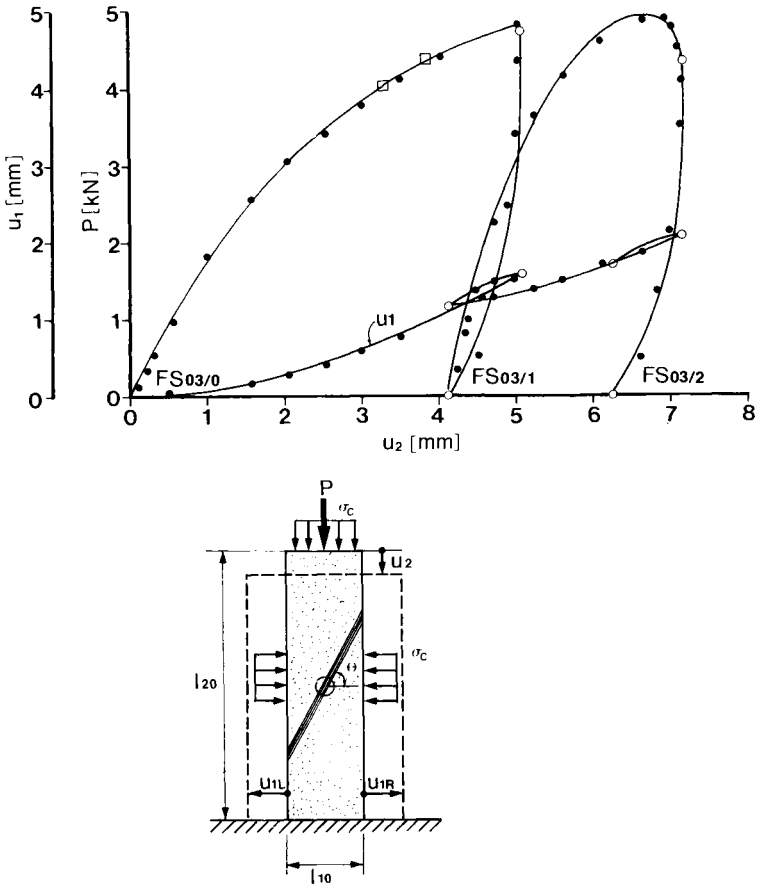

Figure 8.2.2 Data from biaxial tests: u_2 (mm) axial displacement; u_1 (mm) lateral displacement stress; P (kN) axial load (Vardoulakis *et al.*, 1985).

shear modulus:	$G = 50.34\,\text{MPa}$
Poisson's ratio:	$\nu = 0.1$
mobilized friction function:	$\mu = \gamma^{\text{p}}/(c_1 + c_2\gamma^{\text{p}})$; $c_1 = 1.7915 \times 10^{-3}$; $c_2 = 1.3930$
mobilized dilatancy function:	$\beta = \mu - \mu_{\text{cv}}$; $\mu_{\text{cv}} = 0.412$

Using these data, computationally the bifurcation strain γ_{B}, the corresponding critical hardening rate h_{B} and shear-band inclination angle θ_{B} can be found using the formulae in the previous section. Experimental and computational results are summarized in Table 8.2.1.

First, this table demonstrates a typical result of flow theory as applied to granular media: the theoretical estimate for the shear-band bifurcation strain is significantly less than a lower bound for the shear strain at which shear-band formation is observed

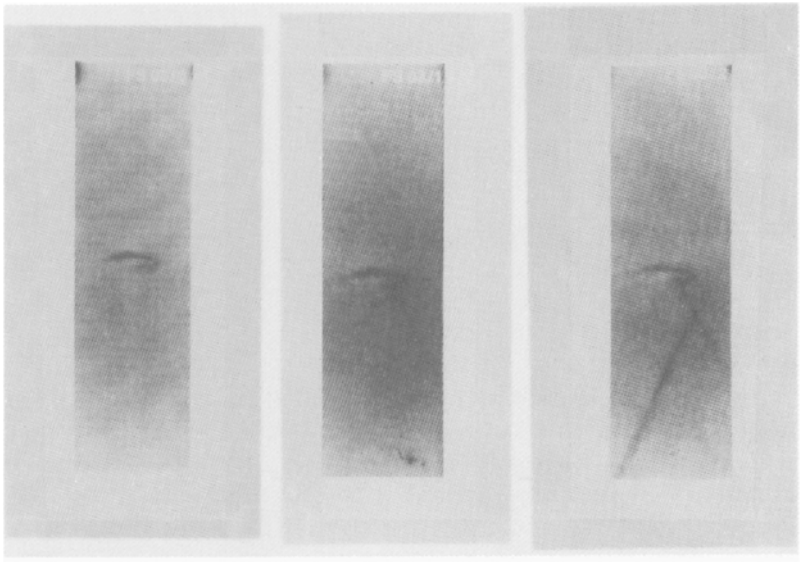

Figure 8.2.3 X-ray plates showing the evolution of the porosity localizations (Vardoulakis *et al.*, 1985).

Table 8.2.1 Experimental and theoretical results on shear-band formation in a biaxial compression test on fine grained Dutch dune sand (σ_c=294.3 kPa)

Result	γ_B	h_B	ϕ_B	ψ_B	θ_B
Experiment					
lower bound	0.06	0.008	44.2°	16.6°	62.5°
upper bound	0.10	–	≈45.0°	–	62.5°
Theory					
exact	0.04	0.025	43.4°	16.0°	59.2°
approximate	–	0.024	–	–	59.8°

experimentally (here a relative error of 33% in bifurcation strain). What is not seen directly from this table, but can be easily demonstrated by parameter analysis, is that the theoretical prediction for γ_B depends sensitively on the assumed value for the elastic shear modulus (see for example Vardoulakis, 1988). All these observations mean that non-associative flow theory of granular media underestimates the shear-band bifurcation strain, and in that sense non-associativity severely destabilizes the constitutive response. This defect of standard flow theory for granular media is undesirable, as far as realistic constitutive modeling is concerned, and suggests searching for further modifications of the standard plasticity model, which have to counterbalance the destabilizing effect of non-associativity; see section 8.4.

Secondly, we observe from Table 8.2.1 that the prediction in the shear band orientation angle is significantly better (with a relative error of 5%). Finally, we remark

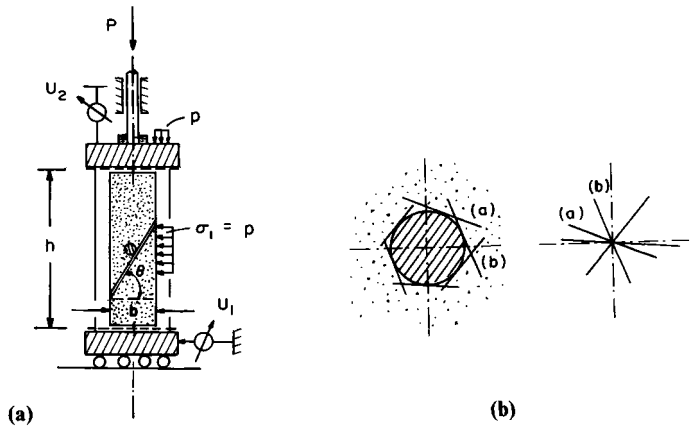

Figure 8.2.4 (a) The biaxial apparatus, (b) hard inclusion as an envelope of possible shear planes.

that the approximate formulae 8.2.11 and 8.2.15 give fairly good approximations of the exact theoretical results. This last observation leads usually to the statement that in bifurcation analyses for granular materials the effect of initial stress is negligible.

8.2.3
Imperfection sensitivity of the biaxial test

Shear bands may emerge out of (a) various disturbances like density imperfections, (b) surface anomalies and (c) hard or soft inclusions, i.e. out of interfaces between soft and hard material. As already mentioned, shear bands are seen in X-ray radiographs as localized zones of higher porosity and may be partially or fully formed. A partially formed shear band does not separate the soil body into two parts and resembles very much a 'crack' (cf. Palmer and Rice, 1973). However, the classical Griffith crack of elasticity theory is a 'cut', and its two faces are stress-free. The partially developed shear band on the other hand carries both normal and shear stresses at its boundaries and is filled with softer material.

Vardoulakis and Graf (1982) performed a series of biaxial experiments on dry sand specimens which contained a small cylindrical wooden inclusion (diameter 8 mm), placed perpendicular to the plane of deformation at the center of the specimen (Figure 8.2.4a). The cylindrical surface of the inclusion is understood as the envelope of the set of possible slip planes, as indicated in Figure 8.2.4(b). Figure 8.2.5 shows the test data from the aforementioned biaxial experiment on dry, medium-grained, dense Karlsruhe sand (Test BSE-7: n_0=0.36,$\phi_C = 45°, \theta_E = 63°$)). Figure 8.2.6 reveals in successive X-ray radiographs (taken at various stages of the experiment) at least qualitatively, any change in the porosity distribution in space. From these pictures we observe that between states III and IV the horizontal displacement of the moving bottom plate commences, indicating the complete development of a shear band, separating the

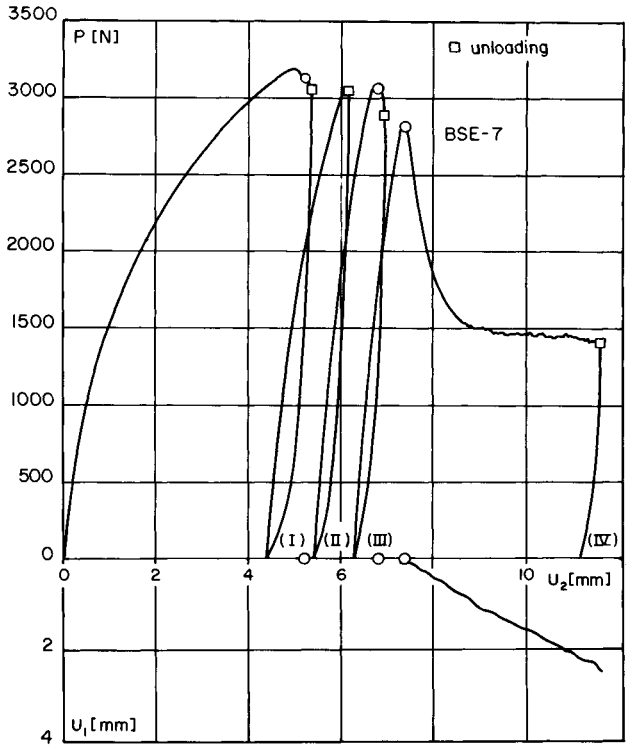

Figure 8.2.5 Test data from a dry, medium-grained dense sand BSE-7 (Vardoulakis and Graf, 1982).

specimen into two distinct blocks sliding relative to each other. The radiographs also show that from the two evolving symmetric porosity localizations one finally dominates and becomes a shear band.

Figure 8.2.7(a) shows a partially formed shear band in a biaxial test emerging out of an interior density imperfection. This band, like the ones shown in Figure 8.2.6, is straight as opposed to the one shown in Figure 8.2.7(b), which is emerging out of surface imperfection, a notch. The latter is curved and flatter towards the free boundaries (cf. Vardoulakis and Graf, 1985). These observations are in qualitative agreement with the theoretical solutions summarized above in equations 8.2.15 and 8.2. 23, respectively.

8.2.4
Spontaneous versus progressive localization

As described above, localization of the deformation in elastoplastic materials is mathematically described by the Thomas-Hill-Mandel theory of equilibrium bifurcation, which gives essentially the shear-band orientation angle θ_B and an estimate for the

critical hardening modulus h_B, equations 8.2.15 and 8.2.11, respectively. The theory considers localized deformation in an initially homogeneously deforming infinite domain and constitutes therefore a local bifurcation analysis. Complementary experiments are limited to initially homogeneous stress and strain fields and failure may be termed as *spontaneous,* meaning that it may occur at any point, most probably out of subliminal imperfections.

Notwithstanding the significance of this theory, one could address its appropriateness in a more general case: that is, in the case of shear bands developing in a non-homogeneous stress and strain field. The prevailing concept in this context is that of *progressive* failure. According to this concept, a structure fails by increasing loads with the gradual (progressive) formation of a shear band. Progressive shear band failure may be linked to the local criterion as follows: It may be assumed that a shear band starts from a given point at a surface or inside the body where the stress field first satisfies the local bifurcation condition. Continued loading leads then further points of the body to satisfy the local bifurcation condition. It is assumed that whenever this happens the shear band is progressing through these points at an angle given by the characteristic equation (Leroy and Ortiz, 1989). In section 8.5 we will return to the problem of progressive failure by discussing a few cases as examples.

8.3
Shear banding in sands: experiment versus theory

Shear band formation in granular media has been investigated extensively in a series of experimental studies by Arthur *et al.* (1977), Vardoulakis and co-workers (1977, 1980, 1982, 1985), Desrues and co-workers (1984, 1985, 1987, 1989, 1991), Tatsuoka *et al.* (1990), and Han *et al.* (1991, 1993). This body of work refers mainly to element tests on sands and focusses on the documentation of a shear-band 'failure criterion' that is a statement on the strain γ_B, at shear-band formation, and on the shear-band orientation angle θ_B with respect to principal stress axes. In granular media, shear banding is influenced by one or more of the following factors:

(a) porosity of the medium;
(b) confining pressure during the test, i.e. the level of effective isotropic stress at bifurcation;
(c) stress-induced or inherent anisotropy of the medium;
(d) size and shape of the grains.

8.3.1
Influence of porosity

As demonstrated in chapter 6, in ordinary flow theory of plasticity the influence of porosity is directly accounted for by selecting appropriately the various material constants and functions:

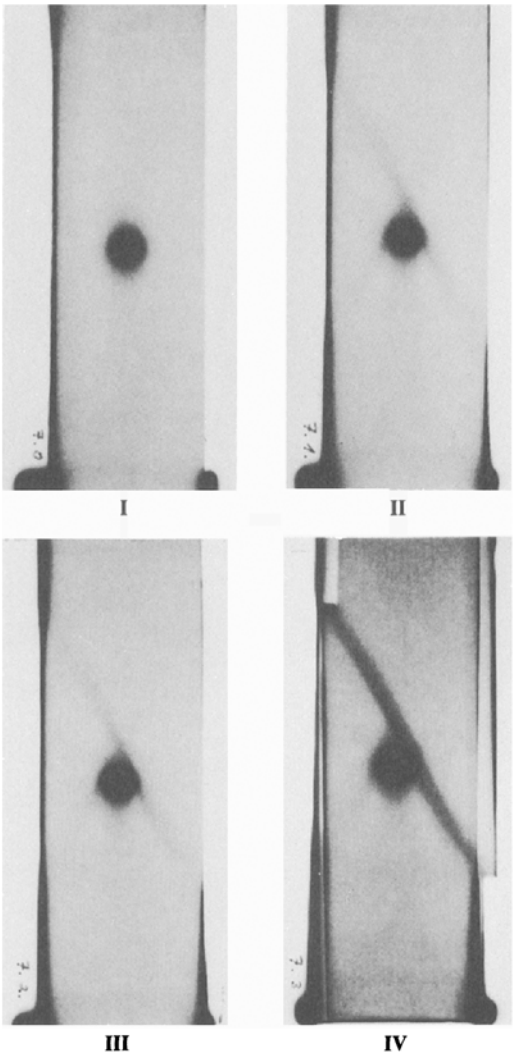

Figure 8.2.6 X-ray radiographs showing the evolution of dilatancy localizations (Vardoulakis and Graf, 1982).

$$G = G(n_0);\ \nu = \nu(n_0)$$
$$\sin\phi_m = \mu(n_0, \gamma^p);\ \sin\psi_m = \beta(n_0, \gamma^p) \tag{8.3.1}$$

Theoretical predictions on shear-band formation, based on flow theory of plasticity are very sensitive to the selection of the elastic shear modulus. Table 8.2.1 demonstrates that it was possible to predict the experimentally measured shear-band orientation only approximately with a larger error in the prediction of γ_B and a lesser error in the prediction of θ_B. With constant elastic shear modulus, the procedure can be repeated for

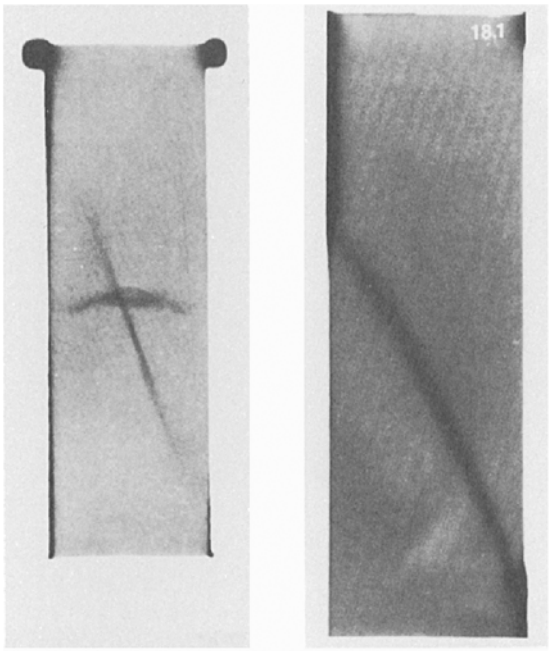

Figure 8.2.7 Shear band emerging out of (a) an interior density imperfection; (b) a surface imperfection.

various values of the confining pressure σ_c of a biaxial test and the theoretical predictions are usually not satisfactory. Bardet (1991) summarized the theoretical and out to the limitations of the elastoplastic Mohr-Coulomb model. Figure experimental work on shear-band orientation in frictional soils and pointed 8.3.1 from Bardet (1991) compares the inclination angle $\theta_B^* = 90° - \theta_B$ of shear bands that are measured experimentally in a series of plane strain experiments by Arthur *et al.* (1977), Vardoulakis (1980) and Desrues (1984) to Vardoulakis' theoretical solution, $\theta_V^* = 45° - (\phi_B + \psi_B)/4.$.

8.3.2
Influence of confining pressure

The influence of the confining pressure on shear banding in biaxial compression tests on sands has been investigated systematically in two doctoral theses by Hammad (1991) and Han (1991). Figure 8.3.2 from Hammad (1991) (see also Desrues and Hammad, 1989) shows the measured dependency of (a) the axial strain ε_{2B} at shear band formation, and (b) the inclination angle θ_B^*, on the confining pressure σ_c in biaxial tests on Hostun sand. The general trend is that ε_{2B} and θ_B^* (θ_B) increase (decreases) with σ_c. In the same figure, Hammad has indicated the lines which correspond to the theoretical

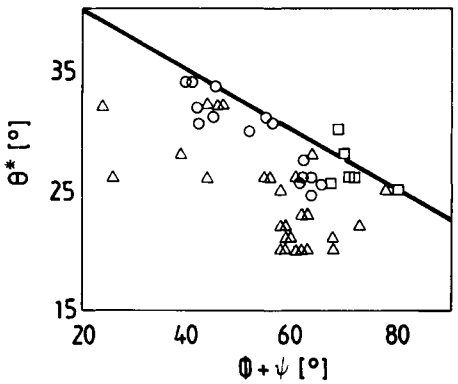

Figure 8.3.1 Shear-band inclination θ_B^* versus $(\phi_B+\psi_B)$. □, Arthur *et al.* (1977); ○, Vardoulakis (1980); Δ, Desrues (1984); ▲, Desrues (1984) local;——, theory. Data after Arthur *et al.* (1977), Vardoulakis (1977), Desrues (1984) and Bardet (1991).

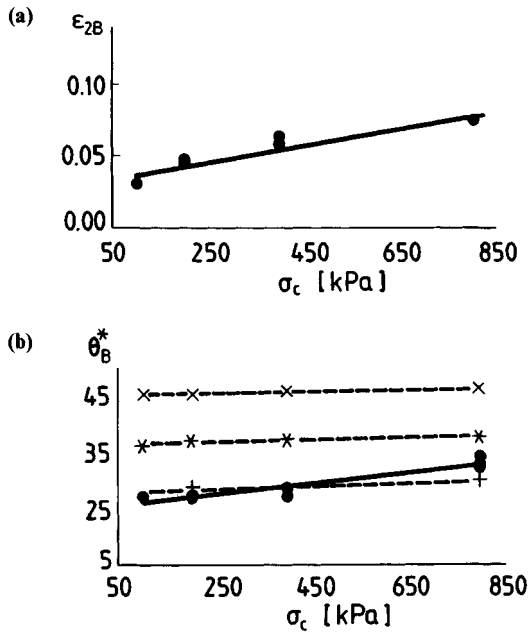

Figure 8.3.2 Influence of confining pressure for dense Hostun sand. (a) Axial strain ε_{2B}, (b) shear-band inclination θ_B^* (Hammad, 1991). ●, θ_B^*; +, $\pi/4-\phi/2$; ×, $\pi/4-\psi/2$; *, $\pi/4-(\phi+\psi)/4$.

solutions of Coulomb, $\theta_C^* = 45° - \phi_B/2$, Roscoe $\theta_R^* = 45° - \psi_B/2$, and Vardoulakis $\theta_V^* = 45° - (\phi_B + \psi_B)/4$. From these plots we deduce that the experiments on Hostun sand yield inclination angles between θ_C^* and θ_V^*.

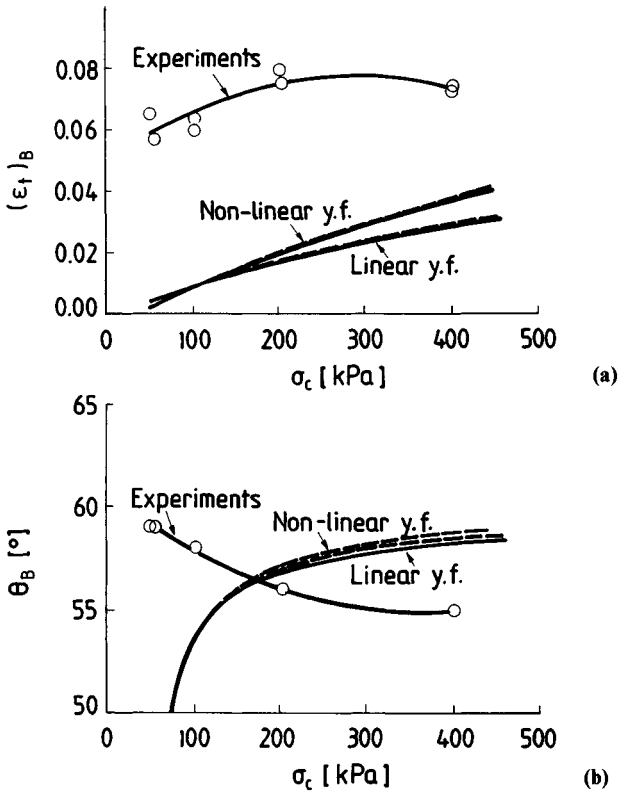

Figure 8.3.3 Influence of confining pressure for dense Ottawa sand. Experiment versus elastoplastic model (flow theory): (a) shear strain intensity at shear banding γ_B, (b) shear-band inclination angle θ_B (Han, 1991).

Similar results are reported by Han (1991), who tested a poorly-graded Ottawa sand. The analysis of Han has shown that the significant difference between the theoretical predictions, based on flow theory of plasticity, and experimental results cannot be remedied by considering only the stress-level dependence of the elastic shear modulus, i.e. by resorting to a flow theory of plasticity, with underlying elasticity a hyperelasticity having stress-dependent elastic parameters. Han confirmed also that consideration of geometric non-linearities which account for the state of initial stress, modify only slightly the theoretical prediction. Moreover, Han found that consideration of a curved yield surface in stress space has little bearing.

In Figure 8.3.3 the experimental results of Han and Drescher (1993) are compared against the theoretical predictions for an elastoplastic model with constant values for the elastic constants, taken as averages over the whole range of tested confining pressures. In Figure 8.3.4, computational results for a rigid-plastic model are plotted against the experimental findings. One can see that the rigid-plastic model provides a better fit than the elastoplastic model; cf. Vardoulakis (1980).

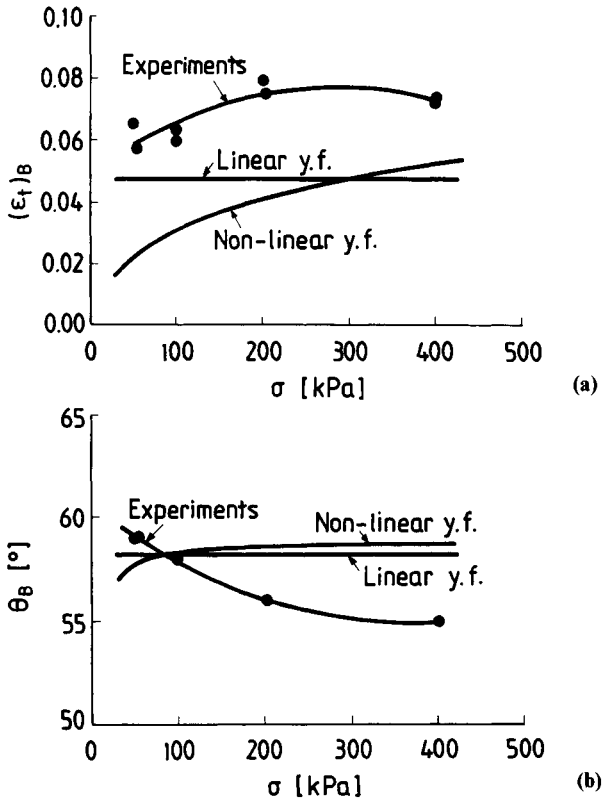

Figure 8.3.4 Influence of confining pressure for dense Ottawa sand. Experiment versus rigid-plastic model: (a) shear strain intensity at shear banding γ_B, (b) shear-band inclination angle θ_B (Han, 1991).

The above results point at a major deficiency of flow theory. In the following we sketch some ideas which have been proposed to modify the flow theory and to provide a better model for the description of the experimental results. It turns out that the flow rule of ordinary plasticity is very restrictive and needs to be modified drastically. For simplicity we restrict ourselves here to 2D considerations, and we start our discussion by recalling the expression of the plastic deviatoric strain rate in the 2D-plasticity model, which is discussed in some length in section 6.5.2. In accordance with the Prandtl-Reuss equations 6.5.40, the deviator of the plastic deformation rate, $D^{p}_{\alpha\beta}$ can be written in the following form,

$$D^{p'}_{\alpha\beta} = \frac{1}{2Gh} A\, m_{\alpha\beta} \tag{8.3.2}$$

where h is the hardening modulus, A is a mixed invariant function of the stress and its (objective) rate

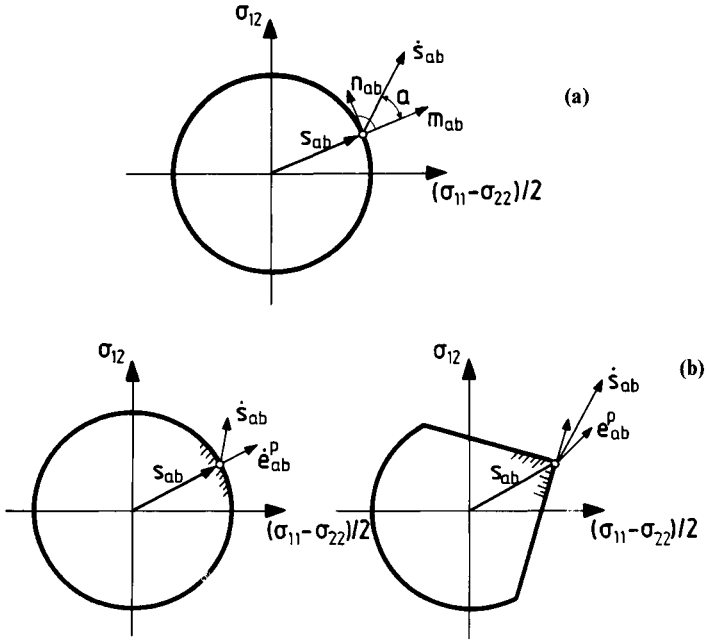

Figure 8.3.5 Deviatoric stress space: (a) definitions of the $m_{\alpha\beta}$ and $n_{\alpha\beta}$; (b) smooth yield function and coaxial flow rule and yield vertex and freedom for non-coaxial flow rule.

$$A = m_{\gamma\delta}\dot{s}_{\gamma\delta} - (1/\sqrt{2})(\tau/\sigma)\dot{\sigma}_{\gamma\gamma} \tag{8.3.3}$$

and $m_{\alpha\beta}$ is a unit vector in stress space which is parallel to the deviator $s_{\alpha\beta}$, (Figure 8.3.5a),

$$m_{\alpha\beta} = s_{\alpha\beta}/(\sqrt{2}\tau);\ m_{\alpha\beta}m_{\alpha\beta} = 1 \tag{8.3.4}$$

Equation 8.3.2 illustrates the fact that in ordinary flow theory of plasticity the plastic deformation rate $D^{p}_{\alpha\beta}$ possesses the same principal axes (it is 'coaxial') as the stress $\sigma_{\alpha\beta}$ tensor. The simplest modification of 8.3.2 is to consider additional terms, which will account for the influence of the stress-rate itself on the direction of the plastic deviatoric deformation rate. The resulting plasticity theory may be called after Kolymbas (1991) a hypoplasticity (see Remark after section 3.2.4, page 73).

In the simplest hypoplastic flow rule in addition to the coaxial term there is a non-coaxial term as well

$$D^{p'}_{\alpha\beta} = \frac{1}{2Gh} A m_{\alpha\beta} + \frac{1}{2Gh_1} n_{\alpha\beta} \tag{8.3.5}$$

where h_1 is a new modulus controlling the deviation from coaxiality, and $n_{\alpha\beta}$ is a vector in stress space which is normal to $m_{\alpha\beta}$

$$n_{\alpha\beta} = \dot{s}_{\alpha\beta} - m_{\gamma\delta}\dot{s}_{\gamma\delta}m_{\alpha\beta};\ n_{\alpha\beta}m_{\alpha\beta} = 0 \tag{8.3.6}$$

$$(n_{\alpha\beta}n_{\alpha\beta})^{\frac{1}{2}} = \pm\sqrt{2}\,\dot{\tau}\sin\alpha \tag{8.3.7}$$

and $\dot{\tau}$ is the intensity of the deviatoric stress rate

$$\dot{\tau} = (\dot{s}_{\alpha\beta}\dot{s}_{\alpha\beta}/2)^{\frac{1}{2}} \tag{8.3.8}$$

In equation 8.3.7, α is the invariant angle in deviatoric stress space which measures the deviation from proportional loading (Budiansky, 1959)

$$\cos\alpha = \frac{s_{\mu\nu}\dot{s}_{\mu\nu}}{(s_{\alpha\beta}s_{\alpha\beta})^{\frac{1}{2}}(\dot{s}_{\gamma\delta}\dot{s}_{\gamma\delta})^{\frac{1}{2}}} \tag{8.3.9}$$

Note that for proportional loading,

$$\dot{s}_{\alpha\beta} = \lambda m_{\alpha\beta} \rightarrow n_{\alpha\beta} = 0 \qquad (\alpha = 0) \tag{8.3.10}$$

and the contribution of the non-coaxial term in equation 8.3.5 is zero. The above modification of the flow theory has been initially suggested by Rudnicki and Rice (1975) and has been motivated by an argument in favor of a 'yield vertex' plasticity model; Figure 8.3.5(b). As pointed out by Stören and Rice (1975), equation 8.3.5 is highly non-linear and it is not clear how to describe the changes in the hardening moduli h and h_1 under continued plastic flow. Moreover, the definition of loading and unloading is not straightforward, although we find in the literature a number of works which deal with these questions; see for example Christoffersen and Hutchinson (1979). Finally we remark that Vardoulakis and Graf (1985) proposed such a modification of the flow rule for a rigid-plastic model on the basis of 'deformation theory' of plasticity (cf. section 7.2.2). In a recent study, Papamichos *et al.* (1992, 1995) have abandoned the concept of yield vertex plasticity and developed a consistent, non-coaxial plasticity model which we will discuss in section 8.4.

The above modifications of the plasticity flow rule result in significant changes in material response for non-proportional loading paths. For example, if one considers shear-band bifurcation out of a plane-strain rectilinear compression, both shear strain at bifurcation and shear-band inclination depend sensitively on the shear modulus G_* for loading to the side,

$$\mathring{\Delta}\sigma_{12} = 2G_*\Delta\varepsilon_{12} \tag{8.3.11}$$

where, as in section 8.2.1 (x_1, x_2) is the Cartesian coordinate system of principle directions of initial stress. In flow theory plasticity with smooth yield surface and coaxial flow rule, the shear modulus for loading to the side coincides with the elastic shear modulus

$$G_* = G \tag{8.3.12}$$

and plastic strain increments are coaxial to the stress vector in stress space, as shown in the deviatoric plane representation of Figure 8.3.5(b). A slightly smaller value of G_* is given by the deformation theory (Vermeer and Schotman, 1986)

$$G_* = G_s = (\gamma^e/\gamma)G \tag{8.3.13}$$

where G_s is the secant modulus. However, the magnitude of G_* can be substantially reduced if the yield surface possesses a vertex. As discussed by Christoffersen and Hutchinson (1979), the sensitivity of the effect of the yield vertex can be examined by introducing an additional material parameter C such that

$$G_* = \{1 - C(\alpha)\gamma\}(\gamma^e/\gamma)G \tag{8.3.14}$$

$C(\alpha)$ in equation 8.3.14 is assumed to be a function of the Budiansky angle α, defined through equation 8.3.9. In Figure 8.3.6 from Han (1991), the influence of $C(\alpha)$ on γ_B and θ_B is shown.

8.3.3
Influence of anisotropy

Anisotropic plasticity models can be constructed by the consideration of additional directors and tensors describing inherent anisotropy. The influence of differences in the bedding plane of deposition of the sand in the specimen on shear band orientation was studied experimentally by Tatsuoka *et al.* (1990) within an extended testing program on Toyoura sand. The influence of inherent anisotropy formed during deposition process or sample preparation is very well reproduced theoretically by the micromechanically motivated constitutive model of 'spatial mobilized plane' by Nakai and Matsuoka (1983).

Stress-induced anisotropy of granular assemblies is reflected in the spatial distribution of interparticle contact force orientation. Anisotropy in the fabric of grain contacts and contact forces influences the flow characteristics of the assembly. In its simplest manifestation stress-induced anisotropy is accounted for if one considers the following hypoplastic modification of the Rudnicki and Rice rule (8.3.5). We recall first that the flow rule of classical flow theory of plasticity is coaxial, $D^{p'}_{\alpha\beta} = (m_{\alpha\beta}/\sqrt{2})\dot{\psi}$. We observe that in this case the plastic multiplier is inversely proportional to the dimensionless hardening modulus, $\dot{\psi} = A/(\sqrt{2}Gh)$, and equation 8.3.2 is recovered. For deviatoric stress probes which lie perpendicular to the stress vector, the nominator A vanishes, since according to equation 8.3.3, A is proportional to the inner product of deviatoric stress and stress-rate tensors. More important is the fact that classical theory is described by a singular flow rule in terms of the hardening modulus h, which simply is describing the physical observation that plastic strains increase with decreasing hardening rate. Thus classical theory is virtually correct as $h \to 0$. If for some reason we expect deviations from proportional loading far in advance of the state of full plastification (e.g. equilibrium bifurcations at relatively small strains), then the classical description may not be accurate enough. These remarks allow the reinterpretation of the

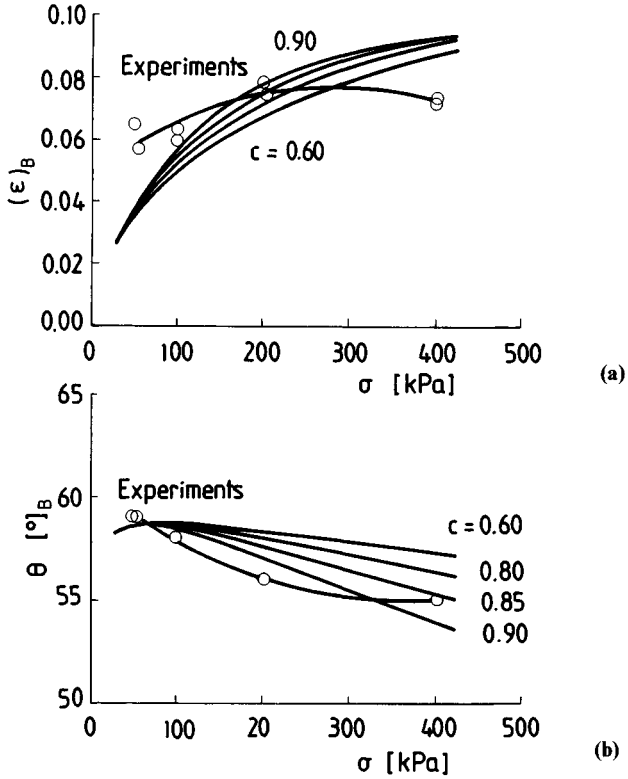

Figure 8.3.6 Influence of confining pressure for dense Ottawa sand. Experiment versus yield-vertex model; (a) shear strain intensity at shear banding γ_B; (b) shear-band inclination angle θ_B (Han, 1991).

deviatoric part of the flow rule of classical flow theory as the leading term of a more general asymptotic power series of the form

$$D^{p'}_{\alpha\beta} = m_{\alpha\beta}\left\{a_0 + \frac{a_1}{2h} + \ldots\right\} \tag{8.3.15}$$

where the coefficients a_i are isotropic scalar functions of the mixed invariants of the stress and stress-rate tensors. Thus a modification of the coaxial flow rule is at hand, so that in the flow rule a regular term a_0 appears, which reflects the effect of the deviation from non-proportional loading on the magnitude of the plastic rate of deformation. In view of the above observations we modify only the deviatoric part of the flow rule as follows,

$$D^{p'}_{\alpha\beta} = \frac{m_{\alpha\beta}}{\sqrt{2}}\{1 + f(\alpha)(2h) + \ldots\}\dot{\psi} \tag{8.3.16}$$

where *f(α)* is an appropriate invariant function of the angular function *α*, measuring the deviation from proportional loading, equation 8.3.9. The flow rule 8.3.16 results together with the consistency condition of flow theory in an expression like 8.3.15 with, $a_0 = (A/G)f(\alpha)$ and $a_1 = (A/G)$. A simple selection for *f(α)* in equation 8.3.16 is the non-negative, bounded function

$$f(\alpha) = \lambda|\sin\alpha| \qquad (\lambda \geqslant 0) \tag{8.3.17}$$

which can be used as a measure for the 'direction' of the stress-rate vector in deviatoric stress space; cf. equation 8.3.7.

Considering, for example, a rectilinear deformation, in the coordinate system of principal axes of initial stress the principal axes orientation angle of the stress-rate tensor is

$$\tan 2\Omega = \frac{\dot{s}_{12}}{\dot{s}_{11}} \tag{8.3.18}$$

Thus we obtain that

$$\sin\alpha = |\sin 2\Omega| \tag{8.3.19}$$

For small deviations from proportional loading ($0<|\alpha|<<1$) it is

$$\sin 2\Omega \approx |\tan 2\Omega| \rightarrow \sin\alpha \approx |\dot{s}_{12}|/\dot{s}_{11} \tag{8.3.20}$$

This modification of the flow rule introduces an anisotropic effect which is seen more clearly if we write down the rate constitutive equations in the coordinate system of the principal axes of initial stress. Within a small strain incremental formulation, instead of equations 8.2.2 we obtain

$$\begin{aligned}
\mathring{\Delta}\sigma_{11} &= L^{u}_{1111}\Delta\varepsilon_{11} + L^{u}_{1122}\Delta\varepsilon_{22} + 2L^{u}_{1112}|\Delta\varepsilon_{12}| \\
\mathring{\Delta}\sigma_{22} &= L^{u}_{2211}\Delta\varepsilon_{11} + L^{u}_{2222}\Delta\varepsilon_{22} + 2L^{u}_{2212}|\Delta\varepsilon_{12}| \\
\mathring{\Delta}\sigma_{12} &= 2G\Delta\varepsilon_{12}
\end{aligned} \tag{8.3.21}$$

where the additional components of the stiffness tensor are

$$\begin{aligned}
L^{u}_{1112} &= GN\{(k\beta)(1-\mu) - h\}/h^{*} \\
L^{u}_{2221} &= GN\{(k\beta)(1+\mu) + h\}/h^{*}
\end{aligned} \tag{8.3.22}$$

$$N = 2\{1 + k\mu(1-\nu)/(1+\nu)\}\lambda \tag{8.3.23}$$

In this case the characteristic equation 8.2.6 results in (Vardoulakis and Graf, 1985; Sulem *et al.,* 1993),

$$a\tan^4\Theta \mp d\tan^3\Theta + b\tan^2\Theta \mp e\tan\Theta + c = 0 \tag{8.3.24}$$

where the upper sign holds for $\Theta>0$ and the lower sign holds for $\Theta<0$.

$$d = L^{u}_{2212}L^{u}_{1111} - L^{u}_{1112}(L^{u}_{2211} - 2\xi)$$
$$e = L^{u}_{1112}L^{u}_{2222} - L^{u}_{2212}(L^{u}_{1122} + 2\xi) \tag{8.3.25}$$

As pointed out earlier by Vardoulakis and Graf (1985), perturbations of rectilinear deformations, which correspond to a small deviation angle α, produce additional volume changes which are proportional to the shear stress increment

$$\Delta\tilde{\varepsilon}^{p} = |\Delta\tilde{\sigma}_{12}|/D_{R} \tag{8.3.26}$$

Note that undrained torsional tests with saturated sand on hollow cylinder specimens (Ishihara and Towhata, 1983) indicated that axes rotations produce an incipient contraction; this would mean that $D_R<0$. The influence of shear-stress increment on the plastic volume dilation or contraction could be called Reiner dilatancy. (Reiner (1960) and Vardoulakis and Graf (1985) called this phenomenon Reynolds' dilatancy; however, we prefer here to call Reynolds' dilatancy the kinematic constraint that relates volume changes of a granular assembly to the magnitude of average slip in that assembly.) For $1/D_R=0$, one recovers the classical dilatancy constraint of flow theory, which holds for isotropic granular assemblies.

Appropriate choice of a measure of anisotropy (like Reiner's dilatancy coefficient D_R) generally allows a better description of the experimental results on shear-band formation in soil specimens which show inherent anisotropy due to the influence of the orientation of the bedding plane of sand deposition. Yatomi *et al.* (1989), for example, analyzed shear banding in clay soil and derived a complete fourth-order characteristic equation, similar to equation 8.3.24. The considered structure of the flow rule, equation 8.3.16, explains the preferred orientation of shear bands in simple shear as indicated in Figures 8.3.7 and 8.3.8 from Annin *et al.* (1987).

8.3.4
Influence of grain size and shape

In Table 8.3.1 and Figure 8.3.9 some typical experimental results are summarized indicating the influence of grain size and shape and shear-band inclination angle θ_E (Vardoulakis, 1977). As follows from this table, generally, the shear-band inclination angle, θ_E, in biaxial tests increases with decreasing grain size and angularity. A theoretical explanation of this finding is given by Vermeer (1990), who performed semi-inversely post-bifurcation computations, taking into account the effect of boundary conditions in the biaxial test and concluded that the Coulomb solution, $\theta_C = 45^\circ + \phi_B/2$, appears to be moreprobable for fine-grained sand. Although Vermeer's analysis could not becorroborated either in element tests or in more complicated boundary-value tests, for example the deformation localization in cavity inflation experiments by Alsiny *et al.* (1992), it now constitutes the only comprehensivestudy of the influence grain size on shear band inclination.

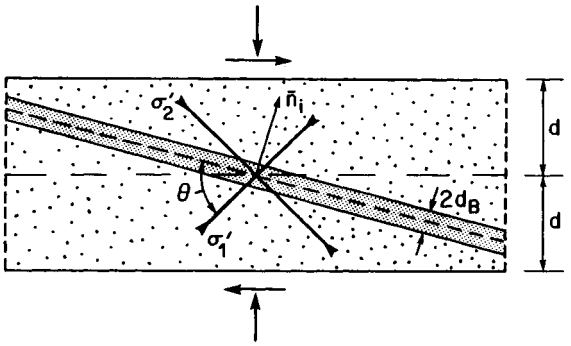

Figure 8.3.7 The dominant shear band in simple shear.

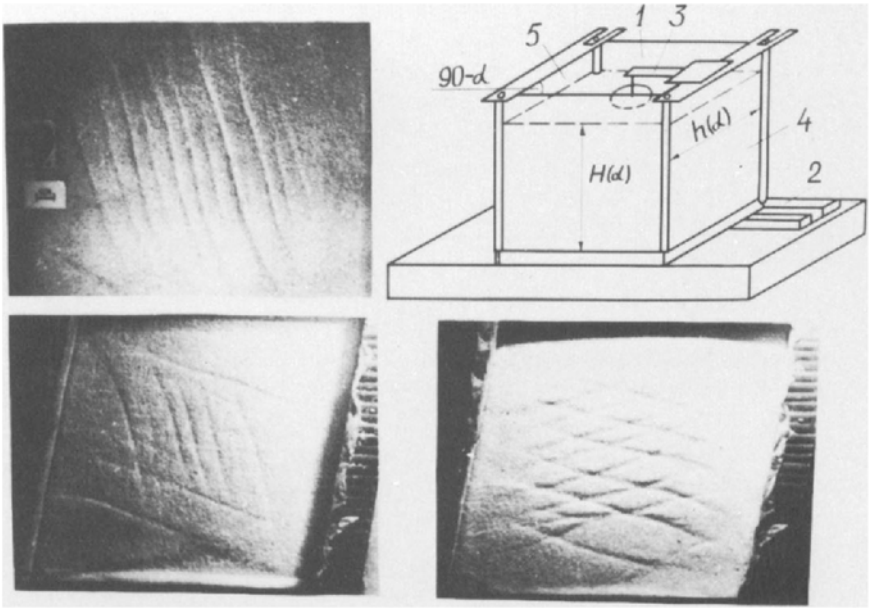

Figure 8.3.8 Dominant (asymmetric) shear banding in simple shear. Echelon and reversed echelon pattern upon shear stress reversal. After Annin *et al.* (1987), courtesy of Academician J. Shemyakin.

8.4
Non-coaxial plasticity model

As already mentioned, in order to arrive at better predictions for the bifurcation strain one has to abandon the concept of classical coaxial plasticity flow rule and resort to hypoplasticity flow rules, which consider one way or the other the effect of stress rate. Following Papamichos *et al.* (1992, 1995) one can formulate a consistent non-coaxial, elastoplastic model, with well-defined loading-unloading conditions. This is a mixed hardening model, where the isotropic part of hardening is based on the coaxial flow theory of plasticity, while the kinematic part is based on a modified Prager's hardening rule.

Table 8.3.1 Influence of grain size on shear-band inclination angle (Vardoulakis, 1977)

Test #	$d_{50\%}$ (mm)	n_0 (—)	ϕ_B (°)	θ_E (°)	θ_C (°)	
XV1.24	0.33	0.356	47.5	64.0	68.75	medium grained with round grains
VV1.08	0.33	0.355	47.6	64.0	68.80	medium grained with round grains
VV1.20	0.20	0.425	46.0	66.0	68.00	fine grained with round grains
VV1.21	0.20	0.384	47.4	70.6	68.70	fine grained with round grains
XV1.25	0.20	0.443	51.9	68.3	70.95	fine grained with angular grains
XV1.26	0.20	0.440	52.8	67.2	71.40	fine grained with angular grains

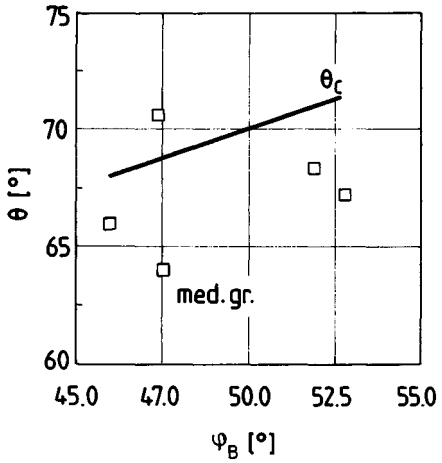

Figure 8.3.9 Experimental results on fine-grained sands by Vardoulakis (1977) and their relation to Coulomb's solution.

For simplicity, a 2D model is presented here since 3D models can be easily constructed following standard definitions of yield and potential functions which include the effect of the third stress invariant; cf. section 6.3.

In accordance with the kinematic hardening rule suggested by Prager (1956), the coaxial plastic deformation is associated with a yield function of the form

$$F = F(\tau_{\alpha\beta}, \psi) = F(\sigma_{\alpha\beta} - \alpha_{\alpha\beta}, \psi) \tag{8.4.1}$$

where ψ is the hardening parameter and $\tau_{\alpha\beta}$ is a 'materially effective' or 'reduced' stress. The difference between the reduced stress, $\tau_{\alpha\beta}$, and the true (equilibrium) stress, $\sigma_{\alpha\beta}$, which shifts the position of the yield surface in stress space is called 'relative' stress,

$$\alpha_{\alpha\beta} = \sigma_{\alpha\beta} - \tau_{\alpha\beta} \tag{8.4.2}$$

For the reduced stress $\tau_{\alpha\beta}$ the deviatoric stress $t_{\alpha\beta}$ and its intensity $\bar{\tau}$ are defined, respectively

$$\tau_{\alpha\beta} = t_{\alpha\beta} + \tfrac{1}{2}\tau_{\gamma\gamma}\delta_{\alpha\beta};\ \bar{\tau} = (\tfrac{1}{2}t_{\alpha\beta}t_{\alpha\beta})^{\frac{1}{2}} \tag{8.4.3}$$

The rate of deformation tensor is decomposed into an elastic and a plastic part

$$D_{\alpha\beta} = D^{\mathrm{e}}_{\alpha\beta} + D^{\mathrm{p}}_{\alpha\beta} \tag{8.4.4}$$

The elastic part is related to the Jaumann stress rate of the Cauchy stress by a Hooke type elasticity law

$$\mathring{\sigma}_{\alpha\beta} = L^{\mathrm{e}}_{\alpha\beta\gamma\delta} D^{\mathrm{e}}_{\gamma\delta} \tag{8.4.5}$$

$$L^{\mathrm{e}}_{\alpha\beta\gamma\delta} = G\left[\frac{2\nu}{1-2\nu}\delta_{\alpha\beta}\delta_{\gamma\delta} + \delta_{\alpha\gamma}\delta_{\beta\delta} + \delta_{\alpha\delta}\delta_{\beta\gamma}\right] \tag{8.4.6}$$

The plastic rate of deformation is further split into two parts, a part coaxial to the reduced stress $\tau_{\alpha\beta}$ and another normal to it

$$D^{\mathrm{p}}_{\alpha\beta} = D^{\mathrm{pc}}_{\alpha\beta} + D^{\mathrm{pn}}_{\alpha\beta} \tag{8.4.7}$$

In accordance with ordinary flow theory, the coaxial part of the plastic deformation is expressed by a (non-associated) flow rule as

$$D^{\mathrm{pc}}_{\alpha\beta} = \frac{\partial Q}{\partial \tau_{\alpha\beta}}\dot{\psi} \tag{8.4.8}$$

where $Q = Q(\tau_{\alpha\beta}, \psi)$ is the plastic potential function and the scalar function $\dot{\psi}$ is the rate of the hardening parameter ψ The normal plastic rate of deformation is expressed by a non-coaxial flow rule in the form

$$D^{\mathrm{pn}}_{\alpha\beta} = \frac{1}{h_1}\bar{n}_{\alpha\beta} \tag{8.4.9}$$

where h_1 is the rate of hardening in the normal to the $\tau_{\alpha\beta}$ direction. The tensor $\bar{n}_{\alpha\beta}$ is assumed to be purely deviatoric

$$\bar{n}_{\alpha\beta} = \dot{t}_{\alpha\beta} - \bar{m}_{\gamma\delta}\dot{t}_{\gamma\delta}\bar{m}_{\alpha\beta};\ \bar{m}_{\alpha\beta} = t_{\alpha\beta}/(\sqrt{2}\bar{\tau}) \tag{8.4.10}$$

The non-coaxial plasticity model is made complete by consideration of an evolution law for the relative stress,

$$\mathring{\alpha}_{\alpha\beta} = c(\psi) D^{\mathrm{pn}}_{\alpha\beta} \tag{8.4.11}$$

These assumptions define a kinematic-type hypoplastic model. According to Mróz (1973) in kinematic plasticity the local dissipation is given in terms of the materially effective stress, which in turn is called dissipative or active stress, and of the plastic deformation rate:

$$\begin{aligned}\rho\theta\eta_{\mathrm{loc}} &= (\sigma_{\alpha\beta} - \alpha_{\alpha\beta})D^{\mathrm{p}}_{\alpha\beta} = \tau_{\alpha\beta}D^{\mathrm{p}}_{\alpha\beta} \\ &= \tau_{\alpha\beta}(D^{\mathrm{pc}}_{\alpha\beta} + D^{\mathrm{pn}}_{\alpha\beta}) = \tau_{\alpha\beta}D^{\mathrm{pc}}_{\alpha\beta} \geqslant 0\end{aligned} \tag{8.4.12}$$

(cf. section 2.3.5). Accordingly, only the plastic-parallel deformation rate contributes to the local dissipation, whereas the plastic-normal deformation rate is neutral. It is emphasized that the normal (neutral) deformation rate $D^{\mathrm{pn}}_{\alpha\beta}$ is irreversible as in the original theory of Rudnicki and Rice (1975) in contrast with the deformation theory of Vardoulakis and Sulem (1993), where $D^{\mathrm{pn}}_{\alpha\beta}$ is part of the elastic deformation rate.

For a Mohr-Coulomb, friction isotropic hardening model, the yield function and plastic potential are written as

$$F = \bar{\tau} + \mu\sigma;\ Q = \bar{\tau} + \beta\sigma \tag{8.4.13}$$

where $\sigma = \tau_{\alpha\alpha}/2 = \sigma_{\alpha\alpha}/2$, is the mean (in plane) normal stress. From the yield and plastic potential functions 8.4.13, $\mu = \mu(\psi)$ and $\beta = \beta(\psi)$, are identified as the mobilized friction and dilatancy functions, respectively. Moreover, $\dot{\psi}$ is equal to the deviatoric intensity of the coaxial plastic deformation rate,

$$\dot{\psi} = \dot{\gamma}^{\mathrm{pc}} = (2D'^{\mathrm{pc}}_{\alpha\beta} D'^{\mathrm{pc}}_{\alpha\beta})^{\frac{1}{2}} \tag{8.4.14}$$

This formulation allows the resolution of the scalar function $\dot{\psi}$, from Prager's consistency condition, $\dot{F} = 0$, or (cf. section 6.2.1)

$$\frac{\partial F}{\partial \tau_{\alpha\beta}} \dot{\tau}_{\alpha\beta} + \frac{\partial F}{\partial \psi} \dot{\psi} = \frac{\partial F}{\partial \tau_{\alpha\beta}} (\mathring{\sigma}_{\alpha\beta} - \mathring{\alpha}_{\alpha\beta}) + \frac{\partial F}{\partial \psi} \dot{\psi} = 0 \tag{8.4.15}$$

Noting that $(\partial F/\partial \tau_{\alpha\beta})\mathring{\alpha}_{\alpha\beta} = 0$ and $(\partial F/\partial \tau_{\alpha\beta}) L^{\mathrm{e}}_{\alpha\beta\gamma\delta} D^{\mathrm{pn}}_{\gamma\delta} = 0$, because $\mathring{\alpha}_{\alpha\beta}$ and $D^{\mathrm{pn}}_{\alpha\beta}$ are both orthogonal to $\tau_{\alpha\beta}$, $\dot{\psi}$, can be solved from equation 8.4.15 as

$$\dot{\psi} = \frac{\langle 1 \rangle}{H} \frac{\partial F}{\partial \tau_{\alpha\beta}} L^{\mathrm{e}}_{\alpha\beta\gamma\delta} D_{\gamma\delta} \tag{8.4.16}$$

where

$$H = \frac{\partial F}{\partial \tau_{\alpha\beta}} L^{\mathrm{e}}_{\alpha\beta\gamma\delta} \frac{\partial Q}{\partial \tau_{\gamma\delta}} - \frac{\partial F}{\partial \mu} h_t;\ h_t = \frac{\mathrm{d}\mu}{\mathrm{d}\psi} \tag{5.4.17}$$

and the following definition of the switch function <1>, expressing the loading criterion for the coaxial plastic deformation rate:

$$\langle 1 \rangle = \begin{cases} 1 & \text{if } F = 0 \text{ and } (\partial F/\partial \tau_{\alpha\beta}) L^{\mathrm{e}}_{\alpha\beta\gamma\delta} D_{\gamma\delta} > 0 \\ 0 & \text{if } F < 0 \text{ or } \{F = 0 \text{ and } (\partial F/\partial \tau_{\alpha\beta}) L^{\mathrm{e}}_{\alpha\beta\gamma\delta} D_{\gamma\delta} \leqslant 0\} \end{cases} \tag{8.4.18}$$

The plastic coaxial deformation rate can now be determined from the flow rule 8.4.8 as

$$D^{\mathrm{pc}}_{\alpha\beta} = \frac{\langle 1 \rangle}{H} \frac{\partial Q}{\partial \tau_{\alpha\beta}} \frac{\partial F}{\partial \tau_{\mu\nu}} L^{\mathrm{e}}_{\mu\nu\gamma\delta} D_{\gamma\delta} \tag{8.4.19}$$

From equation 8.4.9 and with the help of equations 8.4.2 and 8.4.11, the normal deformation rate can be written as

$$D^{\mathrm{pn}}_{\alpha\beta} = \frac{1}{h_1} N_{\alpha\beta\gamma\delta} \dot{t}_{\gamma\delta} = \frac{1}{c + h_1} N_{\alpha\beta\gamma\delta} \dot{\sigma}_{\gamma\delta} \tag{8.4.20}$$

where

$$N_{\alpha\beta\gamma\delta} = \frac{1}{2} \left[\delta_{\alpha\gamma}\delta_{\beta\delta} + \delta_{\alpha\delta}\delta_{\beta\gamma} - \delta_{\alpha\beta}\delta_{\gamma\delta} - \frac{t_{\alpha\beta} t_{\gamma\delta}}{\bar{\tau}^2} \right] \tag{8.4.21}$$

Table 8.4.1 Experimental and theoretical results on shear-band formation in a biaxial compression test on fine grained Dutch dune sand. Coaxial versus non-coaxial modeling (σ_c = 294.3 kPa)

Result	$\overset{*}{\xi}$	γ_B	h_B	ϕ_B	ψ_B	θ_B
Experiment		0.06	0.008	44.2°	16.6°	62.5°
Theory						
coaxial	1.0	0.04	0.025	43.4°	16.0°	59.0°
non-coaxial	0.3	0.05	0.014	43.8°	16.3°	59.4°
	0.1	0.06	0.008	44.3°	16.7°	58.7°

From equations 8.4.4 to 8.4.8 and 8.4.20, $D^{pn}_{\alpha\beta}$ can be expressed in terms of the total deformation rate $D_{\alpha\beta}$ as,

$$D^{pn}_{\alpha\beta} = \frac{1}{2G + c + h_1} N_{\alpha\beta\mu\nu} L^{e}_{\mu\nu\gamma\delta} D_{\gamma\delta} \tag{8.4.22}$$

resulting finally in the following expression for the total plastic deformation rate

$$D^{p}_{\alpha\beta} = \left[\frac{\langle 1 \rangle}{H} \frac{\partial Q}{\partial \tau_{\alpha\beta}} \frac{\partial F}{\partial \tau_{\mu\nu}} + \frac{1}{2G + c + h_1} N_{\alpha\beta\mu\nu} \right] L^{e}_{\mu\nu\gamma\delta} D_{\gamma\delta} \tag{8.4.23}$$

The stress rate can then be determined from equation 8.4.5 using equations 8.4.4 and 8.4.23

$$\mathring{\sigma}_{\alpha\beta} = L^{ep}_{\alpha\beta\gamma\delta} D_{\gamma\delta} \tag{8.4.24}$$

$$L^{ep}_{\alpha\beta\gamma\delta} = L^{e}_{\alpha\beta\gamma\delta} - L^{p}_{\alpha\beta\gamma\delta} \tag{8.4.25}$$

$$L^{p}_{\alpha\beta\gamma\delta} = L^{e}_{\alpha\beta\mu\nu} \left[\frac{\langle 1 \rangle}{H} \frac{\partial Q}{\partial \tau_{\mu\nu}} \frac{\partial F}{\partial \tau_{\kappa\lambda}} + \frac{1}{2G + c + h_1} N_{\mu\nu\kappa\lambda} \right] L^{e}_{\kappa\lambda\gamma\delta} \tag{8.4.26}$$

It can be seen from equation 8.4.26 that the non-coaxial modification of ordinary coaxial flow theory of plasticity results in an additional term in the plastic stiffness tensor, which expresses the non-coaxial character of the model.

In summary, we remark that such a model is a mixed-hardening material model that incorporates an isotropic hardening rule for the coaxial plastic deformation rate and a kinematic hardening rule for the non-coaxial plastic deformation rate. As a consequence of the non-coaxial flow rule 8.4.9, normal plastic deformation is generated only during principal stress rotations. For loading paths without principal stress rotations, only coaxial plastic deformation is generated and the model's response reduces to the response of the isotropic hardening model of ordinary coaxial flow theory. Such a response is in accord with the experimental evidence on non-coaxiality in sands (Gutierez *et al.,* 1991).

This constitutive model requires the specification of the material parameters and functions associated with the isotropic and the kinematic part of hardening. The fact that the model's response reduces to the response of the coaxial flow theory, allows the

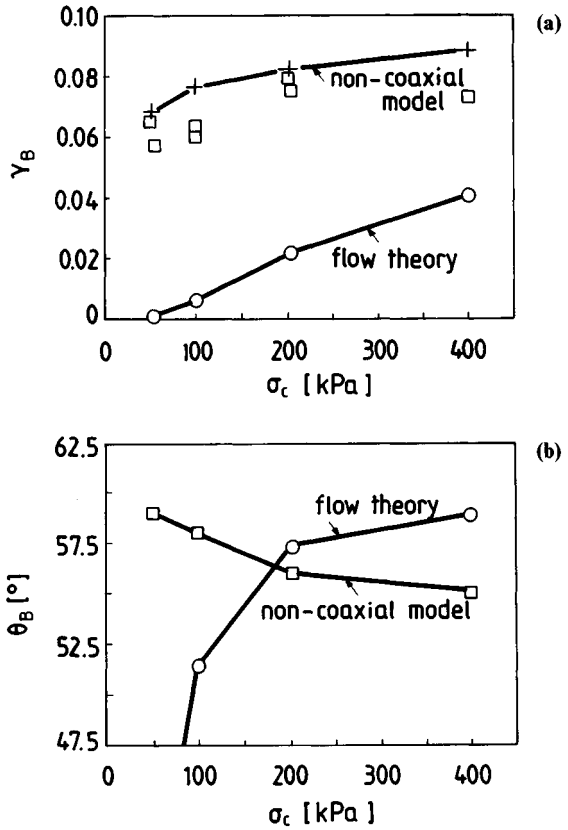

Figure 8.4.1 Influence of confining pressure for dense Ottawa sand. Experiment versus non-coaxial model: (a) shear strain intensity at shear banding γ_B; (b) shear-band inclination angle θ_B (Papamichos *et al.*, 1992).

determination of the isotropic hardening functions $\mu = \mu(\dot{\gamma}^{pc})$ and $\beta = \beta(\dot{\gamma}^{pc})$, from biaxial plane-strain test data or indirectly from triaxial test data. The kinematic part involves the hardening rate h_1 and parameter c, whose identification requires tests where principal stress axes rotate, e.g. the hollow-cylinder torsion test (cf. Ishihara and Towhata, 1983). Alternatively, such a model may be applied in shear-band predictions and the non-observable (in ordinary tests) parameters may be back-calibrated for a best fit. Such a procedure was first suggested by Vardoulakis (1980) and later by Hammad (1991).

As already mentioned above in section 8.3.2, the result of a shear-band bifurcation analysis depends sensitively on the shear modulus G_* for shearing parallel to the principal axes of initial stress; cf. equation 8.3.11. With

$$G_* = \overset{*}{\xi} G \tag{8.4.27}$$

the result depends on the non-coaxiality parameter

$$\overset{*}{\xi} = \frac{c + h_1}{2G + c + h_1} \tag{8.4.28}$$

By an appropriate selection of the non-coaxiality parameter $\overset{*}{\xi}$ the error in predicting shear banding can be optimized (for example, it can be the same for both γ_B and $\tan\theta_B$). For example, for the experiment discussed in section 8.2.2, Table 8.4.1 summarizes some results of such a parameter study, which clearly the stabilizing effect of non-coaxiality. The non-coaxiality parameter $\overset{*}{\xi}$ is found to depend on the confining pressure, reflecting the pressure sensitivity of the non-coaxial model. Figure 8.4.1 from Papamichos *et al.* (1992) shows that Han's experimental results concerning both γ_B and θ_B over a range of confining pressures are reproduced for appropriate selection of $\overset{*}{\xi} = \overset{*}{\xi}(\sigma_c)$.

As already mentioned, the above non-coaxial plasticity model as well as a more general plasticity model based on a flow rule for $D^{pn}_{\alpha\beta}$ of the type of equation 8.3.5, fall in the category of incrementally non-linear plasticity models or hypoplasticity models. Bifurcation analyses on the basis of such rate-independent, non-linear rate-type constitutive equations have been mostly carried out by two research groups in Germany and France, led by Kolymbas and Desrues, respectively. For further reading in this area of research the reader should refer to the papers by Kolymbas (1981) and his treatise of 1988, and to the papers by Desrues and Chambon (1989) and Loret (1987).

Remark on hypoplastic flow rules. The hypoplastic flow rules 8.3.5 and 8.3.16 can be combined into a single one, which combines both stress-induced anisotropy and non-coaxiality

$$D^{p'}_{\alpha\beta} = \frac{1}{2Gh}\left[A + \frac{h}{h_2}N\right]m_{\alpha\beta} + \frac{1}{2Gh_1}n_{\alpha\beta}$$

The effect of non-coaxiality is given by the parameter $\overset{*}{\xi}$, defined above through equation 8.4.28, whereas the effect of anisotropy by the parameter,

$$\hat{\xi} = h/h_2$$

For $\overset{*}{\xi} = 1$ and $\hat{\xi}$, flow theory is retrieved. Parameter studies have shown

the following influence of $\overset{*}{\xi}$ and $\hat{\xi}$ on shear banding: As $\overset{*}{\xi}$ decreases from 1 to 0, γ^p_B while θ_B first increases and then decreases. The direct effect of decreasing $\overset{*}{\xi}$ on θ_B is decrease, but since at the same time γ^p_B also increases one has as result non-monotonous variation of θ_B. Increase of the anisotropy parameter $\hat{\xi}$, on the other hand, in a decrease in γ^p_B and an increase in θ_B. The combined effect of $\overset{*}{\xi}$ and $\hat{\xi}$ can be used to match exactly experimental results on both γ^p_B and θ_B (Vardoulakis and Graf, 1985).

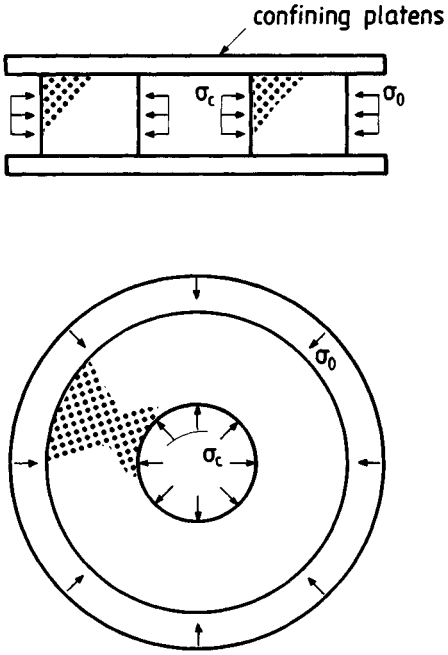

Figure 8.5.1 Principle of the thick-walled cylinder inflation test in plane strain; σ_c, σ_0 internal and external confining pressure.

8.5
Localization in inhomogeneous stress field

8.5.1
The cavity inflation test

In this section we discuss a simple test problem for investigating equilibrium bifurcation in non-uniform stress and strain conditions. This is the thick-walled cylinder inflation experiment, where a thick-walled cylinder is inflated in plane strain, with cavity volume control under constant external pressure and lubricated ends (Figure 8.5.1; Alsiny, 1992; Alsiny *et al.,* 1992). A series of tests was performed on sand specimens of aspect ratio 1/10. The tested material was a dense, poorly graded, coarse and fine Ottawa sand (Figure 8.5.2). From biaxial tests the material constants and functions were determined independently and the results are depicted in Figure 8.5.3 (Han, 1991). The shear modulus and Poisson ratio for the coarse (fine) sand were estimated to $G = 75\,\text{MPa}$ $(G = 110\,\text{MPa})$ and $\nu = 0.2$ $(\nu = 0.1)$ respectively. Finally, Figure 8.5.4 summarizes the measured dependence of the shear-band orientation angle θ_B on the confining pressure in biaxial compression tests.

In the thick-walled cylinder inflation experiments and prior to bifurcation, the stress and strain non-homogeneity is one-dimensional. Figure 8.5.5 shows the measured

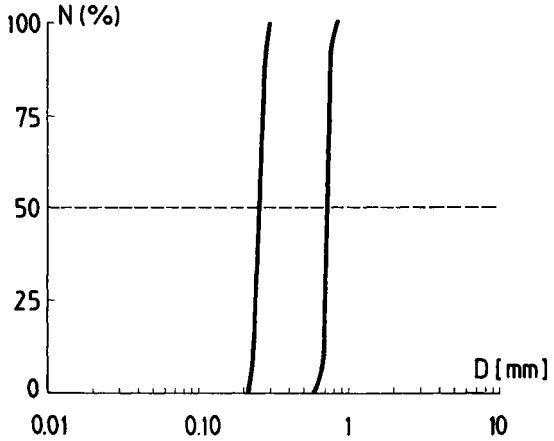

Figure 8.5.2 Grain-size distribution for coarse and fine Ottawa sand.

cavity pressure versus cavity volume change curve, demonstrating, at large strains, the global softening behavior of the thick-walled cylinder under inflation. These tests have shown that both diffuse and localized deformation modes occur. The diffuse deformation mode manifests itself as a cavity surface rumpling, with a dominant wave number of $m = 8$ to 9. The localized deformation mode is seen as a curvilinear shear band extending from the cavity to the outer surface of the specimen (Figure 8.5.6). The measurement techniques used in the tests did not allow accurately detecting either the onset or growth of the deformation modes. It seems, however, that shear banding takes place slightly beyond the peak in the cavity pressure versus cavity volume curve, and is preceded by a diffuse surface rumpling deformation mode.

The plane strain inflation of the thick-walled cylinder is analyzed in an *(r, θ)* natural polar coordinate system, as shown in Figure 8.5.7. Prior to bifurcation, the thick-walled cylinder under internal and external pressure undergoes a uniform expansion in radial direction which is determined by the amount of displacement at the cavity wall (Figure 8.5.8a), i.e. at any time stem Δt the deformation of the material surrounding the cavity is described by an incremental radial displacement field $\Delta\mathring{u}_r$, which in turn constitutes the *trivial* deformation mode. For the determination of the trivial solution, and for a given set of incremental constitutive equations, one must first integrate the equilibrium equation

$$\frac{d\Delta\sigma_r}{dr} + \frac{1}{r}(\Delta\sigma_r - \Delta\sigma_\theta) = 0 \tag{8.5.1}$$

In general, this has to be done numerically, utilizing for example the ring model of Figure 8.5.9 and the transfer matrix technique (see section 4.2.2 and Vardoulakis and Sulem, 1993). In this case, the space surrounding the cavity is discretized in N rings, and for the ith ring, continued equilibrium leads to an Euler differential for the trivial deformation mode

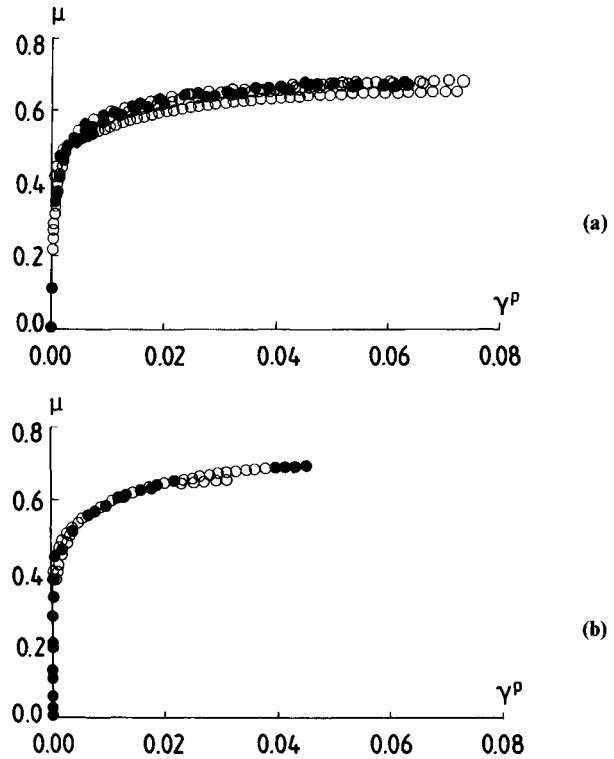

Figure 8.5.3 Mobilized friction coefficient versus plastic shear strain for (a) coarse sand, and (b) fine sand (σ_0=200 kPa; Han, 1991).

$$c_{11}\frac{\mathrm{d}^2\Delta\mathring{u}_r}{\mathrm{d}r^2}+(c_{11}+c_{12}-c_{21})\frac{1}{r}\frac{\mathrm{d}\Delta\mathring{u}_r}{\mathrm{d}r}-c_{22}\frac{\Delta\mathring{u}_r}{r^2}=0 \tag{8.5.2}$$

where the coefficients $c_{\alpha\beta}$ are corresponding non-dimensional principal components of the stiffness tensor of, say, the 2D upper-bound linear comparison solid, given by equations 8.2.2 and 8.2.3, i.e.

$$c_{11}=L^{\mathrm{u}}_{rrrr}/G,\ c_{12}=L^{\mathrm{u}}_{rr\theta\theta}/G \text{ etc.} \tag{8.5.3}$$

Equation 8.5.2 can be integrated in each ring and the matrix transfer technique leads to elimination of the intermediate integration constants and to the evaluation of the initial stress field at any loading step. Figure 8.5.10 shows the computed distribution of the radial and circumferential stresses as well as the corresponding stress path which is followed by the material points along the radius: a point at the cavity surface follows the entire stress path whereas points deeper inside the cylinder follow only a smaller part of it.

If we want to apply Ortiz's model of progressive failure, the thick-walled cylinder is again regarded as a collection of separate rings, with the stresses known from the

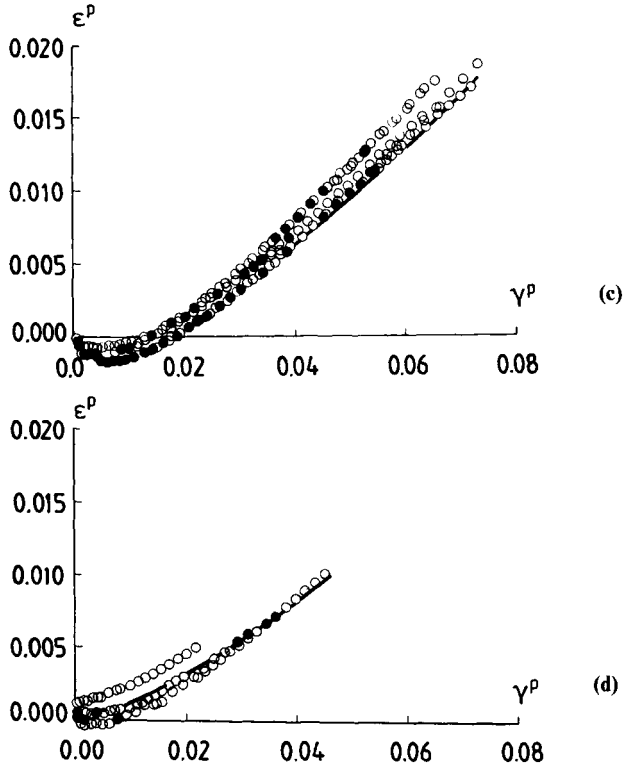

Figure 8.5.3 (continued) Mobilized dilatancy coefficient versus plastic shear strain for (c) coarse sand and (d) fine sand (σ_0=200 kPa; Han, 1991).

axisymmetric solution. It is then possible to determine the local shear-band inclination angle in each ring. The dashed lines in Figure 8.5.6 show the predicted shape of the shear bands at the peak differential cavity pressure recorded in tests. For all the confining pressure applied, the shape of the predicted shear bands differs markedly from that measured in the tests. Finally, a comparison may be done between the recorded shear-band shapes with those resulting from the classical formulae of Coulomb and Roscoe; equations 8.2.17 and 8.2.18. The results, shown in Figure 8.5.6, as solid lines, validate Coulomb's prediction.

According to the local shear-band criterion of bifurcation theory, a shear band has to develop in the region between $(SB)_1$ and $(SB)_0$ points of Figure 8.5.5, so that if the experiment is terminated between these two points one should observe a partial shear band. Since a shear band was observed through X-rays only in the softening regime in the differential cavity pressure versus cavity volume curve, this means that a progressive failure model based on local bifurcation criterion cannot be applied in this non-homogeneous boundary-value problem. It must be remembered, however, that local bifurcation conditions only define the onset of shear banding, and strains must localize significantly before the shear band becomes visible. In order to explain this discrepancy,

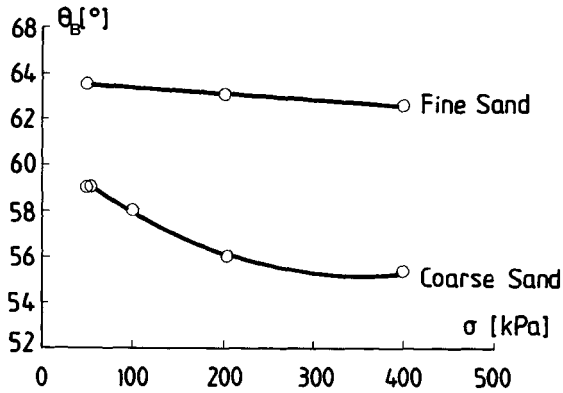

Figure 8.5.4 Shear-band inclination angle θ_B versus confining pressure from biaxial tests; after Han (1991).

we resort to the numerical bifurcation and post bifurcation analysis of Papanastasiou and Vardoulakis (1992). In this work, the shear band in a cavity closure problem emerges naturally from a symmetry-breaking solution in the post-peak regime, when the global stiffness matrix becomes singular (see section 3.3.4).

8.5.2
Global bifurcation analysis of the cavity inflation test

Diffuse bifurcation of the thick-walled cylinder is analyzed by investigating the possibility of warping of the cavity surface (Figure 8.5.8b). The components of the non-trivial displacement field for warping deformation mode are given in terms of two unknown amplitude functions of the dimensionless radius $\rho = r/r_c$.

$$\begin{aligned} \Delta\hat{u}_r &= U(\rho)\cos(m\theta) \\ \Delta\hat{u}_\theta &= V(\rho)\sin(m\theta) \end{aligned} \tag{8.5.4}$$

where m is the wave number of the bifurcation mode (m=1,2,...). With increasing m the wavelength of the corresponding warping modes decreases.

We recall that for non-axisymmetric bifurcations, the physical components of the infinitesimal displacement gradient in cylindrical coordinates are:

$$\{\Delta u_{\alpha|\beta}\} = \begin{pmatrix} \dfrac{\partial \Delta u_r}{\partial \rho} & \dfrac{1}{\rho}\dfrac{\partial \Delta u_r}{\partial \theta} - \dfrac{\Delta u_\theta}{\rho} \\ \dfrac{\partial \Delta u_\theta}{\partial \rho} & \dfrac{1}{\rho}\dfrac{\partial \Delta u_\theta}{\partial \theta} + \dfrac{\Delta u_r}{\rho} \end{pmatrix} \tag{8.5.5}$$

The equations of continued equilibrium for the considered infinitesimal transition can be written as

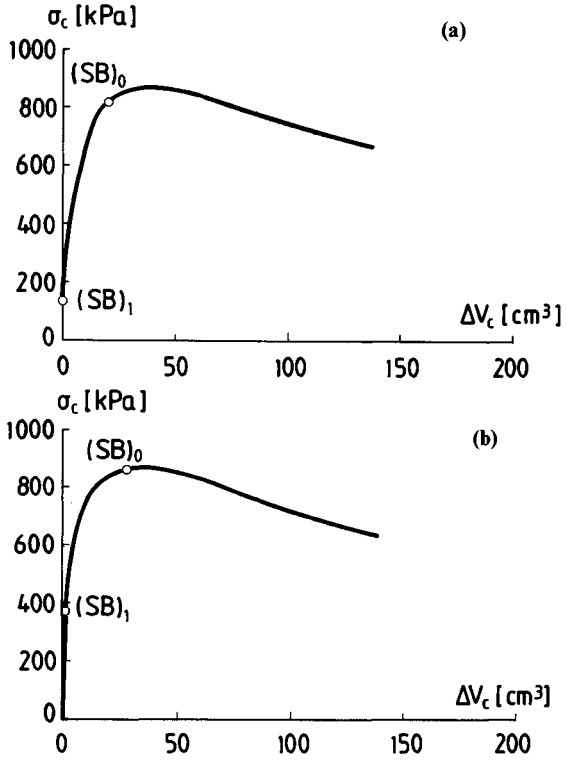

Figure 8.5.5 Measured cavity pressure versus cavity volume-change curves for: (a) coarse and (b) fine sand (σ_0=200 kPa; Alsiny *et al.,* 1992).

$$\frac{\partial \Delta\sigma_{rr}}{\partial \rho} + \frac{\partial \Delta\sigma_{r\theta}}{\partial \theta} + \frac{1}{\rho}(\Delta\sigma_{rr} - \Delta\sigma_{\theta\theta}) = 0$$
$$\frac{\partial \Delta\sigma_{r\theta}}{\partial \rho} + \frac{1}{\rho}\frac{\partial \Delta\sigma_{\theta\theta}}{\partial \theta} + \frac{2}{\rho}\Delta\sigma_{r\theta} = 0 \qquad (8.5.6)$$

The components of the incremental strains and accordingly the incremental stresses can be expressed in terms of the amplitude functions *U(ρ)* and *V(ρ)*. Substituting these expressions into the continued equilibrium equations 8.5.6, we get the following system of differential equations

$$a_1 U'' + a_2 \rho^{-1} U' + a_3 \rho^{-2} U + a_4 \rho^{-1} V' + a_5 \rho^{-2} V = 0$$
$$b_1 V'' + b_2 \rho^{-1} V' + b_3 \rho^{-2} V + b_4 \rho^{-1} U' + b_5 \rho^{-2} U = 0$$

where $(\cdot)' \equiv \mathrm{d}/\mathrm{d}\rho$, and the coefficients a_i and b_i are known functions of the constitutive parameters and of the modal number m

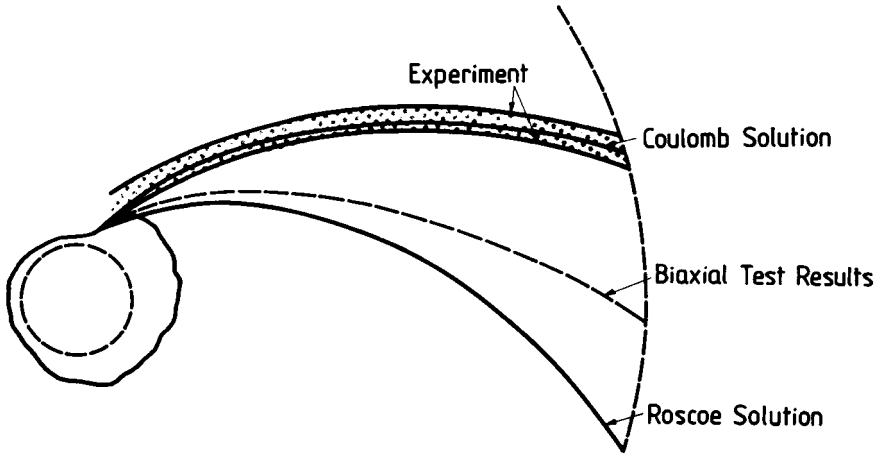

Figure 8.5.6 Experimentally observed and theoretically predicted shear bands in coarse sand with σ_0=200 kPa (Alsiny *et al.,* 1992).

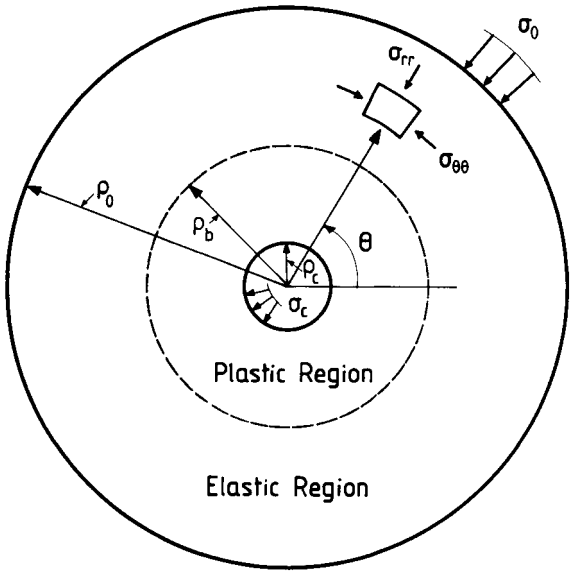

Figure 8.5.7 Transverse section of a thick-walled cylinder subjected to cavity and external confining pressures.

$$
\begin{aligned}
a_1 &= c_{11} & b_1 &= 1 \\
a_2 &= c_{12} + c_{11} - c_{21} & b_2 &= 1 \\
a_3 &= -(m^2 + c_{22}) & b_3 &= -(m^2 c_{22} + 1) \\
a_4 &= c_{12} + 1 & b_4 &= -m(1 - c_{21}) \\
a_5 &= -(1 + c_{22}) & b_5 &= -m(1 - c_{22})
\end{aligned}
\tag{8.5.8}
$$

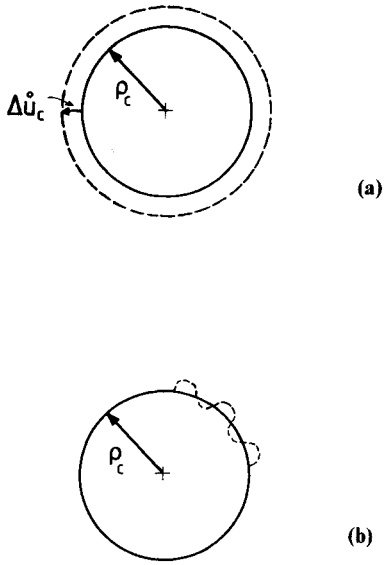

Figure 8.5.8 Cavity deformation modes: (a) uniform cavity expansion (trivial deformation mode); (b) warping of cavity wall (bifurcation mode).

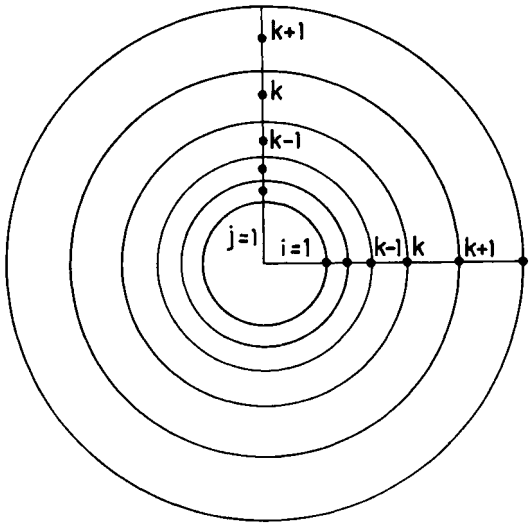

Figure 8.5.9 Discretization of domain—the ring model.

The general solution of the above system of Euler differential equations 8.5.7 is

$$U(\rho) = \sum_{i=1}^{4} A_i U_i;\ V(\rho) = \sum_{i=1}^{4} A_i V_i \tag{8.5.9}$$

where A_i are the integration constants, and

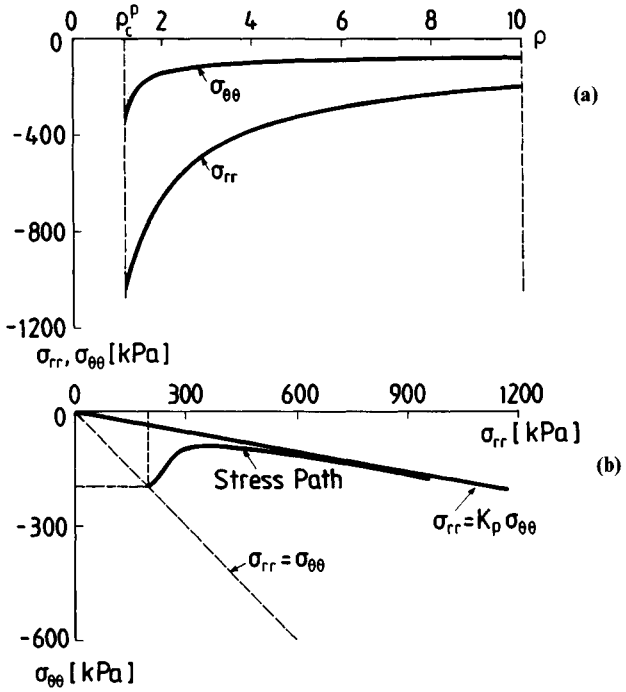

Figure 8.5.10 (a) Radial distribution of radial and circumferential stresses; (b) stress path ($\sigma 0$=200 kPa; Alsiny, 1992).

$$U_i = \exp\{\beta_i \ln(\rho)\};\ V_i = r_i U_i \tag{8.5.10}$$

are the basis functions. The exponents β_i are roots of the characteristic equation

$$c_1\beta^4 + c_2\beta^3 + c_3\beta^2 + c_4\beta + c_5 = 0 \tag{8.5.11}$$

where

$$\begin{aligned} c_1 &= a_1 b_1 \\ c_2 &= a_1(b_2 - 2b_1) + a_2 b_1 \\ c_3 &= a_1(b_1 - b_2 + b_3) + a_2(b_2 - b_1) + a_3 b_1 - a_4 b_4 \\ c_4 &= -a_1 b_3 + a_2 b_3 + a_3(b_2 - b_1) - a_4 b_5 - a_5 b_4 \\ c_5 &= a_3 b_3 - a_5 b_5 \end{aligned} \tag{8.5.12}$$

and the proportionality factor is given by the following equation:

$$r_i = -(a_1\beta_i(\beta_i - 1) + a_2\beta_i + a_3)/(a_4 + a_5) \tag{8.5.13}$$

The transfer matrix technique is utilized to formulate the bifurcation condition as explained in section 4.2.2, resulting in a singularity condition for the global system matrix

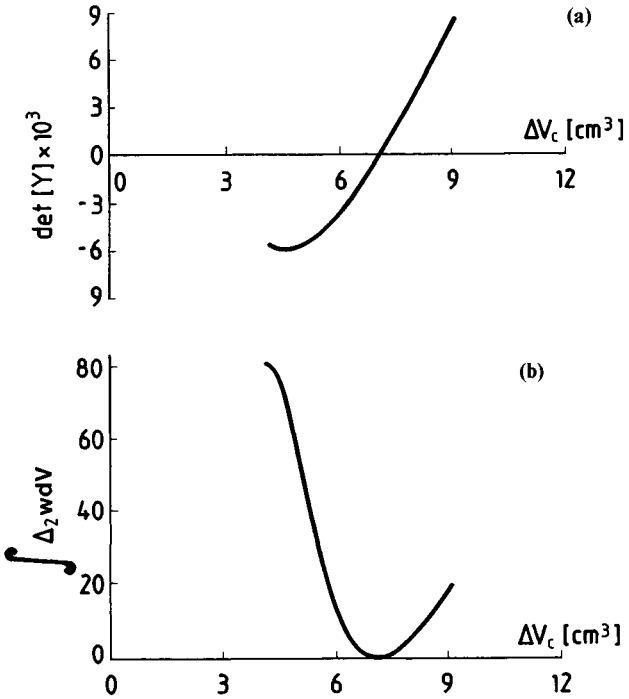

Figure 8.5.11 (a) System determinant. (b) Second-order work versus cavity-volume change (σ_0=200 kPa; Alsiny, 1992).

$$\det([Y]) = 0 \tag{8.5.14}$$

Global bifurcation is detected by monitoring the sign, and the magnitude of the determinant of the system matrix, *[Y]*, during continued loading along the primary solution branch, as shown in Figure 8.5.1 l(a) from Alsiny (1992). Alternatively, loss of uniqueness is detected as soon as the global second-order work for the considered bifurcation mode vanishes,

$$\int_V \Delta_2 w \, dV = \int_V \Delta\sigma_{ij} \Delta\varepsilon_{ij} \, dV = 0 \tag{8.5.15}$$

as shown in Figure 8.5.11(b) (see section 3.3.5).

The numerical results show that for the smallest wave number, min*(m)* global bifurcation is detected in the hardening regime for coarse-grained sand and in the softening regime for fine-grained sand both close to the peak of the differential cavity pressure-cavity volume curve as shown in Figures 8.5.12(a,b) from Alsiny (1992)

$$\max(m) \geqslant m \geqslant \min(m) \tag{8.5.16}$$

with max*(m)*=50 and min*(m)*=8 coarse sand, max*(m)*=25 and min*(m)*=5 for fine sand. It seems that small wavelength modes (m large) are not persistent, and are obviously 'cured' during continued inflation of the cavity, in the global hardening regime. Accordingly, shear bands seem to emerge in this test out of the large wavelength rumpling modes (*m* small) of the cavity surface, since these rumpling modes occur close to the peak, and according to the experiment are persistent in the softening regime of the global system response. These findings are easily understood if one recalls (as explained also in general terms in section 3.3.5) that failure of a local uniqueness criterion does not necessarily imply global non-uniqueness (see also Bigoni and Hueckel, 1990, 1991). However, a definite answer to this question and to the question of global shear band geometry can only be given by computer-aided post-bifurcation analysis similar to the one performed by Papanastasiou and Vardoulakis (1992) for the cavity-closure problem.

8.5.3
Progressive failure

The classical paradigm of progressive failure in soil mechanics is the problem of limiting 'earth pressure' on a vertical wall. This problem was first analyzed by Charles-Augustin Coulomb in his 'Essai sur une application des règles de maximis & minimis a quelques problèmes de statique, relatifs a I'architecture' in 1773. In this section the problem of 'passive' earth pressure is considered and the experiments discussed hereafter were part of a research report by Gudehus *et al.* (1985).

In this experimental program 1*g* model experiments were performed as shown in Figure 8.5.13(a,b). The dimensions of the wall were: height $h = 20\,\mathrm{cm}$; width $b = 15\,\mathrm{cm}$, and the material behind the wall was dry, standard Karlsruhe sand with a uniform density of $\rho = 1.65\,\mathrm{g/cm^3}$. Special care was taken such that the load E on the wall is applied horizontally and that the wall itself undergoes a parallel translation with minimal tilting.

The experimental results are plotted in terms of non-dimensional quantities: the non-dimensional (passive) earth-pressure coefficient

$$K_h = \frac{E_h}{\frac{1}{2}\rho g b h^2} \tag{8.5.17}$$

and the non-dimensional horizontal displacement of the wall

$$\delta_h = u_x/h \tag{8.5.18}$$

At zero displacement the measured 'at rest' earth pressure was, $E_0 \approx 10\,\mathrm{N}$, resulting according to equation 8.5.17 in an at rest earth pressure coefficient, $K_0 \approx 0.202$. In Figure 8.5.14 the results from two tests are plotted in a (K_h, δ_h) diagram and are smoothed by a hardening-softening rational function:

$$K_h = K_0 + (c_1 - c_2\delta_h)\delta_h/(1 + c_0\delta_h) \tag{8.5.19}$$

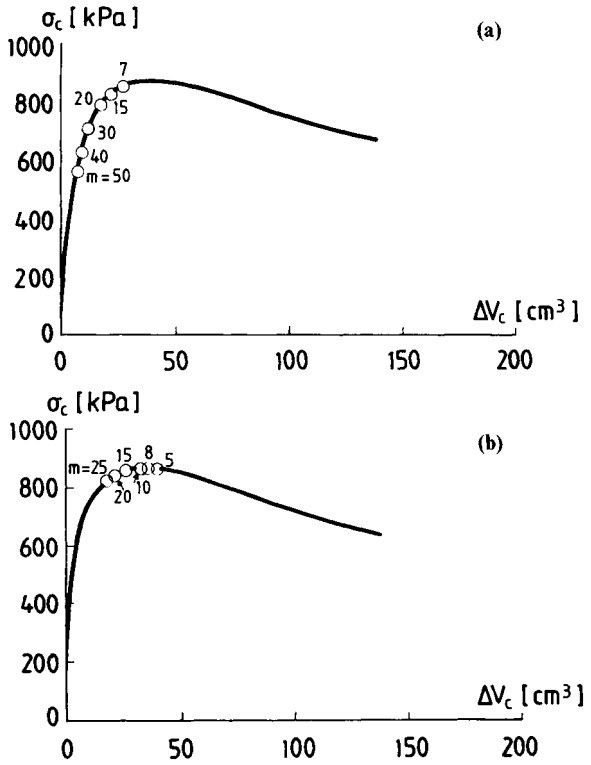

Figure 8.5.12 Theoretical predictions of global bifurcation for (a) coarse and (b) fine sand (σ_0=200 kPa; Alsiny, 1992).

with: $c_0 = 0.1760E + 3$, $c_1 = 0.1921E + 4$, $c_2 = 0.1498E + 5$. The limiting value of the earth pressure is called passive earth pressure, E_{ph}. Here E_{ph} or the corresponding passive earth pressure coefficient K_{ph} are computed from the fit 8.5.19,

$$K_{ph} = 7.4 \tag{8.5.20}$$

which occurred at horizontal wall movement of $\delta_{ph} = 2.2\%$.

In the considered experiments the evolution of porosity localizations were monitored in due course of the movement of the wall. For this purpose, X-rays were taken at regular intervals of the displacement process. It turned out that close to peak load a horizontal precursor localization formed (Figure 8.5.15a), to be followed by the dominant inclined one. More importantly, at about 3% wall displacement the horizontal localization had died out, whereas the inclined one had formed only impartially (i.e. 60% of its full length; Figure 8.5.15b). At about 4% wall displacement, in the softening regime of the load-displacement curve, one could observe a fully developed straight localization (Figure 8.5.15c). This 'failure plane' was inclined with respect to the horizontal at an angle

$$\theta_E^* \approx 25^\circ \tag{8.5.21}$$

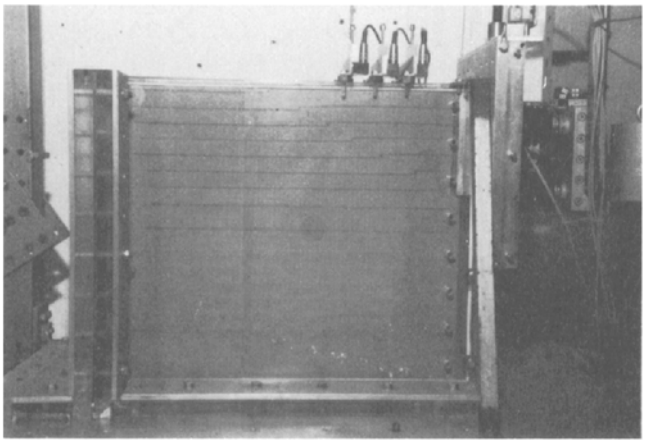

Figure 8.5.13 Experimental set-up for model earth pressure tests after Gudehus *et al.* (1985).

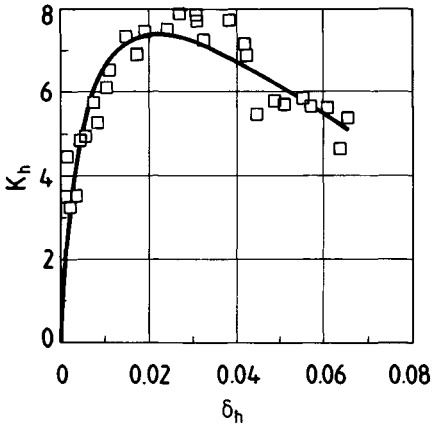

Figure 8.5.14 Passive earth-pressure coefficient versus non-dimensional horizontal wall displacement (Gudehus *et al.*, 1985).

On the other hand Coulomb's earth-pressure theory predicts the following values for the passive earth-pressure coefficient and the corresponding inclination angle of the failure plane

$$K_C = \tan^2(45° + \phi_C/2) \tag{8.5.22}$$

$$\theta_C^* = 45° - \phi_C/2 \tag{8.5.23}$$

From equations 8.5.20 and 8.5.22 follows that $\phi_C \approx 50°$, whereas from equations 8.5.21 and 8.5.23 that $\phi_C = 40°$. If one considers the fact that at peak load no fully developed failure plane was observable, this discrepancy in back-computing ϕ_c really disqualifies Coulomb's earth-pressure theory in particular and puts a question mark on limit analysis computations in general.

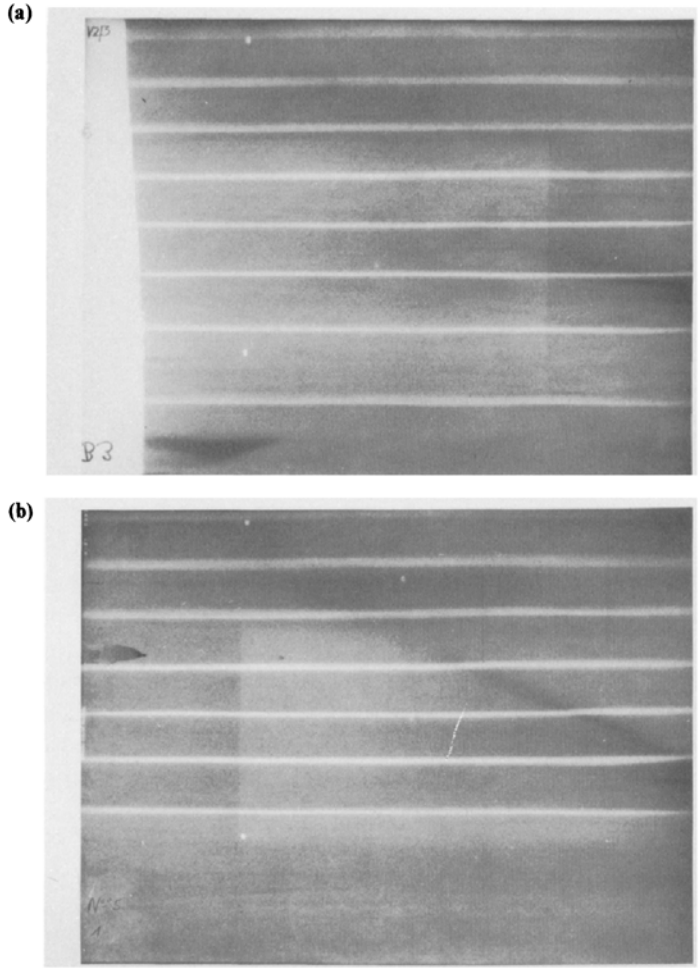

Figure 8.5.15 Evolution of porosity localizations in passive earth-pressure experiments. (a) Precursor 'horizontal' shear band at δ_h=2.5%. (b) Partially developed inclined band at δ_h=2.75% (Gudehus *et al.,* 1985).

The high value of the measured passive earth-pressure coefficient in small, 1g model tests is typical in soil mechanics literature, where it is well recognized that small model tests are always 'stronger' than large ones (Vesic 1963; de Beer 1965). This phenomenon can be related to two basic effects:

(a) *Stress-level effect.* This is the effect of confining pressure on the apparent friction angle of the material. Usually, this effect is thought to be remedied by resorting to centrifuge testing (increased **g** tests), such that the same stresses hold in similar places in the model and in the prototype.

Reliable element tests at low stresses are difficult to perform and more difficult to interpret, due to the influence of self-weight and end-platen friction (see for example

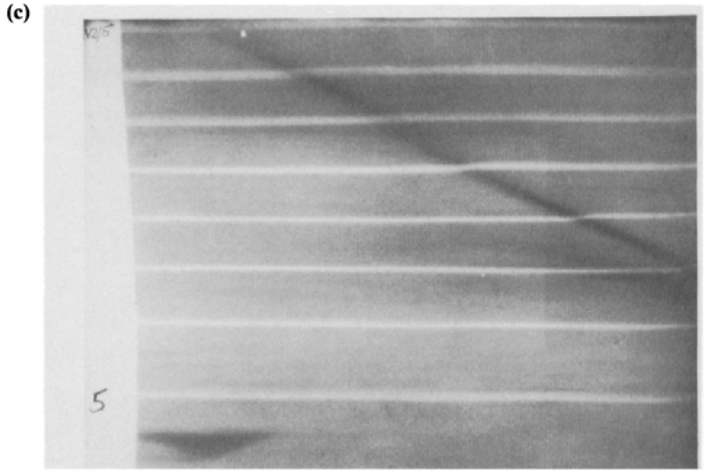

Figure 8.5.15 (continued) (c) Fully developed inclined band at δ_h= 4.2% with inclination angle δ_h= 25° (Gudehus *et al.,* 1985).

Vardoulakis and Drescher, 1985). However, there is little disagreement that at low pressures the apparent friction coefficient f increases, e.g. in a first approximation, hyperbolically with intergranular pressure,

$$\mathrm{f_C} = \mathrm{f_{C\infty}} + \frac{c}{(-p)} + \dots \tag{8.5.24}$$

Then, according to equations 6.3.14 and 6.3.15, we obtain at low intergranular pressures the following limit condition for the shear stress intensity

$$T = c + \mathrm{f_{C\infty}}(-p) \tag{8.5.25}$$

Thus, it is argued, that sand in this regime of low stresses possesses a small apparent cohesion c, due to grain interlocking and capillarity; $f_{C\infty}$ in equation 8.5.25 is then the friction coefficient at elevated pressures.

From triaxial compression tests on the same sand by Hettler and Vardoulakis (1984) it is estimated that $\mathrm{f_{C\infty}} = 0.92$ ($\phi_{C\infty} = 39°$) which is in agreement with ϕ_c from θ_C^*, equation 8.5.23. With this value, and in order to explain the discrepancy between the measured value K_{ph} and K_C from Coulomb's theory, one has to assume an apparent cohesion $c \approx 1.2\,\mathrm{kPa}$. Such a value is rather high, since it corresponds to an unrealistically large (perhaps tenfold higher) free standing height of a vertical cut of dry sand: $h_c = 4c/(\rho g h) \approx 14\,\mathrm{cm}$.

(b) *Scale effect.* As will be shown in chapters 9 and 10, the scale effect manifests itself statically in increased strength. Geometrically, the scale effect is seen in the aforementioned partial development of the shear band at peak load. Accordingly, the length ℓ of the partially developed shear band at peak load is seen as an internal length of the problem, i.e. a length determined by a material length rather than by a geometric length. The only material length of a granular medium is some effective grain diameter.

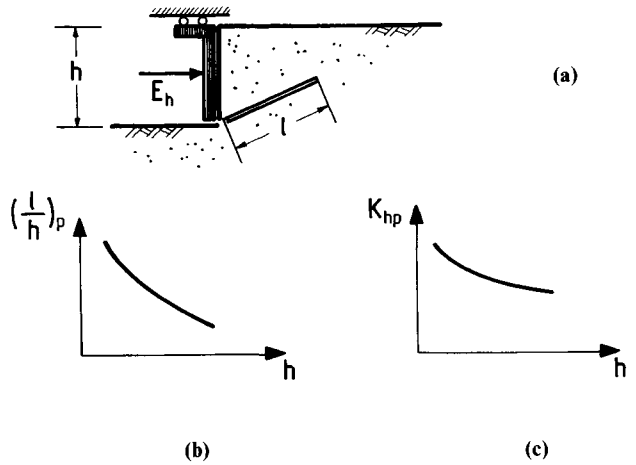

Figure 8.5.16 Progressive failure in the passive earth-pressure experiment: (a) partially developed localization; (b) geometric scale effect; (c) static scale effect.

Thus one may assume that ℓ is a function of the mean grain size d_{50} of the (considered here uniform) sand

$$\ell = \ell(d_{50}) \tag{8.5.26}$$

Under these circumstances, and irrespectively of the **g** value, a family of model tests with the same sand but different heights h of the failing vertical cut are geometrically dissimilar since the model law

$$M_\ell = d_{50}/h \tag{8.5.27}$$

is violated, resulting in a functional dependence (ℓ/h) on h, as indicated in Figure 8.5.16(b) (Graf, 1984). Accordingly, a complete theory of progressive failure should result in correction of K_{ph} due to scale effect, e.g. to a formula of the form

$$K_{ph} = K_C\{1 + f(\ell/h)\} \tag{8.5.28}$$

f(•) in 8.5.28 is seen as a monotonously increasing function, which can be determined from a family of model tests with the same sand and different geometric scale (Figure 8.5.16c). We remark that the scale effect will persist in centrifuge testing, and its consideration constitutes a necessary correction to be accounted for. Moreover, tests with artificial material of scaled-down grain size are not a solution to the problem, since, as it is well known from soil mechanics literature, important material properties depend strongly on grain size and shape; cf. differences between sands (5mm>d_{50}>0.1mm) and silts (0.1 mm>d_{50}).

In chapters 9 and 10 extensions of plasticity theory will be discussed which allow the consideration of material length properties and lead naturally to scale effect.

Literature

Textbooks and monographs

Alsiny, A. (1992). Deformation Modes in Thick-walled Cylinder Experiments on Dry Sand. PhD Thesis, University of Minnesota, 244 pp.

Desrues, J. (1984). La Localisation de la Déformation dans les Matériaux Granulaires. These de Doctorat ès Science, UMSMG & INPG, Grenoble.

Graf, B. (1984). Theoretische und experimentelle Ermittlung des Vertikaldrucks auf eingebettete Bauwerke. Dissertation, Universität Karlsruhe, Veröffentlichungen IBF, Heft Nr. 96.

Hammad, W.I. (1991). Modélisation Non linéaire et Étude Expérimentale des Bandes de Cisaillement dans les Sables. Thèse de Docteure, Université Joseph Fourier-Grenoble I.

Han, C. (1991). Localization of Deformation in Sand. PhD Thesis, University of Minnesota.

Hill, R. (1950). *Mathematical Theory of Plasticity,* Clarendon Press, Oxford.

Kolymbas, D. (1988). Eine Konstitutive Theorie für Böden und andere Körnige Stoffe. Habilitation, Universität Karlsruhe, Veröffentlichungen IBF, Heft Nr. 109.

Reiner, M. (1960). *Deformation, Strain and Flow.* H.K.Lewis, London.

Truesdell, C. and Noll, W. (1965). *Nonlinear Field Theories of Mechanics. Handbuch der Physik,* Vol. III/3, Section 30. Springer-Verlag, Berlin.

Vardoulakis, I. (1977). Scherfugenbildung in Sandkörpern als Verzweigungsproblem. Dissertation, Universität Karlsruhe, Veröffentlichungen IBF, Heft Nr. 70.

Vardoulakis, I. and Sulem, J. (1993). Application of bifurcation theory to rock mechanics. In: *Comprehensive Rock Engineering* (ed. J.A.Hudson), Vol. 1, Section 23. Pergamon Press, Oxford.

References

Alsiny, A., Vardoulakis, I. and Drescher, A. (1992). Deformation localization in cavity inflation experiments on dry sand. *Géotechnique,* **42,** 395–410.

Annin, V., Revuzhenko, A. and Shemyakin, E. (1987). Deformed solid mechanics at the Siberian branch, Academy of Sciences of the USSR. *J. Appl Mech. Tech. Physics,* **28,** 531.

Arthur, J.R.F., Dunstan, T., Al-Ani, Q.A.J. and Assadi, A. (1977). Plastic deformation and failure of granular media, *Géotechnique,* **27,** 53–74.

Bardet, J.P. (1990). A comprehensive review of strain localization in elastoplastic soils. *Computers Geotechnics,* **10,** 163–188.

Bardet, J.P. (1991). Orientation of shear bands in frictional soils. *J. Eng. Mech. ASCE,* **117,** 1466–1484.

Benallal, A., Bilardon, R. and Geymonat, G. (1989). Conditions de bifurcation a l'interieur et aux frontières pour une classe de matériaux non standards. *C.R.Acad. Sci., Paris,* **308,** série II, 893–898.

Bigoni, D. and Hueckel, T. (1990). A note on strain localization for a class of non-associative plasticity rules. *Ingenieur Archiv,* **60,** 491–499.

Bigoni, D. and Hueckel, T. (1991). Uniqueness and localization—I. Associative and non-associative plasticity. *Int. J. Solids Struct.,* **28,** 197–213.

Bigoni, D. and Zaccaria, D. (1992a). Loss of strong ellipticity in non-associative elastoplasticity. *J. Mech. Phys. Solids,* **40,** 1313–1331.

Bigoni, D. and Zaccaria, D. (1992b). Strong ellipticity of comparison solids in elastoplasticity with volumetric non-associativity. *Int. J. Solids Struct.,* **29,** 2123–2136.

Bransby, P.L. and Milligan, G.W.E. (1975). Soil deformations near cantilever sheet pile walls, *Géotechnique,* **25,** 175–195.

Budiansky, B. (1959). A reassessment of deformation theories of plasticity. *J. Appl Mech.,* **26,** 259–264.

Christoffersen, J. and Hutchinson, J.W. (1979). A class of phenomenological corner theories of plasticity. *J. Mech. Phys, Solids,* **27,** 465–487.

De Beer, E.E. (1965). The scale effect on the phenomenon of progressive rupture in cohesionless soils. *6th Int. Conf. Soil Mech. Found. Eng.,* Vol. **2,** 3/**3,** 13–17.

Desrues, J., Lanier, J. and Stutz, P. (1985), Localization of the deformation in tests on sand sample. *Eng. Fract. Mechan.,* **21,** 909–921.

Desrues, J. (1987). Naissance des bandes de cisaillement dans les milieux granulaires: Epérience et Théorie. In: *Manuel de Rhéologie des Geómatériaux* (ed. F.Darve), pp. 279–298. Presses des Ponts et Chaussées, Paris.

Desrues, J. and Chambon, R. (1989). Shear band analysis for granular materials: The question of incremental non-linearity. *Ingenieur Archiv,* **59,** 187–196.

Desrues, J. and Hammad, W. (1989). Etude expérimentale de la localisation de la deformation sur le sable: Influence de la contrainte moyenne. *12th Int. Conf. Soil Mech. Found. Eng.,* **1/9,** 31–32.

Desrues, J., Mokni, M. and Mazerolle, F. (1991). Tomodensitométrie et localisation sur les sables. *10th Eur. Conf. Soil Mech. Found. Eng.,* 61–64.

Gudehus, G., Graf, B. and Vardoulakis, I. (1985). Versuche zur Untersuchung des progressiven Enstehens der scherfuge beim passiven Erddruck. In: 2. Meilen-steinbericht mit technischem Bericht zum Forschungsprojekt 'Sicherheit von Stützbauwerken an Hängen', RG 88 322 6, IBF Universität Karlsruhe.

Gutierez, M., Ishihara, K. and Towhata, I. (1991). Flow theory for sand during rotation of principal stress direction. *Soils Foundations,* **31,** 121–132.

Han, C. and Drescher, A. (1993). Shear bands in biaxial tests on dry coarse sand. *Soils Foundations,* **33,** 118–132.

Hettler, A. and Vardoulakis, I. (1984). Behavior of dry sand tested in a large triaxial apparatus. *Géotechnique,* **34,** 183–198.

Hill, R. (1962). Acceleration waves in solids. *J. Mech. Phys. Solids,* **10,** 1–16.

Ishihara, K. and Towhata, I. (1983). Sand response to cyclic rotation of principal stress directions as induced by wave loads. *Soils Foundations,* **23,** 11–26.

Kanatani, Ken-Ichi (1982). Mechanical foundation of plastic deformation of granular materials. *IUTAM Conference on Deformation and Failure of Granular Materials,* 119–127. Balkema, Rotterdam.

Kolymbas, D. (1981). Bifurcation analysis for sand samples with a non-linear constitutive equation. *Ingenieur Archiv,* **50,** 131–140.

Kolymbas, D. (1991). An outline of plasticity. *Arch. Appl Mech.,* **61,** 143–151.

Leroy, Y. and Ortiz, M. (1989). Finite element analysis of strain localization in frictional materials. *Int. J. Num. Anal Meth. Geomech.,* **13,** 53–74.

Loret, B. (1987). Non-linéarité incrémentale et localisation des deformations: quelques remarques. *J. Mécan. Théor. Appl.,* **6,** 423–459.

Loret, B., Prévost, J.H. and Harireche, O. (1990). Loss of hyperbolicity in elastic-plastic solids with deviatoric associativity. *Eur. J. Mech. A/Solids,* **9,** 225–231.

Mandel, J. (1962). Ondes plastiques dans un milieu indéfini a trois dimensions. *J. Mécan.,* **1,** 3–30.

Mandel, J. (1964). Propagation des surfaces de discontinuite dans un milieu elasto-plastique, In: *Stress Waves in Anelastic Solids,* 331–341. Springer-Verlag, Berlin.

Molenkamp, F. (1985). Comparison of frictional material models with respect to shear band initiation. *Géotechnique,* **35,** 127–143.

Mróz, Z. (1973). Mathematical Models of Inelastic Material Behavior. University of Waterloo Press, Solid Mechanics Division.

Nakai, T. and Matsuoka, H. (1983). Shear behaviors of sand and clay under three-dimensional stress condition. *Soils Foundations,* **23,** 26–42.

Ortiz, M., Leroy, Y. and Needleman, A. (1987). A finite element method for localized failure analysis. *Comput. Meth. Appl. Mech. Eng.,* **61,** 189–194.

Palmer, A.C. and Rice, J. (1973). The growth of slip surfaces in the progressive failure of over-consolidated clay. *Proc. Roy. Soc. Lond., A,* **332,** 527–548.

Papamichos, E., Vardoulakis, I. and Han, C. (1992). Noncoaxial flow theory of plasticity: shear failure prediction in sand. In *Modern Approaches to Plasticity* (ed. D.Kolymbas), 585–598. Elsevier, Amsterdam.

Papamichos, E. and Vardoulakis, I. (1995). Effect of confining pressure in shear band formation in sand. *Géotechnique,* in press.

Papanastasiou, P. and Vardoulakis, I. (1992). Numerical treatment of progressive localization in relation to borehole stability. *Int. J. Num. Anal Meth. Geomech.,* **16,** 389–424.

Prager, W. (1956). A new method of analyzing stress and strains in work-hardening solids. *J. Appl. Mech. ASME,* **23,** 493–496.

Rice, J.R. (1976). The localization of plastic deformation. In *Theoretical and Applied Mechanics* (ed. W.T.Koiter), 207–220. North-Holland, Amsterdam.

Rice, J.R. and Rudnicki, J.W. (1980). A note on some features of the theory of localization of deformation. *Int. J. Solids Struct.,* **16,** 597–605.

Rudnicki, J.W. and Rice, J.R. (1975). Conditions for the localization of deformation in pressure-sensitive materials. *J. Mech. Phys. Solids,* **23,** 371–394.

Schaefer, D.G. (1990). Instability and ill-posedness in the deformation of granular materials. *Int. J. Num. Anal. Meth. Geomech.,* **14,** 253–278.

Shanley, F.R. (1947). Inelastic column theory. *J. Aeronaut. Sci.,* **14,** 261–267.

Shield, R.T. (1953). Mixed boundary value problems in soil mechanics. *Q. Appl. Math.,* **11,** 61–75.

Serrano, A.A. (1972). Generalization del method de los campos asociados. *5th Eur. Conf. Soil Mech. Found. Eng.,* 63–67.

Stören, S. and Rice, J.R. (1975). Localized necking in thin sheets. *J. Mech. Phys. Solids,* **23,** 421–441.

Sulem, J., Vardoulakis, I. and Papamichos, E. (1993). Prediction of shear failure in sandstone. *Geotechnical Engineering of Hard Soils-Soft Rocks* (eds A. Anagnostopoulos *et al.*), Vol. 2, 1663–1669. Balkema, Rotterdam.

Tatsuoka, F., Nakamura, S., Huang, G.-C. and Tani, K. (1990). Strength anisotropy and shear band direction in plane strain tests of sand. *Soils Foundations,* **30,** 35–54.

Vardoulakis, I. (1976). Equilibrium theory of shear bands in plastic bodies. *Mech. Res. Comm.,* **3,** 209–214.

Vardoulakis, I. (1978). Equilibrium bifurcation of granular earth bodies. *Adv. Anal. Geotech. Instabilities,* **13,** 65–120.

Vardoulakis, I. (1980). Shear band inclination and shear modulus of sand in biaxial tests. *Int. J. Num. Anal. Meth. Geomech.,* **4,** 3–119.

Vardoulakis, I. (1981). Bifurcation analysis of the plane rectilinear deformation on dry sand samples. *Int. J. Solids Struct.,* **17,** 1085–1101.

Vardoulakis, I. (1983). Rigid granular plasticity model and bifurcation in the triaxial test. *Acta Mechanica,* **49,** 57–79.

Vardoulakis, I. (1988). Theoretical and experimental bounds for shear-band bifurcation strain in biaxial tests on dry sand. *Res Mechanica,* **23,** 239–259.

Vardoulakis, I. and Drescher, A. (1985). Behavior of granular soil specimens in the triaxial compression test. In: *Development in Soil Mechanics and Foundation Engineering—2* (eds P.K. Banerjee and R.Butterfield), 215–252. Elsevier, London.

Vardoulakis, I. and Graf, B. (1982). Imperfection sensitivity of the biaxial test on dry sand. *IUTAM Conference on Deformation and Failure of Granular Materials,* 485–492. Balkema, Rotterdam.

Vardoulakis, I. and Graf, B. (1985). Calibration of constitutive models for granular materials using data from biaxial experiments. *Géotechnique,* **35,** 299–317.

Vardoulakis, I., Graf, B. and Hettler, A. (1985). Shear-band formation in a fine-grained sand. *5th Int. Conf. Num. Meth. Geomech.,* **1,** 517–521. Balkema, Rotterdam

Vesić, A. (1963). Bearing Capacity of Deep Foundations in sand. Georgia Institute of Technology.

Vermeer, P.A. (1990). The orientation of shear bands in biaxial tests. *Géotechnique,* **28,** 413–433.

Vermeer, P.A. and Schotman, G.J. (1986). An extension to the deformation theory of plasticity. *Proc. 2nd Int. Symp. Num. Models Geomechan.,* 33–41. Jackson and Son, England.

Yatomi, C, Y6ashima, A., Iizuka, A. and Sano, I. (1989). General theory of shear bands formation by non-coaxial Cam-clay model. *Soils Foundations,* **29,** 41–53.

9
Cosserat continuum model for granular materials

9.1
Micromechanical considerations

9.1.1
Motivation

In a zeroth grade approximation step, the shear band is modelled as a stationary velocity discontinuity line as shown in Figure 9.1.1(a), and has found its use in limit equilibrium and limit analysis computations for rigid perfectly plastic continuum models for soils. In first approximation, the shear band is bounded by two stationary discontinuity surfaces of the velocity gradient. In this case, a linearly varying velocity field fully describes the kinematics inside the shear band (Figure 9.1.1b). The band has a thickness tending to zero as compared to any other geometric length scale of the boundary value problem at hand. Such is the Thomas-Hill-Mandel shear band model which is discussed in chapter 8.

The real deformation pattern of a shear band in a granular medium on the basis of microscopic film observations was presented by Dr. G. Mandl in a seminar at the Institut für Boden- und Felsmechanik, Universität Karlsruhe on the 17th of January 1974. In a DFG (Deutsche Forschungs-gemeinschaft) Report Vardoulakis (1974) commented: "…There [i.e. in Mandl's experiment] one could observe, that the shear band (Scherfuge) consists of three parallel layers with different deformation patterns: A central domain of simple shear was bound by two essentially thinner layers of very strong shear deformation. An obvious model of such a shear band (2nd gradient approximation) is shown in Figure 2.1" (this is reproduced here as Figure 9.1.1c). Further in this report, the following shear band model was suggested: "…One considers a structure which consists of two very thin shear zones (Scherzonen, thickness h_2), which are bounding the thin shear band (thickness h_1). In the shear zones *(h_2)* the deformation is in a first approximation non-homogeneous, i.e. if we consider the parallel (to the shear band axis) velocity (component) v_1 of the material points across a shear zone, then according to the mean value theorem (Figure 2.1):

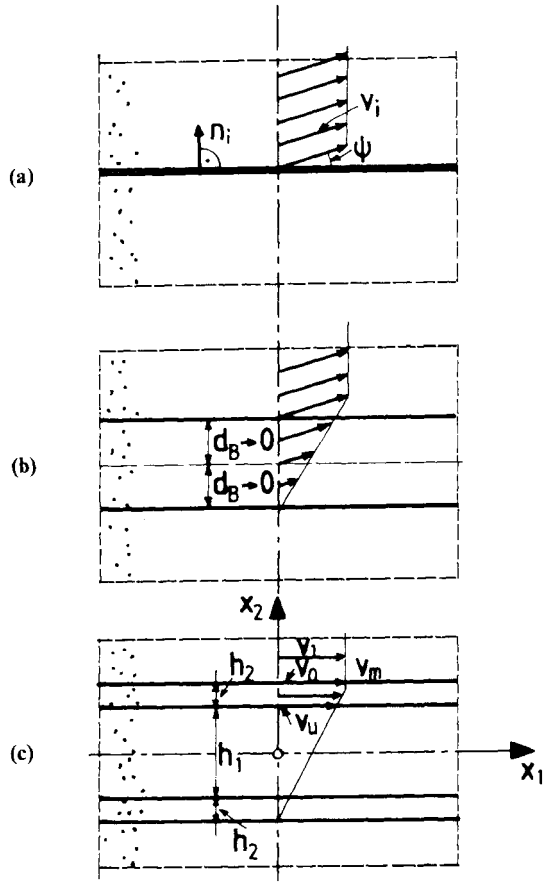

Figure 9.1.1 Shear-band models of increasing complexity. (a) The limit analysis model of velocity discontmuity line (b) The Thomas-Hill-Mandel pair of velocity gradient discontinuity lines at vanishmg distance. (c) The early conceptual shear-band model based on Mandl's experiment (Vardoulakis, 1974).

$$\partial_2 v_1|_0 - \partial_2 v_1|_u \approx \partial_{22}^2 v_1|_m h_2 \neq 0 \tag{1}$$

From (1) follows that concerning the deformation inside the shear zones one has to consider in a first approximation the second-velocity gradient. Accordingly (1) reflects the *non-simple* material behavior within the shear zones (h_2); (1) is an important kinematic property of the shear band."

Mandl's experiment, and other subsequent tests on various granular media have shown that what really dominates in these very thin shear zones is particle rotation. The question naturally arose of how to account best for particle rotation. The answer to this question is to resort to concepts from so-called Cosserat continuum mechanics, i.e.

mechanics of continua with both particle displacement and particle rotation (Becker and Burger, 1975).

In the following section we derive the basic micromechanical properties of a Cosserat continuum model of a granular medium by extending the kinematics and statics of the Schneebelli model material, which has been already discussed in the introduction of chapter 6.

Remarks on pertinent literature on Cosserat continua. 50 years after the first publication of the original work of the Cosserat brothers, Eugène and François (1909), the basic kinematic and static concepts of Cosserat continuum were reworked in a milestone paper by Günther (1958). Günther's paper marks the rebirth of micromechanics in the 1960s. Following this publication, several hundred papers were published all over the world on the subject of micromechanics. A variety of names have been invented and given to theories of various degrees of rigor and complexity, e.g. Cosserat continua or micropolar media, oriented media, continuum theories with directors, multipolar continua, microstructured or micromorphic continua, non-local media and others (Hermann, 1972). The state-of-the-art at this time was reflected in the collection of papers presented at the historical IUTAM Symposium on the 'Mechanics of Generalized Continua', in Freudenstadt and Stuttgart in 1967 (Kröner, 1968). Finally, on the subject of Cosserat elasticity recommendable for their clarity and didactical value are the papers by H. Schaefer (1962, 1967) and Kessel (1964) in German, and Koiter (1964 I & II) in English. For a comprehensive study of Cosserat continuum mechanics one is referred also to the Lecture of Stojanović (1970).

There is no doubt that Cosserat continuum theory is mostly suitable for describing the kinematics of granular media; this was clear in the minds of the scientists of this first period among whom Mindlin (1964) is the most prominent proponent. However, early applications of Cosserat theory for the description of the mechanics of granular media were less encouraging. A criticism arose as far as the meaning and significance of couple stresses in granular media is concerned (Brown and Evans, 1972; Bogdanova-Bontcheva and Lippmann, 1975), and research in this area was briefly halted. It should be mentioned that the theoretical difficulties concerning couple stresses are overcome by adopting Günther's (1958) and later Germain's (1973a,b) 'energy' approach, i.e. a continuum modeling approach which is based on the virtual work equation. Indeed, the kinematics of granular media (particle translation and particle rotation) is easier to grasp, as it is less intuitive to work with the fabric of intergranular forces. Thus one may choose kinematics as a starting point and deduce statics from the virtual work equation. This approach is followed for example in the papers by Mühlhaus and Vardoulakis (1987), and Chang and Ma (1991).

We believe that the new interest in Cosserat theories in the mid '80s and following years is simply because the link was made by Mühlhaus (1986), Mühlhaus and Vardoulakis (1987) between Cosserat continuum description and localization analysis (see also Sluys, 1990; Steinmann, 1992). It was observed that in the post-localization regime structures (shear bands) are formed, whose characteristic dimension (thickness)

is governed by the grain size. This and other observations concerning particle rotations have prompted testing the following conceptual model: In the pre-bifurcation regime of a locally homogeneous deformation the underlying assumption is that the mean grain rotation coincides with the average spin of a representative grain assembly which contains this grain. Beyond the bifurcation point this assumption must be relaxed and the grain must be allowed to rotate differently as its neighborhood. This hypothesis was validated in Distinct Element computer simulations of shear banding in the biaxial test performed by Bardet and Proubet (1992). On the other hand, observations by Oda (1993) suggest that couple stresses are important in the development of the micro-fabric of shear bands in granular media.

9.1.2
Kinematical considerations

At any material point of a Cosserat continuum we assign both a velocity and a spin vector, Figure 9.1.2(a):

$$\mathbf{v} = v_\alpha \mathbf{e}_\alpha \qquad (\alpha = 1,2);\ \mathbf{w}^c = w_3^c \mathbf{e}_3 \tag{9.1.1}$$

Accordingly we introduce the following kinematic fields: (a) The rate of deformation tensor which corresponds to the average particle velocity v_α and the corresponding rotation tensor

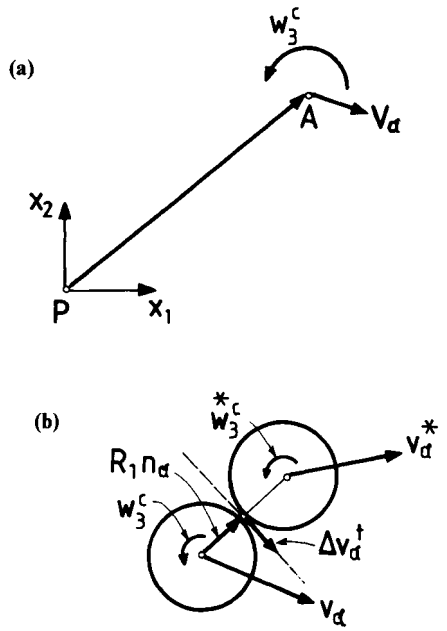

Figure 9.1.2 (a) The kinematic degrees of freedom of the Cosserat continuum; (b) the kinematics of two grains in contact.

$$D_{\alpha\beta} = \tfrac{1}{2}(\partial_\beta v_\alpha + \partial_\alpha v_\beta);\ W_{\alpha\beta} = \tfrac{1}{2}(\partial_\beta v_\alpha - \partial_\alpha v_\beta) \tag{9.1.2}$$

(b) the deformation due to the average particle rotation w_3^c

$$W_{\alpha\beta}^c = -e_{\alpha\beta 3} w_3^c \tag{9.1.3}$$

and (c) the gradient of the particle rotation which is also called the curvature of the deformation,

$$C_\alpha = \partial_\alpha w_3^c \tag{9.1.4}$$

The velocity gradient is identified with a macroscopic measure of deformation, and the particle rotation as a measure of micro-deformation. The difference between micro- and macro-deformation is a relative deformation tensor

$$V_{\alpha\beta} = \partial_\alpha v_\beta - W_{\alpha\beta}^c \tag{9.1.5}$$

We observe that in the Cosserat continuum, the symmetric part of the relative deformation coincides with the rate of the macro-deformation and its antisymmetric part with the difference between the macro- and micro-spin, i.e. with the difference in local spin due to particle displacement and particle rotation

$$V_{(\alpha\beta)} = D_{\alpha\beta};\ V_{[\alpha\beta]} = W_{\alpha\beta} - W_{\alpha\beta}^c \tag{9.1.6}$$

The granular medium is modelled here by a random assembly of rods with the same radius R_g. By assuming two representative particles (rods) in contact as being embedded in the Cosserat continuum, the relative velocity of these two rods at their periphery is (Satake, 1968; Kanatani, 1979; Figure 9.1.2b)

$$\Delta v_\beta = 2R_g(V_{\alpha\beta} + R_g e_{\alpha\beta 3} C_\gamma n_\gamma) n_\alpha \tag{9.1.7}$$

where n_α is the contact plane unit normal vector. The normal and tangential components of the relative velocity at the considered contact point are then given by the following expressions

$$\begin{aligned} \Delta v_\alpha^n &= \Delta v^n n_\alpha;\ \Delta v^n = 2R_g V_{\alpha\beta} n_\alpha n_\beta \\ \Delta v_\alpha^t &= 2R_g(V_{\alpha\beta} - V_{\gamma\delta} n_\gamma n_\delta \delta_{\alpha\beta} + R_g e_{\alpha\beta 3} C_\gamma n_\gamma) n_\beta \end{aligned} \tag{9.1.8}$$

As already discussed in chapter 6, the mean amplitude of the normal component of the relative velocity vector, taken over all contact directions, defines an average measure of the change of the distance of two grains in close proximity to each other, and thus a measure for the dilatancy of the granular medium

$$\dot{\varepsilon} = \frac{1}{\pi}\int_0^{2\pi} \frac{\Delta v^n}{2R_g}\,\mathrm{d}\theta = \frac{1}{\pi}\int_0^{2\pi} D_{\alpha\beta} n_\alpha n_\beta\,\mathrm{d}\theta = D_{\alpha\alpha} \tag{9.1.9}$$

On the other hand, the mean amplitude of the tangential component of the relative velocity vector defines an average measure of the relative slip among the grains in contact

$$\dot{\gamma} = \left[\frac{4}{\pi}\int_0^{2\pi} \frac{\Delta v_\alpha^t}{2R_g}\frac{\Delta v_\alpha^t}{2R_g}\,\mathrm{d}\theta\right]^{\frac{1}{2}} = (g_1 V'_{\alpha\beta}V'_{\alpha\beta} + g_2 V'_{\alpha\beta}V'_{\beta\alpha} + g_3 R_g^2 C_\gamma C_\gamma)^{\frac{1}{2}} \tag{9.1.10}$$

where $V'_{\alpha\beta}$ is the deviator of the relative deformation tensor

$$V_{\alpha\beta} = V'_{\alpha\beta} + \tfrac{1}{2}D_{\gamma\gamma}\delta_{\alpha\beta} \tag{9.1.11}$$

From the above kinematical definition of average interparticle slip, equation 9.1.10, follows that the weights g_i have the particular values, $\{g_i\} = \{3, -1, 4\}$. The corresponding measure for interparticle slip is then denoted as

$$\dot{\gamma}_{\mathrm{kin}} = (3V'_{\alpha\beta}V'_{\alpha\beta} - V'_{\alpha\beta}V'_{\beta\alpha} + 4R_g^2\kappa_\gamma\kappa_\gamma)^{\frac{1}{2}} \tag{9.1.12}$$

Note that for this derivation, the assumption of uniform contact-normal distribution is made. Thus together with the identities 6.1.6 use of the following identity was made

$$\begin{aligned}\overline{n_\alpha n_\beta n_\gamma n_\delta n_\sigma n_\tau} = (\pi^2/48)(&\delta_{\alpha\beta}\delta_{\gamma\delta}\delta_{\sigma\tau} + \delta_{\alpha\beta}\delta_{\gamma\sigma}\delta_{\delta\tau} + \delta_{\alpha\beta}\delta_{\gamma\tau}\delta_{\delta\sigma} + \delta_{\alpha\gamma}\delta_{\beta\delta}\delta_{\sigma\tau}\\ &+ \delta_{\alpha\gamma}\delta_{\beta\sigma}\delta_{\delta\tau} + \delta_{\alpha\gamma}\delta_{\beta\tau}\delta_{\delta\sigma} + \delta_{\alpha\delta}\delta_{\beta\gamma}\delta_{\sigma\tau} + \delta_{\alpha\delta}\delta_{\beta\sigma}\delta_{\gamma\tau} + \delta_{\alpha\delta}\delta_{\beta\tau}\delta_{\gamma\sigma}\\ &+ \delta_{\alpha\sigma}\delta_{\beta\gamma}\delta_{\delta\tau} + \delta_{\alpha\sigma}\delta_{\beta\delta}\delta_{\gamma\tau} + \delta_{\alpha\sigma}\delta_{\beta\tau}\delta_{\gamma\delta} + \delta_{\alpha\tau}\delta_{\beta\gamma}\delta_{\delta\sigma} + \delta_{\alpha\tau}\delta_{\beta\delta}\delta_{\gamma\sigma}\\ &+ \delta_{\alpha\tau}\delta_{\beta\sigma}\delta_{\gamma\delta}) = (\pi^2/48)\delta_{\alpha\beta\gamma\delta\sigma\tau}\end{aligned}$$

We observe that introduction of dimensionless coordinates

$$\overset{*}{x}_\alpha = x_\alpha/\ell \tag{9.1.14}$$

where ℓ is an arbitrary reference length, does not affect the rate of deformation, the microrotation and the relative deformation,

$$D^*_{\alpha\beta} = D_{\alpha\beta};\ W^{c*}_{\alpha\beta} = W^c_{\alpha\beta};\ V^*_{\alpha\beta} = V_{\alpha\beta} \tag{9.1.15}$$

However, the rescaling 9.1.14 is stretching the curvature

$$C^*_\alpha = \frac{\partial}{\partial \overset{*}{x}_\alpha} w_3^c = \ell C_\alpha \tag{9.1.16}$$

Accordingly if we refer the deformation to the grain-radius scale (i.e. if we set $\ell = R_g$ in 9.1.14) the above definition of volume dilatancy remains unaffected, whereas the definition of average interparticle slip becomes

$$\dot{\gamma} = (g_1 V'_{\alpha\beta}V'_{\alpha\beta} + g_2 V'_{\alpha\beta}V'_{\beta\alpha} + g_3 C^*_\gamma C^*_\gamma)^{\frac{1}{2}} \tag{9.1.17}$$

In order to recover from this definition, the classical definition of average interparticle slip, we have to make the following two assumptions: (i) The curvature of the deformation is small even at grain scale, and (ii) the grain rotations coincide with the spin of the deformation. Indeed, under these conditions the last term in equation 9.1.17 is negligible, and, with an appropriate local rotation of the coordinate system, we finally obtain

$$\dot{\gamma} = (2D'_{\alpha\beta}D'_{\alpha\beta})^{\frac{1}{2}} \tag{9.1.18}$$

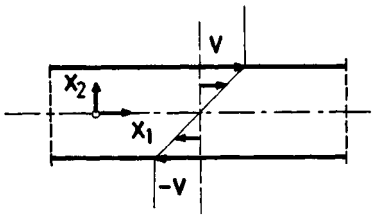

Figure 9.1.3 Simple shear of infinite strip.

Consequently, the above definitions of dilatancy and interparticle slip coincide with or include the corresponding classical definitions as special case. This observation allows us to retain unaltered the fundamental form of internal kinematical constraint, equation 6.1.12

$$\dot{\varepsilon} = \beta\dot{\gamma} \tag{9.1.19}$$

It is worth noting that the curvature terms in the definition $\dot{\gamma}$ introduce through the constraint 9.1.19 a coupling between dilatancy and the gradient of grain rotation (curvature).

Remark on restricted Cosserat continuum. A restricted Cosserat continuum is the one for which the relative spin is vanishing $V_{[\alpha\beta]} = 0$ and thus microrotations coincide with macrorotations

$$W^c_{\alpha\beta} = W_{\alpha\beta}$$

There is an affinity between restricted Cosserat continuum and the so-called 'gradient' models, where higher-order gradients of the deformation are accounted for. To demonstrate this we consider the example of simple shear deformations

$$\partial_2 v_1 = \nabla v; \quad \text{else} \quad \partial_\beta v_\alpha = 0$$

For this motion, in a restricted Cosserat continuum

$$W^c_{21} = W_{21} = -\tfrac{1}{2}\nabla v$$

and from the Cosserat-continuum approximation for the average interparticle slip, equation 9.1.10, we obtain the following expression

$$\dot{\gamma} = \{(\nabla v)^2 + R_g^2(\nabla^2 v)^2\}^{\frac{1}{2}}$$

This shows that a restricted Cosserat continuum results in a definition of the interparticle slip which depends on the strain and on its gradient.

Conversely a micromechanical model for granular material could be developed by disregarding the particle rotations and by emphasizing higher strain gradients at the grain-radius scale. In this case instead of equation 9.1.7 we have,

$$\Delta v_\beta = 2R_g(\partial_\beta v_\alpha + R_g n_\gamma \partial_\beta \partial_\gamma v_\alpha)n_\alpha$$

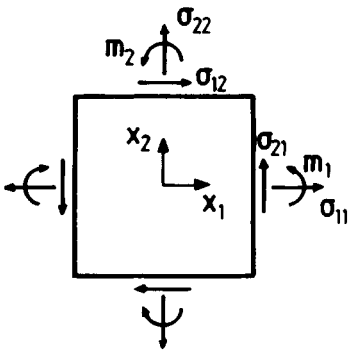

Figure 9.1.4 Stresses and couple stresses in a Cosserat continuum.

From this approximation it follows that the definition of dilatancy remains unchanged, whereas the definition of average interparticle slip becomes

$$\dot{\gamma} = \{2D'_{\alpha\beta}D'_{\beta\alpha} + (R_g^2/3)(\partial_\beta D'_{\alpha\beta}\partial_\gamma D'_{\alpha\gamma} + 2\partial_\gamma D'_{\alpha\beta}\partial_\gamma D'_{\alpha\beta} + \partial_\gamma D'_{\alpha\beta}\partial_\beta D'_{\alpha\gamma})\}^{\frac{1}{2}}$$

For the particular example of simple shear above expression yields to

$$\dot{\gamma} = \{(\nabla v)^2 + (4R_g^2/3)(\nabla^2 v)^2\}^{\frac{1}{2}}$$

This example demonstrates the similarities between 'gradient' models and restricted Cosserat models.

9.1.3
Static considerations

As shown in chapter 6 the macroscopic Cauchy stress $\sigma_{\alpha\beta}$ of a Boltzmann continuum is related to the intergranular stress $\sum_{\alpha\beta}$ of the Schneebelli medium through appropriate averaging over a distance R^*, where $R^* > R_g$ represents the radius of continuum particle. Accordingly in a Cosserat continuum, a macroscopic non-symmetric true stress $\sigma_{\alpha\beta}$ and true couple stresses $\mu_{3\alpha}$ are defined which have the same effect as the intergranular stress over the extent of the considered macro-element (Figure 9.1.4). We notice that the stress tensor $\sigma_{\alpha\beta}$ in a Cosserat medium, in case of symmetry, coincides with the transposed Cauchy stress tensor of the corresponding Boltzmann continuum. This convention in notation has mainly to do with the evolution of these lecture notes. At present we are forced to keep this notation since we want to be mainly consistent with the derivations of chapter 3, where for example the 1.P-K stress increment is defined as $\Delta\pi_{ij} = \pi_{ij} - \sigma_{ji}$ and not as, $\Delta\pi_{ij} = \pi_{ij} - \sigma_{ij}$).

Since the stress tensor $\sigma_{\alpha\beta}$ is the average of $\sum_{\alpha\beta}$ over the considered dimension $2R^*$, equation 6.1.14, couple stresses are defined by the first moment of the normal intergranular stresses,

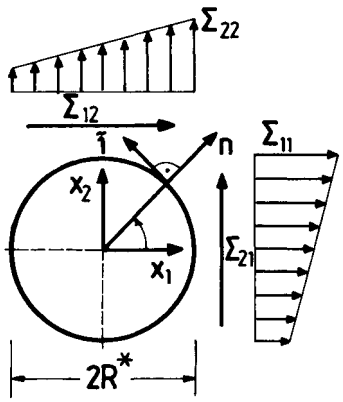

Figure 9.1.5 On the relation between intergranular stresses and stresses in a statical Cosserat model for granular material.

$$\mu_{31} = \int_{-R^*}^{R^*} \Sigma_{11} x_2 \, dx_2, \text{ etc.} \tag{9.1.20}$$

Consequently, the macroscopic stress tensor $\sigma_{\alpha\beta}$ will be in general non-symmetric, provided that the intergranular stress tensor fluctuates over the macroelement in an asymmetric manner. For example, if x_1 denotes the direction of a shear band, the intergranular stress component $\sum_{22}$ is expected to fluctuate asymmetrically in a fashion that the crests of the waves always point in the direction of the applied shear stress σ_{12} (Figure 9.1.5).

Going back to the interaction among macroelements, intercellular contact tractions can be defined by postulating a generalized stress tensor as follows

$$t_\alpha = \bar{\sigma}_{\alpha\beta} n_\beta; \; \bar{\sigma}_{\alpha\beta} = \sigma_{\alpha\beta} + \frac{1}{R^*} e_{\alpha\beta 3} \mu_{3\gamma} n_\gamma \tag{9.1.21}$$

With

$$t_\alpha^{\mathrm{n}} = t^{\mathrm{n}} n_\alpha; \; t^{\mathrm{n}} = \bar{\sigma}_{\alpha\beta} n_\alpha n_\beta; \; t_\alpha^{\mathrm{t}} = (\delta_{\alpha\gamma} - n_\alpha n_\gamma) \bar{\sigma}_{\gamma\beta} n_\beta \tag{9.1.22}$$

being the normal and tangential components of the intercellular tractions (Figure 9.1.6), invariant measures of average, normal and shear contact tractions over the periphery of a macrocell result in the following definitions of mean stress and shear stress intensity, respectively

$$\sigma = \frac{1}{\pi} \int_0^{2\pi} t^{\mathrm{n}} \, d\theta = \sigma_{\gamma\gamma}/2 \tag{9.1.23}$$

$$\tau = \frac{2}{\pi} \left[\int_0^{2\pi} t_\alpha^{\mathrm{t}} t_\alpha^{\mathrm{t}} \, d\theta \right]^{\frac{1}{2}} = (h_1 s_{\alpha\beta} s_{\alpha\beta} + h_2 s_{\alpha\beta} s_{\beta\alpha} + h_3 (1/R^{*2}) \mu_{3\gamma} \mu_{3\gamma})^{\frac{1}{2}} \tag{9.1.24}$$

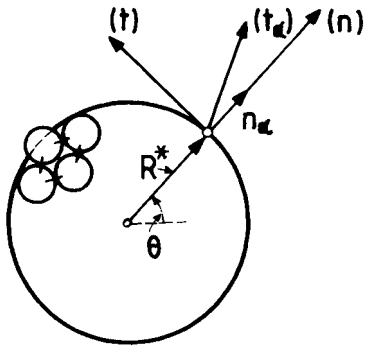

Figure 9.1.6 The equivalent-stress vector at the boundary of a (multigrain) particle.

where again $s_{\alpha\beta}$ denotes the 2D deviator of $\sigma_{\alpha\beta}$. From the above static definition of average shear stress, equation 9.1.24, it follows that the weights h_i have the particular values $\{h_i\} = \{3/4, -1/4, 1\}$, and thus

$$\tau_{\text{stat}} = \{(3/4)s_{\alpha\beta}s_{\alpha\beta} - (1/4)s_{\alpha\beta}s_{\beta\alpha} + (1/R^{*2})\mu_{3\gamma}\mu_{3\gamma}\}^{\frac{1}{2}} \tag{9.1.25}$$

Accordingly the measure for the intergranular normal forces remains unaltered, whereas the measure for the intergranular shear forces is generalized, so as to incorporate the effect of stress asymmetry and that of the couple stresses. The above static definition of shearing stress intensity, suggests replacing the couple stresses by stresses $\overset{*}{\mu}_{3\alpha}$ which with an equivalent lever R^* produce the same couple,

$$\mu_{3\alpha} = R^*\overset{*}{\mu}_{3\alpha} \tag{9.1.26}$$

leading to

$$\tau = (h_1 s_{\alpha\beta}s_{\alpha\beta} + h_2 s_{\alpha\beta}s_{\beta\alpha} + h_3 \overset{*}{\mu}_{3\gamma}\overset{*}{\mu}_{3\gamma})^{\frac{1}{2}} \tag{9.1.27}$$

We observe again that for vanishing equivalent stresses $\overset{*}{\mu}_{3\gamma}$ and symmetric stresses $\sigma_{\alpha\beta}$, the above definition collapses to the classical one

$$\tau = (\tfrac{1}{2}s_{\alpha\beta}s_{\beta\alpha})^{\frac{1}{2}} \tag{9.1.28}$$

The above generalization of the stress invariants, allows the direct adoption of Coulomb's field condition 6.1.20

$$\tau = -\sigma\mu \tag{9.1.29}$$

It should be noted that $\dot{\gamma}_{\text{kin}}$ and τ_{stat}, defined through equations 9.1.12 and 9.1.25, respectively, are *not* dual in energy as the corresponding classical measures are. Therefore we can postulate at least two different theories of plasticity for granular materials, one based on the kinematical definition of interparticle slip $\dot{\gamma}_{\text{kin}}$ and one based on the static definition of average shear contact stress τ_{stat}.

9.2
Basic concepts from Cosserat continuum mechanics

9.2.1
Kinematics of 2D Cosserat continuum

Let x_α (α=1,2) be the Cartesian coordinates of a material point in a 2D Cosserat continuum. To each material point a local, rigid coordinate cross is attached, such that the center of this rigid cross coincides with the position of the material point. During deformation the rigid crosses are moving with the velocity by v_α and at the same time the crosses are rotating with the spin $\dot{\omega}^c$ with respect to a fixed-in-space coordinate system (Figure 9.2.1). The state of deformation is described by the four components of the rate of the so-called 'relative' deformation (Schaefer, 1962)

$$\begin{aligned} \dot{\gamma}_{11} &= \partial_1 v_1;\ \dot{\gamma}_{12} = \partial_2 v_1 + \dot{\omega}^c \\ \dot{\gamma}_{22} &= \partial_2 v_2;\ \dot{\gamma}_{21} = \partial_1 v_2 - \dot{\omega}^c \end{aligned} \tag{9.2.1}$$

and the two components of the 'curvature' of the deformation

$$\dot{\kappa}_1 = \partial_1 \dot{\omega}^c;\ \dot{\kappa}_2 = \partial_2 \dot{\omega}^c \tag{9.2.2}$$

A better understanding of 2D Cosserat kinematics is achieved if one splits the relative deformation into a symmetric and an antisymmetric part:

$$\begin{aligned} \dot{\gamma}_{\alpha\beta} &= \dot{\gamma}_{(\alpha\beta)} + \dot{\gamma}_{[\alpha\beta]} \\ \dot{\gamma}_{(\alpha\beta)} &= \dot{\varepsilon}_{\alpha\beta} \\ \dot{\gamma}_{[\alpha\beta]} &= \dot{\omega}_{\alpha\beta} - \dot{\omega}^c_{\alpha\beta} \end{aligned} \tag{9.2.3}$$

where

$$\begin{aligned} \dot{\varepsilon}_{\alpha\beta} &= \tfrac{1}{2}(\partial_\beta v_\alpha + \partial_\alpha v_\beta) \\ \dot{\omega}_{\alpha\beta} &= -e_{3\alpha\beta}\dot{\omega};\ \dot{\omega} = \tfrac{1}{2}(\partial_1 v_2 - \partial_2 v_1) \\ \dot{\omega}^c_{\alpha\beta} &= -e_{3\alpha\beta}\dot{\omega}^c \end{aligned} \tag{9.2.4}$$

The above definitions can be written also in abbreviated form

$$\dot{\gamma}_{\alpha\beta} = \dot{\varepsilon}_{\alpha\beta} + (\dot{\omega}_{\alpha\beta} - \dot{\omega}^c_{\alpha\beta}) \tag{9.2.5}$$

$$\dot{\kappa}_\alpha = \partial_\alpha \dot{\omega}^c \tag{9.2.6}$$

Following Mindlin's (1964) terminology concerning continuum theories of materials with microstructure we say that the velocity field v_α describes the *macroscopic* deformation of the continuum. Accordingly, the symmetric part of the velocity gradient is called macroscopic strain. The Cosserat rotation plays then the role of *micro-deformation,* and its gradient (curvature) plays the role of micro-deformation gradient. From above equations we observe then that for the considered continuum the symmetric part of the

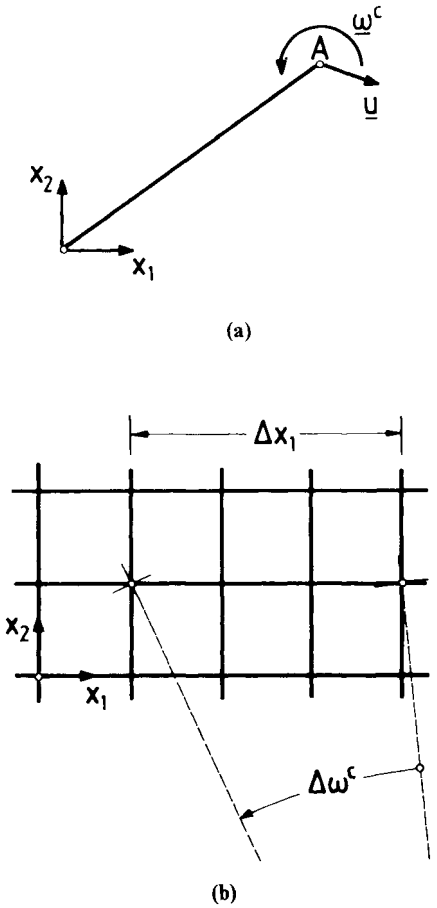

Figure 9.2.1 Visualization of Cosserat-continuum kinematics. (a) Displacement and rotation of rigid cross. (b) Relative rotation of two neighboring rigid crosses (curvature).

relative deformation coincides with the macroscopic strain-rate tensor and that the difference between macro- and micro-deformation appears only in the antisymmetric part of the relative deformation, namely in the possibility that the average rotation of individual grains in a small domain does not coincide with the spin of this domain as this is reflected by the antisymmetric part of the (macroscopic) velocity gradient. If the grains rotate with their neighborhood, then the additional kinematic degree of freedom $\dot{\omega}^c$ disappears, with the consequence that the relative rate of deformation reduces to the classical, symmetric strain-rate tensor,

$$\dot{\omega}_{\alpha\beta} = \dot{\omega}^c_{\alpha\beta} \rightarrow \dot{\gamma}_{\alpha\beta} = \dot{\varepsilon}_{\alpha\beta} \tag{9.2.7}$$

Relative strains and curvatures in a 2D Cosserat continuum obey the following compatibility conditions

$$\begin{aligned} \partial_2\dot{\gamma}_{11} - \partial_1\dot{\gamma}_{12} + \dot{\kappa}_1 &= 0 \\ \partial_1\dot{\gamma}_{22} - \partial_2\dot{\gamma}_{21} - \dot{\kappa}_2 &= 0 \\ \partial_2\dot{\kappa}_1 - \partial_1\dot{\kappa}_2 &= 0 \end{aligned} \tag{9.2.8}$$

Thus the compatibility conditions in a Cosserat continuum are less restrictive than the corresponding compatibility conditions in a classical continuum,

$$\partial_2^2\dot{\varepsilon}_{11} + \partial_1^2\dot{\varepsilon}_{22} - 2\partial_{12}^2\dot{\varepsilon}_{12} = 0 \tag{9.2.9}$$

9.2.2
Dynamics and statics

In a 2D Cosserat continuum, besides the four components of the stress tensor $\sigma_{\alpha\beta}$, there are two couple stresses, $m_\alpha = \mu_{3\alpha}\,(\alpha = 1,2)$. The equations of force equilibrium at the element look formally the same as in classical continuum (Figure 9.2.2a):

$$\begin{aligned} \partial_1\sigma_{11} + \partial_2\sigma_{12} + f_1 &= 0 \\ \partial_1\sigma_{21} + \partial_2\sigma_{22} + f_2 &= 0 \end{aligned} \tag{9.2.10}$$

However moment equilibrium (Figure 9.2.2b) results in:

$$\partial_1 m_1 + \partial_2 m_2 + (\sigma_{21} - \sigma_{12}) + \Phi = 0 \tag{9.2.11}$$

Dynamic effects are included if the volume force and volume couple are identified with the corresponding inertial forces and couple:

$$f_\alpha = -\rho\partial_t v_\alpha \qquad (\alpha = 1,2) \tag{9.2.12}$$

$$\Phi = -I\partial_t\dot{\omega}^c \tag{9.2.13}$$

In these equations the inertia of distributed mass of the macro-medium is given by the partial density ($\rho = \rho_1$)

$$\rho = (1 - n)\rho_s \tag{9.2.14}$$

where ρ_S the density of the grain and n the porosity of the medium.

On the other hand, the inertia per unit volume of the micro-medium due to its micro-rotation is computed as follows (Figure 9.2.3): Let L_g be the angular momentum of a spinning grain,

$$\begin{aligned} L_g &= \int \mathrm{d}L_g \\ \mathrm{d}L_g &= r\,\mathrm{d}F = r\,\mathrm{d}m\dot{v} = r(\rho_s r\,\mathrm{d}r\,\mathrm{d}\theta)(\dot{\omega}^c r)^{\cdot} = \rho_s\ddot{\omega}^c r^3\,\mathrm{d}r\,\mathrm{d}\theta \end{aligned} \tag{9.2.15}$$

and the integration is carried out over the volume V_s of the grain. From equations 9.2.15 we obtain

$$L_g = I_g\ddot{\omega}^c \tag{9.2.16}$$

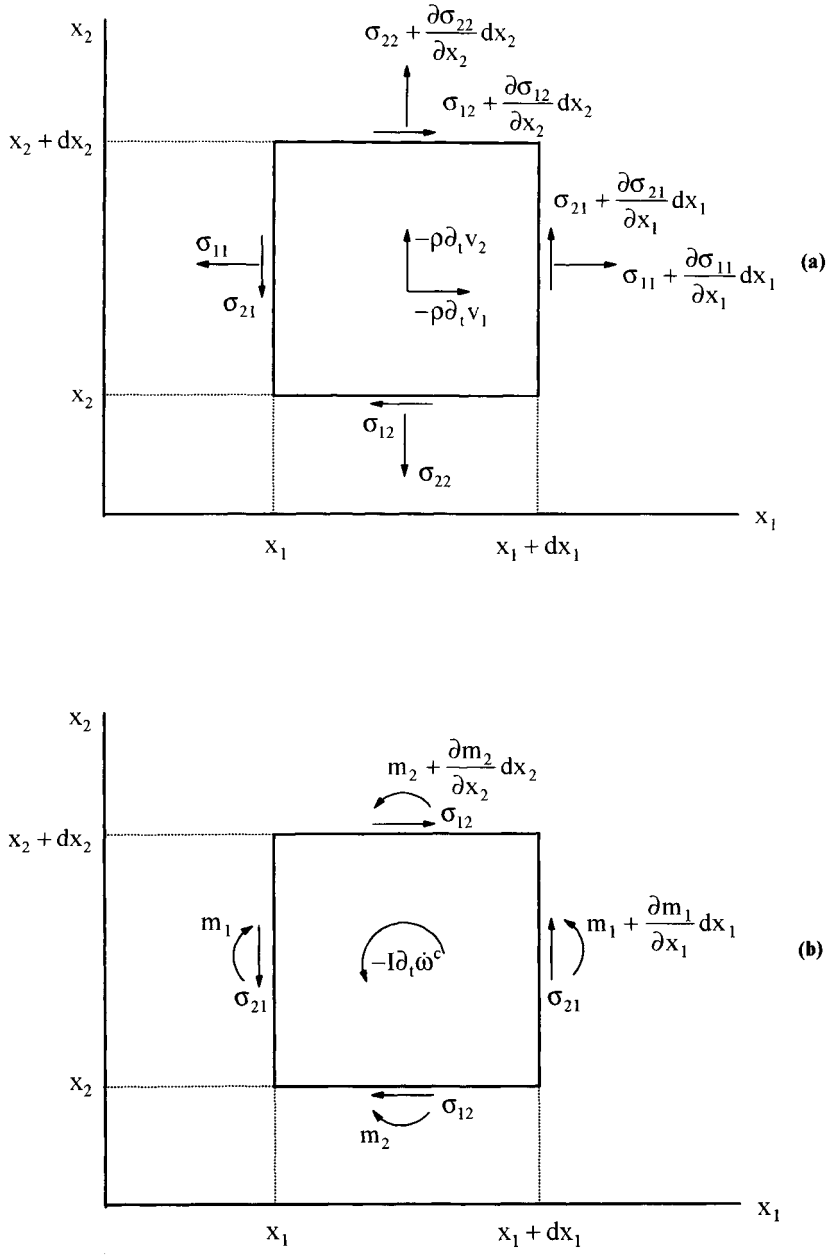

Figure 9.2.2 The derivation of equilibrium equations. (a) Force equilibrium; (b) moment equilibrium.

where I_g is the moment of inertia of the grain,

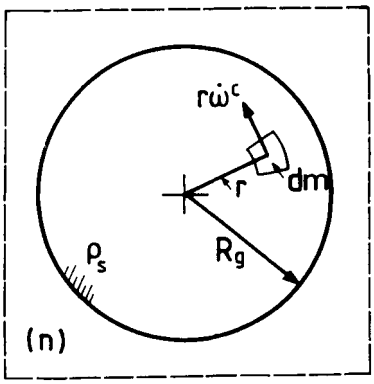

Figure 9.2.3 The computation of the micro-inertia.

$$I_g = \rho_s \int r^3 \, dr \, d\theta = (\pi/2)\rho_s R_g^4 \tag{9.2.17}$$

In 2D the grain occupies a volume $V_s = \pi R_g^2$ and its moment of inertia is distributed over a volume $V' = V_s/(1-n)$. Thus the microelement V′ has a radius $R' = R_g/\sqrt{(1-n)}$. Then the angular momentum of the micro-medium per unit volume of the micro-medium is

$$L = \frac{L_g}{V'} = I\ddot{\omega}^c \tag{9.2.18}$$

where

$$I = \frac{I_g}{\pi R'^2} = \rho(R_g/\sqrt{2})^2 \tag{9.2.19}$$

and ρ is again the partial density of the granular medium given by equation 9.2.14.

From the dynamic equation 9.2.11 with 9.2.13 we observe that in the dynamic case only micro-inertial effects suffice to cause asymmetry of the stress tensor. In the static case the symmetry of the stress tensor follows when the couple stresses are self-equilibrated. Thus, in a Cosserat continuum the stress tensor will be in general non-symmetric.

Remark. Schaefer in his GAMM Lecture in 1967 gives credit to Boltzmann concerning the axiomatic character of the symmetry of the stress tensor (Schaefer, 1967, p. 486 ff): "...Die klassische Kontinuumsmechanik setzt an dieser Stelle ein Axiom: '...Der Spannungstensor σ_{ik} ist auch bei der Bewegung des Kontinuums symmetrisch'. G.Hammel nennt diese Feststellung das Boltzmansche Axiom. Der berühmte Physiker und Philosoph Ludwig Boltzmann hat in seinen Vorlesungen 'Über die Grundprinzipien und Grundgleichungen der Mechanik', gehalten an der Clark-University im Jahre 1899, nachdrücklich darauf hingewiesen, daß die Behauptung der Symmetrie des Spannungstensors axiomatischen Charakter hat. Eine Kontinuumsmechanik mit

nichtsymmetrischen Spannungstensor ist (in Analogie zu einer nichteuk-lidischen Geometrie) als nichtboltzmannsche Mechanik zu bezeichnen. Eine solche Mechanik ist die des Cosserat-Kontinuums...".

In order to appreciate the effect of an asymmetric stress tensor, we first consider the tractions on an arbitrary plane, with unit normal n_i and unit parallel vector m_i (Figure 9.2.4a)

$$\begin{aligned} n_1 &= \cos\alpha;\ n_2 = \sin\alpha \\ m_1 &= -\sin\alpha;\ m_2 = \cos\alpha \end{aligned} \tag{9.2.20}$$

The normal and tangential (shear) component of the traction vector can then be expressed in terms of components of the stress tensor

$$\sigma_n = t^n = \sigma_{\alpha\beta} n_\alpha n_\beta;\ \sigma_s = t^m = \sigma_{\alpha\beta} m_\alpha n_\beta \tag{9.2.21}$$

or

$$\sigma_n = \tfrac{1}{2}(\sigma_{11} + \sigma_{22}) + \tfrac{1}{2}(\sigma_{11} - \sigma_{22})\cos 2\alpha + \tfrac{1}{2}(\sigma_{12} + \sigma_{21})\sin 2\alpha \tag{9.2.22}$$

$$\sigma_s + \tfrac{1}{2}(\sigma_{12} - \sigma_{21}) = -\tfrac{1}{1}(\sigma_{12} - \sigma_{22})\sin 2\alpha + \tfrac{1}{2}(\sigma_{12} + \sigma_{21})\cos 2\alpha \tag{9.2.23}$$

From these expressions we recognize that the expression normal stress is the same as in the classical continuum, and that the shear stress differs only from the classical by the antisymmetric stress

$$\sigma^a_{12} = \tfrac{1}{2}(\sigma_{12} - \sigma_{21}) \tag{9.2.24}$$

Accordingly, the geometric locus of all possible 2D-stress states is a circle, which can be seen as a shifted Mohr (1900) circle. The center of this circle of stresses is shifted perpendicular to the σ_n axis by the amount of antisymmetric stress, as shown in Figure 9.2.4(b). It should be mentioned, however, that in the general 3D case, the geometric locus of stress states is not, as in classical continuum, a set of three Mohr circles (see Unterreiner, 1994).

9.2.3
Principles of virtual work

The stress power in a Cosserat medium is defined such that the symmetric part of the relative deformation $\dot{\gamma}_{(\alpha\beta)}$ is dual in energy to the symmetric part of the stress tensor $\sigma_{(\alpha\beta)}$, the antisymmetric part of the relative deformation $\dot{\gamma}_{[\alpha\beta]}$ is dual in energy to the antisymmetric part of the stress tensor $\sigma_{[\alpha\beta]}$, and that curvatures $\dot{\kappa}_\alpha$ are dual in energy to the couple stresses m_α,

$$F = \sigma_{(\alpha\beta)}\dot{\gamma}_{(\alpha\beta)} + \sigma_{[\alpha\beta]}\dot{\gamma}_{[\alpha\beta]} + \dot{m}_\alpha \dot{\kappa}_\alpha \tag{9.2.25}$$

From this expression and equations 9.2.3 we obtain the following expression for the stress power in a Cosserat continuum

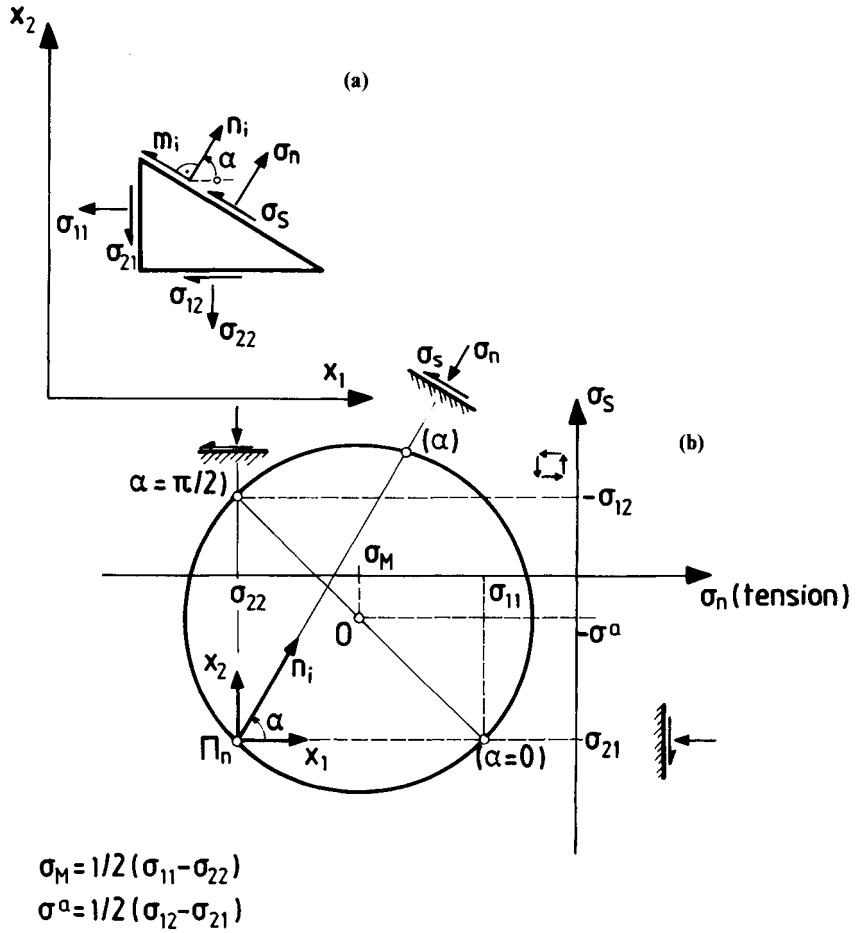

Figure 9.2.4 (a) Stresses at an arbitrary plane. (b) The 'Mohr' circle in 2D for non-symmetric stress tensor.

$$\begin{aligned} P &= \sigma_{(\alpha\beta)}\dot{\varepsilon}_{\alpha\beta} + \sigma_{[\alpha\beta]}(\dot{\omega}_{\alpha\beta} - \dot{\omega}^{c}_{\alpha\beta}) + m_{\alpha}\dot{\kappa}_{\alpha} \\ &= \sigma_{\alpha\beta}\dot{\gamma}_{\alpha\beta} + m_{\alpha}\dot{\kappa}_{\alpha} \end{aligned} \tag{9.2.26}$$

Following again Mindlin's (1964) terminology, the symmetric part of the stress tensor, $\sigma_{(\alpha\beta)}$, may be called the Cauchy stress since it works on the macroscopic strain, and $\sigma_{[\alpha\beta]}$ may be called the relative stress since it works on the relative rotation.

The above expressions for the stress power suggest using instead of m_{α} and $\dot{\kappa}_{\alpha}$, equivalent stresses to the couple stresses and dimensionless curvatures, which are defined through an appropriate characteristic length ℓ, i.e. with

$$m^{*}_{\alpha} = m_{\alpha}/\ell\,;\ \dot{\kappa}^{*}_{\alpha} = \ell\dot{\kappa}_{\alpha} \tag{9.2.27}$$

we obtain from equation 9.2.26

$$F = \sigma_{\alpha\beta}\dot{\gamma}_{\alpha\beta} + m^*_\alpha \dot{\kappa}^*_\alpha \tag{9.2.28}$$

Based on the above expression for the stress power one can define the first-order virtual work of internal forces within a finite volume V with boundary ∂V

$$\delta W^{(i)} = \int_V (\sigma_{\alpha\beta}\delta\dot{\gamma}_{\alpha\beta} + m_\alpha \delta\dot{\kappa}_\alpha)\mathrm{d}V \tag{9.2.29}$$

where $\delta\dot{\gamma}_{\alpha\beta}$ and $\delta\dot{\kappa}_\alpha$ are variations of the relative deformation and micro-rotation gradient respectively.

The boundary ∂V is divided into two complementary parts ∂V_u and ∂V_σ, such that on ∂V_u kinematical conditions and on ∂V_σ static conditions are prescribed. Since v_α ($\alpha = 1, 2$ and $\dot{\omega}^c$ are the kinematical degrees of freedom, the essential boundary conditions on ∂V_u are

$$v_\alpha = \dot{\delta}_i;\ \dot{\omega}^c = \dot{\Omega}^c \tag{9.2.30}$$

The natural boundary conditions on ∂V_σ are to prescribe the tractions t_α and the couples m. Then the virtual work of external forces reads

$$\delta W^{(e)} = \int_{\partial V_\sigma} (t_\alpha \delta v_\alpha + m\delta\dot{\omega}^c)\mathrm{d}S \tag{9.2.31}$$

for arbitrary kinematically admissible fields (δv_α, $\delta\dot{\omega}^c$). The test functions (δv_α, $\delta\dot{\omega}^c$) are said to be kinematically admissible, if

$$\delta v_\alpha = 0;\ \delta\dot{\omega}^c = 0 \tag{9.2.32}$$

on ∂V_u on which kinematic constraints are prescribed.

Let also

$$-\delta K = -\int (\rho\partial_t v_\alpha \delta v_\alpha + I\partial_t\dot{\omega}^c\delta\dot{\omega}^c)\mathrm{d}V \tag{9.2.33}$$

be the virtual work of inertial forces. The virtual work principle states that fields ($\sigma_{\alpha\beta}$, m_α) which are satisfying the virtual work equation

$$\delta W^{(e)} - \delta K = \delta W^{(i)} \tag{9.2.34}$$

they do also satisfy the dynamic equations 9.2.10 and 9.2.11 and appropriate stress and couple stress boundary conditions. Indeed independent variation of the three degrees of freedom of the 2D Cosserat continuum in the variational equation 9.2.34 leads to the local dynamic equations

$$\begin{aligned} &\partial_\beta \sigma_{\alpha\beta} = \rho\partial_t v_\alpha; \\ &-e_{3\alpha\beta}\sigma_{\alpha\beta} + \partial_\alpha m_\alpha = I\partial_t\dot{\omega}^c \end{aligned} \tag{9.2.35}$$

and to the following boundary conditions on ∂V_σ

$$n_\beta \sigma_{\alpha\beta} = t_\alpha;\ m_\alpha n_\alpha = m \tag{9.2.36}$$

According to the above derivations we may conclude that the principle of virtual work provides a natural way to introduce boundary conditions, which are consistent with the generalized continuum at hand (Germain, 1973a,b). Of course the kinematic and static boundary conditions 9.2.30 and 9.2.36 are not the only possible ones for such a medium. The effect of boundary conditions (and especially that of the extra conditions, required for the well-posedeness of the corresponding boundary-value problem) is studied in problems where boundaries are playing the important role. Such problems are interface mechanics problems (cf. Teichmann, 1990; Unterreiner, 1994).

9.2.4
The boundary-layer effect

The stress-strain relationships of a 2D-linear isotropic elastic Cosserat medium are (Schaefer, 1962)

$$\begin{aligned} \sigma_{11} &= (K + G)\varepsilon_{11} + (K - G)\varepsilon_{22} \\ \sigma_{22} &= (K - G)\varepsilon_{11} + (K + G)\varepsilon_{22} \end{aligned} \tag{9.2.37}$$

$$\begin{aligned} \sigma_{(12)} &= \sigma_{(21)} = 2G\varepsilon_{12} \\ \sigma_{[12]} &= -\sigma_{[21]} = -2G^c(\omega - \omega^c) \end{aligned} \tag{9.2.38}$$

$$m_1 = M\kappa_1;\ m_2 = M\kappa_2 \tag{9.2.39}$$

In these constitutive equations, K is the 2D-compression modulus and G is the macroscopic shear modulus that links the (symmetric) macroscopic shear strain to the symmetric part of the shear stress. The Cosserat shear modulus G^c links the antisymmetric part of the relative deformation to the antisymmetric shear stress. Finally, stress couples are linked to the corresponding curvatures through a bending modulus M, which has the dimension of force. Thus in 2D Cosserat elasticity the problem is governed by four material constants. As such we may select the following: (a) the shear modulus G, (b) the material length for bending

$$\ell = \sqrt{(M/G)} \tag{9.2.40}$$

(c) the Poisson ratio, $-1 \le \nu \le 1/2$, with

$$K/G = 1/(1 - 2\nu) \tag{9.2.41}$$

and (d) the coupling number

$$\alpha = 1/\sqrt{(1 + G/G^c)} \tag{9.2.42}$$

We observe that $0 \le \alpha \le 1$, and that the limiting case of $\alpha = 1$ corresponds to the so-called 'constrained' Cosserat continuum. Due to $G^c = \infty$, from equation (9.2.38.2) we obtain

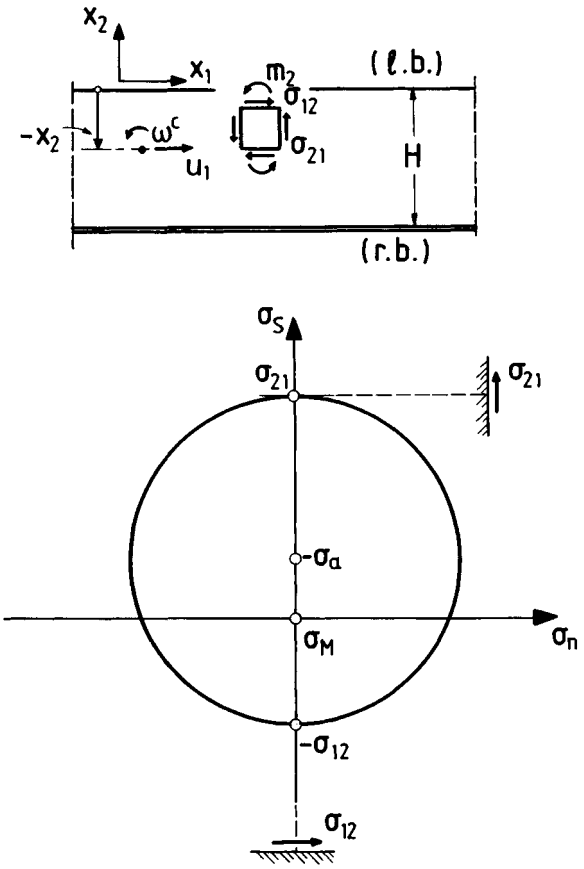

Figure 9.2.5 Simple shear of a strip consisting of linear elastic Cosserat material.

that in the constrained Cosserat medium the micro-rotation coincides with the macro-rotation, $\omega=\omega^c$.

In order to illustrate the effect of Cosserat terms, we consider here the example of small-strain simple shear of a long layer of thickness H consisting of linear-elastic Cosserat material (Figure 9.2.5; cf. Vardoulakis and Unterreiner, 1994). The thickness H of the Cosserat-elastic strip is assumed to be at least one order of magnitude larger than the elastic bending length ℓ In the case of simple shear of a long layer, all mechanical properties are assumed to be independent of the x_1-coordinate, which runs parallel to the considered strip of material, i.e. $\partial/\partial x_1 \equiv 0$, which results directly in $\varepsilon_{11} = \kappa_1 = 0$, and in m_1=0. Assuming also that $\sigma_{22} = 0$ at one boundary and $u_2 = 0$ at the other boundary, then the fields σ_{11}, σ_{22} and ε_{22} vanish identically everywhere in the considered domain. In that case the remaining equilibrium conditions

$$\frac{d\sigma_{12}}{dx_2} = 0 \quad \text{or} \quad \sigma_{12} = \tau = \text{const} \tag{9.2.43}$$

$$\frac{dm_2}{dx_2} + \sigma_{21} - \sigma_{12} = 0 \tag{9.2.44}$$

At the so-called *'interface boundary'*, $x_2 = 0$, and in accordance to equations 9.2.30, we assume here that both displacement and Cosserat rotation are prescribed, i.e.

$$\text{for } x_2 = 0: \qquad u_1 = u_{10};\ \omega^c = \omega_0^c \tag{9.2.45}$$

At the so-called *'remote boundary'*, $x_2=H$, $(H \gg \ell)$ the displacement is set equal to zero and the Cosserat rotation is constrained to be equal to the rigid body rotation, so that conditions for classical continuum are enforced at this boundary:

$$\text{for } x_2 = H \gg \ell: \qquad u_1 = 0;\ \omega^c = \omega \tag{9.2.46}$$

From the last condition and equation 9.2.43 follows that the common rotation at the remote boundary is given by the dimensionless shear stress, which constitutes one of the four integration constants of the problem,

$$\text{for } x_2 = H \gg \ell: \qquad \omega^c = \omega = \omega_H;\ \omega_H = -\tau/(2G) \tag{9.2.47}$$

We observe that in simple shear both macroscopic rigid-body rotation and shear strain are expressed by the macroscopic displacement gradient,

$$\omega = -\varepsilon_{12} = -\frac{1}{2}\frac{du_1}{dx_2} \tag{9.2.48}$$

The problem is simplified if one introduces the quantity

$$\Omega^c = \omega^c - \omega_H \tag{9.2.49}$$

Ω^c measures the amount of Cosserat rotation in excess to the macro-continuum rotation, which is observed at the remote boundary.

With the above notation, the equilibrium conditions 9.2.43 and 9.2.44 result to the following equations for the unknowns of the problem

$$\omega = \omega_H + \alpha^2(\omega^c - \omega_H) \tag{9.2.50}$$

$$\ell^2 \frac{d^2\Omega^c}{dx_2^2} - 4\alpha^2\Omega^c = 0 \tag{9.2.51}$$

The solution of the above boundary-value problem may be expressed in terms of the following quantities: (a) The dimensionless rescaled coordinate of a point in the layer, measured from the interface boundary

$$x = -2\alpha\frac{x_2}{\ell} \tag{9.2.52}$$

(b) the scaling factor

$$\eta = \frac{\alpha}{2}\frac{\ell}{H} \ll 1 \tag{9.2.53}$$

and (c) the interface-boundary data, i.e. the non-dimensional displacement

$$\overset{*}{u}_0 = \frac{u_{10}}{2H} \tag{9.2.54}$$

and the Cosserat rotation ω_0^c.

With this notation the dimensionless displacement $\overset{*}{u} = u_1/(2H)$, is given by the following equation

$$\overset{*}{u} \approx \frac{\overset{*}{u}_0}{1-\eta}\{1-(\eta/\alpha^2)x - \eta e^{-x}\} + \frac{\eta\omega_0^c}{1-\eta}\{1-(\eta/\alpha^2)x - e^{-x}\} \tag{9.2.55}$$

and the Cosserat rotation is expressed as

$$\omega^c \approx \omega_H + (\overset{*}{u}_0 + \omega_0^c)\frac{e^{-x}}{1-\eta} \tag{9.2.56}$$

where the common rotation ω_H of the macro- and micro-medium at the remote boundary is expressed in terms of the interface-boundary data and the scaling factor

$$\omega_H \approx -\frac{\overset{*}{u}_0}{1-\eta} - \frac{\eta\omega_0^c}{1-\eta} \approx -(\overset{*}{u}_0 + \eta\omega_0^c) \tag{9.2.57}$$

From equations 9.2.54 and 9.2.55 one can see clearly that the Cosserat effect is localized close to the interface boundary, x=0. Accordingly, a boundary layer is formed, where the displacement profile is non-linear and micro-rotations differ significantly from macro-rotations. In this boundary layer, asymmetric shear stresses are equilibrated by the gradient of the couple stress.

As an example the so-called 'kinematical' Cosserat material is discussed here ($G^c/G = 2.0;\ \alpha = 0.82$) for $\ell/H = 0.1$ ($\eta = 0.041$) and $\overset{*}{u} = 0.01$. We observe, that, in accordance with equation (9.2.56), the classical continuum solution is retrieved, if the boundary data are restricted such that, $\omega_0^c = -\overset{*}{u}_0$. In this case the condition $\omega^c = \omega$ is enforced also at the interface boundary $x_2 = 0$. This solution is compared with a non-degenerate one with $(\omega_0^c/\overset{*}{u}_0) = -10$, and the result is shown in Figure 9.2.6, where the displacement-and micro-rotation fields are depicted. In Figures 9.2.7(a-c), the Cosserat solution is presented in terms of the variation of strains, spins, shear stresses and couple stresses. We observe that the Cosserat effect is confined in a boundary layer of about 3ℓ thickness. More details about interface mechanics in elastic and elastoplastic Cosserat continua can be found in Unterreiner (1994).

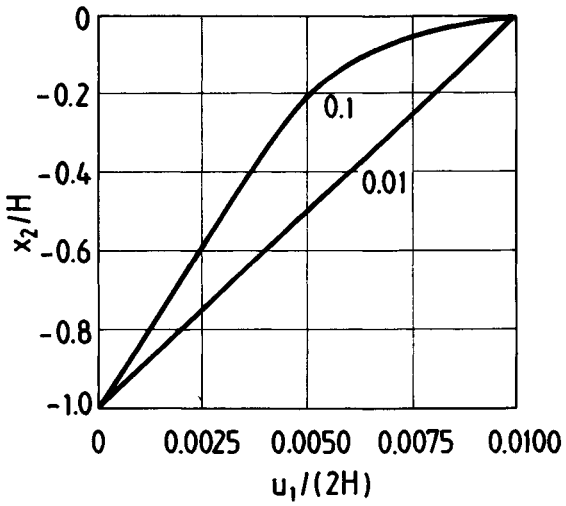

Figure 9.2.6 Interface mechanics. Displacement profile for: (a) linear displacement field for $\omega_0^c = \overset{*}{u} = -0.01$; (b) non-linear field for $\omega_0^c = -0.1$; $\overset{*}{u} = 0.01$ ($G^c/G = 2.0$, $\ell/H = 0.1$).

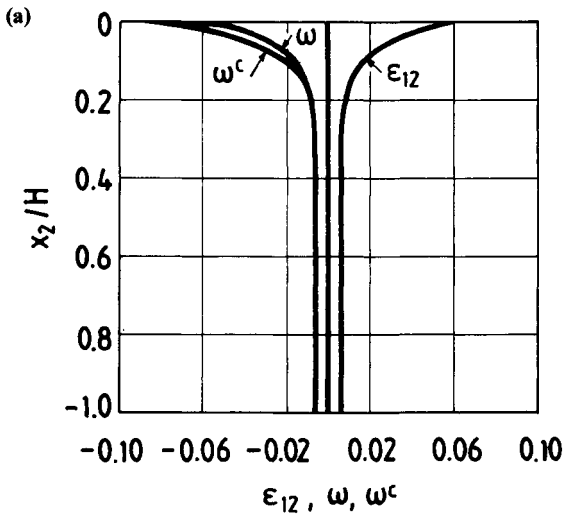

Figure 9.2.7 Interface mechanics. (a) Shear strain ε_{12}, macro-rotation ω and micro-rotation ω^c $\omega_0^c = -0.1$; $u^* = 0.01$; (G^C/G=2.0, ℓ/H=0.1).

9.3
The Mühlhaus Vardoulakis Cosserat plasticity model

The Mühlhaus-Vardoulakis Cosserat plasticity model is conceptually based on the micromechanically motivated Cosserat continuum generalizations of the second deviatoric invariants of stress and plastic strain rate as outlined in section 9.1. A micromechanical generalization of the third invariant is not straightforward as shown in section 6.3.1. Thus this model is basically a 2D-constitutive model.

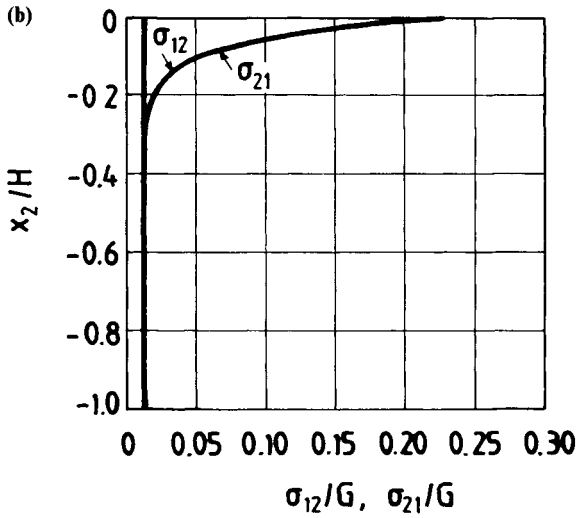

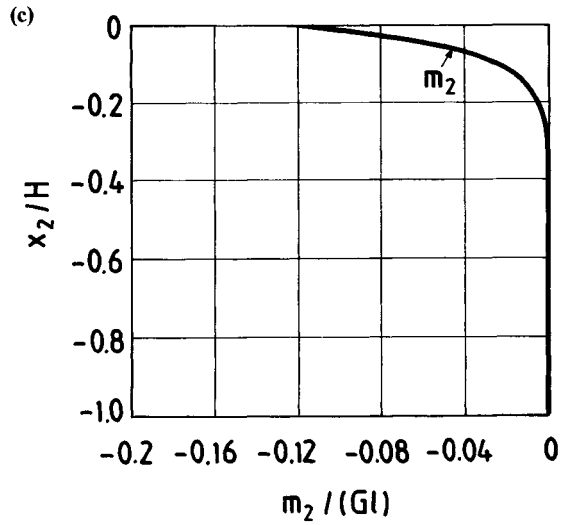

Figure 9.2.7 (continued) (b) Shear stresses σ_{12} and σ_{21} (ω_0^c=−0.1; $\overset{*}{u}$=0.01; G^c/G=2.0, ℓ/H=0.1). (c) Couple stress m_2 (ω_0^c=−0.1; $\overset{*}{u}$=0.01; G^c/G=2.0, ℓ/H=0.1).

9.3.1 Definitions

A 2D flow theory of plasticity for granular media with Cosserat microstructure can be derived by keeping the same definitions for the yield surface and the plastic potential as

in the classical theory and by generalizing appropriately the stress and strain invariants involved in these definitions. As in classical, small-strain plasticity theory, the deformation is decomposed into elastic and plastic parts

$$\dot{\gamma}_{\alpha\beta} = \dot{\gamma}^{\mathrm{e}}_{\alpha\beta} + \dot{\gamma}^{\mathrm{p}}_{\alpha\beta};\ \dot{\kappa}_{\alpha} = \dot{\kappa}^{\mathrm{e}}_{\alpha} + \dot{\kappa}^{\mathrm{p}}_{\alpha} \tag{9.3.1}$$

Moreover the stress and the deformation are decomposed into spherical and deviatoric parts,

$$\sigma_{\alpha\beta} = s_{\alpha\beta} + \tfrac{1}{2}\sigma_{\gamma\gamma}\delta_{\alpha\beta} \tag{9.3.2}$$

$$\dot{\gamma}^{(\mathrm{k})}_{\alpha\beta} = \dot{g}^{(\mathrm{k})}_{\alpha\beta} + \tfrac{1}{2}\dot{\gamma}^{(\mathrm{k})}_{\gamma\gamma}\delta_{\alpha\beta} \qquad (\mathrm{k} = \mathrm{e}, \mathrm{p}) \tag{9.3.3}$$

Based on the micromechanical considerations presented in section 9.1, the following generalized stress and strain invariants are utilized

$$\begin{aligned} &\sigma = \sigma_{\alpha\alpha}/2 \\ &\tau = \{h_1 s_{\alpha\beta}s_{\alpha\beta} + h_2 s_{\alpha\beta}s_{\beta\alpha} + h_3(m_\gamma/R_{\mathrm{s}})(m_\gamma/R_{\mathrm{s}})\}^{\frac{1}{2}};\ h_1 + h_2 = 2 \end{aligned} \tag{9.3.4}$$

$$\begin{aligned} &\dot{\varepsilon}^{\mathrm{p}} = \dot{\varepsilon}^{\mathrm{p}}_{\mathrm{kk}} \\ &\dot{\gamma}^{\mathrm{p}} = (g_1\dot{g}^{\mathrm{p}}_{\alpha\beta}\dot{g}^{\mathrm{p}}_{\alpha\beta} + g_2\dot{g}^{\mathrm{p}}_{\alpha\beta}\dot{g}^{\mathrm{p}}_{\beta\alpha} + g_3(R_{\mathrm{k}}\dot{\kappa}^{\mathrm{p}}_{\gamma})(R_{\mathrm{k}}\dot{\kappa}^{\mathrm{p}}_{\gamma})^{\frac{1}{2}};\ g_1 + g_2 = \tfrac{1}{2} \end{aligned} \tag{9.3.5}$$

We distinguish among a *static* and a *kinematical* plasticity model. It can be shown that a kinematical model which is based on the micromechanical definition of interparticle slip, equation 9.1.12, results in the following set of weighting factors,

$$\{g_i\}_{\mathrm{kin}} = \{3, -1, 4\} \rightarrow \{h_i\}_{\mathrm{kin}} = \{\tfrac{3}{8}, \tfrac{1}{8}, \tfrac{1}{4}\} \tag{9.3.6}$$

A static model is based on the micromechanical definition of interparticle shear, equation 9.1.25, and is given by

$$\{h_i\}_{\mathrm{stat}} = \{\tfrac{3}{4}, -\tfrac{1}{4}, 1\} \rightarrow \{g_i\}_{\mathrm{stat}} = \{\tfrac{3}{2}, \tfrac{1}{2}, 1\} \tag{9.3.7}$$

We note that in the above definitions the symbols R_{s} and R_{k} have been used to denote the internal length of the statical model and that of the kinematical model, respectively. From the considerations presented in section 9.1, only the internal length of kinematical model is identified, namely $R_{\mathrm{k}} = R_{\mathrm{g}}$, the mean grain radius. In view also of the simple identification of the dynamic internal length $R_{\mathrm{g}}/\sqrt{2}$, which according to equation 9.2.16 determines the micro-inertia of the spinning grain, the kinematical model seems to be preferable, as providing a more clear physical picture. In the following derivations we will not distinguish between the two different internal length scales, and the unique symbol R will be used.

9.3.2
Elastic strains

In order to define elastic strains we postulate an elastic complementary energy density function

$$w^c = \frac{1}{2}\left[\frac{\sigma^2}{K} + \frac{\tau^2}{G}\right] \tag{9.3.8}$$

where K and G are the elastic shear and compression modulus. Elastic deformations and curvatures can then be computed as follows

$$\dot{g}^e_{\alpha\beta} = \frac{\partial(w^c)}{\partial s_{\alpha\beta}};\ \dot{\gamma}^e_{\alpha\alpha} = \frac{\partial(w^c)}{\partial \sigma_{\alpha\alpha}};\ \dot{\kappa}^e_{\alpha} = \frac{\partial(w^c)}{\partial m_{\alpha}} \tag{9.3.9}$$

These definitions result in the following expression for the elastic strain and curvature rates:

$$\dot{\gamma}^e_{\alpha\beta} = \left\{2(h_1\delta_{\alpha\gamma}\delta_{\beta\delta} + h_2\delta_{\beta\gamma}\delta_{\alpha\delta}) - \frac{k-1}{2k}\delta_{\alpha\beta}\delta_{\gamma\delta}\right\}\frac{\dot{\sigma}_{\gamma\delta}}{2G};\ \dot{\kappa}^e_{\alpha} = h_3\frac{\dot{m}_{\alpha}}{GR^2} \tag{9.3.10}$$

where

$$k = K/G = 1/(1-2\nu) \tag{9.3.11}$$

By using the notations

$$\begin{aligned}\{\dot{\gamma}\} &= \{\dot{\gamma}_{11}, \dot{\gamma}_{22}, \dot{\gamma}_{12}, \dot{\gamma}_{21}, \dot{\kappa}_1, \dot{\kappa}_2\}^T \\ \{\sigma\} &= \{\sigma_{11}, \sigma_{22}, \sigma_{12}, \sigma_{21}, m_1, m_2\}^T\end{aligned} \tag{9.3.12}$$

equation 9.3.10 can be written as a single matrix equation as follows

$$\{\dot{\gamma}^e\} = [\mathbf{D}^e]^{-1}\{\dot{\sigma}\} \tag{9.3.13}$$

where the matrix $[\mathbf{D}^e]$ contains the elasticities of a two-dimensional, linear elastic, isotropic Cosserat continuum

$$[\mathbf{D}^e] = \begin{bmatrix} K+G & K-G & 0 & 0 & 0 \\ K-G & K+G & 0 & 0 & 0 \\ 0 & 0 & G+G^c & G-G^c & 0 \\ 0 & 0 & G-G^c & G+G^c & 0 \\ 0 & 0 & 0 & M & 0 \\ 0 & 0 & 0 & 0 & M \end{bmatrix} \tag{9.3.14}$$

and

$$G^c/G = h^c = 1/(2(h_1 - h_2));\ M = GR^2/h_3 \tag{9.3.15}$$

9.3.3 Plastic strains

By analogy to the classical flow theory of plasticity for frictional materials, plastic strains are defined by means of a Coulomb yield surface

$$F = -\tau/\sigma - \mu = 0 \tag{9.3.16}$$

where as described in the previous section, σ and τ are generalized isotropic, invariants of the plane Cosserat continuum, equations 9.3.4, and the hardening parameter μ is the identified with the mobilized friction coefficient.

$$\mu = \mu(n_0, \gamma^p);\ \gamma^p = \int d\gamma^p \tag{9.3.17}$$

On the other hand, we postulate a plastic potential surface

$$Q = -\tau/\sigma - \beta \tag{9.3.18}$$

where

$$\beta = \beta(n_0, \gamma^p) \tag{9.3.19}$$

is the mobilized dilatancy coefficient.

In flow theory of plasticity, the flow rule states that plastic strain increments are proportional to a given vector $\{\mathbf{q}\}$ which is coaxial with the stress tensor

$$\{\dot{\boldsymbol{\gamma}}^p\} = \dot{\gamma}^p\{\mathbf{q}\} \tag{9.3.20}$$

where $\{\mathbf{q}\}$ is the vector normal to the plastic potential surface in generalized stress space

$$\{\mathbf{q}\} = -\sigma\frac{\partial Q}{\partial\{\boldsymbol{\sigma}\}} \tag{9.3.21}$$

resulting in

$$\{\mathbf{q}\} = \begin{bmatrix} (h_1 + h_2)s_{11}/\tau \\ (h_1 + h_2)s_{22}/\tau \\ (h_1 s_{12} + h_2 s_{21})/\tau \\ (h_1 s_{21} + h_2 s_{12})/\tau \\ h_3 m_1/\tau \\ h_3 m_2/\tau \end{bmatrix} + \begin{bmatrix} \beta/2 \\ \beta/2 \\ 0 \\ 0 \\ 0 \\ 0 \end{bmatrix} \tag{9.3.22}$$

Similarly we define a vector $\{\mathbf{f}\}$ which is normal to the yield surface in generalized stress space, by replacing in equation 9.3.22 the dilatancy coefficient β with the coefficient of friction μ. Obviously $\{\mathbf{q}\}$ coincides with the normal $\{\mathbf{f}\}$ to the yield surface whenever the friction and dilatancy coefficients coincide. In this particular case the material obeys an *associated* flow rule, otherwise it obeys a non-associated flow rule. The condition $\mu = \beta$ is called again the *normality condition,* because in this case the incremental plastic strain vector in stress space is normal to the yield surface.

9.3.4
Constitutive equations

The actual value of $\dot{\boldsymbol{\gamma}}^p$ is determined from Prager's consistency condition, F=0 and dF=0, the latter equation resulting in

$$\{\mathbf{f}\}\cdot\{\dot{\boldsymbol{\sigma}}\} + \sigma h_t \dot{\gamma}^{\mathrm{p}} = 0 \tag{9.3.23}$$

where

$$h_t = \frac{\mathrm{d}\mu}{\mathrm{d}\gamma^{\mathrm{p}}} \tag{9.3.24}$$

is the plastic hardening modulus.

In view of equations 9.3.13 and 9.3.20 the generalized stress rate $\{\dot{\boldsymbol{\sigma}}\}$ can be expressed in terms of the generalized elastic strain rate $\{\dot{\boldsymbol{\gamma}}^{\mathrm{e}}\}$ or the total strain increment $\{\dot{\boldsymbol{\gamma}}\}$

$$\{\dot{\boldsymbol{\sigma}}\} = [\mathbf{D}^{\mathrm{e}}]\{\dot{\boldsymbol{\gamma}}^{\mathrm{e}}\} = [\mathbf{D}^{\mathrm{e}}](\{\dot{\boldsymbol{\gamma}}\} - \{\dot{\boldsymbol{\gamma}}^{\mathrm{p}}\}) = [\mathbf{D}^{\mathrm{e}}](\{\dot{\boldsymbol{\gamma}}\} - \dot{\gamma}^{\mathrm{p}}\{\mathbf{q}\}) \tag{9.3.25}$$

Combining the last two equations 9.3.23 and 9.3.25, $\dot{\gamma}^{\mathrm{p}}$ can be expressed as

$$\dot{\gamma}^{\mathrm{p}} = \frac{\{\mathbf{f}\}\cdot([\mathbf{D}^{\mathrm{e}}]\{\dot{\boldsymbol{\gamma}}\})}{\{\mathbf{f}\}\cdot([\mathbf{D}^{\mathrm{e}}]\{\mathbf{q}\}) - \sigma h_t} \tag{9.3.26}$$

Loading of the yield surface $F = 0$ takes place whenever $\dot{\gamma}^{\mathrm{p}}$. A switch function is now defined such that

$$\langle 1\rangle = \begin{cases} 1 & \text{if } F = 0 \text{ and } \dot{\gamma}^{\mathrm{p}} > 0 \\ 0 & \text{if } F < 0 \text{ or } (F = 0 \text{ and } \dot{\gamma}^{\mathrm{p}} \leqslant 0) \end{cases} \tag{9.3.27}$$

Finally the elastic-plastic stiffness matrix $[\mathbf{D}^{\mathrm{ep}}]$ is derived by combining equations 9.3.25 and 9.3.26

$$\{\dot{\boldsymbol{\sigma}}\} = [\mathbf{D}^{\mathrm{ep}}]\{\dot{\boldsymbol{\gamma}}\} \tag{9.3.28}$$

where

$$[\mathbf{D}^{\mathrm{ep}}] = [\mathbf{D}^{\mathrm{e}}] - \langle 1\rangle \frac{([\mathbf{D}^{\mathrm{e}}]\{q\}) \times ([\mathbf{D}^{\mathrm{e}}]\{\mathbf{f}\})^{\mathrm{T}}}{\{\mathbf{f}\}\cdot([\mathbf{d}^{\mathrm{e}}]\{\mathbf{q}\}) - \sigma h_t} \tag{9.3 29}$$

In general, rate-type constitutive equations must be formulated in terms of an objective stress-rate measurelike the Jaumann derivative of the Cauchy stress, $\mathring{\sigma}_{\alpha\beta} = \dot{\sigma}_{\alpha\beta} - \dot{\omega}_{\alpha\gamma}\sigma_{\gamma\beta} + \sigma_{\alpha\gamma}\dot{\omega}_{\gamma\beta}$. This reasoning holds also in the considered case of a Cosserat continuum, where $\sigma_{\alpha\beta}$ is the true non-symmetric stress tensor. According to section 2.2.3, a similar definition holds also for the Jaumann derivative of the true couple stress tensor,

$$\mathring{\mu}_{\alpha\beta} = \dot{\mu}_{\alpha\beta} - \dot{\omega}_{\alpha\gamma}\mu_{\gamma\beta} + \mu_{\alpha\gamma}\dot{\omega}_{\gamma\beta} \tag{9.3.30}$$

Accordingly, in the rate constitutive equation 9.3.28, $\{\dot{\boldsymbol{\sigma}}\}$ should be replaced by the Jaumann derivative of the generalized stress.

It should be noted that in elasticity or deformation theory of plasticity Jaumann terms cannot be neglected in general. However, in flow theory of plasticity for granular soils with constant elastic shear modulus G, the Jaumann correction turns out to be insignificant; cf. section 8.2.1.

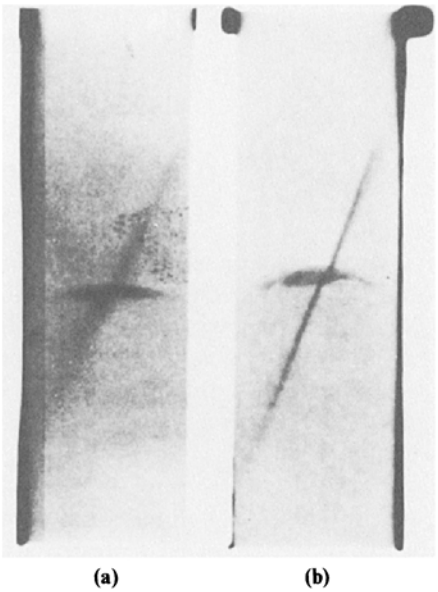

Figure 9.4.1 Shear band emerging out of a density inhomogeneity. (a) Medium-grained Karlsruhe sand (Vardoulakis and Graf, 1985); (b) fine-grained Holland sand (Vardoulakis *et al.,* 1985).

9.4
Prediction of the shear-band thickness

Vardoulakis (1974) conjectured that spontaneous loss of homogeneity in the form of shear-band formation is a clear indication for the existence of an internal (material) length scale. Indeed, there is ample experimental evidence that shear bands in granular materials engage a significant number of grains. Based on direct experimental observations, Roscoe (1970) proposed that the width of shear bands is about 10 times the average grain diameter (see also Vardoulakis, 1977; Scarpelli and Wood, 1982). In Figure 9.4.1 X-ray radiographs of shear bands are shown that are formed in the biaxial tests reported by Vardoulakis and Graf (1985) and Vardoulakis *et al.* (1985). Figure 9.4.1(a) corresponds to a medium-grained sand from Karlsruhe, and Figure 9.4.1(b) corresponds to a fine-grained sand from Holland. Table 9.4.1 summarizes the evaluation of these plates. In this table $d_{50\%}$ denotes the mean grain size of the tested sand and $2d_{\mathrm{E}}$ the measured shear-band thickness. Accordingly, these experiments suggest a shear-band thickness that is about 16 times the mean grain diameter. Figure 9.4.2 from Hammad (1991) shows the experimentally observed dependency of shear band thickness for Hostun RF dense and loose sand on the confining pressure in biaxial tests. The shear band thickness appears again as small multiple of grain diameter, however decreasing with increasing confinement.

Table 9.4.1 Measured shear-band thickness (Vardoulakis *et al.*, 1985a,b)

Sand	$d_{50\%}$ (mm)	$2d_E$ (mm)	$2d_E/d_{50\%}$ (—)
Fine sand (FS)	0.20	3.7	18.5
Medium sand (D)	0.33	4.3	13.0

As discussed in chapter 8, the classical Thomas-Hill-Mandel approach to the shear-band problem involves the consideration of a classical constitutive model and the examination of the existence of discontinuity planes for the velocity gradient, which in turn are identified with the shear-band boundaries. Since the formulation of the problem does not contain a material property with the dimension of length, it is not possible to produce a statement about the shear-band thickness. In order to be able to predict theoretically the dimensions of the shear band, the grain size must be introduced into the constitutive model. This can be done by means of a Cosserat continuum model.

The earlier references in relation to application of Cosserat continuum model for the description of the behavior of granular media are by Satake (1968), Brown and Evans (1972), and Bogdanova-Bontcheva and Lippmann (1975). Later, Kanatani (1979) applied a statistical mechanics approach to describe the kinematics of granular flow. In these analyses, the importance of couple stresses was weakened, primarily because it was assumed that couple stresses are exlusively a consequence of stress non-homogeneities at the grain contact surface. As has been demonstrated, however, by Oda (1993), couple stresses are the result of bend columnar micro-fabric inside the shear band. Oda's experiment supports the earlier analysis of Mühlhaus and Vardoulakis (1987) concerning shear-band thickness. According to the Mühlhaus-Vardoulakis Cosserat plasticity theory, at the bifurcation point of the classical description the predicted shear-band thickness is infinite. This finding should be understood as indicating that no localization is possible at the bifurcation point, i.e. the band at the bifurcation point is indeed invisible. For all post-bifurcation states the predicted thickness is finite, rapidly decreasing towards a stationary value. As the overall strain approaches the experimentally observed upper-bound $\gamma_E^{(u)}$ (cf. section 8.2.2) the predicted shear-band thickness approaches the measured value $2d_E$.

In the next section we present a shear-band bifurcation analysis within the framework of the 2D flow theory of plasticity with Cosserat structure which was originally presented by Vardoulakis (1989).

9.4.1
Governing equations

We consider here the equations that govern continued equilibrium from a configuration C of homogeneous rectilinear deformation. The conditions for continued equilibrium can

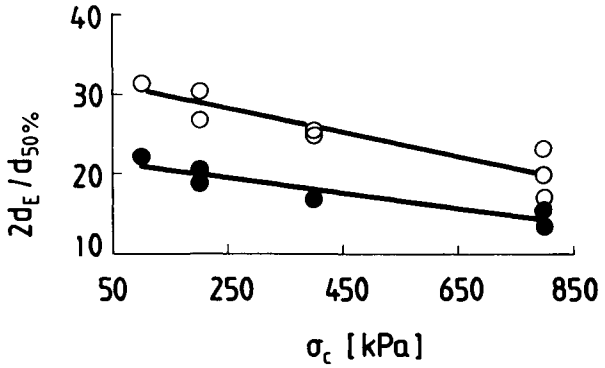

Figure 9.4.2 Shear-band thickness in biaxial experiments for dense and loose Hostun RF sand as function of confining pressure (Hammad, 1991). ●, sable Hostun RF dense; O, sable Hostun RF lâche.

be expressed in terms of the Jaumann time derivatives of the true stresses in C as follows:

$$\partial_1 \mathring{\sigma}_{11} + \partial_2 \mathring{\sigma}_{12} + (\sigma_1 - \sigma_2)\partial_2 \dot{\omega} = 0 \tag{9.4.1}$$

$$\partial_1 \mathring{\sigma}_{21} + \partial_2 \mathring{\sigma}_{22} + (\sigma_1 - \sigma_2)\partial_1 \dot{\omega} = 0 \tag{9.4.2}$$

$$\mathring{\sigma}_{21} - \mathring{\sigma}_{12} + \partial_1 \mathring{m}_1 + \partial_2 \mathring{m}_2 = 0 \tag{9.4.3}$$

In the considered case of deformations that are superimposed to monotonous rectilinear deformations, relatively simple rate constitutive relations can be derived from the general equations 9.3.28. In this case, the initial stress tensor is symmetric and initial moment stresses vanish. Under fully loading conditions we obtain then the following set of constitutive equations

$$\begin{aligned}
\mathring{\sigma}_{11} &= L^{u}_{1111}\dot{\varepsilon}_{11} + L^{u}_{1122}\dot{\varepsilon}_{22} \\
\mathring{\sigma}_{22} &= L^{u}_{2211}\dot{\varepsilon}_{11} + L^{u}_{2222}\dot{\varepsilon}_{22} \\
\mathring{\sigma}_{12} &= 2G\{\dot{\varepsilon}_{12} - h^{c}(\dot{\omega} - \dot{\omega}^{c})\} \\
\mathring{\sigma}_{21} &= 2G\{\dot{\varepsilon}_{12} + h^{c}(\dot{\omega} - \dot{\omega}^{c})\}
\end{aligned} \tag{9.4.4}$$

$$\mathring{m}_{\alpha} = M\dot{\kappa}_{\alpha} \qquad (\alpha = 1, 2) \tag{9.4.5}$$

whereas in equations 8.2.2, L^{u} are the components of the stiffness tensor for the responding upper-bound, linear comparison elastoplastic solid:

$$\begin{aligned}
L^{u}_{1111} &= G\{k(1-\beta)(1-\mu) + (1+k)h\}/h^{*} \\
L^{u}_{1122} &= G\{k(1+\beta)(1-\mu) - (1-k)h\}/h^{*} \\
L^{u}_{2211} &= G\{k(1-\beta)(1+\mu) - (1-k)h\}/h^{*} \\
L^{u}_{2222} &= G\{k(1+\beta)(1+\mu) + (1+k)h\}/h^{*}
\end{aligned} \tag{9.4.6}$$

and

$$h^c = G^c/G = 1/(2(h_1 - h_2)); \; M = GR^2/h_3$$
$$h = (|\sigma|/G)h_t; \; h^* = 1 + h - h_T; \; h_T = -k\mu\beta \tag{9.4.7}$$

Combining the above equilibrium equations with the above constitutive equations results finally in the following system of PDEs for the components of the velocity v_α, the Boltzmann spin $\dot{\omega}$ and the Cosserat spin $\dot{\omega}^c$.

$$L^u_{1111}\partial^2_{11}v_1 + G(1 + h^c - \xi)\partial^2_{22}v_1 + \{L^u_{1122} + G(1 - h^c + \xi)\}\partial^2_{12}v_2 + 2G^c\partial_2\dot{\omega}^c = 0 \tag{9.4.8}$$

$$\{L^u_{2211} + G(1 - h^c - \xi)\}\partial^2_{12}v_1 + G(1 + h^c + \xi)\partial^2_{11}v_2 + L^u_{2222}\partial^2_{22}v_2 - 2G^c\partial_1\dot{\omega}^c = 0 \tag{9.4.9}$$

$$R^2(\partial^2_{11}\dot{\omega}^c + \partial^2_{22}\dot{\omega}^c) + 2(\dot{\omega} - \dot{\omega}^c) = 0 \tag{9.4.10}$$

where

$$\xi = (\sigma_1 - \sigma_2)/2G \qquad (|\xi| \ll 1) \tag{9.4.11}$$

is the parameter accounting for the influence of initial stress.

We recall that equations 9.4.8 and 9.4.9 are derived from the equilibrium conditions for stress rates whereas equation 9.4.10 is from the equilibrium condition for couple stress rates. If one is interested in studying bifurcation modes that involve the global dimensions l_i of a body then the coordinates x_i must be non-dimensionalized by those dimensions and the highest derivatives of the Cosserat spin in equation 9.4.10 are multiplied by numbers $(R/l_i)^2 \ll 1$. In this case this equation reduces to $\dot{\omega}^c = \dot{\omega}$, and the remaining differential equations 9.4.8 and 9.4.9 reduce to those that govern diffuse bifurcations in a classical continuum. If on the other hand, one is interested in determining whether or not shear bands exist, then one has to investigate equilibrium of tractions and couples across two adjacent planes at a distance $2d_B$ that correspond to shear-band boundaries. With $(R/d_B) = 0(1)$, equation 9.4.10 becomes then essential.

9.4.2
Shear-band solution

The above differential equations 9.4.8 to 9.4.10, can be investigated for the special case where solutions are sought that correspond to localization of the deformation into narrow zones of intense shear, the so-called shear bands. According to Figure 9.4.3, the (x_1, x_2)-coordinate system is chosen in such a fashion that the x_1-axis coincides with the minor principal stress σ_1 in C. Let us assume that in $\bar{C}$ a shear band is forming which is inclined with respect to the x_1-axis at an angle θ. A new coordinate system (x, y) is introduced with its axes parallel and normal to the shear band

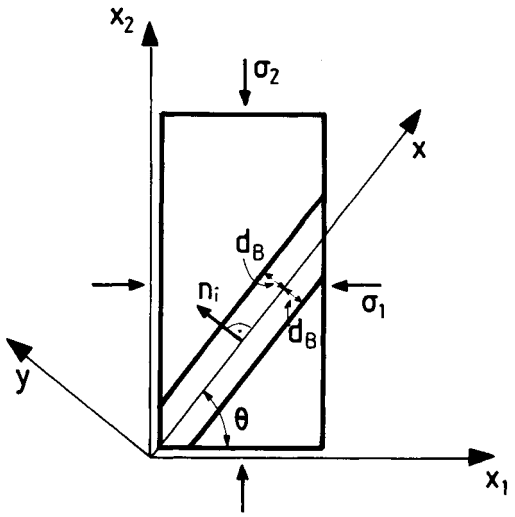

Figure 9.4.3 Specimen with shear band.

$$\begin{bmatrix} x \\ y \end{bmatrix} = [x_1, x_2] \begin{bmatrix} \cos\theta & -\sin\theta \\ \sin\theta & \cos\theta \end{bmatrix} \tag{9.4.12}$$

Let n_α be the unit vector that is normal to the shear-band axis

$$n_1 = -\sin\theta;\ n_2 = \cos\theta \tag{9.4.13}$$

By assuming that all field properties related to the forming shear band do not depend on the longitudinal x-coordinate and setting $(\cdot)' = \partial/\partial x$ equations 8.4.8 to 8.4.10 reduce to the following system of ordinary differential equations

$$A^c_{11} v_1'' + A^c_{12} v_2'' + A^c_{13} \dot{\omega}^{c\prime} = 0 \tag{9.4.14}$$

$$A^c_{21} v_1'' + A^c_{22} v_2'' + A^c_{23} \dot{\omega}^{c\prime} = 0 \tag{9.4.15}$$

$$n_2 v_1' - n_1 v_2' - R^2 \dot{\omega}^{c\prime\prime} + 2\dot{\omega}^c = 0 \tag{9.4.16}$$

where

$$\begin{aligned} A^c_{11} &= L^u_{1111} n_1^2 + G(1 + h^c - \xi) n_2^2 \\ A^c_{12} &= L^u_{1122} n_1 n_2 + G(1 - h^c + \xi) n_1 n_2 \\ A^c_{13} &= 2G^c n_2 \\ A^c_{21} &= L^u_{2211} n_1 n_2 + G(1 - h^c - \xi) n_1 n_2 \\ A^c_{22} &= L^u_{2222} n_2^2 + G(1 + h^c + \xi) n_1^2 \\ A^c_{23} &= -2G^c n_1 \end{aligned} \tag{9.4.17}$$

In looking for exponential solutions,

$$\begin{aligned} v_\alpha &= c_\alpha d_B \exp(\lambda y/d_B) \qquad (\alpha = 1,2) \\ \dot{\omega}^c &= c_3 \exp(\lambda y/d_B) \end{aligned} \tag{9.4.18}$$

the above system of equations 9.4.13 to 9.4.16 yields

$$\begin{bmatrix} b_{11} & b_{12} & 0 \\ b_{21}\lambda & b_{22}\lambda & -1 \\ -n_2\lambda & n_1\lambda & \ell^{*2}\lambda^2 - 2 \end{bmatrix} \begin{bmatrix} c_1 \\ c_2 \\ c_3 \end{bmatrix} = \{0\} \tag{9.4.19}$$

where

$$\{b_{\alpha\beta}\} = \begin{bmatrix} A^c_{11}n_1 + A^c_{21}n_2 & A^c_{12}n_1 + A^c_{22}n_2 \\ (-A^c_{11}n_2 + A^c_{21}n_1)/(2G^c) & (-A^c_{12}n_2 + A^c_{22}n_1)/(2G^c) \end{bmatrix} \tag{9.4.20}$$

and

$$\ell^* = R/d_B \tag{9.4.21}$$

For non-trivial solutions, the matrix equation 9.4.20 results in the following *bifurcation condition*

$$\lambda = \pm i\lambda^* \qquad (i = \sqrt{-1}) \tag{9.4.22}$$

where

$$\lambda^* = a/\ell^* \tag{9.4.23}$$

and

$$a = [(b_{11}n_1 + b_{12}n_2)/b - 2]^{\frac{1}{2}} \tag{9.4.24}$$

$$b = b_{11}b_{22} - b_{12}b_{21} \tag{9.4.25}$$

This solution corresponds to periodic functions for the velocities and the Cosserat spin

$$\begin{aligned} v_\alpha &= d_B c_\alpha \sin(\lambda^* y/d_B) \qquad (\alpha = 1,2) \\ \dot{\omega}^c &= c_3 \cos(\lambda^* y/d_B) \end{aligned} \tag{9.4.26}$$

where

$$c_1 = -\frac{c}{\lambda^*}\frac{b_{12}}{b};\ c_2 = \frac{c}{\lambda^*}\frac{b_{11}}{b};\ c_3 = c \tag{9.4.27}$$

This solution satisfies identically homogeneous conditions at the shear-band boundary for the tractions. With

$$t_\alpha = \dot{\pi}_{\alpha\beta}n_\alpha \tag{9.4.28}$$

we obtain

$$\begin{aligned} t_1 &= A^c_{11}v'_1 + A^c_{12}v'_2 + A^c_{13}\dot{\omega}^c \\ t_2 &= A^c_{21}v'_1 + A^c_{22}v'_2 + A^c_{23}\dot{\omega}^c \end{aligned} \tag{9.4.29}$$

In view of the equilibrium equations 9.4.14 and 9.4.15 and the above expressions 9.4.29, it follows that zero traction rates hold along planes parallel to the shear-band boundaries

$$\dot{t}_\alpha = 0 \qquad (\alpha = 1, 2) \tag{9.4.30}$$

On the other hand, the couple stress that is acting on planes parallel to the shear-band boundaries is only a function of the Cosserat spin

$$\dot{m} = M\dot{\omega}^{c\prime} = -c_3 M(\lambda^*/d_B)\sin(\lambda^* y/d_B) \tag{9.4.31}$$

However, for equilibrium reasons, the couple stress has to be continuous across the shear-band boundaries

$$[\dot{m}] = \dot{m}^+ - \dot{m}^- = 0 \tag{9.4.32}$$

The shear-band solution is based on the assumption that, outside the shear-band couple, stresses are zero,

$$\dot{m}^+ = 0 \tag{9.4.33}$$

which results in vanishing couple stresses along the shear-band boundaries

$$\dot{m}^- = 0 \quad \text{for} \quad y = \pm d_B \tag{9.4.34}$$

equations 9.4.31 and 9.4.34 yield $\lambda^* = \pi$, or, in the following expression for the shear-band thickness

$$\frac{d_B}{R} = \frac{\pi}{a} \tag{9.4.35}$$

The shear-band thickness $2d_B$ is viewed as an *internal length* of the considered problem. According to equation 9.4.35 this internal length is proportional to the material length $D = 2R$, and the proportionality factor (π/a) is a function of the plastic hardening parameter. Equation 9.4.35 is thus an analytical estimate of the internal length of the problem, which in turn is observable in experiments. This estimate can be used to test the assumption that the material length D is equal to the mean grain diameter. It should be finally noticed that the structure of the above analytical estimate for the internal length is very similar to the thickness estimate for interface layers for rigid-plastic Cosserat continua (Vardoulakis and Unterreiner, 1994).

9.4.3
Analytical and experimental results

The shear-band thickness estimate 9.4.35 has to be tested here against the experimental evidence. As an example we select here the biaxial test on fine Dutch dune sand ($\sigma_c = 294.3\,\text{kPa}$; Vardoulakis and Graf, 1985), which was already discussed in section 8.2.2. One is interested in producing theoretical results in the regime past the shear-band bifurcation state. Thus the experimental results from biaxial tests concerning mobilized friction and dilatancy must be extrapolated theoretically into this regime. For

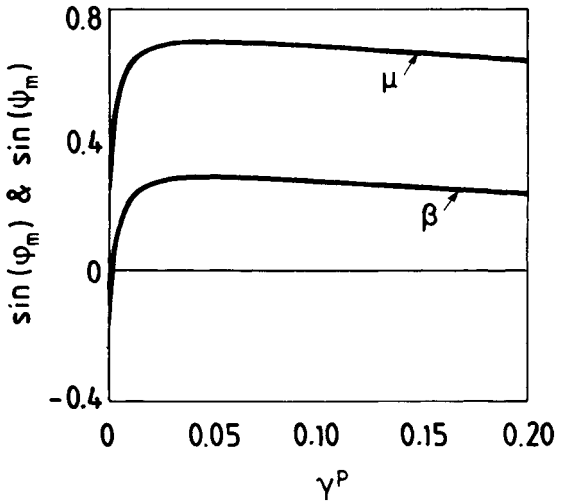

Figure 9.4.4 Mobilized friction and dilatancy functions of plastic shear strain for fine Dutch dune sand, according to the two-phase softening presented in section 6.4.3.

this purpose, we select here the porosity softening theory, discussed in section 6.4.3. Direct fit of the experimental results produced the following material functions and constants:

shear modulus:	$G = 50.34\,\text{MPa}$
Poisson's ratio:	$\nu = 0.1$
mobilized friction of mixture:	$\mu = (1 - n^{\text{f}})\mu^{\text{c}} + n^{\text{f}}\mu^{\text{f}};\ \mu^{\text{f}} = \mu_{\text{cv}}$
mobilized friction of competent fraction:	$\mu^{\text{c}} = \gamma^{\text{p}}/(c_1 + c_2\gamma^{\text{p}});\ c_1 = 2.8582E-3;$ $c_2 = 1.2166E0$
mobilized dilatancy (Taylor rule):	$\beta = \mu - \mu_{\text{cv}};\ \mu_{\text{cv}} = 0.412$
relative porosity:	$n^{\text{f}} = (n - n_{\min})/(n_{\max} - n_{\min})$
initial porosity:	$n_0 = 0.383$
maximum and minimum porosity:	$n_{\max} = 0.482;\ n_{\min} = 0.362$

Figure 9.4.4 shows the mobilized friction and dilatancy coefficients $\mu = \mu(\gamma^{\text{p}})$ and $\beta = \beta(\gamma^{\text{p}})$ for the considered softening model. Shear-band bifurcation (B: $a = 0$ occurred in the hardening regime, at

plastic shear strain:	$\gamma^{\text{p}}_{\text{B}} = 2.68\%$
mobilized friction angle:	$\phi_{\text{B}} = 43.4^\circ$
mobilized dilatancy angle:	$\psi_{\text{B}} = 16.0^\circ$
shear band inclination angle:	$\theta_{\text{B}} = 59.2^\circ$

Figure 9.4.5 shows the evolution of the predicted shear-band thickness

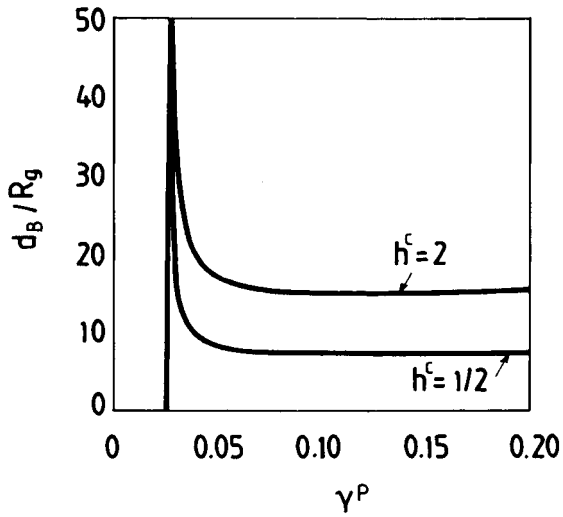

Figure 9.4.5 Computed shear-band thickness for various post-bifurcation states for fine Dutch dune sand and for the kinematical (h_c=2) and statical (h_c=1/2) Cosserat continuum model.

$$\frac{d_B}{R_g} = \frac{2d_B}{d_{50\%}} \tag{9.4.36}$$

in the post-bifurcation regime of the classical description. From this figure, we observe that at the bifurcation point of the classical description d_B is infinite, i.e. no localization is possible at the bifurcation point of the classical description. However, past the bifurcation point the deformation rapidly localizes, with d_B assuming a minimum value at about 10% plastic strain. For larger strains the shear-band thickness increases again.

This stationarity property is important, because we know from the experiment that the shear-band thickness is almost constant. We will thus identify this minimum with the observed shear-band thickness. According to Figure 9.4.5 the shear-band thickness for the kinematical Cosserat model $(h^c = 2)$ found as $(d_B/R_g)_{min} \approx 15$, and for the statical Cosserat model $(h^c = 1.2)$ as $(d_B/R_g)_{min} \approx 7$. X-ray radiographs of the considered Ostershelde sand specimens revealed a shear-band thickness that is about 18.5 times the mean grain diameter; cf. Figure 9.4.1 and Table 9.4.1.

These findings are in complete accordance with the physical experiments and Distinct-Element computations (Cundall, 1989; Bardet and Proubet, 1992). Indeed, in both cases an initial thinning followed by material growth of the band was observed. On the other hand, Cundall's numerical experiments for random assemblies of rods reveal a thickness of about eight grain diameters. Accordingly, the kinematical model is more suitable for approximating the behavior of a true 3D granular medium, whereas the statical model is a better model of a Schneebelli material.

It should be mentioned that this type of behavior of initially decreasing and later increasing shear-band thickness was first reported by Vardoulakis (1978) and Vardoulakis and Goldscheider (1981) and is rather typical for the post-failure measurements in the biaxial apparatus (Vardoulakis and Drescher, 1989). Figure 9.4.6 demonstrates indeed the shear-band thickness evolution as it is seen through an apparent dilation angle (Drescher *et al.,* 1990). It is interesting to note that although the tested sand was dense, an initial apparent contractancy is observed, which in view of our present results speaks for initial shear-band thinning. For larger strains, however, and although the stress obliquity across the shear-band boundary is approximately constant, a residual apparent dilation angle of about 10° is measured. This again is in accordance with our result of a rather prolonged shear-band thickening in the post-bifurcation regime. It should be noted that shear-band thickening is observed in the context of large fault displacements and is of importance to the geophysicist (Watterson, 1986).

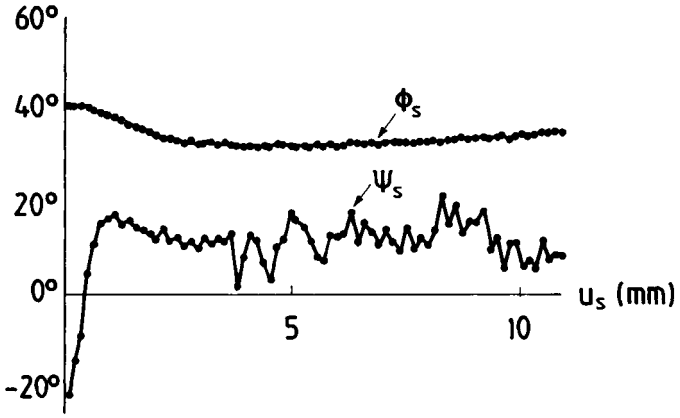

Figure 9.4.6 Measured post-failure variation of the stress obliquity ϕ_s, and the apparent dilation angle ψ_s in biaxial tests on Ottawa sand (Drescher *et al.,* 1990).

9.5
Discussion and numerical implications

Failure in geomaterials is often accompanied by the concentration of deformation into one or more narrow bands of intense shear. During the last two decades numerous researches described localization phenomena in solids by utilizing the Thomas-Hill-Mandel theory of equilibrium bifurcation. Analytical expressions for the critical hardening modulus and the localization band orientation angle at bifurcation have been derived for the infinite domain problem and for various constitutive models; cf. section 8.3. Shear-band analyses for more complicated boundary-value problems and, more importantly, post-localization analyses can only be done numerically.

In the numerical studies of Prevost (1984), Griffiths (1981), Shuttle and Smith (1988) and Cundall (1989), localization was triggered through initial imperfections in the form of strategically placed weak elements. In the studies of Ortiz *et al.* (1986), the onset of localization was detected by the failure of Mandel's material stability criterion (i.e. existence of zero eigenvalues of acoustic tensor) carried out at the element level. De Borst (1988) analyzed the formation of shear bands in materials obeying a non-associated flow rule by implementing eigenvalue analysis of the global stiffness matrix to determine the load at which bifurcations are possible. It is not clear, however, if one can really trigger shear banding by non-associativity only, and de Borst's computations were never confirmed. As we have seen in the previous section, true localization (i.e. minimum in d_B) is related to material strain softening.

As already shown in section 3.3, within a small strain theory, global equilibrium bifurcation occurs when global second-order work vanishes

$$\int_V \Delta^2 w \, \mathrm{d}V = 0 \tag{9.5.1}$$

which in a Finite Element discretization scheme results in the requirement that the *global* stiffness matrix becomes singular

$$\det([\mathbf{K}]) = 0 \tag{9.5.2}$$

It should be noted that unlike the suggestion of Ortiz *et al.* (1986), in inhomogeneous problems, failure of the local stability criterion ($\Delta^2 w = 0$) does not necessarily imply global loss of uniqueness. On the other hand, material strain softening leads to negative second-order work.

A major drawback of classical strain-softening models is that they lead to mathematically ill-posed boundary value problems, whose numerical analysis is sensitive to mesh refinements (Bažant *et al.,* 1984). Since in classical constitutive models there is no material (internal) length, the discretization sets the length scale. The localization region which is associated with strain softening, depends then on the size of the mesh used for spatial discretization, i.e. the thickness of the shear band is governed by the mesh spacing.

It was found that computational analyses based on a classical continuum theories render themselves inadequate for an objective (robust) treatment of the problem of deformation localization. A typical example of the nonrobustness of classical continuum modeling was presented by Veeken *et al.,* (1989), where it was made clear, that classical computations are severely imperfection sensitive in the sense that the imperfection severely dominates the final failure mechanism. It should be noted that for a classical continuum, eigenvalues of the global stiffness matrix are spurious in nature and do not persist on the primary branch past the bifurcation point.

As pointed out by Bažant *et al.,* (1984), a constitutive theory without internal length leads often to a softening zone of negligible thickness and zero energy dissipation. Many different methods for regularizing the quasi-static, boundary-value problem with strain

softening are proposed in the literature. For example, non-local approaches in various forms which include the use of the concept of imbricated continua (Bažant, 1984), and higher-order deformation gradients (de Borst and Mühlhaus, 1992). Alternatively, the problem of mesh dependence can be resolved by resorting to continua with Cosserat micro-structure like for example the plasticity model of Mühlhaus and Vardoulakis, presented in this section. There is not yet a clear consensus on which of the above continuum models is preferable, based on better correlation of computational results with the experimental evidences and on the convenience with which each method can be implemented in a numerical code. In order to decide among the various competing models one has to resort on the physics of the problem. For example, in granular materials and predominant shear failure forms, the Cosserat continuum approach seems physically justified (cf. Ord *et al.,* 1991). This was demonstrated in a paper by Papanastasiou and Vardoulakis (1992) where for the problem of borehole stability in sandstones they confirmed that micro-rotations play an important role in the computation (Cosserat effect). Figure 9.5.1(a) shows the plastic state of the elements close to the borehole wall and at the bifurcation point and the selected warping mode. As can be seen in Figure 9.5.1(b), in the course of post-bifurcation deformation, most of the elements in close proximity to the borehole wall unload elastically except for two regions of localized deformation. Eventually one of these two regions dominates; see Figure 9.5.1(c). Shear bands are characterized as elastoplastic domains of softening material which are surrounded by unloading elastic domains (white). Deeper regions remain in the elastoplastic hardening regime or are deformed elastically below first yield. The next three figures demonstrate the computed failure mode by means of the γ^{p}-isolines (Figure 9.5.1d) the incremental displacement field (Figure 9.5.1e), and the deformed finite element mesh (Figure 9.5.1f). In particular it was found that the trivial (axisymmetric) solution is characterized by vanishingly small micro-rotations whereas they significant for the secondary solution. The difference between the macro- and micro-rotation is given by the relative rotation

$$\Delta\omega^{r} = \Delta\omega - \Delta\omega^{c} \tag{9.5.3}$$

Figure 9.5.2 shows in a 3D-perspective graph the distribution of the incremental relative rotation vector at the end of the localized branch. Upwards-pointing vectors denote a clockwise rotation. The relative rotation is localized at the shear-band boundaries, as expected, and in accordance with the Mandl's experiment mentioned in the introduction.

Finally, it should be pointed out that in a Cosserat continuum, the corresponding incremental boundary-value problem remains always globally elliptic, which results in *numerical stability in the softening regime*. The computational result is imperfection sensitive, however the corresponding failure patterns are persistent. (In the example studied by Papanastasiou and Vardoulakis (1992) one or two 'breakouts' were predicted depending on whether or not there is a slight stress anisotropy.)

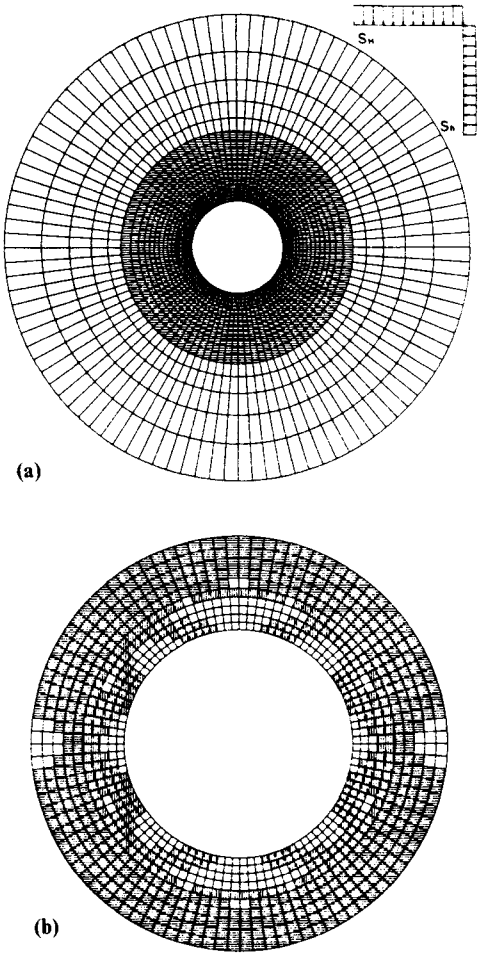

Figure 9.5.1 Detail of plastic and elastic domains at (a) beginning of localization; (b) past the bifurcation indicating progressive localization.

Other investigators have also used Cosserat continuum theory for post-bifurcation analyses. For example, Mühlhaus (1990) used a finite-element formulation with the Cosserat plasticity model to analyze surface instabilities in an elastoplastic, cohesion-softening half-space under compression and he detected the post-failure evolution of tensile zones at some distance from the free surface. De Borst (1990) and Mühlhaus *et al.* (1991), studied localization phenomena in a series of illustrative simple boundary-value problems involving Cosserat plasticity, like the tension test, the shear test and the biaxial compression test, where due to the homogeneity of initial stress field, localization was triggered through initial imperfections in the form of weak elements. Therefore, the mathematically ill-posed boundary problem of strain-softening material can be regularized, successfully, by adopting a Cosserat plasticity theory.

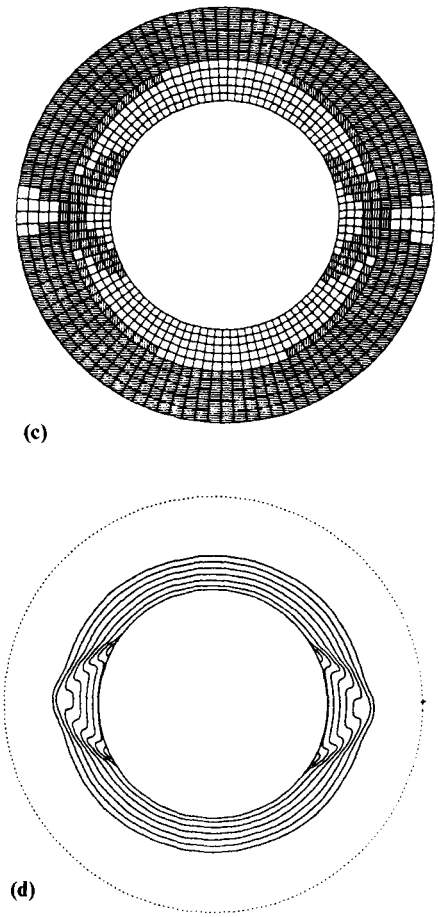

Figure 9.5.1 (continued) (c) end of the secondary branch indicating one-side localization; (d) isolines of accumulated plastic shear strain (γ^p).

For the formulation of well-posed boundary value problems within a Cosserat continuum theory extra boundary conditions are necessary. A set of admissible kinematical and static extra boundary conditions follows directly from the principle of virtual work. These or other types of boundary conditions must be physically meaningful, since close to boundaries the Cosserat effect is more pronounced, leading for example in Cosserat elasticity occasionally to the formation of boundary layers (section 9.2.4) and in Cosserat plasticity to thin plastic boundary layers (Unterreiner, 1994). It turns out in all these cases the type of assumed extra boundary conditions influences significantly some of the observable properties of surface localizations. Figure 9.5.3 from Teichman (1990) illustrates for example the difference in thickness of interface layers for 'rough' and 'very rough' steel-plate interfacing with sand in a biaxial setting. Thus the physical justification and calibration of non-standard boundary

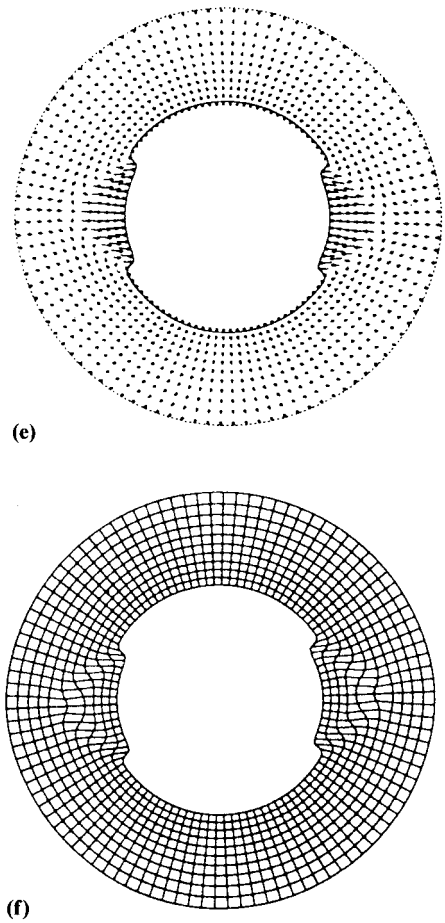

Figure 9.5.1 (continued) (e) incremental displacement field; (f) deformed mesh after localization (Papanastasiou and Vardoulakis, 1992).

conditions can be succeeded by carefully performed interface experiments and corresponding Finite Element Cosserat-continuum back analyses (cf. Unterreiner, 1994).

Literature

Textbooks and monographs

Becker, E. and Bürger, W. (1975). *Kontinuumsmechanik.* Teubner, Stuttgart.

Cosserat, E. and F. (1909). *Théorie des Corps Déformables.* A.Hermann, Paris.

Kröner, E. (ed) (1968). *Mechanics of Generalized Continua. IUTAM Symposium Freudenstadt and Stuttgart* 1967. Springer-Verlag, Berlin.

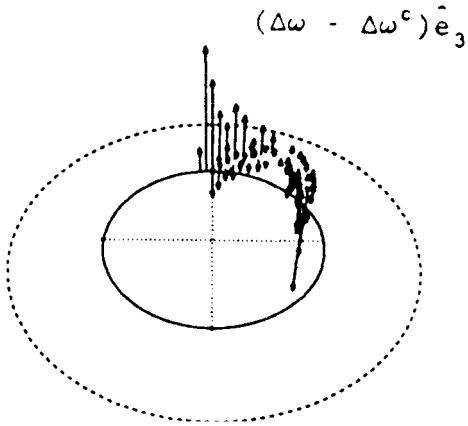

Figure 9.5.2 3D perspective drawing of the incremental relative rotation at the localized zone in a Cosserat-continuum simulation of the borehole breakout (Papanastasiou and Vardoulakis, 1992).

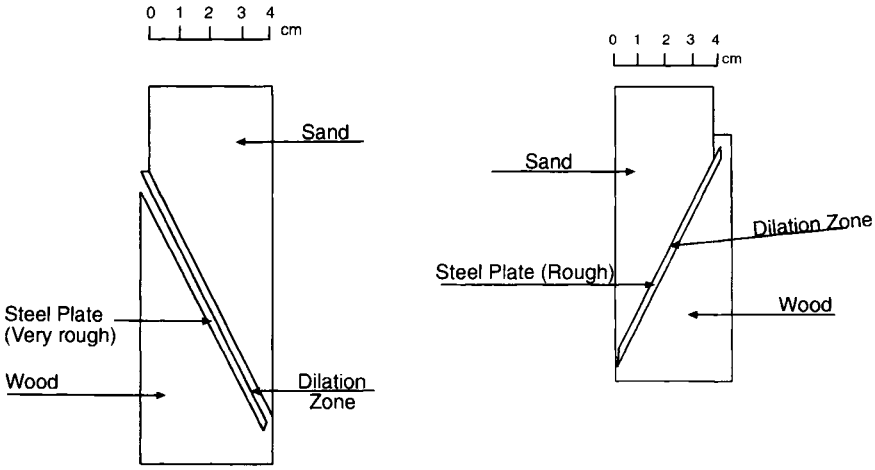

Figure 9.5.3 Interface softening dilatancy localizations for 'rough' and 'very rough' steel interfacing with sand in a biaxial setting (Teichman, 1990).

Stojanovic, R. (1970). *Recent Developments in the Theory of Polar Continua.* International Center for Mechanical Sciences, Course and Lectures No. 27, Udine, Springer-Verlag, Wien, New York.

Vardoulakis, I. (1977). Scherfugenbildung in Sandkörpern als Verzweigungsproblem. Dissertation, Universität Karlsruhe, Veröffentlichungen IBF, Heft Nr 70.

References

Bardet, J.P. and Proubet, J. (1992). Shear-band analysis in idealized granular material. *ASCE J. Eng. Mech.,* **118,** 397–415.

Bažant, Z.P. (1984). Imbricate continuum and its variational derivation. *ASCE J. Eng. Mech.,* **110,** 1693–1712.

Bažant, Z.P., Belytschko, T.B. and Chang, T.P. (1984). Continuum theory for strain softening. *ASCE J. Eng. Mech.,* **110,** 1666–1692.

Bogdanova-Bontcheva, N. and Lippmann, H. (1975). Rotationssymmetrisches Fliessen eines granularen Modellmaterials. *Acta Mechanica,* **21,** 93–113.

Brown, C.B. and Evans, R.J. (1972). On the application of couple-stress theories to granular media. *Geotechnique,* **22,** 356–361.

Chang, C.S. and Ma, L. (1991). A micromechanical-based micropolar theory for deformation of granular solids. *Int. J. Solids Struct.,* **28,** 67–86.

Cundall, P. (1989). Numerical experiments on localization in frictional materials. *Ingenieur Archiv.,* **59,** 148–159.

De Borst, R. (1988). Bifurcations in finite element models with a non-associated flow law. *Int. J. Num. Anal. Meth. Geomech.,* **12,** 99–116.

De Borst, R. (1990). Simulation of localization using Cosserat theory. *2nd Int. Conf. on Computer Aided Design of Concrete Structures, Zell-am-See,* 4–6 April 1990 (eds. N.Bicanic *et al.*) Pieridge Press, Swansea, 931–944.

De Borst, R. and Mühlhaus, H.-B. (1992). Gradient-dependent plasticity: Formulation and algorithmic aspects. *Int. J. Num. Meth. Eng.,* **35,** 521–540.

Drescher, A., Vardoulakis, I. and Han, C. (1990). A biaxial apparatus for testing soils. *Geotech. Test. J.,* **13,** 226–234.

Germain, P. (1973a). La méthode des puissances visuelles en mécanique des milieux continus. Part I *J. Mécanique,* **12,** 235–274.

Germain, P. (1973b). The method of virtual power in continuum mechanics. Part 2: Microstructure. *SIAM, J. Appl. Math.,* **25,** 556–575.

Griffiths, D.V. (1981). Computation of strain softening behaviour. In: *Implementation of Computer Procedures and Stress-Strain Laws in Geotechnical Engineering,* **2,** 591–603 (eds C.S.Desai and S.K.Saxena), Acorn Press.

Günther, W. (1958). Zur Statik und Kinematik des Cosseratscen Kontinuums. In: *Abhandlungen der Braunscheigschen Wissenschaftlichen Gesellschaft*, Vol. 10,. 195–213. Verlag E.Goltze, Göttingen.

Hammad, W.I. (1991). Modélisation Non Linéaire et Étude Expérimentale des Bandes de Cisaillement dans les Sables. These de Doctorat, Université Joseph Fourier-Grenoble I, 331 pp.

Hermann, G. (1972). Some applications of micromechanics. *Exp. Mech.,* **12,** 235–238.

Kanatani, K. (1979). A micropolar continuum theory for flow of granular materials. *Int. J. Eng. Sci.,* **17,** 419–432.

Kessel, S. (1964). Lineare Elastizitätstheorie des anisotropen Cosserat-Kontinuums. In: *Abhandlungen der Braunscheigschen Wissenschaftlichen Gesellschaft,* Vol. 16, 1–22. Verlag E.Goltze, Göttingen.

Koiter, W.T. (1964). Couple-stresses in the theory of elasticity Parts I and II. In: *Proc. Ned. Koninkl. Nederl. Akad. Wet., Ser. B.,* **67,** 14–44.

Mindlin, R.D. (1964). Micro-structure in linear elasticity. *Arch. Rat. Mech. Anal,* **10,** 51–77.

Mohr, O. (1900). Welche Umstände bedingen die Elastizitätsgrenze und den Bruch eines Materials? *Zeitschr. Vereines deutscher Ingenieure,* **44,** 1–12.

Mühlhaus, H.-B. (1986). Scherfugenanalyse bei granularem Material im Rahmen der Cosserat-Theorie, *Ingenieur Archiv.,* **56,** 389–399.

Mühlhaus, H.-B. (1990). Lamination phenomena in prestressed rock. In: *Rockbursts and Seismicity in Mines* (ed. C.Fairhurst), 101–107. Balkema, Rotterdam.

Mühlhaus, H.-B., de Borst, R. and Aifantis, E. (1991). Constitutive models and numerical analyses for inelastic materials with microstructure, *Proc. IACMAG 91, Cairns, Australia* (eds G.Beer, J.R.Booker and J.P.Carter) Vol. 1, 377–386. Balkema, Rotterdam.

Mühlhaus, H.-B. and Vardoulakis, I. (1987). The thickness of shear bands in granular materials, *Geotechnique,* **37,** 271–283.

Oda, M. (1993). Micro-fabric and couple stress in shear bands of granular materials. *Powders & Grains* 93 (ed. Thornton), 161–166. Balkema, Rotterdam.

Ord, A., Vardoulakis, I. and Kajewski, R. (1991). Shear band formation in Gosford sandstone. *Int. J. Rock Mech. Mining Sci/Geomech. Abstr.,* **28,** 397–409.

Ortiz, M., Leroy, Y. and Needleman, A. (1986). A finite element method for localized failure analysis. *Comp. Meth. Appl. Mech. Eng.,* **61,** 189–214.

Papanastasiou, P. and Vardoulakis, I. (1992). Numerical treatment of progressive localization in relation to borehole stability. *Int. J. Num. Anal. Meth. Geomech.,* **16,** 389–424.

Prevost, J. (1984). Localization of deformation in elastic-plastic solids. *Int, J. Num. Anal. Meth. Geomech.,* **8,** 187–196.

Roscoe, K.H. (1970). The influence of strains in soil mechanics. *Géotechnique,* **20,** 129–170.

Satake, M. (1968). Some considerations of the mechanics of granular materials. In: *Mechanics of Generalized Continua, IUTAM Symposium Freudenstadt and Stuttgart,* 1967, 156–159. Springer-Verlag, Berlin.

Scarpelli, G. and Wood, D.M. (1982). Experimental observations of shear band patterns in direct shear tests. In: *Deformation and Failure of Granular Materials*, 473–484. Balkema, Rotterdam.

Schaefer, H. (1962). *Versuch einer Elastizitätstheorie des zweidimensionalen ebenen COSSERAT-Kontinuums. Miszellannenn der Angewandten Mechanik.* Akademie-Verlag, Berlin.

Schaefer, H. (1967). Das Cosserat-Kontinuum. *ZAMM,* **47**(8), 485–498.

Shuttle, D.A. and Smith, I.M. (1988). Numerical simulation of shear band formation in soils. *Int. J. Num. Anal. Meth. Geomech.,* **12,** 6s11–626.

Sluys, L.J. (1990). Localization in a Cosserat continuum under dynamic loading conditions. TU Delft, Report nr. 25.2–90–5–15.

Steinmann, P. (1992). Lokalisierungsprobleme in der Plastomechanik. Dissertation, Universität Karlsruhe.

Teichman, J. (1990). Scherfugenbildung and Vespannungseffekte bei der Siloentlehrung, PhD Thesis, Institute for Soil and Rock Mechanics, University of Karlsruhe, Germany.

Unterreiner, P. (1994). Modélisation des Interfaces en Mécanique des Sols: Applications aux Calculs en Deformation des Murs en Sol Cloué. These de Doctorat de l'ENPC, Paris.

Vardoulakis, I. (1974). Berechnungsverfahren für Erdkörper mit plastischer Ver- und Entfestigung: Entstehung und Ausbreitung von Scherfugen. DFG Report GU 103/16.

Vardoulakis, I. (1978). Equilibrium bifurcation of granular earth bodies. *Adv. Anal. Geotech. Instabilities,* **13,** 65–120.

Vardoulakis, I. (1989). Shear-banding and liquefaction in granular materials on the basis of a Cosserat continuum theory. *Ingenieur Archiv,* **59,** 106–113.

Vardoulakis, I. and Drescher, A. (1989). Bi-axial geomaterial test system. US Patent No. 4,825,700 and 4,885,941.

Vardoulakis, I. and Graf, B. (1985). Calibration of constitutive models for granular materials using data from biaxial experiments. *Géotechnique,* **35,** 299–317.

Vardoulakis, I., Graf, B. and Hettler, A. (1985). Shear-band formation in a fine-grained sand, *5th Int. Conf. Num. Meth. Geomech.,* Vol. 1, 517–521. Balkema, Rotterdam.

Vardoulakis, I. and Goldscheider, M. (1981). A biaxial apparatus for testing shear bands in soils, *10th ICSMFE, Stockholm,* 1981, Vol. **4**(61), 819–824. Balkema, Rotterdam.

Vardoulakis, I. and Unterreiner, P. (1994). Interfacial localisation in simple shear tests on granular medium modelled as a Cosserat continuum. In *Mechanics of Geomaterials Interfaces* (eds A.P.S.Selvadurai and M.Boulon). Elsevier, Amsterdam.

Veeken, C.A., Walters, J.V., Kenter, C.J. and Davis, D.R. (1989). Use of plasticity models for predicting borehole stability. *Rock at Great Depth* (eds V.Maury and D.Fourmaintraux), **2,** 835–844. Balkema, Rotterdam.

Watterson, J. (1986). Fault dimensions, displacements and growth. *Pageoph.,* **124**, 365–373.

10
Second-grade plasticity theory for geomaterials

10.1
Mindlin's formalism of microstructure

Mindlin (1964) formulated a general and powerful theory for micro-structure in linear isotropic elasticity, whose simplest application is Cowin and Nunziato's (1983) linear void elasticity. Such a theory could be used, for example, as a starting point for the formulation of an advanced poro-elasticity theory of fluid-infiltrated media. In this chapter, however, the emphasis lies on plasticity theories and Cowin's work will not be elaborated further. As shown by Vardoulakis and Frantziskonis (1992), the basic formalism of Mindlin's continuum theory can be successfully applied in the formulation of gradient-dependent plasticity theories for geomaterials, like sands and psammitic rocks, which are straightforward generalizations of existing 3D constitutive models.

10.1.1
Kinematics

Consider a body **B,** which at a configuration C*(t)* occupies the volume *V,* with boundary ∂V. Let x_i and $\bar{x}_i (i = 1,2,3)$ be the coordinates of a macro-*material particle* **X** in C*(t)* and $\bar{\mathrm{C}} = \mathrm{C}(t + \Delta t)$, respectively, measured from a fixed-in-space Cartesian coordinate system. The components of the (infinitesimal) displacement vector of the macro-particle **X** are defined as

$$\Delta u_i = \bar{x}_i - x_i \tag{10.1.1}$$

The infinitesimal macro-strain and macro-rotation are defined as usual as the symmetric and antisymmetric part of the displacement gradient,

$$\begin{aligned} \Delta\varepsilon_{ij} &= \tfrac{1}{2}(\partial_i \Delta u_j + \partial_j \Delta u_i) \\ \Delta\omega_{ij} &= \tfrac{1}{2}(\partial_i \Delta u_j - \partial_j \Delta u_i) \end{aligned} \tag{10.1.2}$$

We assume now that the macro-particle possesses a simple micro-structure defined as follows: In each macro-material particle X we assume that there is a micro-volume V' embedded, in which the spatial position vectors of *micro-material particle* X′ are x_i' and $\bar{x}_i'$

in C and $\bar{\mathbf{C}}$, respectively. We assume that the position of the micro-particle is measured with respect to a single Cartesian coordinate system (x_i'), parallel to the x_i-system, such that the origin of the coordinates x_i' moves with the macroscopic displacement Δu_i. A microdisplacement $\Delta u_i'$ is defined, with components,

$$\Delta u_i' = \bar{x}_i' - x_i' \tag{10.1.3}$$

Within the frame of an infinitesimal theory all micro- and macro-displacement gradients are assumed to be small as compared to unity. Moreover, we assume that the micro-displacement can be expressed accurately enough as

$$\Delta u_j' = x_k' \Delta \psi_{kj}(x_i, t) \tag{10.1.4}$$

The quantity

$$\Delta \psi_{ij} = \partial_i' \Delta u_j' \tag{10.1.5}$$

is called the *micro-deformation,* and is accordingly taken to be homogeneous in the micro-medium V'. The symmetric part

$$\Delta \psi_{(ij)} = \tfrac{1}{2}(\Delta \psi_{ij} + \Delta \psi_{ji}) \tag{10.1.6}$$

is called the micro-strain, and the antisymmetric part

$$\Delta \psi_{[ij]} = \tfrac{1}{2}(\Delta \psi_{ij} - \Delta \psi_{ji}) \tag{10.1.7}$$

is called the micro-rotation.

The difference between the macro-displacement gradient and the micro-deformation is called the relative deformation,

$$\Delta \gamma_{ij} = \partial_j \Delta u_i - \Delta \psi_{ij} \tag{10.1.8}$$

Finally the quantity

$$\Delta \kappa_{ijk} = \partial_i \Delta \psi_{jk} \tag{10.1.9}$$

is called the micro-deformation gradient.

All three tensors $\Delta \varepsilon_{ij}$, $\Delta \gamma_{ij}$ and Δk_{ijk} are independent of the micro-coordinates x_i', typical components of which are shown in Figures 10.1.1 and 10.1.2.

We may summarize the above definitions as follows: On a macroscopic level one usually introduces at any point $\mathbf{X}$ the *vector* displacement, Δu_i, and derives from it the displacement gradient, $\partial_i \Delta u_j$. If for some reason this description of the deformation is not sufficiently accurate, then one introduces at any point $\mathbf{X}$ in addition to the vector Δu_i the *tensor* micro-deformation, $\Delta \psi_{ij}$, and derives from it the micro-deformation gradient, $\partial_i \Delta \psi_{jk}$ The deviation between macro- and micro-deformation is measured by the relative deformation tensor $\Delta \gamma_{ij}$.

The basic kinematic quantities Δu_i and $\Delta \psi_{ij}$ are assumed to be single-valued functions of x_i, leading to the following compatibility equations,

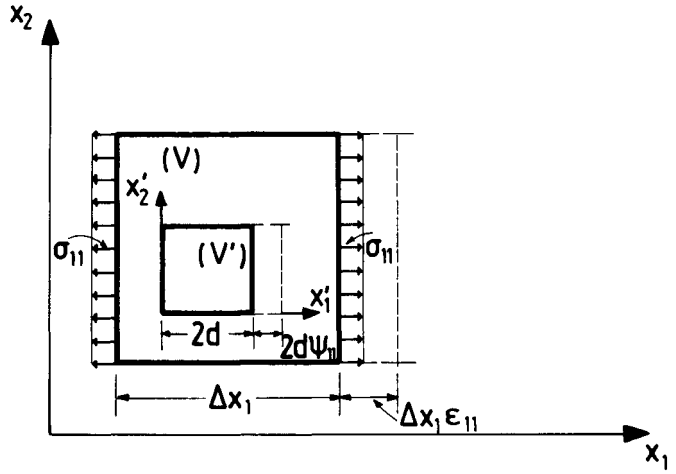

Figure 10.1.1 Total stress σ_{11}, displacement gradient $\partial_1 u_1$, micro-deformation ψ_{11} and relative deformation $\gamma_{11}=\partial_1 u_1-\psi_{11}$

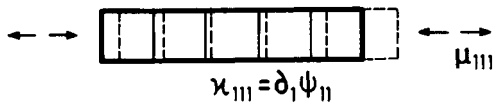

Figure 10.1.2 Double stress μ_{111} and gradient of micro-deformation κ_{111}.

$$\begin{aligned} e_{mik}e_{nlj}\partial_i\partial_j\Delta\varepsilon_{kl} &= 0 \\ e_{mij}\partial_i\Delta\kappa_{jkl} &= 0 \\ \partial_i(\Delta\varepsilon_{jk}+\Delta\omega_{jk}-\Delta\gamma_{jk}) &= \Delta\kappa_{ijk} \end{aligned} \tag{10.1.10}$$

10.1.2 The principle of virtual work

Germain (1973a,b) suggested a general framework for the foundation of consistent higher grade continuum theories on the basis of the virtual work principle. This approach starts with the definition of the virtual work $\delta w^{(i)}$ of internal forces at any point, which for a Mindlin-type continuum is defined as follows

$$\delta w^{(i)} = \tau_{ij}\delta\varepsilon_{ij} + \alpha_{ij}\delta\gamma_{ij} + \mu_{ijk}\delta\kappa_{ijk} \tag{10.1.11}$$

The expression for the virtual work gives in turn rise to the identification of the corresponding stress tensors. Here, according to 10,1.11, the stress tensor, τ_{ij}, which is dual in energy to the macroscopic strain, is symmetric and is called by Mindlin the Cauchy stress. The stress tensor, α_{ij}, which is dual in energy to the relative deformation is called the relative stress, and the higher-order stress tensor, μ_{ijk}, which is dual in

energy to the micro-deformation gradient is called the double stress. By using equations 10.1.2.1 and 10.1.8, the work of internal forces becomes

$$\delta w^{(i)} = \sigma_{ij}\partial_i \delta u_j - \alpha_{ij}\delta\psi_{ij} + \mu_{ijk}\delta\kappa_{ijk} \tag{10.1.12}$$

where

$$\sigma_{ij} = \tau_{ij} + \alpha_{ij} \tag{10.1.13}$$

is called the total stress tensor.

The definition 10.1.11 of the virtual work of internal forces gives rise also to the definition of the virtual work of corresponding external forces, i.e. body forces and surface tractions,

$$\delta W^{(e)} = \int_V f_i \delta u_i \, dV + \int_{\partial V} t_i \delta u_i \, dS + \int_V \Phi_{ij}\delta\psi_{ij} \, dV + \int_{\partial V} T_{ij}\delta\psi_{ij} \, dS \tag{10.1.14}$$

f_i is identified as the body force per unit volume, t_i as the surface traction per unit surface area. Φ_{ij} is the double-force per unit volume, and T_{ij} is double-traction per unit surface area. We notice that double-force systems without movement are stress systems equivalent to two oppositely directed forces at the same point. Within the realm of linear elasticity singularities of this type are discussed, for example, by Love (1927, section 132).

Using d'Alembert's principle, macro- and micro-inertial terms may be included in the above expression for the virtual work of external forces. In this case, in equation 10.1.14 the body force f_i is to be replaced by $(f_i - \rho\partial_{tt}\Delta u_i)$, and the double-body force Φ_{ij} by $(\Phi_{ij} - I_{ijkl}\partial_{tt}\Delta\psi_{kl})$, where I_{ijkl} is an appropriate micro-inertial tensor.

The variations δ_{ui} and $\delta\psi_{ij}$ are treated as independent. Then from the virtual work equation

$$\int_V \delta w^{(i)} \, dV = \delta W^{(e)} \tag{10.1.15}$$

one obtains two integral equations: one concerning the macro-mechanics of the medium

$$\int_V \{\sigma_{ij}\partial_i \delta u_j - f_i \delta u_i\} \, dV = \int_{\partial V} t_i \delta u_i \, dS \tag{10.1.16}$$

and, another concerning the micro-mechanics

$$\int_V \{-\alpha_{ij}\delta\psi_{ij} + \mu_{ijk}\partial_i \delta\psi_{jk} - \Phi_{ij}\delta\psi_{ij}\} \, dV = \int_{\partial V} T_{ij}\delta\psi_{ij} \, dS \tag{10.1.17}$$

In order to evaluate these integral equations, the boundary ∂V is divided into complementary parts $\{\partial V_u, \partial V_\sigma\}$ and $\{\delta V_\psi, \delta V_\gamma\}$, respectively, such that

$$\begin{aligned} &\text{on } \partial V_u\text{: } \Delta u_i = \delta_i \quad \text{and} \quad \delta u_i = 0 \\ &\text{on } \partial V_\psi\text{: } \Delta \psi_{ij} = \theta_{ij} \quad \text{and} \quad \delta \psi_{ij} = 0 \end{aligned} \tag{10.1.18}$$

are prescribed. From equations 10.1.16 to 10.1.18, Gauss' theorem and d'Alembert's principle one finally obtains the following dynamic equations, holding for the macro- and micro-medium respectively:

$$\text{in } V\text{: } \quad \partial_i \sigma_{ij} + f_j = \rho \partial_{tt} \Delta u_j \tag{10.1.19}$$

$$\text{on } \partial V_\sigma\text{: } n_i \sigma_{ij} = t_j \tag{10.1.20}$$

and

$$\text{in } V\text{: } \quad \alpha_{jk} + \partial_i \mu_{ijk} + \Phi_{jk} = I_{jkmn} \partial_{tt} \Delta \psi_{mn} \tag{10.1.21}$$

$$\text{on } \partial V_\mu\text{: } n_i \mu_{ijk} = T_{jk} \tag{10.1.22}$$

Note that according to equation 10.1.19 the total stress tensor, $\sigma_{ij} = \tau_{ij} + \alpha_{ij}$, is identified with the common (macroscopic) equilibrium stress tensor.

In case of vanishing relative deformation the micro-deformation coincides with the macro-deformation

$$\Delta \gamma_{ij} \equiv 0 \rightarrow \Delta \psi_{ij} \equiv \partial_i \Delta u_j \tag{10.1.23}$$

and the corresponding medium may be called a restricted Mindlin continuum. In this case δu_i and $\delta \psi_{ij}$ are not independent variations, and the virtual work equations must be modified accordingly. This will be done in section 10.2.4 in the context of flow theory of plasticity for geomaterials.

10.1.3
Example: Gradient elasticity theory with surface energy

In order to demonstrate the potential of the considered continuum theories with microstructure we select here a rather neglected early application of these concepts done by Casal (1961), which is referenced in the aforementioned papers by Germain (1973a,b). Casal's model cannot be directly embedded in Midlin's linear, isotropic elasticity theory with micro-structure, because it is an anisotropic elasticity model. For demonstration purposes we consider first the 1D example of the simple tension bar, as shown in Figure 10.1.3. In the uniaxial case the strain energy of the tension bar is defined as follows

$$W = \frac{1}{2} \int_0^L E\{\varepsilon^2 + \ell_V^2 (\nabla \varepsilon)^2\} \mathrm{d}x + \frac{1}{2} [E \ell_S \varepsilon^2]_0^L \tag{10.1.24}$$

where

$$\nabla \varepsilon = \frac{\mathrm{d}\varepsilon}{\mathrm{d}x} \tag{10.1.25}$$

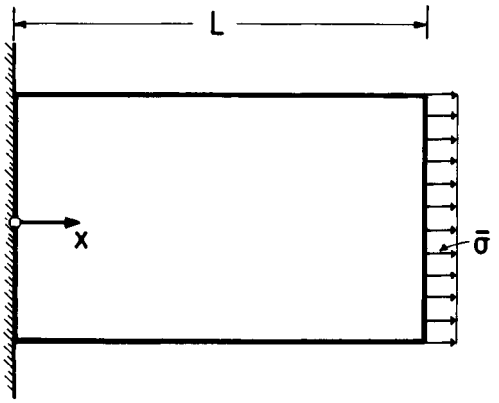

Figure 10.1.3 Simple tension bar with a clamped and free end.

are the various notations for the strain gradient. Casal's expression for the elastic strain energy equation 10.1.24 consists of two terms: (a) a 'volumetric energy' term which includes the contribution of the strain gradient, and (b) a 'surface energy' term. Accordingly, ℓ_v and ℓ_s are material lengths related to volumetric and surface elastic strain energy.

Casal's expression 10.1.24 for the global strain energy of the tension bar is recovered by introducing an appropriate anisotropic, linear elastic, restricted Mindlin-type continuum. Since in a restricted continuum the relative deformation vanishes, the variation of the strain energy density becomes

$$\delta w = \tau \delta \varepsilon + \mu \delta \nabla \varepsilon \tag{10.1.26}$$

In connection with this variation, Casal's model is equivalent to the following constitutive assumptions for the Cauchy and double stress

$$\tau = \frac{\partial w}{\partial \varepsilon} = E(\varepsilon + \ell_s \nabla \varepsilon) \tag{10.1.27}$$

$$\mu = \frac{\partial w}{\partial \nabla \varepsilon} = E(\ell_s \varepsilon + \ell_v^2 \nabla \varepsilon) \tag{10.1.28}$$

From equations 10.1.26 to 10.1.28 the elastic strain energy density is computed, resulting in the following expression

$$w = \tfrac{1}{2} E\{\varepsilon^2 + \ell_v^2 (\nabla \varepsilon)^2\} + \tfrac{1}{2} E \ell_s \nabla \varepsilon^2 \tag{10.1.29}$$

It turns out that for w>0, the material lengths must be restricted, such that

$$0 < \ell_s < \ell_v \tag{10.1.30}$$

This means in particular that if surface energy terms are included then volume strain-gradient terms must be also included. It is worth noticing that in Griffith's (1921) theory

of cracks only surface energy is considered, which is of course inadmissible in the sense of inequality 10.1.30. Strain-gradient terms could be important since in the crack tip region strain gradients are very high. On the other hand Altan and Aifantis (1992) in analysing Mode III cracks have essentially only considered the volumetric strain-gradient energy term and they have ignored the surface energy term, which is admissible within the frame of the considered elasticity theory (cf. Vardoulakis *et al.*, 1995).

Finally we remark that, with

$$W = \int_0^L w \, \mathrm{d}x \tag{10.1.31}$$

from equation 10.1.29, equation 10.1.24 is recovered.

In the uniaxial case equilibrium condition holds for the total stress,

$$\frac{\mathrm{d}\sigma}{\mathrm{d}x} = 0 \tag{10.1.32}$$

where

$$\sigma = \tau + \alpha \tag{10.1.33}$$

and α is the workless relative stress, which in turn is in equilibrium with the double stress

$$\alpha + \frac{\mathrm{d}\mu}{\mathrm{d}x} = 0 \tag{10.1.34}$$

The gradient-elasticity total stress-strain relation is finally derived from equations 10.1.28, 10.1.29 and 10.1.33,

$$\sigma = E(\varepsilon - \ell_{\mathrm{V}}^2 \nabla^2 \varepsilon) \tag{10.1.35}$$

The tension bar problem is thus defined by (a) the constitutive equations 10.1.35 and 10.1.28 for the total stress σ and the double stress μ; (b) the equilibrium condition 10.1.32 for the total stress; and (c) appropriate boundary conditions. As such we select the following:

$$\begin{aligned} &\text{for } x = 0\text{: } u = 0 \quad \text{and} \quad \mathrm{d}u/\mathrm{d}x = 0 \text{ (Dirichlet)} \\ &\text{for } x = L\text{: } \sigma = \bar{\sigma} \quad \text{and} \quad \mu = 0 \qquad \text{(Newmann)} \end{aligned} \tag{10.1.36}$$

The solution of this problem is inhomogeneous strain under constant stress

$$\varepsilon = \left\{ 1 + \frac{\cosh(x/\ell_{\mathrm{V}}) - \sinh[(L-x)/\ell_{\mathrm{V}}] - (\ell_{\mathrm{V}}/\ell_{\mathrm{S}})(\sinh(x/\ell_{\mathrm{V}}) + \cosh[(L-x)/\ell_{\mathrm{V}}])}{[1 - (\ell_{\mathrm{V}}/\ell_{\mathrm{S}})^2]\sinh(L/\ell_{\mathrm{V}})} \right\} \frac{\bar{\sigma}}{E} \tag{10.1.37}$$

As indicated in Figure 10.1.4 both strain and strain energy are constant along the bar except at both ends, where boundary effects are dominant. It should be noted that for the lower limit $\ell_{\mathrm{S}}/\ell_{\mathrm{V}} \to 0^+$, strain gradient effects are least pronounced, while they are notably accentuated for the upper limit $\ell_{\mathrm{S}}/\ell_{\mathrm{V}} \to 1^-$.

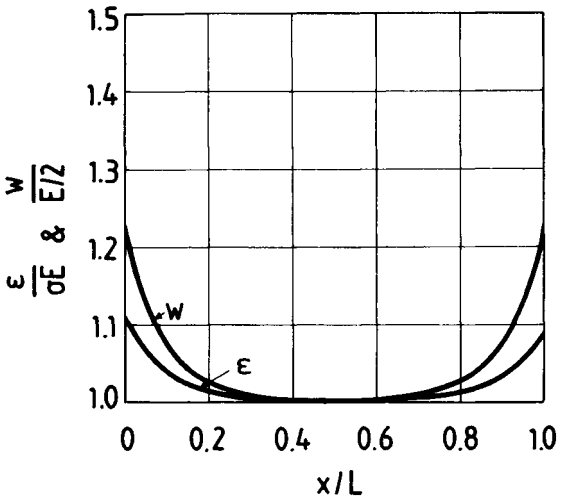

Figure 10.1.4 Gradient elasticity with surface tension: strain and strain energy distribution in a tension bar (L=1; ℓ_v=0.1; ℓ_s=0.01).

Notice that the 3D generalization of the gradient-dependent elasticity with surface energy considered here is straightforward. In 3D, the strain energy density becomes

$$w = \tfrac{1}{2}\lambda\varepsilon_{pp}\varepsilon_{qq} + G\varepsilon_{pq}\varepsilon_{qp} + G\ell^2\partial_r\varepsilon_{pq}\partial_r\varepsilon_{qp} + G\partial_r(\ell_r\varepsilon_{pq}\varepsilon_{qp}) \tag{10.1.38}$$

where λ and G are the Lamé constants, and,

$$\ell = \ell_V;\ \ell_r = \ell_S v_r;\ v_r v_r = 1 \tag{10.1.39}$$

We observe that 10.1.38 leads to a gradient elasticity with constant characteristic directors, v_r. The meaning of the last term as a surface-energy term is obvious, since

$$\int \partial_r(\ell_r\varepsilon_{pq}\varepsilon_{qp})\mathrm{d}V = \ell_S \oint (\varepsilon_{pq}\varepsilon_{qp})(v_r n_r)\mathrm{d}S \tag{10.1.40}$$

and n_r is the unit normal to the boundary.

Finally we remark that from 10.1.38 follow directly the constitutive relations for the stresses,

$$\begin{aligned} \sigma_{pq} &= \lambda\varepsilon_{rr}\delta_{pq} + 2G(\varepsilon_{pq} - \ell^2\nabla^2\varepsilon_{pq}) \\ \mu_{rpq} &= 2G(\ell_r\varepsilon_{pq} + \ell^2\partial_r\varepsilon_{pq}) \end{aligned} \tag{10.1.41}$$

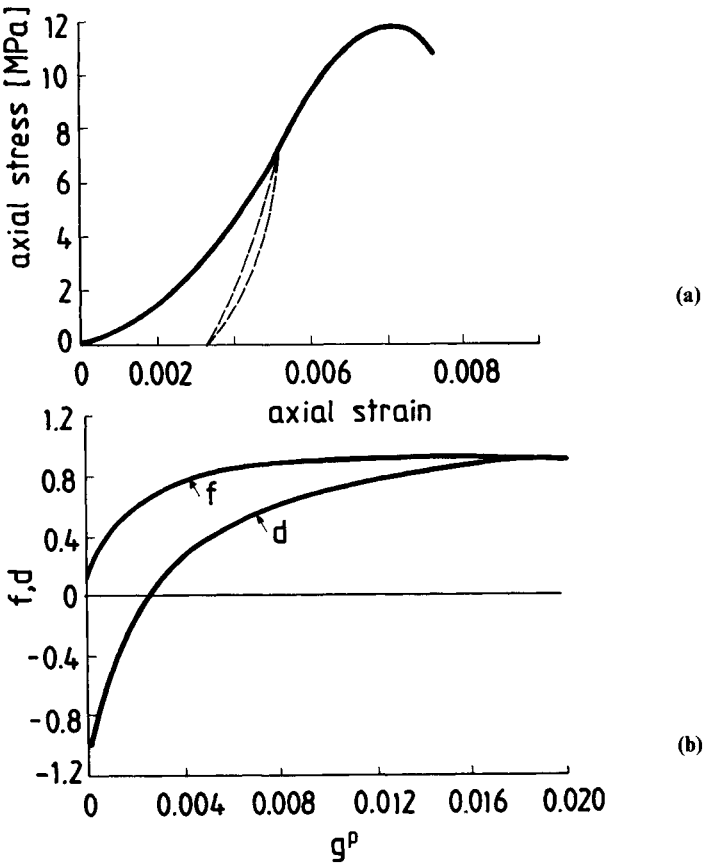

Figure 10.2.1 (a) Typical uniaxial stress-strain curve for sandstone; (b) typical variation of mobilized friction and dilatancy coefficients for sandstone.

10.2
Second-grade plasticity theory for granular rocks

10.2.1
Observational background

Sandstones are psammitic rocks which exhibit elasticity, internal friction, cohesion and dilatancy. Accordingly, they can be modelled within the frame of elastoplasticity theory. Starting from their elasticity it should be mentioned that the experiment indicates that sandstone elasticity is stress-dependent (Santarelli *et al.,* 1986). Stress dependence of the elastic moduli can account for an initially convex upward stress-strain curve in uniaxial compression, which is micro-mechanically attributed to closing of cracks (Figure 10.2.1a). Mathematically, this effect can be modelled by assuming an

appropriate complementary elastic energy density function, which plays the role of an elastic strain potential and leads to a hyperelastic model (see section 6.2.2). In addition, rock elasticity degrades in due course of the deformation due to micro-crack generation; this phenomenon is captured mathematically by introducing plastic strain as an additional internal variable into the appropriate state function (e.g. the free energy; cf. Lemaître, 1992). For simplicity, both phenomena of stress- and plastic strain-dependent elasticity will be neglected here. In particular, linear, isotropic elasticity will be assumed.

The emphasis lies here in modelling plasticity of sandstones. Within the frame of plasticity theory, the experimental data clearly support a mixed, hardening/softening model. In particular, one finds very good agreement with the following assumption. The plastic shearing strain intensity (as already discussed in previous chapters) is a good macroscopic measure of plastic slip, which occurs at intergranular boundaries and across micro-cracks. Past the state of initial yield, friction is mobilized as function of plastic shear strain and reaches saturation at some given peak value. On the other hand, in the course of deformation, new micro-cracks are activated and new ones are formed. We therefore can assume that all observed deviatoric stress softening must be attributed to micro-cracking, which leads to a decrease in tensile strength. This softening mechanism is active during all stages of the straining process. However, it becomes more pronounced when the material loses its capacity to mobilize additional frictional resistance. Thus for simplicity we may assume that during the friction hardening phase all cohesion softening is negligible, and that it becomes noticeable only past the peak of mobilized friction.

The above 'standard' model is corroborated by acoustic emission (AE) data. AE in sandstones under triaxial compression usually starts to increase gradually at about 60% of peak deviator. The maximum rate of AE events is monitored inside the deviator-softening regime, and is followed by a decrease in the rate of AE events. Such an observation indicates that past the point of maximum rate of AE the size of the actual localized softening zone is already a small fraction of the specimen size, with a decreasing tendency as the global deformation continues. Thus the point of maximum rate of AE must correspond to the point of observable localized failure.

Concerning plastic volumetric strains, the experimental data show that at low confining pressures the rock dilates strongly, whereas at higher confining pressures rock dilatancy diminishes. This pressure sensitivity of the plastic volumetric strains indicates that they must be generally split into a part due to dilatancy and a part due to compaction (grain slip and rotation with partial grain crushing). In this section the effect of compaction will be neglected and thus plastic volume changes are assumed to be solely linked to plastic-frictional yield. Thus dilatancy is understood as a constitutive constraint between plastic volumetric and plastic shear strain increments.

As indicated in Figure 10.2.1(b), the mobilized dilatancy coefficient $d = d(g^p)$ is always bound by the mobilized friction coefficient $f = f(g^p)$ $(d \leqslant f)$. Without significant error d may be approximated by *f,* leading to the simple volumetric normality flow rule

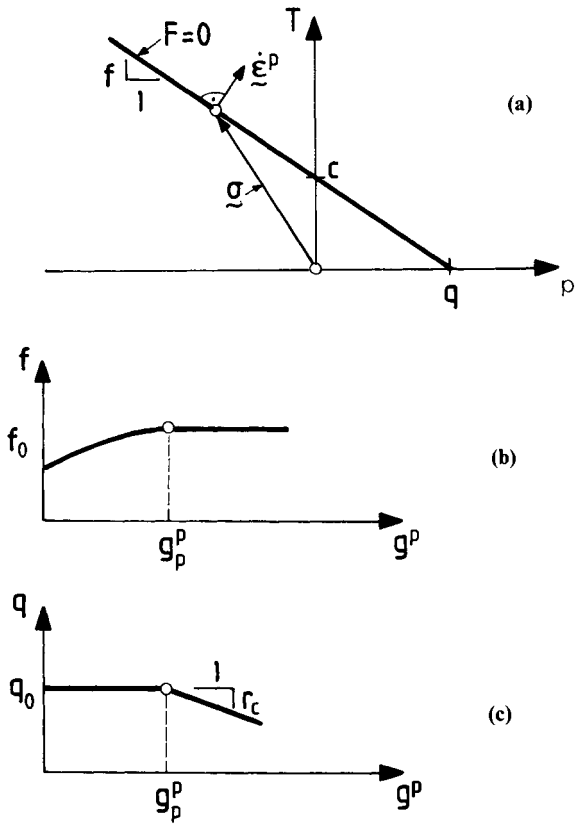

Figure 10.2.2 (a) Coulomb yield surface in the *(T, p)*-plane with the plastic strain-rate vector acting normal to it; (b) friction hardening function; (c) cohesion softening function.

$$d \approx f \tag{10.2.1}$$

Accordingly, such a constitutive model for rock is termed as a friction-hardening/ cohesion-softening model with dilatancy, associated to friction according to the 'normality' rule.

The above basic constitutive assumptions are illustrated graphically in Figure 10.2.2: Figure 10.2.2(a) shows the trace of a Coulomb-type yield surface in a *(p, T)*-plane, with the plastic strain-rate vector $\{\dot{v}^p, \dot{g}^p\}^T$ acting normal to it. The yield surface is depicted in this figure by a straight line

$$F = T - (q - p)f = 0 \tag{10.2.2}$$

which intersects the *T*-axis at a point where we read the actual value of the mobilized cohesion,

$$c = qf \tag{10.2.3}$$

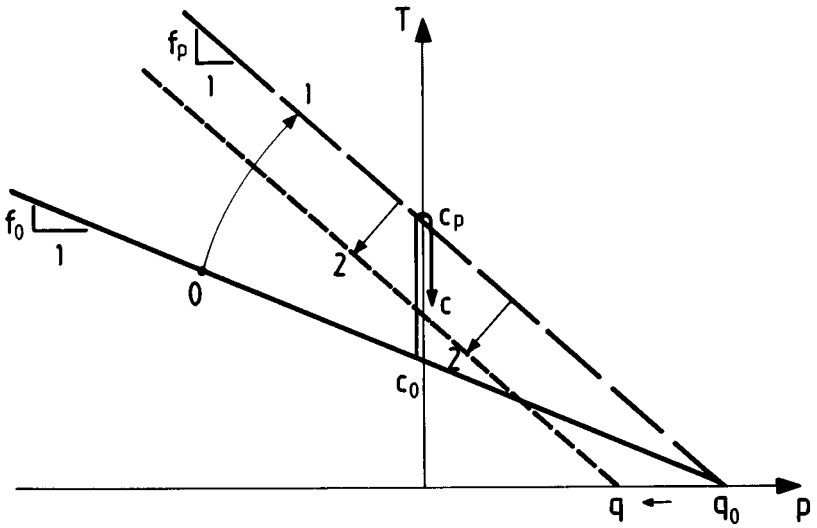

Figure 10.2.3 Motion of the yield surface in stress-space: (0−1) 'isotropic' friction-hardening phase; (1−2) 'kinematic' cohesion-softening phase.

Figures 10.2.2(b,c) show the assumed typical variation of the mobilized friction coefficient f and of the tensile strength parameter q, respectively as functions of plastic shear strain g^p. Due to the assumed rock behavior, depicted in these figures, and the above expression for the cohesion, all cohesion hardening is attributed to the mobilization of internal friction, and all cohesion softening to the degradation of tensile strength, i.e.

$$c = \begin{cases} q_0 f(g^p) & \text{for } 0 \leqslant g^p \leqslant g_p^p \\ f_p q(g^p) & \text{for } g_p^p \leqslant g^p \end{cases} \tag{10.2.4}$$

It should be noted that in Figure 10.2.2(c), a simple linear softening function is depicted. This is because material softening is non-observable but it is indirectly detectable. In these cases it is advisable to start with the simplest function and through back-analysis of experimental data to match the corresponding material parameters (in the considered case these are q_0 and the slope r_c of the descending straight line). Figure 10.2.3 illustrates the corresponding motion of the yield surface in stress-space in due course of plastic deformation. One observes first 'isotropic' friction-hardening (0–1), followed by 'kinematic' cohesion softening (1–2).

10.2.2
Constitutive modeling

Following Prager's (1955, 1956) original ideas, Vardoulakis and Frantziskonis (1992) noticed that the kinematic character of cohesion-softening can be easily modeled by assuming that the yield function depends on a reduced stress

$$\tau_{ij} = \sigma_{ij} - \alpha_{ij} \tag{10.2.5}$$

where σ_{ij} is the true (equilibrium) stress, and α_{ij} is a 'back' stress. Accordingly, the yield function is written as a function of the reduced stress

$$F = F(\tau_{ij}, \psi) \tag{10.2.6}$$

where the explicit reference of the plastic state parameter ψ signifies the isotropic character of friction hardening. For example, if we adopt a Drucker-Prager type of yield function, then equation 10.2.6 becomes,

$$F = \sqrt{(J_{2t})} - (q_0 - I_{1\tau}/3)f \tag{10.2.7}$$

where

$$I_{1\tau} = \tau_{kk};\ J_{2t} = (\tfrac{1}{2} t_{ij} t_{ji})^{\frac{1}{2}} \tag{10.2.8}$$

$$\tau_{ij} = t_{ij} + (\tfrac{1}{3})\tau_{kk}\delta_{ij} \tag{10.2.9}$$

Thus isotropic friction hardening is described by the hardening modulus

$$H_t = -\frac{\partial F}{\partial \psi} = -\frac{1}{3} I_{1\tau} \frac{\mathrm{d}f}{\mathrm{d}\psi} \tag{10.2.10}$$

In order to illustrate the effect of back stress, we specialize the representation further for axisymmetric motions of compression, with

$$\{\sigma_{ij}\} = \begin{bmatrix} \sigma_{11} & 0 & 0 \\ 0 & \sigma_{22} & 0 \\ 0 & 0 & \sigma_{33} \end{bmatrix};\ \sigma_{33} \leqslant \sigma_{11} \leqslant \sigma_{22} \tag{10.2.11}$$

In this case we have

$$p = p_\tau + p_\alpha;\ T = T_\tau + T_\alpha \tag{10.2.12}$$

where

$$\begin{aligned} p &= I_{1\sigma}/3 = (2\sigma_{11} + \sigma_{33})/3 \\ T &= \sqrt{(J_{2s})} = (1/\sqrt{3})(\sigma_{11} - \sigma_{33}) \geqslant 0 \end{aligned} \tag{10.2.13}$$

and with similar expressions holding for p_τ, p_α and T_τ, T_α. Accordingly the yield function, defined by equation 10.2.7, becomes

$$F = T - f(q_\alpha - p) \tag{10.2.14}$$

$$q_\alpha = q_0 + \frac{1}{f}[T_\alpha + fp_\alpha] \tag{10.2.15}$$

We notice that the model is defined in such a way that the back-stress αij does not evolve in the hardening regime of f and that it does evolve as soon as f reaches its peak value, f_p, in the cohesion-softening regime.

In the considered model the flow rule is associated, and accordingly F is serving as plastic strain-rate potential,

$$\dot{\varepsilon}^p_{ij} = \frac{\partial Q}{\partial \tau_{ij}}\dot{\psi}(\dot{\psi} \geqslant 0);\ Q \equiv F \text{ (associativity)} \tag{10.2.16}$$

In the considered case of a D.-P. potential function, $\dot{\psi}$ coincides with the plastic shearing strain-rate intensity,

$$\begin{aligned} \dot{\psi} &= \dot{g}^p = \sqrt{(2\dot{e}^p_{ij}\dot{e}^p_{ji})} \\ \dot{\varepsilon}^p_{ij} &= \dot{e}^p_{ji} + (\tfrac{1}{3})\dot{v}^p\delta_{ij} \end{aligned} \tag{10.2.17}$$

and thus the dilatancy constraint becomes

$$\dot{v}^p = f\dot{g}^p \tag{10.2.18}$$

cf. Figure 10.2.2(a).

The physical meaning of the back stress can be appreciated by considering post-peak states more closely. For g^p_p

$$\begin{aligned} f &= f_p \\ q &= q_\alpha < q_0 \\ c &= f_p q_\alpha < c_p = f_p q_0 \end{aligned} \tag{10.2.19}$$

In this case the first-order plastic stress-power becomes,

$$P^p = \sigma_{ij}\dot{\varepsilon}^p_{ij} = p\dot{v}^p + T\dot{g}^p \tag{10.2.20}$$

However, due to the normality condition,

$$(p - q_\alpha)\dot{v}^p + T\dot{g}^p = 0 \tag{10.2.21}$$

and with that the plastic stress-power, equation 10.2.20, becomes

$$P^p = q_\alpha\dot{v}^p = q_\alpha f_p\dot{g}^p = c\dot{g}^p < c_p\dot{g}^p \tag{10.2.22}$$

If one would equate the local dissipation with the plastic stress power, then from equation 10.2.22 would follow that the local dissipation should decrease in the post-peak regime. This would be in contradiction to acoustic emission recordings, which indicate increasing activity (damage) past the peak point of the stress deviator (cf. Figure 10.2.1). In order to remedy that we assume that the local dissipation consists of two parts,

$$D_{loc} = P^p + S_d \tag{10.2.23}$$

where S_d corresponds to the rate of local entropy production due to damage. In order to specify S_d, we make the following constitutive assumption: In all *post-peak states the local dissipation is constant,*

$$\text{for } g^p \geqslant g_p^p\text{: } D_{loc} = \text{const.} \tag{10.2.24}$$

This assumption, together with the observation that at peak

$$D_{loc} = P^p = c_p \dot{g}^p \tag{10.2.25}$$

results finally in the well-known expression of the local dissipation of kinematic plasticity (Mróz, 1973)

$$D_{loc} = (p - q_\alpha)\dot{v}^p + (T - T_\alpha)\dot{g}^p \tag{10.2.26}$$

This in turn means that

$$S_d = -(q_\alpha \dot{v}^p + T_\alpha \dot{g}^p) = (c_p - c)\dot{g}^p \geqslant 0 \tag{10.2.27}$$

The last finding is generalized to provide an expression for the local entropy production due to damage in the softening regime,

$$S_d = -\alpha_{ij}\dot{\varepsilon}_{ji}^p + \dots \tag{10.2.28}$$

The dots on the right-hand side of this equation stand for higher-grade terms. For example, if the effect of plastic strain-rate gradient is noticeable, then

$$S_d = -\alpha_{ij}\dot{\varepsilon}_{ji}^p + \mu_{ijk}\partial_i\dot{\varepsilon}_{jk}^p + \dots \tag{10.2.29}$$

Here μ_{ijk} may be termed a double stress, since it is an associate thermodynamic variable to the plastic strain gradient. It is expected that their effect is *entropy reduction,* due to structures formation (localization), which in turn will ameliorate the strong effect of entropy increase of the back-stress.

These observations and assumptions allow us (in accordance to the definitions for the kinematics of a Mindlin continuum presented in the previous section) to make the following identifications: The plastic strain-rate tensor is a micro-deformation measure

$$\dot{\varepsilon}_{ij}^p \equiv \dot{\psi}_{ij} \tag{10.2.30}$$

and the plastic strain-rate gradient is the corresponding micro-deformation gradient,

$$\partial_i\dot{\varepsilon}_{jk}^p = \dot{\kappa}_{ijk} \tag{10.2.31}$$

In other words within the frame of plasticity theory, $\dot{\psi}_{ij}$ and $\dot{\kappa}_{ijk}$ describe irreversible changes in the micro-structure of the medium. Consequently the elastic strain rate, which is the difference between the total (macroscopic) and the plastic (microscopic) strain rate, is identified with the relative deformation of a Mindlin continuum,

$$\left.\begin{aligned}\dot{\varepsilon}_{ij}^e &= \dot{\varepsilon}_{ij} - \dot{\varepsilon}_{ij}^p \\ \dot{\gamma}_{ij} &= \dot{\varepsilon}_{ij} - \dot{\psi}_{ij}\end{aligned}\right\} \rightarrow \dot{\varepsilon}_{ij}^e \equiv \dot{\gamma}_{ij} \tag{10.2.32}$$

Having now identified in the sense of continuum mechanics and continuum thermodynamics the state variables and the associate state variables, we may return to

the flow rule, here equation 10.2.16, which plays a central role in plasticity theory. We remark that with the aid of the flow rule the six components of the micro-deformation $\dot{\psi}_{ij}$ are reduced to a single one, the plastic multiplier $\dot{\psi}$,

$$\dot{\psi}_{ij} = \frac{\partial Q}{\partial \tau_{ij}} \dot{\psi}; \; Q \equiv F \tag{10.2.33}$$

Finally, we remark that in ordinary plasticity theory the plastic multiplier $\dot{\psi}$ is eliminated by utilizing Prager's consistency condition for continuous loading. Namely assuming that $F = \dot{F} = 0$, we obtain that

$$\frac{\partial F}{\partial \tau_{ij}} (\dot{\sigma}_{ij} - \dot{\alpha}_{ij}) + \frac{\partial F}{\partial \psi} \dot{\psi} = 0 \tag{10.2.34}$$

The consistency equation can be resolved, if appropriate evolution equations for the true stress and the back-stress are postulated. First we remark that within the frame of small strain theory, and in accordance to classical elastoplasticity, the rate of the true stress is given in terms of the elastic strain rate

$$\dot{\sigma}_{ij} = C^{e}_{ijkl} \dot{\varepsilon}^{e}_{kl} \tag{10.2.35}$$

where C^{e}_{ijkl} is the elastic stiffness tensor, which in the simplest case of Hookean isotropic elasticity, is given by

$$C^{e}_{ijkl} = G\{\delta_{ik}\delta_{jl} + \delta_{il}\delta_{jk} + 2\nu/(1 - 2\nu)\delta_{ij}\delta_{kl}\} \tag{10.2.36}$$

G and υ are the elastic shear modulus and Poisson's ratio, respectively. The meaning of the constitutive assumption 10.2.35 is the following: If plastic strains are not generated, then $\dot{\varepsilon}^{e}_{ij} \equiv \dot{\varepsilon}_{ij}$, and the behavior is (linear isotropic) elastic, i.e. elastoplasticity is modeled as a perturbation of elasticity. In the following section we will demonstrate that gradient elastoplasticity corresponds again to an analogous perturbation of ordinary elastoplasticity.

With the identifications 10.2.30 and 10.2.31 made above for the micro-deformation, consistent models for the rate $\dot{\alpha}_{ij}$ of the back stress are obtained if $\dot{\alpha}_{ij}$ is made to obey a complete balance law of the form 10.1.21 (cf. Aifantis,. 1978, 1985; Vardoulakis and Frantziskonis, 1992). As is common in kinematic plasticity theory, such a balance law is written in the form of an evolution equation for the back-stress,

$$\dot{\alpha}_{ij} = -\dot{\Phi}_{ij} - \partial_k \dot{\mu}_{kij} + I_{ijkl} \partial_{tt} (\dot{\varepsilon}^{p}_{kl}) \tag{10.2.37}$$

The first term in this equation is recognized as describing the effect of kinematic softening. For example, Prager's (1955) kinematic hardening rule reflects a particular constitutive assumption for the double-body force,

$$\dot{\Phi}_{ij} = -r\dot{\varepsilon}^{p}_{ij} \tag{10.2.38}$$

In order to identify the modulus r in the above constitutive equation, we neglect the higher-grade terms in equation 10.2.37, and apply it for axisymmetric compressions. By

restricting again ourselves to post-peak states we get r proportional to the cohesion softening modulus,

$$r = \frac{1}{1/2 + (1/3)f_p^2} \frac{dc}{dg^p} \tag{10.2.39}$$

The second term in the evolution equation 10.2.37 describes the effect of deformation inhomogeneity. According to Vardoulakis and Frantziskonis (1992) this effect is easily modeled by assuming that double stress rates are proportional to the gradient of plastic strain rates. Furthermore, the simplest constitutive model arises if one assumes that consideration of plastic strain-rate gradients introduces only *one* additional material parameter into the material description. Then from dimensional analysis we obtain that a simple isotropic linear relationship for the double stress rate is the following

$$\dot{\mu}_{rij} = C^e_{ijkl} \ell_c^2 \partial_r(\dot{\varepsilon}^p_{kl}) \tag{10.2.40}$$

where ℓ_c is this new material parameter; ℓ_c has the dimension of length and is thus called a *material length.* With the same argument consideration of micro-inertia will introduce in the simplest case another material parameter T_c with dimension of time, i.e. a *material time factor.*

With these constitutive assumptions the evolution law 10.2.37 for the back-stress takes the following form

$$\dot{\alpha}_{ij} = r\dot{\varepsilon}^p_{ij} - C^e_{ijkl}\{\ell_c^2 \nabla^2 - T_c^2 \partial_{tt}\}(\dot{\varepsilon}^p_{kl}) \tag{10.2.41}$$

This is the complete *second-grade* evolution equation for the back stress. If the effect of micro-inertia is negligible, then $T_c \equiv 0$, and 10.2.41 is a *second-gradient* evolution equation for the back-stress. Notice that for modeling cohesionless sand we may neglect both cohesion and micro-inertia. In this case, Vardoulakis and Aifantis (1991) emphasized the effect of porosity localizations, which resulted in the following evolution law for α_{ij},

$$\dot{\alpha}_{ij} = -K\ell_c^2 \nabla^2(\dot{n})\delta_{ij} \qquad \dot{n} \approx \dot{\varepsilon}^p_{kk} \tag{10.2.42}$$

where K is the elastic compression modulus. According to 10.2.42 α_{ij} is an isotropic stress which evolves only then if sufficiently strong (plastic) volumetric strain-rate gradients occur (i.e. porosity localizations).

Remark on gradient plasticity models. In recent publications on gradient dependent plasticity theories (cf. Aifantis, 1984; Coleman and Hodgdon, 1985; Schreyer and Chen, 1986; Mühlhaus and Aifantis, 1991) instead of equation 10.2.6 an explicit dependence of the yield function and of the plastic potential function (Vardoulakis and Aifantis, 1991) on the gradient of the hardening parameter was suggested. In the present case, this would have led for example to,

$$F = f(\sigma_{ij}) - [\tau(\psi) - c_1(\nabla\psi)^2 - c_2\nabla^2\psi]$$

Such a special representation is however unnecessary when gradient terms are implicitly contained in the expression for the yield- and plastic potential function through the contribution of the evolving back stress α_{ij}.

Finally, it should be noted that an attempt to motivate a strain gradient plasticity theory from the concept of residual strain (displacement) and with that from dislocation motions was done following a rather cumbersome formalism in an early paper by Dillon and Kratochvil (1970).

10.2.3
Constitutive equations

With the constitutive equations 10.2.35 and 10.2.41, for the true- and back-stress rates, the consistency condition 10.2.34 results in a differential constraint for the plastic multiplier $\dot{\psi}$. We discuss first this differential consistency condition, and, for simplicity, we neglect here micro-inertial terms (which can be included without affecting the formalism),

$$-\frac{H_0}{H}\ell_c^2\nabla^2\dot{\psi}+\dot{\psi}=\frac{1}{H}\frac{\partial F}{\partial\tau_{ij}}C^e_{ijkl}\dot{\varepsilon}_{kl};\ \dot{\psi}\geqslant 0 \tag{10.2.43}$$

where neglecting non-linear and gradient terms of $(\partial Q/\partial\tau_{ij})$,

$$H_0\approx\frac{\partial F}{\partial\tau_{ij}}C^e_{ijkl}\frac{\partial Q}{\partial\tau_{kl}} \tag{10.2.44}$$

$$H\approx H_0+r\frac{\partial F}{\partial\tau_{ij}}\frac{\partial Q}{\partial\tau_{ji}}-\frac{\partial F}{\partial\psi} \tag{10.2.45}$$

and $Q\equiv F$ for associative plasticity.

The consistency condition is a differential equation which links the plastic multiplier $\dot{\psi}$ to the total strain rate $\dot{\varepsilon}_{ij}$. (In Mindlin's continuum formalism this is a constraint which links the micro-deformation to the macro-deformation.) Thus, if one can resolve this constraint, then as is the case in classical flow theory of plasticity, $\dot{\psi}$ is eliminated. Otherwise, if this is not possible, then one has to carry the consistency condition as an additional field equation together with the balance equations and to treat $\dot{\psi}$ as an additional degree of freedom (Mühlhaus and Aifantis, 1991). Here we suggest an approximate procedure which indeed allows for elimination of $\dot{\psi}$ from the set of governing equations and simplifies the problem drastically (Vardoulakis and Frantziskonis, 1992).

For homogeneous ground plastic-strain states, the first term on the left-hand side of equation 10.2.43 vanishes identically and the consistency condition collapses to that of the classic flow theory of plasticity, i.e. to a monomial equation for the plastic multiplier $\dot{\psi}$. However, within a good approximation, this is also true for inhomogeneous states as well. To demonstrate this we set

$$\ell^2 = \frac{H_0}{H}\ell_c^2 \approx \ell_c^2 \tag{10.2.46}$$

and assume that ℓ_c is a micro-structural length scale, like for example a mean grain or void diameter, and accordingly ℓ_c is small if compared to any geometric length dimension of the deforming solid. Then equation 10.2.43 in operational form becomes

$$(1 - \ell^2\nabla^2)\dot{\psi} = \frac{1}{H}B_{kl}\dot{\varepsilon}_{kl}$$

or

$$\dot{\psi} = \frac{1}{1 - \ell^2\nabla^2}\frac{1}{H}B_{kl}\dot{\varepsilon}_{kl} \approx \{1 + \ell^2\nabla^2 + O(\ell^4)\}\frac{1}{H}B_{kl}\dot{\varepsilon}_{kl}$$

$\dot{\psi}$ whenever loading of the yield surface $F = 0$ is taking place, or else $\dot{\psi} = 0$. Thus we set finally

$$\dot{\psi} = \frac{\langle 1\rangle}{H}\frac{\partial F}{\partial \tau_{ij}}C^e_{ijkl}(\dot{\varepsilon}_{kl} + \ell^2\nabla^2\dot{\varepsilon}_{kl} + O(\ell^4)) \tag{10.2.47}$$

In this equation denote again the McAuley brackets of plasticity theory. With H>0 the switch function is defined as follows

$$\langle 1\rangle = \begin{cases} 1 & \text{if } F = 0 \quad \text{and} \quad (\partial F/\partial\tau_{ij})C^e_{ijkl}(\dot{\varepsilon}_{kl} + \ell^2\nabla^2\dot{\varepsilon}_{kl}) > 0 \\ 0 & \text{if } F < 0 \quad \text{or} \quad \{F = 0 \quad \text{and} \quad (\partial F/\partial\tau_{ij})C^e_{ijkl}(\dot{\varepsilon}_{kl} + \ell^2\nabla^2\dot{\varepsilon}_{kl}) \leqslant 0\} \end{cases} \tag{10.2.48}$$

The plastic strain rate can be expressed as

$$\dot{\varepsilon}^p_{ij} = A_{ijkl}(\dot{\varepsilon}_{kl} + \ell^2\nabla^2\dot{\varepsilon}_{kl} + O(\ell^4)) \tag{10.2.49}$$

$$A_{ijkl} = \frac{\langle 1\rangle}{H}\frac{\partial Q}{\partial \tau_{ij}}\frac{\partial F}{\partial \tau_{pq}}C^e_{pqkl} \tag{10.2.50}$$

Furthermore from the evolution equation 10.2.41 for the back-stress, and neglecting non-linear terms, we obtain

$$\dot{\alpha}_{ij} = rA_{ijkl}\dot{\varepsilon}_{kl} + (rA_{ijkl} - C^p_{ijkl})\ell^2\nabla^2\dot{\varepsilon}_{kl} + O(\ell^4) \tag{10.2.51}$$

where C^P is the plastic stiffness matrix

$$C^p_{ijkl} = \frac{\langle 1\rangle}{H}C^e_{ijmn}\frac{\partial Q}{\partial \tau_{mn}}\frac{\partial F}{\partial \tau_{pq}}C^e_{pqkl} \tag{10.2.52}$$

Thus the plastic strain rate is within an ℓ^4-approximation eliminated from the set of constitutive equations. This means that the extended constitutive equations of elastoplasticity describe a restricted Mindlin-type elastoplastic solid, whose degree of freedom of micro-deformation is linked to its macro-deformation through to the quasi-linear constraint 10.2.49 with 10.2.50. Accordingly, the approximate rate stress-strain relations of the strain-rate-gradient dependent flow theory of plasticity

$$\dot{\sigma}_{ij} = C^{ep}_{ijkl}\dot{\varepsilon}_{kl} - C^p_{ijkl}\ell^2\nabla^2\dot{\varepsilon}_{kl} + O(\ell^4) \tag{10.2.53}$$

where C^{ep} is the common elastoplastic stiffness tensor,

$$C^{ep}_{ijkl} = C^{e}_{ijkl} - C^{p}_{ijkl} \tag{10.2.54}$$

Equations 10.2.53 can be interpreted in many ways. For example:

(a) The *asymptotic character* of elastoplastic constitutive equations as successive approximations of a 'target' material behavior becomes clear if equations 10.2.53 are written in the following form

$$\dot{\sigma}_{ij} = C^{e}_{ijkl}\dot{\varepsilon}_{kl} - C^{p}_{ijkl}\dot{\varepsilon}_{kl} - C^{p}_{ijkl}\ell^2\nabla^2\dot{\varepsilon}_{kl} + \dots \tag{10.2.53a}$$

This form suggests that gradient elastoplasticity is a singular perturbation of ordinary elastoplasticity, which in turn as already mentioned above, can be seen as a regular perturbation of (hypo-)elasticity.

(b) The *non-local character* of gradient elastoplasticity is seen if the constitutive equations are written as follows

$$\begin{aligned} \dot{\sigma}_{ij} &= C^{e}_{ijkl}\dot{\varepsilon}_{kl} - C^{p}_{ijkl}\langle\dot{\varepsilon}_{kl}\rangle \\ \langle\dot{\varepsilon}_{kl}\rangle &= (1/V)\int_V \dot{\varepsilon}_{kl}\,\mathrm{d}V = \dot{\varepsilon}_{kl} + \ell^2\nabla^2\dot{\varepsilon}_{kl} + \dots \end{aligned} \tag{10.2.53b}$$

i.e. that the plastic operator C^{P} acts on the mean strain over a characteristic volume V, which in turn is expressed approximately by value of the strain and its Laplacian at a collocational point inside V (Bažant, 1984).

(c) The *Mindlin continuum character* follows if one rewrites equations 10.2.53 in the following form (Vardoulakis and Aifantis, 1991)

$$\begin{aligned} \dot{\sigma}_{ij} &= \dot{\sigma}^{(0)}_{ij} + \dot{\sigma}^{(2)}_{ij} \\ \dot{\sigma}^{(0)}_{ij} &= C^{ep}_{ijkl}\dot{\varepsilon}_{kl} \\ \dot{\sigma}^{(2)}_{ij} &= -C^{p}_{ijkl}\ell^2\nabla^2\dot{\varepsilon}_{kl} \end{aligned} \tag{10.2.53c}$$

The stress-rate tensor $\dot{\sigma}^{(0)}_{ij}$ coincides with the constitutive stress rate of the classical flow theory of plasticity and is called, by analogy to Mindlin's nomenclature, the Cauchy stress tensor. Similarly, the stress-rate tensor $\dot{\sigma}^{(2)}_{ij}$ is re-interpreted as a relative stress tensor of the considered restricted second-gradient elastoplastic solid. One may introduce a self-equilibrating double stress $\dot{m}_{ijk}$ such that

$$\dot{\sigma}^{(2)}_{ij} + \partial_k\dot{m}_{kij} = 0 \tag{10.2.55}$$

From equations 10.2.53c and 10.2.55 the relative stress rate of the considered restricted Mindlin continuum can be eliminated, yielding

$$\dot{\sigma}_{ij} = \dot{\sigma}^{(0)}_{ij} - \partial_k\dot{m}_{kij} \tag{10.2.56}$$

If finally one assumes that the double stress rate is proportional to the gradient of the strain rate

$$\dot{m}_{ijk} = C^{p}_{jkmn} \ell^2 \dot{c}_{imn} \tag{10.2.57}$$

where

$$\dot{c}_{ijk} = \partial_i \dot{\varepsilon}_{jk} \tag{10.2.58}$$

and neglects non-linear gradient terms, then the internal balance equation 10.2.55 is satisfied.

The above results are summarized in the following statement: The constitutive equation 10.2.5 3c, of gradient-dependent flow theory with yield surface and plastic potential surface, describes the behavior of a restricted Mindlin-type continuum, i.e. a micro-homogeneous material for which the macroscopic strain rate coincides with the micro-deformation rate. This in turn leads to a vanishing relative deformation rate, and, according to equation 10.2.58, to a rate of micro-deformation gradient which coincides with the strain-rate gradient. We observe also that the present Mindlin continuum extension of flow theory involves only *one* new material parameter, the material length ℓ_c. This is unlike the Cosserat-continuum extension of plasticity theory. As discussed in chapter 9, elastoplastic solids with the microstructure of a micropolar continuum in addition to the material length, a shear modulus for the antisymmetric shear stress rates had to be assumed.

10.2.4
Formulation of the rate-boundary value problem

The weak formulation of the balance law of linear momentum together with the appropriate set of boundary conditions for the considered second gradient elastoplastic solid is achieved through the principle of virtual work. First, in accordance with the above observations, we define the virtual second-order work of internal forces in a finite volume V

$$\delta^2 W^{(i)} = \int_V (\dot{\sigma}^{(0)}_{ij} \delta \dot{\varepsilon}_{ij} + \dot{m}_{ijk} \delta \dot{c}_{ijk}) \mathrm{d}V \tag{10.2.59}$$

The surface δV of the considered volume V is divided into two complementary parts ∂V_v and ∂V_σ such that on ∂V_v kinematic data are prescribed whereas on ∂V_σ static data are prescribed. In classical continua these are constraints on velocity and traction rates, respectively. Since in the considered constitutive description second gradients of strain rates appear, additional kinematic data must be prescribed on ∂V_v. With the velocity already given on ∂V_v, according to Hadamard's lemma (section 2.4.1) only its normal derivative with respect to that boundary in unrestricted. This means that on ∂V_v the normal derivative of the velocity should also be given,

$$v_i = \dot{w}_i; \; Dv_i = \dot{r}_i \tag{10.2.60}$$

where $D = n_k \partial_k$ is the derivative in a direction normal to the boundary with local unit outward normal n_k. The boundary is assumed to be smooth; boundary conditions for non-smooth boundaries are derived in Mindlin (1964) and Mühlhaus and Aifantis (1991).

For the computation of the second-order virtual work of external forces $\delta^2 W^{(e)}$ we have to consider not only the rate of surface tractions and double forces but also the work of the usual body and inertial forces. By applying D'Alembert's principle, inertial forces are included in the body forces with opposite sign and are computed from the bulk density ρ and the acceleration $\partial_{tt} v_i$. Following these considerations, the virtual work of external forces becomes

$$\delta^2 W^{(e)} = \int_V (\dot{f}_i - \rho \partial_{tt} v_i) \delta v_i \, \mathrm{d}V + \int_{\partial V_\sigma} (\dot{t}_i \delta v_i + \dot{m}_i D \delta v_i) \mathrm{d}S \tag{10.2.61}$$

where $\dot{f}_i$ are rates of body forces and $\dot{t}_i$, $\dot{m}_i$ are rates of surface tractions and will be derived below. With the equations 10.2.59 to 10.2.61 the virtual work double forces, whose relation to the stress rate and double stress-rate tensor equation becomes

$$\delta^2 W^{(i)} = \delta^2 W^{(e)}$$

or

$$\int_V \{\dot{\sigma}_{ij}^{(0)} \delta \dot{\varepsilon}_{ij} + \dot{m}_{ijk} \delta \dot{c}_{ijk} - (f_i - \rho \partial_{tt} v_i) \delta v_i\} \mathrm{d}V = \int_{\partial V} (\dot{t}_i \delta v_i + \dot{m}_i D \delta v_i) \mathrm{d}S \tag{10.2.62}$$

In order to compute the surface integral on the right-hand side of 10.2.62 we require that the virtual velocity field and its normal derivative vanish on ∂V_v,

$$\delta v_i = 0 \quad \text{and} \quad D \delta v_i = 0 \tag{10.2.63}$$

From the volume integrals one derives the usual dynamic equations for the true stress-rate tensor in V

$$\partial_i \dot{\sigma}_{ij} + \dot{f}_j = \rho \partial_{tt} v_j \tag{10.2.64}$$

In order to derive the corresponding boundary conditions from the remaining terms of the virtual work equation 10.2.62 we have to elaborate on the term

$$I = \int_{\partial V} n_i \dot{m}_{ijk} \partial_j \delta v_k \, \mathrm{d}S \tag{10.2.65}$$

First we decompose $\partial_j \partial v_k$ into a component normal to the boundary ∂V and another tangential to it

$$\partial_j \delta v_k = n_j D \delta v_k + D_j \delta v_k \tag{10.2.66}$$

where

$$D = n_k \partial_k : D_k = (\delta_{k\ell} - n_k n_\ell)\partial_\ell \tag{10.2.67}$$

With that we get

$$n_i \dot{m}_{ijk} \partial_j \delta v_k = n_i \dot{m}_{ijk} D_j \delta v_k + n_i \dot{m}_{ijk} n_j D \delta v_k \tag{10.2.68}$$

The first term on the right-hand side of 10.2.68 becomes

$$n_i \dot{m}_{ijk} D_j \delta v_k = D_j (n_i \dot{m}_{ijk} \delta v_k) - n_i D_j \dot{m}_{ijk} \delta v_k - (D_j n_i) \dot{m}_{ijk} \delta v_k \tag{10.2.69}$$

In order to work out the first term in the right-hand side of 10.2.69 use is made of the identity

$$D_j F_j = D_k n_k n_j F_j - n_q e_{qpm} \partial_p (e_{mkj} n_k F_j) \tag{10.2.70}$$

where e_{ijk} is the alternating tensor. Denoting by

$$A_m = e_{mkj} n_k F_j ; \; F_j = n_i \dot{m}_{ijk} \delta v_k \tag{10.2.71}$$

we get that over a closed surface

$$\oint_{\partial V} e_{qpm} \partial_p A_m n_q \, \mathrm{d}S = 0 \tag{10.2.72}$$

We observe also that

$$n_j \partial_i \dot{m}_{ijk} = n_j D_i \dot{m}_{ijk} + n_i n_j D \dot{m}_{ijk} \tag{10.2.73}$$

If we collect the terms appearing in the surface integrals of the work equation we finally get

$$\int_{\partial V} \{ n_j \dot{\sigma}^{(0)}_{jk} - n_i n_j D \dot{m}_{ijk} - (n_i D_j + n_j D_i) \dot{m}_{ijk} + (n_i n_j D_\ell n_\ell - D_j n_i) \dot{m}_{ijk} \} \delta v_k \, \mathrm{d}S$$

$$+ \int_{\partial V} n_i n_j \dot{m}_{ijk} D \delta v_k \, \mathrm{d}S = \int_{\partial V} \dot{t}_k \delta v_k \, \mathrm{d}S + \int_{\partial V} \dot{m}_k D \delta v_k \, \mathrm{d}S \tag{10.2.74}$$

These surface integrals contain both δv_i and its normal derivative $D\delta v_i$ which is however an independent variation. This observation allows the formulation of the following set of static boundary conditions on ∂V_σ

$$n_j \dot{\sigma}^{(0)}_{jk} - n_i n_j D \dot{m}_{ijk} - (n_i D_j + n_j D_i) \dot{m}_{ijk} + (n_i n_j D_\ell n_\ell - D_j n_i) \dot{m}_{ijk} = \dot{t}_k \tag{10.2.75}$$

$$n_i n_j \dot{m}_{ijk} = \dot{m}_k \tag{10.2.76}$$

The first constraint takes the place of the classical boundary condition for surface tractions. Due to the constitutive equation 10.2.57 for $\dot{m}_{ijk}$, the second constraint means that on some part of the boundary ∂V the second velocity gradient might be given. In order to illustrate further the set of the above boundary conditions we examine the case of a plane boundary. The (x_2, x_3)-plane is chosen parallel and the x_1-axis normal to the

considered boundary, pointing outwards; i.e. $n_1 = 1; n_2 = n_3 = 0$. The $x_1 = 0$ boundary may be seen as a 'long' interface boundary. Kinematic constraints are given on a part ∂V_v of it which according to conditions 10.2.60

$$v_i = \dot{w}_i;\ \partial_1 v_i = \dot{r}_i \qquad (i = 1,2,3) \tag{10.2.77}$$

On the complementary part ∂V_σ of the considered boundary conditions 10.2.75 and 10.2.76

$$\dot{\sigma}_{1i} = \dot{t}_i;\ \dot{m}_{11i} = \dot{m}_i \qquad (i = 1,2,3) \tag{10.2.78}$$

The constitutive equations for $\dot{\sigma}^{(0)}_{jk}$ and $\dot{m}_{ijk}$ (together with the definitions for the yield and plastic potential surface the McAuley brackets and the evolution law for the back stress $\dot{\alpha}_{ij}$) can be combined with the virtual work equation 10.2.62 with constraints 10.2.63 to provide the integral equation formulation of the rate-boundary value problem for the considered second gradient elastoplastic solid

$$\int_V \{C^{ep}_{ijkl}\dot{\varepsilon}_{kl}\delta\dot{\varepsilon}_{ij} + C^{p}_{jkmn}\ell^2\dot{c}_{imn}\delta\dot{c}_{ijk}\}\,\mathrm{d}V = \int_V (\dot{f}_i - \rho\partial_{tt}v_i)\delta v_i\,\mathrm{d}V + \int_{\partial V}(\dot{t}_i\delta v_i + \dot{m}_i D\delta v_i)\mathrm{d}S \tag{10.2.79}$$

This formulation is reduced to the finite-element formulation of the rate initial boundary-value problem of the classical elastoplastic solid

$$\int_V C^{ep}_{ijkl}\dot{\varepsilon}_{kl}\delta\dot{\varepsilon}_{ij}\,\mathrm{d}V + \delta G = \int_V (\dot{f}_i - \rho\partial_{tt}v_i)\delta v_i\,\mathrm{d}V + \int_{\partial V}\dot{t}_i\delta v_i\,\mathrm{d}S + \delta M \tag{10.2.80}$$

with additional entries in the stiffness matrix and the loading vector

$$\delta G = \int_V C^{p}_{jkmn}\ell^2\dot{c}_{imn}\delta\dot{c}_{ijk}\,\mathrm{d}V$$
$$\delta M = \int_{\partial V}\dot{m}_i D\delta v_i\,\mathrm{d}S \tag{10.2.81}$$

which could be easily accounted for in an iterative computational scheme.

10.2.5
Well-posedeness of the rate-boundary value problem

As presented in section 3.3.5, the integrand of the integral 10.2.59, has the character of second-order work, and plays a central role in the formulation of uniqueness theorems,

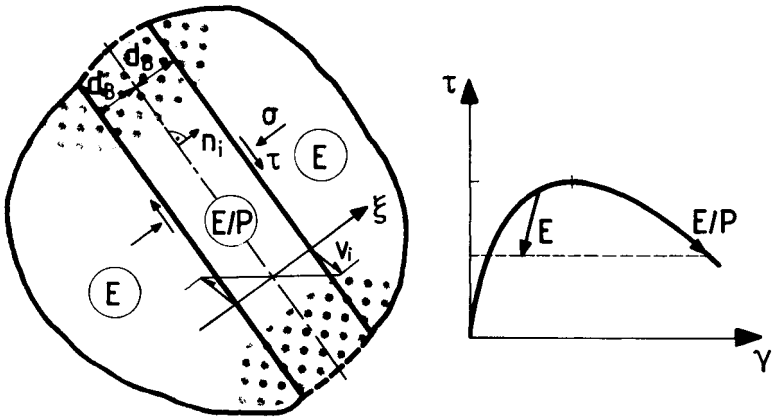

Figure 10.2.4 Shear-band localization in strain-softening elastoplastic solid.

$$\begin{aligned}\Delta_2 w &= \Delta\sigma_{ij}^{(0)}\Delta\varepsilon_{ij} + \Delta m_{ijk}\Delta c_{ijk} \\ &= C_{ijkl}^{ep}\Delta\varepsilon_{kl}\Delta\varepsilon_{ij} + \ell^2 C_{jkmn}^{p}\Delta c_{imn}\Delta c_{ijk}\end{aligned} \tag{10.2.82}$$

For example in the simplest 1D configuration

$$\begin{aligned}&\Delta\varepsilon_{ij}\to\Delta\gamma;\ \Delta c_{ijk}\to\nabla(\Delta\gamma) \\ &C^{e}\to G;\qquad C^{p}\to Gh\end{aligned} \tag{10.2.83}$$

where G is an elastic reference modulus and h is a (dimensionless) softening modulus. Then the second-order work of stresses becomes

$$\Delta_2 w = G\{h(\Delta\gamma)^2 + \ell^2[\nabla(\Delta\gamma)]^2\} \tag{10.2.84}$$

Inside the localized zone the strain term in expression 10.2.84 is non-positive, due to *material strain softening* (h<0), whereas the strain-gradient term is non-negative. However, in spite of the gradient term, locally the second-order work may negative (e.g. in the middle of the localized zone), and the local sufficient criterion for uniqueness, inequality 3.3.74, breaks down. However, under some restrictions global uniqueness is restored: By an appropriate rescaling of coordinates we observe that the gradient term may dominate, provided that the rate of material strain softening is not very large. In order to demonstrate that, let

$$\xi = x/\ell \tag{10.2.85}$$

be the dimensionless coordinate perpendicular to the shear band axis, with the origin on the shear-band axis (Figure 10.2.4). By the same token we observe that with this proposition the extent of the localized zone must scale with the material length, i.e. $d_B = O(\ell)$. Its extent is determined, and the original elastoplastic problem of strain softening material becomes a problem with internal boundaries, which separate the

elastic unloading from the plastic-softening domain. The integral, $I = \int \Delta_2$, inside the localized zone becomes

$$I_{EP} = \int_{-\xi_B}^{\xi_B} G\left\{h(\Delta\gamma)^2 + \left[\frac{d(\Delta\gamma)}{d\xi}\right]^2\right\} d\xi \tag{10.2.86}$$

with $\xi_B = d_B/\ell$. Let us assume for simplicity that $h = -h_s = \text{const.} < 0$, and that the fundamental solution has a leading trigonometric term (Vardoulakis and Aifantis, 1991)

$$\Delta\gamma \approx \gamma_0 \cos(q\xi);\ q = \pi/\xi_B \tag{10.2.87}$$

Then

$$I_{EP} > 0 \rightarrow -(\pi/\xi_B)^2 < h < 0 \tag{10.2.88}$$

Assuming for example that $\xi_B = 15$ (Vardoulakis and Aifantis, 1991), then from 10.2.88 the softening modulus is *limited* to 'small' values; $0<h_s<0.05$.

Outside the localized zone the behavior is elastic and the second-order work is positive. All these observations allow the formulation of the following (Vardoulakis, 1994).

Proposition. Within the frame of elastoplasticity theory, loss of uniqueness in the incremental, boundary value problem of strain-softening material is restored by consideration of at least first grade terms in the expression of the second-order work.

Following this proposition the resulting singular governing equations are regularized through the rescaling (10.2.85) and uniqueness is guaranteed as soon as the rate of strain softening is sufficiently small, cf. inequality 10.2.88. Figure 10.2.5 shows the boundary-value problem of interfacial localization in cohesive-frictional rock, which was analyzed analytically and numerically by Vardoulakis *et al.* (1992). Figure 10.2.5(a) shows the geometry of the problem. Figures 10.2.5(b,c) show the basic constitutive assumptions for the rock (i.e. constant friction, cohesion softening and plastic incompressibility). An elastoplastic softening 'interface layer' (P) of determined extent D forms adjacent to the frictional contact surface. This softening zone is separated from the elastic zone (E) of unloading material by the elastoplastic boundary (E/P). Inside the localized zone (P), gradient plasticity formulation leads to a third-order ordinary differential equation (o.d.e.) for the velocity, whereas in the adjacent elastic zone (E), a first-order o.d.e. for the velocity holds. Accordingly, at both ends of the layer different boundary conditions are specified. Moreover additional compatibility conditions hold at the elastoplastic boundary (E/P). This means that an elastoplastic softening interface layer has some similarity with the common boundary layer as far as boundary conditions are concerned. Its main difference from the boundary layer is that the 'internal' and 'external' solution are not matched in an asymptotic sense but they are made compatible in an exact manner along the (moving) elastoplastic boundary.

Figure 10.2.6 summarizes the computational results concerning the variation of material cohesion T and apparent cohesion at the top of the shear interface layer. This

figure demonstrates the following: Even when the material cohesion T is piecewise linear function of plastic strain, a smooth non-linear cohesion c is observed

$$c = T + \alpha_\tau \tag{10.2.89}$$

T represents the true material cohesion whereas α_τ is the back-stress, due to strong plastic strain gradients. The 'local' term $T(\gamma^p)$ is not directly observable and it must be determined from c through an inverse procedure. This means that the determination of the true cohesion of a material, especially in the softening regime, is an inverse problem.

We remark finally that the analysis showed in addition to a constraint of the form of 10.2.88, extra boundary conditions must obey additional constraints. This observation is strengthening Aifanti's (1978) conjecture of the constitutive character of boundary constraints in materials with microstructure. The problem of constitutive boundary conditions is open and deserves further attention from the theoretical as well as the experimental point of view.

10.3
Bifurcation analysis deep boreholes

10.3.1
Problem statement

Borehole breakouts and exfoliations are important phenomena that influence the engineering design of drilling hardware and can critical for the progress of the drilling process. Breakouts lead in general to progressive deterioration of the borehole. Wellbore breakouts are attributed to the existence of significant deviatoric stresses that act in the horizontal plane at great depth and to the stress concentration around the borehole (Bell and Gough, 1979; Zoback *et al.,* 1986). It should be noticed, however, that not only the stress deviator but also the temperature and pore-fluid flow may influence borehole stability. In this section only stress-induced instabilities will be discussed.

The problem of circular hole bifurcation analysis has been studied first in the context of large-strain formulations for rigid-hardening plastic cohesive-frictional solids by Vardoulakis and Papanastasiou (1988) and Vardoulakis *et al.* (1988). It was found that for classical cotinuum models the critical diffuse bifurcation mode is surface instability. This finding was explained by the high stress gradient at the hole wall. Surface instabilities in converging cavities correspond to the infinitesimally small wavelength limit with respect to the radius of the cavity. This means that the bifurcation solution is affecting only an infinitesimally narrow ring of material close to the cavity surface. Since the short-wavelength limit is an accumulation point of bifurcations, almost all sufficiently small wavelengths of the corresponding 'warping' bifurcation mode are possible, and consequently there is no influence of the borehole radius. However, this indeterminacy of the critical wavelength of the surface instability can be rectified by resorting to continuum theories with material length. For example, for a half-space with

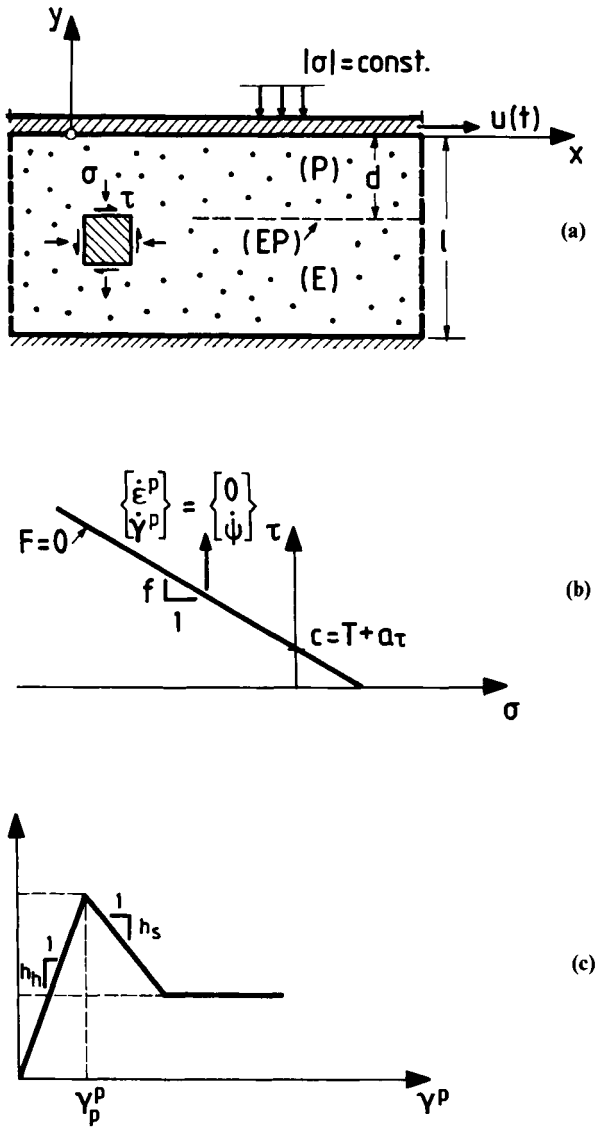

Figure 10.2.5 (a) Long rock strip interfacing with rough 'tool' under constant normal stress and controlled horizontal displacement; (b) Coulomb yield condition for rock; (c) 'True' or material cohesion of rock consisting of hardening/softening and residual branch (Vardoulakis *et al.,* 1988).

bending stiffness and uniform initial strain the critical bifurcation mode corresponds to the infinite wavelength limit with respect to the material length. Thus, the combination of the stress-gradient effect (stress concentration effect) around the cavity with the Cosserat effect resulted in the study by Papanastasiou and Vardoulakis (1989) into *wave number selection* and to a *scale effect.*

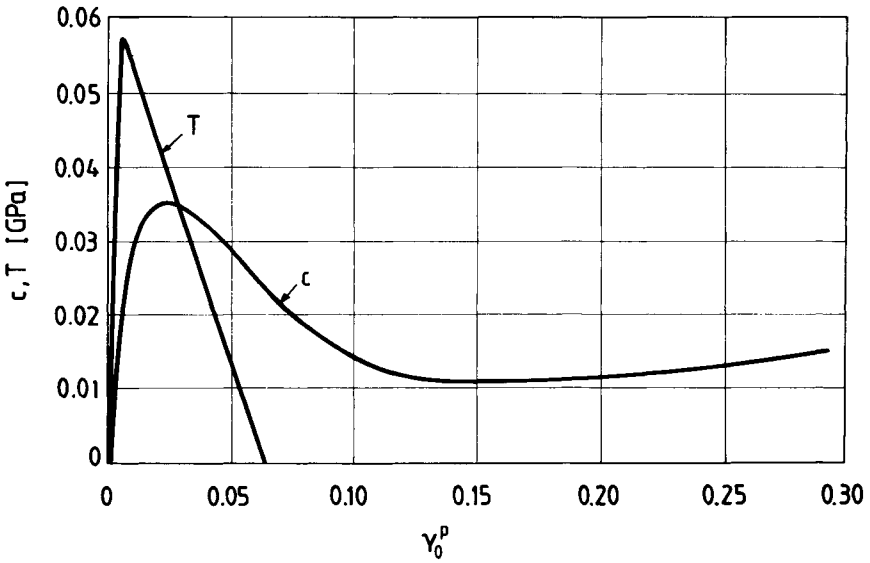

Figure 10.2.6 Variation of material cohesion T and of apparent cohesion c at the top of the interface layer with the plastic strain γ^p at the top of the layer (Vardoulakis *et al.,* 1992).

As already mentioned in section 9.5 Papanastasiou and Vardoulakis (1992) performed large-scale finite-element computations on the basis of a Cosserat continuum formulation (for strain-softening cohesive-frictional material), which followed the evolution of circular hole-wall warping into the post-bifurcation regime. This analysis showed that cavity 'failure' occurs through post-bifurcation, progressive localization of the deformation into shear bands. Moreover, a numerical study on mesh sensitivity for different types of failure showed that the Cosserat model is effective as a regularization method when frictional slip is dominant (Sluys, 1992). In the same study, a gradient-type model appeared to be effective in the description of tensile as well as shear type of failure. In a recent comparative study by Papamichos *et al.* (1994) it was found that the gradient model predicts a stronger scale effect in comparison with the Cosserat model. Furthermore, an important result with respect to the interpretation of laboratory hollow cylinder tests and their extrapolation to large-scale boreholes is the fact that the gradient model scale effect remains present for cavities of much larger radius in comparison with the Cosserat model scale effect.

10.3.2
Bifurcation analysis

In this section the second-gradient elastoplasticity model is applied to the problem of equilibrium bifurcation of a hollow cylinder under external compression. The bifurcation analysis is restricted here to plain-strain deformations on the plane normal to the axis

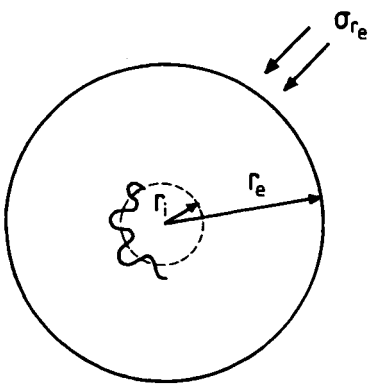

Figure 10.3.1 Geometric layout of the thick-walled hollow cylinder and of the 'warping' bifurcation mode.

of the cavity of a hollow cylinder, and is meant to simulate the laboratory test commonly used to assess stability of deep boreholes (Figure 10.3.1). This assumption is justified by experimental observations of the dominant failure patterns around the cavity (Tronvoll *et al.,*1993).

The analysis was performed in the natural cylindrical (r, θ)-coordinate system. The considered problem was solved by using a one-dimensional discretization along the radius of the thick-walled hollow cylinder. C^1 continuous, two-noded elements with Hermite basis functions of cubic order were used. This is necessary because of the third-order constitutive equations in terms of the velocity components. The degrees of freedom at each node were the velocity and its first derivative (Vardoulakis *et al.,* 1994).

The analysis assumes that the cavity is unstable as soon as, in addition to the trivial deformation of cylindrical convergency of the cavity, another non-trivial, non-axisymmetric deformation mode exists that fulfils homogeneous boundary conditions. This deformation mode corresponds to warping of the cavity surface and its wavelength is inversely proportional to the wave number *(m)* of the bifurcation mode.

The trivial solution of cylindrical convergency of the cavity is obtained by solving incrementally the variational equation 10.2.80 for axisymmetric deformations. Static boundary conditions are imposed on the internal and external boundary of the hollow cylinder,

$$\begin{aligned} &\text{for } r = r_i,\ \dot{\sigma}_{rr} = 0;\ \dot{m}_{rrr} = 0 \\ &\text{for } r = r_e,\ \dot{\sigma}_{rr} = \dot{t}_r;\ \dot{m}_{rrr} = 0 \end{aligned} \tag{10.3.1}$$

where r_i and r_e are the internal and external radius of the hollow cylinder, respectively, and $\Delta t_r = \dot{t}_r \Delta t$, the radial stress increment applied at the external boundary.

On the other hand, the bifurcation condition for the non-trivial solution of warping the cavity is obtained by solving equation 10.2.80 for the non-axisymmetric velocity field

$$v_r = V_r(r)\cos(m\theta);\ v_\theta = V_\theta(r)\sin(m\theta) \tag{10.3.2}$$

For this velocity field at the internal boundary ($r=r_i$) homogeneous static boundary conditions, according to equations 10.2.75 and 10.2.76, were imposed, resulting in the present case to the following equations

$$\begin{aligned} \dot{\sigma}_{rr} = 0;\ \dot{m}_{rrr} = 0 \\ \dot{\sigma}_{r\theta} - \frac{1}{r}\frac{\partial \dot{m}_{r\theta\theta}}{\partial \theta} = 0;\ \dot{m}_{rr\theta} = 0 \end{aligned} \tag{10.3.3}$$

At the external boundary ($r = r_e$) homogeneous kinematic boundary conditions, according to equations 10.2.77, were imposed,

$$\begin{aligned} v_r = 0;\ v_\theta = 0 \\ \frac{\partial v_r}{\partial r} = 0;\ \frac{\partial v_\theta}{\partial r} = 0 \end{aligned} \tag{10.3.4}$$

This results in an eigenvalue problem for the critical bifurcation stress $\sigma_{rr}(r = r_e) = -\sigma_{cr}$.

Within a finite-element discretization scheme the solution to this problem is obtained again by requiring that the *global stiffness matrix* **[K],** becomes singular (cf. section 3.3.4),

$$\det[\mathbf{K}] = 0 \tag{10.3.5}$$

The analysis confirmed the fact that in inhomogeneous problems like the present one, failure of local uniqueness criteria does not necessarily imply global loss of uniqueness. In fact, the obtained bifurcation points corresponded to loading states where the elements close to the cavity wall have entered the softening regime. In other words, although at these elements the local stability criterion is violated, the global stiffness matrix **[K]** remained regular.

10.3.3
The scale effect

The second-gradient elastoplastic constitutive model presented above in section 10.2, was calibrated for the Red Wildmoor sandstone using extensive experimental data from uniaxial and triaxial tests (Tronvoll *et al.*, 1993). For simplicity the constitutive equations of a 2D-associative model with linear Mohr-Coulomb yield function were used,

$$F \equiv Q = \tau - \{q(\gamma^p) - \sigma\}\mu(\gamma^p) \tag{10.3.6}$$

where σ and τ are the 2D first stress and second deviatoric stress invariants, and γ^p the corresponding 2D-plastic shearing strain intensity. As already mentioned above for this type of 'standard' rock plasticity model, the hardening character is modeled by a non-softening mobilized-friction coefficient and a non-hardening parameter q

$$\mu = \begin{cases} \mu_0 + \dfrac{(1 + c_3\gamma^p)\gamma^p}{c_1 + c_2\gamma^p} \\ \mu_p \end{cases}; r = \begin{cases} 0 & \text{for } \gamma^p \leqslant \gamma_p^p \\ -r_0 & \text{for } \gamma_p^p \leqslant \gamma^p \end{cases}$$

with $q = q_0$ prior to peak; cf. equations 10.2.34 and 10.2.39. The values of the elastic and plastic constants of the model used in this analysis are:

$$G = 2.2\,\text{GPa};\ v = 0.2$$

$$q_0 = 6.6\,\text{MPa};\ r_0/G = 0.0227$$

$$\mu_0 = 0.413;\ \mu_p = 0.526$$

$$c_1 = 0.0085;\ c_2 = 6.5;\ c_3 = -18.0;\ \gamma_p^p = 0.007$$

(Vardoulakis *et al.,* 1994). The model requires also the specification of the material length ℓ_c. In the considered calibration the *material length was taken equal to the mean grain radius of the Red Wildmoor sand stone;* i.e.

$$\ell_c = 0.05\,\text{mm}$$

Due to the existence of the material length ℓ_c, one can distinguish between small and large cavities leading to scale effect. Various cavity internal radii r_i were thus chosen in the range of 1.25 cm≤r_i≤25 cm, or

$$0.004 \leqslant (\ell_c/r_i) \leqslant 0.0002$$

In all these cases the ratio between internal and external radii was constant

$$(r_e/r_i) = 5/1$$

In order to achieve mesh insensitivity a fine discretization is required close to the cavity wall by discretizing the domain in 100 elements according to a geometric progression along the radial direction.

The results of this analysis are summarized in Figures 10.3.2 to 10.3.4. In Figure 10.3.2 the cavity-closure curve, corresponding to the trivial solution of cylindrical convergency of the cavity is given, where the externally applied radial stress is plotted as a function of the cavity deformation. It should be noted that the cavity-closure curve depends on the size of the cavity itself, due to the scaling of the geometric length (radius) r_i with the material length ℓ_c. However, the effect of ℓ_c on the primary solution is minimal inappreciable, and in fact the closure curves for different size cavities are almost indistinguishable.

In the cavity-closure curve, the bifurcation points for cylinders with various initial internal radii are depicted. The corresponding critical bifurcation modes are shown in Figure 10.3.3, where the dependency of the bifurcation stress on the considered mode and internal radius is portrayed. Based on the critical bifurcation stress, a plot showing the *scale effect* for the considered rock is shown in Figure 10.3.4. We notice from this figure that the obtained scale effect compares favorably with the experimental results by Tronvoll *et al.* (1993).

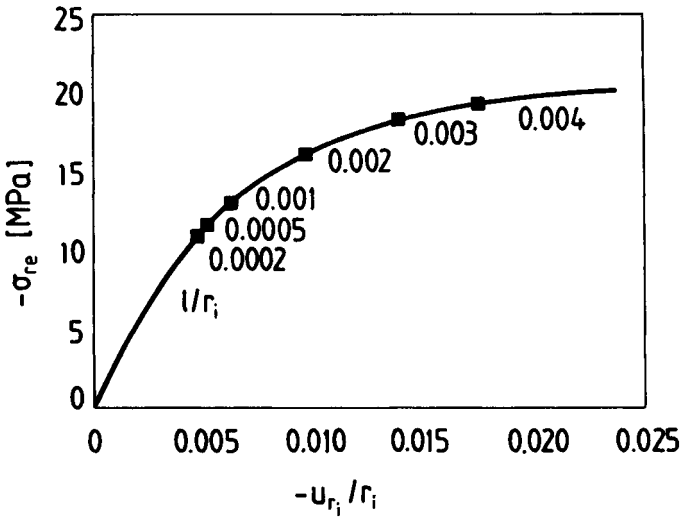

Figure 10.3.2 Cavity closure curve for Red Wildmoore sandstone (Vardoulakis *et al.,* 1994).

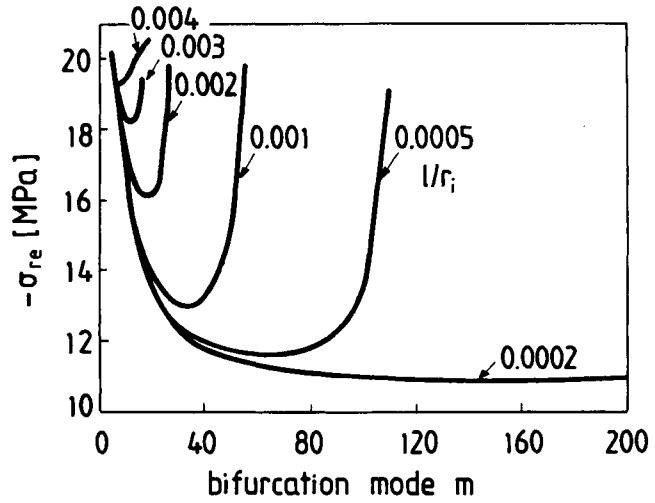

Figure 10.3.3 Wave number selection in bifurcation analysis of the thick-walled hollow cylinder under external pressure (Vardoulakis *et al.,* 1994).

10.4
A 2D-gradient model for granular media

10.4.1
Constitutive equations

As we saw in chapter 9 in the continuum description of the deformation of a granular medium one has to consider, in general, the effects of intergranular slip and rotation.

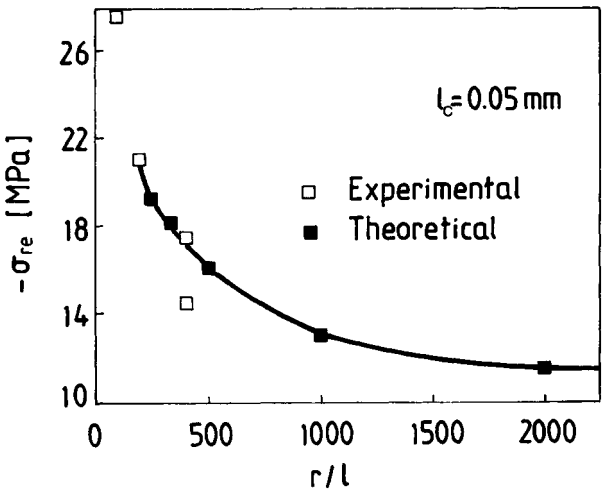

Figure 10.3.4 Theoretical (Vardoulakis *et al.,* 1994) and experimental scale effect (Tronvoll *et al.,* 1993).

However, in granular media under shear, intergranular slip and rotation are linked to porosity changes through the internal (dilatancy) constraint. Thus in order to arrive at a simple non-classical constitutive model one may want to emphasize the effect of porosity changes and its gradient, whereas the effect of grain rotation may be suppressed.

In order to justify the identification of the plastic strain rate with the micro-deformation rate and the elastic strain rate with the relative deformation rate, equations 10.2.30 and 10.2.32, we return to the familiar picture of two-phase granular medium which consists of deformable grains and of voids. The voids are assumed to be filled with gaseous substances or fluids whose interaction with the solid skeleton is disregarded here. Within a small strain theory, and according to equation (5.2.12) mass balance for the solid constituent results in the following condition

$$\dot{\varepsilon} = -\dot{\rho}_s/\rho_s + \dot{n}/(1-n) \tag{10.4.1}$$

The left-hand side term in this equation is identified as the macroscopic volumetric strain rate. In a first approximation one may neglect: (a) all irreversible volume changes, due to grain damage (grain cracking or crushing), and (b) all reversible porosity changes. These assumptions provide a micro-mechanical justification of the strain-rate decomposition of the theory of elastoplastic materials. The volumetric strain rate is decomposed into an elastic (recoverable) and a plastic (permanent) part

$$\dot{\varepsilon} = \dot{\varepsilon}^e + \dot{\varepsilon}^p \tag{10.4.2}$$

where the elastic strain rate is almost due to the reversible volume changes of the solid constituent (elastic deformation of the grains)

$$\dot{\varepsilon}^e \approx -\dot{\rho}_s/\rho_s \tag{10.4.3}$$

and the plastic part is almost due to irreversible porosity changes (rearrangement of the grains)

$$\dot{\varepsilon}^{\mathrm{p}} \approx \dot{n}/(1-n) \tag{10.4.4}$$

The next issue is to give a geometrical meaning to the choice of the plastic multiplier $\dot{\psi}$ and its gradient representation. For demonstration purposes we restrict our analysis in two dimensions and suggest identifying the plastic multiplier $\dot{\psi}$ with the average interparticle slip, among the grains contained in a small but finite material volume V surrounding a material x_α (α=1,2)

$$\dot{\psi} \equiv \langle \dot{\gamma}^{\mathrm{p}} \rangle \tag{10.4.5}$$

This non-local hypothesis is expressed formally by the relation

$$\langle \dot{\gamma}^{\mathrm{p}} \rangle = (1/V) \int_V \dot{\gamma}^{\mathrm{p}}(x_\alpha + \xi_\alpha) \mathrm{d}V \tag{10.4.6}$$

(cf. Aifantis, 1984; Bažant, 1984; Pijaudier-Cabot *et al.*, 1988; Vardoulakis and Aifantis, 1991). A Taylor's expansion of the function $\dot{\gamma}^{\mathrm{p}}(x_\alpha + \xi_\alpha)$ around x_α gives

$$\dot{\gamma}^{\mathrm{p}}(x_\gamma + \xi_\gamma) = \dot{\gamma}^{\mathrm{p}}(x_\gamma) + \partial_\alpha \dot{\gamma}^{\mathrm{p}}(x_\gamma)\xi_\alpha + \frac{1}{2!}\partial^2_{\alpha\beta}\dot{\gamma}^{\mathrm{p}}(x_\gamma)\xi_\alpha\xi_\beta + \dots \tag{10.4.7}$$

where $\partial_\alpha = \partial/\partial x_\alpha$, $\partial^2_{\alpha\beta} = \partial^2/\partial x_\alpha \partial x_\beta$, etc. We assume that the region V is a circle of radius R, which in turn is a small multiple of the grain radius is small compared to any geometrical length scale of the considered material body. For performing the integrations in 10.4.7, the appropriate polar coordinates are $r(0 \le r \le R)$ and $\theta(0 \le \theta \le 2\pi)$. If n_α denotes the outward unit normal of the circle $r = R$, then we have the following relation between the average and local plastic shear strain rate

$$\begin{aligned} \langle \dot{\gamma}^{\mathrm{p}} \rangle &= \dot{\gamma}^{\mathrm{p}} + \frac{1}{\pi R^2}\int_0^R \int_0^{2\pi} \left[\partial_\alpha \dot{\gamma}^{\mathrm{p}} r n_\alpha + \frac{1}{2!}\partial^2_{\alpha\beta}\dot{\gamma}^{\mathrm{p}} r^2 n_\alpha n_\beta + \dots \right] \mathrm{d}r\, r\, \mathrm{d}\theta \\ &= \dot{\gamma}^{\mathrm{p}} + \frac{1}{\pi R^2}\left[\frac{R^3}{3}\partial_\alpha \dot{\gamma}^{\mathrm{p}} \int_0^{2\pi} n_\alpha \mathrm{d}\theta + \frac{R^4}{8}\partial^2_{\alpha\beta}\dot{\gamma}^{\mathrm{p}} \int_0^{2\pi} n_\alpha n_\beta \mathrm{d}\theta + \dots \right] \end{aligned} \tag{10.4.8}$$

with $\int_0^{2\pi} n_i \mathrm{d}\theta = 0; \int_0^{2\pi} n_i n_j \mathrm{d}\theta = \pi\delta_{ij}$, it follows immediatly from this expression that

$$\langle \dot{\gamma}^{\mathrm{p}} \rangle = \dot{\gamma}^{\mathrm{p}} + \ell_{\mathrm{c}}^2 \nabla^2 \dot{\gamma}^{\mathrm{p}} + 0(\ell_{\mathrm{c}}^4) \tag{10.4.9}$$

where the kinematical length scale $\ell_{\mathrm{c}} = R/(2\sqrt{2})$ is unspecified. In passing, we note that the numerical factor in 10.4.9 depends on the dimensionality of the problem, e.g. $R^2/8$ is replaced by $R^2/10$ if the calculation is carried on in three dimensions.

On the other hand, for the yield surface and the plastic potential we assume the simplest generalizations of the corresponding mobilized friction and dilatancy laws

$$F = -\tau - (\sigma - \alpha_\sigma)\mu(\bar{\gamma}^{\mathrm{p}}) \tag{10.4.10}$$

$$Q = -\tau - (\sigma - \alpha_\sigma)\beta(\bar{\gamma}^{\mathrm{p}}) \tag{10.4.11}$$

with $\bar{\gamma}^{p} = \int \langle \dot{\gamma}^{p} \rangle$.

Furthermore, the following evolution law for the back-stress is postulated (Vardoulakis and Aifantis, 1991)

$$\dot{\alpha}_{\sigma} = -K\ell_{c}^{2}\nabla^{2}\dot{\varepsilon}^{p} \tag{10.4.12}$$

where K is the 2D-compression modulus and ℓ_c is a material length.

The physical meaning of equations 10.4.10 to 10.4.12 is straightforward: Inside the localized zone γ^p varies rapidly and assumes a maximum value somewhere at the center of it, if we deal with a shear band, or at a boundary of it, if we deal with an interface band. Consequently, within a zone of localized deformation we expect that,

$$\dot{\gamma}^{p} > 0 \quad \text{and} \quad \nabla^{2}\dot{\gamma}^{p} < 0 \tag{10.4.13}$$

Since localization is accompanied by rarefaction and material softening, any decrease in $\bar{\gamma}^{p}$ is counterbalanced by the increase of the gradient term. In other words, in regions of material softening, a larger than local region contributes to the overall strength. This means that in the present theory non-local effects lead to strengthening of the material, since the gradient-dependent relative stress produces effectively an increase of the local confining pressure.

In the considered case Prager's consistency condition becomes

$$-K'\mu\beta\ell_{c}^{2}\nabla^{2}\langle\dot{\gamma}^{p}\rangle + H\langle\dot{\gamma}^{p}\rangle - b_{\alpha\beta}^{F}\dot{\varepsilon}_{\alpha\beta} = 0 \tag{10.4.14}$$

where

$$\begin{aligned} b_{\gamma\delta}^{F} &= G(s_{\alpha\beta}/\tau + k\mu\delta_{\alpha\beta}) \\ L_{\alpha\beta\gamma\delta}^{e} &= G\{(k-1)\delta_{\alpha\beta}\delta_{\gamma\delta} + \delta_{\alpha\gamma}\delta_{\beta\delta} + \delta_{\alpha\delta}\delta_{\beta\gamma}\} \\ H &= Gh^{*} = G(h + h_{0});\ h_{0} = 1 - h_{T} \\ h &= (|\sigma - \alpha_{\sigma}|/G)(\mathrm{d}\mu/\mathrm{d}\bar{\gamma}^{p});\ h_{T} = -k\mu\beta;\ k = K'/G \end{aligned} \tag{10.4.15}$$

cf. section 6.5.2.

As already shown in section 10.2.3 the differential consistency condition may be reduced into an ℓ^4-algebraic condition for local interparticle slip $\dot{\gamma}^{p}$

$$\langle\dot{\gamma}^{p}\rangle \approx \frac{\langle 1\rangle}{h_{0}} b_{\alpha\beta}^{F}\{\dot{\varepsilon}_{\alpha\beta} + \ell^{2}\nabla^{2}\dot{\varepsilon}_{\alpha\beta}\} \geq 0 \tag{10.4.16}$$

and the back-stress rate is given by

$$\dot{\alpha}_{\sigma} \approx -\frac{\langle 1\rangle}{\mu}\ell^{2} b_{\alpha\beta}^{F}\nabla^{2}\dot{\varepsilon}_{\alpha\beta} \tag{10.4.17}$$

where denote again the McAuley brackets. Since, $\dot{\gamma}^{p}$, whenever loading of the yield surface $F = 0$ is taking place and zero otherwise.

Accordingly, the approximate rate stress-strain relations of the strain-rate gradient dependent flow theory of plasticity are recovered

$$\dot{\sigma}_{\alpha\beta} = L^{ep}_{\alpha\beta\gamma\delta}\dot{\varepsilon}_{\gamma\delta} - L^{p}_{\alpha\beta\gamma\delta}\ell^2\nabla^2\dot{\varepsilon}_{\gamma\delta} \tag{10.4.18}$$

where $L^{ep}_{\alpha\beta\gamma\delta}$ is the elastoplastic stiffness,

$$L^{ep}_{\alpha\beta\gamma\delta} = L^{e}_{\alpha\beta\gamma\delta} - L^{p}_{\alpha\beta\gamma\delta} \tag{10.4.19}$$

$$L^{p}_{\alpha\beta\gamma\delta} = \frac{\langle 1\rangle}{H} b^{Q}_{\alpha\beta} b^{F}_{\gamma\delta} \tag{10.4.20}$$

The tensor $b^{Q}_{\alpha\beta}$ is defined. in analogy to $b^{F}_{\alpha\beta}$, in terms of the mobilized dilatancy coefficient, $b^{Q}_{\alpha\beta} = G(s_{\alpha\beta}/\tau + k\beta\delta_{\alpha\beta})$. These constitutive equations are a straightforward singular perturbation of the ones of classical flow theory, equations 6.5.42. Finally we remark that as far as the weak or strong formulation of the rate boundary value problem is concerned, the formalism of section 10.2.4 can be directly applied.

10.4.2
Shear-band analysis

We will consider here the differential equations that govern continued equilibrium from a given configuration C of a soil body; these are the rate-constitutive equations 10.4.18 and the rate-equilibrium equations

$$\begin{aligned} \partial_1\dot{\sigma}_{11} + \partial_2\dot{\sigma}_{21} &= 0 \\ \partial_1\dot{\sigma}_{12} + \partial_2\dot{\sigma}_{22} &= 0 \end{aligned} \tag{10.4.21}$$

We assume that at C the fields of initial stress and hardening parameter vary slowly in space. Accordingly, the components of the stiffness tensors $L^{ep}_{\alpha\beta\gamma\delta}$ and $L^{p}_{\alpha\beta\gamma\delta}$ may be treated as constants. For convenience, the governing equations are written in the coordinate system of the principal axes of the stress tensor in C. Under fully loading conditions we obtain the following set of constitutive equations

$$\begin{aligned} \dot{\sigma}_{11} &= L^{u}_{1111}\dot{\varepsilon}_{11} + L^{u}_{1122}\dot{\varepsilon}_{22} - M_{11}\nabla^2\dot{\varepsilon}_{11} - M_{12}\nabla^2\dot{\varepsilon}_{22} \\ \dot{\sigma}_{22} &= L^{u}_{2211}\dot{\varepsilon}_{11} + L^{u}_{2222}\dot{\varepsilon}_{22} - M_{21}\nabla^2\dot{\varepsilon}_{11} - M_{22}\nabla^2\dot{\varepsilon}_{22} \\ \dot{\sigma}_{12} &= \dot{\sigma}_{21} = 2G\dot{\varepsilon}_{12} \end{aligned} \tag{10.4.22}$$

where L^{u}_{ijkl} are the components of the stiffness tensor of the 'upper bound' comparison solid, given explicitly by equations 8.2.3, and

$$\begin{aligned} M_{11} &= \ell^2 G(k\mu + 1)(k\beta + 1)/h^* \\ M_{12} &= \ell^2 G(k\mu + 1)(k\beta - 1)/h^* \\ M_{21} &= \ell^2 G(k\mu - 1)(k\beta + 1)/h^* \\ M_{22} &= \ell^2 G(k\mu - 1)(k\beta - 1)/h^* \end{aligned} \tag{10.4.23}$$

Introducing these expressions into the equilibrium equations results finally in the following system of partial differential equations for the components of the velocity v_i

$$
\begin{aligned}
M_{11}\nabla^2(\partial_{11}^2 v_1) + M_{12}\nabla^2(\partial_{21}^2 v_2) - L_{1111}\partial_{11}^2 v_1 - G\partial_{22}^2 v_1 \\
- (L_{1122} + G)\partial_{12}^2 v_2 = 0 \\
M_{21}\nabla^2(\partial_{12}^2 v_1) + M_{22}\nabla^2(\partial_{22}^2 v_2) - (L_{2211} + G)\partial_{12}^2 v_1 \\
- G\partial_{11}^2 v_2 + L_{2222}\partial_{22}^2 v_2 = 0
\end{aligned}
\tag{10.4.24}
$$

These partial differential equations constitute a singular perturbation of the classical ones, i.e. they reduce to the classical ones if the material length ℓ is allowed to go to zero. If one is interested in studying boundary-value or eigenvalue problems which involve some geometric dimension L of a structure, then the coordinates x_α must be non-dimensionalized properly (by L) and the highest derivatives in equations 10.4.24 are then multiplied by the number $(\ell/L)^2 \ll 1$. In this case, the above equations reduce to the ones that govern deformation in a classical continuum. If, on the other hand, one is interested in determining whether or not shear bands exist, then one has to investigate equilibrium across two adjacent planes at a distance $2d_B$ that correspond to shear-band boundaries. With the assumption that $\ell/d_B = 0(1)$, the higher-order derivatives in equations 10.4.24 become then essential. The shear-band thickness $2d_B$ is called then an internal length of the problem, and above consideration means simply that an internal length scales with the material length per definition.

Accordingly the above differential equations 10.4.24 can be investigated for the special case where solutions are sought that correspond to the localization of deformation into narrow zones of intense shear, the so-called shear bands. According to Figure 10.4.1, the (x_1, x_2)-coordinate system is chosen in such a fashion that the x_1-axis coincides with the minor minimum principal stress σ_1 in C. Let us assume that a shear band is forming that is inclined with respect to the x_1-axis at an angle θ A new coordinate system $(x, y) = (n_2 x_1 + n_1 x_2, -n_1 x_1 + n_2 x_2)$ is introduced with its axes parallel and normal to the shear band, where $(n_1, n_2) = (-\sin\theta, \cos\theta)$ is the unit vector that is normal to the shear-band axis. By assuming that all field properties related to the forming shear band do not depend on the longitudinal x-coordinate and setting $(\cdot)' = \partial/\partial y$, above equations reduce to the following system of ordinary differential equations

$$
\begin{aligned}
M_{11}n_1^2 v_1^{(4)} + M_{12}n_1 n_2 v_2^{(4)} - \Gamma_{11}v_1'' - \Gamma_{12}v_2'' = 0 \\
M_{21}n_1 n_2 v_1^{(4)} + M_{22}n_2^2 v_2^{(4)} - \Gamma_{21}v_1'' - \Gamma_{22}v_2'' = 0
\end{aligned}
\tag{10.4.25}
$$

where $\Gamma_{\alpha\beta}$ is the 2D-acoustic tensor

$$
[\Gamma_{\alpha\beta}] = \begin{bmatrix} L_{1111}n_1^2 + Gn_2^2 & (L_{1122} + G)n_1 n_2 \\ (L_{2211} + G)n_1 n_2 & Gn_1^2 + L_{2222}n_2^2 \end{bmatrix}
\tag{10.4.26}
$$

In searching for periodic solutions we set

$$
v_\alpha = c_\alpha \sin(Qy)
\tag{10.4.27}
$$

and the above system yields

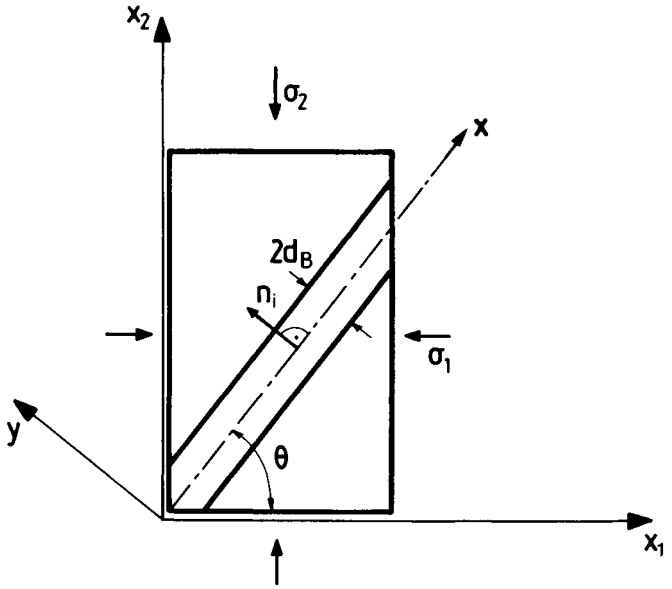

Figure 10.4.1 Specimen with shear band.

$$\begin{bmatrix} b_{11} & b_{12} \\ b_{21} & b_{22} \end{bmatrix} \begin{bmatrix} c_1 \\ c_2 \end{bmatrix} = [0] \tag{10.4.28}$$

where

$$[b_{ij}] = \begin{bmatrix} M_{11}n_1^2Q^4 + \Gamma_{11}Q^2 & M_{12}n_1n_2Q^4 + \Gamma_{12}Q^2 \\ M_{21}n_1n_2Q^4 + \Gamma_{21}Q^2 & M_{22}n_2^2Q^4 + \Gamma_{22}Q^2 \end{bmatrix} \tag{10.4.29}$$

For non-trivial solutions the matrix equation 10.4.28 results in the following condition for the shear-band thickness $2d_B = \pi/Q$

$$(Q\ell)^2 = -a_1(n_1, n_2)/a_0(n_1, n_2) \tag{10.4.30}$$

where

$$a_1 = \det(\Gamma_{\alpha\beta}) \tag{10.4.31}$$

$$a_0 = R_{11}\Gamma_{22}n_1^2 - (R_{21}\Gamma_{12} + R_{12}\Gamma_{21})n_1n_2 + R_{22}\Gamma_{11}n_2^2;\ R_{\alpha\beta} = M_{\alpha\beta}/\ell^2 \tag{10.4.32}$$

It should be noted that a_1=det ($\Gamma_{\alpha\beta}$) is a quadratic form in the orientation cosines n_α and that the condition det ($\Gamma_{\alpha\beta}$)=0 coincides with the classical bifurcation condition,

$$L_{1111}n_1^4 + ((1/G)(L_{1111}L_{2222} - L_{1122}L_{2211}) - L_{1122} - L_{2211})n_1^2n_2^2 + L_{2222}n_2^4 = 0 \tag{10.4.33}$$

Prior to classical bifurcation, and for any n_α, $a_1(n_1, n_2)>0$, whereas $a_1<0$ for any state past the classical critical bifurcation point. On the other hand, $a_0(n_1, n_2)$ is a quadratic form

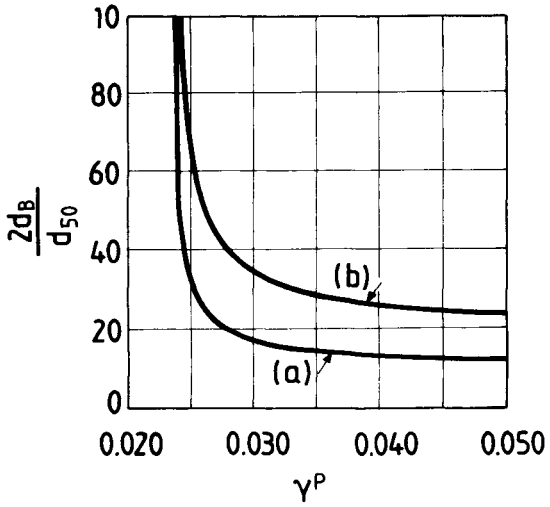

Figure 10.4.2 Evolution of shear-band thickness in the post-bifurcation regime of the classical description: (a) $2R=d_{50\%}$, (b) $2R=2d_{50\%}$.

in the orientation cosines which is characteristic for the type of the governing partial differential equations. It turns out that always $a_0>0$ which means that the system of partial differential equations (10.4.24) is always elliptic, as opposed to the classical system of governing equations which is of changing type, namely turning from elliptic to hyperbolic at the point of classical bifurcation.

Following these observations we conclude that: (a) prior to classical bifurcation there is no real solution for the shear band thickness, (b) at the classical bifurcation point the shear-band thickness is infinite as compared to the material length ℓ, rapidly decreasing in the post-bifurcation regime. This is a well-established qualitative result that should hold for any linear analysis that is based on a physically sound constitutive theory; cf. chapter 9.

In order to provide an estimate of the material length ℓ we will analyze here some experimental results from a biaxial test on a fine-grained Oestershelde sand which were also analyzed in sections 8.2.2 and 9.4.3. We recall that classical-type bifurcation occurs at a critical plastic shear strain $\gamma_B^p \approx 2.7\%$ with $\phi_B = 43.4^\circ$; $\psi_B = 16^\circ$; the corresponding inclination of the shear-band $\theta_B = 59.2^\circ$. X-ray radiographs of the considered Oestershelde sand specimens revealed a shear-band thickness that is about 18.5 times the mean grain diameter $d_{50\%}$ (Table 9.4.1). In order to match this finding we have to assume that the domain of integration for the evaluation of the non-local interparticle slip, equation 10.4.8, has a diameter

$$2R = d_{50\%} \text{ to } 2d_{50\%} \tag{10.4.34}$$

Figure 10.4.2 shows the corresponding predictions of the admissible shear-band thickness ($2d_B/d_{50\%}$) in the post-bifurcation regime of the classical description. This figure demonstrates that no localization is possible at the bifurcation point of the classical description and that the deformation rapidly localizes in the post-bifurcation regime. According to this figure the material length ℓ_c, which appears in equation 10.4.9 and the following equations is such that $\ell_c = R/\sqrt{8}$, and thus $\ell_c \approx d_{50\%}/4$.

Literature

Textbooks and monographs

Love, A.E.H. (1927). *A Treatise on the Mathematical Theory of Elasticity.* Cambridge University Press, Cambridge.

Lemaître, J. (1992). *A Course on Damage Mechanics.* Springer-Verlag, Berlin.

References

Aifantis, E.C. (1978). A proposal for continuum with microstructure. *Mech. Res. Comm.,* **5,** 139–145.

Aifantis, E.C. (1984). On the microstructural origin of certain inelastic models. *J. Mat. Eng. Tech.,* **106,** 326–330.

Aifantis, E.C. (1985). Mechanics of microstructures—I. In: Continuum Mechanics, Thermodynamics and Microstructures. *Proc. Int. Centre Theor. Phys., Trieste, Italy* (eds V.Balakrishnan and C.E.Botani), 316–346.

Altan, S.B. and Aifantis, E. (1992). On the structure of the mode II crack-tip in gradient elasticity. *Scipta Metallurgica,* **26,** 319–324.

Bažant, Z.P. (1984). Imbricate continuum and its variational derivation. *ASCE J. Eng. Mech.,* **110,** 1693–1712.

Bell, J.S. and Gough, D.I. (1979). Northeast-southwest compressive stress in Alberta: evidence from oil wells. *Earth Planet. Sci. Lett.,* **45,** 475–482.

Casal, P. (1961). La capilarité interne. *Cahier du Groupe Français d'Études de Rhéologie C.N.R.S.,* **VI** (3), 31–37.

Coleman, D.B. and Hodgdon, M.L. (1985). On shear bands in ductile materials. *Arch. Rat. Mech. Anal,* **90,** 219–247.

Cowin, S.C. and Nunziato, J.W. (1983). Linear elastic materials with voids. *J. Elast.,* **13,** 125–147.

Dillon, O.W. and Kratochvil, J. (1970). A strain gradient theory of plasticity. *Int. J. Solids Struct.,* **6,** 1513–1533.

Germain, P. (1973a). La méthode des puissances virtuelles en mécanique des milieux continus. Part I *J. Mécanique,* **12,** 235–274.

Germain, P. (1973b). The method of virtual power in continuum mechanics. Part 2: Microstructure. *SIAM J. Appl. Math.,* **25,** 556–575.

Griffith, A.A. (1921). The phenomena of rupture and flow in solids. *Phil. Trans. Roy. Soc. London,* **A221,** 163–198.

Mindlin, R.D. (1964). Micro-structure in linear elasticity. *Arch. Rat. Mech. Anal,* **10,** 51–77.

Mróz, Z. (1973). *Mathematical Models of Inelastic Material Behavior.* University of Waterloo Press, Solid Mechanics Division.

Mühlhaus, H.-B. and Aifantis, E.C. (1991). A variational principle for gradient plasticity. *Int. J. Solids Struct.,* **28,** 845–857.

Papamichos, E., Vardoulakis, I. and Sulem, J. (1994). Generalized continuum models for borehole stability analysis. SPE/ISRM 28025, Proc. EUROCK '94, SPE/ISRM *Rock Mechanics in Petroleum Engineering,* Delft, 37–44, Balkema, Rotterdam.

Papanastasiou, P. and Vardoulakis, I. (1989). Bifurcation analysis of deep boreholes: II. Scale effect. *Int. J. Num. Anal Meth. Geomech.,* **13,** 183–198.

Papanastasiou, P. and Vardoulakis, I. (1992). Numerical analysis of progressive localization with application to borehole stability. *Int. J. Num. Anal. Meth. Geomech.,* **16,** 389–424.

Pijaudier-Cabot, G., Bazant, Z. and Tabbara, M. (1988). Comparison of various models for strain softening. *Eng. Comp.,* **5,** 141–150.

Prager, W. (1955). The theory of plasticity: a survey of recent achievements. *Proc. Inst. Mech. Eng.,* **169,** 41–57.

Prager, W. (1956). A new method of analyzing stress and strains in work-hardening solids. *J. Appl Mech. ASME,* **23,** 493–496.

Santarelli, F.J., Brown, E.T. and Maury, V. (1986). Analysis of borehole stresses using pressure dependent, linear elasticity. *Int. J. Rock Mech. Min. Sci. Geomech. Abstr.,* **23,** 445–449.

Schreyer, H.L. and Chen, Z. (1986). One-dimensional softening with localization. *J. Appl. Mech.,* **108,** 791–797.

Sluys, L.J. (1992). Wave propagation, Localization and Dispersion in Softening Solids. PhD Thesis, Delft Technical University.

Tronvoll, J., Papamichos, E. and Kessler, N. (1993). Perforation cavity stability: Investigation of failure mechanism. *Proc. Int. Symp. Hard Soils and Soft Rocks.* (eds A Anagnostopoulos *et al.*) **2,** 1687–1693.

Vardoulakis, I. (1994). Potentials and limitations of softening models in geomechanics. *Eur. J, Mech./Solids,* **13,** 195–226.

Vardoulakis, I. and Aifantis, E.C. (1991). A gradient flow theory of plasticity for granular materials. *Acta Mechanica,* **87,** 197–217.

Vardoulakis, I. and Frantziskonis, G. (1992). Micro-structure in kinematic-hardening plasticity. *Eur. J. Mech./Solids,* **11,** 467–486.

Vardoulakis, I., Sulem, J. and Guenot, A. (1988). Stability analysis of deep boreholes. *Int. J. Rock Mech. Min. Sci. Geomech. Abstr.,* **25,** 159–170.

Vardoulakis, I. and Papanastasiou, P. (1988). Bifurcation analysis of deep boreholes: I. Surface instabilities. *Int. J. Num. Anal Meth. Geomech.,* **25,** 158–170.

Vardoulakis, I., Shah, K.R. and Papanastasiou, P. (1992). Modelling of tool-rock interfaces using gradient-dependent flow theory of plasticity. *Int. J. Rock Mech. Min. Sci. Geomech. Abstr.,* **29,** 573–582.

Vardoulakis, I., Papamichos, E. and Sulem, J. (1994). A second-gradient plasticity model for granular rocks. *Europe-U.S. Workshop on Fracture and Damage in Quasibrittle Structures: Experiment, Modeling and Computer Analysis, Prague, September 21–23, 1994* (eds Z.Bažant *et al.*), 99–111. E. & F.N.Spon, London.

Vardoulakis, I., Exadactylos, G. and Aifantis, E. (1995). Gradient elasticity with surface energy—Mode III crack problem. Submitted for publication.

Zoback, M.D., Moos, M. and Mastin, L. (1986). Well bore breakouts and *in situ* stress. *J. Geoph. Res.,* **90,** 5523–5530.

11
Stability of undrained deformations

11.1
Monotonic biaxial tests on water-saturated sand

The behavior of water-saturated granular materials subjected to undrained deformations has been thoroughly investigated by several authors in past years. Typical examples of this type of work are the papers by Castro (1969), Casagrande (1976) and later by Vaid and Chern (1983). Most of the published work which concerns us here is based on the static or cyclic behavior of sands tested in the triaxial (cylindrical) apparatus. Some papers deal with tests in the torsional (Tatsuoka *et al.,* 1982) or the simple shear apparatus (Alarcon-Guzman *et al.,* 1988). Professor Ishihara (1993) in his Rankine Lecture on 'Liquefaction and Flow Failure during Earthquakes' gives a thorough and exaustive reference to published works in the subject.

The evaluation of experiments and the description of observed phenomena is always done within the frame of a continuum and constitutive theory. Here, water-saturated granular soil is modeled as a mixture of a solid and an aqueous phase, which may or may not share common velocities. For the interpretation of the resulting partial stresses Terzaghi's effective stress principle is utilized. The behavior of the skeleton is described in terms of effective stresses by the elastoplasticity theory for cohesionless materials with internal friction and dilatancy; cf. Peters (1984), Vardoulakis (1985, 1986) and Nova (1991).

In this section, we discuss results from undrained biaxial experiments published earlier by Han and Vardoulakis (1991) and Vardoulakis (1995). Table 11.1.1 summarizes some data related to these tests, which were run under axial displacement control and constant confining pressure. Initially, a well-prepared sand specimen is deforming homogeneously and its evaluation and interpretation within a constitutive theory is straightforward. We call this phase of the deformation of the soil specimen, the constitutive phase of soil behavior. Except for the very loosely packed sand specimens (e.g. test DC-09) the constitutive phase was terminated by a spontaneous shear-band formation.

The following sections are mostly based on some recent work of Vardoulakis (1995) where the issues of uniqueness, stability and well posedeness, in relation to undrained

Table 11.1.1 Monotonic, displacement-controlled, undrained biaxial tests on St. Peter Sandstone sand (Han and Vardoulakis, 1991)

Parameter	DC-11	DC-04	DC-16	DC-09
Initial density, ρ_{d0} (g/cm^3)	1.660	1.608	1.594	1.495
Initial porosity, n_0 (—)	0.374	0.393	0.399	0.436
Confining pressure, σ_c (kPa)	501.2	750.3	502.3	501.1
Initial back-pressure, p_{w0} (kPa)	295.6	345.5	297.6	296.5
Initial effective mean stress, σ'_0 (kPa)	205.6	404.8	204.7	204.6
Degree of saturation, S (%)	99.98	99.95	99.95	99.95

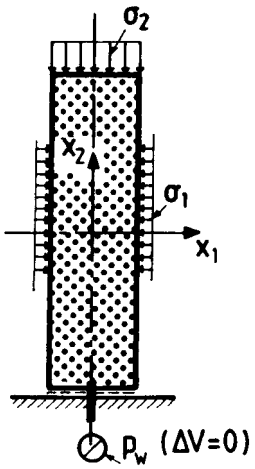

Figure 11.1.1 Biaxial set-up.

deformations of sands are discussed. This analysis includes a simple mathematical model for undrained monotonic biaxial tests under constant confining pressure and the condition for globally undrained shear banding.

11.1.1
Experimental basis

Let (x_1, x_2) be the coordinates in the plane of deformation in the directions of principal stretches, and let x_3 be the coordinate perpendicular to it (Figure 11.1.1). During a homogeneous plane, rectilinear deformation these directions are fixed in space. Let λ_α and σ_α $(\alpha = 1,2,3)$ be the corresponding principal (logarithmic) strains and Cauchy stresses, with $\lambda_3 = 0$ and σ'_α. The total stresses σ_α are decomposed into effective stresses and pore-water pressure

$$\sigma_\alpha = \sigma'_\alpha - p_w \tag{11.1.1}$$

with compressive stresses σ_α (σ'_α) being negative and p_w>0, if the pore fluid is under pressure. In the considered plane-strain tests the pore-water pressure p_w was

monitored, whereas the out-of-plane principal stress σ_3 was not measured. In order to resolve the indeterminacy of σ_3 the assumption of elastoplastic behavior is adopted. Thus principal strain increments, $\Delta\lambda_\alpha = \Delta\varepsilon_\alpha$, are decomposed into an elastic and a plastic part

$$\Delta\varepsilon_\alpha = \Delta\varepsilon_\alpha^e + \Delta\varepsilon_\alpha^p \tag{11.1.2}$$

Furthermore we make the following assumptions:

(a) Elastic strain increments are associated with the effective stress increments.
(b) The plastic strain rate potential does not depend on the intermediate (effective) stress.
(c) σ_3' is always the intermediate effective stress (σ_2').

These assumptions result in $\Delta\varepsilon_3^p = 0$,, which together with the plane-strain condition, $\Delta\varepsilon_3^e = 0$, to $\Delta\varepsilon_3 = 0$,, or to

$$d\sigma_3' = \nu(d\sigma_1' + d\sigma_2') \tag{11.1.3}$$

where υ is the Poisson ratio. Equation 11.1.3 suggests the application of a 2D theory of plasticity, whose material constants and functions are easily derived from or related to the ones of a corresponding 3D theory (cf. section 6.5.1). However, here only results from the aforementioned plane-strain experiments will be used. Accordingly, the results from the constitutive phase of biaxial experiments are represented in terms of the following 2D invariant stress and strain measures:

$$\begin{aligned} \sigma' &= (\sigma_1' + \sigma_2')/2;\ \tau = |\sigma_1' - \sigma_2'|/2 \\ \varepsilon &= \lambda_1 + \lambda_2;\ \gamma = |\lambda_1 - \lambda_2| \end{aligned} \tag{11.1.4}$$

Figure 11.1.2 shows the deviatoric stress-strain curves for the medium dense sand specimens (DC-04 and DC-16), which had almost the same initial porosity but were sheared at different initial effective stresses. The corresponding effective stress paths are shown in Figure 11.1.3. Figures 11.1.4 and 11.1.5 show the experimental curves for the group of tests which were sheared at the same initial effective stress (DC-09, DC-16 and DC-11).

In undrained tests, due to the inevitable membrane penetration error volumetric strains should be estimated indirectly from the storage equation 5.4.14. The pore fluid contains, in general, a small amount of air and thus it is more compressible than the de-aired fluid. Accordingly, the compressibility of the fluid-air system depends on the degree of saturation S and on the pore-fluid pressure as expressed by equation 5.4.9. In addition to the storage equation 5.4.14 one should also consider equation 5.4.15, which accounts for minor corrections in the porosity. However, almost perfect saturation ($\Delta\varepsilon_3^e = 0$) and small solids and water compressibilities result in volumetric strains which are two and three orders of magnitude smaller than the corresponding shear strains. Thus, in general, and without significant error, the deformation may be considered isochoric

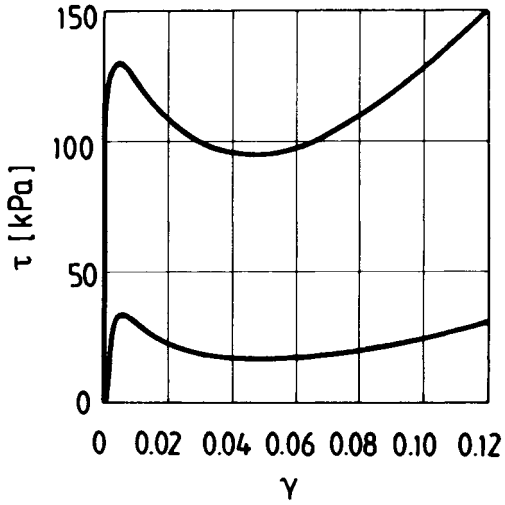

Figure 11.1.2 Deviatoric stress-strain curves for medium dense sand at different initial confining pressure (DC-04 and DC-16).

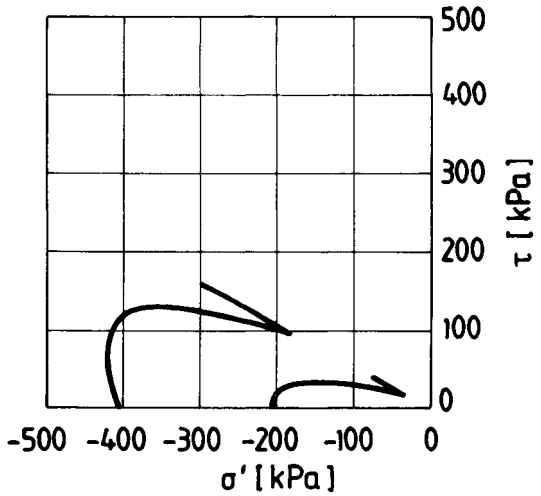

Figure 11.1.3 Effective stress paths for medium dense sand at different initial confining pressure (DC-04 and DC-14).

$$\Delta\varepsilon = 0 \rightarrow n \approx n_0 \tag{11.1.5}$$

According to 11.1.2, volumetric and shear strain increments are also decomposed into an elastic and a plastic part

$$\Delta\varepsilon = \Delta\varepsilon^e + \Delta\varepsilon^p;\ \Delta\gamma = \Delta\gamma^e + \Delta\gamma^p \tag{11.1.6}$$

with elastic strains given by a simple incremental elasticity law,

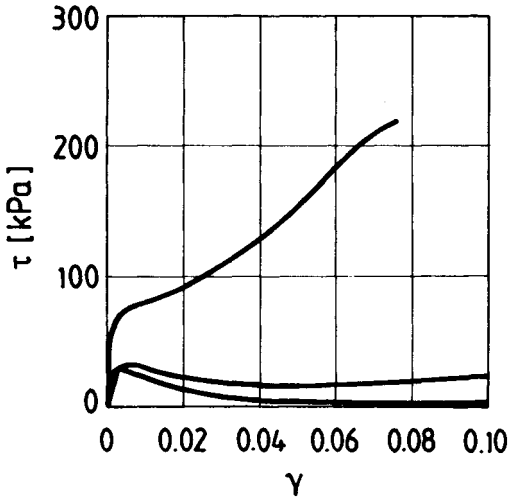

Figure 11.1.4 Deviatoric stress-strain curves for loose (DC-09) medium dense (DC-16) and dense sand (DC-11).

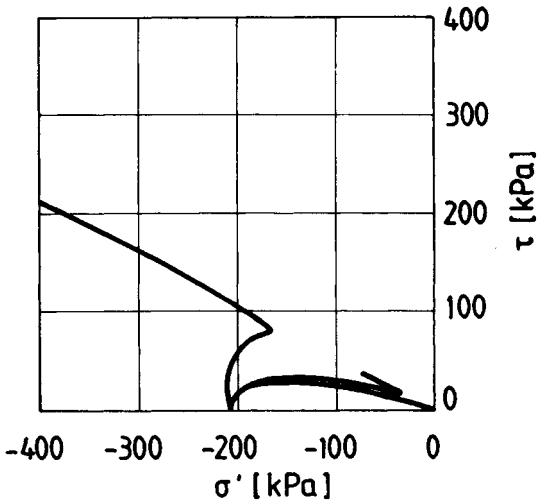

Figure 11.1.5 Effective stress paths for loose (DC-09), medium dense (DC-16) and dense sand (DC-11).

$$\Delta\varepsilon^e = \Delta\sigma'/K'; \; \Delta\gamma^e = \Delta\tau/G \tag{11.1.7}$$

Due to 11.1.3, the 2D elastic compression modulus K' is related to the elastic shear modulus G according to equation 6.5.15.

As presented in section 6.5, sand is described here by a linear, single strain hardening Mohr-Coulomb non-associative elastoplastic constitutive model,

$$F = \tau + \sigma'\mu(\gamma^p);\ Q = \tau + \sigma'\beta(\gamma^p) \tag{11.1.8}$$

where the mobilized friction and dilatancy coefficients are functions not only of the accumulated plastic shear strain but also of the porosity and the effective stress. We consider first in a *(σ′, τ)*-plot the effective stress path for a typical undrained test (cf. Figures 11.1.3 and 11.1.5). The angle between the σ'-axisand the radius, connecting the origin and a point on this graph, defines the mobilized Mohr-Coulomb friction angle $\phi_m = \arcsin(\tau/|\sigma'|)$. Similarly, the mobilized dilatancy angle after Hansen and Lundgren is defined as $\psi_m = \arcsin(\Delta\varepsilon^p/\Delta\gamma^p)$. It should be noted that the best way to determine the dilatancy coefficient was through the deviatoric stress rather than the effective stress data. Obviously for plastic stress states

$$\mu = \sin\phi_m \quad \text{and} \quad \beta = \sin\psi_m \tag{11.1.9}$$

In order to arrive at a simple mathematical description of the evolution of the mobilized dilatancy coefficient for the general non-associative case, $\beta<\mu$, Taylor's (1948) stress-ratio dilatancy rule was adopted

$$\bar{\mu} = \mu - \beta = \text{const.} \geqslant 0 \tag{11.1.10}$$

(cf. sections 6.3.3 and 6.5.3). For the evaluation of $\bar{\mu}$ we proceed with the observation that this constant can be identified with the effective stress ratio at which the soil behavior turns from contractant to dilatant. It is customary to call the corresponding state the 'point of phase transformation' (Ishihara *et al.,* 1975). We may call this state also a state of constant plastic volumetric strain, and denote it by the abbreviation (cv)

$$\bar{\mu} = \mu_{cv};\ \mu_{cv} = \left.\frac{\tau}{|\sigma'|}\right|_{\beta=0} \tag{11.1.11}$$

The curve-fitting procedure for the mobilized friction coefficient was based on a four-parameter function which allows for sufficiently accurate description of strain hardening/softening behavior

$$\mu = \mu_0 + \frac{(1 - c_1\gamma^p)\gamma^p}{c_2 + c_3\gamma^p} \tag{11.1.12}$$

The curve-fitting parameters c_i (i=1, 2, 3) are taken constant for all tests. The influence of porosity, initial effective stress enters only through the mobilized friction coefficient at initial yield μ_0. This procedure yielded c_1=1.704, c_2=0.047, c_3=2.947 and the values for the constants listed in Table 11.1.2. Figure 11.1.6 shows the measured and fitted values for the mobilized friction and dilatancy coefficients for test DC-04.

11.1.2
Simulation and discussion

In order to model the biaxial compression experiments, we assume that the deformation of the soil specimen is homogeneous. In particular, we assume that the deformation of

Table 11.1.2 Curve-fitting parameters, displacement-controlled, undrained biaxial tests on St. Peter Sandstone sand (Han and Vardoulakis, 1991)

Test	n_0	ν	G (MPa)	μ_0	μ_{cv}
DC-11	0.374	0.2	60.0	0.311	0.465
DC-04	0.393	0.2	57.2	0.300	0.525
DC-16	0.399	0.2	45.5	0.240	0.470
DC-09	0.436	0.2	30.0	0.110	0.354

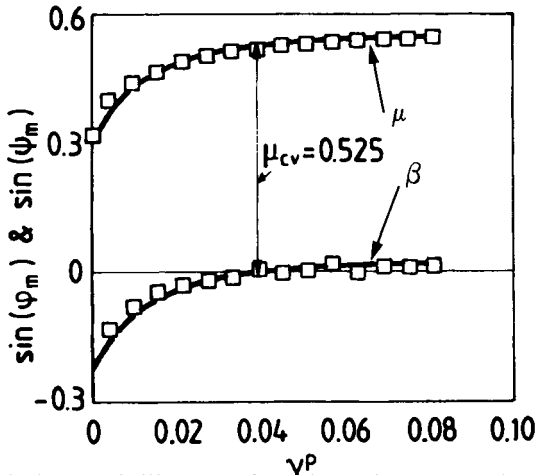

Figure 11.1.6 Mobilized friction and dilatancy functions demonstrating Taylor's stress-dilatancy rule, equation 11.1.10.

the specimen is a plane-strain, undrained rectilinear deformation under constant confining pressure and controlled axial displacement. As already mentioned such tests are described in terms of the deviatoric stress τ and effective stress σ' and the deviatoric strain γ, since the volumetric strain is practically zero (ε=0). Results are usually plotted in terms of the deviatoric stress-strain curve

$$\tau = f(\gamma) \tag{11.1.13}$$

and the effective 'stress path'

$$\tau = g(\sigma') \tag{11.1.14}$$

With the given evolution of the deviatoric and mean effective stress, the pore-water pressure can be computed from the boundary condition, which here corresponds to constant lateral stress

$$\sigma_1 = \text{const.} \rightarrow \mathrm{d}p_w = \mathrm{d}\sigma'_1 = \mathrm{d}\tau + \mathrm{d}\sigma' \tag{11.1.15}$$

In the elastic regime (F<0)

$$\mathrm{d}\tau = G\,\mathrm{d}\gamma \tag{11.1.16}$$

In order to remove the indeterminacy of the effective stress, the incompressibility constraint 11.1.5 must be relaxed. The effective stress path follows then directly from the storage equation 5.4.14 and equations 11.1.15 and 11.1.16, leading to

$$\frac{d\tau}{d\sigma'} = -\left[1 + \frac{2}{3}(1+\nu)\frac{c - c_s}{c_m}\right]; c = 1/K \tag{11.1.17}$$

Accordingly in the elastic regime the slope of the undrained stress path turns out to be relatively steep and approximately constant. For the considered tests $(d\tau/d\sigma')_E \approx 16$

In the elastoplastic regime the effect of solids and fluid compressibility may be neglected without significant error. In this regime the effective stress path can be represented in parametric form, with the plastic shearing strain intensity γ^p as the curve parameter

$$\frac{d\sigma'}{d\gamma^p} = -K\beta \tag{11.1.18}$$

$$\frac{d\tau}{d\gamma^p} = G(h - h_T) \tag{11.1.19}$$

where h is the dimensionless hardening modulus

$$h = \frac{|\sigma'|}{G}\frac{d\mu}{d\gamma^p} \tag{11.1.20}$$

and h_T is a hardening parameter defined as,

$$h_T = -k\mu\beta;\ k = K'/G \tag{11.1.21}$$

We notice that since $d\gamma = d\tau/G + d\gamma^p$, one can replace γ^p by γ and vice versa.

The evolution of the effective stress σ' and the deviatoric stress τ in the elastoplastic regime of undrained deformations is determined by the dilatancy coefficient β and hardening parameter $(h - h_T)$. Figure 11.1.7 shows the evolution of the parameters h and h_T for the set of material parameters corresponding to test DC-04. Equations 11.1.25 and 11.1.26 can be thus integrated to compute the behavior of specimens of water-saturated sand subjected to monotonic undrained biaxial tests. Figures 11.1.8 and 11.1.9 show the computed and measured deviatoric stress-strain curve and effective stress path for test DC-04. It should be noted that the computed stress-strain curves are extended here past the regime that corresponds to the aforementioned 'constitutive' phase of the test, since in the considered test DC-04 a shear band was definitely observed at $\gamma = 12\%$, i.e. slightly prior to the second peak of the deviatoric stress-strain curve.

Water-saturated, relatively medium-dense sand specimens of ordinary size show in displacement-controlled undrained tests a typical 'hardening-soft-ening-rehardening' deviatoric behavior (Figure 11.1.8). In the soil mechanics literature this type of soil behavior is called 'flow with limited deformation'. This means that, unlike other more fine-grained materials (e.g. clays) a typically 'unstable' behavior is indeed observable in

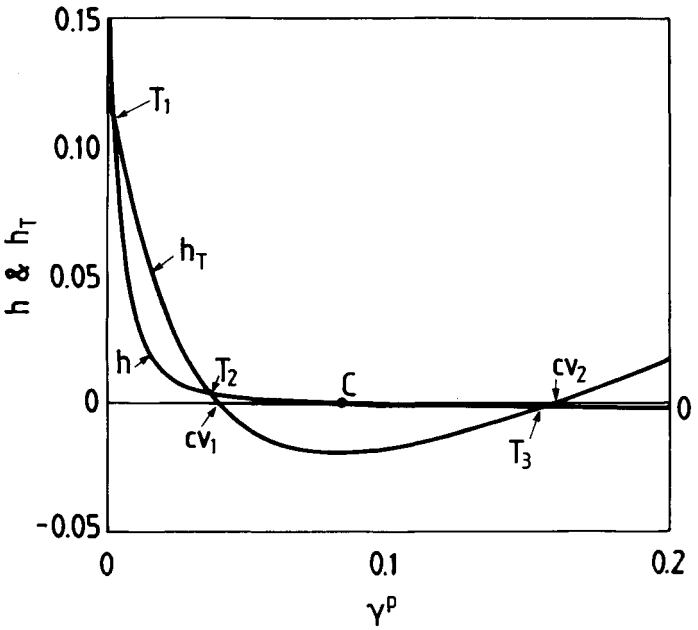

Figure 11.1.7 Evolution of parameters h and h_T for the set of material parameters corresponding to test DC-04.

undrained sand element experiments. The first peak in the deviatoric stress-strain curve marks a state, which is called a Tresca' state, in order to denote a limit point of maximum principal stress difference. The limit state (T_1) is reached at small strains ($\gamma \approx 0.3\%$) and at an effective stress ratio ($\phi_m = 21^\circ$) which is significantly smaller than the maximum effective stress ratio ($\phi_C \approx 33^\circ$). The effective stress ratio at (T_1) is sometimes called the 'critical stress ratio' (Vaid and Chern, 1985). The background soil behavior is definitely contractant ($\psi_m = -10^\circ$), the plastic hardening modulus is positive and it assumes its critical value ($h_T = 0.115$)

$$d\tau/d\gamma^p = 0 \rightarrow h = h_T > 0 \tag{11.1.22}$$

Depending on the type of boundary conditions instabilities may or may not occur at (T_1). In the experimental program considered here, instabilities at (T_1) were only observed in the case of load-controlled tests, since at (T_1) the axial load assumes a local maximum.

The limit state (T_1) of the first maximum of the deviatoric stress is followed by a state (T_2) of minimum deviator, where a second solution of equation 11.1.22.2 exists. The state (T_2) is usually called a 'quasi-steady state'. It is reached at moderate strains, as can be seen from Figure 11.1.8. At (T_2) the soil is hardening and is sightly contractant (**DC-04/T_2**: $\gamma \approx 4\%$, $\phi_m = 31^\circ$,, $\psi_m = -0.5^\circ$, $h_T \approx 0.01$). State (T_2) slightly precedes the aforementioned state of (first) 'phase transformation' (cv_1), where the dilatancy coefficient β changes sign from negative to positive. This means that at (cv_1)

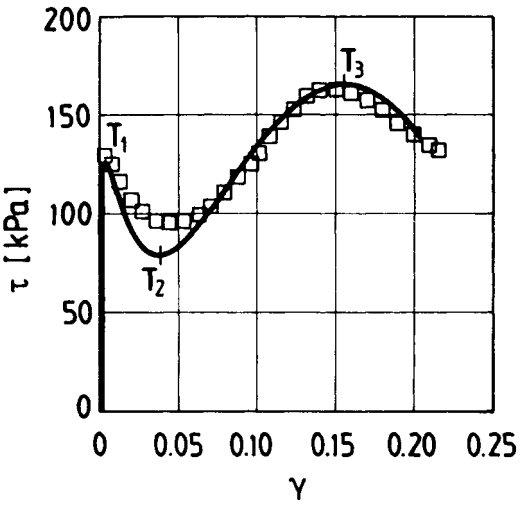

Figure 11.1.8 Measured and computed deviatoric stress-strain curve for test DC-04.

$$d\sigma'/d\gamma^p = 0 \rightarrow \beta = 0 \quad \text{or} \quad \mu = \mu_{cv} \tag{11.1.23}$$

$$(\text{DC-04/cv}_1\text{: } \gamma \approx 5.5\%,\ \phi_m = 32^\circ,\ \psi_m = 0^\circ,\ h_T = 0).$$

In plane-strain experiments, a second maximum (T_3) in the axial load (represented here by the 'nominal' principal stress difference τ) is observed, which fairly well corresponds to a third solution of equation 11.1.22.2. The state (T_3) occurs for dilatant behavior (β>0) inside the softening regime of the background effective stress ratio ($h = h_T < 0$). It turns out that in the discussed typical experiment prior to reaching state (T_3) a shear band has formed, and accordingly the corresponding segment of the stress-strain can only be seen as describing some sort of global (or nominal) behavior. Again, soon after state (T_3) another 'phase transformation' state (cv_2) is reached which indeed marks a transition from dilatant to contractant behaviour, occurring inside a narrow band of strain softening material.

The above described sequence of stress states can be also followed on the effective stress-path diagram, shown in Figure 11.1.9. In this figure the early maximum in deviatoric stress (T_1) is clearly seen as a local maximum of the corresponding curve. The state (T_2) or 'quasi-steady-state' is not clearly seen in this diagram and, as already mentioned, it should not be confused with the state of 'phase transformation' (cv_1), which indeed coincides with the 'elbow' of the effective stress path, i.e. the point with vertical slope ($d\tau/d\sigma' = \infty$). Past this state the effective stress path moves quickly toward its ultimate slope, or 'steady state', which is attained at a state (C) of zero plastic strain hardening ($h = 0$). Accordingly at (C)

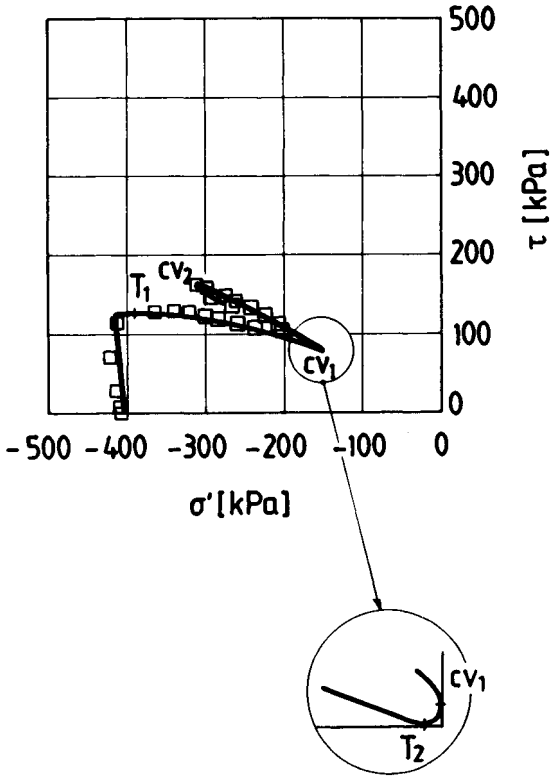

Figure 11.1.9 Measured and computed effective stress path for test DC-04.

$$\frac{d\tau}{d\sigma'} = \frac{\tau}{\sigma'} \rightarrow \mu = \mu_C \tag{11.1.24}$$

This state was termed in section 8.2 a 'Coulomb' state, and signifies the limit state of maximum effective stress ratio

$$h = 0 \rightarrow \mu_C = \max\{\mu\} \tag{11.1.25}$$

Since soils are assumed to obey Coulomb's 'failure' criterion, the corresponding straight line through the origin with slope $(-\mu_C)$ is sometimes called the 'failure line'.

Finally the second 'elbow' in the effective stress path of Figure 11.1.9 corresponds to the ultimate 'phase transformation state' (cv_2). Continued plastic strain softening leads to a 'backwards' tracing of a 'failure line' with slightly smaller slope as the ultimate one.

In Figure 11.1.10 the deviatoric response of a 'loose' sand specimen (DC-09) is reproduced. A 'loose' or 'undercritically dense' specimen reaches at large strains a steady state, which is usually termed the state of 'flow with unlimited deformation'. This is the state of proper soil 'liquefaction', because for continued shearing the soil provides constant resistance, very much like a viscous fluid. This state can be called accordingly a 'critical state' (cs) in the sense of Casagrande, because both stresses and density are

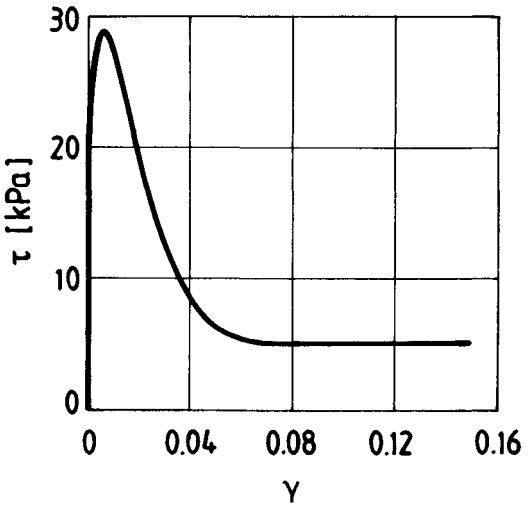

Figure 11.1.10 Computed deviatoric stress-strain curve for a typical loose sand specimen (DC-09).

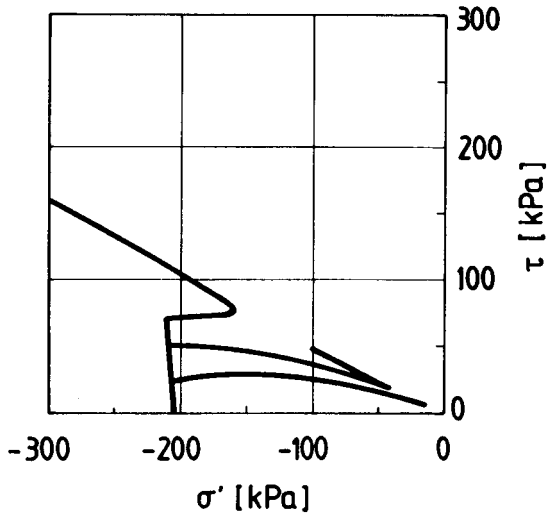

Figure 11.1.11 Computed effective stress paths for three typical behaviors: relatively loose, medium dense and dense sand.

stationary. However, state (cs) is reached asymptotically, i.e. prior to (cs) the behavior of the material is always strain hardening ($h>0$) and contractant ($\beta<0$), with diminishing hardening rate and rate of contractancy. At (cs):

$$d\sigma' = d\tau = 0 \rightarrow \mu_{cs} = \mu_C = \mu_{cv};\ \beta_{cv} = 0 \tag{11.1.26}$$

Finally Figure 11.1.11 summarizes the computational results for the simulation of the three typical behaviors. We observe that the steady state for relatively 'dense' specimens is the Coulomb state, where condition 11.1.24 is satisfied.

11.2 Theoretical implications

Following the above mathematical description of the homogeneous isochoric plane strain rectilinear deformation, the question of uniqueness of such a deformation mode arises. In classical plasticity theory uniqueness is guaranteed by resorting to Drucker's 'stability postulate', which requires that for all possible stress probes the second-order plastic work is non-negative,

$$\Delta_2 w^{\mathrm{p}} = \Delta\sigma'_{ij}\Delta\varepsilon^{\mathrm{p}}_{ij} \geqslant 0 \tag{11.2.1}$$

with the equal sign holding for $\Delta\varepsilon^{\mathrm{p}}_{ij} = 0$; cf. section 6.2.5. We recall that if Drucker's postulate is satisfied at a given state of an elastoplastic body and for all points in the volume that it occupies, then the corresponding incremental boundary value problem possesses under dead loading a unique solution.

In the case of associative material the assumption of Drucker's postulate precludes softening of underlying effective stress ratio, and a material obeying Drucker's postulate is sometimes called a 'stable material'. Indeed, $\Delta_2 w^{\mathrm{p}}$ becomes negative in the softening regime of the effective stress ratio strain curve, since then the plastic increment vector is normal to the yield surface and pointing outwards to this yield surface, whereas the stress increment vector is pointing inwards, and the inner product is negative.

In case of non-associative frictional material, Drucker's stability postulate is violated even in the hardening regime of the material behavior. For continued plastic loading the stress increment is pointing into the exterior domain of the yield surface (F>0), and we distinguish among two sets of possible stress probes (Figure 11.2.1):

$$\text{set (I)} \quad \text{with: } \Delta_2 w^{\mathrm{p}} \geqslant 0$$

$$\text{set (II)} \quad \text{with: } \Delta_2 w^{\mathrm{p}} < 0$$

Undrained, displacement-controlled tests provide realizations of stress probes which lie in the above set (II); that is, for states with $\mu<\mu_{\mathrm{cv}}$, plastic strain contractancy (β<0) results through the constant-volume constraint to an effective stress drop and consequently to pore-water pressure increase. The corresponding effective stress paths turn towards the origin as shown in Figure 11.1.11. The effective stress path can be seen as the envelope in stress space of these effective stress increments. If we imagine the stress and the plastic strain increment vectors attached at some given stress point on the stress path, we can easily visualize the actual value of the second-order plastic work, as their inner product as shown in Figure 11.2.1. For states during an undrained test the actual value of the second-order plastic work can be computed analytically

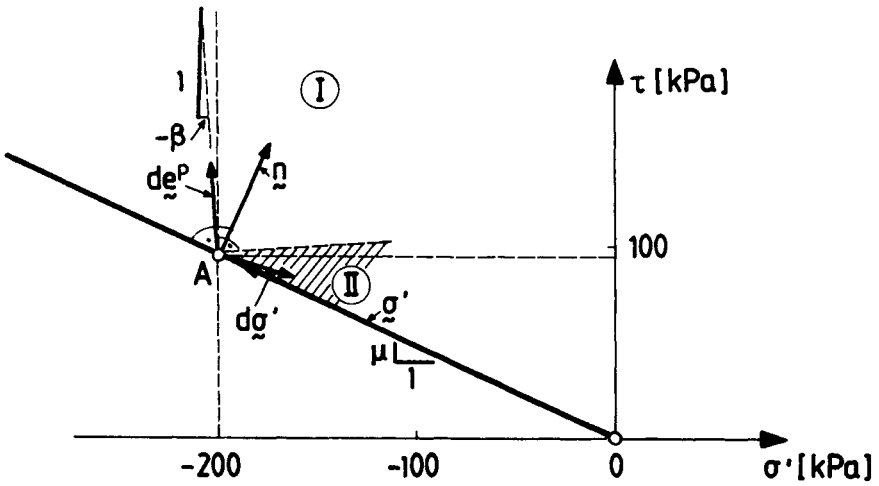

Figure 11.2.1 Yield surface and flow rule for frictional non-associative material and the various sets of stress probes with positive and negative second-order plastic work.

$$\Delta_2 w^p = d\tau \Delta\gamma^p + d\sigma' \Delta\varepsilon^p = G h_w (\Delta\gamma^p)^2 \tag{11.2.2}$$

where

$$h_w = h + k(\mu - \beta)\beta = h + k\mu_{cv}\beta \tag{11.2.3}$$

Notice that in case of normality $(\mu = \beta;\ \mu_{cv} = 0)$, $h_w = h$. In Figure 11.2.2 the hardening parameter h_w is plotted versus γ^p, together with the hardening moduli h and h_T for test DC-04. From the sign of the actual second-order plastic work we conclude that the effective stress path in the considered test follows a track which in the initial and final part of the test corresponds to $\Delta_2 w^p<0$. The initial part with $\Delta_2 w^p<0$ corresponds to (effective stress ratio) strain-hardening material, with $0<h<-\kappa\mu_{cv}\beta$. $\Delta_2 w^p$ becomes positive at a state slightly after the state (T_2) of minimum deviator and before the first 'elbow' of the effective stress path (the state cv_1). $\Delta_2 w^p$ stays positive even past the state (C) of maximum effective stress ratio, in the softening regime, and for all $h>-k\mu_{cv}\beta$. It becomes negative again at a state close to the second deviator maximum (T_3) prior to the second 'elbow' (cv_2) of the effective stress path.

Accordingly, the analysis of such experiments, within the frame of non-associative plasticity, provides empirical proof that for large portions of an undrained test the second-order plastic work is negative ($\Delta_2 w^p<0$). Moreover, under the considered conditions of axial displacement control and constant confining pressure, no visible instabilities took place in the regime with $\Delta_2 w^p<0$. This observation was discussed and validated experimentally in the past by Lade (1989) and Lade *et al.* (1987, 1988). All these observations mean that under certain boundary conditions a deformation process may be unique and homogeneous even if the second-order plastic work is negative.

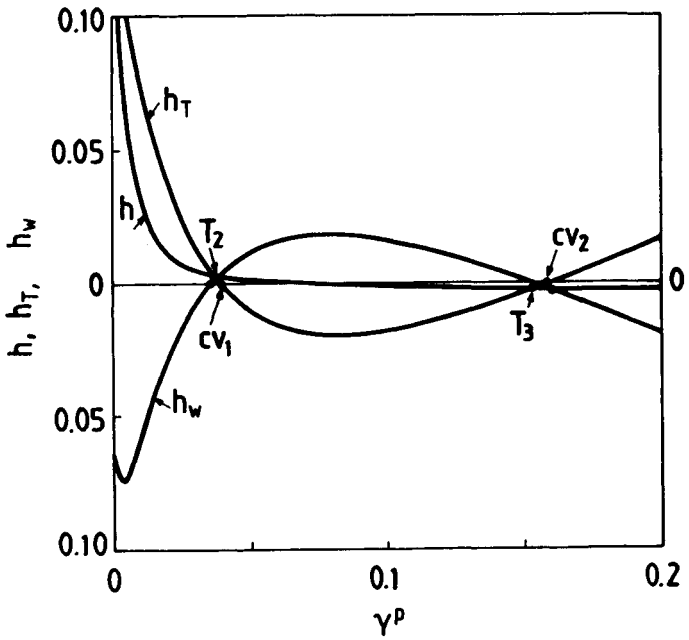

Figure 11.2.2 Evolution of hardening parameters h, h_T and h_w, indicating that the second-order plastic work is negative (approximately) for all contactant states and for states within the softening regime.

11.3
Bifurcation and stability

11.3.1
Undrained shear banding

We consider here a fluid saturated soil body at time t=0, in a given configuration C. Let this body be subjected to an infinitesimal deformation, and let C be the reference configuration. It is assumed that during this deformation process the various mechanical properties of the body change but little, for example the porosity changes from its value $n(x_k, 0)$ in C to $\bar{n} = n + \Delta n(x_k, t)$ in $\bar{\mathbf{C}}$, with $\Delta n(x_k, 0) = 0$ and $|\Delta n|/n \ll 1$ (cf. section 5.7). The incremental displacement of the solid for the considered transition $\mathbf{C} \rightarrow \bar{\mathbf{C}}$ is Δu_i and the relative specific discharge vector of the fluid in $\bar{\mathbf{C}}$ is $\bar{q}_i = q_i + \Delta q_i$. Since connective terms will be neglected for both the solid phase (superscript 1) and the fluid phase (superscript 2), material time derivatives coincide with partial time derivatives, and

$$\begin{aligned} v_\alpha^{(1)} &= \partial_t \Delta u_\alpha \\ v_\alpha^{(2)} &= \partial_t \Delta u_\alpha + \Delta q_\alpha / n \end{aligned} \tag{11.3.1}$$

For incompressible fluid and solids the storage equation becomes

$$-\partial_\alpha \Delta q_\alpha = \partial_t \Delta \varepsilon_{\alpha\alpha} \tag{11.3.2}$$

In a fluid-saturated medium, local uniqueness (and stability) is studied with the undrained deformation mode as the ground mode. The ground mode is denoted here by a (°). Undrained deformations are characterized by remote boundary conditions which preclude in- or outflow of water. Such a type of boundary conditions implies that, under homogeneous deformations, the fluid flow is zero everywhere in the considered domain,

$$\Delta \mathring{q}_\alpha = 0 \tag{11.3.3}$$

This condition means that under locally undrained conditions both phases share common velocity,

$$\mathring{v}_\alpha^{(2)} = \mathring{v}_\alpha^{(1)} \tag{11.3.4}$$

From this condition and the storage equation 11.3.2 it follows that the ground deformation mode is isochoric (volume preserving)

$$\partial_t \Delta \mathring{\varepsilon}_{\alpha\alpha} = 0 \tag{11.3.5}$$

The uniqueness question is posed as follows: at any given state of an undrained deformation, small perturbations $\Delta \tilde{u}_\alpha$, $\Delta \tilde{p}_w$, $\Delta \tilde{q}_\alpha$ and $\Delta \tilde{q}_\alpha$ of the displacements of the skeleton, the pore-water pressure and the relative specific discharge vector are considered. The total displacement, pore-water pressure and discharge are then the sum of the ground mode and the perturbation mode,

$$\Delta u_\alpha = \Delta \mathring{u}_\alpha + \Delta \tilde{u}_\alpha \quad \text{etc.} \tag{11.3.6}$$

In this section we restrict ourselves to (locally undrained) isochoric deformation modes, i.e. we assume that

$$\Delta \tilde{q}_\alpha = 0 \rightarrow \Delta \varepsilon_{\alpha\alpha} = 0 \tag{11.3.7}$$

Note that for the considered (globally) undrained deformations, $q_\alpha = \Delta \mathring{q}_\alpha = 0$, and thus always $\tilde{q}_\alpha = \Delta \tilde{q}_\alpha$.

Linear equilibrium bifurcation analysis is based on the assumption that the perturbation mode is sufficiently 'small' such that nowhere in the domain unloading takes place. In other words, the analysis is not performed for the true (quasi-linear) elastoplastic solid but for another linear 'comparison' solid, which corresponds to full loading conditions. For the considered set of isochoric deformation modes the incremental constitutive equations in the coordinate system of principal axes of initial stress become,

$$\begin{aligned} \Delta \sigma_{11} &= \Delta \sigma + 2G^* \Delta \varepsilon_{11} \\ \Delta \sigma_{22} &= \Delta \sigma + 2G^* \Delta \varepsilon_{22} \\ \Delta \sigma_{12} &= 2G \Delta \varepsilon_{12} \end{aligned} \tag{11.3.8}$$

where

$$G^* = \frac{h - h_T}{1 + h - h_T} G \tag{11.3.9}$$

is the tangent shear modulus, which reflects the dependence of the stress deviator $\tau = (\sigma_{11} - \sigma_{22})/2$ on the strain deviator $\gamma = \varepsilon_{11} - \varepsilon_{22}$ (cf. Figure 11.1.8). Accordingly G^* becomes zero at the state (T_1) of maximum deviator, and is negative in the softening regimes of the deviatoric stress-strain curve. In the constitutive equations 11.3.8,

$$\Delta\sigma = \Delta\sigma' - \Delta p_w \tag{11.3.10}$$

is the mean stress increment. We observe that the mean effective stress increment is determined

$$\Delta\sigma' = \frac{-K\beta}{1 + h - h_T} \Delta\gamma \tag{11.3.11}$$

This means that, in general, the pore-water pressure increment Δp_w is kinematically undetermined to accommodate the incompressibility constraint imposed by equation 11. 3.7.2. Note that for the analysis of the ground mode, Δp_w is determined by a boundary condition, equation 11.1.15, which of course cannot be invoked here, in a local bifurcation analysis.

In particular, we examine here the existence of a special type of non-uniqueness in the form of discontinuities in the strains $\Delta\varepsilon_{ij}$. Let n_i be the unit normal vector to the shear-band axis and let g_i be the jump of the normal derivative of the incremental displacement vector. The geometric jump conditions for the incremental strain are

$$[\Delta\varepsilon_{\alpha\beta}] = (g_\alpha n_\beta + g_\beta n_\alpha)/2 \tag{11.3.12}$$

In particular the constant volume condition results in the following restriction

$$g_1 n_1 + g_2 n_2 = 0 \tag{11.3.13}$$

The bifurcation condition for shear banding is expressed in terms of jump conditions for the stress increments, as

$$[\Delta\sigma_{\alpha\beta}] n_\alpha = 0 \tag{11.3.14}$$

If we introduce in this equation the constitutive equations 11.3.8 and the geometric compatibility conditions 11.3.12 with the constraint 11.3.13, we obtain the classical characteristic equation for the direction cosines n_α by asking for non-trivial solutions for the jump vector g_α. First bifurcation is predicted whenever this equation provides for the first time real characteristics. In the case considered we obtain the following condition for first bifurcation,

$$h = h_T \tag{11.3.15}$$

The characteristic direction for the shear band is expressed in terms of an angle θ, which measures the inclination of its axis with respect to the minor principal stress σ_2. With

$$n_1 = -\sin\theta;\ n_2 = \cos\theta;\ n_3 = 0 \tag{11.3.16}$$

in the present case we have

$$\tan\theta = \pm 1 \rightarrow \pm\theta = 45^\circ \tag{11.3.17}$$

This means that first isochoric shear-band bifurcation is occurring at the state T_1 of first maximum of the deviator, and at critical angles of $\pm 45^\circ$, which correspond to planes on which the shear stress is maximum. The corresponding jump in total stress is zero,

$$[\Delta\sigma] = 0 \rightarrow [\Delta p_w] = [\Delta\sigma'] = -\sqrt{2K\beta}\, g_1 \tag{11.3.18}$$

The above bifurcation solution is slightly modified if the effect of initial stress is included. In this case $\Delta\sigma_{\alpha\beta}$ in the statical compatibility condition 11.3.14 is replaced by $\Delta\pi_{\alpha\beta}$, the increment of the nominal (1. P.-K.) stress tensor referred to the current configuration C, and the stress increments appearing in the constitutive equations 11.3.8 are seen as the corresponding Cauchy/Jaumann stress increments. At this approximation level the characteristic equation yields (Hill and Hutchinson, 1975),

$$(1+\xi)n_1^4 + 2(2G^*/G - 1)n_1^2 n_2^2 + (1-\xi)n_2^4 = 0 \tag{11.3.19}$$

where $\xi = \tau/G \ll 1$ measures the effect of initial stress. First bifurcation is predicted slightly prior to (T_1), at

$$h = h_T + \xi^2/2 \tag{11.3.20}$$

with

$$\pm\tan\theta = 1 - \xi/2 + O(\xi^2) \tag{11.3.21}$$

and the pore-water jump is in general non-zero,

$$[\Delta p_w] \approx -\sqrt{2G}\{k\beta - \xi + O(\xi^2)\} g_1 \tag{11.3.22}$$

These results imply that, even for plastically incompressible poro-elastoplastic material (β=0), undrained shear banding goes hand in hand with pore-water pressure shocks. In metal thermo-elastoplasticity the analogous phenomenon is called 'adiabatic shearing', which is physically meaningful under rapid loading conditions. Accordingly, in order to justify solutions 11.3.18 or 11.3.22 we have to estimate how long such pressure shocks may be sustained and compare this characteristic time with the ordinary testing time scale. In order to do this we first consider the complete storage equation

$$-\partial_\alpha \bar{q}_\alpha = -c_s \partial_t \Delta p' + c_m \partial_t \Delta p_w + \partial_t \Delta\varepsilon_{\alpha\alpha} \tag{11.3.23}$$

Interstitial fluid flow is governed by Darcy's law

$$\bar{q}_\alpha = -\frac{1}{f}\partial_\alpha \Delta p_w \tag{11.3.24}$$

For the limiting case of isochoric skeleton deformation then the resulting equation is a pore-pressure diffusion equation

$$\partial_t p_w = c_p \nabla^2 p_w;\ c_p = 1/(fnc_w) \tag{11.3.25}$$

According to test data reported in Han and Vardoulakis (1991) for the typical test DC-04, f is estimated as: $f = 3 \times 10^6\,\mathrm{g\,cm^{-3}\,sec^{-1}}$, and with that the pore-pressure diffusivity coefficient results in: c_p=2m^{2}sec^{-1} With this estimate we can examine the possibility of locally undrained shear banding. From X-ray radiographs the thickness of the shear band is estimated as $2d_B \approx 22D_{50}$, with a mean grain size of $D_{50} = 0.165\,\mathrm{mm}$. Thus the corresponding characteristic time for pore pressures to diffuse across the shear band is indeed very small: $t_{chr} = (d_B^2/c_p) \approx 100\,\mathrm{msec}$. This allows us to conclude that *in ordinary soil mechanics testing situations no pore-pressure shocks can develop across shear-band boundaries.*

With the assumption of continuity for the pore-water pressure,

$$[\Delta p_w] = 0 \tag{11.3.26}$$

equations 11.3.18 or 11.3.22 result in

$$g_1 = 0 \tag{11.3.27}$$

i.e. to the condition that excludes the possibility of locally undrained shear banding. In other words, the analysis supports the assumption that in the considered tests (locally) undrained shear banding cannot be sustained, and the herein considered bifurcation mode at state (T_1) is under the given circumstances unrealistic. This finding is supported by experiment, since no shear bands at an angle of $\pm 45^\circ$ close to (T_1) are observed.

11.3.2
Linear stability analysis

In the context of a poro-elastoplasticity theory for dilatant hardening/softening frictional material linear stability analysis was first performed by Rice (1975). Vardoulakis (1985) showed that Rice's linear stability analysis at the state of maximum deviator (T_1) leads to a sharp transition from infinitely stable to infintely unstable behavior, which indicates that the underlying mathematical problem is ill-posed. All these observations force us to discuss questions of existence, uniqueness and stability in a more detailed manner.

Linear stability is done here if the fluid-saturated medium is treated along the lines of section 5.7.3. The strict zero drainage condition is relaxed by allowing internal flow to take place. Flow is governed by the storage equation, where both fluid and solid phase are assumed to be incompressible. We recall that the storage equation derives from mass balance and that its consideration introduces the time scale into the problem. Having done so, one may consider balance of linear momentum for the inertialess limit,

$$\partial_\alpha \Delta\sigma_{\alpha\beta} = 0 \tag{11.3.28}$$

where the total stress increment is split according to Terzaghi's effective stress principle into effective stress and pore-water pressure, $\Delta\sigma_{\alpha\beta} = \Delta\sigma'_{\alpha\beta} + \Delta p_w \delta_{\alpha\beta}$. The effective stress increment is determined by the deformation of the soil skeleton through the

elastoplastic stiffness tensor L^{ep}; cf. equation 6.5.42ff. Linear stability analysis is performed on the basis of the upper-bound, linear comparison solid, described by the corresponding stiffness tensor $\mathbf{L}^{u} = L^{e} - L^{p}$.

Elimination of the total stress increment from the set of governing equations leads finally to the following set of linear partial differential equations for the perturbation mode

$$L^{u}_{ijkl}\partial_j\partial_l\Delta\tilde{u}_k = \partial_i\Delta\tilde{p}_w$$
$$\partial_t\partial_k\Delta\tilde{u}_k = \frac{1}{f}\partial_m\partial_m\Delta\tilde{p}_w \tag{11.3.29}$$

The coefficients of $\mathbf{L}^{u}$ are only functions of the plastic strain-hardening parameter γ^{p}, whereas f is treated as a constant. However, through the mass-balance equation for the solid phase, one could compute changes of the porosity, which in turn would affect the physical permeability k and with that f. This additional non-linearity is suppressed here as well.

For the roller bifurcation mode (Figure 5.7.1) linear stability is described by the dispersion equation for the growth coefficient of the instability

$$(fS) = -\frac{\Gamma(\gamma^{p}; n_1, n_2)}{\Delta(\gamma^{p}; n_1, n_2)}Q^2$$

cf. equation 5.7.49. We recall that coefficients Δ and Γ are biquadratic forms in the direction cosines n_i

$$\Delta = \Gamma_{11}n_2^2 - (\Gamma_{12} + \Gamma_{21})n_1n_2 + \Gamma_{22}n_1^2 \tag{11.3.31}$$

$$\Gamma = \det(\Gamma_{\alpha\beta}) \tag{11.3.32}$$

where $\Gamma_{\alpha\beta}$ is the corresponding acoustic tensor.

As mentioned in section 5.7.3, linear stability analysis becomes questionable, if (for some values of the plastic hardening parameter γ^{p} and) some directions n_i, the coefficient Δ in equation 5.7.49 becomes zero. In this case the algebraic (dispersion) equation 11.3.30 is meaningless, and a solution for the corresponding linear stability problem does not exist. To discuss a little further this tantalizing case, the coefficient Δ is written explicitly

$$\Delta/G = n_1^4 + Rn_1^2n_2^2 + n_2^4 \tag{11.3.33}$$

where

$$R = 2\left\{2\frac{h - h_T}{1 + h - h_T} - 1\right\} \tag{11.3.34}$$

We observe that

$$\{\forall n_i\colon h > h_T\} \rightarrow \Delta > 0$$

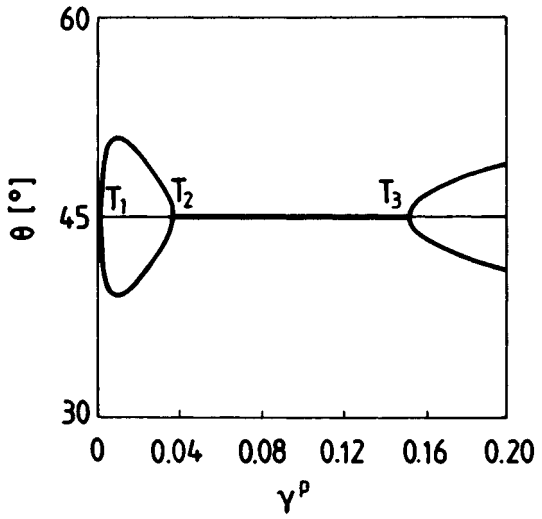

Figure 11.3.1 Real solutions for 'ill-posedeness' directions.

and accordingly existence of solution is guaranteed. As already mentioned, the condition $h = h_T$ holds whenever the deviator becomes stationary, i.e. at states (T_1), (T_2) and (T_3); cf. Figure 11.1.8. For states between the first maximum deviator (T_1) and minimum deviator (T_2) and past the second maximum deviator (T_3), $h<h_T$ and the biquadratic equation

$$\Delta(\Theta) = 0 \tag{11.3.35}$$

has real solutions in Θ. For all these states the underlying initial boundary value problem is mathematically ill-posed. We notice that for stationary deviator $(h = h_T)$ the critical angle from 11.3.32 is again $\Theta_T = \pm 45^\circ$, corresponding to the pattern of Figure 5.7.1. This means that the initial problem for incremental perturbations of the isochoric (volume preserving) deformation becomes for the first time ill-posed at maximum deviator (T_1) along characteristic directions which correspond to the planes of maximum shear stress. Past this state two sets of symmetric solutions of equation 11.3. 35 exist, as depicted in Figure 11.3.1.

Finally we notice that nullity of the determinant of the acoustic tensor,

$$\Gamma(\Theta) = 0 \tag{11.3.36}$$

may occur in the regime of mathematical ill-posedeness. For example, in the discussed test DC-04, $\Gamma = 0$, is predicted at $\gamma_B^p \approx 0.8\%$ and for a critical angle of $\Theta_B \approx \pm 50^\circ$, which coincides with one of the two solutions of Δ=0 at this state.

11.3.3 Regularization

The ill-posedeness of the underlying initial value problem for states with $h<h_T$ cannot be remedied by considering regularizations of the type which introduce only an additional material length into the problem. In this category fall for example extensions of either the constitutive equations of the soil (e.g. Cosserat or second-gradient models; cf. Vardoulakis, 1989; Vardoulakis and Aifantis, 1989; Vardoulakis and Frantziskonis, 1992) or of the fluid flow (e.g. extensions of Darcy's law; cf. Brinkman, 1947; Aifantis, 1986; Vardoulakis and Aifantis, 1994). If, however, in addition to the characteristic length, a characteristic time is introduced into the problem, through for example viscous or micro-inertial effects, then regularization is achieved. In order to demonstrate this, we resort to the complete second-grade extension of the classical flow theory of plasticity discussed here. As explained in chapter 10 the constitutive equations of flow theory of plasticity can be rigorously extended so as to consider the effect of high-strain gradients and accelerations,

$$\Delta\sigma'_{\alpha\beta} = L^{ep}_{\alpha\beta\gamma\delta}\Delta\varepsilon_{\gamma\delta} - L^{p}_{\alpha\beta\gamma\delta}\{\ell^2\nabla^2 - T^2\partial_t^2\}\Delta\varepsilon_{\gamma\delta} \tag{11.3.37}$$

where ℓ and T are material characteristic length and time scales (Vardoulakis and Aifantis, 1994).

In this case, linear stability considerations result in a third-degree polynomial 'dispersion' equation

$$Mb_0\overset{*}{s}^3 + b_7\overset{*}{q}^2\overset{*}{s}^2 + M(a_0 + b_0\overset{*}{q}^2)\overset{*}{s} + (a_1 + b_1\overset{*}{q}^2)\overset{*}{q}^2 = 0 \tag{11.3.38}$$

for dimensionless growth coefficient and wavenumber,

$$\overset{*}{s} = ST;\ \overset{*}{q} = Q\ell \tag{11.3.39}$$

The coefficients of the above dispersion equation are as follows

$$M = \frac{f\ell^2}{GT} \tag{11.3.40}$$

$$\begin{aligned} b_0 &= \{L^p_{1111} - (L^p_{1122} + L^p_{2211}) + L^p_{2222}\}n_1^2n_2^2/G \\ b_1 &= \{\Gamma_{11}L^p_{2222}n_2^2 - (\Gamma_{12}L^p_{2211} + \Gamma_{21}L^p_{1122}) + \Gamma_{22}L^p_{1111}n_1^2\}/G^2 2 \end{aligned} \tag{11.3.41}$$

$$\begin{aligned} a_0 &= \Delta/G = \{\Gamma_{11}n_2^2 - (\Gamma_{12} + \Gamma_{21})n_1n_2 + \Gamma_{22}n_1^2\}/G \\ a_1 &= \Gamma/G^2 = (\Gamma_{11}\Gamma_{22} - \Gamma_{12}\Gamma_{21})/G^2 \end{aligned} \tag{11.3.42}$$

The regularization is meaningful if the leading coefficient of the dispersion equation is different from zero.

Since

$$b_0 = \{4/(1 + h - h_T)\}n_1^2n_2^2 > 0 \tag{11.3.43}$$

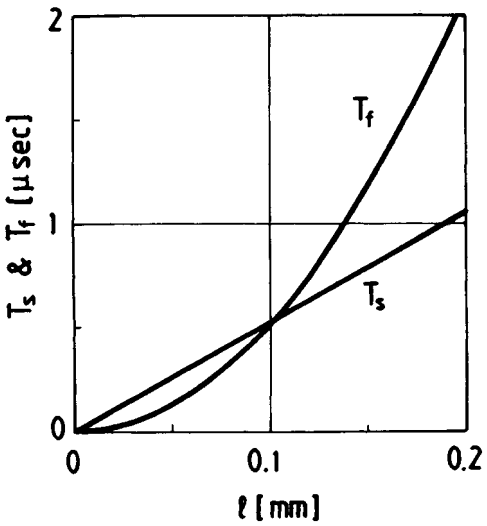

Figure 11.3.2 Time scaling factors: (a) $T_s = \ell/v_s$ of the micro-inertial effects; (b) $T_f = \ell^2/c_f$ of the interstitial fluid flow.

for $n_i \neq 0$, this results in a requirement for the number M, equation 11.3.40. Indeed, one can get an estimate of this coefficient as follows: If we want to introduce *only one* additional material constant into the second-grade constitutive model 11.3.37, say the internal length ℓ, then the intrinsic time $T \doteq T_s$ due to micro-inertial effects in the solid follows from dimensional analysis by assuming that it corresponds to the time necessary for an elastic body wave to travel the distance ℓ; i.e. if we assume that

$$T_s = \ell/v_s;\ v_s = \sqrt{(G/\rho)} \tag{11.3.44}$$

On the other hand, as in ordinary consolidation theory, the time scale of interstitial fluid flow is governed by a 'consolidation' coefficient c_f such that

$$T_f = \ell^2/c_f;\ c_f = G/f \tag{11.3.45}$$

We remark that T_s is linear and that T_f is quadratic in ℓ

$$T_s = O(\ell);\ T_f = O(\ell^2) \tag{11.3.46}$$

(Figure 11.3.2) and that the intrinsic time factor

$$M = \frac{T_f}{T_s} \tag{11.3.47}$$

If we set $\ell = D_{50}$ (D_{50}=0.165mm, mean grain size) then for the above values for test DC-04 of f, G and ρ we obtain, c_0=1.63. Accordingly, in the microscale the two characteristic times are small but of the same order: $T_f \approx 1.43$, $T_s \approx 0.88\,\mu\text{sec}$. In this regime the consideration of strain gradients and accelerations removes the mathematical ill-

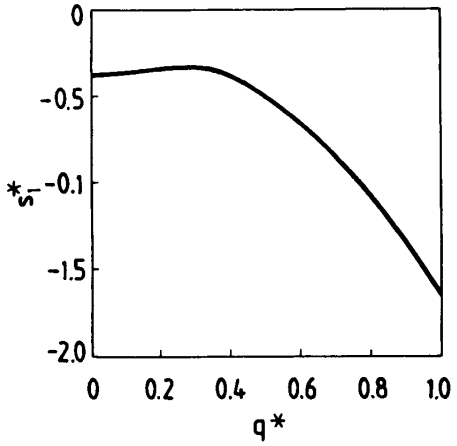

Figure 11.3.3 The stable mode, $s_1^* < 0$.

posedeness at state (T_1); Figures 11.3.3 and 11.3.4 show the corresponding dispersion curves:

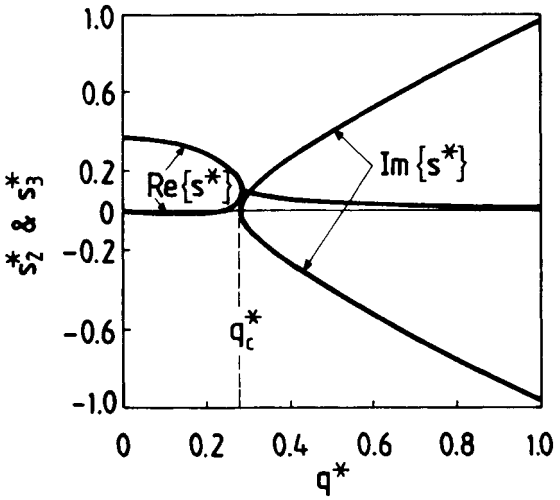

Figure 11.3.4 The unstable mode Re{s}>0, with flutter instabilities Im {s}≠0, at short wavelengths.

Figure 11.3.3 One mode is stable throughout since it corresponds to a negative root of the cubic dispersion equation 11.3.38, $(0 < q^* < q_c^*)$.

Figure 11.3.4 The other two modes show two regimes: (a) Large wavelength regime ($s_2^* < 0 < s_3^*$) with two real solutions ($q_c^* < q^* < \infty$), i.e. stable second and unstable third mode. (b) Short wavelength regime ($q_c^* < q^* < \infty$) with two conjugate complex solutions and positive real part Re{s*}>0, i.e. in this regime, flutter instabilities are predicted.

With sufficiently small spatial discretization (q_c^*) and a scaling law for the time such that ($T_f \approx T_s$) instabilities in regime 11.3.4 should be suppressed. Flutter instabilities which are predicted in this regime seem to be an artifact of linear analysis and that they should disappear in a fully non-linear elastoplastic consideration.

Summary. The constitutive equations used here to describe the corresponding linear comparison solid under loading are in reality successive asymptotic approximations of the 'true' behavior:

$$\begin{aligned} &\text{hypoelasticity:} && \Delta\sigma' = L^e\Delta\varepsilon \\ &\text{zeroth-grade elastoplasticity:} && \Delta\sigma' = L^e\Delta\varepsilon - L^p\Delta\varepsilon \\ &\text{second-grade elastoplasticity:} && \Delta\sigma' = L^e\Delta\varepsilon - L^p\Delta\varepsilon - L^p\{\ell^2\nabla^2 - T^2\partial_t^2\}\Delta\varepsilon \end{aligned} \tag{11.3.48}$$

Consequently, in the case of *deviator softening* poro–elastoplastic soil, we remark that linear stability for zeroth-order flow theory results in ill-posedeness, whereas second-grade flow theory results in instability, i.e. consideration of sufficient terms in the asymptotic constitutive expansion results in regularization of the system of governing partial differential equations 11.3.30.

11.3.4
Globally undrained shear banding

In order to illustrate the possibility of shear-band formation under *globally* undrained conditions we consider here as an example shear banding in a medium dense specimen, namely in test DC-04. As already mentioned in the previous section, drained shear banding is governed by the nullity of the determinant of the acoustic tensor, condition 11.3.37, which for the considered test resulted in a bifurcation prediction: $\gamma_B^p \approx 0.8\%$, $\theta_B \approx \pm 50°$, $\gamma_E \approx \gamma_E^p \approx 12\%$ in the hardening regime of the underlying effective stress ratio versus plastic strain curve. In the considered biaxial tests shear band formation was signaled by appreciable horizontal displacement of the movable bottom plate of the biaxial apparatus; cf. Figure 11.3.5. Shear banding was found experimentally for the considered test DC-04 at $\gamma_E \approx \gamma_E^p \approx 12\%$ with $\theta_E = 57°$, in the softening regime of the (μ, γ^p)-curve. This means that we may say the globally undrained conditions seem to delay shear banding. In order to explain this we examine the situation in the test more closely.

The hodograph of the measured rigid-body displacements is inclined at an angle $\theta' = 53.5°$, which after correction becomes 55.4°. This indicates that in post-failure, the

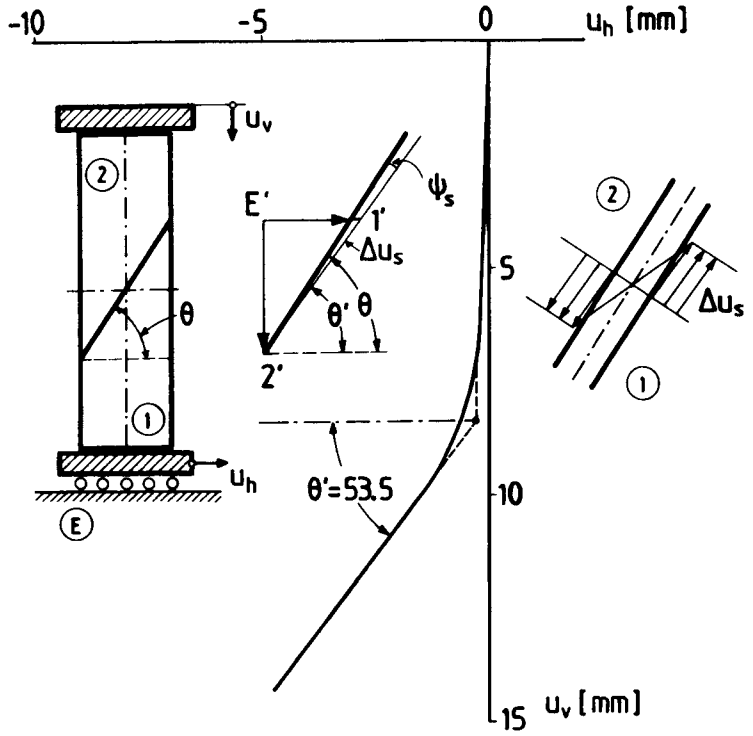

Figure 11.3.5 Specimen with shear band and hodograph.

shear band is dilating by $\psi_s = \theta - \theta' = 1.6°$. However, if we want to investigate the point of incipient shear-band formation, we must assume that the dilatancy angle

$$\psi_s = \psi_m \tag{11.3.49}$$

and accordingly,

$$\theta' = \theta - \psi_m \tag{11.3.50}$$

Globally undrained shear banding is only then possible, if the amount of water that has to flow across the shear-band boundaries due to small shear-band dilation or contraction can be accommodated by elastic deformation of the surrounding band soil mass. Let dV_B be the change in volume of the shear band due to plastic dilatancy, and let dV be the corresponding volume contraction of the specimen due to increasing effective mean stress

$$dV_B = V_B \, d\varepsilon_B = \frac{du_s}{d_B} \sin\psi_s \, 2d_B \frac{B}{\cos\theta} \tag{11.3.51}$$

$$dV = V \frac{d\sigma'}{K} = BH \frac{d\sigma'}{K} \tag{11.3.52}$$

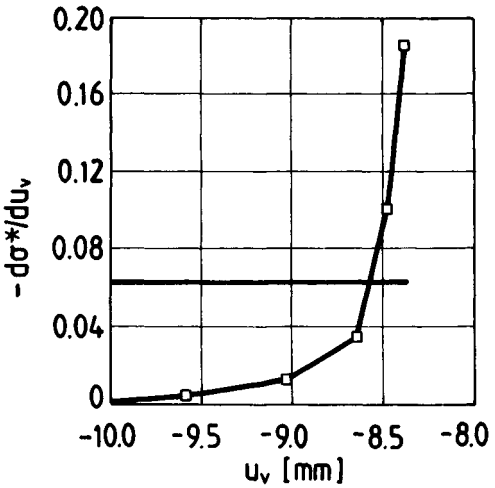

Figure 11.3.6 Graphical representation of the undrained shear-band condition.

where $H \approx 141\,\text{mm}$ and $B \approx 39\,\text{mm}$ are the height and width of the specimen. Globally undrained shear banding requires that

$$\mathrm{d}V_{\mathrm{B}} = \mathrm{d}V \tag{11.3.53}$$

With the $\mathrm{d}u_{\mathrm{v}}$ being the vertical displacement and $\mathring{\sigma} = \sigma'/K'$, we obtain the following constraint

$$-\frac{\mathrm{d}\mathring{\sigma}}{\mathrm{d}u_{\mathrm{v}}} = \frac{2\sin\psi_{\mathrm{s}}}{H\cos\theta\sin\theta'} \tag{11.3.54}$$

In Figure 11.3.6 the directly measured quantity in the left-hand side of 11.3.54 is plotted against the vertical displacement u_{v}. The horizontal line corresponds to the quantity in the right-hand side of equation 11.3.54. This figure demonstrates that globally undrained shear banding is only possible at a later stage of the deformation, which in the particular experiment was past the Coulomb state of maximum effective stress ratio. The analysis of the experimental results seems to indicate that, although the local condition for instability may be satisfied, remote boundary conditions preventing drainage together with displacement control result in global stability. In other words, the fact that the specimen is relatively 'small' results in suppression of the fully drained shear-band bifurcation mode. However, for very densely packed specimens, and in the vicinity of the Coulomb state, maximum plastic dilatancy causes a sharp drop of the pore-water pressure, which occasionally may even become sufficiently negative to cause cavitation. On this occasion, drained shear banding is possible and does actually occur.

11.4
Grain size and shape effect

The response of the specimens in the experiments on sand reported above was obviously dominated by the boundary conditions, since the condition of zero fluid flux across the boundaries of the specimen seems to prohibit internal fluid flow, and to suppress accordingly the herein discussed internal instabilities. Assuming that the material length is determined by the mean grain size D_{50} (here $D_{50} = 0.165\,\text{mm}$), it seems that the considered specimens with a smallest geometric dimension B=40mm and a scale factor $B/D_{50} \approx 250$ are still too 'small'. This dominance of the boundary conditions and the resulting stabilizing effect is not observed in (normally, anisotropically consolidated) clays where the corresponding characteristic material length (particle size) is 100 times smaller; cf. Vardoulakis, 1982, 1985.

Figure 11.4.1 shows a microscopic view of the shear band in a kaolin specimen subjected to direct shear as presented by Morgenstern and Tschalenko (1967). According to this figure the thickness $2d_B$ of the shear band is of the order of few hundreds of microns; $2d_B \approx 200\,\mu\text{m}$. Accordingly, shear banding cannot be suppressed at all in clays by external control. Moreover, shear bands occur in clays in rhombic pattern formation, as shown in Figure 11.4.2, for normally, anisotropically consolidated kaolin clay in plane strain and axisymmetric, undrained compression experiments after Kuntsche (1982). Shear-band patterning, on the other hand, illustrates the volume of material which is sufficient to accommodate shear-band dilation.

These observations prompt the question as to whether in fine-grained materials like clays, instabilities are indeed observed at the state (T) of maximum deviator, whenever this state is reached in undrained tests. In undrained triaxial compression tests of water-saturated specimens under constant confining pressure σ_c, pore-water pressure changes are usually expressed by Skempton's pore-pressure parameter A_f,

$$A_f = \frac{\Delta p_w - \Delta\sigma_c}{\Delta\sigma_a - \Delta\sigma_c} \tag{11.4.1}$$

In this definition, σ_a is the axial stress, and the index f denotes the state of 'failure'. In Figure 11.4.3, A_f is plotted as a function of the 'overconsolidation' ratio (OCR), which in turn measures the degree of compaction prior to shear (Graham and Li, 1985).

In undrained tests of (highly plastic) structured, normally to lightly overconsolidated clays, the state (f) coincides with the Tresca state (T), of maximum deviator. Due to the platelet shape of clay particles, 'structure' may be induced by anisotropic preconsolidation, resulting in preferred particle bedding, normal to the major preconsolidation stress. This anisotropic structure of the clay fabric seems to lead to the fact that at state (T) pore-water pressure generation is high, and it becomes unstable for normally (anisotropically) consolidated clays (Parry and Nadarajah, 1974). This can be seen also in Figure 11.4.4(a), which shows that a normally, anisotropically consolidated, highly plastic clay reaches the (T), under definite pore-water pressure generation,

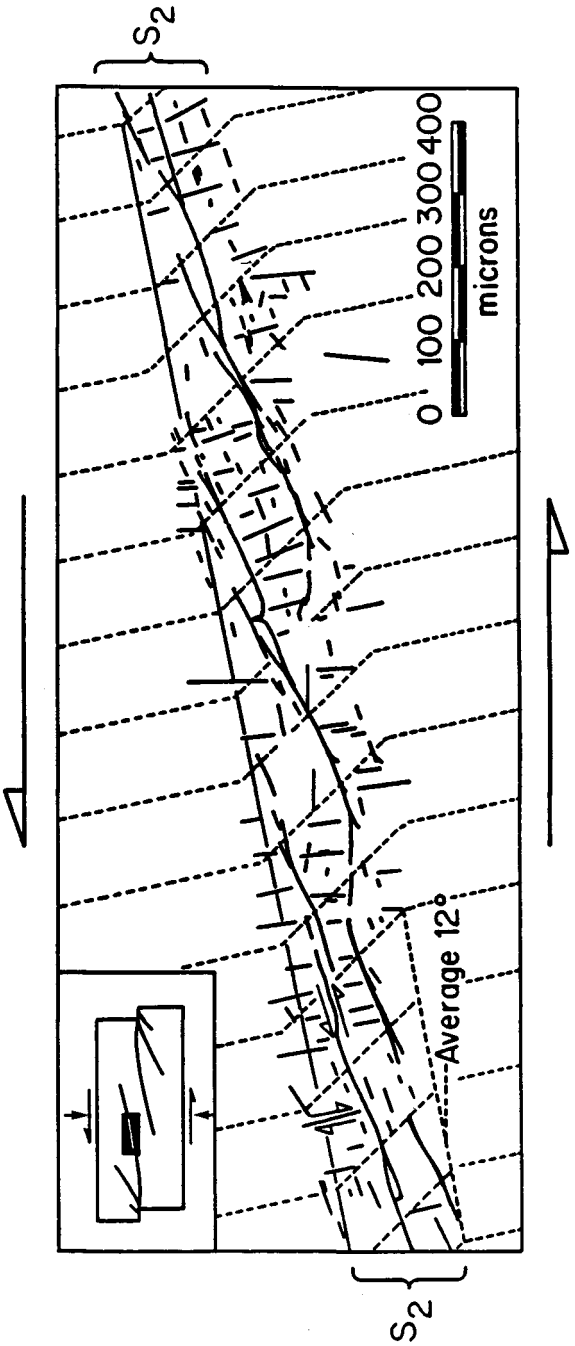

Figure 11.4.1 Detail of a shear band in a kaolin specimen subjected to direct shear; after Morgenstern and Tschalenko (1967).

indicating in turn that the background drained behavior is contractant at (T). Figure 11.4.5(a) demonstrates clearly that for a material like this the pore-pressure

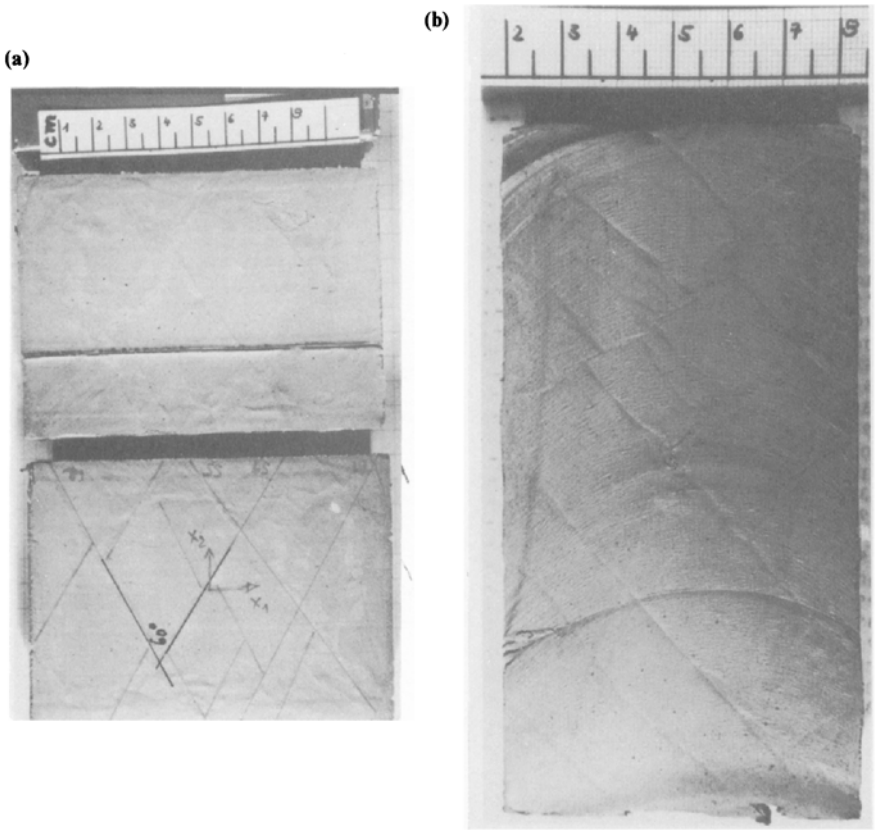

Figure 11.4.2 Deformation patterning in normally consolidated kaolin specimens: (a) plane-strain constant volume-controlled test; (b) undrained.

generation at (T) becomes unstable.

In normally, isotropically consolidated or significantly overconsolidated clays the failure state coincides practically with the Coulomb state (C), of maximum effective stress ratio. Such specimens reach first the state (C) with the pore-water pressure decreasing, indicating dilatant behavior; Figures 11.4.4(b) and 11.4.5(b). As already mentioned above, in this case the failure mode is patterned shear banding (Figure 11.4.2).

Literature

Textbooks and monographs

Casagrande, A. (1976). *Liquefaction and Cyclic Deformation of Sands—A Critical Review.* Harvard Soil Mechanics Series, 88. Harvard University Press.

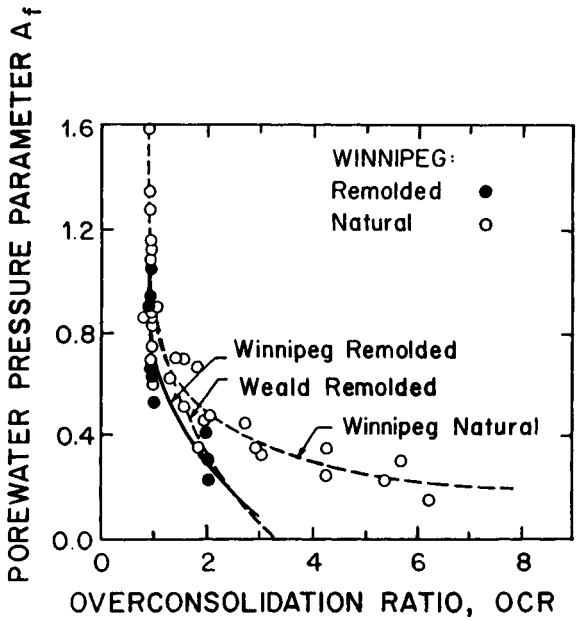

Figure 11.4.3 Skempton's pore-pressure parameter A_f versus overconsolidation ratio (Graham and Li, 1985).

Castro, G. (1969). *Liquefaction of Sands.* Harvard Soil Mechanics Series, 81. Harvard University Press.

Kuntsche, K. (1982). Materialverhalten von wassergesättigtem Ton bei ebenen und zylindrischen Verformungen. Dissertation Universität Karlsruhe, Veröffentlichungen IBF, Heft Nr. 91.

Taylor, D.W. (1948). *Fundamentals of Soil Mechanics.* John Wiley, New York, London.

References

Aifantis, E.C. (1986). Application of mixture theory to fluid saturated geologic media. In: *Compressibility Phenomena in Subsidence (Proc. of the Engineering Foundation Conference, New Hampshire, 1984)* (ed. S.K.Saxena), 65–78, 1986.

Alarcon-Guzman, A. *et al.* (1988). Undrained monotonic and cyclic strength of sands. *J.Geotech. Div. ASCE,* **114,** 1089–1109.

Brinkman, H.C. (1947). A calculation of the viscous force exerted by a flowing fluid on a dense swarm of particles. *Appl. Sci. Res.,* **A1,** 27–34.

Graham, J. and Li, E.C.C. (1985). Comparison of natural and remolded plastic clay. *J. Geotech. Div. ASCE,* **111,** 865–881.

Han, C. and Vardoulakis, I. (1991). Plane-strain compression experiments on water-saturated fine-grained sand. *Géotechnique,* **41,** 49–78.

Hill, R. and Hutchinson, J.W. (1975). Bifurcation analysis in the plane tension test. *J. Mech. Phys. Solids,* **23,** 239–264.

Ishihara, K., Tatsuoka, F. and Yasuda, S. (1975). Undrained deformation and liquefaction of sand under undrained cyclic stresses. *Soils Foundations,* **15,** 29–44.

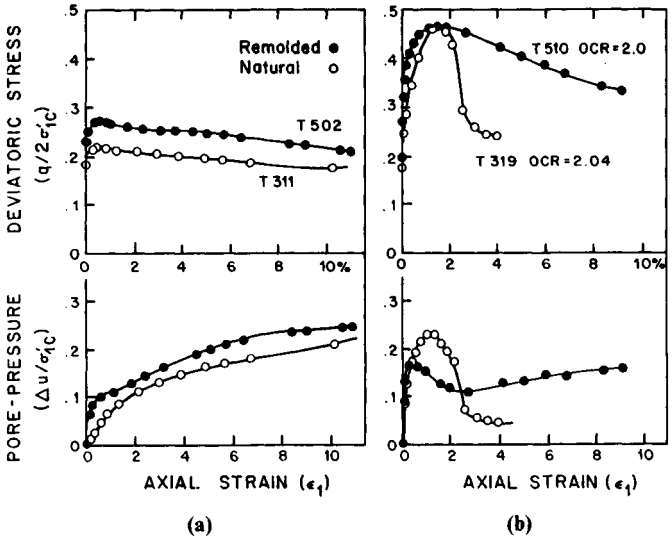

Figure 11.4.4 Stress-strain and pore-water pressure curves for undrained triaxial tests on anisotropically (structured) consolidated clay specimens: (a) normally consolidated; (b) over-consolidated (Graham and Li, 1985).

Ishihara, K. (1993). Liquefaction and flow failure during earthquakes. The Rankine Lecture. *Géotechnique,* **43,** 351–415.

Lade, P.V. (1989). Experimental observations of stability, instability and shear planes in granular materials. *Ingenieur Archiv.,* **59,** 114–123.

Lade, P.V., Nelson, R.B. and Ito, Y.M. (1987). Nonassociated flow stability of granular materials. *J. Eng. Mech. ASCE,* **113,** 1302–1318.

Lade, P.V., Nelson, R.B. and Ito, Y.M. (1988). Instability of granular materials with nonassociate flow. *J. Eng. Mech. ASCE,* **114,** 2173–2191.

Mandel, J. (1966). *Conditions de Stabilité et Postulat de Drucker. IUTAM Symposium on Rheology and Soil Mechanics, Grenoble April 1–8, 1964,* 58–67, Springer-Verlag, Berlin.

Morgenstern, N.R. and Tschalenko, J.S. (1967). Microscopic structures in kaolin subjected to direct shear. *Géotechnique,* **17,** 309–328.

Nova, R. (1991). A note on sand liquefaction and soil stability. In: *Constitutive Laws for Engineering Materials* (eds C.S.Desai, *et al*), 153–156. ASME.

Parry, R.H.G. and Nadarajah, V. (1974). Observations on laboratory prepared, lightly overconsolidated specimens of kaolin. *Géotechnique,* **24,** 345–358.

Peters, J.F. (1984). Instability of loose saturated sands under monotonic loading. In: *Engineering Mechanics in Civil Engineering* (eds A.P.Boresi and K.P.Chong) **2,** 945–948. ASCE.

Rice, J.R. (1975). On the stability of dilatant hardening for saturated rock mass. *J. Geophys. Res.,* **80** (11), 1531–1536.

Tatsuoka, F., Masashige, M. and Tsumo, S. (1982). Cyclic undrained stress-strain behavior of dense sands by torsional simple shear test. *Soils Foundations,* **22,** 55–70.

Vaid, Y.P. and Chern, J.C. (1983). Effect of static shear on resistance to liquefaction. *Soils Foundations,* **23,** 47–60.

Vaid, Y.P. and Chern, J.C. (1985). Cyclic and monotonic undrained response of saturated sands. Advances in the art of testing soils under cyclic conditions, ASCE Annual Convention, Detroit, Michigan, 120–147.

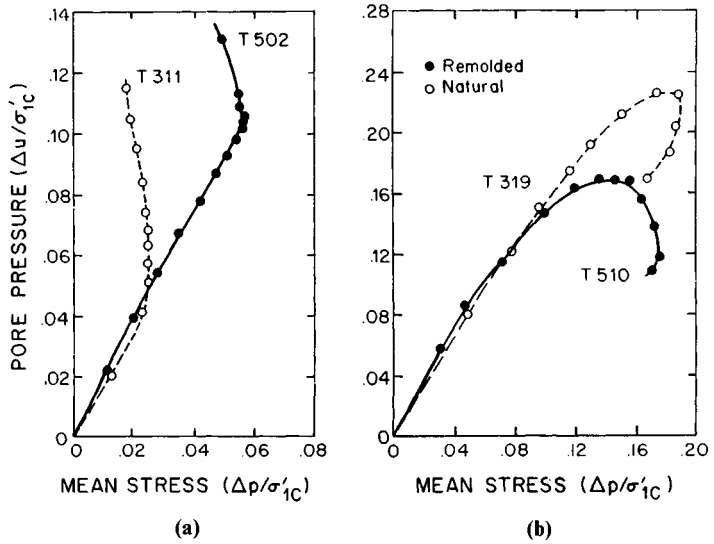

Figure 11.4.5 Relationships between pore-water pressure changes and mean principal stress changes; (a) normally consolidated; (b) over consolidated (Graham and Li, 1985).

Vardoulakis, I. (1982). Stability and bifurcation of soil samples. In: *Constitutive Relations for Soils* (eds G.Gudehus *et al.*), 477–483. Balkema, Rotterdam.

Vardoulakis, I. (1985). Stability and bifurcation of undrained, plane rectilinear deformations on water-saturated granular soils. *Int. J. Num. Anal Meth. Geomech.,* **9,** 339–414.

Vardoulakis, I. (1986). Dynamic stability of undrained simple shear on water-saturated granular soils. *Int. J. Num. Anal. Meth. Geomech.,* **10,** 177–190.

Vardoulakis, I. (1989). Shear-banding and liquefaction on the basis of a Cosserat continuum theory. *Ingenieur Archiv,* **59,** 106–113.

Vardoulakis, I. (1995). Deformation of water saturated sand: I Uniform undrained deformation and shear banding. II The effect of pore-water flow and shear banding. *Géotechnique,* in print.

Vardoulakis, I. and Aifantis, E.C. (1989). Gradient dependent dilatancy and its implications in shear banding and liquefaction. *Ingenieur Archiv.,* **59,** 197–208.

Vardoulakis, I. and Aifantis, E.C. (1994). On the role of microinertia in the behavior of soils: Effects of higher order gradients and inertial effects. *Mech. Mater.,* in press.

Vardoulakis, I. and Frantziskonis, G. (1992). Micro-structure in kinematic-hardening plasticity. *Eur. J. Mech. A/Solids,* **11,** 467–486.

Index